JOINT EUROPEAN TORUS JET

JET
JOINT
UNDERTAKING
PROGRESS
REPORT
1996

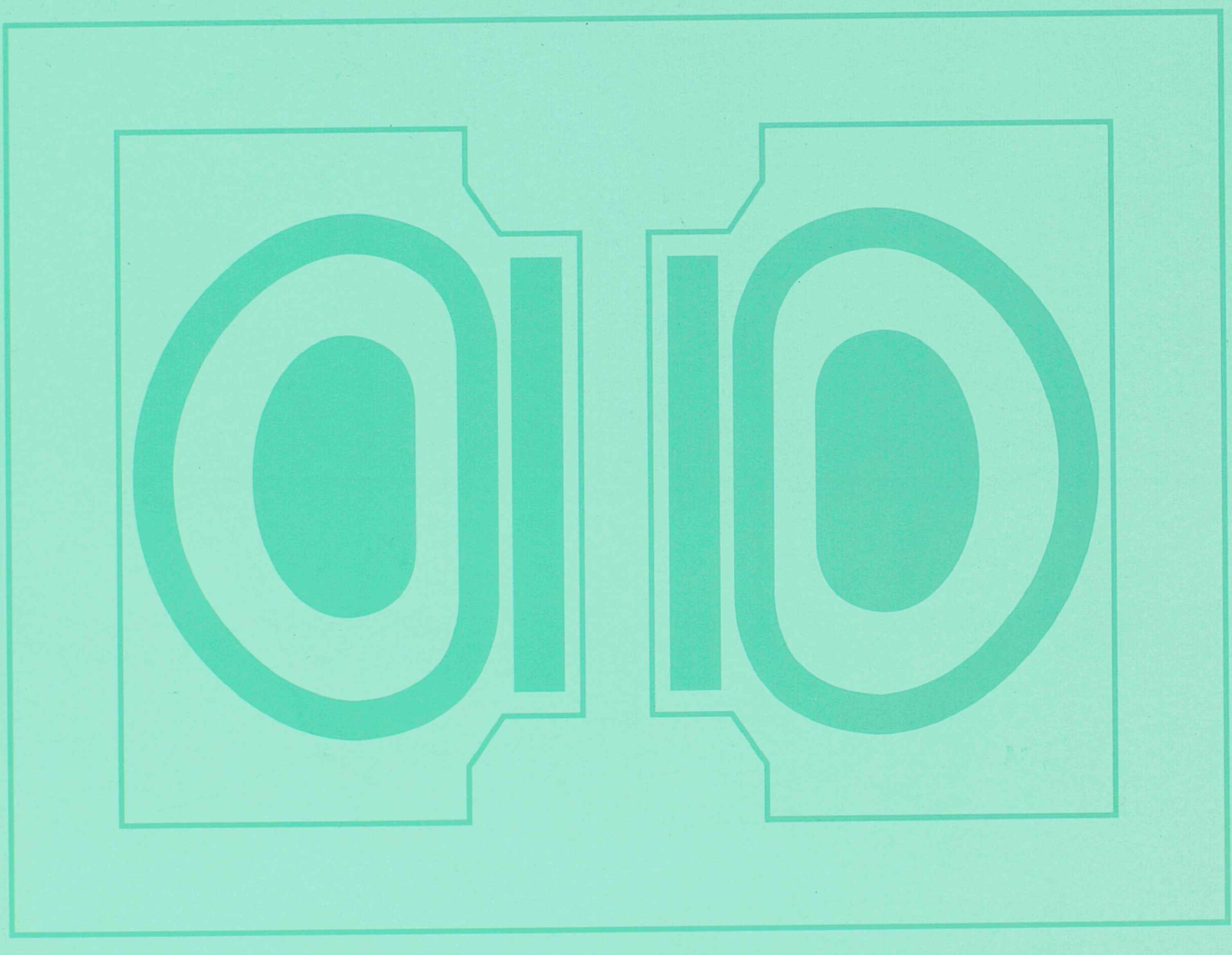

EUR 17619-EN-C
EUR-JET-PR14

JET
JOINT
UNDERTAKING

PROGRESS
REPORT
1996

APRIL 1997

EUR17619-EN-C (EUR-JET-PR14) April 1997.
Editorial work on this report was carried out by B.E.Keen.
The preparation for publication was undertaken by
JET Publications Group, JET Joint Undertaking, Abingdon, UK.

Catalogue number : CD-NB-17619-EN-C for the Report EUR 17619-EN-C

Printed in England

Contents

Foreword

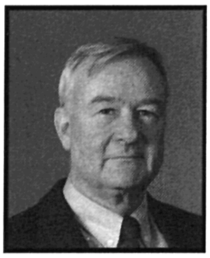

This is the fourteenth JET Progress Report, which provides an overview summary and puts into context the scientific and technical advances made on JET during 1996. This Report presents a more detailed account of JET's Progress than that contained in the JET Annual Report. It is aimed not only at specialists and experts engaged in nuclear fusion and plasma physics, but also at a more general scientific community. To meet these aims, the Report contains a brief summary of the background of the Project, and describes the basic objectives of JET, its role in the world fusion programme and its principal design features.

At the beginning of 1996, JET had entered the ITER-EDA Support Phase of its International Thermonuclear Experimental Reactor (ITER) Support Programme. Before that JET had already completed its Pumped Divertor Characterisation Phase, the objective of which had been to establish reliable methods of plasma purity control and plasma exhaust in operational conditions relevant for the Next Step tokamak. Since the geometry of the divertor is an important aspect in achieving these objectives, a pumped divertor which allowed the test of various configurations had been installed. Tests on the first divertor configuration, the Mark I pumped divertor, had proven to be most effective and allowed a broad-based and highly ITER-relevant research programme to be pursued. This campaign had addressed the central problems of the ITER divertor: efficient dissipation of the exhausted power; control of particle fluxes; and effective impurity screening.

JET started 1996 in shutdown for the installation of the Mark II divertor support structure, which forms the basis for all future divertor work at JET. In addition, the "more-closed" Mark IIA divertor target assembly was installed. During the shutdown, work was also undertaken on various systems in preparation for the next period of D-T operation (DTE-1), scheduled for Spring/Summer 1997, and for the Remote Tile Exchange shutdown after DTE-1. In particular, thirty three carriers and associated tiles were successfully installed by remote handling, giving confidence in operational procedures, tooling, support management and time estimates.

The shutdown was completed on schedule at the end of March 1996 and was followed by pumpdown, leak testing and bake out which were the quickest and most effective after a major shutdown, reflecting the quality of the in-vessel and ex-vessel preparations and the experience gained. The restart programme to commission JET for the start of the experimental programme began at the beginning of April and ended as planned in early June with the routine operation at 2 to 3MA plasma current with up to 20MW of additional heating power.

The 1996 experimental campaign then concentrated on specific ITER-relevant issues related to the "more-closed" Mark IIA divertor and, due to their importance for predicting ITER's ignition margin and fusion power output, the scaling of the H-mode threshold power and the energy confinement. In addition, preparation of high performance scenarios for DTE-1 was a high priority of the campaign.

The Mark IIA divertor behaved as expected for a "more-closed" device. It offered improved power handling over the Mark I divertor, pumped the plasma 2-3 times more rapidly and showed signs of increased neutral recycling in the divertor region. The latter feature showed up particularly well in the detachment of the divertor plasma from the target at significantly lower main plasma density than the Mark I divertor, in agreement with predictions.

In ITER-relevant scaling studies, the threshold power for the H-mode was found to be independent of the type of additional heating (neutral beam or ion cyclotron resonance frequency (ICRF)) and no hysteresis was found. In conjunction with DIII-D (General Atomics, USA), confinement in the plasma core was shown to depend on three dimensionless parameters (normalised Larmor radius, ρ^*, collisionality, ν^* and normalised plasma pressure, β). Precise experiments confirmed the ρ^* and ν^* dependence of the ITER93H-P scaling law used at present for ITER, but the β dependence turned out to be more favourable. With increasing radiated power to reduce the heat load to the divertor target plates, confinement degraded progressively and no longer followed the ITER93H-P scaling law.

An empirical scaling law for plasma purity was also established and showed that only slightly better impurity control would be required for ITER operations with radiative plasmas. Furthermore, steady-state ITER-like plasmas were achieved at high current and heating power.

Fusion performance during 1996 showed a strong dependence on neutral beam heating power, but was restricted by the available power levels of up to 17MW. Combined neutral beam and ion cyclotron resonance frequency heating was also effective in producing high fusion power. Ultimately, hot-ion H-modes were limited by magnetohydrodynamic (MHD) phenomena, when the edge pressure gradient approached the ideal ballooning and kink stability limits.

During 1996, a new and significant mode of high performance optimised shear plasmas were developed. Internal transport barriers were produced in the plasma. Under these conditions, H-mode levels of confinement were obtained during the L-mode phase of the discharge, and fusion performance was already comparable to that obtained in the best hot-ion H-modes of 1996.

A five week shutdown commenced at the end of September to plug divertor bypass leaks, clad the inner wall of the vacuum vessel with graphite tiles and to replace three of the sixteen neutral beam PINIs, which had prevented full power operation. The experimental programme recommenced in November with the aim of optimising performance in preparation for DTE-1 but was interrupted during the second half of December due to a water leak in the Octant No. 8 neutral beam injection box. This was repaired ready for operations to be restarted in early January 1997.

The further reduction of the bypass leakage conductances in October 1996 resulted in a further reduction in the neutral recycling in the main chamber, but did not change significantly the plasma performance or its intrinsic carbon content (perhaps due to the increased carbon tile coverage of the inner wall).

During 1996, the neutral beam heating system operated routinely up to 16-17MW, but technical difficulties with three PINIs prevented operation at the full power of ~20MW. ICRF heating operated routinely with ~8MW in all modes of combined heating operation and up to 17MW in radio-frequency only heated discharges. Real time control of the heating power was used extensively to help maintain steady-state conditions and to economise on neutron production. Overall, the JET machine demonstrated a high level of availability and reliability during 1996. Nonetheless, the reliability of the machine for future operations continues to be assessed, with recent work concentrating on the amelioration and/or accommodation of vertical displacement events which produce the highest vertical forces and sideways vessel displacements.

The first period of D-T operation (DTE-1) is scheduled for Spring 1997, following an intervention to make the necessary final adjustments for D-T operations. The content and duration of DTE-1 has been defined to take account of the developing needs of ITER and the experience gained in JET and TFTR. The extent of DTE-1 is a compromise between studying essential D-T physics for the ITER-EDA and minimising the delays in the experimental programme that could result from certain component failures during DTE-1.

The physics mission of DTE-1 will last about four months and could produce up to 2×10^{20} neutrons. In this case, the activation of the JET vessel would prevent normal manned in-vessel intervention for up to one year after D-T operation. However, in-vessel components which are accessible could be repaired using the remote handling equipment developed for the Mark IIGB (Gas-box) target assembly change. This equipment has demonstrated a very high level of reliability and is now fully proven for the planned remote handling tasks. Its versatility and ability to perform a wide variety of other tasks has also been demonstrated, provided access can be obtained. For ex-vessel repairs, normal manned access will be possible after DTE-1.

The extension of JET to the end of 1999 was officially approved in May 1996. The purpose of the extension is to provide further data of direct relevance to ITER, especially for the ITER-EDA, before entering into a final phase of D-T operation. In particular, the extension will: make essential contributions to the development and demonstration of a viable divertor concept for ITER; permit carrying out experiments using D-T plasmas in an ITER-like configuration, which will provide a firm basis for the D-T operation of ITER; and allow key ITER-relevant technology activities, such as the demonstration of remote handling and tritium handling.

This programme will include studies aimed at providing data in support of the ITER divertor, while satisfying the requirements of high performance D-T operations. The subsequent programme would progress to divertor/plasma optimisation studies before a more extensive period of D-T operation (DTE-2) in 1999. In DTE-2, D-T plasmas would be studied with substantial alpha-particle heating, capitalising on the performance improvements achieved in preceding experimental campaigns. DTE-2 experiments could produce up to 5×10^{21} neutrons, but efforts would be made to reduce activation while still satisfying JET's role in supporting ITER and the World Fusion programme.

JET is still making substantial advances in its scientific and technology programme. With continued dedication of the staff, I am confident that the Project will meet the challenges ahead and will continue to provide crucial information to ensure that fusion will become an important source of energy for future generations.

Dr M Keilhacker
Director
April 1997

Introduction, Background and Summary

Introduction

JET Progress Reports are aimed both at specialists in plasma physics and nuclear fusion research and at the more general scientific community. This contrasts with the JET Annual Reports, which provide overview descriptions of the scientific, technical and administrative status of the JET programme, and is directed at the average member of the public.

To meet these general aims, the Progress Report contains a brief summary of the background to the Project, describes the basic objectives of JET and sets out the principal design aspects of the machine. In addition, the Project Team structure is detailed, since it is within this framework that machine activities and responsibilities are organized and the scientific programme is executed.

The main part of the 1996 Report provides overview summaries of scientific and technical advances made during the year, supplemented by detailed cross-references to the more important JET scientific and technical articles produced during the year. The final part of the Report briefly sets out developments underway to further improve JET's performance and plans for future experiments through to its foreseen completion.

Background

Objectives of JET

The Joint European Torus (JET) is the largest single project of the nuclear fusion research programme of the European Atomic Energy Community (EURATOM). The project was designed with the essential objectives of obtaining and studying plasma in conditions and with dimensions approaching those needed in a fusion reactor. These studies are aimed at defining the parameters, the size and working conditions of a tokamak reactor. The realisation of this objective involves four main areas of work:

(i) the scaling of plasma behaviour as parameters approach the reactor range;
(ii) the plasma-wall interaction in these conditions;
(iii) the study of plasma heating; and
(iv) the study of alpha-particle production, confinement and consequent plasma heating.

Two of the key technological issues in the subsequent development of a fusion reactor are faced for the first time in JET. These are the use of tritium and the application of remote maintenance and repair techniques. The physics basis of the post-JET programme will be greatly strengthened if other fusion experiments currently in progress are successful. The way should then be clear to concentrate on the engineering and technical problems involved in progressing from an advanced experimental device like JET to a prototype power reactor.

Basic JET Design

To meet these overall aims, the basic JET apparatus was designed as a large tokamak device with overall dimensions of about 15m in diameter and 12m in height. A diagram of the apparatus is shown in Fig.1 and its principal parameters are given in Table I. At the heart of the machine, there is a toroidal vacuum vessel of major radius 2.96m having a D-shaped cross-section 2.5m wide by 4.2m high. During operation of the machine, a small quantity of gas (hydrogen, deuterium or tritium) is introduced into the vacuum chamber and is heated by passing a large current through the gas. Originally, the machine was designed to carry 4.8MA, but has been modified to achieve 7MA. This current is produced by transformer action using the massive eight-limbed

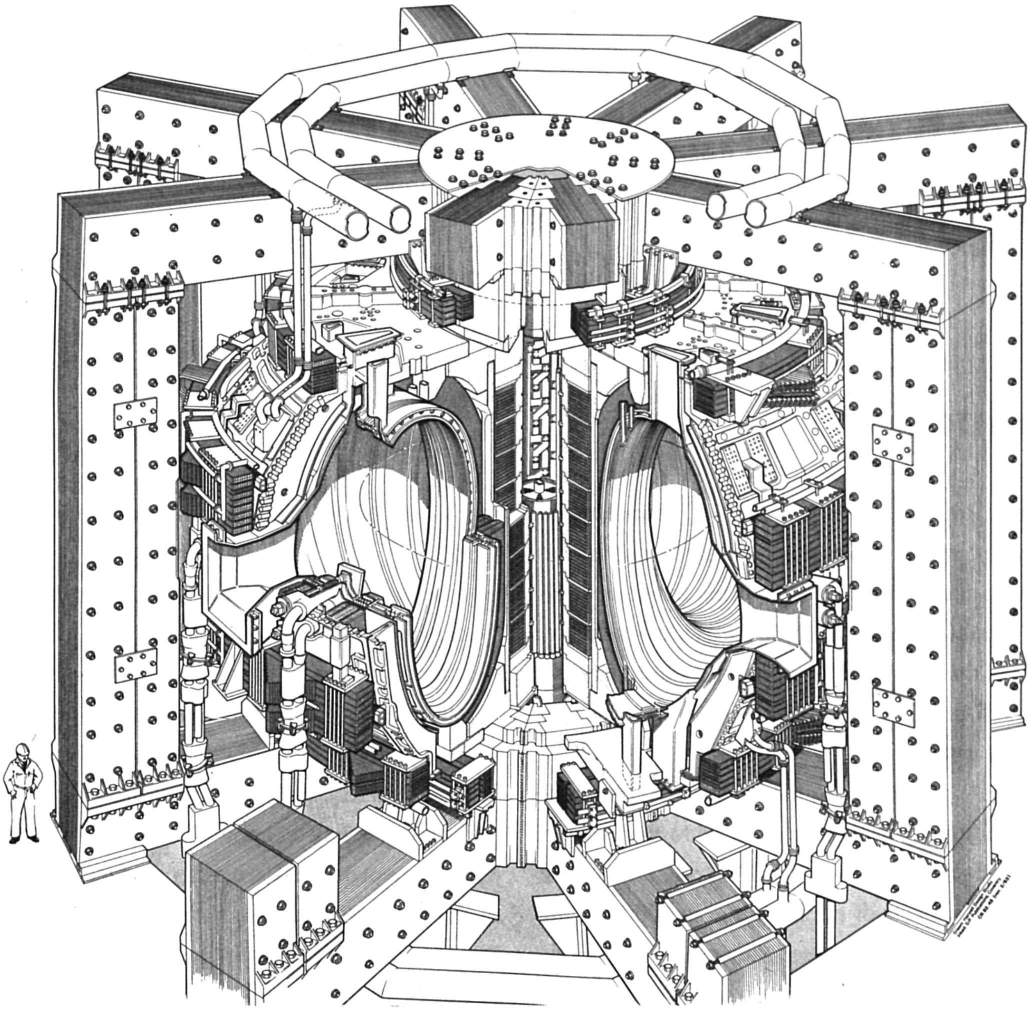

Fig.1: Diagram of the JET Tokamak.

Table I

Principal Parameters

Parameter	*Value*
Plasma minor radius (horizontal), a	1.25m
Plasma minor radius (vertical), b	2.10m
Plasma major radius, R_0	2.96m
Plasma aspect ratio, R_0/a	2.37
Plasma elongation ratio, $\varepsilon=b/a$	1.68
Flat top pulse length	60s
Toroidal magnetic field (plasma centre)	3.45T
Plasma current, D-shaped plasma	7.0MA
Volts-seconds available	54Vs
Toroidal field peak power	380MW
Poloidal field peak power	300MW
Additional heating power (into torus)	~50MW
Weight of vacuum vessel	108t
Weight of toroidal field coils	364t
Weight of iron core	2800t

magnetic circuit, which dominates the apparatus (see Fig.1). A set of coils around the centre limb of the magnetic circuit forms the primary winding of the transformer with the plasma acting as the single turn secondary. Additional heating of the plasma is provided by the propagation and absorbtion of high power radio frequency waves in the plasma and by the injection of beams of energetic neutral atoms into the torus.

The plasma is confined away from the walls of the vacuum vessel by a complex system of magnetic fields, in which the main component, the toroidal field, is provided by 32 D-shaped coils surrounding the vacuum vessel. This field, coupled with that produced by the current flowing through the plasma, forms the basic magnetic field for the tokamak confinement system, which provides a full design field at the plasma centre of 3.45T. The poloidal coils, positioned around the outside of the vacuum vessel, shape and position the plasma in operation.

Experiments have been carried out mainly using hydrogen or deuterium plasmas, although during 1991, experiments were performed in helium-3 and helium-4 and a preliminary experiment was performed using 10% tritium in deuterium. In the final stage of the programme, it is planned to operate with deuterium-tritium plasmas so that abundant fusion reactions occur. The alpha-particles liberated from the reactions should produce significant heating of the plasma. During this phase, the machine structure will become radioactive to the extent that any repairs and maintenance would have to be carried out using remote handling systems.

To reach conditions close to those relevant to a fusion reactor, plasma densities of $\sim 10^{20}m^{-3}$ at temperatures of 10-20keV would be needed. Even with plasma currents up to 7MA in JET, this would be inadequate to provide the temperature required using ohmic heating alone. Consequently, additional heating is required and two main systems are being used at JET, as follows:

- Injection into the plasma of highly energetic neutral atoms (Neutral Injection Heating);
- Coupling of high power electromagnetic radiation to the plasma (Radio Frequency (RF) Heating).

In 1991, the lifetime of the Project was extended to the end of 1996 to allow JET to implement a new Pumped Divertor phase of operation. This would assist the aim of establishing in deuterium plasmas "reliable methods of plasma purity control under conditions relevant for the Next Step Tokamak". During 1992/93, an axisymmetric pumped divertor (Mark I) was installed inside the vacuum vessel, together with all necessary auxiliary equipment.

The new plasma shapes of the divertor configuration required a complete redesign of the vacuum vessel first wall to accommodate the relevant plasmas. Upon completion, the inside of the vessel had been almost completely rebuilt and JET was effectively a new machine.

In the 1995/96 shutdown, a "more closed" Mark IIA divertor was installed. Since the Mark II divertor will become radioactive during its use with tritium plasmas, it was engineered to allow replacement of the divertor target structure by full remote handling techniques. The Mark II divertor configuration is intended to lead to enhanced particle and impurity retention in the divertor chamber.

Table II

JET Departmental and Divisional Structure

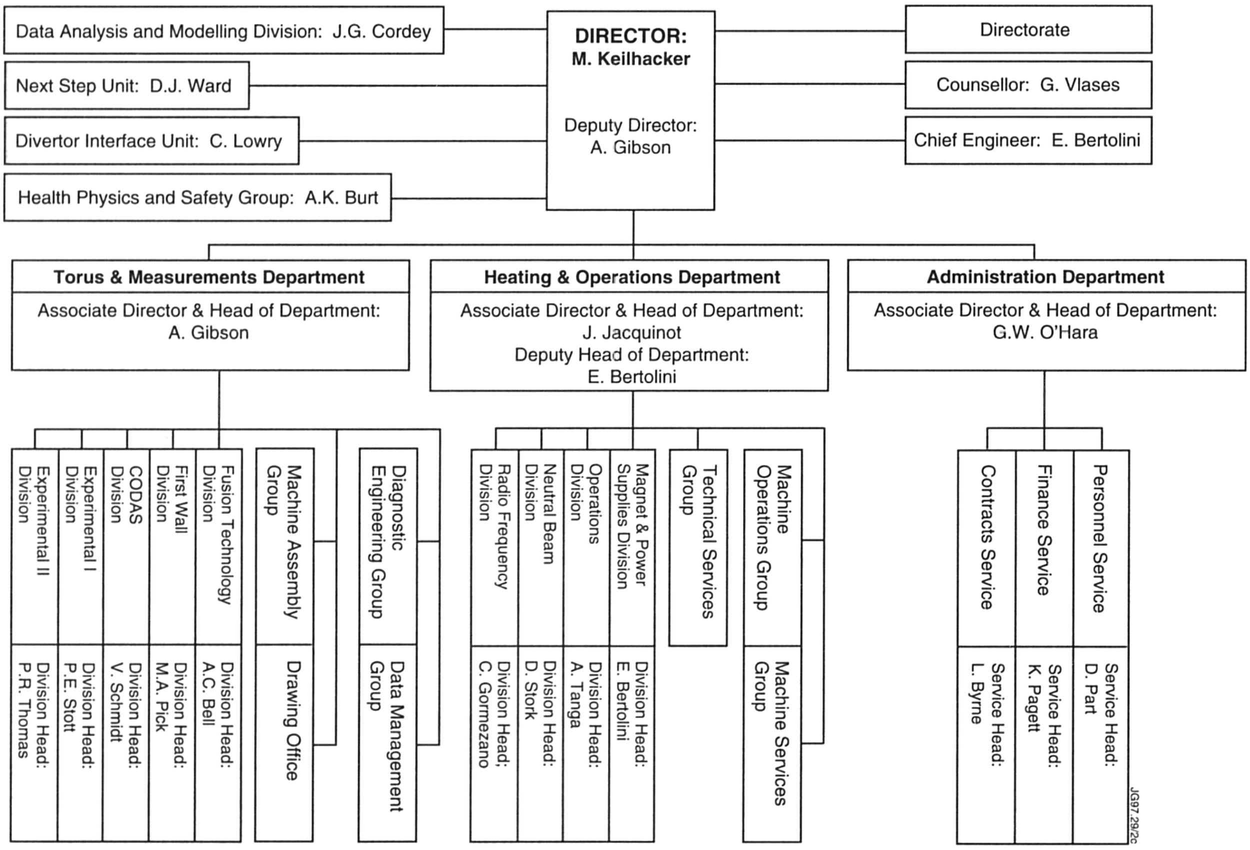

In mid-1996, the lifetime of the Project was officially extended to the end of 1999, to enable the Project to provide further data of direct relevance to ITER. In particular, the Project should contribute significantly to the development and demonstration of a viable divertor concept for ITER. It should undertake experiments using D-T plasmas in an ITER like configuration, which should provide a sound basis for the D-T operation of ITER. In addition, the extension would permit key ITER relevant technology activities to be carried out, such as the demonstration of remote handling and tritium handling.

Project Team Structure

The Project structure adopted, for management purposes, is divided into three Departments (see Table II):

- Torus and Measurements Department;
- Heating and Operations Department;
- Administration Department.

In addition, some scientific and technical duties are carried out within the Directorate and in Supporting Units.

The main duties of the Administration Department have been described in previous JET Annual Reports. This Report concentrates on progress made in the scientific and technical areas during 1996. To aid this description, the functions of these Departments are described below.

Torus and Measurements Department

The Torus and Measurements Department has overall responsibility for the performance capacity of the machine: this includes enhancements directly related to this (excluding heating) and the long term planning associated with integration of these elements to achieve ultimate performance. The Department is also responsible for: fusion technology requirements for the active phase including tritium handling and processing; for construction and operation of necessary measurement diagnostic systems and the interpretation of experiment data; and for data systems comprising data control, acquisition and management. The main functions of the Department are:

- to design, procure and implement enhancements to the JET device;
- to provide and maintain clean conditions inside the vessel which lead to high quality plasma discharges;
- to conceive and define a set of coherent measurements;
- responsible for construction of necessary diagnostics;
- to be responsible for diagnostics operation, quality of measurements and definition of plasma parameters;
- to organise and implement data acquisition and computing;
- to design and develop remote handling methods and tools to cope with JET requirements;
- to design and construct facilities for handling tritium and for waste management.

The Department consists of five Divisions and four Groups (Machine Assembly, Diagnostic Engineering, Data Management and the Drawing Office):

(a) *First Wall Division*, which is responsible for the vital area of plasma wall interactions. Its main tasks include the provision and maintenance inside the vacuum vessel of conditions leading to high quality plasma discharges. The Division develops, designs, procures and installs the first wall systems and its components such as limiters, wall protections and internal pumping devices. The area of responsibility encompasses the mechanical integrity of the vacuum vessel as a whole and the development and implementation of mechanical and Remote Handling techniques;

(b) *Fusion Technology Division*, is responsible for all nuclear engineering aspects of this Project including tritium and gas handling, vacuum systems, waste management and regulatory approvals;

(c) *Control and Data Acquisition System Division (CODAS)*, which is responsible for the implementation, upgrading and operation of computer-based control and data acquisition systems for JET;

(d) *Experimental Division 1 (ED1)*, which is responsible for specification, procurement and operation of about half the JET diagnostic systems. ED1 undertakes electrical measurements, electron temperature measurements, surface and limiter physics and neutron diagnostics;

(e) *Experimental Division 2 (ED2)*, which is responsible for specification, procurement and operation of the other half of the JET diagnostic systems. ED2 undertakes all spectroscopic diagnostics, bolometry, interferometry, the soft X-ray and neutral particle analysis.

The structure of the Torus and Measurements Department to Group Leader level is shown in Fig. 2 and the list of staff within the Department is shown in Fig. 3.

Heating and Operations Department

The overall responsibility of the Heating and Operations Department is for the efficient and effective day-to-day operation of the machine. In addition, the Department has

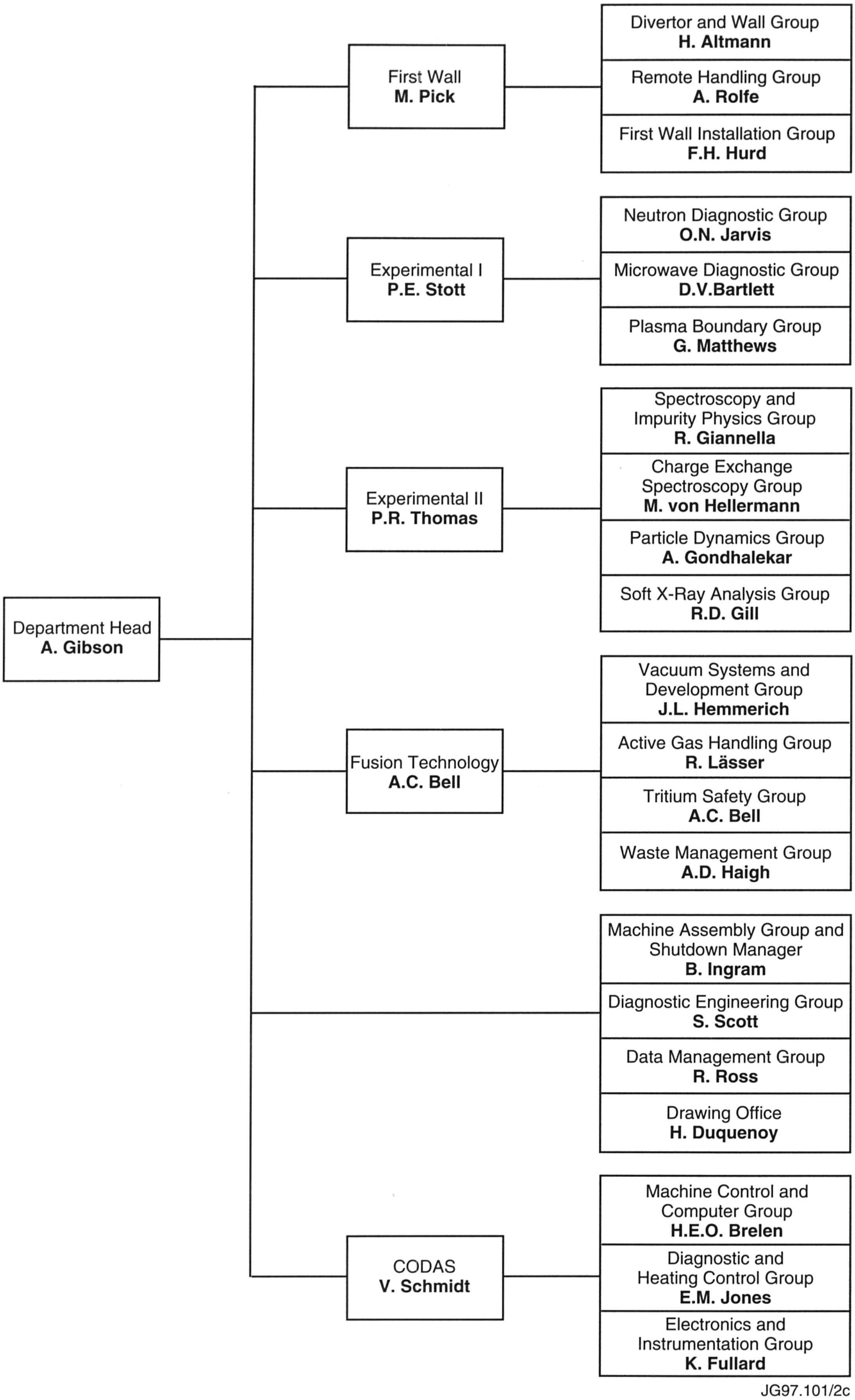

Fig.2: Torus and Measurements Department, Group Structure (December 1996)

TORUS AND MEASUREMENTS DEPARTMENT

Head of Department: A. Gibson

H. Duquenoy
C. Hancock
B. Ingram
Mrs. P. Longworth
J. Lundquist
H. Panissie
J. Reid
Mrs. J. Roberts
R. T. Ross
P. Sagar
Miss. D. Samuel
S. Scott
A. Tiscornia
C. Wilson

FUSION TECHNOLOGY DIVISION

Head: A.C. Bell

C. Birks
S. Bryan
P. Brennan
C. J. Caldwell-Nichols
C. Callaghan
Mrs. J. Campbell
N. Green
A. Haigh
J. L. Hemmerich
D. Holland
H. Jensen
Mrs. M. E. Jones
J. F. Jaeger
S. Knipe
R. Lässer
J. Lupo
J. Mart
A. Miller
G. Newbert
J. Orchard
R. Pearce
Mrs J. Pointer
S. Scales
K. D. Walker
R. Warren
T. Winkel

FIRST WALL DIVISION

Head: M.A. Pick

H. Altmann
P. Brown
T.V. Businaro
R.A. Cusack
Mrs. D. Cranmer
E. Deksnis
C. Froger
L. Galbiati
F. Hurd
Mrs. I. Hyde
G. Israel
M.A.Irving
L.P.D.F. Jones
J.F. Junger
A.B. Loving
B. Macklin
A. Nowak
J. Palmer
A. Peacock

CONTROL AND DATA ACQUISITION SYSTEMS DIVISION

Head: V. Schmidt

M. B. Baronian
Mrs. A. M. Bellido
H. E. O. Brelen
W. J. Brewerton
T. Budd
P. J. Card
J. J. Davis
S. Dmitrenko
S. E. Dorling
K. Fullard
E. M. Jones
F. J. Junique
N. G. Kidd
J. G. Krom
C. Perry
C. Terella
G. Wolfers
I. D. Young

EXPERIMENTAL DIVISION I

Head: P. E. Stott

S. Ali-Arshad
D. Bartlett
H. Bindslev
B. W. Brown
S. Clement
J. P. Coad
S. Davies
J. Ehrenberg
J. Fessey
G. Fishpool
C. Gowers
P. J. Harbour
J. Hoekzema
M. Hone
I. Hurdle
O. N. Jarvis
G. Kaveney
M. Loughlin
F. B. Marcus
G. Matthews
R. Monk
G. Neill
P. Nielsen
H. Oosterbeek
Mrs N. Povey
R. Prentice
P. Roberts
G. Sadler
A. Stevens
D. Summers
P. Tegg
P. van Belle
J. Vince

EXPERIMENTAL DIVISION II

Head: P. R. Thomas

B. Alper
P. Beaumont
Mrs. K. Bell
G. Braithwaite
P. Breger
A. Edwards
R. Giannella
R. Gill
A. Gondhalekar
L. D. Horton
A. Howman
H. Jäckel
R. König
C. Maggi
P. Morgan
C. Nicholson
R. Reichle
R. Robins
P. Smeulders
M. Stamp
S. A. Staunton-Lambert
W. Studholme
M. von Hellermann
B. Viaccoz
R. Webb

Fig.3: Project Team Staff in the Torus and Measurements Department (December 1996)

JG97.101/3c

responsibility for plasma heating and auxiliary equipment and related physics; the design and operation of power supplies as well as contributing to the execution and evaluation of JET's experimental programme. The main functions of the Department are:

- preparing and co-ordinating operation of the machine across Departments and Divisions;
- heating and current drive and analysis of its effects in the plasma;
- plasma fuelling, including pellet injection;
- designing and employing power supplies for ensuring efficient operation and control of the machine.

The Department consists of four Divisions and three Groups (Machine Operations, Machine Services and Technical Services):

(a) *Operations Division* plays a major role in efficient planning and execution of JET's experimental programme and in the integration of systems into an

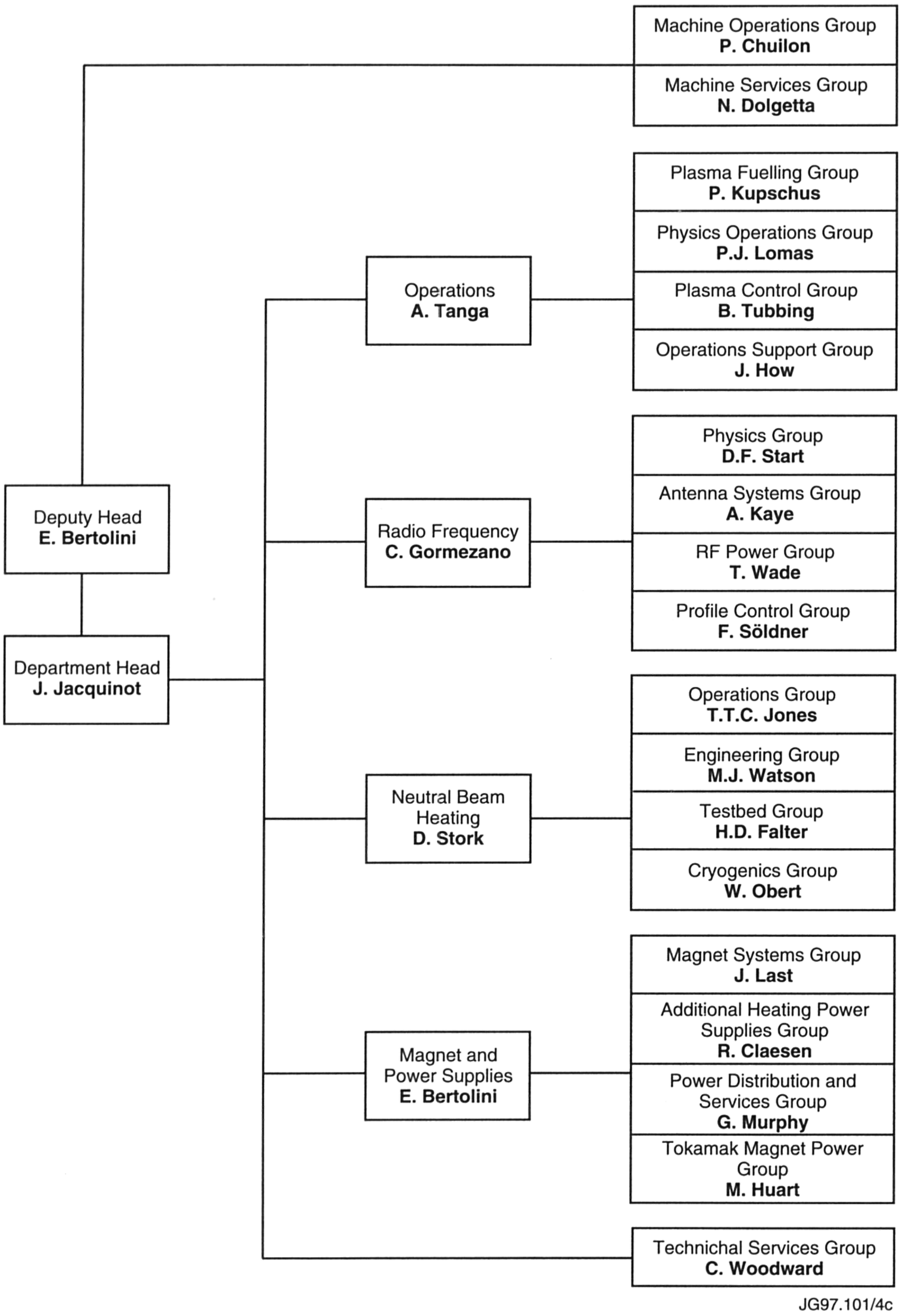

Fig.4: Heating and Operations Department, Group Structure (December 1996)

HEATING AND OPERATIONS DEPARTMENT

Head of Department: J. Jacquinot
Deputy Head of Department: E. Bertolini

M. Axton
P. Barker
V. Bhatnagar
M. Bolton
P. Chuilon
T. Dale
N. Davies
N. Dolgetta
J. Green
R. Greenfield
M. Hughes
H. Jones
M. Macrae
S. McLaughlin
R. Meadows
C. Rayner
B. Regan
Miss. V. Shaw
W. Smith
K. Taylor
J. Watt
C. Woodward
B. Workman

MAGNET AND POWER SUPPLIES DIVISION

Head: E. Bertolini

A. Barnard
T. Bonicelli
D. Chiron
R. Claesen
E. Daly
P. Doyle
C. Folco
J. Goff
D. Graham
M. Huart
F. Jensen
J. Jeskins
H. McBryan
J. McKivett
V. Marchese
G. Marcon
Mrs. H. Marriott
G. Murphy
R. Ostrom
P. Presle
S. Shaw
J. van Veen
C. R. Wilson

OPERATIONS DIVISION

Head: A. Tanga

S. Cooper
M. Gadeberg
J. How
M. Johnson
P. Kupschus
M. Lennholm
P. J. Lomas
S. Puppin
L. Rossi
G. Saibene
A. Santagiustina
R. Sartori
B. Schunke
A. C. C. Sips
M. Tabellini
B. Tubbing

NEUTRAL BEAM HEATING DIVISION

Head: D. Stork

P. Ageladarakis
A. Bickley
A. Browne
D. Ciric
C. D. Challis
S. Cox
J. F. Davies
A. Dines
H. P. L. de Esch
D. Ewers
H. Falter
D. Godden
L. Hackett
Mrs. S. Humphreys
T. T. C. Jones
F. Long
D. Martin
T. Martin
C. Mayaux
W. Obert
S. Papastergiou
A. J. Parfitt
R. Parkinson
D. Raisbeck
L. Svensson
J. Waterhouse
M. J. Watson

RADIO FREQUENCY HEATING DIVISION

Head: C. Gormezano

S. C. Booth
M. Brandon
G. Cottrell
P. Crawley
Mrs. R. Dietrich
T. Dobbing
D. T. Edwards
A. Franklin
P. Finberg
M. Gammelin
M. Graham
R. Horn
A. Kaye
J. Plancoulaine
F. Rimini
P. Schild
M. Schmid
A. Sibley
M. Simon
F. Söldner
D. F. Start
C. Steele
M. Timms
T. Wade
G. Whitehurst

Fig.5: Project Team Staff in the Heating and Operations Department (December 1996)

JG97.101/5c

effective experimental programme. In addition, it is responsible for effective methods of fuelling including the development of methods based on solid high speed hydrogen pellets; development of new plasma wall conditioning techniques; plasma control systems; development of disruption control methods; training operations staff; and monitoring machine operations;

(b) *Neutral Beam Heating Division*, which is responsible for construction, installation, commissioning and operation of the neutral injection system, including development towards full power operation. The Division is also responsible for all cryo-systems and also participates in studies of physics of neutral beam heating;

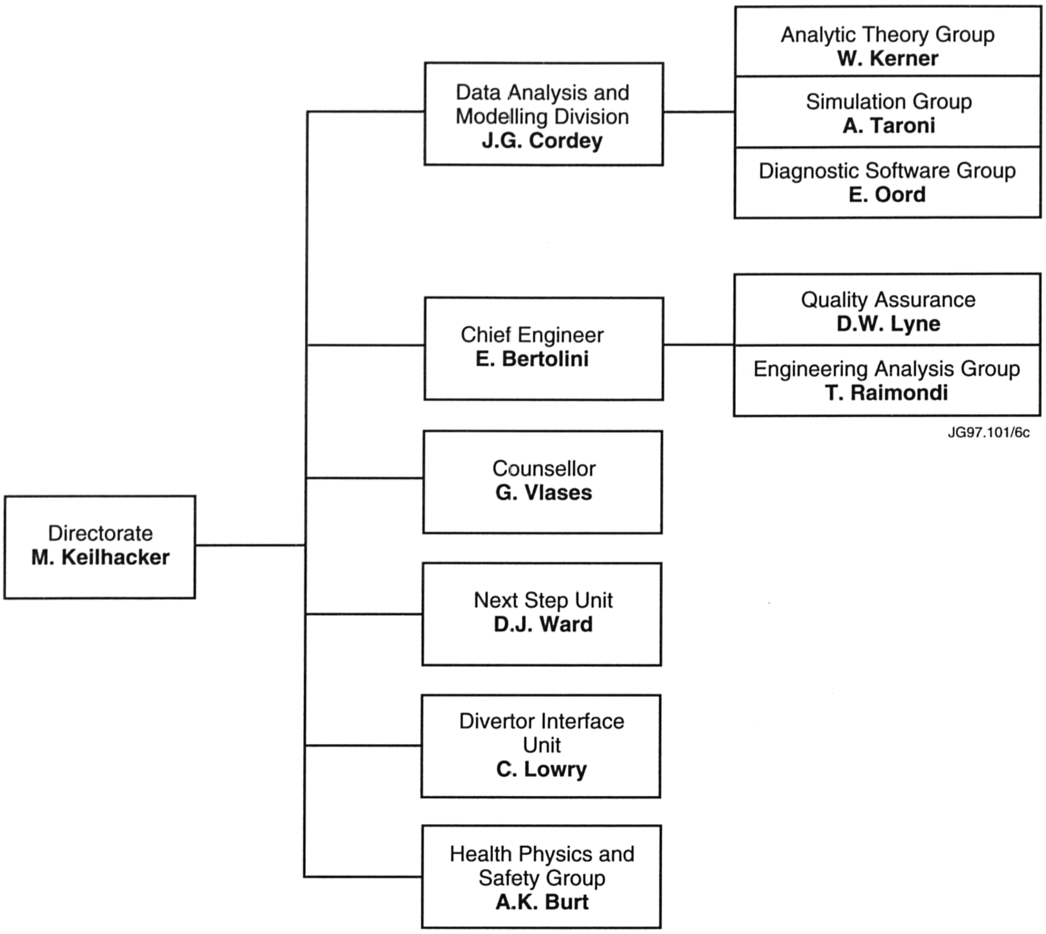

Fig.6: Directorate and Support Units, Group Structure (December 1996)

(c) *Radio Frequency Heating Division*, which is responsible for the design, construction, commissioning and operating RF heating and current drive systems during the different stages of its development to full power. The Division is also responsible for the TAE excitation system and also participates in studies of the physics of RF heating;

(d) *Magnet and Power Supplies Division* is responsible for the design, construction, installation, operation and maintenance of the electromagnetic system and plasma control. The area of responsibility encompasses the toroidal, poloidal and divertor magnets, mechanical structure; and all power supply equipment needed for magnets, plasma control, additional heating and auxiliaries.

The structure of the Heating and Operations Department to Group Leader level is shown in Fig. 4 and the list of staff in the Department is shown in Fig. 5.

In addition, both Departments are involved in:

- execution of the experimental programme;
- interpretation of results;
- making proposals for future experiments.

Directorate

Within the Directorate, there are three technical units, one Division and a Chief Engineer, reporting directly to the Director. The main responsibilities are as follows:

(a) *The Data Analysis and Modelling Division* is responsible for the provision of software for the acquisition and processing of the data from JET diagnostics; for confirming the internal consistency of the processed data and assembling it into public databases; and the development and testing of theoretical models against JET data. In addition, the Division is responsible for prediction by computer simulation of JET performance, interpretation of JET data and the application of analytic plasma theory to gain an understanding of JET physics.

It comprises three Groups:

- Analytic Theory Group;
- Simulation Group;
- Diagnostic Software Group.

(b) *The Next Step Unit* is responsible for co-ordinating contributions from JET to the European effort in

DIRECTORATE AND SUPPORT UNITS
Director: Dr M. Keilhacker

Mrs. L. Ashby
A.K. Burt
D. Campling
A. Gibson
Mrs. C. Johnson
R. Litchfield
C. Lowry
Miss. K. Luker
J. McMahon
P. Macheta
C. Manning
T. O'Hanlon
M. Page
B. Patel
Mrs. P. Reeve
Mrs. J. Reid
K. Sandland
P. Schofield
M. Scotcher
Ms. R. Thormahlen
G. Vlases
D.J. Ward
M. L. Watkins

CHIEF ENGINEERS UNIT
Head: E. Bertolini

T. Raimondi

DATA ANALYSIS AND MODELLING DIVISION
Head: J. G. Cordey

B. Balet
K. Blackler
J. Christiansen
L. G. Eriksson
J. Jeral
W. Kerner
D. O'Brien
E. Oord
M. Ottaviani
R. Simonini
K. Slavin
E. Springmann
Mrs. P. Stubberfield
A. Taroni
K. Thomsen
D. Wilson
W. Zwingmann

NEXT STEP UNIT
Head: D.J. Ward

DIVERTOR INTERFACE UNIT
Head: C. Lowry

Fig.7: Project Team Staff in Directorate and Support Units
(December 1996)
JG97.101/7c

support of the ITER-EDA. This responsibility includes drawing up proposals, initiating relevant work programmes on JET and taking part in their execution and evaluation.

(c) *The Divertor Interface Unit* is responsible for assessing the impact of developments in the experimental programme and operation on the design requirements for JET divertors. This includes a high level of participation in the JET experimental programme on divertor physics, thermomechanical analysis of plasma induced loads on the divertor, and the definition of advanced divertor concepts.

(d) *Health Physics and Safety Group* is responsible for a comprehensive health physics and safety project organisation.

In addition, there is a *Chief Engineer*, who reports to the Director, and is responsible for ensuring the overall coherence of technical aspects of JET operations.

The structure of the Directorate to Group Leader level is shown in Fig.6 and the list of staff is shown in Fig.7.

Report Summary

The first section of this Report gives a brief introduction and background information relevant to the Report. The second and third sections set out an overview of progress on JET during 1996 and with a survey of scientific and technical achievements during 1996 sets these advances in their general context. This summary is specifically cross-referenced to reports and articles prepared and presented by JET staff during 1996.

The fourth section is devoted to future plans and certain developments which might enable enhancements of the machine to further improve its overall performance. Some attention has been devoted to methods of surmounting certain limitations and these are detailed in this section.

In addition, Appendix I contains a list of work topics which have been carried out under Task Agreements with various Association Laboratories. A full list is included in Appendix II of all Articles, Reports and Conference papers published by JET authors in 1996. Copies of particular papers can be obtained from the JET Publications Office.

Technical Achievements during 1996

Introduction

In June 1995, JET had started the major shutdown for the installation of the Mark II support structure (which will be the basis for all future divertor work at JET and is the key to the JET programme to 1999) and the more-closed Mark IIA divertor target assembly, together with modifications to the ICRF antennae. JET entered 1996, nearing the conclusion of this work.

During the shutdown, work was also undertaken on various systems in preparation for the next period of D-T operation (DTE-1), which is scheduled for early 1997, and for the Remote Tile Exchange shutdown after DTE-1. In particular, thirty three carriers and associated tiles were successfully installed by remote handling, giving confidence in the operational procedures, tooling, equipment, support management and time estimates. The shutdown was completed on schedule by the end of March 1996 and was followed by pumpdown, leak testing and bake out which were the quickest and most effective after a major shutdown, reflecting the quality of the in-vessel and ex-vessel methods and the experience gained.

The restart programme to commission JET for the start of the experimental programme began at the beginning of April and ended as planned in early June with the routine operation at 2-3MA plasma current, with up to 20MW of additional heating power into the plasma.

The 1996 experimental campaign then concentrated on specific ITER-relevant issues related to the more closed Mark IIA divertor and, due to their importance for predicting ITER's ignition margin and fusion power output, the scaling of the H-mode threshold power and the energy confinement. In addition, the preparation of high performance scenarios for DTE-1 was a high priority of the campaign.

A five week shutdown commenced at the end of September to plug divertor bypass leaks, clad the inner wall of the vacuum vessel with graphite tiles and to replace three of the sixteen Neutral Beam PINIs, which prevented full power operation.

The experimental programme recommenced in November with the aim of optimising performance in preparation for DTE-1 but was interrupted in the middle of December due to a water leak in the Octant No.8 Neutral Injection box. After this had been repaired operations restarted in early January 1997.

The Mark IIA configuration behaved as expected for a "more-closed" divertor. It offered improved power handling over the Mark I divertor, pumped the plasma 2-3 times more rapidly and showed signs of increased neutral recycling in the divertor region. The latter feature showed up particularly well in the detachment of the divertor plasma from the target as significantly lower main plasma density than in Mark I, in agreement with code predictions.

During 1996, the Neutral Beam heating system operated routinely up to 16-17MW, but technical difficulties with three PINIs prevented operation at full power (≈20MW). ICRF heating operated routinely with ≈8MW in all modes of combined heating operation and up to 17MW in ICRF-only heated discharges. Real-time control of heating power was used extensively to help maintain steady-state conditions and to economise on neutron production.

Prior to the water leak in the Octant No.8 Neutral Beam injection box, the machine had demonstrated high levels of availability and reliability. Nonetheless, the reliability of the machine for future operations continues to be assessed with recent work concentrating on the amelioration/accommodation of vertical displacement events which produce the highest vertical forces and sideways vessel displacements.

First Wall Systems

The main activities on First Wall Systems throughout 1996 were related to: completion of the shutdown to install the Mark II Support Structure and Mark IIA Divertor Tile Carriers; design and manufacture of the inner wall CFC cladding components and the components to prevent divertor gas leakage, as well as the preparations for and installation of these components; and manufacture of the Mark II Gas-box (GB) Divertor components. In addition, the preparations were undertaken for the fully remote replacement of Mark IIA Divertor Tile Carriers with the Mark II GB tile carriers immediately after the Deuterium-Tritium Experiment (DTE1).

The Gas-box Installation Shutdown, during which the Mark IIA tile carriers will be exchanged for the Mark IIGB tile carriers, will be the first fully remote task undertaken on the JET tokamak and the most significant fully remote handling task undertaken on any fusion device in the world. Accordingly, extensive preparations are being made for the proving of equipment function, performance and reliability. In addition, the design and manufacture of tools and ancillary equipment to execute the tasks, as well as the derivation, development and proving of task procedures and operator training had been undertaken.

Interventions in the Vessel during 1996

In 1996, there was one intervention in addition to the conclusion of the main Mark II installation shutdown. This intervention was carried out in October 1996 and was used to install a system to prevent the divertor gas bypass leakage and to clad the inner wall of the machine with CFC tiles.

Completion of Mark II Installation Shutdown

The start of 1996 coincided with critical operation of the divertor installation, namely the welding of the water cooling system for the divertor structure. In terms of management and coordination of operations, it involved the Installation Group, which had overall control and was responsible for critical inert gas purging of the intricate cooling water system; the Remote Handling Group, which was responsible for the welding tools and equipment; the Welding Group for technical input; and the Quality Group for coordinating the third party inspection by British Engine.

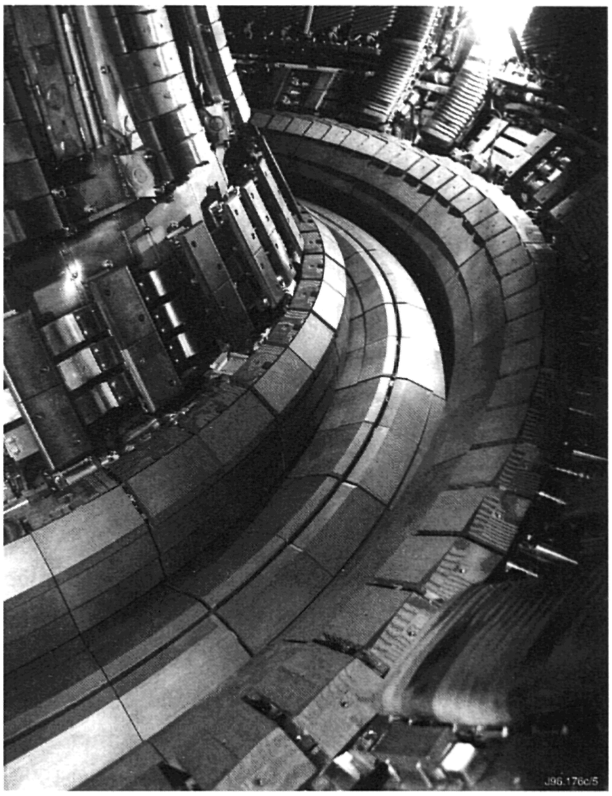

Fig.8: The installed Mark IIA Divertor

The welding consisted of 144 butt welds all requiring 100% radiography, which was carried out on night shift. The successful welding including all required re-welds, took a total of 34 entries (11 days). This was followed by the installation, to the top of Coil 1, of the complex conduit which carries all the diagnostic cabling from the divertor to the relevant feedthroughs. Some additional work was carried out including the installation of new upper sections of the inner wall guard limiters (IWGL) which were replaced to conform better with the required plasma configurations.

The installation of the Mark IIA tile carriers was carried out successfully, about one quarter being installed remotely using the Boom and MASCOT. These carriers were installed following a detailed procedure previously tested and proven on the In-Vessel Training Facility (IVTF) in the Assembly Hall. The Boom manoeuvring and operating positions were first derived off-line using the CATIA Robotics facility in the Drawing Office and were then downloaded to the Boom control system where they were adjusted and refined during the IVTF preparations. An additional six carriers were installed at Octant No.8, where the Boom was fully extended and where preparatory IVTF validations were not possible.

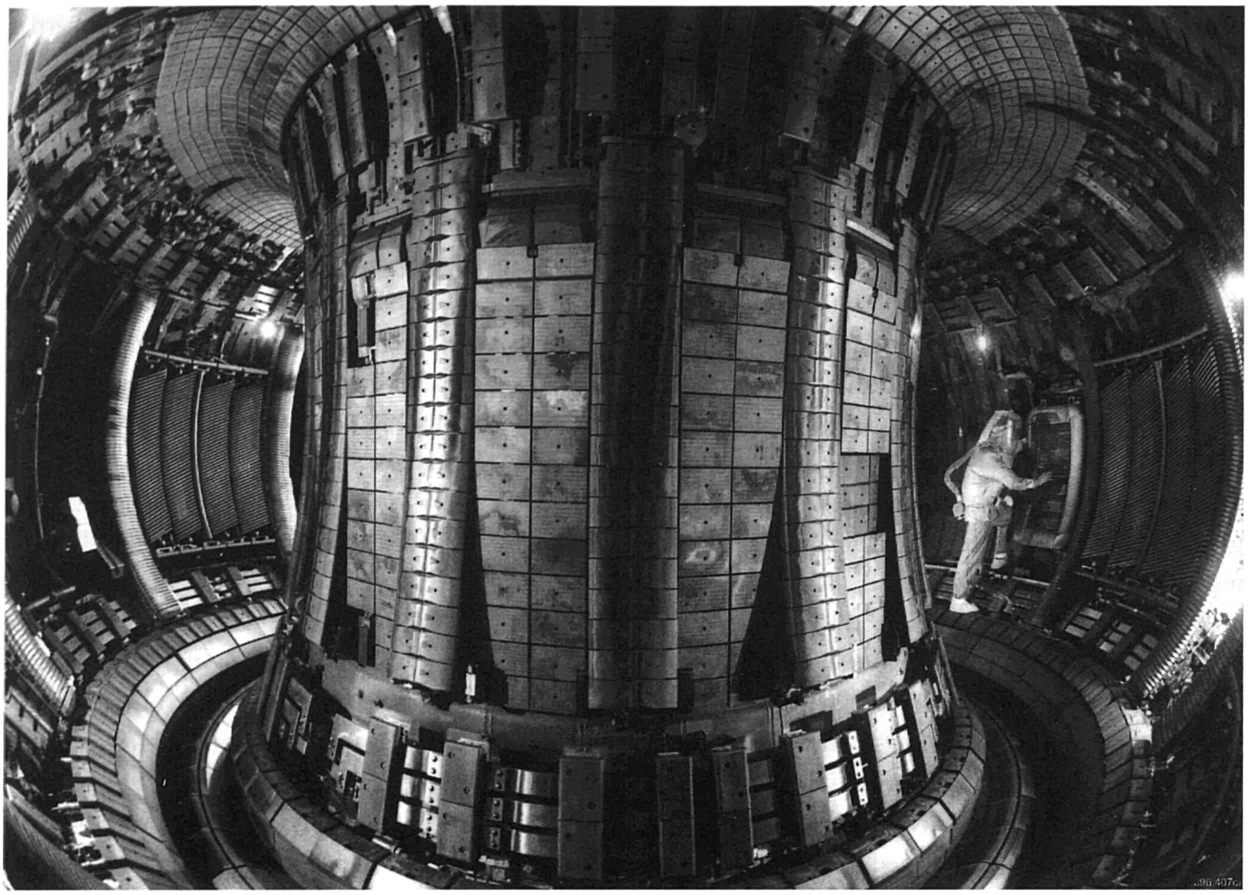

Fig.9: The new inner wall of JET showing the installed CFC cladding

At these locations, the raw data from CATIA was used to position the Boom and a generic operating procedure was followed. In all locations, the tile carriers were successfully and safely installed within the time allotted.

In addition to the installation work, some time was taken to calibrate the general Boom teach files which will be used to position the Boom at all 48 tile carrier sector operating locations during the real tile carrier installation in 1997 and to confirm the effectiveness of the new Remote Handling In-Vessel Viewing System, which will be fundamental to all remote operations.

Surveys of the installed Mark IIA divertor tile carriers showed that after installation the gap between the tiles and the tile-to-tile steps were all well within the tight design parameters. The Mark II Divertor Installation Shutdown was completed on 28th March as planned. Figure 8 shows the divertor installed in the vessel.

Survey and Inspection during Mark II Shutdown

Installation of the Mark II divertor structure was completed in late-1995, using the Computer Aided Theodolite system (CAT) to assist with alignment. In 1996, the CAT system was used to confirm the correct position of the in-vessel installed components relative to the vessel datum system, which is concentric with the magnetic centre of the machine.

Following completion of the installation of the main in-vessel components, a videogrammetry survey of the vacuum vessel interior was carried out. The purpose was to provide an 'as-built' record of the in-vessel components between the upper and lower saddle coils on the outer wall and the lower coils and upper coil supports on the inner wall. For this survey, the in-vessel datum system and some components were fitted with special retro-reflective targets.

The survey permits coordinates of features of other components to be determined by interrogating the digital photographic model resulting from the survey. The model is stored on CD-ROM. It is intended that a remote survey of the divertor structure using this videogrammetry technique will be carried out during the Gas-box Installation Shutdown to verify positional accuracy of the divertor structure prior to the installation of the new tile carriers.

October 1996 In-Vessel Intervention

The intervention carried out in October 1996 was used to install a system to prevent the divertor gas bypass leakage and to clad the inner wall of the machine with CFC tiles. To minimise in-vessel time during installation, the design of the cladding system consisted of beams in Inconel 600 to support the tiles. These beams are attached to the inner wall restraint rings.The cladding of the inner wall with CFC tiles was successfully completed, no major modifications were required to either the beams or the complex tooling required to install them and the individual supports. This was due to the detailed "as built" design available in the Drawing Office and the extensive trials and operator training performed in the In-Vessel Training Facility prior to installation. Figure 9 shows the inner wall with the new CFC cladding.

The control of neutral gas leakage out of the divertor around the coils relied upon thin metal plates with labyrinth gaps between them. It was found that additional preventive measures were required and this was undertaken effectively in the October intervention.

A number of materials were tested for their compatibility with high vacuum conditions up to 350°C. The obvious candidates such as glass fibre, carbon fibre and ceramic cloth were rejected on grounds of fibre shedding, electrical conductivity and water retention, respectively. Trials with polymers showed that Aramid (e.g. Kevlar, Twaron) cloth had the correct properties of vacuum compatibility, ease of handling, radiation resistance and low tritium uptake.

The gaps to be closed were those between the Divertor Coils Nos.1 and 4 and the vessel wall, between Coil No.1 and the divertor structure inner ring, and above the cryopump. Seals were made from two layers of folded Aramid cloth, sewn with Aramid thread, to form rectangular pads with rows of pockets along the edges. These pockets located 10mm wide stainless steel strips, which were shaped to give the cloth seal a U-form. This shape allowed it to be sprung into the relevant gap and then located by locking strips spot welded to the vessel wall. Other gaps such as those above the cryopump were closed either with polymide sheet clipped in place or flat Aramid seals laid on top of the existing metal gas shields.

Some additional work was performed during this intervention including the exchange of a number of poloidal limiter tiles which had some surface cracks due to overheating. These were changed where possible for CFC tiles. Some remedial work was undertaken on the Lower Hybrid Launcher and some Langmuir probes, which had failed in the divertor region. These were brought back into operation by removing, re-wiring and replacing three sections of the electrical conduit on Coil No.1.

In preparation for the forthcoming remote tile carrier exchange and to investigate the effect of a six-month operational period on the unfastening torques of those bolts which needed to be remotely handled, all the tile carrier hold down bolts were inspected, the unfastening torques measured, and subsequently re-tightened to a predetermined torque.

The October intervention was characterised by relatively high levels of radiation (~250μSv/h) which meant careful monitoring of individual dose rates and the extensive use of the IVTF to minimise the in-vessel time required for each task.

The Mark II Gas-box Divertor Components

The Mark IIGB Tile Carriers will be installed in the Mark II support structure during the 1997 remote installation shutdown. The novel feature of the Gas-box divertor is the first use of CFC material for structural purposes in JET. The primary reason behind the choice of CFC material is the relatively high heat flux ($\leq 2\text{MWm}^{-2}$) falling onto some structural components from the radiating gas target plasma.

1996 saw the completion of the detailed design of the Gas-box divertor and the beginning of the manufacturing of the Gas-box tile carriers from CFC material previously delivered. The manufacture of the CFC target tiles has been completed.

Production of the series inner carriers started in November and will be followed by the septum, base and outer carriers. A test septum was assembled with different bolting systems to study their behaviour under cyclic load in a test laboratory. This proved the effectiveness of the copper coated bolts and the use of Spiralock nuts against seizure and loosening due to vibrations. Detailed mechanical stress calculations including 3D finite element calculations were performed which predict adequate reserve factors for the structural CFC components.

High heat fluxes are expected to the various tiles of the gas box configuration that are not structural parts. Computations show that for a wide range of plasma parameters fluxes of up to 18MWm^{-2} are expected for non-radiating divertor plasmas in the gas-box. It is expected that even for 10MW/leg total conducted power, the gas-box divertor will allow 3 - 6s of operation before the surface temperature reaches 1600 °C.

The In-Vessel Training Facility

The In-Vessel Training Facility (IVTF) was continually kept up-to-date and used extensively and effectively for:

- the training of in-vessel workers;
- to develop and test all in-vessel procedures;
- to develop and test all handling and installation tools;
- to check details and interfaces of new components;
- for remote handling trials and the training of remote handling operators.

The In Vessel Training Facility (IVTF) was enlarged to accommodate the trials of the Tile Carrier Transfer Facility (TCTF) and Boom working together. The following additions were made: two additional Octants in the form of D-shaped sectors, one and half Octants of divertor structure, Coil No.1 and Coil No.1 conduit including plugs and sockets, inner wall guard limiters (IWGL), antennae and poloidal limiters. In the middle of this build programme the IVTF was extensively used to prepare for the October Shutdown. By the end of the year, the IVTF had been rebuilt and the final alignment completed. The start of 1997 should see completion of Octant No.1 with divertor structure, antennae and poloidal limiters and IWGLs.

In the Assembly Hall, the boom and short boom were positioned accurately on the training facility exactly as on the torus. This is essential to ensure that 'teach and repeat' files created for the boom and MASCOT in the IVTF are valid for use in-vessel.

This requirement is regarded as an essential aspect of the IVTF as a detailed replica of the real vacuum vessel. It has required the creation of a datum system for the IVTF, similar to that used in-vessel, which allows the use of the CAT system for component installation in the IVTF using in-vessel 'as installed' co-ordinates. While IVTF build has been on-going throughout 1996, it has been a major task of the inspection team throughout November and December.

The Boom itself has been the subject of a major refurbishment, during which the CAT system was extensively utilised. This including setting the Boom carriage and guide rail accurately to the Octant No.1 - No.5 axis of the IVTF, as well as initialising new resolvers on the Boom joints. Measuring accuracy of ±0.015° was achieved on the included angle at a joint.

Survey and Inspection Activities

The routine monitoring of the position and movement of the vacuum vessel during baking and after plasma disruptions has become a major activity in the area of surveying and inspection. Datum points were established on some of the main horizontal ports to allow monitoring of the position of the vacuum vessel both routinely, e.g. on maintenance days, and also in the event of a large disruption when there is some concern about how the vacuum vessel moves and whether it recovers to its original position. The benefit of CAT for this application is that movement is measured relative to independent (or 'off-machine') datums and is reported within an established datum system. Another objective is to quantify accurately the actual movement due to thermal expansion in order to calibrate the 'hot' positions of the magnetic pick-up coils on the vacuum vessel walls used to measure the position of the plasma. The CAT system was used to measure the positions of upper and lower main vertical ports throughout a range of temperatures. Measurements were made with reference to the Torus Datum System which had been expanded from the original floor datum to provide targets on the walls suitable for use with CAT. The survey results improved the accuracy of the 'hot' position of the magnetic pick-up coils.

The CAT system was used extensively in conjunction with the manufacturing, assembly and installation of numerous diagnostic systems. For example, the diagnostic KJ5 (active phase soft-X-ray cameras) collimator lines-of-sight were surveyed to check the focal point, which was then used as a basis for a datum system on the assembly which would later be used to install this large piece of equipment in the Torus Hall. Positions of the KJ5 assemblies at Octants No.4 and No.8 were fine-tuned throughout commissioning to take account of the effect of temperature and vacuum. The object of these surveys has been to establish the position of the equipment with reference to the Torus Datum Systems (i.e. the system to which all in-vessel components have been aligned).

Preparations for the Remote Installation of the Mark II Gas-box

Remote Handling Trials in the IVTF and JET Vessel

A full scale mock-up testing programme has been embarked upon to prepare the equipment and operators for the fully remote exchange of Mark II tile carriers. The programme includes the testing and proving of the task feasibility both under normal operating conditions and under failure case conditions. This mock-up programme,

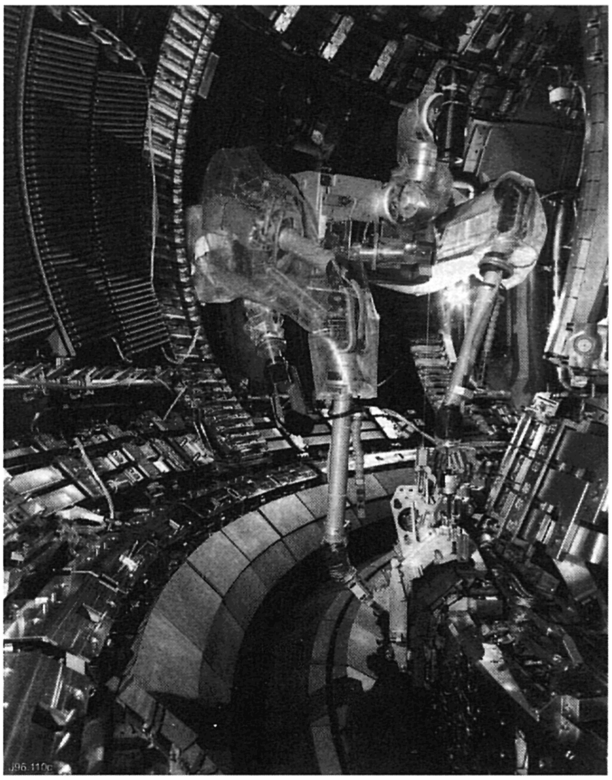

Fig.10: Mascot inside the torus during February 1996

executed in the In-Vessel Training Facility as well as in the actual JET vessel, has been a major part of the Remote Handling work. At the beginning of 1996, final preparations were being made using the full scale torus mock-up (IVTF) for the fully remote installation of one quarter of all the Mark IIA divertor tile carriers. A fixed period was allocated during the shutdown to undertake this first fully remote activity inside the torus. The mock-up preparations were successfully concluded at the beginning of February in the Assembly Hall, the Boom and MASCOT were transferred to the Torus Hall and installed on the torus at a location within 1mm of its correct position relative to the torus co-ordinate reference system. The systems were commissioned and the tooling was deployed into the torus by hand in readiness for operations to start in February.

The operations were performed over a fourteen day period by two teams of operators achieving 15 hours in-vessel operations per day using the MASCOT servomanipulator mounted on the end of the JET articulated boom and making use of a variety of special tools (see Fig.10). Nine base, nine inner and nine outer carriers were progressively installed in the Octant No. 5/ Octant No.6 region where the Boom manoeuvering was particularly difficult.

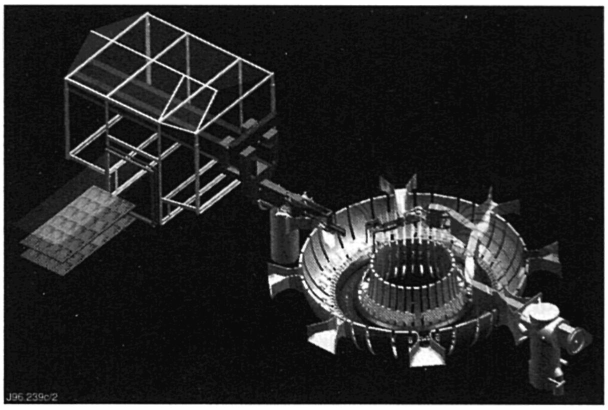

Fig.11: Overall remote handling operational scenario

Remote Handling Equipment - Design and Development

The Articulated Boom was utilised extensively in 1996 for remote handling trials. In August 1996, the system was taken out of operation to undergo upgrading and modification. The upgrading work has comprised modifications to many sub-systems resulting from 1000hr trial recommendations, experience from the mock-up operational programme, results of the failure recovery analysis and results of operational analysis with CATIA/KISMET. The major modifications include a new Boom section with improved range of movement, a new Boom Control System based on a proprietary motion control system and incorporation of many features to facilitate Boom recovery after potential worst case failures.

The new Tile Carrier Transfer Facility (TCTF) comprising a short articulated Boom with a special end-effector, a pair of servo controlled storage trolleys and a contamination control enclosure surrounding the entire hardware has been delivered during 1996 (Fig.11), and installed in the Assembly Hall. The control system for the TCTF is based on the same proprietary motion control system used in the new boom controller. This also has been delivered and commissioned during 1996.

A new 50kg winch system has been designed and built to fit on the front of the JET standard MASCOT force reflecting servomanipulator. This winch was used extensively during the handling of Mark II divertor tile carriers.

A large number of types of tool are required for use during the fully remote handling of the Mark II divertor tile carriers and the associated tasks. During 1996, these tools have been progressively specified, designed, prototype tested and manufactured. The tools required to

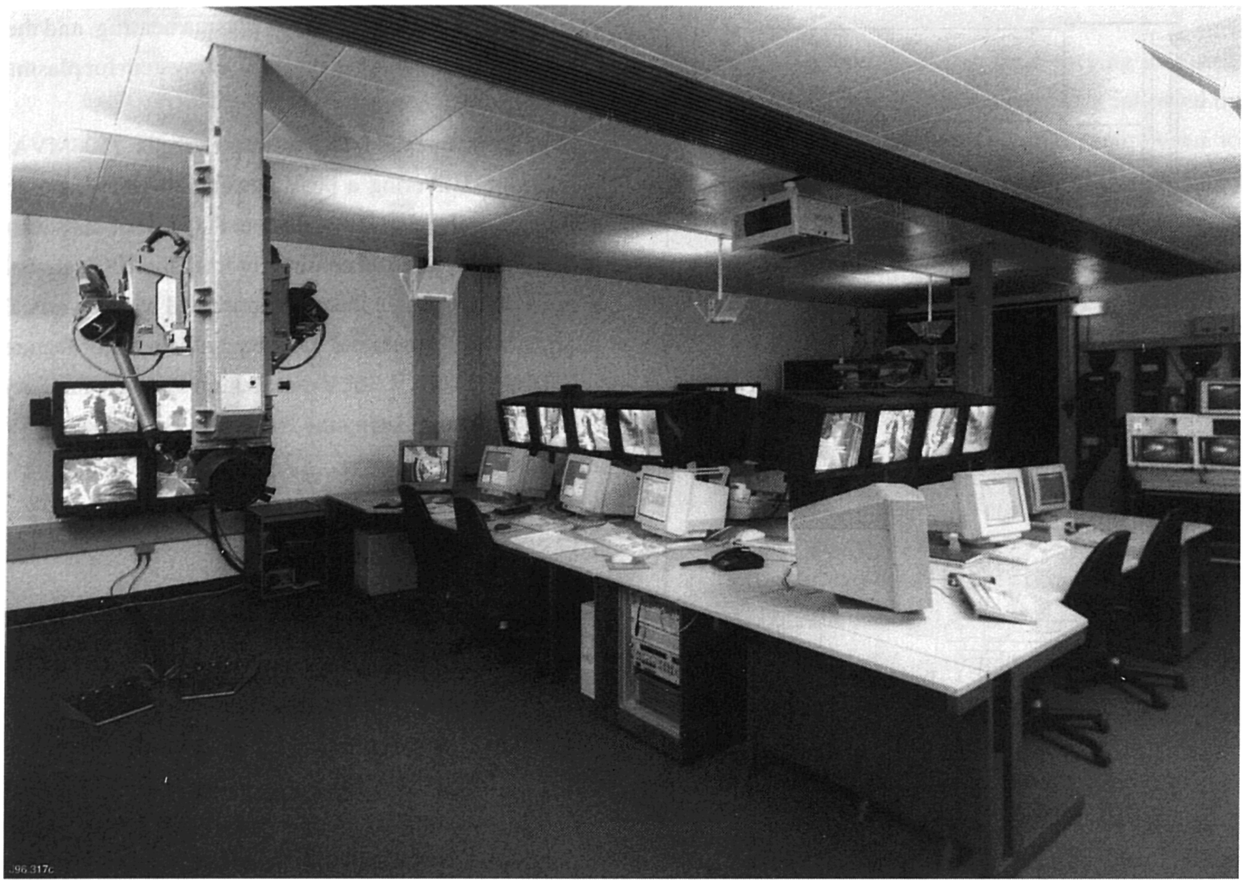

Fig.12: Remote Handling Control Room

handle the Mark II divertor tile carriers have been designed to suit a number of requirements.

The tile carriers are held by a tool which is manipulated by the MASCOT system on the articulated boom. The delicate surfaces and edges of the protruding CFC tiles make it necessary for the tool to align the tile carrier during insertion with only 1mm clearance from its adjacent tile carriers. The tool is also required to provide guidance for the allen key wrenches, as these are used to manipulate the fixing bolts, which are themselves hidden behind the tiles. Finally, the tool is required to provide temporary storage for the bolt handling tools and allen keys. The tools have interface features to suit the TCTF transfer system and level indicators visible to the MASCOT operator during handling.

Fourteen types of tile carrier handling tools have been designed, manufactured and tested. Eight types of tool for the handling of other components such as individual tiles, diagnostic wave-guides and bolometers and videogrammetry equipment have also been designed, manufactured and tested. Finally, a suite of storage trays for the components and the tools have been designed and manufactured.

Remote Handling Human-Machine Interface Development

Work has been proceeding in parallel with the equipment development on the creation of a standard style and implementation for the Human-Machine Interface (HMI). The HMI system is an integral part of the overall remote handling control room (Fig.12). The remote handling HMI system comprises a Pentium PC hardware platform running under Windows NT and communicating with the equipment and other HMI through a dual Ethernet network and a limited number of dedicated serial links.

The Human Machine Interface equipment is presented to operators in a standard form with a Windows "look and feel". The menu structure, MIMIC and dialog layouts, use of colours and the terminology are standardised across the range of equipment HMI to ease their use and the training of operators. The software is structured to facilitate the building of new HMI quickly and reliably.

The serial links are dedicated to specific equipment for real time command and control whilst one Ethernet network is dedicated to equipment control functions

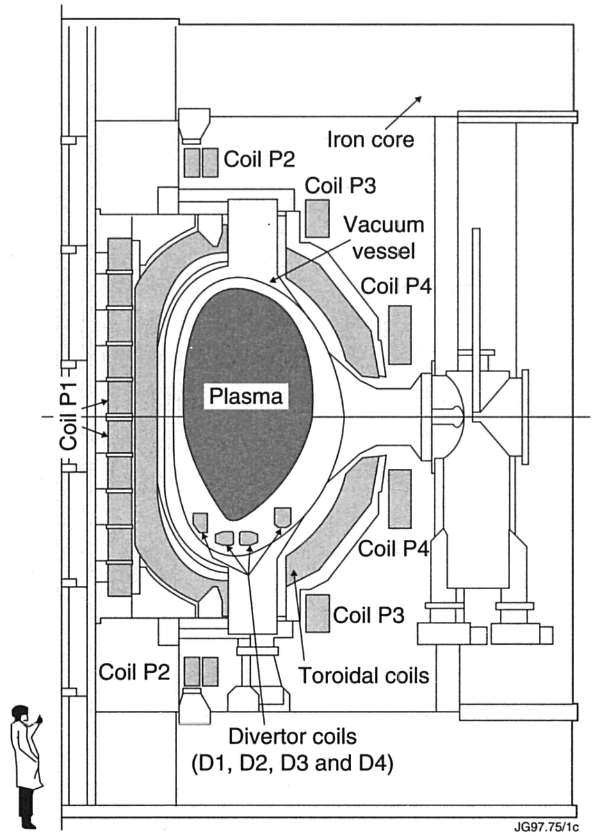

Fig.13: Cross-section showing the toroidal, poloidal and divertor coils

where real time response is not a safety critical issue and the other Ethernet network is used for file transfer, procedural/documentation communications and multimedia applications.

Power Supplies and Magnet Systems

The purpose of the JET electromagnetic system is to establish, maintain and control the tokamak magnetic configuration (Fig.13). It includes: the toroidal coils, which establish the toroidal magnetic field; the Poloidal Coils P1, acting as primary winding of the tokamak transformer, the Coils P2, P3 and P4 to control plasma radial position, vertical position and shape; and the Divertor Coils D1, D2, D3, D4, to establish and control the divertor configuration. The shell mechanical structure resists the large forces generated by the interaction of the currents in the toroidal coils and the poloidal magnetic fields. To perform their functions, the coils are energised by suitable power supplies. Voltages and currents of the poloidal coils are controlled in real-time by the plasma position and current control (PPCC) system. Other DC power supplies energise the Neutral Beam injectors (NB) and Ion Cyclotron Radio Frequency (ICRF) systems for plasma heating, and the Lower Hybrid Current Drive (LHCD) system for plasma current profile control.

The total installed DC power exceeds 1500MVA, capable of delivering a peak power >1000MW and an energy per pulse >10,000MJ. More than half of the power and of the energy is taken directly from the UK National Grid at 400kV, while the rest is provided by two vertical shaft flywheel generators. Consequently, a major feature of JET is the 400kV-36kV distribution system. Auxiliary AC power is supplied by the 20MVA, 11kV/3.3kV/415V distribution system.

Magnet System

Installation and Maintenance

Remote Turn Changing for Shaping Circuit

The number of turns on the poloidal coils are adjusted to enable desired plasma configurations to be produced. These changes require access to the coils and are normally made overnight a few times each week. During and after the DTE experiments, access to the Torus Hall will be much more difficult. Bus-bars have therefore been modified to allow turns changes without direct access to the coils.

For the P3 coils, turns will be changed at link boards at the outer ends of the magnetic circuit limbs. These link boards are shielded from the torus by the limbs so that the radiation level will be very low. For the P2 coils, turns will be changed at link boards in the Basement. These new bus-bars and link boards were installed and commissioned during the June and October shutdowns and have been operational during the latter part of the year.

Replacement of Rafix Connectors in P1

The quick release Rafix water connectors used in the P1 coil were considered insufficiently reliable for D-T operation. Therefore, these were replaced by screwed connectors. New fittings were welded on to manifolds and attached to the coil. All hoses were replaced by new hoses with screwed end fittings.

Replacement of Bolts in Magnetic Circuit

Inspection showed that several bolts holding the vertical limbs of the magnetic circuit in position were cracked under the heads. These failures were due to stress corrosion. The forces acting on the limbs were investigated by means of a 3D magnetic field computation. The computed

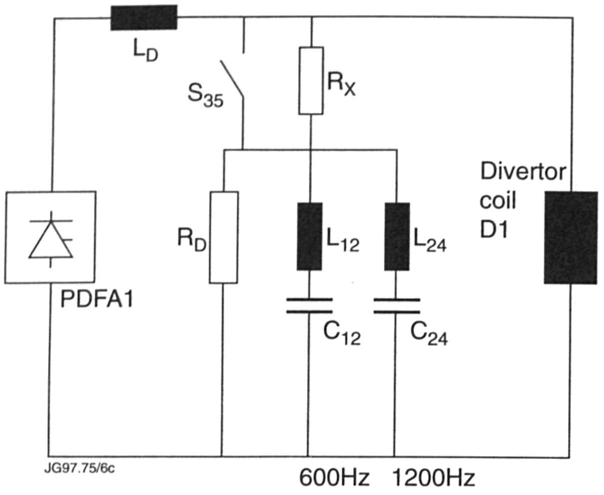

Fig.14: Circuit diagram of the new divertor power filter (four units in total)

horizontal force on a limb for a 6MA scenario was 9 tonnes compared with the allowable force of 26 tonnes confirming that the failure was not due to excessive stress.

Therefore, all bolts of this type were replaced by studs made of a more ductile but still high strength material. The new allowable force is 35 tonnes per limb. The studs were tensioned hydraulically and checked ultrasonically.

Machine Protection and Instrumentation

Engineering experience gained in operating the machine in a variety of new plasma configurations suggested further development of the Coil Protection System(CPS) and of machine instrumentation.

Machine Protection

The coil protection system (CPS) performs protective actions for the poloidal and toroidal coil systems. During 1996, CPS was upgraded with new processors and improved algorithms. CPS now includes:

- Voltage, current and I^2t checks on all circuits;
- Ampere turn checks on all coils;
- Transverse forces on TF coils;
- Circuit model for TF circuit.

Machine Instrumentation

The measurements made on the vacuum vessel have been extended and upgraded and now include:

- Forces on main vertical ports, main horizontal ports and octant joint supports;
- Displacements at main vertical, intermediate vertical, inner vertical and main horizontal ports;
- Acceleration of main horizontal ports.

To avoid interference due to time-varying magnetic fields the transducers use a carrier at 5kHz followed by demodulation. The demodulators are synchronised to avoid noise generated from beating frequencies. A VME based data acquisition system (slow ADCs) samples up to 192 channels with a resolution of 16-bit. The data are sampled at 5kHz and stored at 25Hz every pulse and at 5kHz in cases of plasma disruption.

Magnet Power Supplies

New Equipment

New Divertor Power Filter

The magnetic measurements used to detect the plasma vertical position have been strongly affected by coupling with the four in-vessel divertor coils. The operation of the Poloidal Divertor Field Amplifiers generates voltage harmonics mainly at frequency multiples of 600Hz.

Four new power filters have therefore been installed to substantially reduce the amplitude of the voltage ripple. Each filter is based on two LC circuits resonating at 600Hz and 1200Hz, respectively. A damping resistor ensures that the positive resonance is maintained within an acceptable level. A large series smoothing reactor provides the voltage drop at the harmonic frequencies (Fig.14).

Attenuation factors in excess of 40 have been achieved for the 600Hz and 1200Hz components and in excess of 10 for all the other characteristic components. The filters are essentially disconnected during the initiation of the plasma discharge by opening an HV DC contactor thus avoiding circulating currents in the divertor coils, which would have a detrimental effect on the magnetic configuration.

Load Interface Cubicles - PF and TF systems

Load Interface Cubicles (LIC's) have been installed for the poloidal field power supply system and the toroidal field system during the 1995/1996 shutdown.

The Load Interface Cubicles provide:

- an interface between the JET coil protection system on one side and the power supplies on the other side, for direct intertripping (CPS, DMSS);
- PPCC with essential measurements from power supply transducers;
- control of the "load" earthing switches and other load protection devices (crowbar switches);

- monitoring the access/exit doors giving access to the DC busbars;
- monitoring of all recognised busbar links providing either isolation, polarity or configuration functions;
- control, monitoring and protection functions for a power supply dummy load (where applicable).

The two cubicles were successfully commissioned during January and February 1996 with CODAS, CISS and the coil protection system. A similar cubicle was installed for the divertor field system during the 1992/93 shutdown.

PF and TF Crowbar Switches

Fast make switches (closing time ~ 5ms) are used in both the magnetising field circuit and the toroidal field circuit as mechanical crowbar switches. These are designed to close and provide a short-circuit across the coil terminals in the event of a coil internal fault or an excessive coil current. The trip signals are issued by the respective coil protection systems (CPS, DMSS). The PF crowbar switch and the TF crowbar switch were installed during the 1995/96 shutdown and commissioned with the JET coils.

A failure of the switch occurred in July. A comprehensive investigation concluded that the failure resulted from an internal arcing within the switch, when a high voltage was applied (fast rise phase). A review of the control and interlock is currently underway.

Earth Fault Monitoring Cabinets (EFMC's)

Earth Fault Monitoring Cabinets (EFMC's) have been upgraded in the poloidal vertical field circuit, poloidal shaping field circuit and the toroidal field circuit. The new cabinets provide the following functions:

- measurement of the earth leakage current and transmission of the analogue signal to CODAS;
- measurement of the earth leakage current and trip detection by means of a separate transducer;
- selector switch to connect the neutral cable from the power supply equipment to either a local earth, the remote earth or an internal high voltage power supply;
- a high voltage power supply module (test mode) with a DC output voltage selectable in the range 1-5kV in 1kV steps;
- a local display of the H.V. power supply output voltage/current for diagnostic purposes.

During the recovery from isolation, the PF and TF circuits referred to above are now regularly tested at voltages between 2.0 and 5.0 kV DC to check the integrity of the complete DC circuits (AC/DC rectifier, DC busbar, JET coils) with respect to earth. Similar systems were installed during the 1992/93 shutdown in the radial field circuit (FRFA) and the divertor field circuits (PDFA's).

Improvement of Existing Equipment

PVFA I Thyristor Snubbers

The PVFA amplifiers were originally fitted with an AC "bucket" type snubber aiming at removing voltage spikes (deadly for thyristors) caused by the forced turned-off of the thyristors themselves or by the switching-off the supply transformer. Over the years, this technology has shown many serious problems requiring shutdowns to give access to the HV areas during operation campaigns. The main problems identified have been:

- resistances damaged by surges of current during energisation of the amplifier;
- series resistors regularly going open-circuit due to overloading in particular for the long plasma pulses;
- explosion of non-linear resistors.

The design of a new snubber was undertaken in the course of 1995 and has been implemented during the 1995/96 shutdown on PVFA 1 first, to gain operational experience on a limited scale. After almost one year of operation , the new type of snubber has proven to be very satisfactory. This new design will be extended to the other PVFA amplifiers in 1997.

FGC DC Circuit Breakers

During the operational period before the 1995/96 shutdown, the DC circuit breakers installed in the field circuit of the two flywheel generators showed signs of mechanical fatigue after several years of service. They had achieved ~7,000 cycles of operation well in excess of the 2000 cycles for which they were designed. These were replaced during the shut-down with new fast DC circuit breakers which are of more compact design and faster action, designed specifically for large numbers of operations (50,000 cycles).

The control circuitry was also modified to match the features of the new circuit breakers. Both circuit breakers have successfully performed during 1996, eliminating one of the sources of failures identified during the previous operational period.

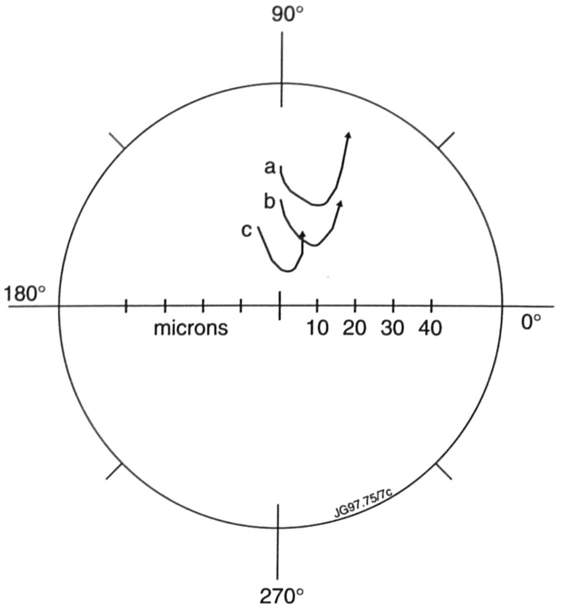

Fig.15: Shaft displacement in top bearing of the Toroidal Flywheel Generator

Internal Bridge Freewheeling as Protection Action for Thyristor Converters

The New Protection Coil System is designed with two protection actions:

- immediate removal of the voltage across the coil;
- immediate removal of the voltage across the coil and in addition, trip of the High Voltage Circuit Breaker.

Initially the PVFA system (Poloidal Vertical Field Amplifiers) had been designed without such facility; the voltage could be removed from the coil, but only when the current in the coil had decayed to a value close to zero, namely after the corresponding circuit time constants had elapsed. For urgent actions, the only way to remove the voltage quickly was to trip the High Voltage Circuit Breaker with the risk of causing its premature wearing.

Since the PVFA amplifiers had been upgraded in the past to higher current ratings, and the original thyristors replaced by new ones with higher capabilities, it has been possible during the 1995/96 shutdown, by extensive modifications of the control electronics, to modify the way the amplifiers were "turned-off". After modifications, when a voltage-off request is issued from the Coil Protection System, one branch of the thyristor bridges is automatically selected and controlled by the electronics to offer a low impedance path to the coil current without giving any voltage output: this is the Freewheel action. This new facility was used successfully during 1996. In addition, it suppressed the excessive number of High Voltage Circuit Breaker trips.

Maintenance and Support

The operational and maintenance support for the Tokamak Magnet Power Supplies is supplied under a service contract. In addition to routine maintenance which was carried out on all magnet power supplies, other work was also completed during the main shutdown:

- replacement of all control and protection devices in the Flywheel Generator 415V switchboard;
- complete overhaul of the speed control liquid resistors;
- complete overhaul of all generator auxiliary pumps.

Flywheel Generators

During the October 1996 shutdown, improvement on the balancing of the TFGC was achieved by fitting balance weights within the pony-motor rotor frame.

A total of 40kg was fitted. Figure 15 shows the shaft displacement in the top bearing in three cases, with the generator free-wheeling from 225 rpm to 112 rpm:

- prior to fitting balance weight (curve (a));
- with 20kg fitted (curve (b));
- with 40kg fitted (curve (c)).

The vibration at the top bearing has been reduced while motoring at high speed, from 150μm to 100μm. This vibration level is now well below the alarm level (160μm).

Saddle Coil Crowbars

The Saddle Coil Crowbar protects the Saddle Coils and is independent of the operation of the Disruption Feedback Amplifier. These crowbars are installed in the Basement and are connected to the Saddle Coils with busbars. During last operation, the Saddle Coils act as antennae for the ICRF frequencies emitted by the ICRF generators. These high frequencies were perturbing the electronics which control the crowbar action. High frequency suppression circuits were added for evaluation during the last shutdown. The result of these changes is being evaluated.

Operation and Commissioning

Recommissioning after the 1995/96 shutdown

At the end of the 1995/96 shut-down, the magnet power supplies and the associated coil protections were comprehensively re-commissioned. The power re-commissioning programme from the main Control Room took place in two phases. Firstly, the power supplies were tested, before being re-connected to the coils, in March 1996 and about one hundred and forty pulses were performed over a period of two weeks.

The second phase, after re-connecting the power supplies to the coils, took place between April/May over four weeks. More than four hundred pulses were executed during that period completing the testing of all power supplies up to their full rated performance.

Commissioning of the new Divertor Power Filter

The new power filters for reduction of voltage harmonics generated by the Poloidal Divertor Field Amplifiers were commissioned from the Control Room in their basic configuration with their essential controls and protections in July, over four dedicated shifts and ~50 pulses.

The second phase of commissioning, which included the final arrangement for the controls and protections and the additional HV DC contactors and resistors, took place at the beginning of November. About forty pulses were executed making use of three dedicated shifts.

Work for ITER

Design Tasks D318

Following the design activities carried out in 1994/95, JET remains involved, as a participant to the European Home Team, with the design activities for the ITER pulsed power supplies system.

In particular, JET defined the overall technical organisation of the Design Task D318 and its subdivision in packages of work. In addition, JET is acting as supervisor, on behalf of NET, for Package C "Pulsed distribution system", Subpackages D1 and D2 "Rectifier transformers, AC/DC busbars, chokes, switchgear, etc. for the AC/DC converter system" and Package E "Switching and Discharging Networks".

R&D Task

On behalf of the European Home Team (NET), JET is in charge of the technical supervision of the R&D Task on a by-pass switch for the ITER discharging and switching networks. The specification for the call for tender, the technical evaluation of the proposal from Industry and the revision of the specifications for the contract were carried out in 1996. JET is also assessing the feasibility of the execution of some of the high current tests at the JET site, making use of the Toroidal Field Generator Convertor.

Additional Heating Power Supplies

The Additional Heating Power Supplies consist of the Power Supplies for the Neutral Beam, the ICRF and the LH systems. These are maintained, modified, upgraded and also operated by the AHPS Group.

Neutral Beam Power Supplies

During the early-1996 shutdown, the new filament detection circuit was installed on the Octant No.4 and the Octant No.8 systems. Prior to this installation, the circuit was fully tested and commissioned in the Hot Cell. On the Octant No.8 system, the circuit worked correctly. However, on the Octant No.4 system, high voltage peaks, most probably generated by breakdowns inside the PINI, blew the protective resistors at the input of the detection card. The PINIs on the Octant No.4 system are high current PINIs which require very high arc currents. Since all these systems are installed at high voltage potentials, a special measuring circuit was build to investigate. After analysis, a protective circuit at the input of the card was installed. Evaluation of the correct working of this circuit is in progress.

When the cooling water to the PINI buckets was switched early in the year a low resistance path between Grid 1 and Arc+ was measured. This suggested a short inside the SF_6 Tower. A deliberate short was installed at the power supply side and at the PINI side to bypass a possible bad contact. Operation with a short between Grid 1 and Arc+ was possible with the PINIs installed, but would be impossible with the high current PINIs.

During the mid-year shutdown, it was decided not to try to repair the Grid 1 to Arc+ short. The PINI had been working correctly and it was judged to be more dangerous to open the SF_6 Tower due to disturbance of other parts leading to problems of otherwise healthy circuits.

ICRF Power Supplies

The ICRF power supplies continue to operate without major problems. Routine maintenance is performed at regular intervals. The supplies are used during operation with the RF generator connected to the antenna and during the shutdown with the RF generator connected to their dummy load. As far as the power supplies are concerned, both operational modes are the same so that these power supplies are operated almost continually.

LHCD Power Supplies

Operation of these power supplies follows similar lines as the ICRF power supplies. These are used either with the klystrons connected to the launcher or to the dummy load.

Routine maintenance is performed at regular intervals but no major changes have been necessary since their early commissioning.

GDC Power Supplies

The Glow Discharge Cleaning (GDC) Power Supply is used extensively at the start of an operational period after a shutdown. At the end of the shutdown, these were switched on and performed without fault. These Power Supplies are current sources, the voltage depends on the load impedance. Originally, striking the glow was obtained by RF generators after which the DC power supply would maintain the glow. Since the RF generators have been removed, striking the glow is now achieved by lowering the gas pressure at the start resulting in a striking voltage close to the maximum limit of the DC supply. This scenario is now routinely used without any problems.

Power Distribution and Electrical Services

Pulsed Power Distribution (400/33kV)

The 36kV power supply system for the Gyrotron of the diagnostic KE4 was completely replaced following damage caused by an electrical flashover and subsequent fire. This installation involved major civil work as the replacement equipment was considerably larger than that used originally. The extra equipment gave rise to additional high voltage areas, and this in turn had implications for the access control system which also required modifications to ensure personnel safety. Commissioning of all newly installed equipment has now been completed.

UKAEA Culham Laboratory have requested a second 36kV supply for the forthcoming MAST project. This will operate on an interpulsed basis with JET and does not therefore have any serious implications as far as loading of the JET 400kV/36kV transformers is concerned. However, it is a problem in that the range of 36kV switchgear currently manufactured by Groupe Schneider (formerly Merlin Gerin) is not mechanically compatible with the switchgear installed at JET, and an "adapting cubicle" is required to overcome this, despite the attendant disadvantage that twice as much space is needed in the J5 Substation to accommodate the equipment.

Local testing and troubleshooting of the Reactive Power Compensation System has been difficult because of the need to simulate CISS and CODAS signals and to ensure that all such simulations are removed before the system is returned to service. To simplify this, a local test kit has been constructed and a fail-safe plug-in test facility has been provided in the local control cubicles.

Very occasional incorrect operation of one of the Reactive Power Compensation Units was eventually traced to spurious opening of one of its Vacuum Switches, (i.e. opening of the switch even though no command to open had been issued). The switch was returned to the manufacturer for investigation of a possible mechanical fault, followed by repair and/or adjustment.

Non-Pulsed Power Distribution System

The principal new loads connected to the non-pulsed power distribution system were the diagnostic KM9 system and the extension to the air conditioning system in Building J1D. Connection of smaller new loads and modification of supplies to existing loads were also undertaken on both the Experimental and the Building Services supply systems.

A major programme of protection relay testing was undertaken at primary board and section board level on the 415V distribution system. This involved widespread service interruptions and extensive co-ordination was needed to minimise inconvenience to plant users. The testing proved to be a most useful exercise, and highlighted the need for further testing on a regular basis.

Routine maintenance was performed on all 11kV circuit breakers, on the main 415V circuit breakers and on all of the Uninterruptible Power Supply units on site.

Electrical Services

A public address system covering all outdoor areas of both the JET and Culham sites was installed in preparation for the DTE1 operational campaign. In the event of an incident involving a possible release of tritium, this system will be used to broadcast safety related information throughout the site.

Electricity Supply Contracts

Cost and usage details of the various electrical supplies to JET are shown in the Table III. The supply from National Power is taken at 400kV, and that from Southern Electric at 132kV. UKAEA Culham Laboratory provides electricity at 415V for some building services, and at 11kV for the standby supply to JET. The charges associated with National Grid are connection charges, and are not related to the amount of electricity consumed.

Table III - Expenditure on Electricity in 1996

	Units Consumed (kWh)	Cost (£)
National Power	17,660,860	662,303
Southern Electric	48,695,300	1,702,210
Culham Laboratory	2,007,070	126,280
National Grid	-	105,797

Machine Services

New modifications on the'in-vessel components water cooling system (D&RS) to satisfy safety requirements for D-T operation, were identified and carried out. Further modifications were performed to improve the reliability of the PF water system and to meet new requests for cooling water.

In-Vessel Water Cooled Component Protections

The protective actions on these cooling loops, in case of 'high in-vessel pressure' (above 15mbar), were substantially changed. To test if any of the cooling systems might cause a significant water leak, associated with a pressure rise, pressure switches were fitted to all cooling loops, connected to a new hardwired protection logic, backed by PLC. In case of an in-vessel pressure higher than 15mbar, the system would isolate, undergoing a pressure test sequence, and draining down automatically only those systems where the water pressure had dropped to the level of the pressure switch trip. Healthy systems would automatically reflow, thus avoiding unwarranted drain actions.

In-Vessel Water Cooled Components Drain Vacuum

The drain rings and waste water holding tank, for the water drained off the in vessel water cooled components, were modified, to be maintained at an absolute pressure of 150mbar at all times while in operation. This allowed a more efficient and faster action whilst maintaining an intermediate vacuum in case any of these systems were to rupture in vessel. Two 'liquid ring' type vacuum pumps were installed, (one main and one stand-by), capable of pumping any mixture of liquid and vapour down to the required pressure. Commissioning was successfully completed with the first installed pump and the system is about to be operational.

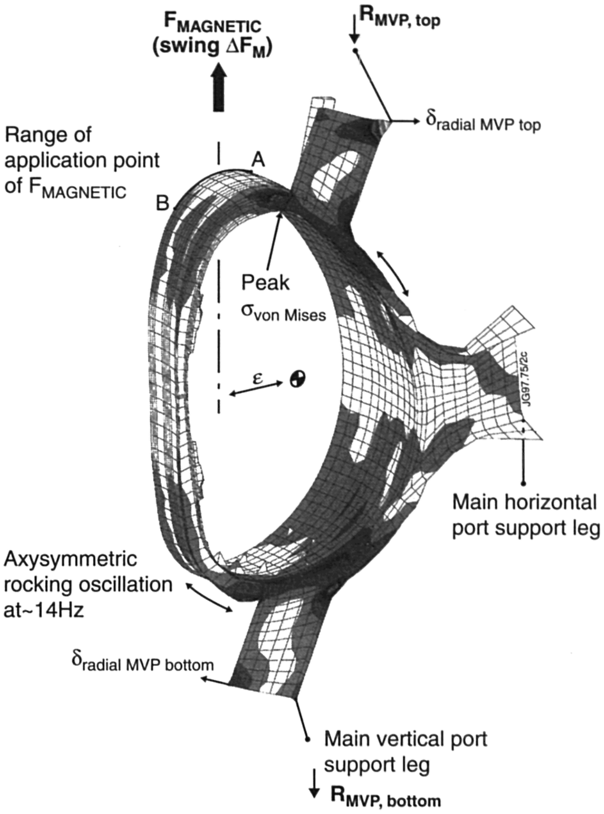

Fig.16: Finite Element model of the Vacuum Vessel Rolling Motion

NIB Cooling Systems

The PLC control logic on these cooling systems (NIB Octant No.4 and NIB Octant No.8) was modified to include the 'Leak detection' mode of operation. This mode is automatically initiated from the NIB vacuum pressure rising to a level of 5mbar. In this condition, the NIB cooling system would operate, closed loop, isolated from the PF system. Water leaks larger than 1 litre/hr could be assessed and monitored via the level on the respective expansion tank. Should the water level in the expansion tank reach a low level in a time less than a preset value (8 minutes), this would allow the manual selection of the 'Full Down' mode, which stops all pumps, and an emergency drain down could then be initiated.

PF Water System

Further modification took place to improve the reliability of the PF water system. In particular, the diesel driven emergency pump was replaced by a new pump with pressure-flow characteristics to meet the requirements of the up to date PF system. Designed to supply essential in-vessel water cooled components, the emergency pump operation is coupled to the isolation of systems for which

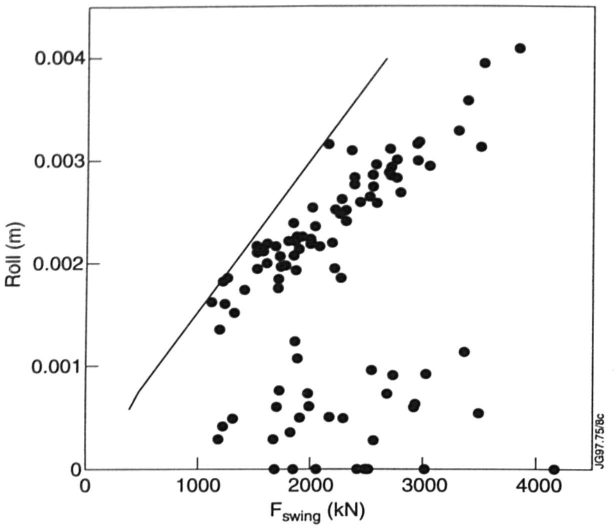

Fig.17: Swing of Radial Displacement of a MVP versus swing of Vertical Force measured at the MVPs

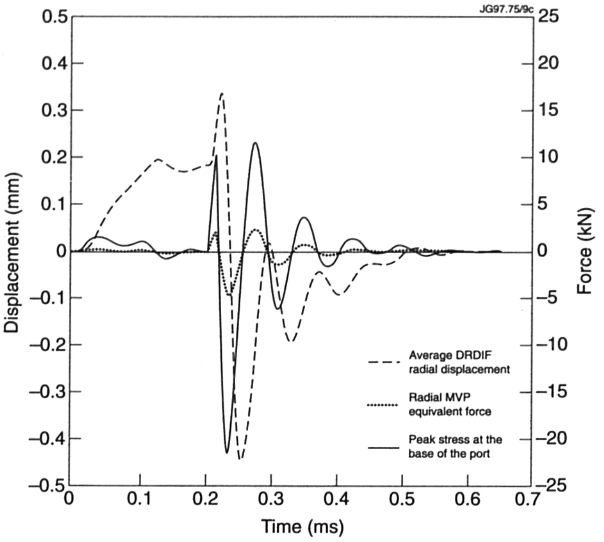

Fig.18: MVP Rolling Motion with 1 MN Vertical Vessel Force Swing

cooling is not essential in emergency conditions (i.e. the PF coils), to maximise delivery to the desired water loops. The appropriate control modifications, involving interconnections between the PF water management control cubicle and local controllers, were performed and the system is about to undergo final commissioning.

Engineering Analysis

Routine work includes assessment of compatibility of any new operating scenarios with existing Operating Instructions, which define the conditions for safe operation of the machine, and assessment of thermal and electromechanical stresses in on-vessel components. Other main activities focussed on the assessment of toroidally non-uniform disruption forces and on the prospects of 4T operation.

Vacuum Vessel and Electromagnetic Forces

Mechanical Behaviour of the Vessel

The response of the vessel to both vertical and horizontal forces has been analysed in a considerable number of disruptions. Use was made of old and newly installed transducers to measure the radial displacement of all ports and vertical forces on the main vertical and horizontal ports (MVP and MHP). Signal-to-noise ratio was improved by revision of the conditioning equipment.

"Rolling" Motion

The rolling motion response of the vessel to vertical forces has been analysed statically and dynamically with the help of the FE model, including the effects of the refurbished MVP dampers. Output from these simulations has also been used in support of a lumped-parameter Simulink model which was developed and used to give quick, though approximate, answers when sounding out the effects of changes of parameters such as the damping factors of MVP dampers.

A series of analyses has been carried out to check the consistency of simulations with observations of forces and displacements during the last campaign. Typically, both observed and calculated ratios of port displacement/support force are in the range 0.9~1.1mm/MN, depending on position and timescale of the load. Also, the measured support force and magnetic force applied to the vessel may differ by a factor up to 2 (in both directions), depending on the application point of the magnetic force (see Fig16).

From the models, confirmed by statistical data, operating limits have been defined. An example in Fig.17 shows a statistical upper bound relationship between the swings of the vertical force and the radial MVP displacement (roll). Since the latter determines the maximum forces on the MVPs (Fig.18), hence the maximum strains at their root, the allowable force swing can be derived. This can be predicted from the pulse parameters using the "F" number correlation. Fatigue life has been estimated as more than 1000 worst vertical displacement events at 6MA with 9MN max. vertical force and 11MN max. swing, causing a ±0.5% strain.

The response of the vessel to non-toroidally symmetric loads has also been addressed by using the 180° FE model

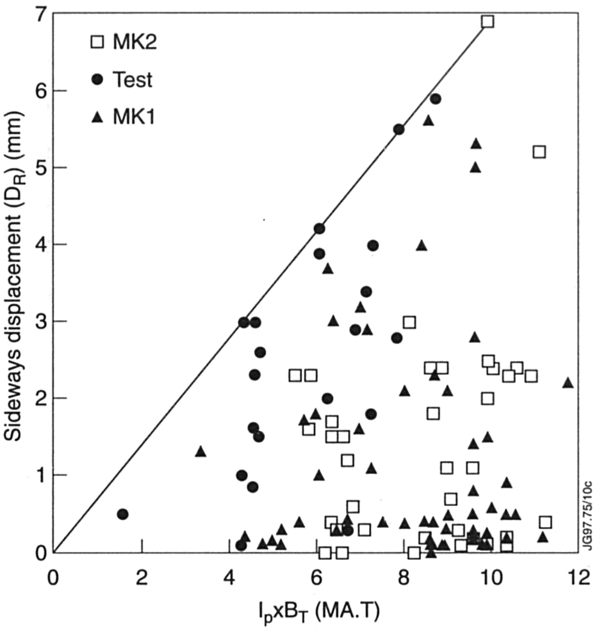

Fig.19: Scaling of Sideways Torus Displacements

and a Simulink model. It has been shown that the torsional stiffness of the vessel has a great beneficial effect in smoothing out the response. For instance, a non-uniform vertical force with peaking factor 2 would produce port displacements (and hence stresses at the port's root) with a peaking factor of only about 1.2.

Sideways Motion

Considerable horizontal movements were observed during the Mark II campaign, in spite of new horizontal restraints on the MHPs. Displacements are not substantially less than previously observed, and in one case somewhat larger, even if analysis showed that the horizontal restraints were working as expected from the design, supporting up to 80 tonnes sideways force. The movement of the vessel was much more heavily damped than could be accounted for by the MVP dampers. In addition, the vessel showed a residual displacement after a sideways disruption of up to ±1.5mm. This indicates an equivalent friction of ~15 tonnes. Magnetic damping was found to be a major restraining force in addition to vertical and horizontal port restraints. It followed that the horizontal forces applied to the vessel by the disruption were about double those originally assumed.

A simple Simulink model has been developed, taking into account the MVP radial hydraulic dampers, the MHP tangential hydraulic dampers, the magnetic damping, the NIB masses and friction effects. Assuming a typical disruption pulse duration of 20ms, the model indicates that a horizontal force applied to the vessel by the disruption of about 400 tonnes is required to produce the record displacement observed in Pulse No.38705. This pulse gave 6.8mm movement (with 6mm displacement of the NIBS) despite 150 tonnes reaction on the various restraints.

The damping effects due to the magnetic field have been evaluated analytically in a simple configuration and more precisely with a 3D FE model. Assuming a rigid plasma ring model for the "kink" mode, its tilt angle from magnetic measurements and the corresponding horizontal force applied to the vessel is calculated. The impulse of the force has been found to correlate satisfactorily with the sideways motion in a number of disruptions.

According to the model, the maximum sideways motion is anticipated to scale with the product of plasma current and toroidal field. The present database, supports this scaling (Fig.19). Extrapolation of the present database to high current, high field operation gives 15mm vessel side movement at 5MA, 3.4T. To avoid or minimise impacts, a radial gap of 15mm has been ensured between MVP and mechanical structure. The kink mode which determines the horizontal forces may however be more stable at high fields and a more favourable scaling would apply.

Vessel Forces and Displacements

Asymmetric Electromagnetic Forces during Disruptions

Disruptions of the plasma are usually associated with vertical displacement events (VDEs) due to saturation of the vertical stabilisation circuit. In many disruptions, the vessel forces and displacements are toroidally non-uniform and peaking factors (local/average) of the forces measured at the vertical vessel supports of up to 1.8 have been observed. These asymmetries produce, in general, global sideways displacements of the vessel. The largest sideways displacement recorded so far was 6.8 mm in a disruption during Pulse No.38705 at $I_p = 3.6$MA. The displacements are restrained by the stiffness of the main vertical ports, by the additional dynamic supports at the main horizontal ports, and also by the magnetic damping due to the movement relative to the toroidal magnetic field Nevertheless, these give cause for concern for some elements attached to the vessel, such as the rotary valves, and for the vessel, itself, in the case that the vertical ports would hit the mechanical shell.

Significant sideways displacements were only observed in upward VDEs and in those cases where the vertical

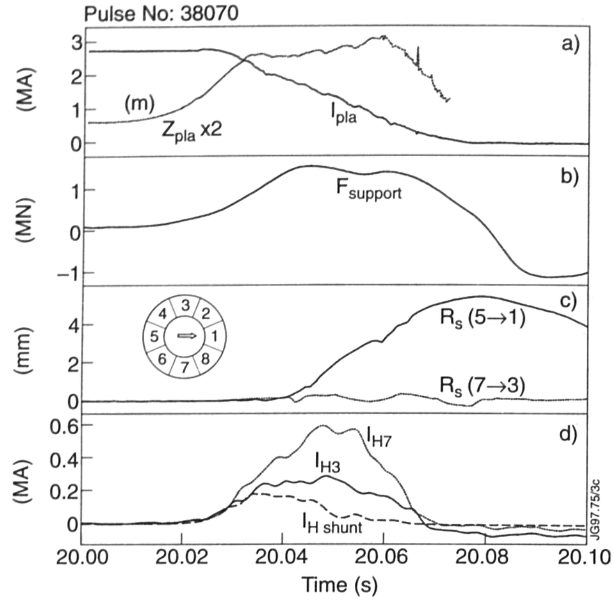

Fig.20: Experimental data for Pulse No. 38070: (a) $R_s \Rightarrow$ torus sideways displacement in direction Octant No. 5 ⇒ No.1 and No.7 ⇒ No.3: (b) $I_H \Rightarrow$ halo current evaluated at Octants No. 3 and No.7: (c)$I_{Hshunt} \Rightarrow$ halo current scaled from mushroom tile currents

stabilisation was lost well before the start of the current quench. The vertical current moment ($M_{IZ} = I_p x Z_p$) and hence, the vertical force can then reach high values. At the peak of the current moment the plasma force balance is mainly obtained by the repelling halo current force between the plasma and the vessel. A deliberate 'worst case' VDE is presented in Fig.20 showing the evolution of the plasma current, plasma displacement, vertical force at the vessel supports, sideways torus displacement, and of the halo current obtained from toroidal field measurements at Octants No.3 and 7. The halo current is strongly non-uniform, the torus is displaced in the direction Octant No.5 (see Fig.20).

The asymmetry of the vertical and radial current moments measured at Octants Nos.1,3,5 and 7 is shown in Fig.21. The current moment differences ΔM_I at opposite Octants may be interpreted as evidence of an m/n = 1/1 kink mode, where the plasma is tilted around an axis Octant No. 5 to No. 1 with an amplitude, $\delta Z_{max} \approx \pm 0.15$m and displaced along that axis by a smaller amount ~0.02m.

The sideways force and tilt moment at the plasma arising from the current moment differences have been estimated on the basis of a simplified model. These are mainly caused by the interaction with the toroidal magnetic field. For Pulse No.38070 a sideways force is estimated, using current moment differences averaged over 30ms and $B_T = -3$T at R = 2.7m: $F_x \approx +2.4$MN

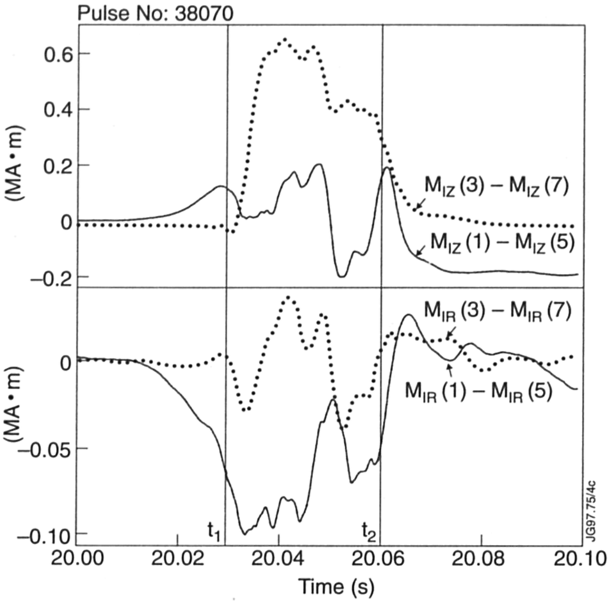

Fig.21: Differences of vertical and radial plasma current moments between opposite Octants

The sideways magnetic force is assumed to be balanced and transmitted to the torus mainly by halo current forces with strong asymmetry as indicated in Fig.20. It is very substantial and of similar order of magnitude as the estimated global destabilising force at the plasma, $F_z \sim +3.4$ MN. A dynamic analysis of the vessel shows that the estimated horizontal impulse 2.4MN.30ms is consistent with the observed torus sideways displacement of 5.5mm.

Large lateral torus displacements can only be expected when:

(a) the vertical current moment becomes large during the VDE (large displacement before current quench);

(b) the plasma boundary q-value decreases to about unity, permitting kink instability; and when

(c) the kink mode is essentially locked, giving an impulse in one direction.

The suspected dependence of lateral displacements on the minimum boundary q-value is illustrated in Fig.22, using $q^* \approx 5B_T a^2 / I_p R_I$ as a rough approximation. Large displacements are only seen when $q^*_{min} \leq 1.5$. However, small q^* did not always give a large displacement. In particular, downward VDEs never produced displacements exceeding 1 mm, even though conditions (a) and (b) were well satisfied. It was noted that in downward VDEs the mode amplitude is smaller and the current quench is generally faster than in upward VDEs.

It has been attempted to identify the plasma configurations and parameters before the disruption which produce large torus displacements. The success was very

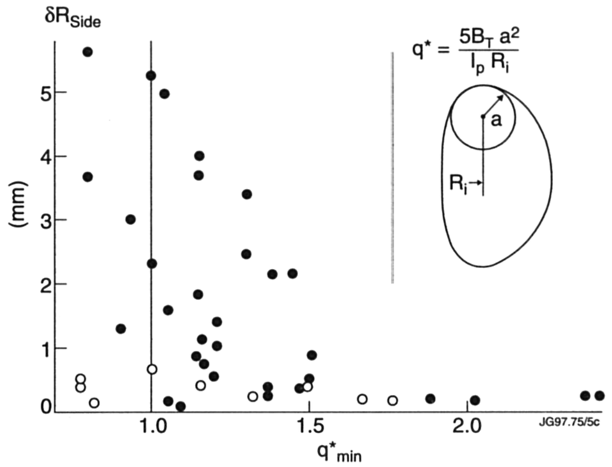

Fig.22: Statistics of sideways torus displacements plotted versus minimum q: Open circles are downward VDEs*

limited. From statistics, there is an indication that large displacements occur mainly at low initial beta and when the elongation ratio is ~1.7 giving smallest average plasma wall gap. During operation with the Mark I divertor, it was concluded that large displacements occurred only with small initial upper triangularity. This latter conclusion was not confirmed during in operation with Mark II.

It is of interest to establish a scaling of sideways displacements in preparation of operation at high current. The theoretical estimate suggests a scaling S $\delta R_{side\ max}$ in proportion to $I_p.B_T$ (or I_p^2 for cases with the same q-value), but there is no estimate of the scaling of the kink amplitude.

Figure 19 indicates that the envelope of sideways displacements with the present vessel support system may be represented by $S(mm) \approx 0.7.I_p(MA).B_T(T)$. At 5MA and 3.4T, $S_{max} \approx 12mm$ could be expected. However, it should be noticed that only two spontaneous disruptions in the life of JET have reached this envelope, and that there are prospects for avoiding the particular causes of premature loss of stabilisation in these two pulses (Pulse Nos.34078 and 38705), by some improvement of the feedback signal generation (decoupling from effect of current changes and of n = 2 mode pick-up).

Magnetic Damping of Torus Displacements

The forces arising from interaction of the lateral torus movements with the toroidal magnetic field were assessed analytically and by FE computations. The forces are produced by both, poloidal and toroidal vessel currents induced by the movement. The anisotropic resistivity of the vessel caused by the presence of bellows was taken into account. To lowest order in the inverse aspect ratio, a/R_o and for moderate elongation ratio κ (not >> 1), the damping coefficient was derived as $f_d \approx 5.8 MNm^{-1}$.

FE computations gave $f_d = 6.0\ MNm^{-1}s$:

The stiffness was derived as

$K_m \approx 340\ MNm^{-1}$ (high frequency limit).

Assessment of Increase of Toroidal Magnetic Field to 4T

Toroidal Field Coils

The electrically faulty TF Coil 3.1 has been cut and used to examine the insulation condition. Tests revealed the following:

- Corrosion was caused by a water leak;
- In areas where water corrosion was not present, the insulation was in good condition;
- From more than 40 specimens extracted from the coil, the average shear strength was 38MPa, with a standard deviation of ±8MPa. The shear modulus Γ was 1000MPa, considerably lower than originally anticipated, and leads to low peak stresses. The ultimate shear strain was considerable at 7%. This resilience ensured a good collaboration of the material and avoided brittle fracture and crack propagation. This appeared also from a stress analysis indicating that the stress intensity decreased assuming cracks of increasing length. A quite safe allowable shear value could therefore be assumed as (a) less than half of the average ultimate shear and (b) less than the average ultimate shear reduced by twice the standard deviation.

A beam model of the whole coil shows that the maximum shear stresses in the coil insulation arose at the collar tooth in the worst assumed scenario. A similar result was obtained in 1988 using a Pafec model. The stresses computed are average values in the cross-section adjacent to the tooth evaluated with "smeared" (averaged) properties of the coil components.

To evaluate the actual value of the stress a second detailed model has been created using Abaqus, considering the composite nature of the structure with the actual properties of the epoxy layers and the copper turns. This model gave a maximum shear stress of 10MPa at the third interturn layer. To verify the accuracy of this value, a computation of the peak stress using "smeared" properties was undertaken, obtaining values (17MPa) coherent with those obtained in 1988. The reduction from 17 to 10MPa was explained by the fact that the peak values were attenuated in the epoxy layers, which were much softer than the adjacent copper layers.

Effects on Vessel Displacements

The effect of increasing B_T on sideways motion has also been evaluated. The damping effect, proportional to B_T^2 effectively limits the increase of impulse force, leading to a maximum sideways motion of 15.6mm with acceptable impacts, if any. The effect on rolling motion is not expected to be significant since the maximum vertical forces depend on the maximum current moment which could be affected only to a minor extent by B_T.

Quality Assurance

The quality assurance activities underwent a major managerial re-assessment during 1996, to align with the new phase of the JET programme and a restrained budget.

Efforts are now more concentrated on operational activities rather than on new equipment, and a corresponding reduction in manpower has been achieved. The main responsibilities for Quality Control at the operating level rest with the Responsible Officers, who can request Quality Assurance Group (QAG) assistance, through their Division Heads, within the limits of the constrained manpower resources.

The main function of the Group are to:

- maintain the JET Quality manual of procedures and propose changes or new procedures as appropriate;
- perform internal Audits to an agreed programme;
- maintain a Central Archive of technical contracts, commissioning and assembly procedure documents, and to establish an interface to local document archives;
- maintain a library of Quality Standards;
- assist in all quality matters on request;
- advise on minimum Third Party Inspection requirements and to coordinate activities with the Welding Section of the Machine Assembly Group;
- log and control issue of Technical Control Documents and participate in technical review panels.

Neutral Beam Heating

Overview

During 1996, the Neutral Beam heating system once more played a major role in the successful and diverse experimental programme of JET. There was heavy involvement in the operational programme and most of the year was spent in bringing the NB system towards its 'nominal' installed power of >19MW. By the end of the year, reliable operation had been achieved at 17.5MW, and a number of problems had been overcome.

The Engineering Group was involved in reinstallation of the injectors early in the year, and then in preparing for the upgrade of spares and in remedying the mechanical failure on the Octant No.8 injector at the end of the year.

The Cryogenic Group continued to improve plant performance on both the NB injector and pumped divertor cryopumps. It was also involved in significant control system upgrade. The Test-bed Group continued important work on beam diagnostics, and establishing the NB Test-bed as the foremost installation of its kind.

In addition, all Groups were, committed to the preparations for tritium beam injection for the DTE1 experiment. In particular, the tritium gas introduction modules (piglets) were installed and tested and commissioned in parallel with injector operation. This involved substantial overnight and weekend work.

Neutral Beam Operations

NB Operation and Performance

The technical commissioning of NB systems for DTE1 was carried out in parallel with normal operation. Despite this, the number of discharges during 1996 with NB injection was the highest of any campaign. Due to the emphasis on establishing regimes of high fusion performance in preparation for DTE1, the proportion of pulses with high power NB injection (>15MW) was also the highest during this period. Only at the highest power levels (>18MW) has the number and proportion of pulses been less than in the 1994/95 campaign; comparison with that period is appropriate since the injectors were configured similarly with respect to the number of installed PINIs of each type. The distribution of NB injection pulses at various power levels for the last ten years is summarised in Table IV.

Most of the installed PINIs at the start of re-commissioning in April 1996 had been modified during the 1995/96 shutdown for incorporation of the 'grid-gas' feed. Due to restrictions on operating the NB Test-bed in deuterium during the shutdown period, most of the high-current 80kV tetrode PINIs were pre-conditioned in hydrogen, thus restricting the maximum voltage to about 65kV at the power supply current limit of 60A. Therefore, these PINIs had to be conditioned on the JET injectors during extended periods of pulsing asynchronous from the tokamak. The new inertial calorimeter, onto which the beams impinge during asynchronous operation, was described in the 1995 Progress Report, and gives a useful

Table IV: Distribution of Neutral Injection Pulses for 1986-1996

				>5MW			>10MW			>15MW			>18MW		
Year	JET	NBI	%JET	No	%JET	%NB	No	%JET	%NB	No	%JET	%NB	No	%JET	%NB
1986	3153	707	22	327	10	46	3	0	0	0	0	0	0	0	0
1987	1412	86	6	62	4	72	0	0	0	0	0	0	0	0	0
1988	2954	993	34	789	27	79	292	10	29	100	3	10	54	2	5
1989	1301	621	48	442	34	71	225	17	36	99	8	16	31	2	5
1990	1567	813	52	465	30	57	211	13	26	72	5	9	17	1	2
1991	2350	1265	54	749	32	59	359	15	28	78	3	6	0	0	0
1992	776	339	44	187	24	55	55	7	16	12	2	4	0	0	0
1994	2664	1312	49	1075	40	82	736	28	56	351	13	27	20	1	2
1995	1770	1122	63	881	50	79	633	36	56	289	16	26	77	4	7
1996	2493	1709	69	1376	55	81	958	38	56	432	17	25	11	0	1
Total	**20440**	**8967**	**44**	**6353**	**31**	**71**	**3472**	**17**	**39**	**1433**	**7**	**16**	**210**	**1**	**2**

increase in maximum pulse length (for asynchronous pulses) from 0.4s to 0.7-1.0s at full power (depending on beam profile). However, the Test Bed conditioning statistics show a further ~1000s of integrated beam-on time were sometimes necessary to obtain reliable operation at 80kV. In the period June-September 1996, it was not possible to establish reliable operation on two of the high-current tetrodes at voltages >70kV within the limited time available for asynchronous conditioning during the experimental programme. Furthermore, a persistent problem with one of the 80kV HV power supplies resulted in some shortfall in power from the high-current injector box during the first part of the campaign.

During the October 1996 shutdown, the two unreliable high-current PINIs were replaced with refurbished spares which had been fully pre-conditioned to 80kV in deuterium on the Test-bed, and the HV power supply fault was rectified during the subsequent re-start phase. Initial re-commissioning in November was performed using the conventional gas supply, but changeover to the Piglet system occurred prior to resumption of the experimental programme. For reasons of Piglet commissioning, problems of operating the high-current PINIs on the 'grid-gas' feed again limited the power available reliably to about 17.5MW until the end of the year. Power >19.5MW was available following restoration of the conventional gas supply on the high-current injector, (i.e. about 90% of the theoretical maximum for the present PINI configuration operating in deuterium).For experiments which did not require full NB power, extensive use was made of the Neutral Beam Local Manager (NBLM) which ensures delivery of the required power by energising reserve beam-sources in case of HV breakdowns or terminating power supply trips. This technique has been extensively used especially in divertor characterisation experiments which required reproducible pulses typically at the 12MW level.

The flexibility of NB injection over a very wide range of plasma configurations and conditions was enhanced by the extended Duct Protection (against power from re-ionisation losses) and in-vessel Shinethrough Protection (described in the 1995 Progress Report). Injection at low currents ≥1MA is now safe for all standard configurations and beam gases, and the minimum safe plasma density for injection is lower than in the previous campaign. This enhanced flexibility is illustrated in Fig.23 in the parameter space of plasma density and current for high-power injection (>10MW). This has been a major factor in the accessibility and successful development during 1996 of the regime of optimised central magnetic shear, which requires high NB power to be applied in the early part of the plasma current rise at low density.

Operational Problems relating to Mechanical Failure

During operation to September, a number of filaments in the PINI plasma sources failed. The failures occurred in several ion sources on both injectors. During the October shutdown, the source which had lost most filaments (10 out of 24) on the high-current injector was removed for inspection and re-filamenting. Preliminary investigation suggests that the failures were fatigue related. In general,

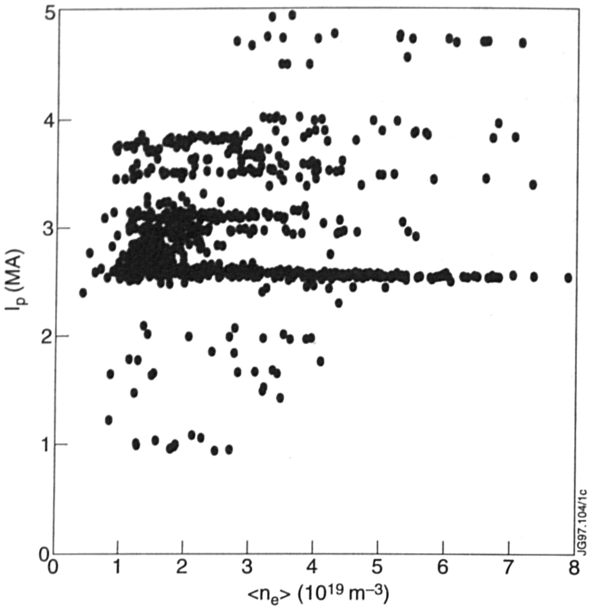

Fig.23: Distribution of high power NB pulses (>10MW) during the 1996 campaign in the parameter space of plasma density and current

the sources with the most failures had accumulated the most running time.

In early December, a small in vacuo water leak occurred in one of the four flexible inconel bellows supplying cooling water to the fast shutter doors located at the box exit on the high-voltage (Octant No.8) injector. An intervention was made to dismantle the injector system and the failure was precisely located using standard vacuum leak detection techniques. The bellows, which failed had been in service since the original commissioning of the injector in 1986, but the failure appeared not to be purely fatigue related since it occurred away from the position of maximum stress and after only 20% of the fatigue lifetime. This failure was attributed to a material defect, and all four bellows were replaced with newer stainless steel ones as already fitted to the Octant No.4 injector in the 1991/92 shutdown. The system was mechanically complete following the repair by Christmas and was used in the subsequent experimental programme.

During this December intervention, the opportunity was taken to re-filament all the high-voltage PINIs, which are now back in full operation, and it is planned to re-filament a further three high-current PINIs before DTE1.

Neutral Beam Engineering

Upgrade of third Central Support Column

The third Central Support Column is a complete unit with Central Column, Ion Dumps, Deflection Magnets and Calorimeters, which was removed from the Octant No.8 injector during the 1992/94 shutdown. Work has now begun on upgrading this Column as a spare. After the tritium experiments in DTE1, a Central Support Column with tritium contamination will take some time to repair. To increase operational availability of the whole injection system, a straight swap of one central column by another is foreseen in case of faults arising in such a column.

PINI Grids and Ion Sources

In addition to the engineering analysis work done to prove the safety of the proposed neutral beam enhancements, finite element analysis work has been carried out in-house to evaluate the membrane stresses and displacements of the PINI grids under enhanced operational scenarios. Results from these simulations will increase substantially the information available towards the understanding of beam optics during the initial non-steady state period as the grids warm up after beam initiation. A novel design for the manufacture of a mechanically more reliable ion source has been completed. A pre-production prototype will be built and tested during the first quarter of 1997.

Be-faced Mock-ups for ITER

Under an ITER Support Task Agreement, mock-ups have been produced to test the feasibility of bonding a beryllium plasma facing layer to a copper/chromium/zirconium substrate. The process yielding most promise at present comprises Cu/Cr/Zr with an electro-plated layer of copper laid onto the base material. The beryllium is faced with ion implanted copper. A silver-free braze foil is placed between the Cu/Cr/Zr and Be components and the assembly placed in a sealed container and subjected to a Hot ISO static pressure (HIPing) process. Initial shear test results have proved to be most encouraging

Cryogenic Systems

Maintenance and Plant Improvement

The divertor shutdown during early 1996 was used for the execution of an extensive maintenance and plant improvement programme. All valves and instruments were recalibrated and all statutory high pressure store vessel were tested. A series of hardware changes were introduced to enhance the cryoplant reliability and to enable switching between the two refrigerators. This switching is required for the implementation of 'back-up' scenarios for plant operation, in particular, to ensure the

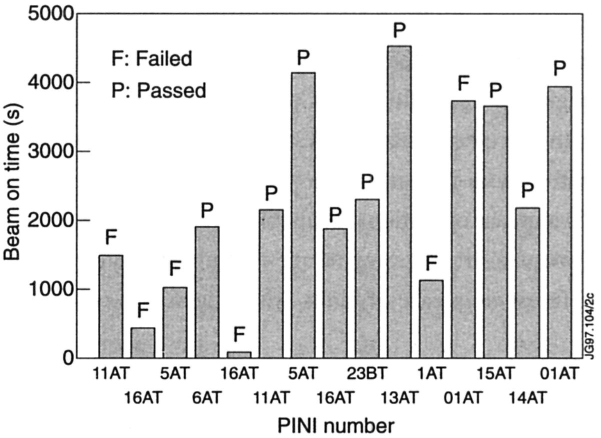

Fig.24: 1996 PINI conditioning statistics

closed loop supercritical helium supply of the pumped divertor cryopumps can be supplied from both compressors.

The supply of liquid helium to various bulk liquid helium users such as the AGHS, Pellet Centrifuge and NB Test-bed had been further improved and automated. A new cryostat for the Gas Collection System has been installed, connected to the cryoplant and commissioned.

The gaseous nitrogen loop has been extended by a new vaporiser to provide gaseous nitrogen for the torus fire suppression system. A new pressurising system has also been installed and commissioned to eliminate the possibility of tritium being released into the environment through the nitrogen vent stack in the event of an in-vessel breakage of the LN_2 system. The impurity monitoring system of the helium plant has been extended and improved.

Control System

The main plant enhancement was the installation of an upgraded control system using a new PC based supervisory system. The central elements of the control system are new Programmable Logical Controllers with a new communication software package. The PLC is connected to the local PC based supervisory system to provide a user friendly operator interface. A direct serial link allowing input/output to the UNIX based central data acquisition system (CODAS) allows all the cryogenic data to be displayed in the main Control Room and to have the basic sequences of the operation of the torus cryopumps (such as cooldown, warm-up or regeneration) initiated from the main Control Room.

An improved software program on the CODAS UNIX system (so-called 'Level 2' programme) has been implemented and commissioned to have the regeneration cycles automatically performed including the checking of potential interfaces to any other torus subsystems.

For the preparation of the DTE1 phase, extensive documentation and training of the various aspects of the cryoplant and its cryopumps have been carried out.

Neutral Beam Test-bed

PINI Conditioning

In the process of converting all PINIs to the tritium compatible configuration, 15 PINIs had to be cycled through the Test-bed in 1996. Before a beam source is installed at one of the torus beam injectors, it is run up to full performance in the Test-bed. On six occasions, PINIs had to be returned to the workshop for reassembly,

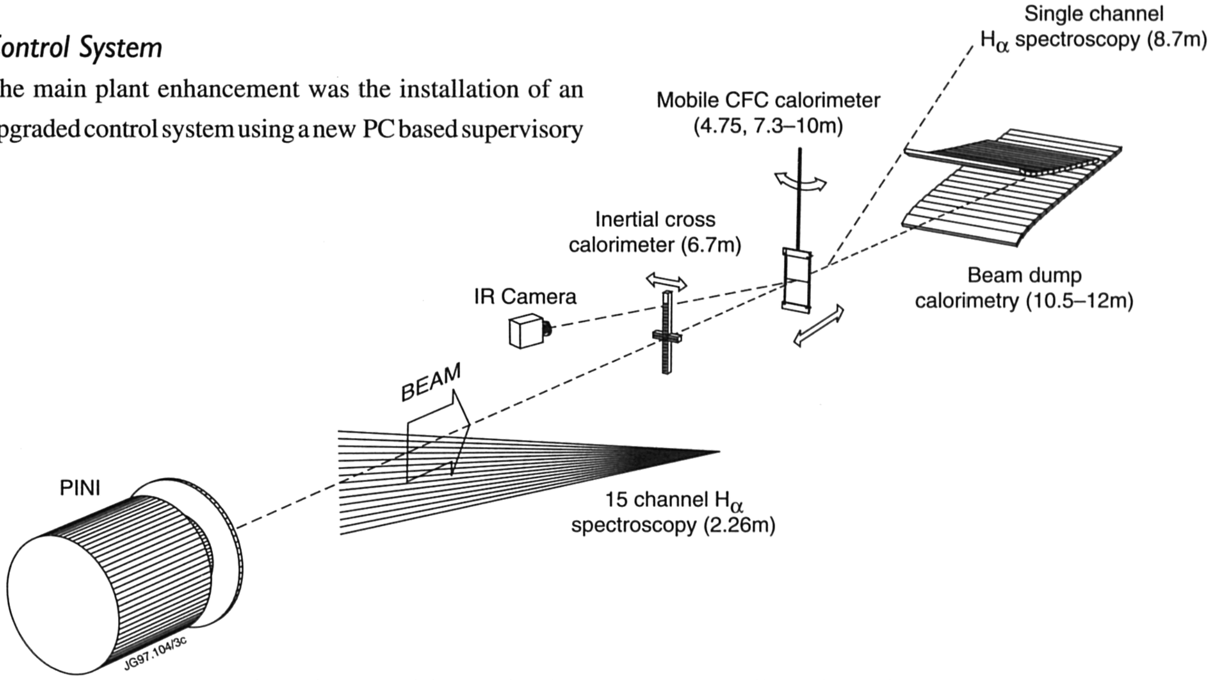

Fig.25: Schematic of the Test-bed beamline showing different beam diagnostics. Numbers in brackets denote the distance from the PINI extraction grid.

mainly to improve the beam alignment. A new diagnostic, based on thermal imaging of the beam footprint on a one directional CFC target, has shown that the two grid halves are frequently misaligned relative to one another. This leads to increased loading on the beam confining scrapers with a risk of excessive power loading. In particular, the 80kV high current PINIs are very sensitive to grid alignment due to the small gap between the grids.

Another observation is that the time required to get a PINI working reliably has become longer - in some cases in excess of 4000 beam seconds. This effect is not fully understood, but it is feared that this is an ageing effect of the highly stressed grids. It has been observed that the grid surface gets damaged probably by implantation of hydrogen which forms bubbles in a front layer of a few micron thickness. The 1996 conditioning statistics are summarised in Fig.24.

Beam Diagnostics

Previous work has raised the possibility that the filter plasma source of the PINI's has a larger plasma non-uniformity than previously thought. The NB Test-bed now has a unique set of diagnostics (Fig.25) to investigate such phenomena. A new beam diagnostic (multi-channel H_α spectroscopy) has been recently commissioned (Fig.25). The light emission from the beam interaction with the residual hydrogen gas is observed close to the exit of the second stage neutraliser (2.26m from the extraction electrodes). Emitted light is focussed on a vertical array of optical fibres, transported using 15 fibre links (50m long), and focused again at the entrance slit of a 0.5m monochromator.The monochromator is equipped with a CCD array detector (600 x 400 pixels) which enables simultaneous acquisition of 15 spectra (Fig.26(a)). The lens-fibre arrangement determines the observation region of the diagnostic: 15 circular areas of 10mm diameter with 32mm displacement along the vertical beam axis. The angle of observation is around 46° with respect to the beam centre line allowing Doppler Shifted Spectroscopy. Each of the light emission images is converted into a spectrum (Fig.26(b)), which is used to determine various beam parameters. The high signal intensity combined with high signal-to-noise ratio, high resolution and well defined geometry allows:

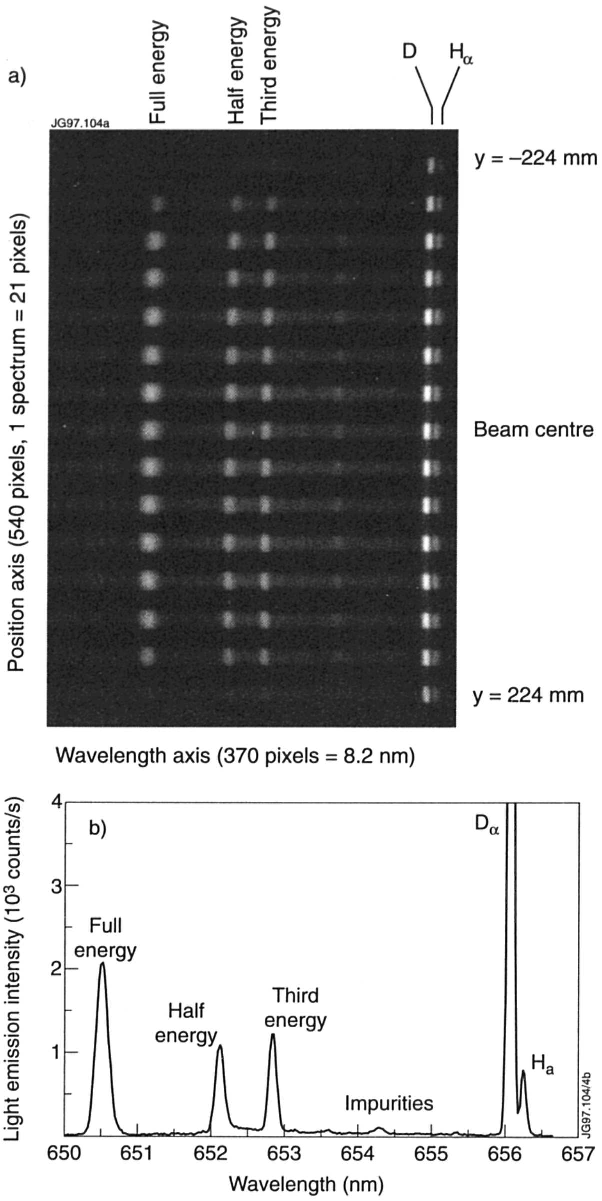

Fig.26: (a) Beam emission image (Balmer-α region) of a 142kV, 30A deuterium beam at perveance match; (b) Beam emission spectrum of a 142kV, 30A deuterium beam at perveance match. The spectrum corresponds to beam centre and was derived from the image shown in (a).

- Spatially resolved measurement of extracted ion species composition from the areas of Doppler shifted Balmer lines;
- Spatially resolved measurement of the beam divergence from the width of Doppler shifted Balmer lines;
- Measurement of the beam steering from vertical beam profiles;
- Time resolved measurement of species composition and beam divergence at fixed position (single fibre);
- Measurement of hydrogen isotope exchange in beamline components from the ratio of unshifted D_α and H_α lines (Fig.26(b)).

The new multi-channel H_α spectroscopy has confirmed the suspicion, that the filter plasma source used in the PINI's has a larger plasma non-uniformity than previously

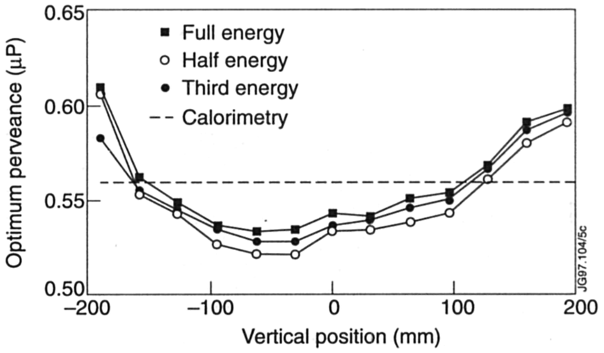

Fig.27: Optimum perveance of a PINI as a function of vertical position at the extraction grid. This defines the extracted current that gives the narrowest beam overall, or as in this graph a minimum in the beamlet divergence. The graph shows that the smallest beamlet divergence is in the centre at a lower perveance (ie. at a lower integral current) than at the fringes.

assumed. During the development of the plasma source, the uniformity was measured with Langmuir probes inserted into the source [1]. These measurements were undertaken without beam extraction and showed the non-uniformity to be less than 10% overall. With the new H_α diagnostic, a ±8% variation was measured in the optimum perveance along the vertical axis of the extracted beam (Fig.27). It was also observed that the fraction of full energy ions had a maximum in the centre. The fraction of third energy ions (from the breakup of D_3^+) had a minimum in the beam centre (Fig.28). The diagnostic has 15 lines of sight in the vertical plane and, therefore it averages over the width of the beam. It can be assumed that a similar distribution exists in the horizontal direction. The non-uniformity is probably caused by the magnet filter field in the plasma source, a configuration which was designed to increase the full energy component of the beam [1]. By modifying the volume of the plasma source and the strength and location of the filter field it should be possible to reduce the source non-uniformity further and match the species composition to the requirements for injection. This would result in a higher beam transmission into the plasma and a reduced loading of the beam confining scrapers.

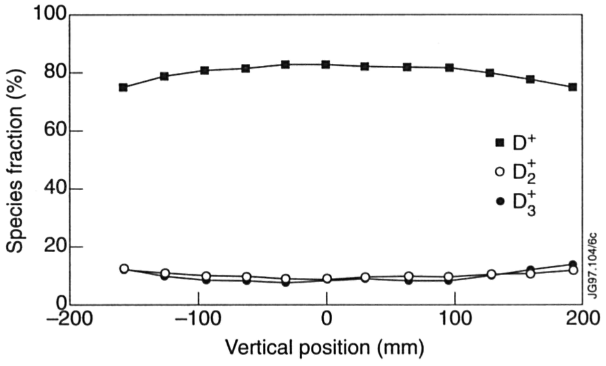

Fig.28: Species fraction from a PINI as a function of vertical position averaged over the beam width. Due to the averaging, the actual D^+ concentration in the centre is close to 90%.

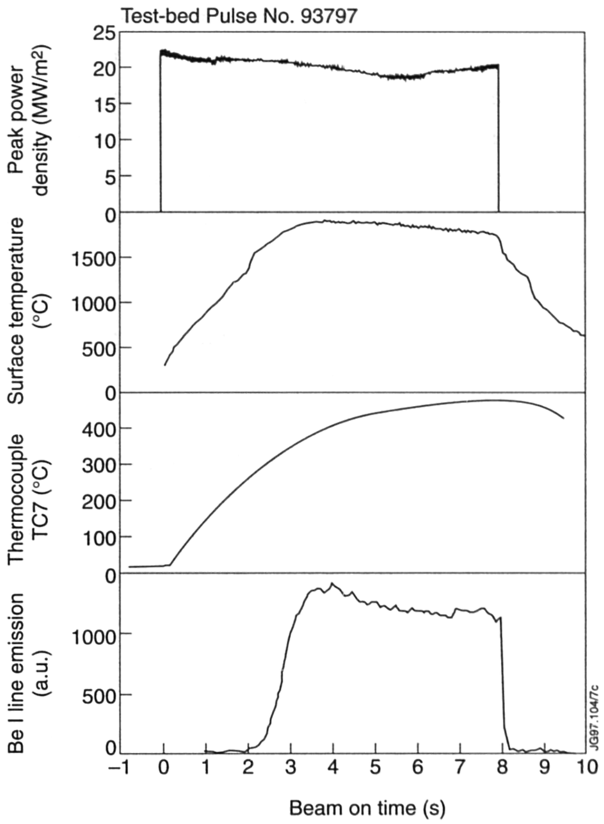

Fig.29: Characteristic data of a beryllium monoblock during exposure to $20MWm^{-2}$. The surface goes into melting after 2s and the cooldown is delayed by 0.6s due to recondensation. Surface temperature and Be vapour pressure come into equilibrium 2s after the onset of melting, well before the thermocouple 10mm below the surface comes into equilibrium.

Another benefit from the new diagnostic is that it gives a direct measure of the beam steering.The beam is extracted from 236 holes in two grid halves. The grid halves are inclined against other and the drillings in one of the accelerating grids slightly offset providing a steering effect to a common focal point. The value of the actual offset and correlation between offset and steering angle are important design parameters. In the vertical H_α profile, the individual rows of beamlets are visible. This allows a direct measure of the steering angle of the outer beamlets in the vertical plane. Power loading on the beam defining scrapers and transmission are strongly influenced by the beam steering and firm knowledge of the beam steering is essential for any upgrade of the beam power which would drive the power loading even closer to the limits.

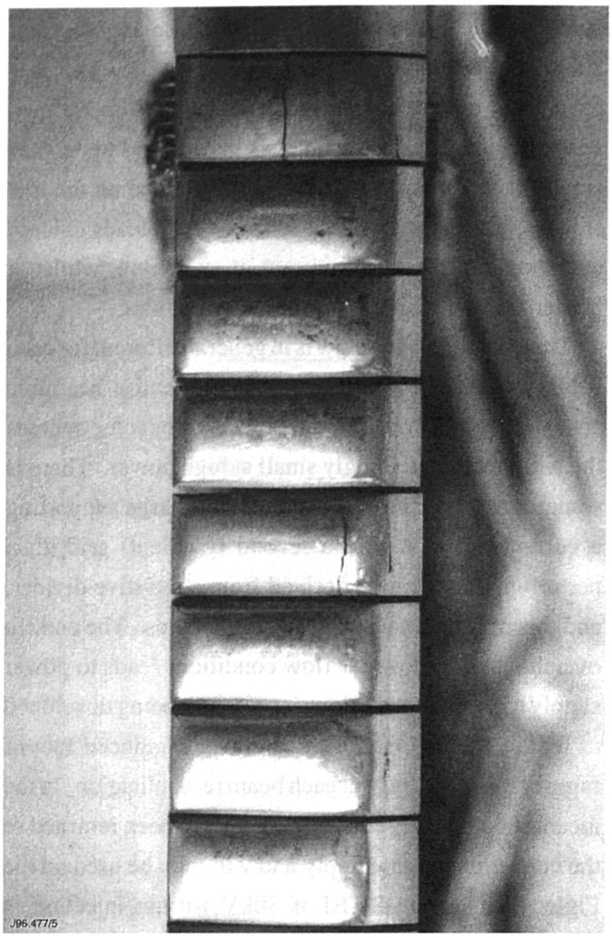

Fig.30: Surface of the beryllium after the test. The melted area is characterised by the meniscus. There are cracks over the full height of two blocks. In the blocks with cracks, the right edge is slightly displaced. This indicates a deep crack.

Power Loading Tests on Actively Cooled Beryllium Armour

As a spin-off of the earlier work on a 33 cooled divertor, a very reliable brazing between beryllium armour and copper heat sink was developed. This has led to actively cooled components with 10mm thick beryllium armour. On exposure to power densities of 20MWm^{-2} the surface of the beryllium is driven into melting two seconds after the start of the power loading. One and a half seconds after the onset of melting the surface temperature and the beryllium vapour pressure came into equilibrium (Fig.29). The surface of the vertically installed beryllium armour forms a smooth meniscus and does not show evidence of missing material. This is demonstrated in Fig.30, which shows a photograph of the surface of beryllium monoblocks exposed to surface melting for 65s in 25 pulses. Some cracks can be observed which are assumed to penetrate through the material.

The amount of deuterium implanted into the beryllium surface by charging the actively cooled test section with a deuterium fluence of 2x10^{19}atoms/cm^2 has also been measured. The energy of the full energy beam component was 60keV. The amount of implanted deuterium is measured as 1.5x10^{18} atoms/cm^2 with NRA, which is sensitive within a depth of 5mm. The measurement also shows, that the implanted deuterium is peaked within this range. The implanted deuterium is quantitatively removed when the surface is driven above liquidus temperature. This has important consequences for the use of beryllium components in devices such as ITER.

Commissioning of Systems for DTE1

The 1995 JET Progress Report described in detail the systems under development for tritium operation of the NB injectors. In particular, the active gas introduction modules (known as 'Piglets'). Their function is to receive tritium and deuterium gas from the central Active Gas Handling System (AGHS) in Building J25, via a distribution box (called the 'Pig'), located in the Central Basement of the Torus Hall, and to supply each pair of NB sources (which share a common acceleration voltage and deflection magnet) with the selected gas at accurately constant pressure and flow. Each of the two neutral injector boxes is served by a separate Piglet module. During early-1996, the mechanical installation of the Piglets was completed, together with the associated systems of control, instrumentation and interlocks. Preliminary calibration and testing of each Piglet assembly was carried out prior to installation of the completed modules, but precise setting of flow rates and accurate determination of internal pipework volumes, necessary for proper accounting of eventual tritium movements, had to be performed in situ. For these measurements, a local gas bottle source of deuterium was initially installed in place of the supply from the Pig.

No dedicated commissioning time for the Piglets was scheduled prior to the October shutdown, but all end-to-end testing and *in situ* calibrations nevertheless had been completed in parallel with operations by the time the Pig transfer lines were connected in October. Fully integrated NB operation together with the Piglets was established during re-start following the October shutdown, without adding significantly to the duration of that re-start phase. Figure 31 shows time traces for a normal beam pulse with gas supplied from the Piglet. Routine operation of both beamlines with the Piglets continued until the end of 1996, although at 15%-20% reduced power on the high-

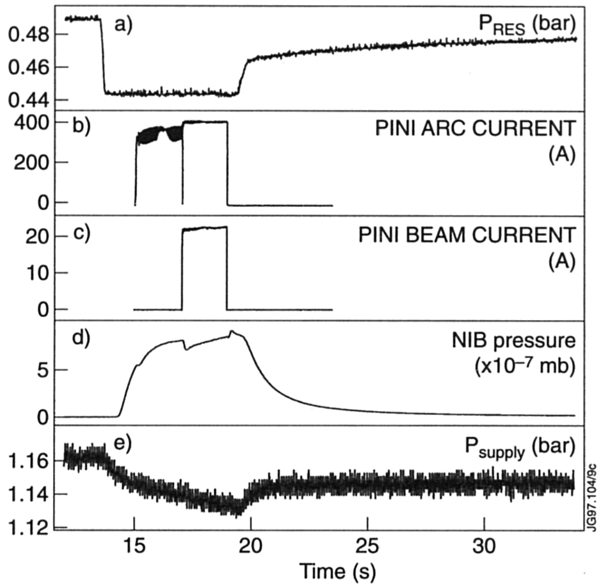

Fig.31: Evolution of (a) Piglet manifold pressure, showing the degree of stability and hence delivered flowrate to the PINI; (b) arc current; (c) extracted beam current; (d) injector box pressure, illustrating the rise and decay times of the gas flow at the PINI; and (e) Pig supply pressure during a pulse.

current 80kV tetrode beam sources (see below). At that stage, the source of deuterium gas in the AGHS plant was a temporary bottled supply to avoid the possibility of potential slight tritium contamination of the internal surfaces of the Piglet before DTE1 (since the AGHS had already operated extensively with active process gas).

All NB operation with active gas will be carried out according to formally approved Tritium Plant Operating Instructions (TPOI). All of the TPOI documents covering Piglet operation have been prepared and reviewed, and it has been possible to test all operations covered by these procedures, except specific actions which require the gas to be supplied from a hot uranium bed within the AGHS plant. These remaining operations will be tested, using deuterium, at the start of the DTE1 operational phase.

In addition to technical commissioning of the Piglet gas supply, the need for some optimisation of beam source operation was foreseen. Instead of using separate gas feeds for the plasma source and neutraliser cell, the Piglet gas is introduced just downstream of the earth grid thus eliminating the frangible glass insulating break, which supplies gas to the plasma source at high voltage. During the development of the ground potential 'grid gas' feed in 1991, prior to the Preliminary Tritium Experiment [2], it was mainly tested on the 160kV triode PINI without problems, and routine operation with Piglet gas on the Octant No.8 injector box equipped with this type of PINI has been quickly and reliably established at full performance. However, operation of the high-current 80kV tetrode PINIs on the Octant No.4 Injector has proven to be unexpectedly difficult. The operational window for the gas flow rate has been found to be very small for the high-current tetrodes, bounded on the low side by gas starvation of the source, which leads to large overshoots in the beam current at switch-on, whilst at higher flows it is limited by HV breakdowns.

The operational window is in general different for each PINI, making the optimisation of the entire beamline costly in terms of operational time, and for some sources the window is vanishingly small at high power. There is sometimes evidence of a sustained discharge supporting a current of ~10A to the second (gradient) grid, thus perturbing its potential derived from a resistive divider, and this may be a cause of HV breakdowns. The current overshoot under low gas flow conditions leads to power supply trips, and a technique is presently being developed to reduce this overshoot by applying a reduced rate of ramp of the arc voltage at each beam re-application. In the meantime, the high-current injector has been returned to the conventional gas supply and will only be used on the Piglet feed during DTE1 if 80kV tritium injection is required (e.g. for additional plasma tritium fuelling) on a small number of selected PINIs. This is a minor change of plan, as it has, however, always been expected that all tritium injection requirements will be met by the 160kV injector alone during DTE1.

Beamline Safety Systems

Several beamline safety protection systems have been upgraded to meet the requirements of tritium operation. In some cases, the need for upgrading was a direct consequence of the hazard mitigation requirements set out in the Safety Case Documentation for Tritium Operation (PCSR) [3]. The NB Direct Plant Interlock System (DPIS) is a PLC based, 24-hour safety protection system which was originally designed to prevent the supply of cryogenic fluids unless the appropriate cooling water flow requirements were satisfied and to raise alarms at the control room incident desk if conditions developed which might pose a freeze-up risk. Extra state logic and plant connections have now been incorporated which provide new functionality in the case of a large pressure rise in the NB injector box (>5MB), which could be attributable to a substantial internal water leak. The new functionality causes the NB cooling water plant to enter

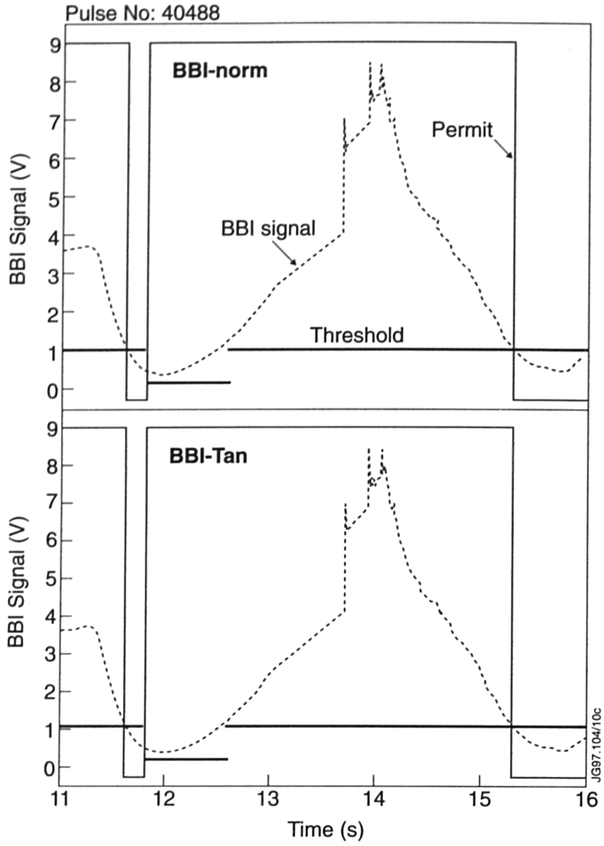

Fig.32: Traces of BBI intensity and change of state of derived NB permits for Normal Bank and Tangential Bank PINIs during a commissioning pulse.

an automatic leak detect mode and, if necessary, to remain isolated from the main cooling loop prevent the amount of water released into the NB box exceeding a safe limit.

There is a second DPIS system which provides safety protection for the in-vessel water circuits and the pumped divertor cryopump. Similar functionality has been incorporated into that system. Further hard-wired protection has been implemented, which acts in the case of large pressure rise in the vacuum systems (>200MB), attributable to large air or cryogenic leaks, to maintain an under pressure by automatically opening the turbomolecular pump bypass valves.

All these safety protection systems have been subjected to rigorous approved written commissioning procedures. Other safety interlock systems, whilst not formally credited in the PCSR, act in normal operation to avoid the risk of damage (e.g. to a water cooled component). These safety systems, which include the Fast Beam Interlock System (FBIS) and Central Interlock and Safety System (CISS) have also been modified, where required, and are subject to a similar standard of commissioning as the PCSR-credited systems. The relevant approved commissioning procedures have been repeated after interventions and during re-start periods following each planned modification. In this way, an incremental and traceable record of the commissioning tests on each protection system has been maintained. The modifications to CISS and FBIS were mainly associated with incorporation of the Piglet gas supply. The FBIS network has been expanded further to include an independent interlock to ensure minimum plasma density for beam injection, based on the Bremsstrahlung emission from the plasma.

The Bremsstrahlung Beam Interlock (BBI) was initially commissioned using a single telescope, fibre optic and detector. The other main system which guarantees that the NB power is applied above set plasma densities is the microprocessor based Plant Enable Windows System (PEWS). The BBI has the same functionality as the central PEWS, as shown in Fig.32. There are separate density thresholds for tangentially and normally aligned PINIs, each with an additional low-level density threshold subject to a 0.5s timeout at the start of beam injection. The motivation for implementing the BBI, which is entirely hardwired and of simple electronic design, was to provide a direct interlock path as an alternative to the complex processing chain of deriving the density in PEWS, which includes the KG1 interferometer signal and PEWS microprocessor. However, to make the BBI active-phase compatible, a second 'blind' compensation fibre and heated fibre jacket with associated controls have been prepared for final installation in the pre-DTE1 shutdown. The heated jacket maintains the fibres at 300°C in order to anneal radiation damage, whereas the 'blind' fibre is used to remove the neutron induced luminescence. The 'blind' and live fibre signals are detected by matched photo-diode detectors in a differential configuration. Following commissioning and re-calibration in the new configuration, it is intended to enable the BBI before DTE1.

An active-phase absolute pressure manometer system has been developed for use on the NB vacuum systems. The electronics normally incorporated in the head have been replaced by a passive resonant network, which includes the pressure-sensitive head capicitance. Following an excitation pulse, the resonant frequency is analysed by pulse counting techniques in the specially developed remote signal processing network [4] whose output is an analogue voltage proportional to the measured pressure. Data obtained using the prototype electronics

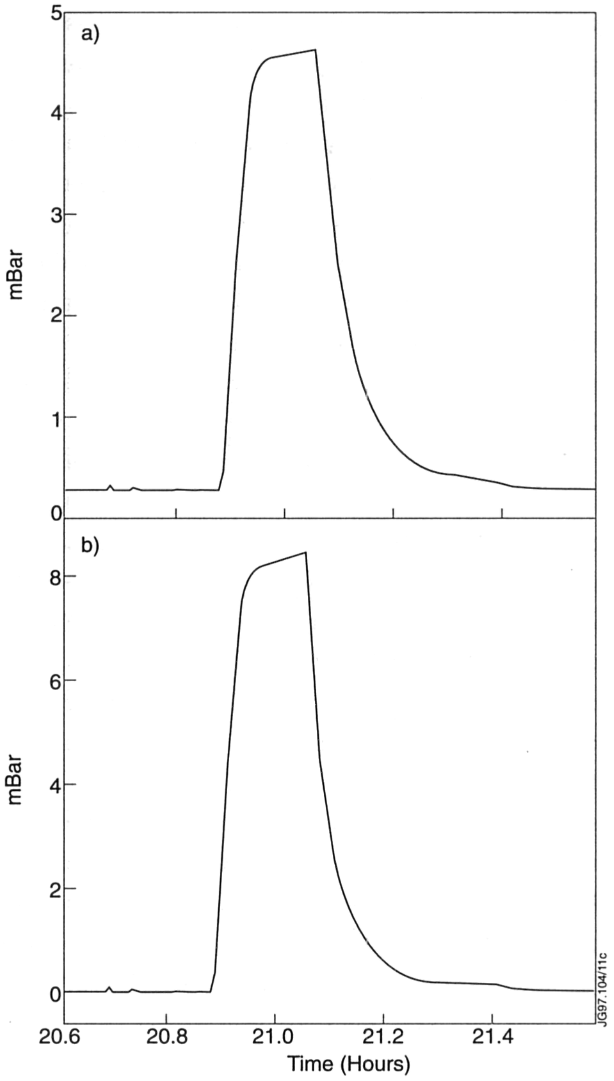

Fig.33: Pressure traces obtained from (a) the active-phase compatible absolute pressure manometer and (b) a Pirani gauge during a NB cryopump regeneration.

during pumpdown and cryo-regenerations have demonstrated the value of this system for obtaining absolute pressure measurements in the pressure range 10^{-3}mbar to several mbar, where a Pirani gauge would otherwise have to be used. An example of such data is shown in Fig.33. Multiple heads covering different pressures have been mounted on the injector boxes and production versions of the electronics will soon be installed.

Upgraded Filament Status Detection circuitry has been extensively tested following installation of current-limiting protection resistors for the 24 status-sensing connections on the PINI and improved jumper cables at the SF_6 tower interface, together with surge protectors on the monitoring electronics located in the filament power supply. These modifications have successfully eliminated damage to the filament monitoring system observed in previous campaigns and attributed to large voltage transients during HV breakdowns. The alarm and protection actions in the case of filament fault detection with the modified system will be fully re-instated before DTE1.

References

[1] R S Hemsworth and A J T Holmes, JET Report, JET-P(90)52, (1990).

[2] JET Joint Undertaking Progress Report - 1991, EUR-14434-EN, vol 1, pp 83-84.

[3] 'Safety Report for the Deuterium-Tritium Operation of JET (PCSR)', Rev 0, March 1996, JET Joint Undertaking, Abingdon, Oxon, OX14 3EA (1996)

[4] A Browne et al, Contrib, paper 19th Symposium on Fusion Technology (SOFT), Lisbon, Portugal (1996).

RF Heating Systems

JET is equipped with two different high power radio frequency systems: the Ion Cyclotron Resonance Frequency (ICRF) heating and the Lower Hybrid Current Drive (LHCD) systems. In addition, a low power system exciting Toroidal Alfven Eigen Modes (TAEE) has been routinely operated. These have very distinctive roles.

The ICRF heating system is used for high power central heating of the JET plasma, with the capability of producing Fast Wave Current Drive (FWCD) with the A2 antenna. The localisation depends mainly on the magnetic field and is insensitive to parameters such as density and temperature. Wide band operation between 23-57MHz allows variation in both the choice of minority ion species heated and the local position of the heating. So far, with the previous A1 antennae, up to 3.5MW on one antenna and 22.7MW total coupled power (in L-mode) for 2s had been achieved. Preliminary experiments on Fast Wave Ion Current Drive with the A1 drive have also been successful showing that the plasma current gradients near the q=1 surface were modified by changing the phase between straps of the antennae. New ICRF antennae optimised to the geometry of the divertor plasmas have since been installed in JET in 1993. Their location in the torus have been chosen to give four arrays of two adjacent antenna. Each array has four RF radiating conductors, or straps, which provide an enhanced radiated spectrum. Variation in the relative phase of the RF currents in the straps allows this spectrum to be adjusted for both heating and current drive experiment. In addition, the control

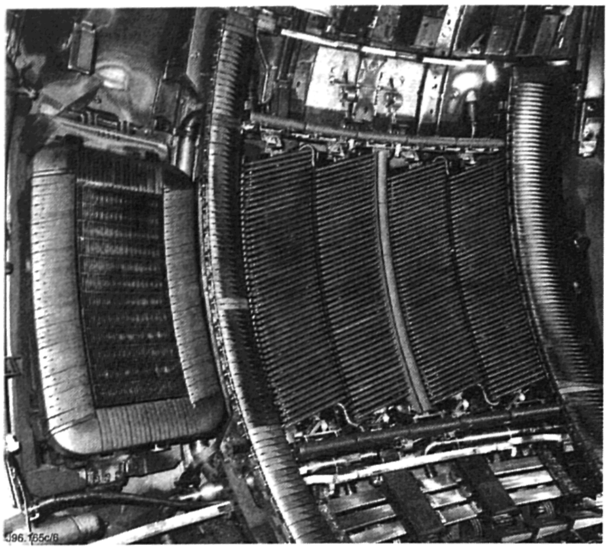

Fig.34: The LHCD launcher together with one module of the ICRF antenna

electronics has been completely rebuilt in order to allow operation with four straps closely coupled and to improve the reliability of the ICRF plant by reducing the crosstalk between modules. 1994 operations were made difficult by the fact that both the control electronics and the antennae were new systems and required a large amount of commissioning time. Several problems were identified and remedial actions were either taken or are in preparation. In spite of these early difficulties, a record power of 16.5MW was launched in a divertor (H-mode) plasma, compared to 12MW in X-point plasmas in the 1991/92 campaign. Combined heating powers of 32MW including 15MW of ICRF power was launched for several seconds into radiative divertor plasmas.

The LHCD system operates at 3.7GHz and is capable of driving a substantial fraction of the plasma current. This is achieved by launching an RF wave predominantly in one toroidal direction. This wave accelerates the high energy electrons in the plasma and so drives a current. This may be used to stabilise sawtooth oscillations, thereby increasing central electron temperatures. The system can modify the JET plasma current profile and is the main tool for stabilising high beta poloidal plasmas with a large proportion of bootstrap current, the so-called advanced tokamak scenarios. It has also been used to optimise JET performance. With a prototype launcher, L0, up to 2.3MW of LHCD was coupled to the plasma. This prototype provided engineering, operational and physics experience with LHCD on JET in a variety of plasma configurations. An upgraded launcher, L1, was installed in JET in 1993 and has been in full operation for the 1994-95 campaign. Power of 7.3MW has been coupled to plasmas and full current drive up to 3MA has been achieved. Up to 6MW of LHCD power have been launched for 13s for profile control experiments. A photograph of the LHCD launcher together with one module of the A2 ICRF antennae is shown in Fig.34.

Alfven Eigenmodes (AE) are discrete global modes of Alfven waves in confined toroidal plasmas. In particular, AE appear in the frequency gaps for shear Alfven waves corresponding to toroidicity, ellipticity or triangularity induced harmonic coupling (whence the denominations TAE, EAE, ...). Modes based on finite β coupling between Alfven and sound waves also exist in the Alfven frequency range ($2\pi f \sim v_A/2qR$) with frequency ranging from 20kHz to 500kHz for the different TAE and EAE. AE have been predicted to be of fundamental importance in tokamak reactor relevant conditions, since they can be destabilised by fast particles (such as fusion produced alphas) and, in turn, may expel fast particles from the plasma core via resonant wave-particle interaction. The saddle coil antennae in JET, in conjunction with the ICRF and NBI heating methods, offer the unique possibility of exploring in a systematic way the importance of these modes, which can be excited in a controlled way by a dedicated RF system, the TAEE system. This system has been successfully put into operation within the framework of a Task Agreement with CRPP-Lausanne, Switzerland. The excitation of TAE modes has been assessed and a large data base of AE activity and damping rates has been collected and are being analysed. In addition, new modes including kinetic Alfven Eigenmodes have been identified. These modes have also been excited by using two modules of the ICRF system with a "beat" frequency, i.e. a frequency difference, corresponding to the TAE frequency.

ICRF Technical Achievements

ICRF Heating

JET has a powerful and highly versatile ion cyclotron resonant heating system with the potential for delivering up to 20MW power to the plasma. The operating frequency range is 23 to 57MHz which allows fundamental heating of hydrogen, deuterium, He^3 and He^4 minority ions, and second harmonic heating with hydrogen, deuterium, tritium and He^4 ions. The power deposition can be located on-axis or off-axis depending only on the ion species and the frequency chosen with respect to the magnetic field. The fast magnetosonic wave excited by the antennae can

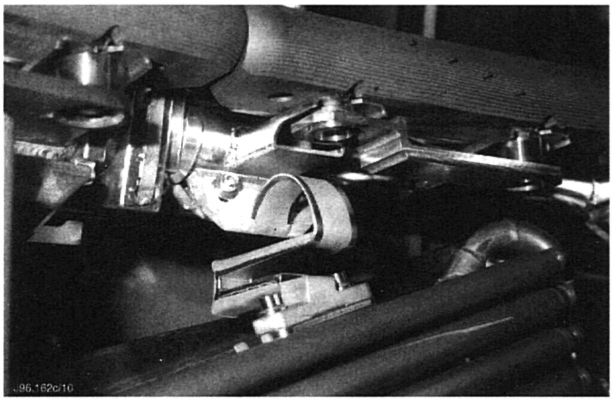

Fig.35: Resistive link connecting the antenna housing to the protection rails

access dense plasmas. Therefore, there is no difficulty in providing central heating at the high densities relevant for reactor operation. The antennae are multi-strap units in which the currents can be phased to launch waves either with no net toroidal directivity for heating purposes, or with up to 75% toroidal directivity for both ion and electron current drive applications.

Antenna Modifications

The A2 antennae were all removed from the torus during the Mark II divertor shutdown and various modifications were carried out to improve the coupling to the plasma. These modifications included fitting of additional capacitance plates to better match the crossover strap inside the antennae, and displacement of the antenna 6mm towards the plasma, reducing the gap to the poloidal limiters to 10-11mm. In addition, changes were made to facilitate operation at low $k_{//}$, including fitting of additional rails to the housing to reduce flux leakage around the back to the antenna, replacement of the top and bottom protection rails with new Inconel 625 rails, which in turn enabled the fitting of comprehensive earth straps to the protection rail/limiter system. Furthermore, new CFC limiters (separators) have been installed between two pairs of straps in each antenna to better reproduce the A1 antennae. In addition to these modifications, it was necessary to replace all of the earth straps on the antenna supports and the associated ceramic insulated connecting plates.

A new so-called "resistive link" was also designed to connect the antenna housing to the top and bottom protection rails, in line with the top and bottom of each of the two current straps. These links allow a low impedance return path for RF currents induced in the protection rails/ limiters. The design of the links needed to allow substantial RF currents, whilst maintaining significant (5mW) DC resistance in order to limit the disruption forces on the antennae. Further, the link had to accommodate up to 3mm relative movement in any direction between the antenna and the protection rail, and to support the forces appearing on the link itself due to disruption currents. The resulting component is shown in Fig.35. It is fabricated in high strength Inconel 718, with nickel plating of the edges to reduce local RF losses. The link has an S-shape to increase the length, with half of the S being a rigid box section to support the forces. The other half is flexible to accommodate the displacements, but stable against buckling under predicted inwards forces. Four of these links have been fitted to each antenna, the support brackets being welding in-situ in-vessel.

All eight modified antennae and associated transmission lines have been re-installed in the torus, and subsequently used during plasma operations. The balance in plasma coupling between inner and outer straps has been found to be improved as expected, with the imbalance reduced from about a factor of four to a factor of two at 42MHz. The coupling is a little higher for a given plasma/limiter gap. The ability to operate with the plasma close to the limiter has also improved the coupling. Operation with efficient heating has been demonstrated at low k// in 00ππ and 90° phasing: operation in 0000 (supermonopole) phasing has not been possible at high power.

The system is limited by the voltage sustainable This improves slowly with conditioning but is ~30kV as before. The causes of this voltage limit, in particular the position of the arc, are being investigated. A new RF window is being developed as part of a programme to improve the voltage capability of the system.

DTE1 Preparations

In preparation for DTE1, various modifications to the RF system have been implemented.

RF System

- Each of the 16 so-called APTL, which is the last metre or so of the transmission line connecting to the antenna window, has been isolated from the line by a ceramic gas barrier to form a secondary volume. In the event of a torus leak at the window or vacuum transmission line, the volume of gas entering the torus is restricted to the volume of the APTL. This volume can also be evacuated to enable torus operations to resume;

- The RF vacuum windows are double with an evacuated interspace. The pressure in the interspace is now monitored continuously, as well as being interlocked with the RF generator, to prevent operation in the event of failure of either ceramic; this system is class 1 IOPS;
- The remaining secondary volumes on the RF system are now all connected to standard JET manifolds for control of such volumes, enabling isolation and pumping in the event of a leak.

ICRF Heating

The ICRF heating during the 1996 campaign has benefited substantially from the modifications to the A2 antennae. These changes included matching the crossover links to the feed-lines, adding a separator to the centre of each antenna, installing flux excluders to prevent arcing, reducing the distance between the screen and limiter and improving the shape of the lower poloidal limiter to increase the connection length, and, hence, the coupling for plasmas with a strongly curved last closed flux surface. As a result, the ICRF plant has operated more reliably and has contributed strongly to both high performance and physics programmes. Up to 17MW of RF power has been coupled to a divertor plasma with a current of 2.5MA and a toroidal field of 3.1T. The RF frequency was 52MHz and the antenna was operated in the 00ππ mode. The smoothness of the RF power waveform is a consequence of a further improvement to the operation. The coupled power can be controlled by the CODAS RF local manager such that if any generator trips, the power deficit is made up by the remaining modules. Thus the power requested for a specific experiment can be more reliably achieved, often avoiding the need for repeat a pulse to obtain the desired conditions.

The ICRF heating efficiency obtained for different phasing of the antennae are shown in Fig.36 where the plasma energy content is plotted versus RF power. Prior to the modifications, the efficiency for 00ππ phasing was 50% of that for dipole, whereas now it is closer to 75%. Note also that the efficiency for monopole phasing is 50% of that for dipole; previously it was difficult to detect any central plasma heating at all with monopole.

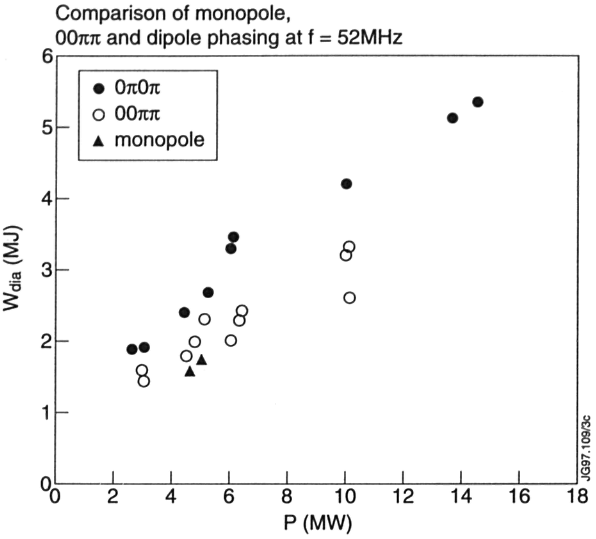

Fig.36: Comparison of stored energy between 0000,00ππ, and 0π0π phasings of the antennae

Wideband Matching

The occurrence of ELMs during ICRF heating leads to particular problems for the RF system. ELMs increase the edge density in front of the antenna and substantially increase the coupling of the antenna, from about 2Ω to 8Ω in severe cases. This occurs in a time of ~0.1ms and recovers in a further 3-5ms. This is too fast for the matching system to respond, the resulting mismatch leads to a trip and possible crowbar of the generator. Various matching schemes which are tolerant of this excursion in coupling, have been considered. Finally, a system has been adopted which uses a quarter wavelength of a 105Ω line inserted into the main 30Ω line. This 105Ω line must be positioned precisely relative to the antenna short-circuit (within a few centimetres) and is adjustable both in length and in position. It is referred to as a SLIMP (SLiding IMPedance). With such a SLIMP correctly located, the change in coupling can be compensated by a change in frequency alone, with no adjustment of the various line lengths. This frequency adjustment can be carried out within typically 1ms, not fast enough to follow the initial rise but sufficient to track the subsequent recovery. With such a system, the loss of power due to trips, and also the voltage (and thus losses) on the main line on the generator side of the SLIMP, are strongly reduced.

The mechanical design of the SLIMP is largely complete. The design allows adjustment of the start and final positions of the 30Ω line, and also adjustment of the length of the 105Ω line by sliding of the trombone. A range of 1m in start position, and 3m in length is provided. The adjustment is via electrically driven leadscrews and is slow (20mm.s^{-1}). Contracts have been placed for the supply of two such units to equip one antenna, and also for the associated modified transmission lines to enable

Table V: Lower Hybrid System on JET

Plant	
Frequency	3.7GHz
Number of klystrons	24
Power (generator)	12MW, (15MW)
Pulse duration	20s, (20s)
Duty cycle	1/30
Efficiency	42%
Phase control	10kHz
Phase accuracy	10°
Maximum VSWR	1.8
Transmission line	
Length	40m
Insertion loss	1dB
Launcher	grill type, 48 multijunctions (copper coated stainless steel)
Number of waveguides	384 (12 rows x 32 columns)
Dimensions of waveguides	height=72 mm, width= 9 mm, wall: 2 mm
Position control	hydraulic actuators
Radial movement	5 ms^{-2}, 33mms^{-1}
Radial stroke	210mm
Baking temperature	450°C
Pumping	cryopump, 85,000ℓs^{-1}
Total weight	15 tonnes
Coupling control	launcher position control plasma position control local gas puff
Wave spectrum	
Maximum	$N_{\parallel}$ = 1.4 - 2.3, adjustable
Full width	$\Delta N_{\parallel}$ = 0.46

installation at the correct distance from the antenna. It is anticipated to fit these at the end of the Gas-box divertor shutdown. High power RF tests have been carried out on the sliding contact with good results.

LHCD Overview

Lower Hybrid Current Drive (LHCD) has been used during the 1996 experimental campaign mainly for current profile control in shear optimisation scenarios. Reliable plasma formation with a fast plasma current ramp rate and control of the internal inductance have been supported by applying LHCD during the current ramp-up phase. Formation of an internal transport barrier and improved central thermal electron confinement have been obtained with LHCD alone. LHCD modelling and transport code analysis have been further developed to describe complete shear optimisation scenarios with all heating and current drive systems on JET. Reliability and flexibility of LHCD operation have been improved by various upgrades of the plant and the control systems. Active coupling control has been expanded to plasma position and shape control on the LH reflection coefficient. Gas puffing through a dedicated feed near the LHCD launcher allowed good coupling to be achieved with larger plasma-launcher distance and the launcher being kept retracted behind protection limiters.

LHCD Generator

The Lower Hybrid Current Drive (LHCD) generator consists of 24 klystrons operating at up to 500kW each with a fixed frequency of 3.7GHz. The main parameters of the LHCD system are given in Table V. The full plant was installed in 1991 and has been operating with good reliability since then. During 1996, a number of improvements were made to further increase hardware reliability and enhance the system control.

Real time software has been implemented to control the output power of a klystron on a pre-settable maximum electric field in the multijunction launcher. This reduces the number of arcs occurring in the multijunctions. A local system manager has also been commissioned. It can be used to control the total output power of the generator, so that if one klystron trips the power on the others is increased to maintain constant generator output. It also provides the interface with the Real Time Central Controller that can be used for feedback control of plasma parameters such as the loop voltage. In addition, the interface to the Plasma Position Central Controller, PPCC, is routed via the LH Local Manager. PPCC can be used for feedback control of the LH Launcher reflection coefficient by adjusting the plasma position.

CODAS Level 1 control has been implemented for the LH system. Complete sets of all control parameters and waveforms are stored for each LH pulse and can be reloaded. This reduces the number of parameters the operator has to set and provides a clearer indication of the plant settings.

Coupling Control

Active coupling control in LHCD applications has been obtained on JET in the past by controlling the launcher position in real-time with a hydraulic system. Additional developments aimed at greater flexibility with respect to different plasma configurations and operation at large plasma-launcher distance. The existing LHCD launcher position control has been upgraded. A new plasma position and shape control system on the LH reflection coefficient

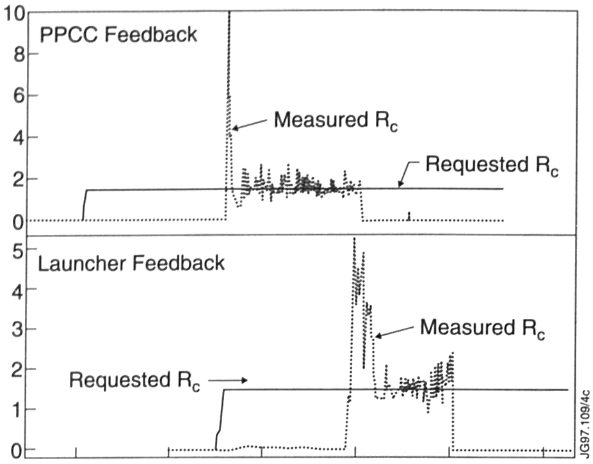

Fig.37: Feedback control of the reflection coefficient R_c with launcher and plasma position control.

has been implemented. Long distance coupling has been improved by a dedicated gas puff system with distributed feeding near the LHCD launcher.

The LHCD launcher position control has been upgraded to a new PC-based digital control system to improve reliability and flexibility. This replaces the previous analogue control system and has been implemented without any modification of the hydraulic system. The new system has allowed the rapid implementation of new operating sequences and alarms for a safer operation of the LH launcher position control. The feedback control system of the launcher position on the reflection coefficient R_c has been also converted to a digital system.The improvement of the feedback loop software and a linearisation of the R_c response function resulted in a more robust R_c feedback (Fig.37).

A new plasma position and shape control system with feedback on the LH reflection coefficient R_c has been implemented. The radial plasma position is controlled on a mean value of R_c averaged over the whole launcher cross section. The vertical plasma position can be controlled to symmetrize the reflection coefficients from upper and lower waveguide rows. The new control loops make use of the LH local system manager and the Real Time Control system. With the new plasma position control good coupling has been achieved, with the LHCD launcher kept retracted behind the poloidal protection limiters. The response of both the launcher position and the plasma position control systems are compared in Fig.37. In both cases, a reflection coefficient of $R_c = 3\%$ was requested. In the discharge with plasma position feedback control activated, the LHCD launcher was kept at a constant position of 10mm behind the poloidal limiters.

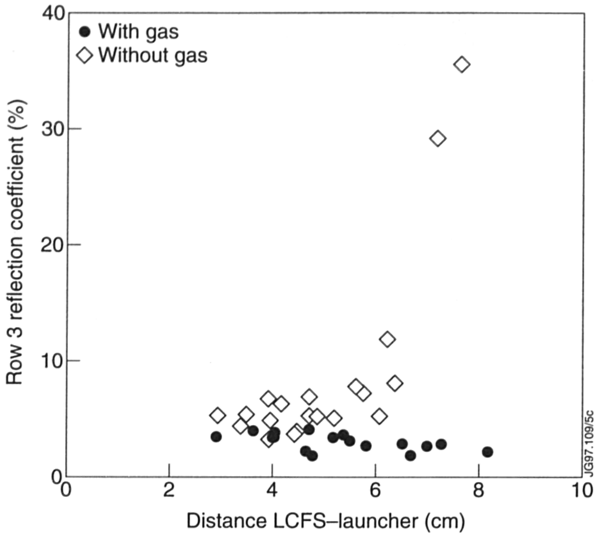

Fig.38: LH reflection coefficient versus plasma-launcher distance

Long distance coupling of LH waves to the plasma at low reflection has been achieved by injecting gas through a feeding system close the LH launcher. This increases the operational range of the LH system, since the power can be coupled also when the plasma configuration is not well matched to the shape of the launcher and the launcher is located behind the poloidal limiters (Fig.38).

The dedicated LH gas feed is located at the outer wall of the vacuum vessel, 1.3m from the launcher on the electron drift side. A pipe has been installed with holes equally spaced along its poloidal extent. Coupling experiments with the near gas feed were carried out on X-point plasmas with gas flow ranging from 1×10^{21}el/s to 9×10^{21}el/s. The minimum gas flow required to see an improvement in coupling is 2.5×10^{21}el/s. With this flow, an average reflection coefficient of 4% has been obtained at a plasma launcher distance of 5cm, in conditions where ≤3cm is required to maintain the same reflection coefficient without the gas feed. With a large gas flow (9×10^{21}el/s), the average reflection coefficient was maintained at 5% while the launcher was located 1cm behind the poloidal limiters and the plasma was moved 7cm away from the limiters (Fig.39). The effect of the near gas feed was also confirmed by comparison with a discharge supplied with gas from another valve located far away from the launcher. In this discharge the coupling could not be maintained when the plasma was moved away (Fig.39).

The fast electron signals, measured by both hard X-ray and ECE diagnostics, were not affected by a low gas flow sufficient to improve coupling. However, these decreased with increasing gas flow. In a discharge with large gas

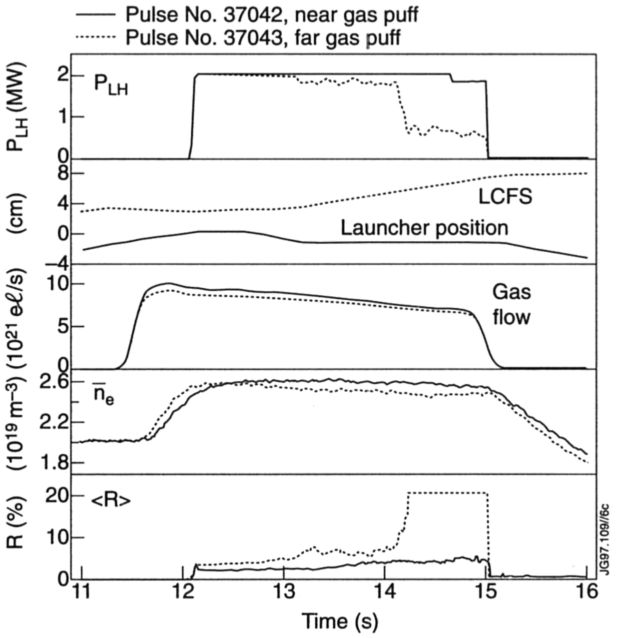

Fig.39: LH coupling with gas puffing near and far to the launcher

flow (5x10^{21}el/s), the fast electron signals decreased by ~30% and the degradation in current drive efficiency was estimated to be of the ~20%. There seemed to be a correlation between the loss of fast electrons and the improvement in coupling, suggesting that the power which was not absorbed in the main plasma was coupled to the scrape-off layer. Direct ionisation of the gas by a fraction of the LH power is a possible mechanism to explain the improvement in coupling.

In experiments in mid-1996, coupling on the middle and the bottom row of the launcher improved significantly when the near gas feed was used. The effect was less pronounced on the top row and was attributed to the fact that there were no holes in the upper part of the gas pipe. In the October shutdown, extra holes were added in the upper part of the pipe, to allow gas to be injected near the top of the launcher. Experiments with the gas feed after October indicated that the coupling was more poloidally uniform than before the modification of the gas pipe. Coupling across the whole launcher can now be actively controlled and improved with the dedicated gas feed.

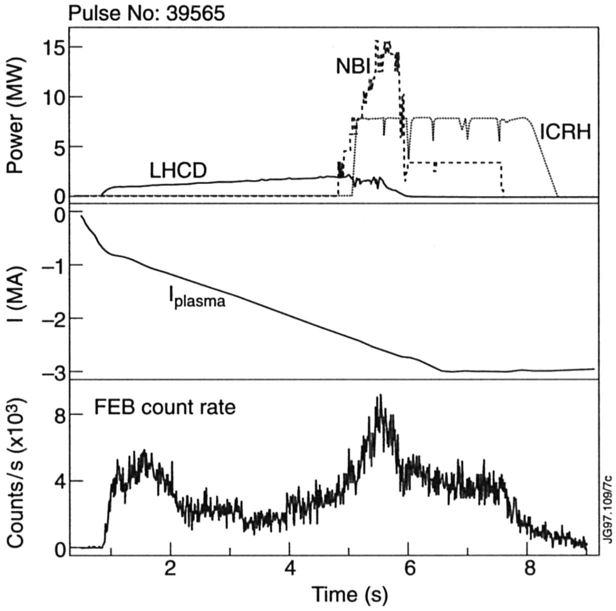

Fig.40: Injected power waveforms, plasma current and the count rate of the central FEB channel.

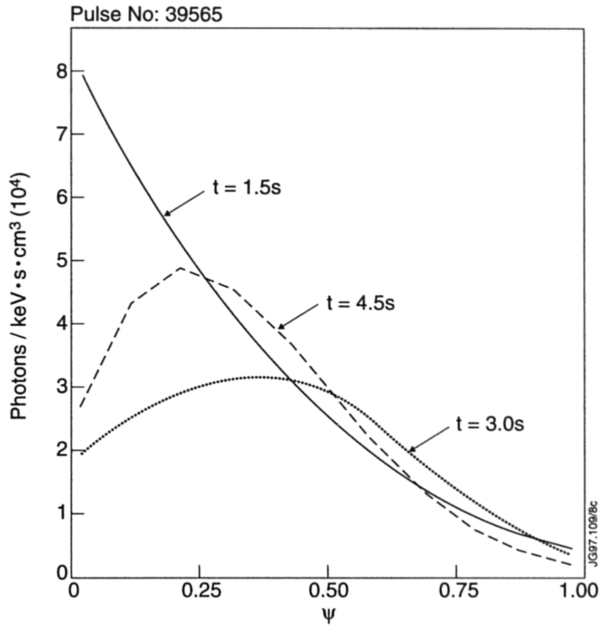

Fig.41: LH deposition profiles from hard X-ray emission FEB measurements

Deposition Profiles

LHCD has been applied in a series of optimised shear experiments for preheating of the plasma during the initial current ramp-up (Fig.40). The LHCD deposition in these experiments was peaked within half radius, slightly off-axis (Fig.41) as shown by Fast Electron Bremstrahlung (FEB) measurements. Good agreement was found between the experimental profiles and the modelling predictions of the transport code JETTO and the Baranov Ray Tracing code. In the initial breakdown phase of the pulses, slide-away conditions often prevailed, resulting in rather high hard X-ray emission. Since the runaway tail is, in general, localised in the centre of the discharge, the FEB emission is observed to be more centrally peaked than the LHCD deposition (Fig.41).

LHCD antenna phasing studies in those experiments showed that the broadest deposition profiles were observed at +90° phasing, whereas the deposition at 0° phasing was

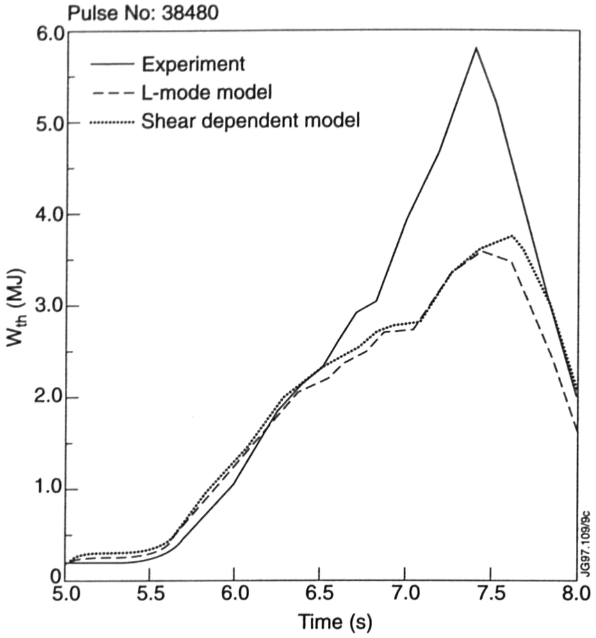

Fig.42: Thermal energy content from experiment and modelling.

most central. This is in contrast to simplified accessibility and absorption considerations based on the plane wave characteristics. Calculations with the full Baranov ray tracing/Fokker-Planck code reproduce well the observed behaviour in these experiments. The initially centrally peaked LH deposition profiles broaden in the course of the discharge with increasing plasma current and density as required for the current profile control with off-axis current drive in the shear optimised scenarios.

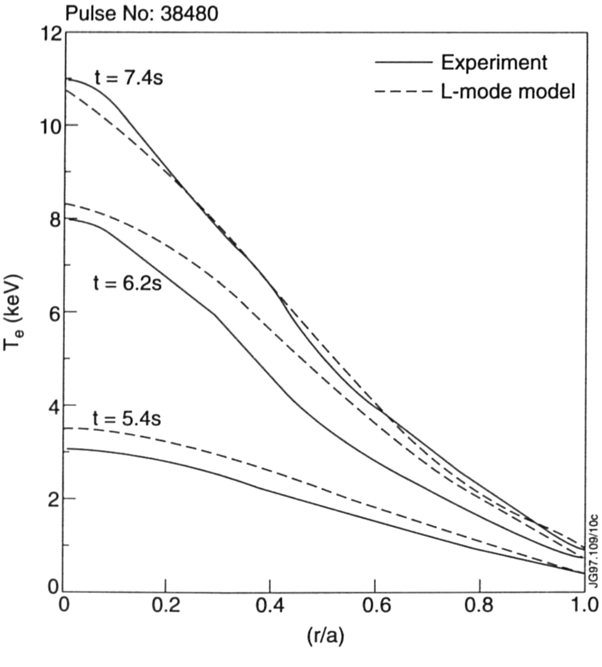

Fig.43: Electron temperature profiles from experiment and modelling.

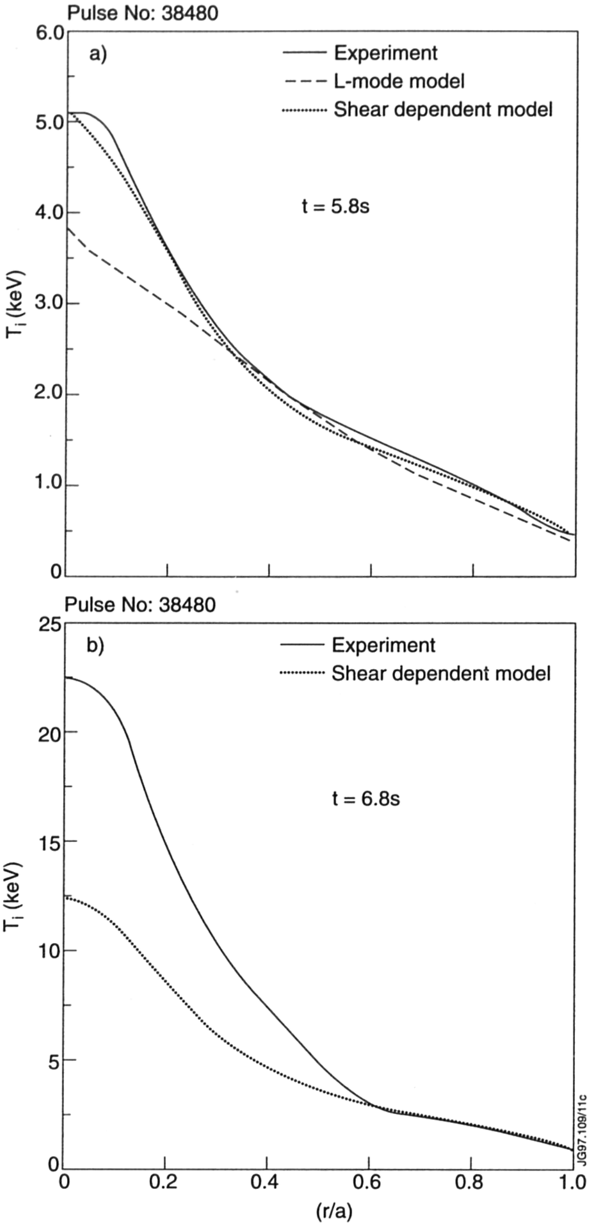

Fig.44: Ion temperature profiles from experiment and modelling.

Transport Code Modelling

The modelling activities have focussed on shear optimisation experiments. A detailed analysis using the JETTO transport code was performed on Pulse No.38480 which achieved the highest neutron yield in 1996 with a combined additional heating power of 17MW by NB and 10MW by ICRF heating Experimental data were compared with results of predictive runs, applying the mixed Bohm/gyro-Bohm model for standard L- and H-mode adaptations as well as a shear dependent model. The latter basically cancels the Bohm term in the region of low or negative magnetic shear.

The standard L-mode model and the shear dependent model clearly underestimate the total thermal energy content at peak performance (Fig.42). The standard

Table VI: Profile Control Scenarios on ITER

		ITER-H	ITER-N	ITER-A
I_p	(MA)	10	21	13
B_t	(T)	5.7	5.7	5.7
n_e	($10^{20}m^{-3}$)	0.27	1.35	1.15
P_{aux}	(MW)	0	50	50
P_{LHCD}	(MW)	25	50	50

(a) Commissioning phase in hydrogen: ITER-H
(b) Nominal operation scenario: ITER-N
(c) Advanced steady-state scenario: ITER-A

H-mode model, on the other hand, over-estimates it, regardless of the deposition models used in the transport modelling. Analysing the confinement of each of the species separately, the electron thermal conductivity was reasonably well described by the standard L-mode model (Fig.43). In Pulse No. 38480, an internal transport barrier was clearly observed for the ion thermal conductivity. The shear dependent model described the improvement in the central ion heat conductivity reasonably well only, as long as the width of the transport barrier coincided with the flat shear region (Fig.44(a)). In the phase of maximum performance, however, the region of improved central confinement grew perceptibly larger than the central flat shear region, as computed by the code (Fig.44(b)). Furthermore, a reduction in the ion gyro-Bohm term was then required to describe the observed confinement behaviour.

Improved central thermal electron confinement was observed also in shear optimisation discharges heated in the central region with LHCD alone. Transport code calculations for these cases can reproduce the experimental results only with a complete suppression of the Bohm term in the electron heat conductivity over the central region. In addition, the gyro-Bohm term had to be reduced.

Code Development

The LHCD code development has been driven towards full treatment of experimental conditions in a wide parameter range and towards modelling of integrated experimental scenarios on JET and on ITER.

LHCD applications to deuterium-tritium plasmas in burn conditions require the simultaneous treatment of wave interaction with fast electrons and fast ions, predominantly alpha-particles. An advanced version of the Fast LHCD code has been developed. It includes fast ray tracing and Fokker-Planck calculations for the electron and α-particle distribution functions. A version of this code has been installed on the IBM mainframe computer. The three moment approximation of the magnetic field configuration in this code is being replaced by a proper description of the X-point magnetic field topology. The code has been used to model deuterium/tritium experiments in JET and pulsed and steady-state scenarios in ITER.

A relativistic 3D Fokker-Planck code has been implemented into the LHCD code. It gives solutions for the electron distribution function in parallel and perpendicular momentum ($p_{//}$, $p_{\wedge}$) space and the radial component ρ, taking into account fast electron spatial diffusion. It has been validated on experimental data by comparison with calculations with a 2D solver in ($p_{//}$, $p_{\wedge}$) previously used in the code for zero diffusion cases. The 3D Fokker-Planck code consumes a factor ten more CPU time than the 2D code and is mainly used for the validation of case studies performed with the 2D code.

Profile Control Scenarios on ITER

Profile control scenarios with non-inductive current drive in ITER have been studied with the transport code JETTO. Lower Hybrid waves and Fast Waves are used to cover the whole profile. The LHCD deposition profiles are determined with the stand-alone Baranov ray tracing code and a beam tracing code implemented into the JETTO transport code. Both codes have been extensively validated on existing experimental results. The Fast Wave deposition profiles are determined with the stand-alone ray tracing code BRAYCO.

Three types of scenarios have been investigated for the three main phases of ITER, the first phase of hydrogen discharges, the nominal ignition case and steady state operation in an advanced scenario. The main parameters are summarised in TableVI.

In the commissioning phase of ITER with hydrogen discharges the pulse length can be considerably prolonged by non-inductive current drive with the LHCD system. High current drive and heating efficiency can be provided by LHCD in this operation regime where the heating power density is low in the absence of alpha-particle heating. Up to 7keV central electron temperatures were obtained with 25MW LH power. The LH power deposited in the central plasma region with a profile peaked slightly off-axis (Fig.45). Profile control scenarios for the subsequent high performance operation can be conveniently tested in this phase.

In the standard ITER case with pulsed operation at 21MA current, current profile optimisation throughout

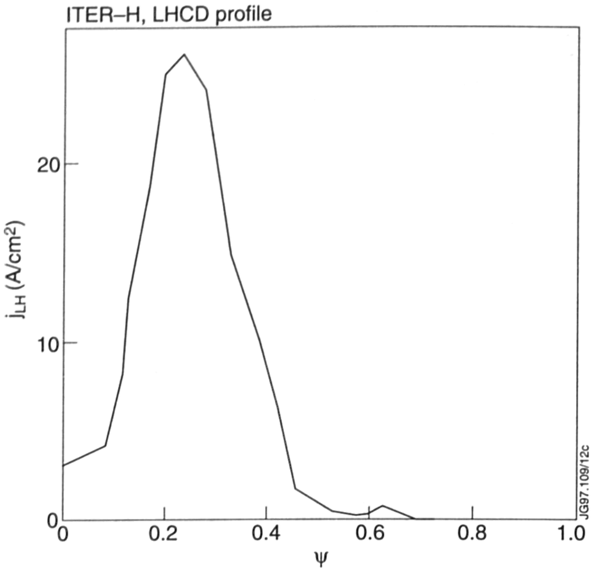

Fig.45: Lower Hybrid current deposition profile during the current flat-top in low density hydrogen discharge on ITER.

the discharge can be achieved by supplementing non-inductive current drive with LH waves. Ramping up the LH power to 50MW during a 0.15MAs^{-1} current rise phase provides non-monotonic q(r)-profiles with a wide central region of flat shear at the beginning of the flat-top phase. Then, over the long resistive diffusion time in the burning phase, the negative magnetic shear zone shrinks slowly and the current profile reverts to a monotonic shape, but q-values can be kept above unity over the whole plasma cross-section up to 1000s. Sawteeth are therefore avoided throughout the whole discharge duration. The q-profiles during flat-top at t = 500s are compared in Fig.46 for Ohmic ramp-up only and LH-assisted ramp-up, both with 50MW ICRH heating started at the begin of the current flat-top. The ohmic power during ramp-up is significantly reduced with LHCD due to the large enhancement of the current drive efficiency from the electric field in the outer half of the plasma. A total of about 70Vs are saved in the ohmic flux consumption. This reduction in flux consumption from the ohmic transformer has to be taken into account for the operation of the poloidal field system.

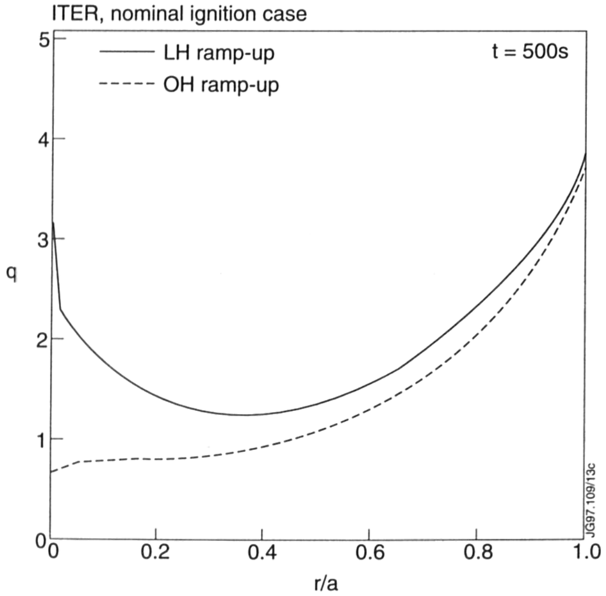

Fig.46: Comparison of the q(r) profiles during current flat-top in an LHCD-assisted ramp-up scenario and in an Ohmic ramp-up case.

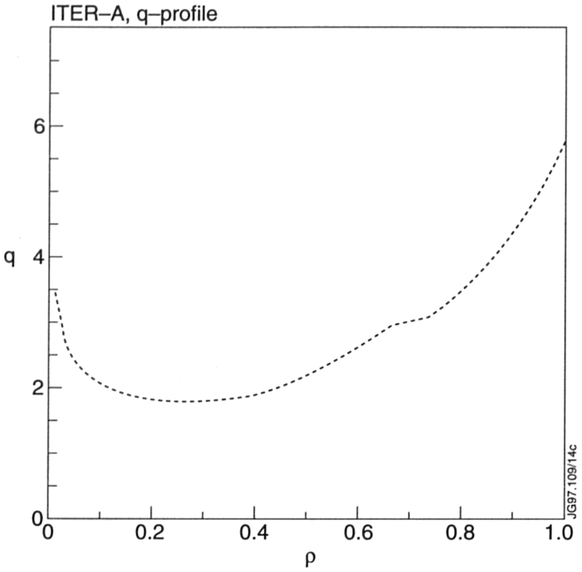

Fig.47: q-profile during the current flat-top in an advanced scenario with LHCD current profile control on ITER.

In an advanced scenario of steady-state operation at 13MA plasma current, off-axis LHCD is used to create and maintain a wide magnetic shear reversal zone and to provide full current drive together with the bootstrap current. LHCD started at a power level of 10MW during the initial current ramp and then ramped to the full power of 50MW at the beginning of the current flat-top phase. The q-profile during current flat-top is shown in Fig.47.

The early application of LHCD is required to avoid a misalignment of the current profile. Large corrections during the high performance phase might entail local non-inductive current overdrive and long inductive time scales for the profile redistribution.

The transport model used in the JETTO calculations links the heat conductivities to the magnetic shear, reducing transport in the region of flat shear. This model has been validated on shear reversal discharges on DIII-D and JET. The temporal evolution of central ion and electron temperatures into steady-state conditions is shown in

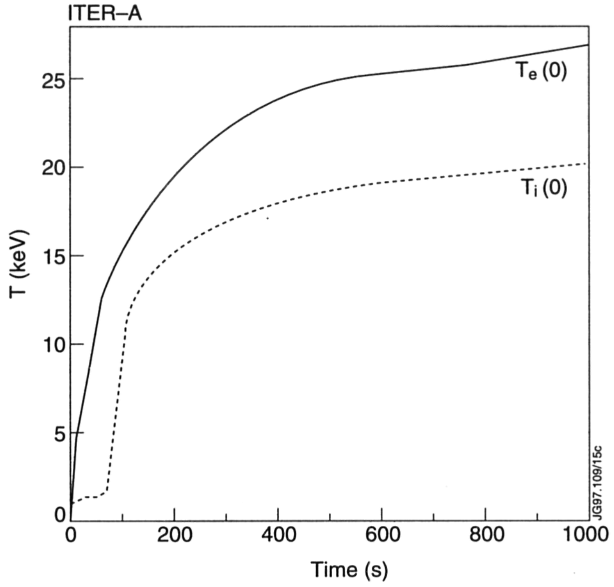

Fig.48: Rise of central ion and electron temperatures to steady-state in an advanced scenario with LHCD current profile control on ITER

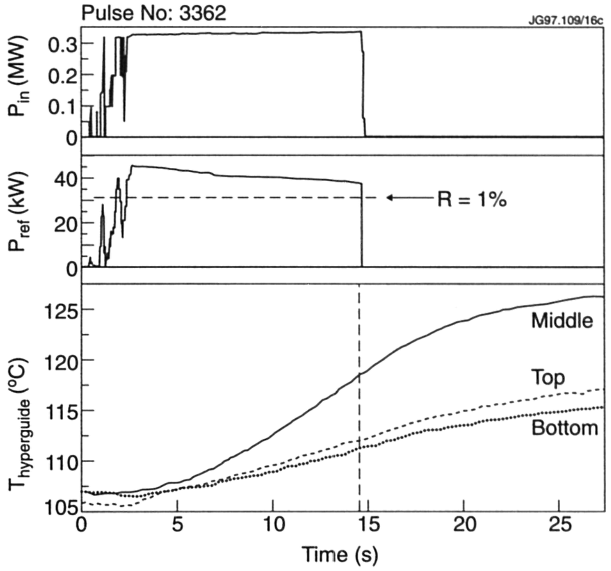

Fig.49: High power pulse at 320kW/13s through a TE03 hyperguide.

Fig.48. A fusion power output of ~1GW is produced in steady-state.

Coupler Development

As part of the development of the next generation LHCD launcher, a high power hyperguide was designed, built and tested. The component was designed in collaboration with Tore Supra, Cadarache, France. A poloidal mode converter has been used as input module to the hyperguide to provide the conversion from the TE_{01} mode of the standard size waveguides of the transmission line to the TE_{03} mode of the hyperguide. A power recombiner was mounted to the other end of the hyperguide connecting through standard size waveguides to a high power load. This allowed a test of the novel hyperguide concept for the first time with high power in transmission and under high reflection. The complete assembly, with two interface components from Cadarache, was installed in the vacuum vessel of the JET LHCD test-bed. The vessel was baked up to 400°C. About 1000 pulses were applied at various power levels to test the power handling capability and the behaviour around resonances found at low power. Up to 320 kW for 13s were applied, representing $42MWm^{-2}$ at the hyperguide input, with a reflection coefficient of 1-2% (Fig.49). No resonances were seen when the hyperguide was operated between 80°C and 350°C. At the output of the hyperguide, up to 99% of the forward power was detected, confirming the results from simulation runs. These results show the reliability and the robustness of the hyperguide which is planned to be used in new LHCD launchers under study for Tore Supra and JET.

Alfvèn Eigenmode Exciter

The Alfvèn Eigenmode active excitation system was designed and installed on JET before the 1994/95 campaign to study the physics of Alfvèn waves in tokamak plasmas. It is based upon the use of the saddle coils as external antennae and of synchronous detection of the electromagnetic perturbations induced in the plasma in the frequency range 30-500kHz. In 1996, while being operated routinely to investigate the stability of the various classes of AE in the different D-D plasma configurations, the apparatus was progressively upgraded for the DTE-1 campaign. A number of minor modifications to the hardware of the exciter were implemented. As the four top saddle coils were dismantled, leaving the bottom set of four in use, below the divertor structure, several parts of the AE exciter, including the impedance matching networks and the isolation unit, were modified. The electrical isolation of the system was increased from ~7kV to ~9kV. Synchronous detection was applied to the measurements of parasitic currents to earth and of sudden changes in the antenna voltage, used in relation to the saddle coil protection systems. This enabled active excitation throughout the entire discharge, including the high performance phase, even in the presence of large edge instabilities.

In the presence of additional heating, the saddle-coil driven perturbations appearred to be masked by intrinsic plasma activity, effectively reducing the sensitivity of the active diagnostic. Therefore, effort was dedicated to increasing the power coupled to the plasma. The wide band hybrid amplifier was reconfigured from class A to class B. The maximum output power on a 50W load was increased from 3kW to ~5kW, while maintaining relatively good spectral properties. Oscillating currents up to 20A were driven in the saddle coils for voltages not exceeding 1300V. The complex character of the exciter circuit, encompassing several series and parallel resonances in the frequency range of interest, motivated the use of a feedback control loop on the saddle coil current to minimise the variation of the driven perturbation amplitude over a frequency scan. On the detection side, some additional non-magnetic diagnostic channels were connected to the synchronous detection system, including signals from fast X-ray cameras and from X-mode reflectometer, yielding fluctuation measurements in the plasma core.

Besides these various minor improvements, the potential of the AE active diagnostic was significantly enhanced by the application of a real-time control system to perform individual resonance tracking. This device constitutes part of the general real-time digital system developed for feedback control of macroscopic plasma parameters, such as the total stored plasma energy or the global fusion reaction rate. The particular application to the AE exciter encompasses two main modes of operation, both controlled by the AE Local Manager (AELM). In the first mode, the expected AE resonance frequency, f_{TAE}, is calculated from real time measurements of density and magnetic field. The controller, run at 1ms clock rate, drives the AE function generator as a voltage controlled oscillator, varying the frequency linearly around the expected resonance. Scans of 100kHz around a central f_{TAE} of 200kHz, at a rate of 300kHz/s, are typical. In the second mode of operation, the AE resonance is tracked by the exciter frequency. The controller imposes feed forward frequency scans around f_{TAE} until an AE resonance, identified in real time via a number of conditions on the measured complex plasma response to the perturbed magnetic field, is met. At that point, and as long as the resonance conditions from the AE signals are satisfied, the exciter frequency is swept back and forth around the full AE resonance width. As a result, AE frequencies, mode structures and, most importantly, damping rates, can be measured with high time resolution (<50-100ms) along their dynamical evolution throughout a discharge. A number of plasma and engineering variables are linked to an ELM via the real-time signal server, enabling the AE operational parameters, such as the conditions for resonance identification or the frequency scan rate, to be defined according to the specific experimental conditions. This resonance tracking technique, demonstrated successfully in 1996 will become important in connection with D-T experiments, in which the measurement of variations in the AE damping rate due to fast particles, in particular, fusion produced alpha-particles, will be undertaken.

Operations Systems

Plasma Position and Current Control

The Plasma Position and Current Control (PPCC) system has undergone a number of enhancements. The system, based on VME masterboards with multi-processor TMS320C40 chips, takes the data from the magnetic diagnostics as input. The hardware architecture of the system is shown in Fig.50. The system calculates the plasma boundary in real-time, which is characterised by the location of the X-point (if present), the location of the two strike zones, and a number of distances (Gaps) between the plasma and the vacuum vessel. Outputs are current request signals to each of the poloidal field power supplies, which control the currents in the primary coils, vertical field coils, shaping field coils, and the four divertor coils.

The control algorithm in PPCC is configurable. The current request for a given power supply can be chosen simply proportional to the plasma current, where the proportionality factor is a programmable waveform in time. Alternatively, current requests can be controlled by the Gap Controller. This is a feedback algorithm which controls one or more of the plasma boundary characteristics to equal a programmable waveform in time, subject to power suppy limits. Routinely, a mixed configuration is used. For example, the shaping field coil current is often made proportional to plasma current, while the vertical field coil current and the divertor coils currents are controlled by the Gap Controller to maintain the gap between plasma and poloidal limiter and the divertor strike zone locations, respectively. The Gap Controller is a linear decoupling controller. The gap control facilities are routinely used in operation. In Fig.51, an example is shown in which outer gap control is continously enabled, while strike zone control is enabled during a time window.

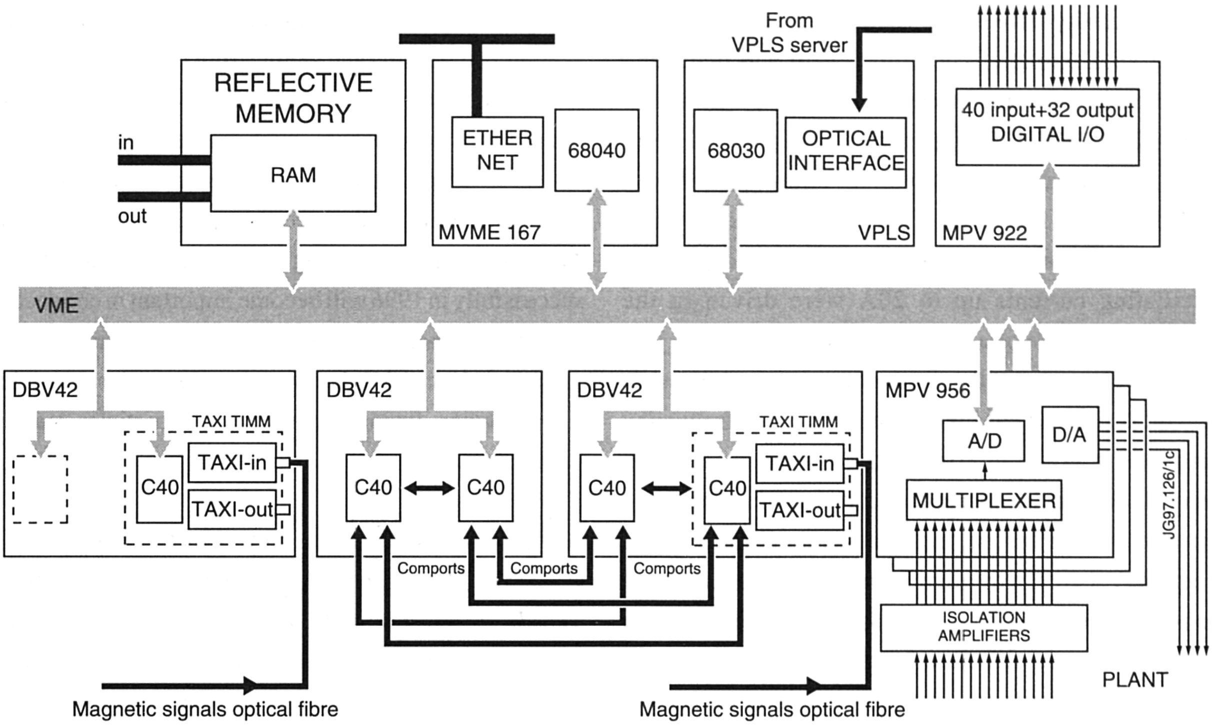

Fig.50: Hardware architecture of the Plasma Position and Current Control System

To improve the reliability of the control system to an algorithm, which identifies the plasma boundary (XLOC) in real-time, has been improved by pre-calculating the fluxes due to the divertor coil currents. This is turn allows the use of a smaller set of magnetic sensors. In particular, a relatively unreliable set of sensors near the divertor has now been excluded.

Vertical Stabilisation

The vertical stabilisation system has been significantly enhanced with a new "adaptive control" algorithm. To obtain an optimum vertical position control, it is necessary to tune the gain of the controller approximately inversely proportional to the growth rate of the plasma vertical instability. Doing this, maintains approximately constant overall system gain. In the past, this was done by manual tuning. In the new algorithm, the overall system gain is obtained from the switching rate of the radial field amplifier, where the switching rate is the rate at which the amplifier delivers its "up" or "down" kicks to the plasma. The algorithm maintains a constant switching rate by feedback control. Together with a lower limit on the controller gain, the system has been highly successful in minimising the number of interventions by the operator in the control system, and in improving the consistency of the vertical position control in plasmas with different elongation.

The new notch filters in the divertor coil power supplies have successfully removed the 600Hz and 1200Hz thyristor switching noise from the plasma position sensors at the bottom of the machine. The vertical stabilisation system is now able to use a larger set of sensors. However, the planned extension of the system to a "full current moment" system has not yet been possible. This is due to remaining high frequency thyristor switching noise on the signals representing the current derivative in the

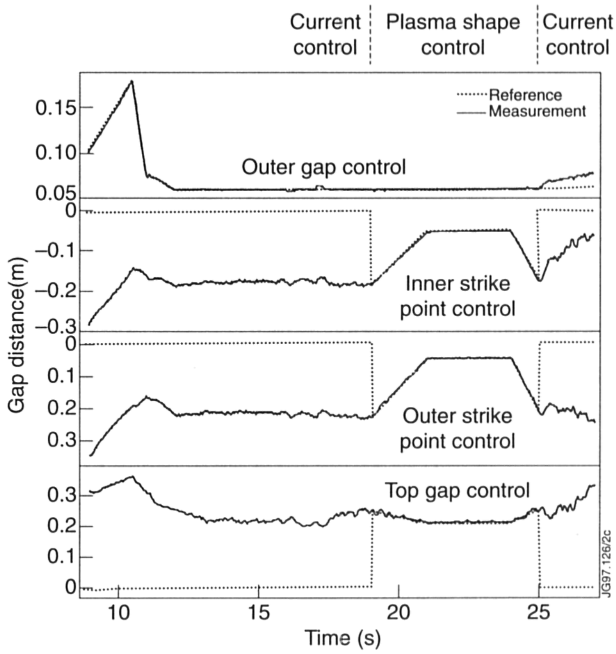

Fig.51: Example in which gap control is continuously enabled

divertor coils. These derivatives are required in the determination of the plasma vertical speed from the current moment. The situation is still under study, with attention focussing on the use of various filter strategies, or the use of alternative signals for the current derivatives.

Progress has been made on the vertical stabilisation with the aid of the soft X-ray signals. The algorithms have been implemented in the vertical position control. The soft X-ray diagnostic is capable of determining in real-time the vertical position of the plasma centroid. Tests with a closed loop system are imminent.

Disruption Prediction and Prevention System

The Disruption Prediction and Prevention System is under construction. The objective of this system is to study advanced methods for predicting disruptions in real-time. In its first implementation, the system will not be enabled to modify the control waveforms. However, plasma termination and modification functions are foreseen, and are compatible with the hardware. The system is built using the same type of hardware as the Plasma Position and Current Control. First results are expected by mid-1997.

The first algorithms to be implemented are as follows:

- a neural network to determine the safety factor q_{95} and the internal inductance ℓ_i from the magnetics data. This will then be combined with a q versus ℓ_i diagram to predict the probability of a disruption;
- a neural network to determine, for a given plasma configuration, the force on the vessel that would arise from a vertical disruption;
- a neural network for disruption prediction. Input data will be, initially, the safety factor q, internal inductance ℓ_i, the radiated power and the total input power.

Saddle Coil System

The Saddle Coils have been operated to investigate several aspects of plasma MHD activity: the generation of error field modes; the excitation and characterisation of Alfven Eigenmodes; and the stabilisation of rotating tearing modes by magnetic feedback.

The Coil's instrumentation has been upgraded to monitor arcs, earth currents and induced currents in the coils during disruptions. Rogowski Coils have been designed and built in collaboration with ENEA, Frascati, Italy, and have been installed on each turn of two Saddle Coils, inside the vacuum vessel. These transducers, a few 10cms from the plasma, measure a few 100A induced current in the coils. These are 5kV insulated from the coil's busbars and made with special radiation and high temperature (400°C) resistant materials. Transducers have been added ex-vessel to monitor earth currents and induced currents.

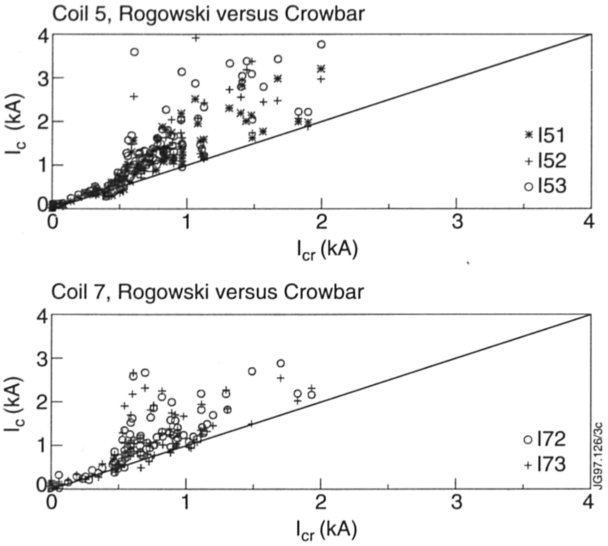

Fig.52: Internal Rogowski coil peak current at disruptions plotted versus the crowbar current. The fact that the two currents are different implies internal arcing of the coils which occurs when the current of the crowbar is larger than 500A and the coil terminal voltage is larger than 50V

A disruption database that includes all data from the transducers has been built and has been regularly updated. The database shows that, during disruptions, just after the energy quenches or during downward VDEs, arcs strike on the coils and generate earth faults and short-circuits between turns (Fig.52). These currents are within the coil's mechanical capabilities.

New protections have been procured to keep the AC coil currents within the prescribed limits and avoid over-stresses generated by the coil's mechanical resonances. A new protection system, capable of switching off and then re-applying the voltage to the coils upon detection of a fault, is under procurement. The new protections will increase the overall reliability of the system

The Disruption Feedback Controller (supervising the tearing mode magnetic feedback system) has been upgraded by adding the following facilities:

- control of the phase of the feedback field as a function of time and of the tearing mode speed, to investigate and avoid the early locking of the tearing modes during feedback experiments;
- control of the feedback gain as a function of time and of the tearing mode amplitude, to optimise the feedback

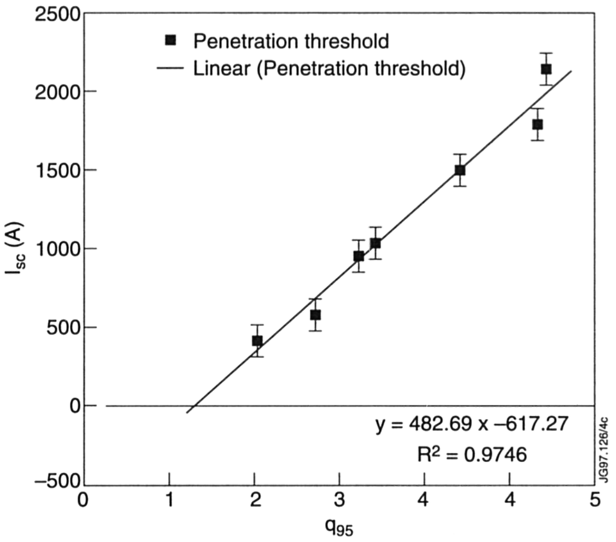

Fig.53: Locked mode threshold versus q_{95}

gain and try to control the amplitude of error field rotating modes;

- automatic compensation of the "fast plasma response" in order to simplify the feedback set-up procedures and to investigate the dependence of this response on the safety factor and on the plasma current profile.

Disruption Feedback Stabilisation System

A series of parasitic experiments on DC error fields has been completed recently. The plasma current was 1.5MA, and the plasma configuration was either X-point or Limiter. Saddle coil currents of up to about 1kA was generated in a three seconds ramp. The plasma conditions were kept constant from at least 2s before the start of the ramp onward, ensuring stable and reproducible conditions.

In X-point configuration, the critical error field for the generation of a locked mode was determined as a function of the safety factor q_{95} by comparing pulses with different toroidal fields. The toroidal field was varied between 0.91T and 2.6T, corresponding to q_{95} between 2.1 and 5.4. The plasma density was constant throughout this scan at $\sim 1.0\times10^{19}$ m^{-3}. The results are shown in Fig.53. There is a clear and approximately linear scaling of the critical error field with the safety factor.

As a part of these experiments, the natural n = 1, m = 2 error field in JET (for the particular combination of shaping currents) was determined. This error field is here expressed as a saddle coil current of 345±40A, at an angle of 277° (anti-clockwise from above with respect to the Octant No.1 and Octant No.8 joint.

Physics Operations

The twin roles of the Physics Operation Group continues to be the development of new plasma scenarios and the support of Task Forces and Session Leaders in plasma development. During the Mark I pumped divertor phase, plasma scenarios were developed to exploit the new plasma configurations over a wide operational domain from ELMy H-modes to ELM-free H-modes up to the full

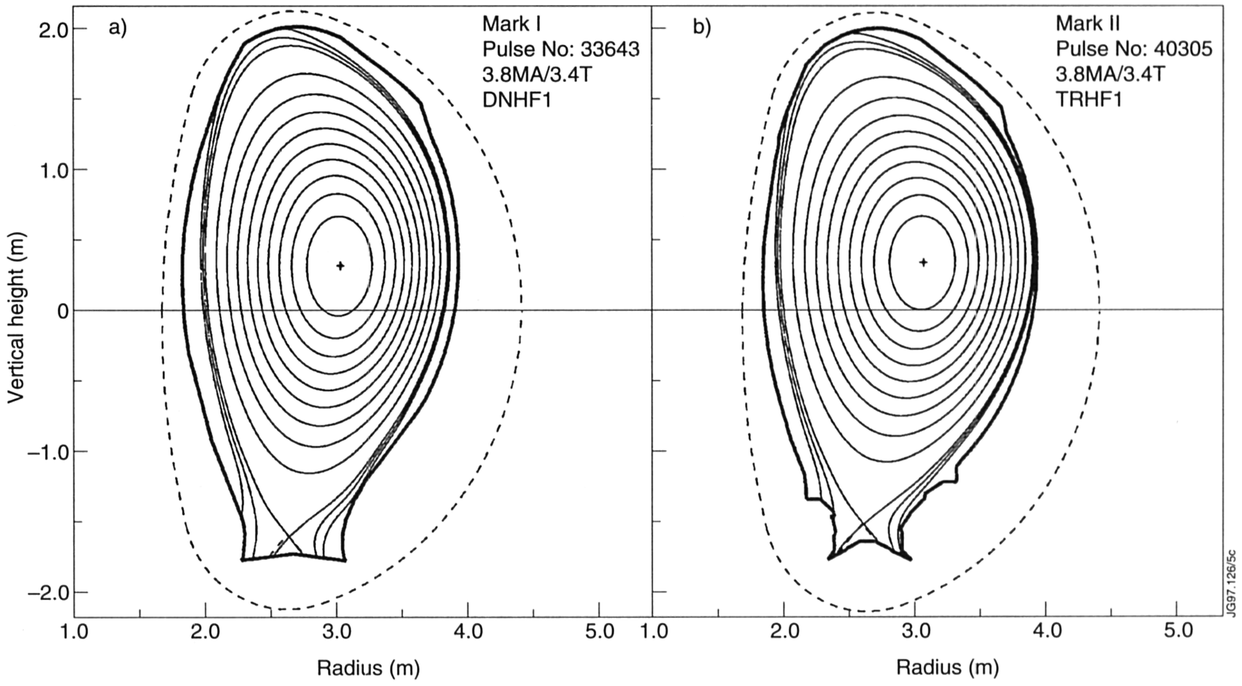

Fig.54: High flux expansion in (a) Mark I and (b) Mark II divertor configurations (ELM-free hot-ion situation)

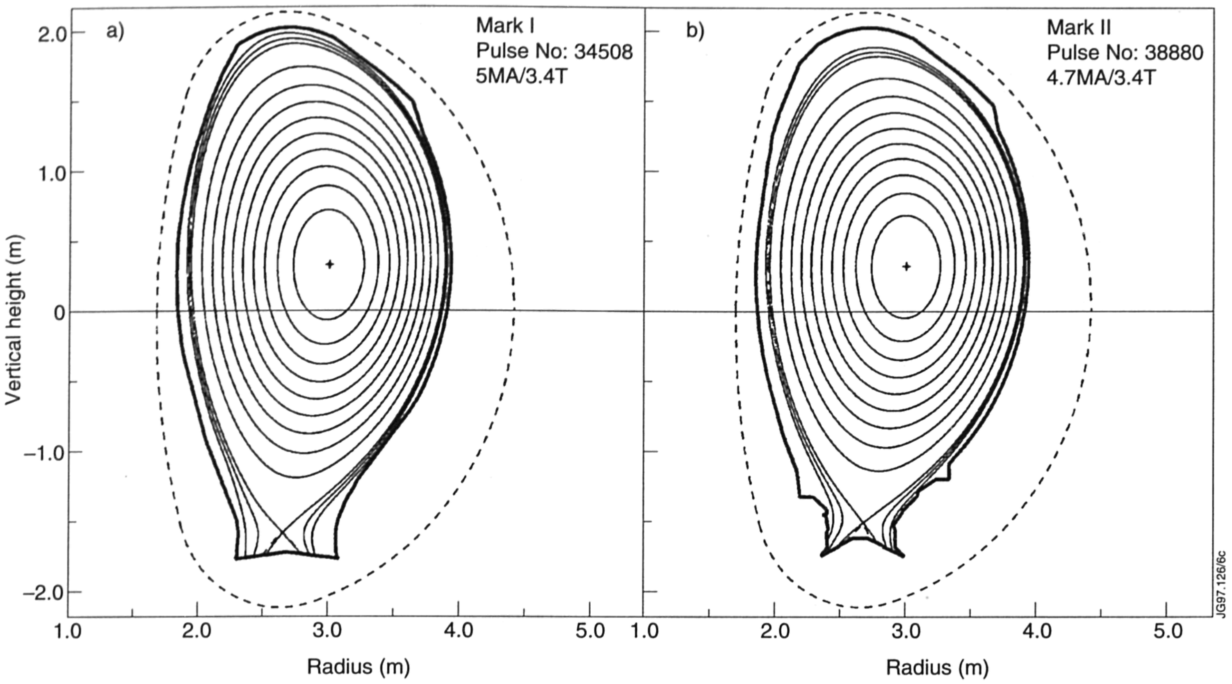

Fig.55: High plasma current pulses in (a) Mark I and (b) Mark II configurations

design capability of 6MA. The knowledge gained was disseminated to all Session Leaders over the following shutdown by means of a lecture course and course notes.

The differences between Mark I and Mark II were much less dramatic and many basic scenarios were translated from Mark I to Mark II with only modest plasma re-engineering. Figure 54 shows this redesign for the high flux expansion highly-shaped configuration used for ELM-free hot-ion studies. In addition to the changes to plasma shape necessary to accommodate the tighter divertor geometry, the plasma elongation was reduced for similar edge stability (shear) to minimise the occurrence of vertical disruptions at giant ELMs. Together with improvements to vertical stabilisation, this reduction in elongation has all but eliminated disruptions at ELMs. At the same time, this scenario has been optimised to minimise transverse forces on the TF coils and as such would be suitable for operation at higher fields than 3.4T.

A similar re-engineering has been performed for high plasma current as shown in Fig.55. These and related configurations have been designed to examine the influence on ELMy H-mode behaviour on triangularity and wall separation.

The most significant impact of Mark II has been on breakdown where the stray fields from induced currents in the Mark II baseplate are sufficient to cause severe problems during the avalanche phase. Considerable effort was devoted to studying this problem before operation commenced and the preferred option was to back the radial field amplifier off the radial field from the baseplate with a proportional waveform for the radial field amplifier (FRFA). This strategy was finally successful with reliable breakdown rapidly established during the first operation with Mark II. Figure 56 illustrates the stray field pattern at breakdown (a) with and (b) without the correction.

Mode B breakdown (i.e. without pre-magnetisation) was re-established. Additional technical commissioning was necessary and two scenarios prepared permitting earlier X-point formation which were exploited for plasma current profile.

Plasma Fuelling

The Plasma Fuelling Group is responsible for the control and monitoring of the torus plasma density by control of the torus gas introduction systems, the pellet injection system and the analysis of the torus exhaust gas.

Torus Plasma Gas Introduction and Density Control

The entire control system came into operation as planned and required little maintenance during operation. The control of the pellet centrifuge pellet injection, which is operated as one of the gas inlet regulator valves despite the discrete nature of the pellet events, was successfully implemented in plasma operation and was used several times in density feedback to limit the pellet rate.

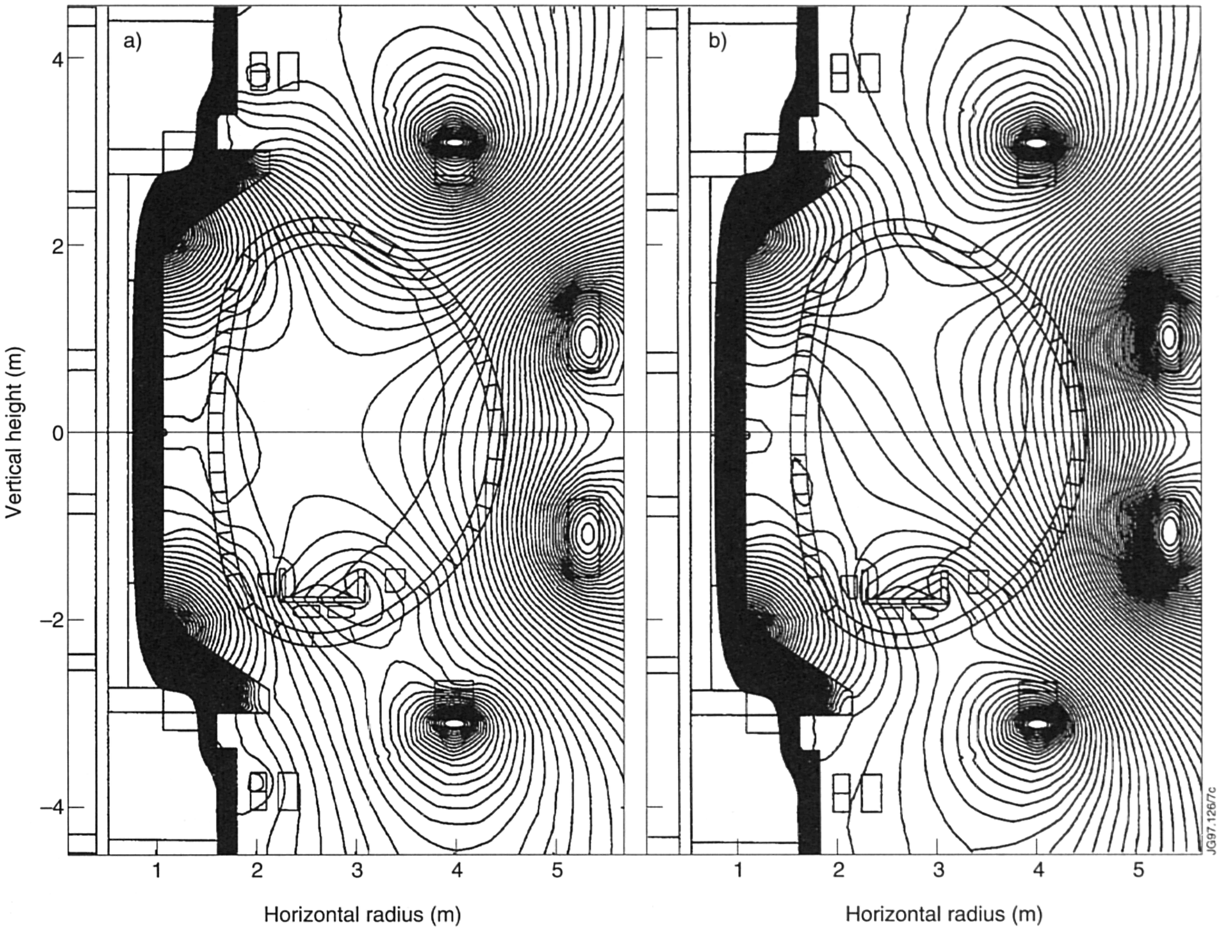

Fig.56: Stray field patterns (a) with and (b) without correction

The Pellet Centrifuge

The pellet centrifuge for the shallow deposition of the pellet fuelling mass, beyond the recycling layer at high equivalent flow rates, is an intermediate radius particle source tool for divertor pumping investigation. This year, the second extruder unit for 4mm pellets was commissioned and the centrifuge with two extruders was brought into operation on the machine with pellet injection into the plasma. A more detailed description of the design and the functions of the various components of the pellet centrifuge can be found in the previous Progress Reports.

Basic Systems Characteristics

The centrifuge has been designed to deliver long strings, ~1 minute duration, of deuterium pellets of 2.7 and 4mm cube size at repetition frequencies of up to $40s^{-1}$ with velocities between 50 and $600ms^{-1}$. It performs this operation by accelerating pellets mechanically from the hub to the tip of a rotor arm (R = 0.35 m) from which the pellets leave at about 1.4 times the rotor speed. Each size of deuterium ice pellet is launched from one of up to four possible individual extruder units into the centre part of the centrifuge rotor hub, into which protrudes, hanging from the stationary crown on top of the rotor housing, the stationary stop cylinder. The latter features a hole that can be azimuthally adjusted and towards which the inner rotor blade guides the pellet to its proper starting conditions for the pellet on the outer rotor arm.

The design of the centrifuge rotor and stop cylinder follows very closely that of the centrifuge developed for ASDEX-Upgrade by IPP Garching, Germany. The extruders (the pellet formation units) are of a new design by JET to provide a much larger quantity of pellets per tokamak pulse, and fresh in the approach in that they use "dynamic cooling". A length of rod of extruded deuterium ice, equivalent to the pellet dimension, is cut off by a chopper magnet, pushing the resultant pellet with the same stroke onto the hub of the rotor. In the vacuum vessel, a large built-in LHe cryopump of more than $10^5\ell s^{-1}$ pumping speed copes with the gas losses stemming from pellet acceleration and guidance and is to keep the pressure below 10^{-3}mbar. To operate on the machine for a two days without regeneration, the capacity of the cryopump is designed for 2500barℓ of deuterium.

Ice pellet formation

A water-driven hydraulic piston at room temperature which is entirely situated within the vacuum of the main vessel, exerts a force of up to 30kN onto the 15cm^2 of the deuterium ice block, which has a maximum content of 150cm^3 (or ~170barℓ) and is enclosed in a helium cooled cylinder. The ice is pushed towards the nozzle which leads into the extrusion channel. To create the cubic pellets, an ice rod is extruded through the nozzle reducing the ice cross-section by a factor of 100 to 200 to that of a pellet. While being extruded the ice is cut off in sections of pellet dimensions at the appropriate rate. The cooling of LHe flow of 10 to 15ℓ/hr is introduced at the tip of the extruder and runs up the channel between the inner section containing the ice and the other stainless steel envelope. The heat flow is regulated by staged electrical heaters spun around the inner copper. The deuterium ice can only be extruded at temperatures >14K, higher than the ideal temperature for the pellet in the range of 8 - 12K suitable for acceleration. Therefore, the deuterium ice is cooled dynamically while it is sliding along the wall of the sufficiently long channel (~200mm to the tip of the extruder), so far successfully up to 4cms^{-1} ice rod extrusion speed.

In 1996, the already previously reported performance of the 2.7mm pellet extruder was improved to give the full extrusion at 5Hz pellet frequency (i.e. 13.5mms^{-1}), the improvement being in the tuning of the temperature circuits and that of the hydraulics. The extrusion speed, achieved at pressure of 80–100bar, is finely regulated by two-point switching within the PID loop. In the commissioning tests, 7000 pellets have been produced at the rate of 5Hz over about 20 minutes continuously or in smaller batches, e.g. over 10-20s as required currently on JET. By the end of the year, the pellet rate was raised to 10Hz.

The 4mm pellet extruder had its piston pressure capability enhanced a factor of 10 by an insert reducing the area. The reduction of the reservoir volume was by about the same factor but the limited number of pellets would still be sufficient for JET within experimental requirements. This extruder was operated by using the extrusion speed feedback control on the hydraulic regulator valve, leading within the narrow temperature band of the nozzle circuits to smooth and reproducible extrusion. The pellet production could be performed at 5Hz (with some preliminary and encouraging results at 10Hz) and required virtually the same pressure range as quoted above for the 2.7mm extruder. In retrospect, it can be concluded that the insert is not needed and that the 4mm extruder can be restored to its full inventory capability of 150barℓ. Comparing the two extruders of different pellet size equipped with and without insert has thus clarified some of principal extrusion characteristics of interest for a further design upgrade to pellet feed ITER-like machines [1].

For ease of operation, the extruders so far have been operated in a batch-wise continuous mode at highest extrusion speed. The cutter now constantly produces pellets which will be either passed on to the torus or eliminated by an electromagnetically driven mechanical gate ("pellet guillotine") in the flight tube section, permitting essentially all modes of pulse sequencing, inclusive of feed-back fuelling which has been demonstrated in plasma experiments.

Some problems have been encountered with the design of the cutter magnet which is open to the centrifuge main vacuum (eddy current heating of LHe cooled metal parts, partial iron powder core disintegration and electrical insulation). A new magnet design with closed magnetic field configuration is in progress in which coils and core are firmly seated into a weld closed stainless steel housing.

Pellet Launching

The microwave pellet diagnostic (consisting of two resonant cavities at 1.4 and 3.2GHz about 2m apart and forming part of the pellet track towards the torus) came into operation. The passage of the pellet causes the de-tuning of the cavities and the corresponding signals are evaluated in real-time while limited storage of original signal traces is provided in transient recorder fashion for reference. The size and speed of the pellets are determined from the amplitude and timing of the signal.

This diagnostic has shown that pellets were missing from the sequences even in the cases of otherwise perfect extrusion, leading to ~20-30% loss on average but there were also continuous periods of missing pellets. The problem was traced to problems with the acceptance of pellets by the rotor hub. In video pictures of the hub region of the centrifuge in stroboscopic flash light, pellets could be seen bouncing off and escaping their intended turn of the rotor or off the rotor hub altogether. Evidence suggests that the cutting timing jitter, the initial speed and the variation of that speed of the pellet after cutting may be too large compared to the design values. These effects may also contribute to the increasing fraction of broken

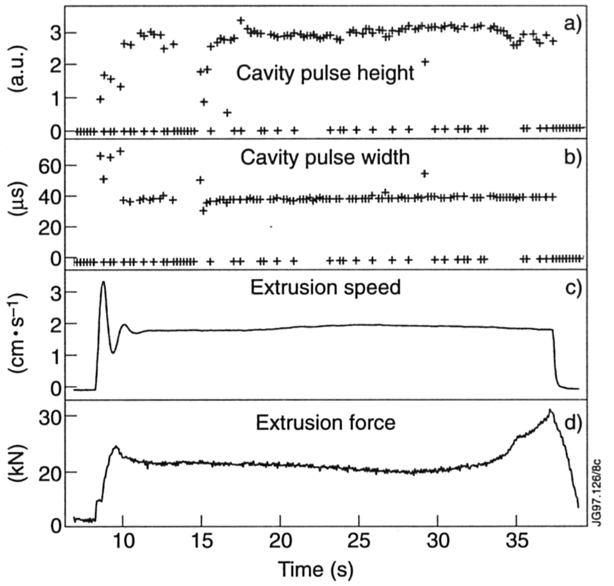

Fig.57: 4mm pellet performance for a 20s pulse at 250ms-1: (a) size and (b) width of microwave signals versus time; (c) extrusion speed; (d) extrusion Force

pellets at progressively higher speed compared to the 250 ms^{-1} at which most of the operation has been carried out. The solution of this problem is to force the guidance of the pellet all the way to the inner rotor blade.

An in-flight photography station close to the second microwave cavity is under assembly. Pellets trigger by means of a light barrier a ~10s flash whose light generates an image of the pellet on a CCD camera, recorded by synchronous reading to video tape. In the absence of this diagnostic, the only close feedback information about pellet integrity came from the plasma generated D_α light of the pellet plume.

An example of the 4mm pellet performance at 5Hz for a 20s pulse at 250ms^{-1} is shown in Fig.57. The upper two traces are the evaluated size and width of the microwave signals versus time where each cross represents a pellet cut from the extrusion. The lower two traces show the speed of the extrusion and the force on the piston extruding the ice. The good pellets (77% of the 20s pellet sequence from 56 to 76s) have their maximum size within 3.5% standard deviation; the width signal is the time for traversing the cavity in use.

Summary of Achieved Pellet Performance

The current pellet centrifuge system performance at the end of 1996 is the following: 2.7mm pellets are available with repetition rates of up to 5Hz. The estimated fuelling rates is about 110mbarℓs^{-1} for full size pellets. This flow rate is reduced by the 20 - 30% of lost pellets due to the hub acceptance. As to the unavoidable gas losses from each pellet due to acceleration and guidance, the latter seem to be more in the vicinity of 20-30% than the initially expected much larger values. Pellet sequence pulses length can be considered unlimited (usable 150barℓ of ice, the condensation of which is performed in about 30 minutes). Pellets have been accelerated at speeds of 150 to 625ms^{-1}. However, at speeds considerably higher than the 250ms^{-1} at which most plasma experiments have been conducted the number of pellets in the sequence as well as their individual integrity deteriorated.

4mm pellets are available with repetition rates of up to 5Hz. Equivalent fuelling rates are about 350mbarℓs^{-1}. The length of pellet sequence was limited to ~120 pellets in accordance with the ice inventory limit caused at the insert. Systems operation is available every day over the full two shifts of operations (~14 hours) and regeneration is usually required only once a week. Extruder re-filling with deuterium (condensing) is possible in between shots (~20 minutes) for the 10barℓ of the 4mm extruder, but for the filling of the entire 150barℓ of the 2.7mm extruder the interval between shots is barely sufficient.

Summary of Operation on the Torus

First plasma injection experiments with the pellet centrifuge were performed with the 2.7mm pellet extruder and showed in ohmic discharges the well known density build-ups seen in JET almost a decade ago with the repetitive pneumatic pellet launcher. In these cases, pellets showed very high fuelling efficiencies of up to 88%, despite the shallow deposition (λa) of about 0.3 (λ is penetration depth, a is minor radius) at 250ms^{-1} pellet speed. Together with the build-up of the plasma density some profiles were peaked and this peaking lasted for about 1s after the termination of the pellet string. However, in a series of pulses most of which were heated by 12MW of neutral beam injection and went into ELMy H-mode, the signature of the pellets was hardly visible in the interferometer density trace.

With the 4mm pellets various refuelling scenarios were investigated with the aim of enhancing the flexibility in density control. Pellet sequences, without and with additional gas puffing, were injected during quasi-stationary L- and H-mode phases of neutral beam and ICRF heated discharges up to a level of 12MW. The observed decrease in l with increasing auxiliary heating power was accompanied by a decrease in fuelling efficiency. In general, pure pellet fuelling acted faster and more efficiently than gas puffing but did not exceed by much the density obtained by gas fuelling. Combining both methods showed advantages for fast density rises to values of ~70% of the Greenwald limit.

As a general observation it was found for H-modes that for almost all pellet injection events, the plasma reacted with an ELM or ELM-like feature, the size of which seems to depend on the time period since the last ELM. At these power levels, pellet induced particle losses did not seem to contribute essentially to the bulk plasma energy losses connected with ELM activity. In high triangularity discharges without gas fuelling during the heating phase, where long ELM-free periods occurred without pellet injection, the controlled release of ELMs by pellet injection was demonstrated at moderate power levels. Pellet injection was applied with a frequency larger than that of the ELMs occurring without pellets. In this case, only pellet triggered ELMs were obtained. With the time delay between pellets varying over a factor of 3, it was observed that the amount of energy and particles lost by each triggered ELM was decreased with decreasing pellet delay.

Gas Collection System:

The Gas Collection System (GCS), measured the time evolution, absolute amount and chemical composition of the gas released from the vacuum vessel by wall outgassing, after plasma pulses, divertor cryopump regeneration and during glow discharge cleaning. The main tools are pressure and mass spectrometer measurements complemented with gas sampling to external analysis stations.

The GCS was used in the Mark I Divertor campaign [2]. A similar measurement effort was ongoing during the Mark II Divertor campaign, but it is too early to summarise the results. In this case, a more global analysis will be made, since the GCS did carry out not only short term pulse measurements (i.e. for a 600s period from the start of the pulses) but also over a full day by collecting all the gas released from the vessel onto the GCS cryopump.

On the technical side, some enhancements were carried out: the measurement cycle was made automatic and remote controlled, and the data are now archived all the way to the IBM mainframe; the completed installation of the heating jackets on the GCS has resulted in a much improved background of the mass spectrometer readings; and the preliminary enclosures for the membrane pumps have been prepared to aback the polymer membranes of the pump with a gas (foreseen is Krypton), which does not interfere with the measurements even if it should leak into the system. No effort was available to design and build the final version of the pump enclosures; in previous years, the GCS cryopump (which is intended to absorb the gas load of the torus pump under regeneration) was tested at high pumping pressure to its capacity and was found somewhat short of the intended 1000barℓ capacity. In 1996, it was integrated into the GCS and, in the initial tests, it failed to pump the torus vacuum foreline to the desirably low pressures. It is suspected that the lack of sufficiently effective heat transfer in its design (bath cryostat with intermediate gas) is the cause for both of these shortcomings. The inability of the GCS to store the total maximum design load of the torus regeneration has so far not hampered the analysis.

Operations Support

Operations Support Group has continued to specify, support and upgrade the many utilities used to drive JET as detailed below.

Level-1 Software

The JET Level-1 System for pulse specification, validation and loading is now in much wider use. Several Pulse Schedule structures are in place: The Main JET Pulse Schedule; Expert JET Pulse Schedule; Expert CPS Schedule; Expert PPCC Schedule; Real-time Central Control; RF Plant Control; etc. This system allows users to build, off-line, required parameter and waveform pulse schedules and compare these with any existing pulses or schedules. Numerous hooks have been included to validation and “flight simulation” software.

The same software is used by the operators in the Control Room to actually load and review the forthcoming pulse, allowing all the same validation and checking routines, and giving instantaneous comparison to any old pulse or schedule. The Level-1 software is used throughout JET. However, in principle, it could be used anywhere in the world to define a JET experimental programme.

Real-Time Central Control

In 1996, the possibility has been introduced to control any of the Heating (NB, RF, LH) or Gas Introduction Systems directly from measured signals. Over 160 diagnostic signals have been routed to a central VME Controller with a modular programmable logic, to feedback directly on the requested heating or requested gas supplies. Hooks have been provided into the Plasma Protection System to close the pulse down in the case of undesirable conditions arising. This system has been used successfully to optimise the plasma energy and neutron yield, to avoid disruptions, and to avoid unnecessary neutron production.

Plasma Protection System

This system has been upgraded to interface with new and changed computer and plant sub-systems. It continues to be reliable in terminating plamas in the case of undesirable conditions. It has significantly reduced the stresses on the vacuum vessel during disruptions.

Neutron Monitoring

The utility NPLAN is used to budget the plasma neutron yield with the aim of controlling vessel activation. This system has been upgraded to improve its reliability and to include the 14MeV D-T neutron yield in preparation for DTE-1 operation.

Gas Inventory

A new utility, GasPlan, has been written to record the amounts and types of gas injected into the torus. This information is necessary to know how much and what gases will be recovered from the torus each time the torus cryo-pump is regenerated.

Jotter

JET Protocol requires the Session Leader to enter pre-and-post pulse and pre-and-post session comments into the JET database. This has traditionally been done by the Control Room Assistant transcribing a hand written report into the computer after each session via the Jotter utility. This year, the Jotter programme has been integrated into the new suite of "JET Logging" programmes, with automatic transfer to the IBM mainframe for archiving. This has allowed Session leaders to enter and edit the information directly.

References

[1] P. Lang, P Cierpka, and P Kupschus, High repetitive pellet injectors for plasma density control, 19th Symposium on Fusion Technology, Lisbon, Portugal, September 1996.

[2] A. Rossi, et al., First measurements of gas balance and chemical composition in the Mark I pumped divertor phase of JET using the Gas Collection System, 23rd EPS Conference on Controlled Fusion and Plasma Physics, Kiev, Ukraine, 1996.

Vacuum Systems

Operations

The vacuum systems performed very well during 1996 - reliability was the best since the start of operations. This coupled with the prompt dedicated action of the "on-call" team ensured that very little JET operational time was lost due to vacuum system problems.

Vessel Baking

A new gas baking control system was commissioned at the end of the Mark IIA shutdown. Cascade control is utilised to give accurate control of the torus temperature and a programmable profiler enables constant rates of heating and cooling. The torus temperature, for the control, is computed by a new high reliability measurement and interlock system from 16 torus thermocouples. The normal operating temperature of the torus (320°C) can be maintained to within 1°C by the new control system. The normal heating and cooling ramp rate for the torus has been set at 10°C/hour. Previously there was only limited control of the heating and cooling rates and some leaks occurred after cycling of the vessel temperature. Using the new controlled rate, there have been no leaks on the torus which could be attributed to thermal cycling.

In preparation for DTE1, the circulating gas of the baking plant gas loop has been changed from air to helium. This is primarily to stop the transport of activated air (gamma emission from N16 decay) into unshielded areas. To maintain a low inlet to outlet temperature differential at the torus interspace, while preserving the heat transfer, a higher blower speed is required with helium than with air. The blower has been successfully commissioned to run with helium at 4800 rpm, twice the previous speed in air.

Gas Introduction

The high gas pumping speeds of the divertor cryo-pump have meant that for some operating scenarios it was difficult to maintain the desired fuelling rate. The ten main torus gas introduction modules have been upgraded to provide a flow of up to 2barℓs^{-1} each . This was achieved

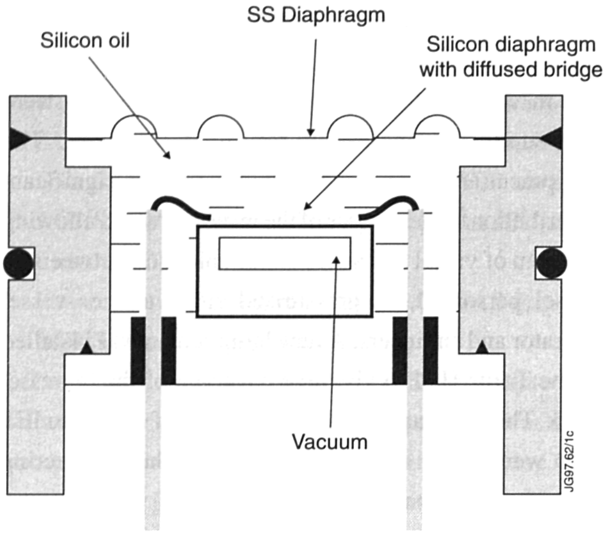

Fig.58: Piezo-resistive sensor

by increasing the operation pressure of the system from 1bar to 2.5bar and by increasing the travel of the piezo-ceramic actuator of the piezo-dosing valve (by the application of higher excitation voltage). To cope with the increase in gas introduction module reservoir pressure and prepare for the higher radiation levels expected in tritium operation, a new high accuracy pressure gauge was developed. The gauge sensor (Fig 58) uses a silicon diaphragm with a diffused piezo-resistive bridge. High doping levels ($\sim 10^{19}$ boron atoms cm^{-3}) are used to give the bridge a good level of radiation tolerance. The bridge is constructed and operated to give high sensitivity enabling the first stage of conditioning electronics to be moved away from the sensor head to a shielded position behind the iron limbs, where the electronics is further shielded from neutrons using polythene. The excellent performance of these gauges has been proven during the 1996 operation and hence they will continue to be used in future.

In preparation for DTE1, a piezo-valve was prepared for tritium gas introduction. The valve is located in a separate secondary containment and connected to the AGHS gas distribution system by means of a secondary-contained line. This gas introduction module (Fig 59) will be used for gas puffing (up to $\sim 500 mb\ell s^{-1}$). The gas from this module can be either injected through a main horizontal port at Octant No.6 near the plasma mid-plane. Alternatively, selection valves downstream of the piezo-valve permit gas injection into the divertor region.

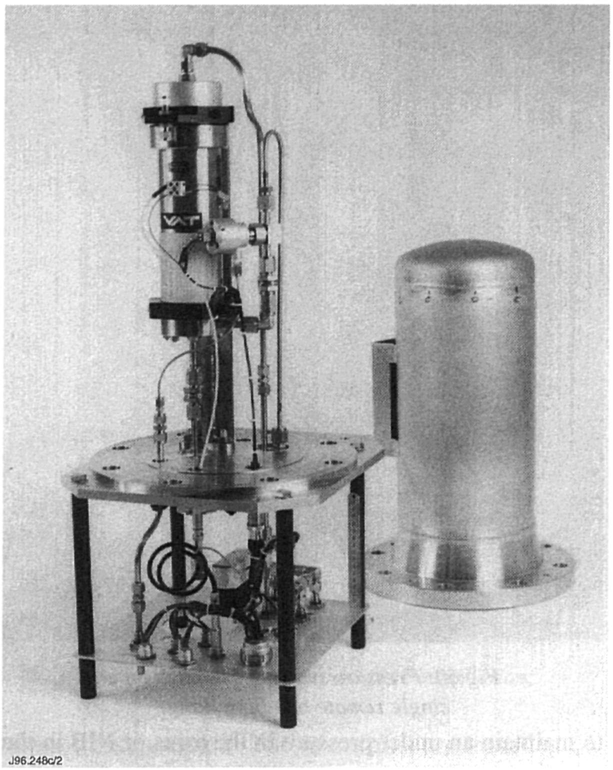

Fig.59: Tritium gas introduction module (GIM-15) - Piezo-valve with secondary containment and control equipment;

Glow Discharge Cleaning

The new glow discharge cleaning gas introduction system was commissioned during restart period following the Mark IIA shutdown. The system, through its new control cubicle, allows flow control of up to four different gases into the torus for glow discharge cleaning (GDC) and lithium beam alignment. New GDC control sequences take advantage of the this new system to make GDC an automated process. GDC has been used extensively to help recover the vacuum conditions following the two shutdowns. In addition, it is used routinely following regeneration of the divertor helium loop and prior to beryllium evaporation. In this case, the most effective scenario has been to do about two hours of D_2 GDC followed by two hours of He GDC. The deuterium glow is most effective at oxygen removal and the He glow is most effective at removal of hydrocarbons and deuterium depletion. The new control sequences and the gas introduction system have allowed this to be an automated process with the changeover of gases being done without local manual intervention.

Interlocks

In preparation for DTE1 and for greater machine safety, new interlocks have been commissioned. Of particular importance are the torus and NIB 200mbar interlocks, which open the relevant turbomolecular bypass valves to enable the active gas handling exhaust detritiation system

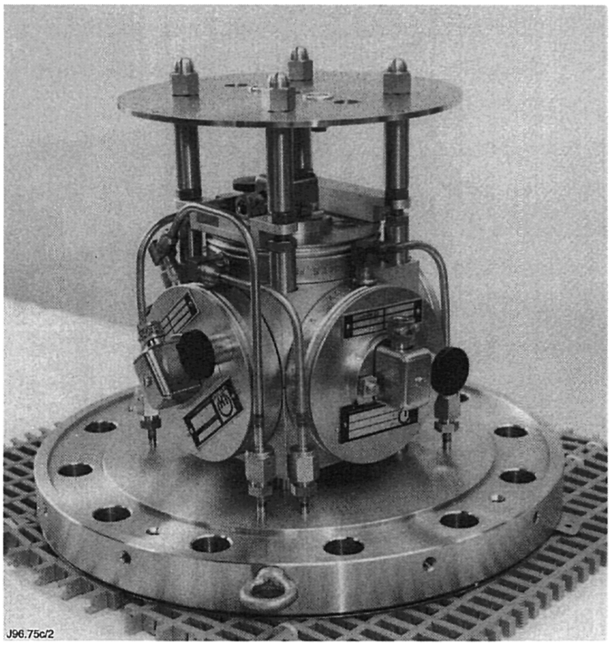

Fig.60: Pressure switches mounted on a single remote handling flange

to maintain an under pressure in the torus or NIB in the case of a large leak. These interlocks form part of the torus safety case for DTE1 and hence have been tested to formal and rigorous procedures. These interlocks have been implemented via new pressure switch modules.

Up to five pressure switches are mounted on a single remote handling flange (Fig.60). The modules are of all-welded construction and are UHV compatible.

In-vessel Communications and Video Systems

The in-vessel video and communications systems were reinstated and maintained for shutdown work. The equipment and support continued to make a significant contribution to the success of the in-vessel work, allowing freedom of visual and audio communication between in-vessel personnel, in pressurised suits, and ex-vessel operator and engineers. A new large screen was installed in the Torus Hall to give live coverage of the in-vessel work. This was particularly appreciated by visitors to JET who were given a unique insight into the engineering activities being performed inside the JET vessel.

Radiation Hard Mass Spectrometers

The design of the JET radiation hard mass quadrupole mass spectrometer has been upgraded to include electron multipliers to provide greater sensitivity. In addition, the control electronics has been upgraded to provide greater computing power. This allows the parameters of the quadrupole filter to be controlled on a mass-by-mass basis giving greater diagnostic potential.

Exhaust Monitoring System

To provide central data collection and some control related to pulses, the AGHS distributed control system has been

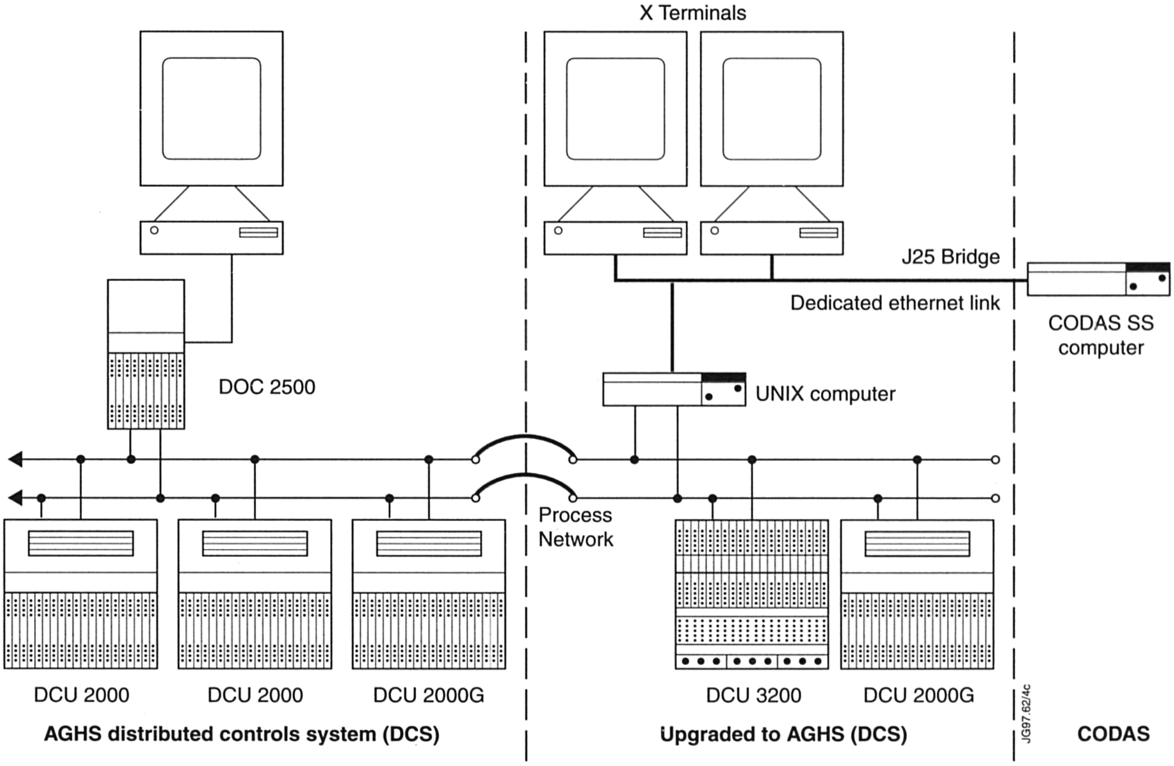

Fig.61: Exhaust monitoring computer systems;

upgraded to link it to CODAS through an ETHERNET (TCP-IP) connection (Fig 61). A protocol has been developed so that the following new facilities are available:

- AGHS plant status available on CODAS mimics;
- Data from CODAS data available for AGHS mimics;
- AGHS data available at rates up to 1 Hz for JET pulse files on CODAS;
- Indirect control of AGHS plant by CODAS through AGHS control sequences.

The interface will be used in DTE1 to isolate the torus backing line from the AGHS pumping over a 10 minute period of a tritium pulse. During this time, the torus exhaust gas will be collected and analysed with ion chambers, pressure gauges, and a residual gas analyser.

Torus Overpressure Relief Flap Valve

As part of DTE1 preparation, the JET safety case required the inclusion of a relief flap valve at the exhaust port of the beryllium filter to act as back-up pressure relief, which was pre-set at an overpressure greater than that of the rupture disc. Currently, the rupture disc perforates at ~1060mbar, whilst the flap valve is adjusted to 1230mbar. The flap valve will provide additional protection against the release of tritium into the Basement following a major in-vessel water leak. Additionally, the self closing property of the flap valve would facilitate pumping of the exhaust vapours/gases by the AGHS EDS from the active gas handling system.

JET Interspace System

For the tritium phase of JET, all items on the torus which could lead to a significant leak in the event of failure, are required to have double containment. Then, if the primary side (the side with a direct interface to the torus main vacuum), developed a leak there would be a secondary barrier to prevent ingress of air and, in the worst case, egress of tritium. Thus all windows, and a majority of bellows and feedthroughs, were designed and installed with a double barrier, making a total of some 330 interspaces. These are then interconnected to form the interspace system of JET.

A system of manifolds with the facility to connect up to eight interspaces, is installed on the machine as close as possible to the interspaces to which they are attached, each manifold being equipped with a pressure monitor, an output valve and blow off valve to prevent overpressure. The manifolds are installed on the upper and lower main vertical ports and the main horizontal ports of all octants, and number 45 in total. A typical main vertical port installation is shown in Fig 62. The interspaces are hard piped to the manifolds with insulating breaks installed, where main bellows are crossed to prevent eddy currents. Each manifold sub-system is back-filled with 500mbar of neon to provide a trace gas indication on the torus mass spectrometer should any primary side develop a leak.

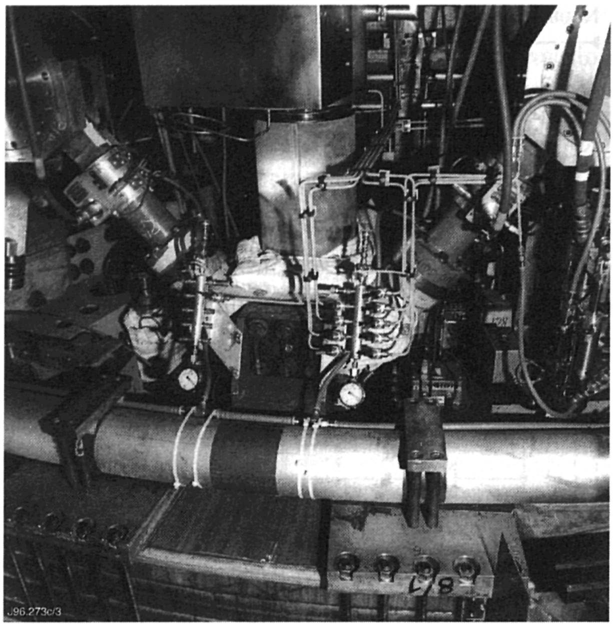

Fig.62: A typical main vertical port installation;

Vessel Ventilation System

The requirement for a vessel ventilation system for remote handling operations originates from the post-DTE phase, when man-access into the vessel is not possible and all in-vessel operations will be undertaken remotely using the pumping chamber access on Octants Nos.1 and No.5. Hence, the need for a facility which would maintain an underpressure in the vessel during these operations.

The output facility consists of two separate systems coming from the lower main vertical ports on Octants No.6 and No.8, to the torus crown. The crown will be connected for the operation of the ventilation system to the exhaust detritiation system in the AGHS. The valves used are the standard JET type-remotely operable spring closed single action. The filter unit consists of a vacuum vessel fitted with DN100 V-band input and outlet flanges and an array of seven HEPA or

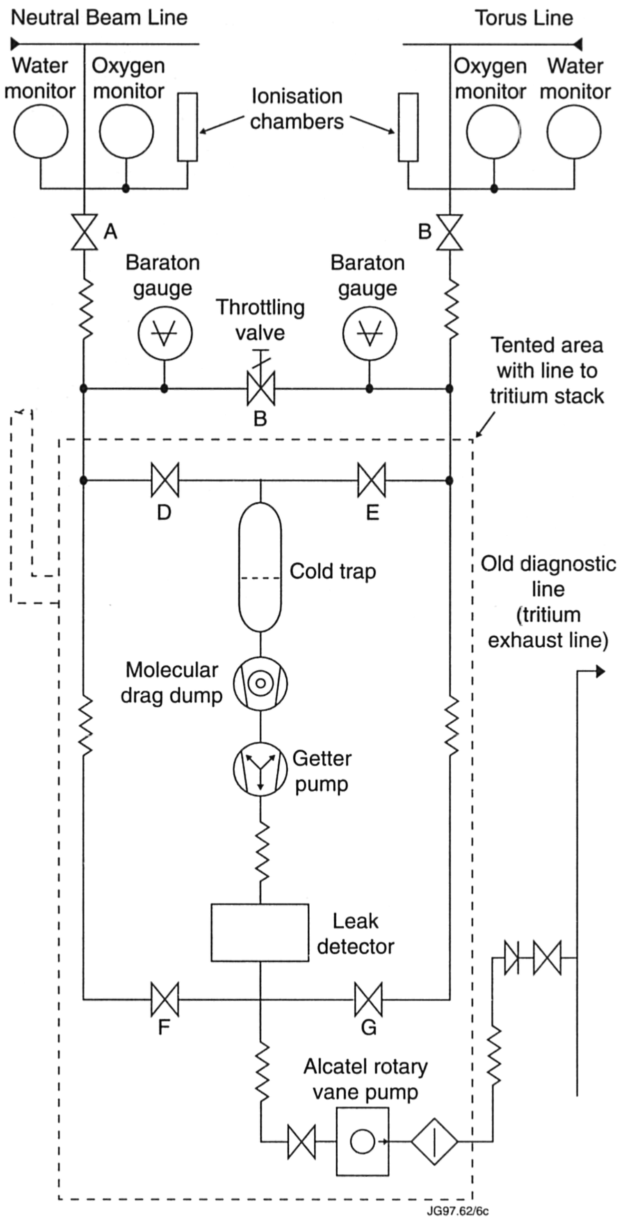

Fig.63: Schematic of the leak detection set-up;

equivalent filters installed inside to prevent dust migration into the crown and to permit the design flow of air to be maintained. The filter unit is installed at a sufficient distance from the torus to permit manual filter change after DTE1 and remote handling filter change after DTE2 should this be required.

The input system of the vessel ventilation system is designed to enable the vessel to be maintained at a set level of depression by admitting air to the vessel through a valve situated on the upper limiter tube, the D-sector of Octant No.4. The atmosphere side of the valve will be connected to a filter unit to prevent ingress of particles to the vessel and egress in the unlikely event of an accidental overpressure.

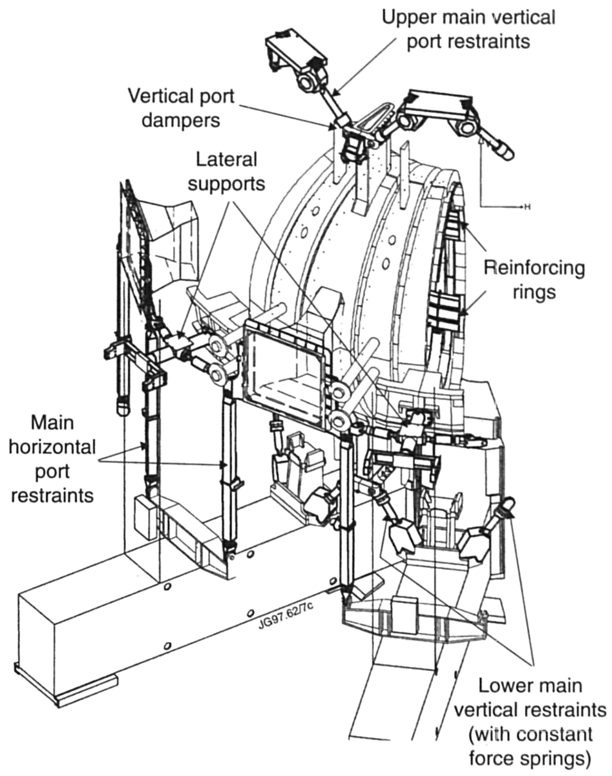

Fig.64: Restraints connected to the main horizontal and vertical ports of the vacuum vessel;

Leak Detection Rig and Remote Reference Test Leak System

Due to limited access to the Torus Hall during the tritium phase, a leak detection rig (Fig 63) is installed in the west wing/roughing pump area connected to the torus and neutral beam pumping lines via valves. If an air leak occured in the torus, the neutral beam boxes and pellet injection box would be valved off, the gas from the torus would flow, through the leak detection rig, into the neutral beam crown to Building J25. If a leak occurs in the neutral beam boxes, the process would be reversed with gas flow to the torus crown.

A throttling valve is installed, as the system may not be able to take all the gas load through the leak detector, so some of the gas is bypassed. The rotary vane pump is only for initial pump-down of the system.

Due to anticipated complications of leak testing during and after the tritium phases, and the effect of the divertor cryopump on the torus pressure, a torus remote reference test leak system is being developed to enable a greater understanding of operational leak situations. The system should, when required, remotely mimic an actual torus leak of about 10^{-4}mbarls^{-1} in air, N_2, He^4 or Ne.

The system design will include remote operation via the CODAS VC computer system to:

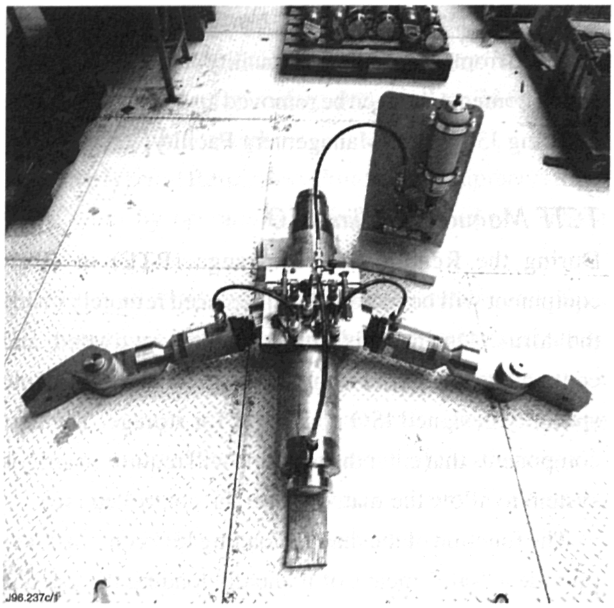

Fig.65: One sub-assembly of the lateral support: bridge between mechanical structure and transformer links with hydraulic cylinders and links to main horizontal ports.

- provide a quick, reliable cross reference of the torus mass spectrometer (RGA) systems;
- enable the calibration of the west wing tritium phase leak detection system;
- enable calibration of the Neon-filled interspace leak detection system.

The reference test leak will be manufactured by laser drilling a 2mm diameter hole in a 50mm thick gold foil mounted in a fitting on the torus behind a pneumatic isolation valve, and supplied with various gases from a local gas distribution box.

Vessel Supports

The main vertical port restraints were fitted with pneumatically actuated brakes, replacing the previously installed thermomechanical locking devices. The new system is free of backlash and can be engaged at any vessel temperature. This has resulted in substantial gains in available operating time.

Hydraulic dampers were modified to implement internal pressure relief valves to avoid excessive stress on main vertical ports during fast lateral vessel displacements. Horizontal restraints were fitted connecting the main horizontal ports via a hydraulic damper system to fixed bridges between mechanical structure and transformer limbs.

All systems (Figs 64 and 65) were installed during the 1995/96 shutdown, commissioned and proven to meet their design requirements.

Waste Management

The Waste Management Group is responsible for provision of facilities in support of interventions and shutdowns, respiratory protection equipment and disposal of radioactive and beryllium wastes. This involves the operation of five controlled areas, including the Torus Access Cabin (TAC), Building K7 complex, the two Beryllium Handling Facilities and the Waste Handling Facility (WHF) in Building J30, together with operation of the liquid waste drainage system.

Preparation for DTE-1

The Waste Management Group have continued to contribute to preparations for DTE1 and the subsequent Remote Tile Exchange (RTE), support for in-vessel work, and routine beryllium and radioactive waste handling.

At the beginning of 1996, the group had a complement of 45 personnel due to the additional staff that were employed to provide support for the Mark II divertor shutdown. By the end of 1996, the staff numbers had fallen to their base level of 24. This level of staffing is required to operate four facilities with radiation and beryllium hazards, the site active drain system, a plastics workshop, a suit maintenance and training facility, with the ability to respond quickly to support any in-vessel interventions required during operational phases.

DTE1/RTE Preparations

Environmental Agency Authorisation

A review of the site authorisation to hold radioactive material and dispose of radioactive waste has been carried out. A draft authorisation has been prepared and its introduction is in train via the recently formed Environmental Agency which now incorporates the former Her Majesty's Inspectorate of Pollution (HMIP).

Procedures for Emergency Response

Procedures and techniques have been developed in conjunction with the Patrol Service to address the use of self contained breathing apparatus with gas-tight suits. An extensive training and familiarisation programme has been carried out to ensure that appropriately trained staff are available to deal with any foreseeable incident or occurrence.

Detritiation

A research and development contract has been placed to study the processes involved in reducing the tritium content of graphite tiles after removal from the vacuum vessel. This will enable a wide variety of options to be explored for re-use or disposal of the tritium or substrate material. In 1996, work was carried out in conjunction with AEA Technology, Winfrith, to identify suitable graphite tiles for this study from the existing waste stream.

Mobile Controller Unit

As part of the pre DTE planning, it was determined that some jobs in the Torus Hall and Basement, following DTE, may have to be carried out in full pressurised suits. A mobile pressurised suit controlling station was manufactured allowing breathing air to be supplied to a maximum of four suited operators. This mobile unit also has audio communications to each suited operator and a monitor to allow a suited operator to carry a camera and relay pictures back to the control station.

Active Handling Enclosure

As part of the preparations for DTE, an assessment was made of the facilities that may be required to be able to maintain equipment that might be removed from the machine after the introduction of tritium. The main facility where maintenance of contaminated equipment is maintained is the Beryllium Handling Facility, which is being upgraded by a ventilated enclosure to allow contaminated components that are outgassing tritium to be placed inside and be maintained. A high airflow rate would be established away from the operator to reduce as much as possible the level of airborne tritium exposure.

AGHS Airlock ISO

The AGHS required an airlock to allow materials to enter and leave the building without breaking the containment boundary of the building. To provide more flexibility than a conventional airlock, a design based around a freight ISO container was produced. The ISO container was designed with double doors at both ends to allow it to act as an airlock with additional features to allow the container to be attached to the building and become an extension. This allows the container to act as an airlock for new materials entering the facility and for packages leaving the facility where the external surfaces of those packages can be shown to be free of contamination.

If packages need to be removed from the facility whose external surfaces cannot be shown to be free from contamination the container airlock can be filled from the facility. Once full, its doors can be closed and then detached from the Building J25 facility so that the container and its contents can then be removed and checked onto the Building J30 Waste Management Facility.

TCTF Manual Handling ISO

During the Remote Tile Exchange (RTE) in 1997, equipment will be removed and replaced remotely inside the torus. During this shutdown, the activated and contaminated material from the vessel will be loaded into specially designed ISO containers for storage. The new components that enter the machine will require an airlock system to allow the material into the controlled area.

The function of the manual loading ISO container is to provide a "safe" means of manually loading the gas box modules into the TCTF and onto the end of the short boom. To do this requires two functions to be addressed. Firstly transferring the modules into the facility without allowing potential contamination from spreading beyond the boundaries of the facility ("safe" transfer). Secondly, providing handling equipment to allow these modules to be loaded onto the short boom.

Safe transfer of modules into the TCTF can be achieved by using the manual loading ISO container as an "airlock". Once the double doors have been removed, the manual loading ISO container has been exposed to the TCTF environment and must be considered as potentially contaminated. Before opening the rear or side doors, the manual loading ISO container must be cleaned and a contamination survey conducted by Health Physics, then be isolated from the TCTF environment by closing the zipped membrane. If the clearance smears show there was no contamination present when the smears were taken and the container has remained isolated from the TCTF environment, then it is safe to open the rear and side doors to re-load the container with a the next load of modules.

Once the container has been restocked with material, the rear and side doors are closed and access from the TCTF can be re-established by unzipping the membrane and thus potentially re-contaminating the container. This sequence can then be repeated as new batches are required to be transferred into the TCTF.

Shutdown Support

Mark II Divertor Shutdown

The first three months of 1996 where taken up with the end of the Mark II Divertor Shutdown which was nine months long with almost 4000 man-entries into the vessel in total. These last few months saw the change in working from 20 hours per day, 6 days per week to, 24 hours per day 13 days per fortnight.

Three types of Respiratory Protective Equipment (RPE) were worn by operatives during this shutdown. These were:

- Powered Half Suits: Used for initial and final inspections, their advantage being that they are battery powered and do not require a trailing airline which may damage in-vessel components, then protection was not fitted at the start and end of the shutdown;
- Polyurethane (PU) Airline Fed Full Suit: Used for the bulk of entries and where heavy work was being undertaken;
- Airline Fed Disposable Half Suit: Used for inspection or difficult access jobs that only involve light industrial work. To protect the suit from damage, a reusable PU oversuit was designed and manufactured in the PVC Workshop that protected the arms and torso.

Both the full- and half-suits use the same PU airline for air supply and communications.

Inner Wall Cladding and Divertor Leakage Shutdown

The Torus Access Cabin (TAC) was installed in its full configuration, with the first entry on the 3 October 1996. The initial plan accounted for 17 days of in-vessel work with the ROs controlling the work from ex-vessel. With the TAC in its full configuration, there are 24 hours of consecutive lifting operations to remove all the components. The removal of the TAC at the end of this shutdown was once again spread over three days with some of the peripherals being removed before in-vessel operations had ceased.

Due to the limited time available, the in-vessel work consisted of four entries per day; this required the TAC to be manned for 20 hours per day for 21 of the 22 days from 3-26 October.

Plastic Workshop

Items manufactured by the workshop fall into two categories: In Vessel-related; and Ex-vessel work. Requests by Ex-vessel Responsible Officers placed the largest demand on the Plastic Workshop services in 1996.

The main users were Diagnostic and Vacuum Groups, both of whom use a large number of isolators, which are of a relatively simple design. In addition, a large number of small components manufactured by the Workshop can be found in all the facility's operated by the Waste Management Group.

Due to the Workshop's continuing development programme, a number of technical problems involving the covering of component before they are placed in a contaminated environment were overcome. This included the production of Pyrophric Powder Bags for incident response, the development of Gaiters and End Effectors for the Mascot Servo Manipulator System, and more recently the development of an oversuit for use with the Gas Tight Suits.

In the weeks leading up to the Divertor Leakage and Inner Wall Cladding Shutdown about 75% of the PVC Workshop output was In-Vessel related. To manufacture the components produced by the Plastic Workshop a total of 2.25km of plastic was required. This represents approximately 36,000 separate RF welding operations, which is ~5km of RF welding.

Waste Operations

JET Active Drainage System

The Radioactive Drainage System collects potentially radioactive aqueous wastes from various sources such as machine cooling systems, Torus Hall air conditioning systems and active handling contamination control areas. It pumps the arisings from the collection tanks through pipework to the monitoring tanks, which are situated at the far west end of the Culham site. The waste water is monitored for radioactivity, beryllium contamination and other contents to ensure that all the discharges off-site are within regulatory limits.

In October, a major series of function tests on the radioactive drain were undertaken in preparation for DTE1. The function tests were carried out to replicate, demonstrate and formally record that all aspects of the radioactive drain functioned as required, such as the normal routine operation of the radioactive drain at all of the collecting, transfer and discharge tanks, the operation of the abnormal condition alarm system, and the non-routine operation of the radioactive drain when under exceptional conditions.

Building J30 Operations

The Waste Handling Facility in Building J30 is the building where potentially radioactive waste, collected from the various active handling facilities and radiologically controlled areas set up to maintain the machine, is handled prior to its disposal. The major services provided in Building J30 are the compactor, ventilated slit box for waste sampling and all facilities to enable personnel to work in a beryllium and radiologically controlled area. Groups of waste are sampled, assessed for radioactivity and beryllium content, compacted or packed into drums for despatch to the Harwell Radwaste Service. An important element of the radioactive waste handling is the quality system to ensure that the correct steps are followed and correct and relevant information concerning the waste is maintained throughout the process of waste generation, collection, handling, packaging and despatch. This provides efficient planning and working and correct despatch documentation that is acceptable to Harwell and BNFL, the owners of the final disposal site.

The major innovation in Building J30 operations was bought about by the introduction of the "Cutting Room". The usual drum into which solid radioactive waste is packed at JET for off-site despatch is an industrial type package which meets the IP2 type requirements. Such drums have a certificate of approval for transport package design. A critical requirement in the use of the drum is the restriction of on contents to the length of each individual item must not exceed the drum diameter and the weight of any individual item must no exceed 10kg. Long items of waste such as pipework were, in earlier years, put to one side whilst other waste was handled in anticipation of suitable facilities to handle them. The "Cutting Room" is a separate ISO container that can be docked onto Building J30, to enable its access and the general support of the Waste Handling Facility. The working centre of the cutting room is a ventilated machine bench to hold cutting tools and vice clamps to hold material.

Tritium Safety

1996 has seen the satisfactory conclusion of the safety analysis of the planned DTE1 experiment. A Safety Case extending to six volumes with a total of ~2300 pages was presented for peer review and finally accepted by the JET Safety Committee. This is expected to lead to the granting of approval for DTE1.

The Safety Case includes both a deterministic section, which demonstrates that dose limits will be complied with and identifies the key safety systems necessary; and a probabilistic section which analyses the frequency and consequences of accidents to demonstrate that the ALARP (as low as reasonably practicable) principle can be met in relation to accidents involving radioactivity.

Control and Data Acquisition System

The JET Control and Data Acquisition System (CODAS) is a fully integrated computer-based system. A network of computers is used for control, monitoring, data acquisition and storage of data. This network is also used to analyse the data from the tokamak, its power supplies, auxiliary equipment and diagnostic devices. CODAS also provides the following common services: Network Information Services, Mail, file servers, printing, network monitoring and off-line program development. These services have grown and this year over 120 systems are in use.

JET components and diagnostic devices are grouped into a number of sub-systems. Sub-systems which control/monitor parts of the tokamak and its auxiliary systems are referred to as control sub-systems; diagnostic devices are grouped in a similar way into diagnostic sub-systems. Each sub-system is controlled and monitored by one dedicated computer interfaced to the machine and its diagnostics through CAMAC and/or VME instrumentation. Real-time applications are implemented in front-end CAMAC and VME-based processors.

Networks and Computers

Networks

The networks are functionally split into two main parts. The first part (Off-line Network) is the site-wide network (JETnet), which supports the PC and UNIX connections from the offices and laboratories on site. The second part (On-line Network) consists of all the sections required to support the control of, and data collection from, VME and PC-based systems distributed across the site. The various connections provide the structure of the client/server UNIX system and the data collection and transfer medium. Also included in this part are some dedicated sections of Ethernet which are used for real-time systems.

Isolation between Off-line and On-line Networks

In preparation for tritium operation, it was decided that access from outside the main Control Rooms to the on-line computers should be more strictly controlled.The aim is been to prevent unauthorised operations on the on-line

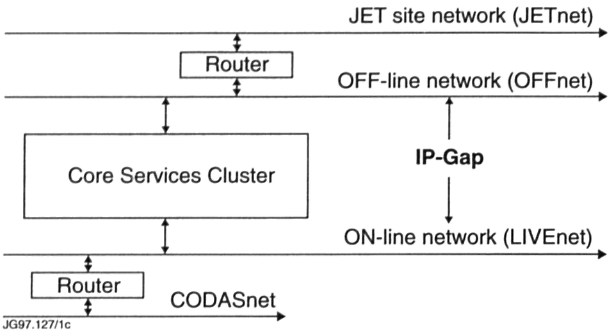

Fig.66: JET Computer Network Structure

CODAS computers due to user error. The initial idea was to have a simple "air gap" between the operational and off-line systems. This was considered too drastic a solution (shared services/resources would have to be duplicated on both sides of the gap; mimics would only be usable anywhere except in the Control Rooms and there was still a requirement for site-wide access to the operational networks for commissioning and monitoring purposes). These considerations let to the design and implementation of what has come to be known as the IP-Gap.

The IP-Gap blocks any IP (Internet Protocol) traffic between the off-line and the on-line networks. It consists of a number of CODAS computers (the core services) that are connected to both the on-line networks and the off-line networks, and as such can communicate with all the CODAS computers (Fig.66). However, direct communication between the off-line and on-line machines is not possible when the gap is 'open'. All cross-gap traffic across the IP-Gap ismust be handled by proxy servers in the core services computers. The implementation of the IP-Gap is now completed and it has been in routine operation for some time in preparation for DTE1.

Table VII: CODAS computer inventory at end of 1996.

Category	Quantity end 1995	Quantity end 1996	Machine Type end 1996	Memory MBytes	Disk GBytes
Server	6	0	Sun SPARCserver2	64	5.2
	4	1	Sun SPARCserver5	64	45
		9	Sun SPARCserver4	64	5.2-27
		1	Sun SPARCserver20	128	4
		2	NAC FAS1400		16
MMI	7		Sun SPARCserver2	64	0.4
	4	9	Sun SPARCstation2	32	0.4
	5		Sun SPARCserver5	64	0.5
		5	Sun SPARCstation5	64	0.5
		15	Sun SPARCserver4	160	0.5
Host Systems	4	8	Sun SPARCserver2	32	0.4
		3	Sun SPARCserver5	64	0.5
Control Systems	16	23	Sun SPARCserver2	32	0.4
		2	Sun SPARCserver5	256	0.5
Diagnostic systems	9	13	Sun SPARCserver2	32	0.4
Communication	2	2	Sun 4/670	128	1.6
	4	5	Sun SPARCserver2	32	0.4
Off line development	22	17	Sun SPARCserver	64	0.4
	4	1	Sun SPARCserver5	32	0.5
		3	Sun SPARCserver4	160	1
		3	Sun SPARCserver20	128	2
Computer totals	87	122			
X-terminals	112	121			

Table VIII
Quantitative Information on CODAS Installation

ITEM	End 1995	End 1996
CODAS Interface Cubicles	173	175
CAMAC Crates	211	208
CAMAC Modules	2,718	2,726
Eurocard Modules (Signal Conditioning and Power Supplies)	7,095	7,405
VME modules	406	539
CAMAC Serial Loop (Fibre Optic)	24	24
On-line Computers	57	92
Off line and Commissioning Computers	32	30

Network Performance Upgrades

The site-wide computer network, JETnet, used to be a shared Ethernet network with bridges connected to hubs in each building. To improve the bandwidth and to facilitate subnets an Ethernet Switch/IP Router was introduced. This switch provides the full Ethernet bandwidth for in each building branch concurrently. The switch is in turn connected to the CODAS Off-line systems, the IBM Mainframe and the Analysis Cluster by means of two FDDI rings. FDDI rings, being ten times faster than Ethernet, are needed to accommodate the concentrated traffic from the switched Ethernet branches.

Similar upgrades have been applied to the internal CODAS On-line networks on the on-line side. CODASnet (network interconnecting all on-line CODAS systems), JPFnet (network for Jet Pulse File transfer) and DATAnet (network connecting the UNIX host systems to the front-end equipment) also used to be shared Ethernet networks with bridges and are now configured with Ethernet switches/IP Routers as well. The JPFnet upgrade will be followed up with an upgrade to the IBM mainframe interface to further increase the efficiency of the JPF transfer further.

Computer Performance and Upgrades

The load on the CODAS computers has again significantly increased over the year. Several subsystems showed signs of overloading due to the increase in the number of points being monitored, and general increase in functionality. To alleviate this situation, a computer hardware upgrade programme has been defined and will be implemented by the beginning of DTE1. A large part of this upgrade was completed by the end of 1996 (see Table VII).

Table IX
Review of CODAS Electronics Stock Holding
(Installed, pre-procurement, loaned and spares)

ITEM	End 1995	End 1996
CAMAC system modules	911	911
CAMAC digital I/O modules	848	875
Timing system (CAMAC, VME & Eurocard)	1,726	1,725
CAMAC analogue I/O modules	1,475	1,492
CAMAC auxiliary controllers	150	149
CAMAC powered crates	280	278
U-port adapter	213	213
CISS modules	1,339	1,339
CCTV	683	683
Cubicle frames	406	414
Power supply modules	2,165	2,164
Intercom, Public Address, Computer terminal network	895	972
Pool instruments	1,030	1,026
Analogue I/O in Eurocard	3,384	3,681
Digital I/O in Eurocard	5,102	5,106
Eurocard sub-racks	1,044	1,048
Network active devices	598	871
VME modules and sub racks	894	1,052
PROFIBUS Components	-	45
Totals	**23,143**	**24,044**

Electronics

Most growth in CODAS' installed electronic hardware has used VME and related technology. CAMAC systems have grown little, leading to an overall hardware growth of 4% (Tables VIII and IX for quantitative details).

During 1996, five new cubicles were designed, constructed and installed, 248 fully-documented hardware improvements were made and 207 maintenance interventions were recorded. Two of the new cubicles were for the safety system, CISS, as part of a gradual introduction of the Siemens 115F programmable logic controller.

The Composite Timing and Trigger Signal, CTTS, is now used for most new timing signals. Its data is encoded onto a single widely-distributed data stream, to which has been added a secure method of resetting any VME system from the Control Room. This is particularly valuable in restricted areas because it avoids a personal visit to the VME crate.

The new CPL1 CAMAC module became available this year. It uses a Xilinx 4013 gate array, so that it can be programmed to perform different functions. The first design emulates a CTM2 stopwatch module that is no longer in production.

A new fibre-optic link for analogue signals has been introduced. It is based on two Eurocard modules of JET design, a pair of which provide four precision connections. The two modules are a UVF3 and a UFV3. These are of flexible design, but in the basic mode the input voltage signal is converted into a train of light pulses whose repetition frequency represents the voltage. The pulse train is reconverted in the receiving module. The novel aspect is the inclusion of programmable controller, various switches, references and converters so that the link can trim itself in gain and offset on command.

Control Systems

Plasma Protection Systems

The Plasma Protection System (PPS) has been reorganised and the latched and unlatched parts have been separated. This simplifies the protection system giving a better overview and a more reliable operation. The main parts of the PPS have been changed, as follows:

- the Plasma Enable Windows System (PEWS) now handles all the unlatched digital and analogue signals that used to be divided between two different parts in PPS;
- the Plasma Termination Network PTN is limited to handling digital latched signals only;
- the Plasma Fault and Protection System (PFPS) now handles latched analogue signals only.

Real-Time Power Control

The Real-time Power Control system has proven to be very successful when configuring and conducting different feedback control scenarios. In particular, important achievements been made within burn control, RDD control and l_i control.

The real time power control system consists of three main parts: the Real-time Plasma Protection (RTPP); the Real-time Central Controller (RTCC) and the Real-time Signal Server (RTSS):

- RTPP is a new implementation of what used to be the Plasma Fault and Protection System, PFPX;
- RTCC is now upgraded to provide six independent controller networks and one simulated network. Each network can be configured to perform controller, filter and logic functions as and when required for feedback control experiments;
- RTSS has the same functionality as previously, but is now expanded to provide more signals.

Downstream of the RTCC are six local controllers which can either be cascaded to RTCC or take their reference from waveforms and control the plant locally. The local controllers are:

- Neutral Beam Local Manager (NBLM), which has had its control algorithm improved. JPF logging has also been included in this function;
- Radio Frequency Local Manager (RFLM) is now a full implementation of the local control of the ICRF plant replacing the previous hardware based control system;
- Lower Hybrid Local Manager (LHLM) is implemented according to an adaptive feedforward principle. This is to achieve fast response from the system despite sampling rate limitations in the local instrumentation;
- Alfven Eigenmode Local Manager (AELM) is made for the specific purpose of tracking Alfven Eigenmode resonances in the plasma;
- Plasma Density Local Manager (PDLM) is an inclusion of the Plasma Density Feedback System.

Vacuum System.

Several activities under the vacuum heading have been completed in preparation for the DTE1 campaign:

- A link for communicating commands and data between the control system of the Active Gas Handling System (AGHS) and CODAS has been installed;
- Control of the GIM15 tritium introduction module;
- Interface to new GDC system;
- Control of insulated line breaks on West Wing gas lines;
- Various new pressure gauges monitoring, interlocks etc.

Vessel Systems.

A new monitoring system (Machine Diagnostic System - MDS) for monitoring accelerations and displacements of the torus has been built. The system provides 196 transient-recorder channels at up to 10kHz, using a combination of UXD1 and VPL1 modules. The VPL1's processor is programmed to give, for each signal, recording at high rates for transient analysis, medium speed permanent storage for the whole JET pulse, and continuous low speed trend recording indefinitely. An extension was made to the KC1 magnetic measurements diagnostic using similar equipment.

Diagnostic Support

During 1996, design and implementation of several CODAS for new diagnostics (KT7D - Divertor VUV and

Table X
JET Pulse File Sizes

Pulse File Type	maximum size 1994/95 campaign (MBytes)	maximum size 1996 campaign (MBytes)	increase 1995/96
JPF (JET Pulse File, after each pulse)	135	145	+7%
LPF (Late Pulse File, from subsystem computers daily)	30	275	+916%
DPF (Delayed Pulse File, late modifications)	<1	~2	not available

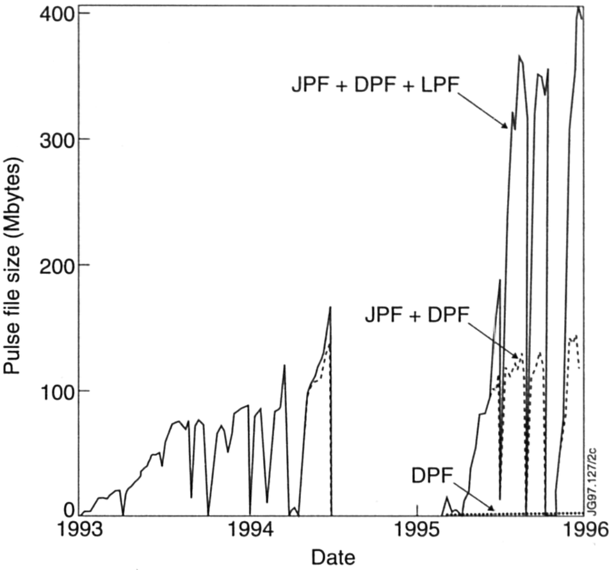

Fig.67: Maximum pulse file size: 1994-1996;

XUV Spectroscopy, KM2 - 14 MeV Neutron Spectrometer, KM9 - Magnetic Proton Recoil Neutron Spectrometer 14 MeV) have been undertaken.

Major changes have been applied to about 20 existing systems. This includes a new version of the KF1 (High Energy Nuclear Particle Analyzer) system as well as a complete rebuild of the KC1D (Magnetic Pick-up Coils) data acquisition. The new KC1D system not only copes with 50% more signals but the new system has been structured as a two crate system allowing for the separation of the KC1D magnetic signals from the auxiliary signals (e.g. halo current).

Data Collection and Transfer

The data collection system has continued to operate well. The amount of data collected has again considerably increased. Table X gives the maximum file sizes for the various Pulse File components during the 1994/5 and 1996 campaigns in table form, whereas Fig.67 plots the weekly maximum sizes over time for the last three years. Figure 68 shows the time evolution of the total JET data storage from beginning of operation in 1982. This passed the 1 TeraByte (240 Bytes) mark at the end of September 1996.

This dramatic increase in data collection caused some performance problems on CODAS computers and networks. These were partially compensated by a modest increase in computing power and by the above described network restructuring, but mainly by deferring data collection to the late pulse file phase, which only takes place as time permits between pulses and (mainly) at the end of the day's session. Local disks to hold the JPFs on the diagnostic system have been increased in size to cope with the extra volume and disks have been added to some of the control systems for similar reasons.

Plant Essentials Monitoring System

CODAS is now heavily dependent on network communications and shared resources. This sharing is very efficient and effective, but it does increase the (small) probability of several subsystems simultaneously failing to gather data. The Plant Essentials Monitoring System (PEMS) is an auxiliary distributed data acquisition system that has been installed during the year. It provides uninterrupted service to track critical signals from the JET plant in the case of outage of the central CODAS control computers.

PEMS has been conceived with a modular approach, using mainly off-the-shelf hardware and software components. It uses on two PC-based monitoring stations in the Control Rooms and a data-acquisition network based on PROFIBUS-DP field-bus technology, which is now a recognised European standard (EN-50170).

PEMS is, by design, easily expandable and modifiable. A star-shaped fibre-optic backbone is used to interconnect five separate network segments. Along each segment, digital and analogue peripheral input modules are interlinked by means of shielded twisted pairs. Connection to the backbone is via a media converter.

The current configuration supports 28 analogue and 40 digital direct inputs. In addition, two RS232-to-PROFIBUS protocol converters extract multiplexed data streams from pre-existing PLCs (DPIS system). The

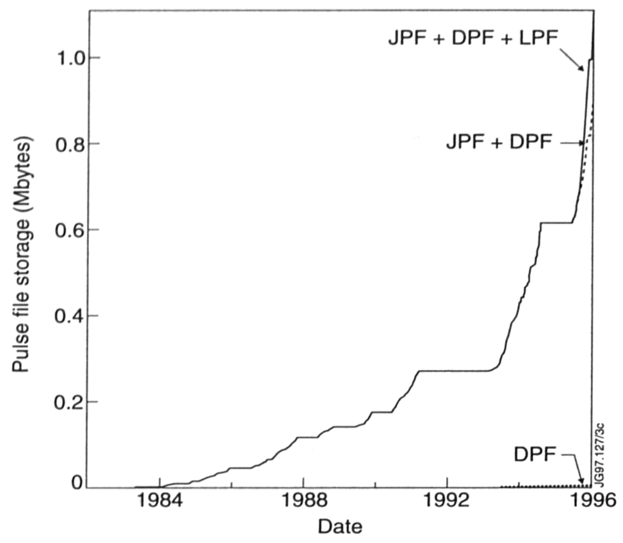

Fig.68: Pulse file storage: 1982-1996.

signals currently being monitored include torus pressures and temperature, plus various other parameters and status variables from the cryogenics, water cooling and compressed air systems.

Auxiliary Systems

For reasons of compatibility between various emergency services, the site mobile radio system was rebuilt to use UHF frequencies. New aerials were mounted on the highest buildings to improve the coverage between buildings and off-site. A set of five base-station transceivers placed close to the aerials are now controlled through long audio link cables by small control units in various Control Rooms. New arrangements were needed also to allow two mobile-radio users to communicate through the 3m-thick biological shield. This is achieved by using audio cables to link transceivers on either side of the shield.

The Public Address system has been extended to cover all outside areas as well as within buildings. This is so that emergency messages can advise people to enter buildings. Messages can be pre-recorded or spoken into a microphone, and can be directed to various zones and buildings. For other messages, the internal zones themselves have been sub-divided. The Control Room itself has been added as a zone so that the Engineer-in-Charge can alert various controllers to imminent events.

Regeneration of cryo-panels is a critical process in JET. It often occurs at night when staff presence is at a minimum. So dedicated intercom stations have been installed close to five critical plant items to give immediate direct communication with the Control Room for a patrolman.

Control Rooms

The J2 Control Rooms' desk layout has remained unchanged, the modified Session Leader suite introduced last year having been well received. More screens have been added, so that there are now 125 terminal screens and 40 non-interactive screens. The terminals are a mixture of X-terminals, IBM terminals and SPARC Workstations.

The connection of terminals to computers has been made more flexible by the commissioning of a structured wiring scheme. A few sockets are provided near every desk. Each socket is permanently wired to a central patch-panel in the Computer Room. Every computer port is separately cabled to the same patch-panel. To add a new terminal, it is simply connected to a local desk socket, and a jumper cable inserted in the patch-panel to connect it to the appropriate computer or network. The new cabling scheme is compatible with all the types of terminal in use, so that a quick response can be made to changed operational needs.

Operations-related Databases

CODAS maintains all its operations-related data in a databases, which use the Mimer software product. The databases covers a wide range of information. It is used to hold all information about CODAS hardware and a number of operations-related pages (e.g. shift rosters). The CODAS Mimer database software has been upgraded to the latest version and is now running under the SOLARIS2 operating system.

This move has allowed newer technologies to be used for interfacing to the CODAS data including MS*Query, MS*Access, MS*Word, MS*Excel via ODBC from PC platforms and TK/Tcl from UNIX platforms. There is also a general trend towards using web-based technology for the distribution of data.

For many years, CODAS has used computer based logging as its record of operations. The log consists of a structured mix of manually entered data concerning the actual operation (e.g. description of fault events) and of machine entered data (e.g. the start time of a JET pulse count-down). The JET logging operational support application has been completely upgraded and now uses a Mimer database as its data repository. The logging application is now available with different user front-ends for different operational groups. Web technology is used to automatically distribute generated operational reports inside JET. In addition search engines are available to query the structured data. As the other logging reports the search engine uses Web technology which makes the user interface platform-independent.

Data Management

The Data Management Group is responsible for the provision of the Central Computing Services based on three separate networked computing environments: the IBM mainframe system; a cluster of high performance UNIX systems; and the site-wide network of PCs and Apple Macintoshes. The Group is also responsible for the management of JET data and for organisation and control of routine data processing.

IBM Mainframe

This computing service is based on an IBM 3090/300J three way processor mainframe with two vector facilities. There are 360 Gigabytes (GB) of disc storage and a further 7200 GB of automated cartridge tape storage. The service has been operating since June 1987, initially based on an IBM 3090/200E dual processor mainframe. This was replaced in February 1990 with the present 3090/300J, almost doubling the processing capacity. The system was upgraded in 1995 to increase the central memory to the maximum of 256MB with a further 256 MB of expanded memory.

A Memorex-Telex automated cartridge tape library (ATL) with eight cartridge tape drives was installed in February 1992 and upgraded in November 1993 to 3490E (36 track) tape technology, doubling the storage capacity to about 2400 GB. This ATL provided storage for all the raw JET data (JPFs), archived processed JET data (PPFs), and the backup and dump tapes. The ATL, together with the introduction of automated operations via the product AutoMate/MVS completely eliminated the requirement for operator cover.

In early 1996, the original disk storage subsystems comprising 110 GB of 3380D/E disks was replaced by 300GB of 3390-2 disks, both to provide a much needed increase of storage capacity and to improve operational reliability. In April 1996, a StorageTek automated tape library with eight 3490E compatible tape drives and a capacity of ~ 6000 tape cartridges (~ 4800GB) was installed in addition to the original Memorex Telex ATL, to provide capacity for the predicted large increase in JET data. The raw data (JPF) and dump tapes have been moved into the new ATL, releasing space in the original ATL for the increasing backup and archive tape load.

The JET IBM Computer Centre was originally established at the UKAEA Harwell Laboratory but was relocated to Building J2 at JET in July 1992. The service has since run very successfully from the JET location, providing the expected improvement in communications, integration with the UNIX and PC systems, and a reduction in staff. The integration was further improved early in 1994 with the introduction of TCP/IP services on the mainframe using the Interlink SNS/TCPaccess software to provide more efficient means of data transfer between the mainframe and the UNIX and PC/Mac systems. It also improved the terminal emulation access from the PCs and UNIX systems. During 1995, the operating system (MVS/ESA) was upgraded to the latest version, providing enhanced facilities in various areas, including the data management software.

The mainframe plays a major role as the data server and archiver, and also provides a powerful computer facility used by about 200 staff. The workload includes the main Drawing Office CAD system (CATIA) supporting 32 CAD stations, interactive data manipulation and extensive scientific data processing including the high priority Intershot data processing.

JET Analysis Cluster

The JET Analysis Cluster (JAC) is a networked cluster of IBM RS/6000 workstations running AIX/UNIX (version 4.1). The service was established in 1994 to provide computing power for the more CPU intensive applications that were previously run on the IBM mainframe. The cluster runs close to 100% utilisation on each system seven days per week and demand for this type of numerically intensive computing, together with high performance graphics grows each year. The initial configuration consisted of three model 370 RS/6000s. During 1994 and 1995, four model 380s were added together with a model C10 as a central server, and a model 3AT dedicated for CAD robotics use. During 1996, a further six model 390s were added together with three 42Ts for Drawing Office use, giving a total computing power estimated as about 750 megaflops, (Linpack 100 DP benchmark) compared with 50 Mflops (scalar) or peak theoretical of 300 Mflops (vector) on the mainframe.

Following upgrades in 1996, the standard memory configuration is now 128 MB RAM, and the total disk space is 96 GB. Groups of machines are allocated for priority work to specific user groups (Simulation, Analytical Theory, Structural Analysis, etc), but all the systems (including the Drawing Office CAD stations outside working hours) are controlled by the Loadleveller Software, making all resources available to all users, if the priority users are not using the system.

A variety of codes are run on the JAC Cluster. These include plasma edge modelling (EDGE2D), plasma core modelling (JETTO) and transport analysis (TRANSP). Other modelling codes commonly used are DIVIMP, CASTOR and FIDO. Structural Analysis studies are also undertaken, using PATRAN, NASTRAN and ABAQUS, and four RS/6000s are used by the Drawing Office to run the major CAD system CATIA.

Client-server database services include the PPF system for the access and storage of all JET processed data, CATIA Distributed Systems which access engineering models stored on the mainframe. 1996 has seen considerable progress in client-server applications between the JAC cluster and the IBM mainframe, including intershot EFIT. This is in line with the philosophy that workloads should be assigned to the most appropriate platform: CPU intensive applications or interactive visualisation are generally best suited to the JAC cluster, whilst the mainframe is far superior as a data server or general multi-user environment.

The IBM ADSM client-server data-management product was installed in 1996, enabling the JAC Cluster to be backed-up automatically overnight to the IBM mainframe, improving the reliability and speed of data restoration. ADSM also allows users to archive data to the mainframe, releasing local disk space for current data.

Management of JET Data

JET has passed two symbolic milestones in this area in 1996 the total raw JET data collected and archived has exceeded 1 Tera-byte (~ 1.1×10^{12} bytes), and the number of public PPFs written has exceeded one million. During 1996 operations, there was a continuing increase in the amount of JET data with JPF sizes up to 405 MB per pulse (140MB in the main JPF and the rest in DPF's and LPF's), yielding up to about 8 GB of data each day of operation. The data is transmitted from the CODAS UNIX systems to the IBM at speeds of about 600 kilobytes per second ensuring that the JET data are available for analysis on the mainframe promptly after collection on the CODAS systems. The development of a very sophisticated data archiving and retrieval system based on a cache of 50 GB of on-line disc backed by tape storage on the ATL currently accommodates over 1200 GB of raw JET data (JPF), which is compressed by a factor of about 2.5 for storage. The total data collected in 1996 was 524 GB, compared with less than 200 GB in each of the previous two years. The system gives almost instant access to any JPF data that is available on disc (typically about 3 weeks data production). Data less recently accessed is restored automatically from cartridge tape and average time to access data is less than 1 minute for any shots back to day one (1983).

The Intershot Analysis is run automatically when the data is received on the IBM and the analysed results are stored in the Processed Pulse File (PPF) database system This corresponds typically to about 20 MB of analysed data per shot. A major upgrade to the PPF system was made in 1994, converting the system to a client server architecture. This has led to the full PPF system on the mainframe being available on the CODAS and JAC UNIX systems and Windows NT PC systems, to provide an essential centralised data storage and retrieval system for use within a distributed analysis environment. An application of this, implemented in 1996, has been to port EFIT, the most CPU intensive Intershot program, to the JET Analysis Cluster. This is synchronised with the mainframe Intershot processing steps via the PPF event notification system and provides faster results while freeing resources on the mainframe.

The Central Physics File (CPF), stored and used under the SAS environment, forms a complete higher level data selection and storage system. A subset of all data is extracted at time points of interest, determined by the Time-slice program and the interactive time slice editor, TED, and stored in the SAS databases. These data are the basis for extended statistical analysis, and the source for other extracts such as the TRANSPORT and EDGE data base. During 1996, TED was updated to allow authorised users to mark time points at which events of interest occurred during a pulse: this information can also be accessed in the CPF.

The widely used JET data display facilities (JETDSP) on the mainframe have been continuously enhanced in response to user requests, to provide a versatile data display and manipulation environment. In addition, an interface to allow users on the JAC and Windows NT systems to read PPF data into the visualisation package IDL via a simple command has been developed.

The real-time analysis systems installed last year and the Intershot PPF analysis programs, have been substantially modified to reflect the changes to the torus with the introduction of the Mark IIA divertor. In particular, this has affected analysis of data from the magnetics diagnostic KC1D, which is used to deduce the basic plasma parameters.

PC and Apple Macintosh and PC Network Services

There are about 600 Personal Computers (PCs) and 80 Apple Macintosh systems on site. The vast majority are connected to the site-wide Ethernet (JETnet). The Data Management Group is responsible for the support of these systems and for the provision of networked PC services. The Apple Macs are mainly used by the secretarial and typist staff for word-processing. The PCs are used for a wide variety of tasks including word processing, data analysis, data acquisition, program development, terminal emulation, CAD, project planning and circuit design and analysis. There is an increasing use of PC systems for the analysis and display of data. The networked services are presently provided from six servers running the Banyan Vines network operating system. This provides services such as electronic mail (integrated with mail systems on UNIX, the mainframe and the Administrative Department PCs), shared file access with central backup service, centrally provided software, access to shared printers and to the UNIX and IBM computer systems. The number of users on the PC network continues to increase, with typically over 350 simultaneous users logged on. The PC network services have become essential tools for many JET staff and the reliability of the network over the past year has been high, although there have been occasional service interruptions to sections of the site, and the performance at times is variable. Continued maintenance on the software, hardware and data management has been required during 1996 to deliver this level of service.

During 1996, there has been extensive preparatory work for the planned move to new servers running the Microsoft Windows NT Server Network Operating System, which will replace the Banyan Vines servers and support a variety of client systems (PC and Mac) operating systems, including Windows 3.11, Windows 95, or Windows NT depending on the level of the desktop client hardware, and the user requirements. The NT services were established in 1996, and some user groups such as Reprographics are supported from these servers. A growing number of high performance PCs are now running Windows NT workstation, and the Group is providing support for several different NT based network services.

The Group has worked closely with CODAS in the provision of the computing services over the sitewide network, coordinated by the regular NeST (Network Service Team) meetings. These services include the secure connection to the external world via the Internet connection through the commercial provider, Pipex (UK) Ltd. In addition to e-mail services, this provides File Transfer (FTP) and remote computer access (Telnet) services from essentially all off-line computers on the JET site networks, and incoming access to the IBM mainframe for authorised users subject to a number of security restrictions. A major increase in the use of World Wide Web services has taken place during 1996. This 'platform independent' technology has also been used extensively for the propagation of information within the Project, with the growth of the JET Intranet.

Diagnostics Systems

The status of JET's diagnostic systems at the end of 1996 is summarized in Table XI and their general layout in the machine is shown in Fig.69. The staged introduction of the diagnostic systems onto JET has proceeded from the start of operation in June 1983. Operational experience on the existing diagnostics has been good and most of the systems have operated automatically with minimal manual supervision. The resulting measurements have been of high quality in terms of accuracy and reliability, and have provided essential information on plasma behaviour in JET. Further details on specific diagnostics systems are given below.

Plasma Viewing

Video camera systems operating in the visible have been routinely as one of the primary diagnostics on JET. There are seven video cameras installed:

- two wide angle view endoscope cameras which cover ~60% of the inner torus surface (unfiltered);
- one wide angle view CID camera which covers the full height of the plasma (unfiltered);

Table XI: Status of JET Diagnostics Systems, December 1996 - Existing Diagnostics

System	Diagnostic	Purpose	Association
KB1	Bolometer cameras	Time and space resolved total radiated power	IPP, Garching
KB3D	In-vessel divertor bolometers	Time and space resolved radiated power	JET
KB4	In-vessel main plasma bolometer	Time and space resolved radiated power	JET
KC1	Magnetic diagnostics	Plasma current, loop volts, plasma position, shape of flux surfaces, diamagnetic loop, fast MHD	JET
KC1D	Magnetic pickup coils	Plasma geometry in divertor region	JET
KD1D	Calorimetry of Mark I divertor target	Power balance of divertor plasma	JET
KE1E	Edge Thomson scattering	T_e and n_e in scrape-off layer	JET
KE3	LIDAR Thomson scattering	T_e and n_e profiles in core plasma	JET and Stuttgart University
KE4	Fast Ion and alpha-particle diagnostic	Space and time resolved velocity distribution of alpha particles and fast ions	JET
KE9D	Divertor LIDAR Thomson scattering	T_e and n_e profiles in divertor plasma	JET
KF1	High energy neutral particle analyser	Ion energy distribution up to 3.5MeV (ICRF minority and fusion products)	Purchased from Ioffe, St Petersburg
KG1	Multichannel far infrared interferometer	$\int n_e d\ell$ on four vertical chords and four horizontal chords – electron density	CEA, Fontenay-aux-Roses
KG3	O-mode microwave reflectometer	n_e profiles and fluctuations	JET and FOM, Rijnhuizen
KG4	Polarimeter	$\int n_e B_p d\ell$ on four vertical and four horizontal chords – poloidal magnetic field	JET and CEA, Fontenay-aux-Roses
KG6D	Divertor microwave interferometer	$\int n_e d\ell$ on sightline across the divertor plasma	JET
KG7D	Divertor microwave comb reflectometer	Peak n_e on sightline across divertor plasma	JET
KG8A	E-mode reflectometer	Measurement of n_e fluctuations and profiles in edge and SOL	JET and CFN IST, Lisbon
KG8B	Correlation reflectometer	Density fluctuations	JET
KH1	Hard X-ray monitors	Runaway electrons and disruptions	JET
KH2	X-ray pulse height spectrometer	Monitor of T_e, impurities and LH fast electrons	JET
KJ3	Compact, re-entrant soft X-ray camera	MHD instabilities, mode identification, plasma shapes and impurity transport	JET
KJ4	Compact, in-vessel soft X-ray camera	MHD instabilities, mode identification, plasma shapes and impurity transport	JET
KJ5	Active phase, soft X-ray cameras	MHD instabilities and vertical position sensing, DT compatible	JET
KJ6	Compact VUV camera	Divertor view in VUV	JET
KK1	Electron cyclotron emission spatial scan	$T_e(r,t)$ with scan time of a few milliseconds	NPL, UKAEA Culham and JET
KK2	Electron cyclotron emission fast system	$T_e(r,t)$ on microsecond time scale	FOM, Rijnhuizen
KK3	Electron cyclotron emission heterodyne	$T_e(r,t)$ with high spatial resolution	JET
KK4D	Electron cyclotron absorption	$n_e T_e$ profile on sightline across divertor plasma	JET
KL1	CCD viewing and recording	Plasma viewing	JET
KL1E	Endoscopes	To allow an unrestricted view of the divertor in the visible and IR	JET
KL2	Impurity flux camera	Impurity influx from the divertor targets with high spatial resolution	JET
KL3A	Infra-red camera (1 dim)	Divertor tile temperature profiles	JET
KL3B	Infra-red camera (2 dim)	Divertor tile temperature profiles with high dynamic range	JET
KL4	Infra-red protection diodes	Machine protection – divertor tile temperature	JET
KL5	Fast spectroscopic cameras	Fast D_α measurements at two toroidal locations for ELM studies	JET
KL6	Colour view of divertor tiles	Colourimetry – used for erosion/redeposition measurements	JET
KM2	14MeV neutron spectrometer	Neutron spectra in D-T discharges, ion temperatures and energy distribution	UKAEA Harwell
KM3U	2.4MeV time-of-flight neutron spectrometer	Neutron spectra in D-D discharges, ion temperatures and energy distributions	JET and NFR, Studsvik

JG96.94/1

Table XI (continued): Status of JET Diagnostics Systems, December 1996 - Existing Diagnostics

System	Diagnostic	Purpose	Association
KM5	14MeV time-of-flight neutron spectrometer	Neutron spectra in D-T discharges, ion temperatures and energy distribution	NFR, Gothenburg
KM7	Time-resolved neutron yield monitor	Triton burnup studies	JET and UKAEA, Harwell
KN1	Time-resolved neutron yield monitor	Time resolved neutron flux	UKAEA, Harwell
KN2	Neutron activation	Absolute fluxes of neutrons	UKAEA, Harwell
KN3U	Neutron yield profile monitor and FEB	Spatial and time resolved profiles of neutron flux and fast electron Bremsstrahlung	JET and UKAEA, Harwell
KN4	Delayed neutron activation	Absolute fluxes of neutrons	Mol
KR2	Active phase, neutral particle analyser	Ion distribution function, T(r) and H/D/T flux ratios	ENEA, Frascati
KS1	Active phase spectroscopy	Impurity behaviour in active conditions	IPP, Garching
KS3	H-alpha and visible light monitors	Ionisation rate, Z_{eff}, impurity fluxes from wall and divertor	JET
KS4	Charge exchange recombination spectroscopy (using heating beam)	Fully ionized light impurity concentration, $T_i(r)$ and rotation velocities	JET
KS5	Active Balmer alpha spectroscopy	Neutral beam deposition, plasma effective charge and motional Stark measurement (for internal magnetic field)	JET
KS6	Bragg rotor X-ray spectroscopy	Monitor of low and medium Z impurity radiation	UKAEA, Culham
KS7	Edge charge exchange	Multichannel measurement of edge poloidal rotation, ion temperature and impirity density	UKAEA, Culham
KS8	Motional Stark effect diagnostic	Uses polarisation of Stark components of beam emission to measure pitch angle of magnetic field	JET, UKAEA, PPPL
KS9	Polarisation resolved passive spectroscopy	Radially localised source measurements from Zeeman splitting of lines	JET
KT1D	VUV spatial scan of divertor	Time and space resolved impurity densities	JET
KT2	VUV broadband spectroscopy	Impurity survey	UKAEA, Culham
KT3	Active phase CX spectroscopy	Fully ionized light impurity concentration, $T_i(r)$, rotation velocities and divertor sources	JET
KT4	Grazing incidence XUV broadband spectroscopy	Impurity survey	UKAEA, Culham
KT5P	Divertor gas analysis	Analysis of divertor exhaust gasses	
KT6D	Poloidal view, visible spectroscopy of divertor plasma using periscopes	Impurity influx, 2D emissivity profile of spectral lines	JET
KT7D	VUV and XUV spectroscopy of divertor plasma	Impurity influx, ionization dynamics, electron temperature and density	JET
KX1	High resolution X-ray crystal spectroscopy	Central ion temperature, rotation and Ni concentration	ENEA, Frascati
KY3	Plasma boundary probes	Vertical drives for reciprocating Langmuir and surface collector probes	JET and UKAEA, Culham
KY4D	Langmuir probes in divertor target tiles and limiters	n_e and T_e at the divertor and limiters	JET
KY5D	Fast pressure gauges	Neutral flux in divertor region	JET
KY6	50kV lithium atom beam	Electron density in scrape-off layer and plasma edge	JET
KY7D	Thermal helium beams	n_e and T_e in the divertor plasma (together with KT6D)	JET
KZ3	Laser injected trace elements	Particle transport, τ_p, impurity behaviour	JET
Kα1	Thin foil charge collectors	Lost alpha-particle detection	JET
Kγ5 & 8	Gamma rays	Fast ion distribution	JET

JG97.151/1

- one divertor endoscope camera which views the divertor from the outer midplane (interference filter CII);
- two divertor view cameras which cover the full radial extent of the divertor at two different Octants (interference filters for D_α, CII);
- one toroidal view camera which covers a substantial part of the toroidal extent of the divertor (interference filter for D_α).

A selection of the seven camera signals is automatically stored on six video recorders. The videos can be replayed between discharges in the Control Room. The video information stored on the tapes can be digitised using an image analysis system and stored in the form of standard PPFs on the mainframe. A main application of the new wide angle view cameras has been the investigation of areas of energy deposition during ELMs. A substantial part of the total energy

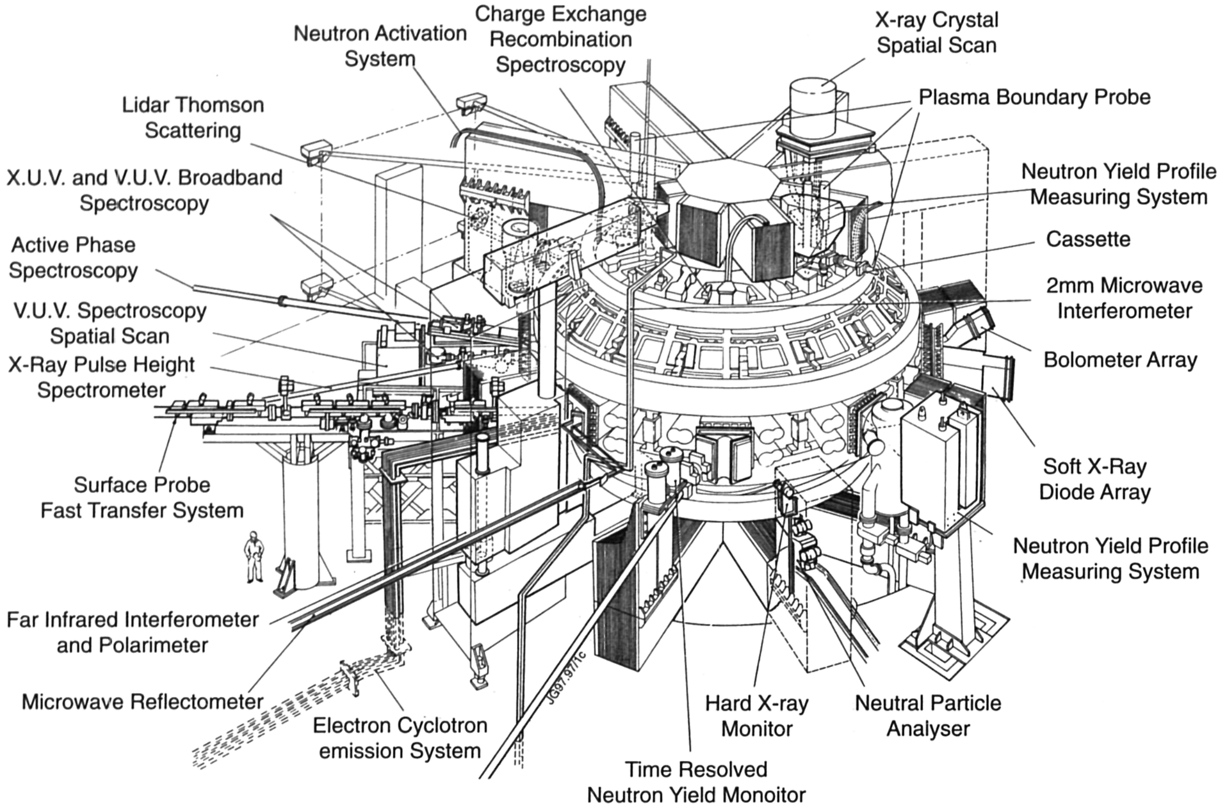

Fig.69: General layout of diagnostics in the machine

released during an ELM is deposited randomly on parts of the inner wall, well outside the divertor.

For direct quantitative measurement of the radiation intensity in the divertor region with high spatial and moderate time resolution ($\delta R \sim 3mm$, $\delta t=5ms$), three spectroscopic thermoelectrically cooled cameras (KL2) have been used. These cameras are looking on the same divertor region and use interference filters to measure the intensities at different wavelengths (D_α, CII, background at 523.5nm). The camera output is directly digitised, thus making the data more readily available for quantitative analysis than the conventional camera systems which use video tape. However, in order to keep the data storage requirements to a manageable size, the data is compressed to one-dimension by averaging the pixels toroidally. The camera data have been extensively used to study erosion mechanisms, ELMs, plasma detachment, etc. An example is given in Fig.70.

For the investigation of ELM events a fast linear CCD camera has been commissioned. It views the radial extent of the divertor from the top of the torus and is capable of a time resolution of 60ms.

Infra-red Measurements and Analysis

The infra-red diagnostics have been substantially upgraded during1996. The existing near infra-red linear array has been mounted with improved optics, which have resulted in lower background levels and better signals, despite the radiation damage sustained by the detector after two long

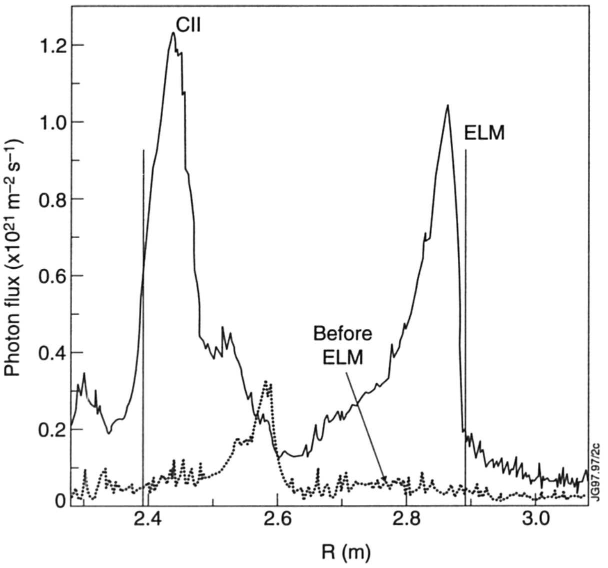

Fig.70: Radial profile of the divertor CII photon flux before and during an ELM

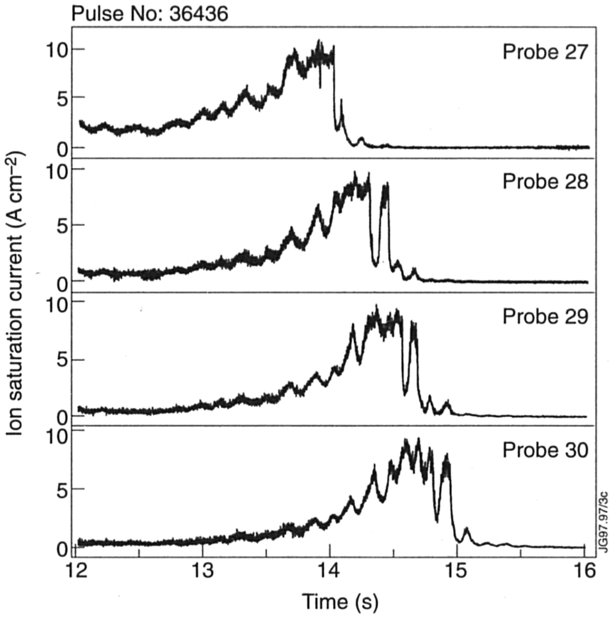

Fig.71: Current signal recorded by consecutive probes as the separatrix was swept across the outer divertor floor. The main plasma parameters were kept constant during this time. Note the similarity in the signals from each probe indicating that a constant (and known) area was exposed to plasma.

operational campaigns. The speed of the frame rate has also been augmented to achieve a scan time of 1.4ms.

The greatest advance has been in the installation of a second infrared camera. This is a custom built staring 2D camera. The controller uses multiple DSP architechture and high speed data transmission. The two dimensional detector, with 128x128 pixels of CdHgTe (CMT) works in the 3.4 to 3.5mm band. It provides a more linear response to temperature, and a better dynamic range than the linear array, as well as full 2D information on the temperature distribution on the target.

Other features of the diagnostic are its high speed (1.4µs full frame rate) and the possibility of subscanning a part of the array to increase the frame rate. In this way, the temperature of a thin region along the radial direction can be measured with a time resolution of 150µs. This feature is being used to study fast events such as ELMs.

Analysis tools have been developed for a PC and UNIX environment, using the commercial programme MATLAB. This ensures an easy visualization of otherwise huge datafiles (120MB/shot). Power calculations and surface temperature reconstruction were performed on the 12 processor PowerXplorer parallel computer system. The system has been adapted to the Mark II large tile design, and the processors have been divided to perform power deposition calculations with data from both the linear and the 2D camera.

Fixed Langmuir Probes

The target Langmuir probes continue to be a key diagnostic in the Mark IIA divertor campaign providing information essential for understanding the physics of divertors and to benchmark the accuracy of the EFIT and XLOC equilibrium codes. For the Mark IIA divertor several upgrades to the diagnostic system were implemented to extend its usefulness in the understanding of divertor physics and these are outlined below. The current design activity is the modification of the probes for inclusion in the Mark II-GB divertor with further optimisation of the probe tips.

The installation of 40 probes each in three 10mm gaps between the divertor tiles presented many technical difficulties despite which accurate installation tolerances were achieved. Figure 71 illustrates the ion-saturation current (I_{sat}) signal from a series of outer target probes as the separatrix was swept across the divertor floor with the main plasma parameters held constant. The remarkable similarity in the amplitude of these signals shows that each probe had the same known projected area when exposed to plasma. Pulses, in which the two strike points are swept across the divertor floor with the same main plasma parameters, are routinely run to provide an assessment of the erosion rate of the probe tips. Comparison of I_{sat} measurements for a particular probe over a period of ~2000 pulses indicate that the probes were initially eroded at the beginning of plasma operations and then stabilised with a much reduced erosion rate. Measurement of the probe tip heights before installation and in-situ after a period of operation have allowed the change in probe area to be accounted for so that the ion-flux can be quoted with certainty.

During the Mark IIA divertor shutdown the so-called 'fast' system was also implemented to enhance fluctuation studies started with the Mark I divertor probes. With the new system it was possible to remotely switch I_{sat} or floating potential signals individually from 16 probes to the 250kHz CATS data acquisition system. Ten probes were evenly distributed about the corner of the Mark IIA divertor in one toroidal location and a further six at the same relative poloidal location but at a different toroidal location were also used. This arrangement meant that both studies of turbulent transport and of the spatial distribution of ELMs could be undertaken, which were further enhanced through the simultaneous use of the reciprocating probe systems.

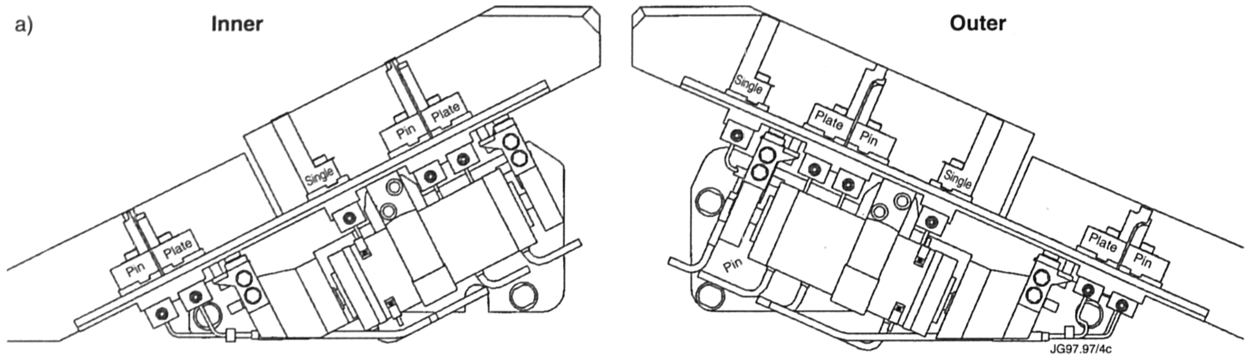

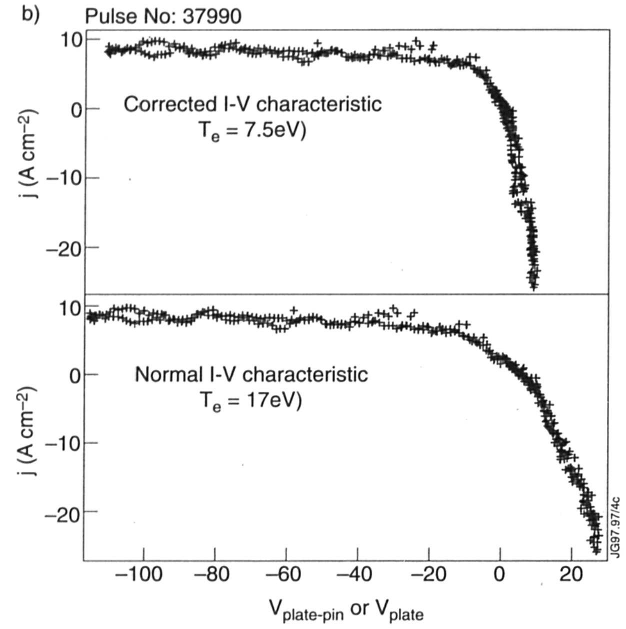

Fig.72: (a) Cut away view of the "pop-up" probe systems in Mark IIA divertor with plate-pin and single probes installed; (b) I-V characteristics with and without correction for the sheath potential drop recorded by the pin-plate probe during the high recycling phase of an ohmic plasma.

To provide information on the effect of the plasma sheath resistivity on the probe derived electron temperature under high recycling conditions, when the electron-to-ion saturation current ratio approaches unity, ''plate-pin' probes, which were installed on the pop-up probe system in the divertor, were used Fig.72(a). The system uses the ambient magnetic field to act on the current carrying coil to pop up a rail containing the probe tips. In this way, measurements could be made at pre-determined times of interest, thus minimising the exposure of the probe tips. This system is particularly useful when measurements are made with the pin-plate probes as the plate has a relatively large effective area and would become severely eroded if continuously exposed. The pin-plate arrangement allowed measurement of the potential drop across the sheath between the pin and current measuring plate from which a sheath resistance could be obtained. An example of the characteristics with and without correction for the sheath potential drop recorded by such a probe arrangement is shown in Fig.72(b). Correcting for the sheath resistance in the analysis of the probe data gives an electron temperature of 7.5eV which, with no correction applied, it would be 17eV.

Elsewhere within the machine, the inner and outer poloidal limiter Langmuir probes were upgraded. In addition, eight Langmuir probes were successfully installed above the RF antenna. These limiter and RF probes provide electron temperatures and densities in the main scrape-off layer useful for the optimisation of the coupling of RF and LHCD power to the plasma. The probes were also used to assess the uniformity of the glow-discharge cleaning at the beginning of operations. The probes now routinely record data for every pulse when a particular probe measures a current signal above a threshold level set within the control software.

Reciprocating Probe Systems

The two reciprocating probe systems were extensively used during the Mark IIA divertor campaign. The systems continued to provide data on the variation of scrape-off layer thickness as a function of main plasma parameters for comparison with the Mark I data and to provide experimental data as boundary conditions for the upstream scrape-off layer parameters calculated from "onion-skin" and EDGE2D model calculations which use target probe data, at different stages of detachment, as initial parameters. From these data and the modelling, the cross-field heat diffusivity, χ, can be calculated. Current activities now include comparison of scrape-off layer thickness and cross-field heat diffusivity with various collisional and collisionless models for cross-field transport.

A significant enhancement of the systems has been the use of boron-nitride body probe heads with graphite

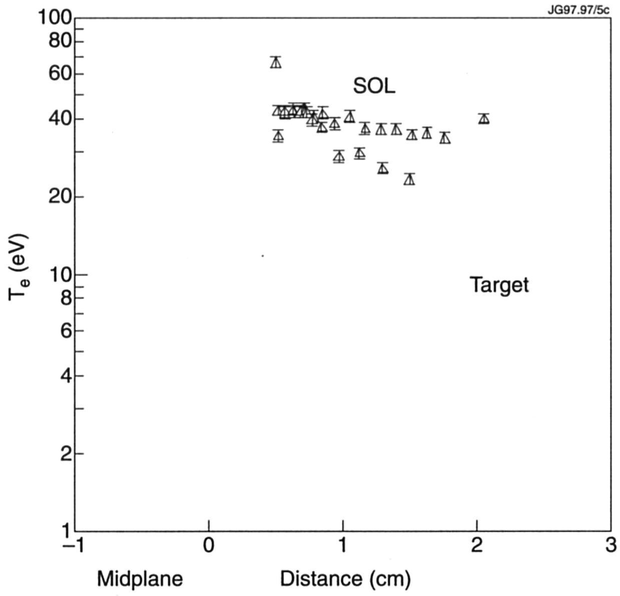

Fig.73: Target and main scrape-off layer profiles recorded during a neutral beam heated ELM-free H-mode plasma.

Langmuir tips and the successful utilisation of the new 400mm stroke system. Both systems can now be viewed by the wide-angle camera systems when reciprocating into plasma. The lack of jxB forces on the boron-nitride and its immunity to thermal stress fracture has meant that the probe could be routinely used to perform scrape-off layer measurements in high input power ELMy and ELM-free H-mode phases of a pulse in which previously only a few data were available. In the Mark IIA divertor campaign, most of the reciprocating probe measurements have been made under these conditions. Typical target and scrape-off layer profiles obtained in an ELM-free H-mode are illustrated in Fig.73. The 400mm stroke system now means that all equilibria can be reached and extends further the region in which the probe determined separatrix position can be compared with the EFIT and XLOC equilibrium code calculated positions. This benchmarking of the magnetic equilibrium codes is also now more accurate following an in-vessel survey and accurate height setting during the Mark IIA divertor shutdown.

As well as using Langmuir probe heads, the Retarding Field Analyser (RFA) and a new fluctuation probe head were used during the Mark IIA divertor campaign. The RFA, which measures ion temperatures in the scrape-off layer, was used during the ELM-free phase of carbon pulses. A probe head was configured for the study of fluctuations in the main plasma scrape-off layer to complement measurements made with the 'fast' target probe system. The arrangement of the probe tips means that radial transport due to fluctuating ExB drifts at two radial positions can be recorded, using the CATS system, simultaneously. Used in conjunction with the 'fast' target probe system in ELMy H-Mode pulses the spatial distribution of ELMs in the divertor and main scrape-off layer can be obtained.

Thermal Helium Beams

This system provides measurement of the electron density and temperature from the inner and outer target plates towards the X-point. Such data are important for the understanding of divertor physics and serve to place more severe boundary conditions on models such as EDGE2D which previously had no experimental data to confirm its predictions. Following its introduction in the Mark I divertor, it has proven to be a versatile diagnostic which can relatively easily provide useful information.

The position of the helium injection points were modified in the Mark IIA divertor to ensure that the periscope systems (KT6D) could still be used to view the relevant HeI lines. In addition, another injection point from the outer-side of the divertor, which uses the KT3 system to view the HeI lines from above, was installed. This arrangement of nozzles gives flexibility to the system to make measurements relevant to a particular experiment. For example, the inner-base and outer-side nozzles are fed from the same gas feed so that electron densities and temperatures in the inner and outer divertor legs can be determined simultaneously. The amount of helium injected has little effect on the main plasma parameters and data have been recorded for a variety of target configurations under different plasma conditions. By using fewer fibres, it is possible to sample faster so as to investigate ELM behaviour in the divertor plasma.Using spectrometers has also meant that HeI lines at different wavelengths were used to determine electron densities and temperatures.

Following collaborative work with the TEXTOR team at KfA Jülich, Germany, where the diagnostic was originally developed, electron densities and temperatures can now be calculated automatically from the line ratio data. This makes it easier to compare the helium beam derived data with other diagnostic systems such as the target Langmuir probes and divertor LIDAR to assess the accuracy of the different methods under varying divertor conditions. Related to this, there is now extensive effort on the development of an interpretative model utilising the DIVIMP code linked to the atomic database ADAS.

A potentially large source of error in the determination of the electron densities and temperatures is the accuracy of the atomic data and extensive work is underway to ensure that the most accurate atomic data are used.

Development of de Laval nozzles is continuing. Initial results indicate that a more directed beam is obtained with such a nozzle and efforts are underway to find ways in which the design can be further refined. The de Laval nozzles will be used in the Mark II-GB divertor, where helium will be injected from the top of the septum as well as from the outer-side wall of this divertor.

Magnetics

Following problems during operations with in-vessel wiring on the magnetics sensors, a set of new magnetic sensors has been installed with wiring that does not include any connectors using sliding contacts inside the vessel. Combined with a modified version of the plasma boundary idenfication code XLOC, it is now possible to calculate the boundary accurately while excluding any sensors using connectors with sliding contacts inside the torus. This has led to a more robust system for real-time control of the plasma position and shape. The improvement in reliability has been evident in recent operation.

Divertor Neutral Pressure

Ionisation gauges were used for neutral gas pressure measurements in the subdivertor volume and the torus main chamber. There are a total of 15 gauges distributed in similar groups of five in two different Octants. In Octant No.4, only four gauges were placed in the divertor area, and one gauge was at the inner wall. Except for the gauge which sits in front of the cyro-pump or at the inner wall, the neutral particle flux, or equivalent pressure, is sampled through lengths of tube, which limits the time response to about 5ms. The data acquisition and analysis system is fully operational and automatically processes the results intershot.

Comparison of divertor gauge measurements with the main chamber gauge measurements as well as main chamber D_α photon flux measurements yielded results on the neutral particle retention capability of the Mark I and Mark II divertor. Mark II divertor exhibits improved particle retention. Residual gaps in the divertor structure of Mark II caused the neutral flux in the main chamber not to decrease as the baffling improved. Only the plugging of these gaps resulted in a substantial decrease (30% to 50%) of main chamber neutral fluxes, but not without reducing the divertor fluxes as well. This suggested that plugging the by-pass leaks also reduced the main plasma edge density, which in turn reduced the plasma flux at the divertor targets.

Real-time Partial Pressure Analysis of Divertor Gases

A new JET diagnostic was installed in 1996 that allowed different masses in the divertor neutral gas to be distinguished. The diagnostic comprises a pumped vacuum tube attached to the sub-divertor volume. It allows divertor gas to enter a Penning gauge, from which emitted light is analysed by a spectrometer. Detection of He, N, Ne, Ar, as well as H, D, and T will be possible allowing, for instance, divertor He and impurity retention studies as well as measurements of the D/T plasma composition during the tritium experiments. After extensive testing in the laboratory prior to installation on the machine, the system is now being commissioned and has successfully undergone leak testing. It is expected that first data can be measured during the D/T phase allowing an assessment of the D and T composition of the divertor neutral gas and thus an indication on the plasma fuel composition.

Neutron Diagnostics

Neutron Yield Measurements

The calibration of the instantaneous neutron yield monitors (KN1) has been checked repeatedly during the year and, independently, some minor discrepancies between the two diagnostics (KN2 and KN4) used for deriving the absolute calibration, were uncovered. Consequently, an extensive investigation into the techniques and procedures was undertaken. This work confirmed the validity of the calibrations provided.

The sets of circumstances that gave grounds for doubting the KN1 calibration are summarized. The first is the data discrepancy encountered for hot-ion H-mode discharges, for which TRANSP analyses predict neutron emissions 40% greater than those measured. The fact that no such discrepancy was found for lower performance discharges demonstrates that an erroneous KN1 calibration is not the source of the problem. The second is the measurement of the in-vessel dose-rate, which was 20% higher than predicted for the September 1996 machine opening. While of great interest, the comparison of dose-rate prediction with measurement is subject to numerous uncertainties: (i) the KN1 calibration; (ii) the neutron transport calculation on which the prediction is based refers to the 1983 condition of the vacuum vessel; (iii) the assumption that only 2.45MeV neutrons are released, pertinent because the 58Ni(n,p)58Co reaction - the sole important reaction - has a steep excitation curve so that any higher energy neutrons associated with ICRF heating will have a disproportionate importance (lower energy neutrons may also be produced), (iv) the Health Physics instrument used for dose-rate measurements may produce uncorrected readings in error by as much as 15% in spite of annual recalibrations. The overall comparison accuracy is probably no better than +30% and may vary erratically with time. Thus, these two areas of concern should not be interpreted as indicating an incorrect overall calibration for KN1.The discrepancy between KN2 and KN4 calibrations is potentially more serious, however.

The instantaneous neutron emission from JET discharges is monitored with three sets of fission chambers, each being attached to a different limb of the transformer magnet at the level of the vacuum vessel midplane. These monitors exhibit little sensitivity to neutron energy, so that 2.5MeV neutrons from D-D reactions cannot be distinguished from 14MeV neutrons from D-T reactions. Their neutron detection responses are dependent on the size and weight of diagnostic and plasma heating equipment situated on the adjacent horizontal diagnostic port, but exhibit little sensitivity to in-vessel components. Since the external hardware near each port is likely to be modified during each major shut-down, a new calibration of the detector response in terms of plasma neutrons emitted must be determined for each operating period. This calibration is derived from the activation of standard neutron dosimetric samples that are subsequently assayed through gamma-ray detection (KN2) or delayed neutron detection (KN4). These two diagnostics actually determine the neutron fluence passing through suitable samples exposed to the neutron radiation field of the tokamak just inside the vacuum vessel. The local fluence is then related to the global neutron emission by computation using appropriate neutron transport codes. The resulting calibration is insensitive to hardware outside the vacuum vessel and is only weakly sensitive to internal features such as the pumped divertor but it does depend on the position of the plasma within the vessel. Over the past decade, numerous transport calculations have been performed using two contrasting computational methods, for three irradiation positions offering responses differing by a factor of 3, and for numerous nuclear materials. After some initial difficulties, excellent overall consistency was obtained and the calculations are considered reliable, with a claimed accuracy of ±7% prior to the installation of the pumped divertor, when vertically opposed pairs of irradiation positions could be used to cancel the dependence on plasma position.

It should be mentioned that the absolute efficiency of the KN2 detector (a high purity germanium diode) is determined anew during each campaign using standard radioisotope sources, since it is possible that the detector efficiency might change with time. This constrasts with the KN4 delayed neutron assemblies, which are exceptionally well instrumented and stable systems, with all numerical aspects enshrined in a computer code. For D-D measurements, KN4 is regarded as the reference diagnostic, with KN2 being used for confirmation. Both diagnostics should offer absolute measurement uncertainties of +3% or better. For physics reasons, the roles of these two diagnostics are reversed for D-T neutron measurements.

The definitive absolute calibration measurements were performed in 1990, since when the two diagnostics KN2 and KN4 have returned fluence measurements that apparently agreed within a few percent. However, measurements during August 1996 were found to be discrepant - an unacceptable difference (of about 10%) being found. To discover the reason for this discrepancy, an investigation was made into all pertinent aspects of the hardware and experimental procedures. Three errors were uncovered, as follows:

(a) although the KN2 detector can be calibrated to ±3% accuracy, this requires considerable care and attention to detail. In practice, it is clear that since 1990, these calibrations were being carried out to only ±7% accuracy (but have now been improved, retrospectively);

(b) the KN4 counter-ends were found to be about 6cm below their optimum positions within their counter assemblies, a fact wholly unsuspected. Evidently, this displacement was introduced during a routine, but undocumented, maintenance. An error of about 8% had been introduced. This change had not been detected during efficiency checks using a standard radio-isotope neutron source;

(c) finally, two corrections that nearly cancelled up to 1990 were neglected subsequently although after the in-vessel irradiation end was lowered in 1991 these should have introduced a 4% adjustment in the opposite direction to the error described above.

The final result of this investigation was that the two techniques were once more in good agreement. Fortuitously, the corrected fission chamber calibrations for 1990 to 1996 appear to have differed by less than 3% from the released figures (used in construction the PPFs) - a small error in relation to the overall claimed uncertainty of +10% for post divertor installation measurements.

Additional confusion arose during the above investigation when the position of a massive diagnostic (KJ5 on Octant No.8) was adjusted during the operational campaign, despite the declaration that it was already in its final position. This temporarily disturbed one of the three fission chambers (the averaged response is adopted) and contributed to the general lack of confidence in the KN1 calibration.

The above account emphasises the use of the KN2 and KN4 diagnostics for determining the absolute calibration figures. This information only becomes available weeks after the start of a new campaign. Thus, at the start of a campaign, the KN1 relative calibration is derived from that for the previous campaign based on a assessment of the physical changes that have been made during the intervening shutdown (e.g. no changes near a diagnostic port implies the calibration of the adjacent fission chamber should not alter) and by independent measurements using the KN3 neutron profile monitor. Taken together, these two sources of information essentially guarantee that the KN1 calibration cannot depart systematically by more than 10% from its previous value without giving obvious cause for concern.

Neutron Profile Monitor

The upgraded Neutron Profile Monitor, KN3U, has been used routinely throughout the year for 2.5MeV (D-D) neutron measurements and for fast electron bremsstrahlung (FEB) measurements during periods of lower hybrid current drive (LHCD) experimentation. The neutron and bremsstrahlung measurements were performed simultaneously.

In the 1995 Progress Report, it was mentioned that the absolute yields initially provided by the upgrade profile monitor (KN3) when installed in May 1995 fell 30% below those determined with the activation system (KN2) and it was suggested that this might be due light response functions used being inappropriate for the new batch of scintillators. This conclusion was only partially correct, the full explanation being as follows. The prototype instrument did not have the FEB detectors installed during neutron measurements and a discrimination bias of 2.0MeV was employed. The apparent 30% drop in yield was determined with the upgrade instrument operated with the FEB detectors in position (at the time, they could not be moved out) and with the bias was reduced to 1.8MeV. It has now been established that: (i) the attenuating effect of having FEB detectors in the lines-of-sight is 23%, substantially greater than the 9% expected, (ii) by setting up the two sets of signal conditioning electronics (one normally used for 2.5MeV neutrons, the other for 14MeV neutrons) with effective discrimination biases of 1.8 and 2.0MeV, the calculated efficiency ratio is found to be in error by about 8%. Taken together, these changes account for the discrepancy and the corrected KN3 neutrons yields agree with the KN1 yields to within a few percent (the absolute, and independent, experimental uncertainties being about +10% for each diagnostic).

Some difficulties have been experienced during 1996 with the rotatable collimators used to control the neutron flux incident on the neutron detectors. These collimators consist of massive cylinders of stainless steel through which two sets of collimating apertures are drilled. They are rotated using pneumatic actuators. Unfortunately, the cylinders could build up considerable angular momentum during the 90° rotation before being brought to rest rapidly on the air cushions in the actuators, generating considerable torque on the locating pins which connect the cylinders to their drive shafts. One of the four pins became deformed (that for the uppermost collimator of the vertical camera). Consequently, the effective solid angle for that camera reduced gradually over a period of months before the matter could be rectified by installing strong oil-filled dampers. Once this problem was resolved, it was again found that the KN3 and KN1 estimates of neutron yields agreed within a few percent.

An analysis programme has been developed to convert the raw KN3 data into processed pulse files (PPFs) suitable for general use. The two cameras are separate instruments, each providing its own estimate of the total neutron yield, which should be in agreement with the yield from the fission chambers (KN1). The PPF generator enforces agreement with KN1, thereby effectively resolving the problem of the out-of-alignment collimator

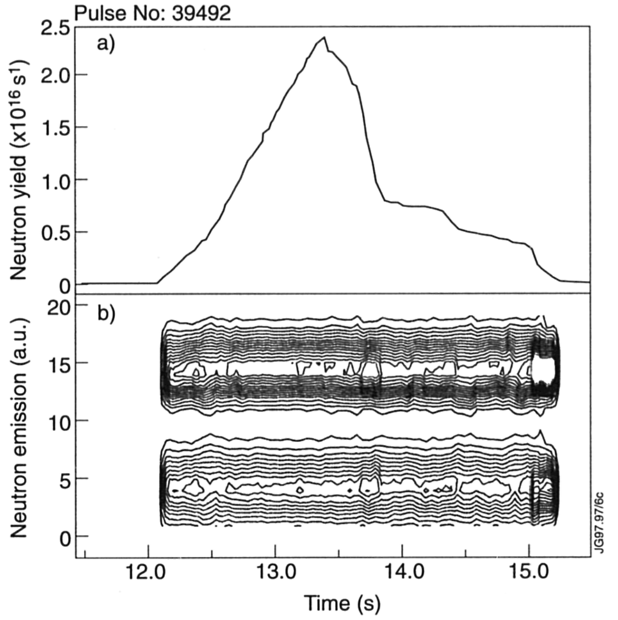

Fig.74: (a) measured time-resolved neutron yield for Pulse No.39492; (b) contours of line-integrated neutron emission from the 19 channels of the neutron profile monitor. Channels 1-10 correspond to the horizontal-viewing camera, and show the vertical profile, while Channels 11-19 correspond to the vertical-viewing camera and show the radial profile. The neutron profiles are normalized to constant global neutron emission strength. The profile shape is defined at the start of the beam heating period and remains essentially constant thereafter.

for the vertical camera. This normalization also addresses the problem of neutron detection efficiencies that change with intensity in the prototype diagnostic (which employed photomultipliers with gains that increased slightly with current drawn). It also makes some allowance for occasional misbehaviour of individual detectors, in particular, their failure to discriminate correctly neutron from gamma-ray-induced events caused by electronic level drifts within the discrimination circuitry. The PPF generator is basically a least-squares fitting procedure that fits a parametrized neutron emission profile to the line-integrated measurements using a geometry based on nested ellipses. This assumes constant emissivity around the surfaces, which appears to be a good approximation for high performance discharges but is certainly not a general result. In particular, it does not hold for certain high-power ICRF-heated discharges. The code outputs its results in the form of a time-dependent set of 19 reprocessed line-integrals, which will exhibit a more regular behaviour than the original data and which are correctly normalized to KN1. In this form, the data are ideally suited for comparison with the predictions from TRANSP and similar codes. As an example of Fig.74 presents the time-resolved neutron yield and the contours of line-integrated neutron emissivity against time for Pulse No.34500. The upper figure (Fig.74(a)) shows the growth and decay of the neutron yield throughout the discharge whereas the lower figure (Fig.74(b)) is a contour plot of the variation of the profile shapes, after normalizing to a total neutron emission rate of 1ns^{-1}. The normalized contour plot shows that the profile shape remains remarkably constant throughout the entire duration of the beam heating period. This is the normal behaviour for high performance (hot-ion H-mode) discharges. Different discharges in this class possess profile shapes that are broadly similar, although there are obvious differences.

The data consistency problem, relates to the finding that TRANSP predictions of the global neutron yield are appreciably greater than the measured values for hot-ion ELM-free H-mode discharges. Data from the neutron profile can shed some light on the origin of this inconsistency. The key observation is that the TRANSP predicted neutron profiles are broader than the measured profiles and that if, for example, the width of the experimental ion temperature profile is adjusted so as to bring the predicted profile into agreement with the measured profile, then consistency between the neutron yields is achieved. Such an adjustment cannot be justified in terms of knowledge of the ion temperature measurements. An alternative explanation could be a lower than measured deuterium concentration in the outer half of the plasma.

The profile monitor is equipped with a separate set of detectors specifically for use with 14 MeV (D-T) neutrons. These detectors employ Bicron scintillators with sensitive volumes reduced such that the separation of neutron from gamma-ray events can be made on the basis of pulse-height alone. Unfortunately, this very feature has impeded the setting up of the signal conditioning electronics, which is usually performed using ^{22}Na gamma-radiation. Thus, the final settings can only be made when sufficiently strong fluxes of 14 MeV neutrons become available, probably requiring 1% tritium-in-deuterium gas mixtures fed to the neutral beam injectors at the start of DTE1.

14 MeV Neutron Spectrometers

The proposals for the 14MeV neutron spectrometers to be used during the D-T phase of operations were accepted over ten years ago, when it was thought that this was the only practical means of determining the central ion temperature for high-temperature discharges with very low impurity contents. The main difficulty is that of separating thermal-thermal from beam-thermal fusion reactions to extract the background ion temperature. Subsequently, the charge-exchange recombination spectroscopy (CXRS) technique was developed, providing full ion temperature profile data during periods of beam heating. Consequently, the present motivation for the neutron spectrometers now resides primarily in the investigation of special effects of ICRF heating which can significantly perturb neutron spectra, although confirmation of CXRS measurements would be very welcome. For the next generation of tokamaks, specifically ITER, it is not obvious that the CXRS technique will be feasible. Neutron spectrometry, on the other hand, will be relatively easy due to the interference from non-thermal reactions being minimal. With this perspective, the comparison of the performances of the three 14-MeV neutron spectrometers during DTE1 will be of particular interest.

There are three major spectrometers installed at JET for DTE1. These include the two spectrometers, KM2 and KM5, constructed by the UKAEA and Swedish Associations, respectively. A third spectrometer, KM9, provided by the Swedish Association, has recently been installed; KM9 has been designed strictly with ITER in mind and JET is being used as a test-bed for evaluating its performance.

All three spectrometers utilize n-p scattering reactions in thin hydrogenous foils and differ in the techniques used for measuring the energies of the recoiling particles. The current status of each of these spectrometers is as follows:

- KM2, a simple proton recoil, tandem-radiator spectrometer is installed in a large concrete blockhouse in the Diagnostic Hall, with a line-of-sight which views the plasma through Octant No.7. It is almost fully commissioned, although it is intended to replace the four large silicon diodes whose characteristics have become impaired during storage. Testing of signal acquisition from the spectrometer via CODAS has commenced although final testing will only be possible when significant fluxes of 14MeV neutrons are available;
- KM5, an associated-particle, time-of-flight, spectrometer is installed in the Roof Laboratory. The hardware commissioning is complete but final tuning cannot be performed until significant fluxes of 14MeV neutrons are produced. The data-analysis programme still requires substantial work and is unlikely to be completed until after DTE1 experiment is completed;
- KM9, a proton recoil, magnetic analysis, spectrometer has been installed in the Torus Hall and hardware commissioning is complete. However, the diagnostic will be operated from a stand-alone computer although data-acquisition through CODAS may be possible in time for the DTE1 experiment.

Lost Alpha-Particle Detector

A pair of lost alpha-particle detectors (essentially, a charge collector) was installed during the October 1996 shutdown. One detector consists of a substantial housing containing four Nickel foils each 2.5×10^{-3}mm thick with an area of 29cm^2, stacked in parallel with 3mm separation. Thus, 3.5MeV alpha-particles can be identified by exploiting their range-energy relationship. The other detector has just a single, relatively thick and therefore robust, charge collection foil. These detectors are situated near Octant No.7, outboard and below the machine midplane. To be recorded, alpha-particles with large gyro-radii must enter the detector on the side away from the plasma. There is a restricted range of alpha-particle pitch angles that will permit the particles to reach the foils after passing through the entrance apertures without first being intercepted by plasma limiting surfaces outside the last closed flux surface. The electronics for this diagnostic are currently being installed.

Modelling of Neutron Yields

The simple 0-D computer code was prepared for predicting the neutron emission in the initial phase of beam-heated hot-ion H-mode discharges in JET. This code has been developed further. It can now be used to model the entire discharge, including the termination, when fuelling of the plasma core with cold neutrals is adopted as a first-order approximation for edge recycling effects. Specifically, given the time traces for the beam heating power, average electron density, Z_{eff} and D_α signals as input data the code can satisfactorily reconstruct the global neutron emission, core volume rotation rate, ion temperature and electron temperature for the entire duration of the discharge, and it also provides an explanation for the anomalously low burnup of D-D fusion product tritons that is sometimes observed. The code provides insight into the relative intensities of the three contributing reaction mechanisms to the total neutron

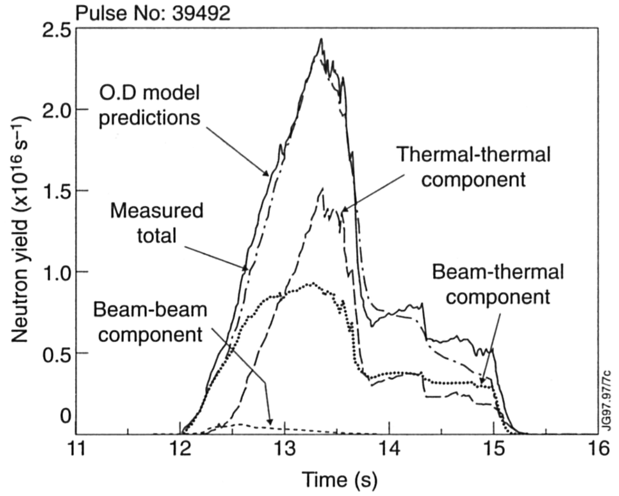

Fig.75: The measured time-resolved neutron yield for Pulse No.39492 compared with the yield calculated using the simple 0-D model. The breakdown of the emission into thermal-thermal, beam-thermal and beam-beam components is shown.

emission (thermal-thermal, beam-thermal and beam-beam reactions) as an aid to interpretation of data from the various neutron diagnostics on JET, including the neutron profile monitor and the neutron spectrometers. Tritium fuelling and beam injection are also implemented, so the code can be used to extrapolate the neutron emission from existing D-D discharges to that expected from similar D-T discharges.

A typical example of the use of the code is shown in Fig.75, which compares the modelled time-resolved neutron yield with the measured yield for Pulse No.39492. The only truly free parameter used in obtaining this fit was the normalization factor for the D_α signal, which is interpreted as an influx of cold deuterium neutrals. Some minor embellishments are included in the code to allow for peaking of the electron density profile, hollowness of the Z_{eff} profile and for sawteeth. Bearing in mind the use in the code of top-hat temperature profiles and thermal neutron emission restricted to a constant volume core region, the agreement is surprisingly good. Naturally, the computed profiles have shapes that change little during the beam-heated portion of the discharge since the core volume is considered time-invariant, which is compatible with the experimentally determined profiles which vary little during this period, as shown in Fig.74.

ITER Neutron Radial Camera Design

The outline design of the radial, horizontally viewing, neutron camera for ITER has been further developed following identification of problems related to neutron streaming inside the cryostat due to the large penetrations through the neutron blanket required for the camera. Accordingly, the design has been modified to include a re-entrant cryostat boundary, the external void being filled with a bioshield plug having lengthened collimator tubes embedded within. This eliminates neutron streaming inside the cryostat and brings the front of the collimation closer to the blanket, permitting reduced blanket penetration. The ITER camera design is proceeding at the Joint Design centre.

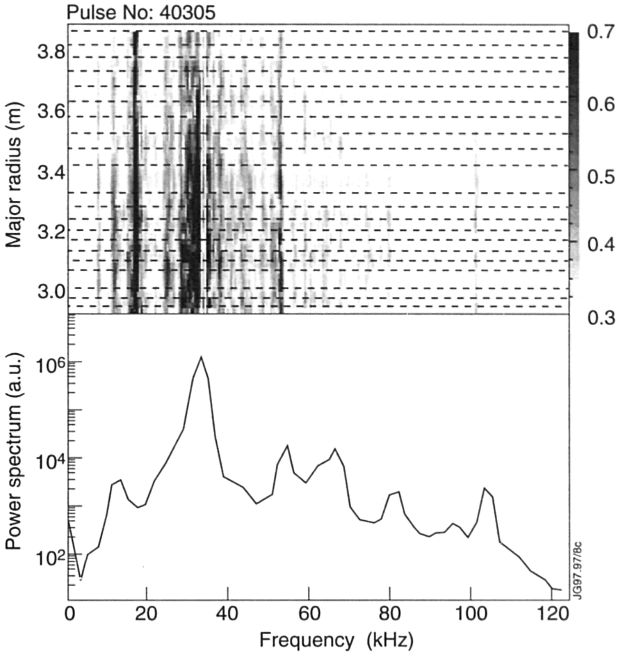

Fig.76: Cross-correlation analysis using data from the ECE heterodye radiometer, KK3: (a) coherence between this signal and radiometer channels at a number of radii is plotted as a grey-scale contours. The strong feature at ~32 kHz is seen to be located near the q=1 surface; (b) power spectrum of the signal from a magnetic pick-up coil at t=13.21s on Pulse No.40305.

Electron Cyclotron Emission System

Near the end of the Mark II divertor shutdown, an absolute spectral calibration of the Michelson interferometer (KK1) was made, with a calibration source in the vacuum vessel. This provided the reference which allowed absolute electron temperature measurements to be made with the other instruments in the Electron Cyclotron Emission (ECE) measurement system: a grating polychromator (KK2) and the heterodyne radiometer (KK3). All three instruments were used routinely throughout 1996 operations. Substantial effort was devoted to the development of sophisticated display and analysis software development for KK3 so that the large quantities of fast data recorded by the CATS data acquisition system could be fully exploited. Figure 76 is an example of the the type of correlation analysis which can be performed.

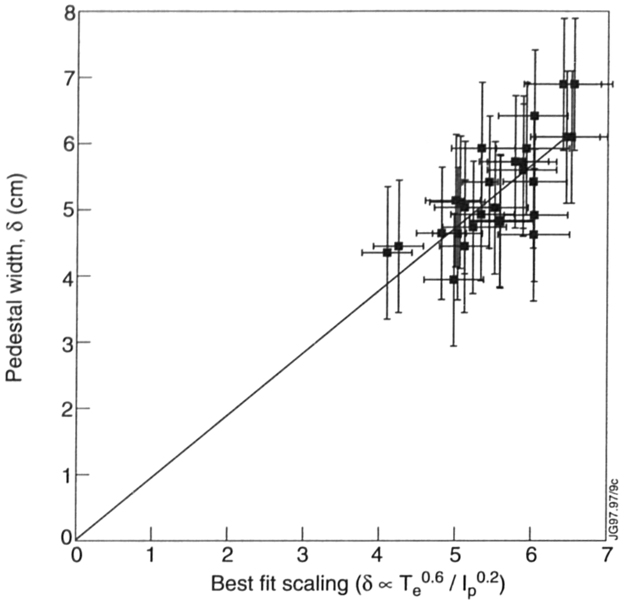

Fig.77: Measured edge electron temperature pedestal width, δ_{ped} plotted against the best fit scaling ($\delta_{ped} \propto T_e^{0.6}/I_p^{0.2}$).

The heterodyne radiometer has also been used to obtain measurements in the edge plasma with high spatial resolution. These measurements have been used to investigate the scaling properties of the edge pedestal in high performance ELM free H-modes. This scaling has been compared with a neoclassical model of H-mode confinement [1]. Figure 77 shows the measured pedestal width (δ_{ped}) plotted against the best fit scaling, which is quite different to the model prediction ($\delta_{ped} \propto T_i^{0.5}/I_p$). The substantial discrepancy between the measured and predicted pedestal width scaling is a subject of continuing investigation.

Microwave Reflectometry

The O-mode multi-channel reflectometer (KG3) routinely provides electron density profiles, as well as being used for observation of turbulent and coherent density fluctuations. Further improvements have been made in the algorithm used for the reconstruction of density profiles from the reflectometer phase measurements.

Coherent density fluctuations, associated with an external kink mode that may be driven unstable by high edge current density, have been observed. The CATS fast data acquisition has been used for a detailed study of fast phenomena occurring before and after Giant ELMs [2]. Time-resolved frequency spectra have been obtained from the phase fluctuations of two reflectometer channels, before and after a Giant ELM. Coherent fluctuations are observed before the ELM, followed by broadband fluctuations after the ELM.

It has been known for some time that the density profile measurements from this reflectometer are limited by drifts in the microwave source frequencies, the susceptibility of the fringe counters to noise and the slow frequency sweep. A novel scheme employing fast frequency modulation of the microwave sources has been developed and tested. It uses a high modulation frequency (65MHz), which reduces the susceptibility to plasma fluctuations and allows instantaneous measurements of phase and hence group delay time to be made. The upgrade is now ready for assessment with plasmas and significant improvements in the density profile measurements are expected.

The E-mode correlation reflectometer system (KG8B) produced results on the behaviour of ELMs, coherent modes and turbulence throughout the 1996 campaign. The KG8B system consists of three separate reflectometers: one is a swept frequency reflectometer (92 - 96GHz) providing radially separated fluctuation measurements, and there are two dual-frequency reflectometers which can be configured to give poloidally or toroidally separated measurements. One of the fixed frequency instruments has two channels at 75GHz for measuring in the edge region, and the other has two channels at 105GHz for measuring in the core plasma. The three reflectometers share a common antenna cluster of two transmit and two receive horns positioned slightly above the mid-plane on the low-field side. The poloidal or toroidal separation is obtained by changing the allocation of transmitters and receivers to different antennae. An important feature of the system is the combination of a fast (2MHz) data acquisition for studying high frequency turbulence, the CATS (250kHz) co-ordinated data acquisition, and a slow (<250kHz) CAMAC system which provides information on the gross fluctuation levels during the whole plasma discharge. In addition some of the KG8B signals are used in the coherent detection of externally excited toroidal Alfven eigenmodes (TAEs).

The heterodyne detection and analysis procedures allow the reflected phase fluctuations (mostly cut-off layer movement) to be separated from the signal amplitude fluctuations (mostly scattering effects). Recent results from a two-dimensional simulation model of reflectometer signals [3] show that measurements of both amplitude and phase fluctuations are necessary to reconstruct the true density fluctuation spectra. For example, moving from the ohmic phase to the high performance ELM free

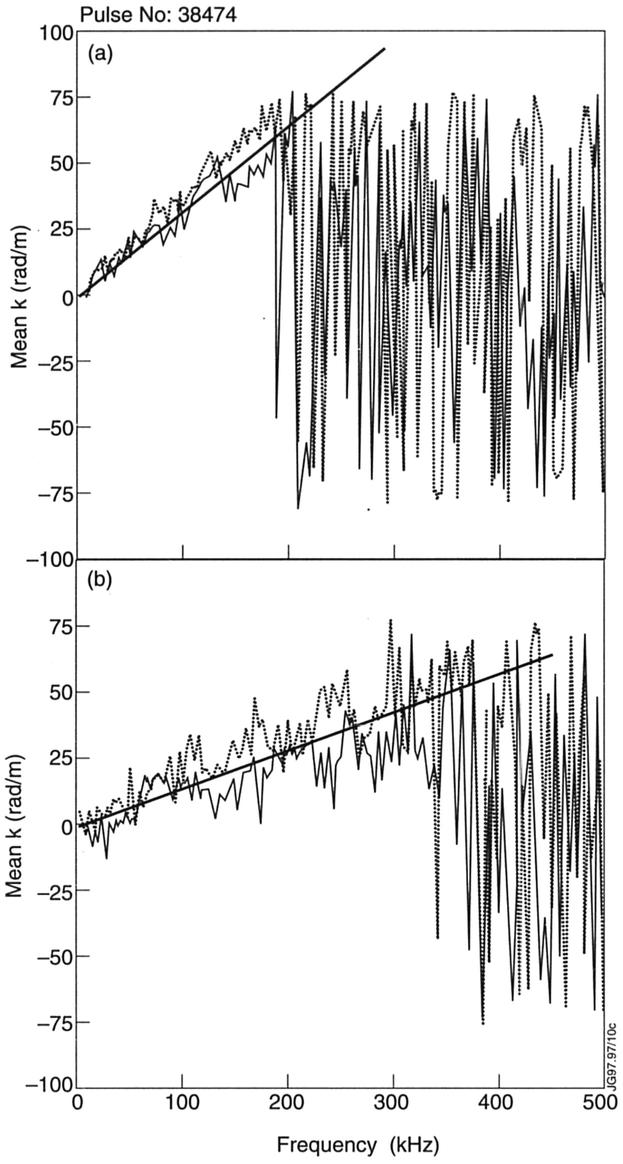

Fig.78: Dispersion relations (frequency-wavenumber spectra) compiled from phase (dashed line) and power (solid line) fluctuations from (a) ohmic phase, (b) RF H-mode phase of discharge, Pulse No.38474. Between the ohmic and H-mode phases the mean fluctuation phase velocity increases from 18kms-1 to <40kms-1 and the toroidal correlation length decreases from >5.5cm to <4cm.

hot-ion H-mode through to the slow R_{DD} "roll-over" phase, KG8B shows that in the plasma edge there is first a collapse then a recovery in both the low and high frequency phase fluctuations, but in the signal amplitude only the low frequency fluctuations are reduced. In the plasma core there is a corresponding increase in the high frequency amplitude fluctuations. According to the behaviour seen in the model, these results imply that it is predominantly low frequency turbulence at the separatrix that affects global confinement. Many high performance discharges also show evidence of a coherent MHD mode forming at the separatrix during the R_{DD} rise and slow roll-over.

Figure 78 shows an example of the change in propagation and coherence properties of turbulent edge fluctuations with various heating scenarios. The two contour plots show the frequency - wavenumber spectra compiled from phase and amplitude fluctuations, respectively. The ohmic phase, marked (a), and an RF H-mode phase, marked (b), are in the same discharge, and show that the mean fluctuation phase velocity V_{ph} increases from 18kms^{-1} to greater than 40kms^{-1}, while the toroidal correlation length decreases from L_c >55mm to less than 40mm, probably as a result of the increased ExB shear in the H-mode phase.

Microwave Divertor Diagnostics

The antennae for the microwave divertor diagnostics are mounted in the divertor structure and has had to be changed for the Mark II divertor configuration. One of the original three sightlines has been lost due to access constraints. The systems now have one sightline through the inboard leg of the divertor plasma and one through the outboard leg.

These two sightlines must be shared by all three microwave divertor diagnostics: a dual frequency density interferometer (KG6D), a "comb" reflectometer (KG7D), and an electron cyclotron absorption diagnostic (KK4D). Polarising beamsplitters, integrated into waveguide mitre bends, enable the two ordinary mode systems (KG6D and KG7D) to share a waveguide with KK4D, which uses the orthogonal extraordinary mode polarisation. Separation of the KG6D radiation from that of KG7D is more difficult because they use the same polarisation. It requires frequency selective beamsplitters which reflect the radiation of one diagnostic and transmit the other. A design study, which predicts that the required separations can be achieved, has been completed by a specialist company and measurements made at JET on a test sample. Manufacture and installation of the final components is planned for the shutdown in the second half of 1997.

The KG6D interferometer, which measures line integrated electron density in the divertor plasma, has been operated throughout the operational campaign. It has been found that the density is almost always too high for measurements to be made on the inboard sightline, and even on the outboard side there are limitations associated with high density and the effects of ELMs. Improvements to both hardware and software have been initiated in an effort to ameliorate these effects.

The interferometer employs two microwave frequencies (130GHz and 200GHz) so that phase shifts due to movement of the antennae (which are mounted on the divertor coils and structure) can be distinguished from plasma induced phase shift. The lower frequency channel often suffers signal loss due to severe refraction, or even cut-off. To overcome this, replacement sources and receivers at 304GHz have been procured. Several technical problems associated with the difficulties of operation at this high frequency are in the course of being resolved.

Software for the routine production of PPFs from KG6D data has been developed. The code incorporates extensive data checking and correction, with user adjustable sensitivities. Various defects (for example, incorrect phase measurements during rapid density transients such as ELMs) are detected, and either corrected or the data flagged as unreliable. By imposing physical constraints (such as that the relative movement of the antennas cannot be too rapid) and by also analysing the data backwards in time from the end of the discharge, reliable output is obtained for the maximum time. Nevertheless, some high performance discharges still produce unexpected failures, and this is being investigated.

The Electron Cyclotron Absorption (ECA) diagnostic, KK4D, is a microwave interferometer with rapid sweeping of the source frequency (110GHz to 190GHz in ~1.3ms). The source radiation is split between the two arms of the interferometer, one of which is the 100m long waveguides to and from the plasma, and the other a reference arm of almost the same length. The beat signal which results from mixing the radiation in these two arms contains both transmission loss information (the envelope) and electron density information (the phase). Narrow band filtering around the beat frequency allows standing wave effects (due to waveguide resonances) to be removed.

The hardware has been upgraded to allow simultaneous measurements on the inboard and outboard sightlines by two independent systems. At typical toroidal fields, ~2.8T, the ECA frequencies are too high on the inboard line, but it can be used for density measurements. A substantial modification of the cryogenically cooled microwave detectors, to reduce reflections from the detector back into the optical system, has significantly improved the signal quality. However, standing waves with their origin elsewhere, still affect the ECA measurement and efforts to reduce them are continuing.

In some circumstances, the electron density is high enough, particularly on the inboard sightline, to cause cut-off at frequencies in the KK4D sweep range. The frequency at which the abrupt transition in transmission occurs gives a reliable estimate of the peak density along the sightline. Using this technique, it has been found that the peak density along the outer sightline is generally $<5x10^{19}m^{-3}$, and the inboard peak density is usually 2 to 4 times higher. At suitable values of toroidal field, KK4D measures peak densities in the same range as the KG7D comb reflectometer. The comparison shows good agreement.

Fast Ion and Alpha Particle Diagnostic

After first successful collective scattering measurements made in 1995, the emphasis was on technical improvements of the system during 1996 to optimize for alpha-particle measurements and on theoretical developments to facilitate interpretation of results.

A different transformer/rectifier, on loan from LLNL, was installed which will allow the use of the full pulse length capability of the gyrotron (0.5s at 500 kW). Changes were made to the detection system to blank out the stray light at spurious frequencies during switching (modulation) of the gyrotron, which led to some saturation effects during the initial measurements. The antenna directions and the detection system were carefully calibrated.

On the basis of original expectations, confirmed by first measurements, the signal-to-noise for alpha-particle measurements would at most be <S/N> ~ 10 (using O-mode, 100ms integration time and Δn /5 channel width) at a magnetic field ~3.3T and even lower at higher magnetic field values. The noise for the measurement is dominated by a relatively high background radiation level, due to ECE which is generated near the edges of the plasma and detected via wall refections. It is possible to reduce the background radiation level (by an order of magnitude) by directing the receiver towards an efficient viewing dump. To obtain detailed information on the alpha-particle velocity distribution, a <S/N> ~30 would be required. Two viewing dumps were installed in the vessel, which should increase the <S/N> to the desired level, at least for two viewing directions. The dumps use carbon cloth as the absorbing material, which is mounted out of sight of the plasma and the Be evaporators using a reflector arrangement.

Diagnosing fast ions by collective Thomson scattering requires inversion of the relation $\mathbf{y} = \mathbf{Kx}$ where $\mathbf{x} \in e\mathbf{X}$

represents the fast ion distribution function and $\mathbf{y} \in e\mathbf{Y}$ is the measured spectral density of the received scattered light and the operator K represents the non-linear mapping from **X** to **Y**. In past years, the theory of collective Thomson scattering has been considerably refined so that it is now believed that an appropriately accurate mathematical representation of **K** has been implemented in codes. The collective scattering operator, **K**, is singular (i.e. more than one element of **X** maps into the same element of **Y**) and K does not span **Y**. In addition, there are uncertainties in the measured values of y. The inverse problem thus presents all the usual difficulties against which standard maximum likelihood estimation with regularization can be brought to bear. An added difficulty encountered in fast ion diagnosis by collective scattering is that there are also uncertainties in the operator K. These uncertainties arise because the definition of K requires the specification of a range of parameters such as electron temperature and density, scattering geometry, calibration coefficients etc., all of which are known but only with finite accuracy.

It is well documented that incorrect values for the operator parameters can seriously affect the estimate of **x** when standard inversion is applied. It is easy to show that the standard estimators neglecting uncertainties in K can be far from optimal. This problem is not unique to collective scattering but common to many fusion plasma diagnostics and indeed to diagnostic problems throughout the physical sciences, yet mostly it is ignored due to the difficulty in accounting for uncertainties in the operator. In statistical inference, the uncertain operator parameters are generally referred to as nuisance parameters and there is an extensive literature on finding optimal estimators for the parameters of interest when nuisance parameters are present. These techniques are, however, mainly geared towards the problems encountered in the fields of biology (medicine) and economics. Therefore, a simple yet powerful generalisation of the χ^2 fitting has been developed which provides the optimal estimator in the presence of uncertainties in the operator K.The increase in computational requirement as compared with the standard χ^2 is modest, the dimension of the search space X being unchanged except when the uncertainty in one or more operator parameters is so large that the effect on K is non-linear. In this case, the dimension of X is increased by their number. The technique has been implemented for KE4 and has been found to the stable and efficient.

A further benefit of this generalisation of the c2 is that it provides an efficient tool for investigating theoretically the diagnostic capabilities of complex diagnostics accounting fully for the effects of uncertainties in K i.e. uncertainties in the definition of the system. Extensive investigations of this nature have been carried out for the fast ion collective scattering system at JET and the systems proposed for ITER.

Main LIDAR Thomson Scattering System

The main LIDAR Thomson Scattering System remained fundamentally the same as in 1995, with operation at 4Hz. Two changes were successfully implemented at the beginning of the year. The line-of-sight was changed to pass through the plasma centre and the digitizers were replaced with new fully digital, 1GHz bandwidth, transient recorders.

The change in line-of-sight and fitting of double windows on the collection system resulted in a small reduction of signal level. The accuracy of measurements is accordingly slightly reduced. Nevertheless, the comparison with the ECE central temperature, over the year, has shown good agreement with peak temperatures up to 15keV. The absolute density is normalised to the interferometer signals at regular intervals. During the year, this calibration has not changed significantly indicating that the build-up of a coating on the collection windows was not a serious problem.

The change of the recording system was very successful. With a fully digital system, writing speed problems are no longer a difficulty when fast transients are encountered. This means that the inter-channel timing can be determined more accurately, with a consequent improvement in the fit of the data. In addition, the new digitizers are more robust instruments and the reliability of the entire system was also significantly improved. LIDAR data was available in more than 95% of JET discharges.

Divertor LIDAR Thomson Scattering System

The front end of the Divertor LIDAR System was completely rebuilt before 1996 operation. With some minor modifications early in the year, both the laser beam delivery system and the collection optics were stable against vessel movements.

The streak camera requires gating off shortly before the arrival of the "inner wall" stray light pulse. A new pulser with <2ns rise and fall times was purchased. Even at this short fall time the transit time slow-down caused problems at the end of the 5ns sweep. If maximum gate-off was used, it was not possible to measure nearer than ~0.8m from the strike-point of the laser on the wall. A partial gate-off could be accepted, if the optical signal was reduced from the inner wall. This was done by setting the focal point of the collection system ~1m from the inner wall, effectively vignetting the strike point out of view.

In this arrangement, data was collected routinely from the plasma near the lower X-point. Temperatures in the range 30eV to 1keV were observed. The small étendue resulting from using a streak camera caused a significant change of solid angle of collection even over the ~ 0.75m scattering length. This in turn meant that it was only possible to make spatially resolved temperature measurements at the highest observed densities. The vignetting problem and the non-linear sweep problem coupled with generally low signal levels mean that it was not possible to generate routine analysis of the recorded data.

Edge Thomson Scattering System

The installation of this system is nearing completion. The optics inside the Torus Hall were completed in time for operation at the beginning of the year. The spectrometer and recording systems have been built and characterised. The laser beam path and safety system are installed. The system is now ready for final commissioning.

Soft X-Ray Systems

In 1996, the new visible/UV soft X-ray camera (KJ6) was brought into operation and the construction and installation of the radiation hardened cameras (KJ5) were completed. These are for future D-T campaigns and also for plasma vertical stabilization. The existing sets of soft X-ray cameras (KJ3, 4) continued to take data through 1996 with many improvements to the CATS data collection and triggering system with data collection also into the JPF. The Si(Li) pulse height analysis system (KH2) unfortunately suffered a Be window failure, but is now back in operation. Data has been obtained with all diagnostics for a wide variety of plasma conditions.

Visible/UV Camera (KJ6)

This is designed to look at radiation over a wide energy range in the divertor at high time resolution (10^{-5}s). The camera uses an X-UV sensitive 16-element silicon array.

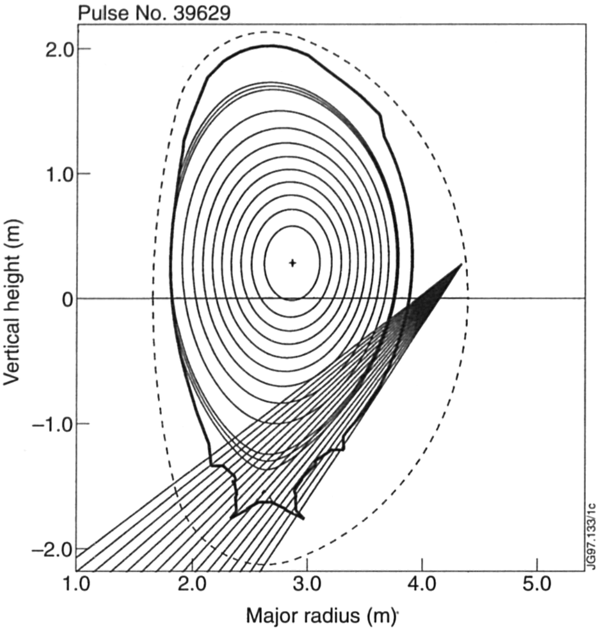

Fig.79: Lines-of-sight for the visible/UV camera

The camera has longer focal length that the soft X-ray cameras to provide good spatial resolution (7cm) in the divertor region (Fig.79). The data is collected by CATS. The diagnostic has provided interesting data during ELM's where it complements data from other diagnostics.

This diagnostic has also made high time resolution measurements of the light emitted when pellets are injected into JET. These pellets are injected in the same port as KJ6 in the median plane. Although there is no direct view of the pellet ablation zone, light from this zone is reflected from the internal surfaces of the camera assembly onto the centre of the detector chip. Very fast and complex modulations are seen with $f \sim 25$kHz. It is believed that these arise from instabilities in the protective cloud which shields the pellet.

Radiation Hardened Soft X-Ray Camera (KJ5)

Two new radiation hardened soft X-ray cameras have been constructed and installed to be used for vertical stabilization of the plasma and during D-T operation when existing cameras will not operate due to very high neutron fluxes. These both damage and destroy the silicon detectors and produce unacceptably high noise levels in the measured signals. Both problems have been overcome in the new design by embedding the detectors in massive barytes concrete shields which are effective for both neutrons and gamma rays.

The complete diagnostic has very similar assemblies on the main horizontal ports of Octants No.4 and No.8.

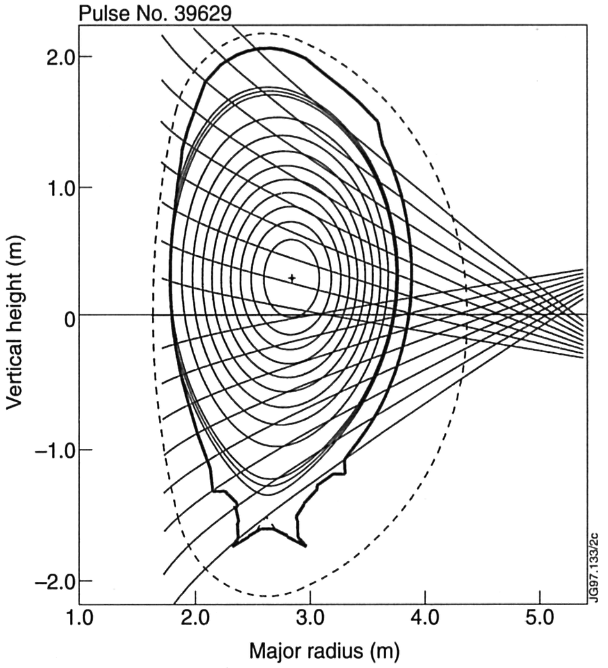

Fig.80: Lines-of-sight of the detectors in the radiation hardened camera

Each assembly has an upper and lower shielding block containing 8 and 9 detector assemblies, respectively. Each shield is 75 cm thick in the direction of the plasma centre. The shielding blocks contain accurately machined collimator holes into which the detector assemblies are inserted from the rear. The detectors do not view the plasma through the machine centre so that their view, projected into a poloidal plane, are not straight lines (Fig.80). The front is connected to the machine by a 250mm Be window and a bellows assembly to allow relative movement during disruptions and thermal expansion of the machine. The Be window, which can withstand more than 1bar pressure from either direction, separates the machine high vacuum from the low vacuum maintained in the diagnostic. Each detector assembly has a coaxial sequence of two PIN diodes, a plastic scintillator and a further PIN diode. The first of these detects the X-rays from the plasma and the second, shielded by the first, detects neutron and gamma ray background signals which can be used to correct the first signal. The scintillator produces light mainly from n - p interactions and this is detected in the third PIN diode. The system is designed so that this neutron signal will have a low noise level in D-T operation and should display MHD activity.

The entire system has been delivered and installed on JET to a tight time schedule in 1996 and brought into operation in the late Autumn. The detector signals are all recorded by CATS and have the expected low noise levels. The efficacy of the shield has not yet been evaluated due to insufficient neutron fluxes, but data taken following the generation of fast neutrons in a disruption show that the individual channels are well shielded in the case of a very localised source.

Compact Soft X-Ray Cameras (KJ3 and KJ4)

These cameras have operated reliably during 1996 and have continued to collect very large data volumes. The cameras use 35 element silicon PIN diodes and view the plasma through pinholes, which include 250mm Be windows to separate the machine and diagnostic vacuum. The detectors are water-cooled to 20°C to reduce noise. The cameras are situated around the outer and upper sides of the plasma in Octant No.2 except for an additional vertical camera installed in Octant No.7 to provide information on toroidal mode numbers.

As anticipated, the detector chips have started to suffer from degradation caused by radiation damage from the D-D and tritium burn-up neutrons. Experience has shown that the damage starts to become a problem after two years of operation, with about 2 x 10^{19} neutrons per year, and a total fluence at the detector approaching 10^{13} n.cm^{-2}. The detectors were originally operated with zero bias, and a decrease of 25% in efficiency was seen together with a rise in the forward voltage from 0.5 to 2V. However, applying a reverse bias to the detectors has reduced the fall in efficiency and improved the bandwidth. Some improvement in detector performance results from self-annealing and partial benefit was obtained from high temperature (150°C) annealing for 24 hours. It is planned to replace all of the detector elements following the 1997 D-T campaign.

CATS Data Acquisition System

This system has been developed to collect data at rates up to 250kHz from the many channels of the soft X-rays system. It is also used to collect data from many other diagnostics including ECE, Langmuir probes, D_{α}, magnetics and reflectometry. The data (~ 500 channels) is collected with accurate time synchronization between the different diagnostics. Data is also collected in response to triggers detected in the data streams and continuous data streams are also recorded into the JPF.

The block diagram (Fig.81) shows the main features of the system. The signal sources can be either voltage or current. The signal can be amplified with a gain which is adjustable between $\times 1$ and $\times 10^4$, and is then filtered with

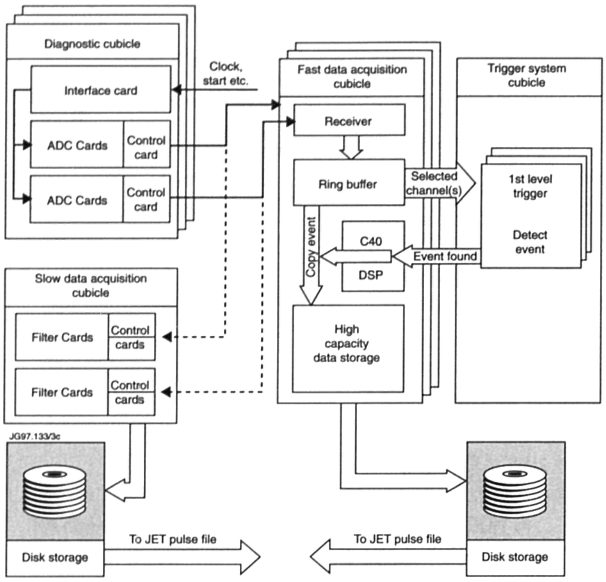

Fig.81: Schematic of the CATS system

an eight-pole analogue filter to prevent aliasing. The ADC is a 12 bit device sampling at 1MHz. Its output is digitally filtered down to 250kHz with a pass-band of 100kHz, and optically isolated before being passed onto the backplane. Data from each ADC is sent down an optical fibre via a TAXI interface. Each control card contains a programmable transputer to change the amplifier gains and DC offsets of each channel before a plasma pulse. Many of the racks of ADCs are in the Torus Hall some distance (~ 200m) from the station at which the data is initially stored. The data from the optical fibres is first reconverted to electrical signals and then processed and stored by a C40 based system which can record data for more than 3s for all channels at the full digitization rate.

It is intended that the trigger system will be split into two levels. The first implements a number of simple fast algorithms which process data in real-time from a few channels and this identifies interesting events within the plasma. The times at which positive identifications are made are passed on to the second level trigger system. The second level system can also contain many routines and can access data from any diagnostic on the CATS system. These routines can be quite complex and be interrelated with one routine dependent on obtaining a positive result from another. This system determines which data is actually stored and is implemented in a C40 system.

The incoming data streams from the soft X-ray channels are also used to provide data for the JPF. The digitised data in optical form at 250kHz is split and digitally filtered down to the desired frequency which is then stored in a transputer before being passed to the JPF after the plasma pulse.

Charge Exchange Spectroscopy

Overall Summary and Global Data Consistency

The activities in Charge Exchange (CX) Spectroscopy in 1996 were determined largely by the spectroscopic diagnostic requirements for the Mark II divertor plasma performance: (i.e. radiative cooling experiments, impurity compression and retention and exhaust studies). In reversed shear experiments, where profile shaping based on the assessment of the transport barrier requires immediate, between pulse analysis of ion temperature profiles, neural network techniques have contributed significantly for the progress of the experimental programme.

On the instrumental side, significant progress has been made by the simultaneous use of two observation ports in Octant No.7 and Octant No.1, respectively, for the observation of CX spectra along the neutral beams in Octant No.8. This dual observation and the addition of one more CX spectrometer (KS5C) has enabled the complete coverage of the main low-Z impurity density profiles. This has been an important asset, particularly in radiative cooling experiments with carbon, beryllium and helium present as intrinsic impurities and neon or nitrogen added as seeded impurity. Distinctive differences in the radial shapes of impurity concentration profiles could be established. A modified observation port for the bremsstahlung in torus mid-plane (KS3-AD14) has ensured a greater protection against window contamination. A broad-band spectrometer (KT3B) for the deduction of local ne and Te values from line-intensity ratio measurements was successfully commissioned in connection with a thermal helium gas inlet nozzle at the vertical target plates. In preparation for DTE1, the spectroscopic instruments needed for the analysis of the new Penning gauge exhaust diagnostic (KT5P) have been tested. Most of the CX diagnostic systems, except the KY6 lithium beam diagnostic, were given heated fibre links to the torus to avoid radiation induced transmission losses during DTE-1.

Corresponding developments have been made in the Charge Exchange Analysis Code (CHEAP), which was modified to cope with specific radial profile shapes for each of the analysed impurities. A further aspect was to ensure overall data consistency required in the deduction of plasma dilution, energy content and neutron production. A further addition to the CHEAP code was the implementation of a subroutine for the calculation of line-of-sight averaged Z_{eff} values, corresponding to the same vertical (and horizontal) lines-of-sight used for the averaged Z_{eff} measurements from visible bremsstrahlung, but which are based on the radial impurity density profiles (C, Be, He, N and Ne) from CX measurements. The agreement of $\langle Z_{eff}\rangle_{vertical}$ and $\langle Z_{eff}\rangle_{horizontal}$ as derived from the CX densities is an indication for the correct magnetic mapping of the horizontal and vertical lines of sight respectively.

Numerous calibration updates and data reprocessing of electron density and magnetic data (LIDAR, KG1, EFIT) have led to distinctive modifications and changes of plasma data derived from spectroscopic measurements. The validity of the electron density profiles provided by the LIDAR diagnostic, which are cross-calibrated in CHEAP by the line-integrated density signals from the far-infra red interferometer, plays a central role in the deduction of impurity density data from spectroscopic photon fluxes. Fringe-jumps in interferometric data need to be corrected interactively prior to the CHEAP reprocessing.

In general, global data consistency has been established for the 1996 campaign. The diamagnetic energy, (i.e. the sum of thermal and non-thermal energies) can adequately be reconstructed from the electron and ion energy content and the fast particle energy derived from CX data and neutral beam deposition profiles. In radiative cooling plasmas, Z_{eff} derived from CX data, agrees well with line-averaged Z_{eff} from bremsstrahlung. However, in hot-ion-mode pulses, the Z_{eff} reconstructed from individual ion densities is below the corresponding bremsstrahlung Z_{eff} value.

New Developments in CHEAP

One result of the quantitative analysis in the CHEAP code is the neutral beam attenuation along the beam axis. The beam deposition profile per flux surface is required to calculate fast particle pressure, power and torque profile as well as beam-thermal reaction rates. CHEAP is in the unique position to calculate these quantities for each pulse for which charge-exchange spectroscopy data have been analyzed. Two main improvements in CHEAP are highlighted:

a) The beam deposition calculation proceeds in two steps. First, local plasma parameters are mapped on the beam path to derive the number of beam particles deposited per unit length. In a second step, this areal distribution of particles is mapped on the one dimensional flux surface grid. For distances of beam axis from plasma centre large compared with the beam diameter, this procedure could be replaced by a simple Gaussian smoothing of the beam deposition calculated for pencil shaped beams. Previously, this simplification was adopted across the whole profile to make the calculation more efficient. Near the torus axis this resulted in an unphysical shape of the deposition profile, which has now been corrected;

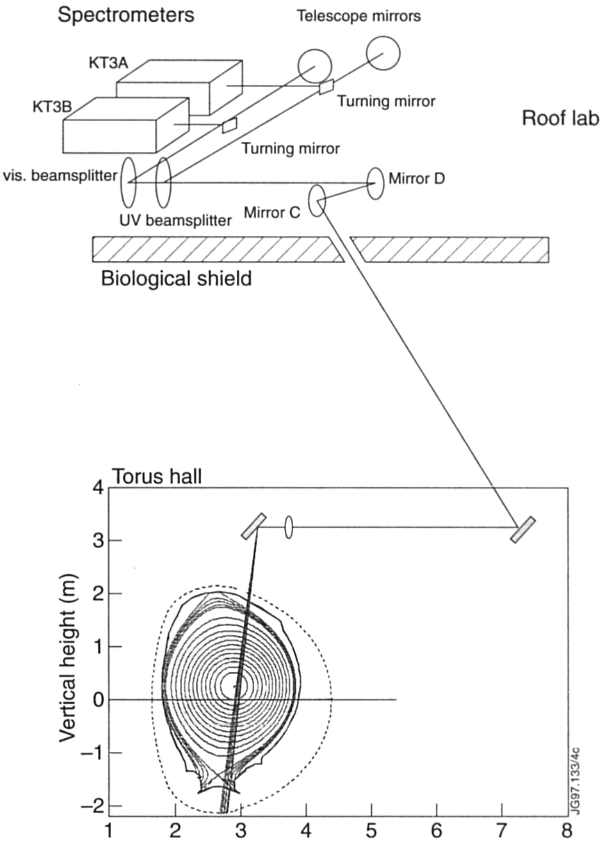

Fig.82: Layout of KT3D optical system

b) At the onset of neutral beam injection, the toroidal angular momentum rises instantaneously in the outer plasma. The toroidal angular momentum in the centre, where the fast ions are injected into passing orbits, and the thermal energy rises on the slowing-down time-scale of the fast ions. The behaviour can be explained by three mechanisms for momentum transfer from fast ions to the bulk. This model of the torque has been incorporated in the Fokker-Planck description of the fast ion behaviour.

Beam Emission Spectroscopy

At the centre of the CHEAP code is the calculation of the neutral beam attenuation, which requires a high degree of accuracy in all input data. The precise shape of the electron density profile plays a decisive role. For high

Table XII: Active Phase Charge Exchange Spectroscopy System (KT3A and KT3B)

	KT3A	**KT3B**
System description	Mirror link divertor spectroscopy system	
Viewing position	Outer divertor strike point	R_{major}= 2.880 m
	standard position:	r_{major}= 2.600 m
	Centre position furthest inward:	R_{major}= 3.200 m
Spatial coverage of divertor	150 mm around central position (75 mm)	
Spectrometer	1-metre Toroidal Mirror Corrected Czerney-Turner	
Detectors	2 Dimensional CCD camera	
Size	770x1152	1242x1152
	(755 x 360 pixels used for imaging)	(1222x 360 pixels used for imaging)
Main purpose	Near-UV spectroscopy of impurities	Visible spectroscopy
Accessible wavelength	2000 to 7000 Å	4000 to 7500 Å
Standard grating	1200 l/mm	300 l/mm
Dispersion	0.187 Å/pixel	0.73 Å/pixel
Wavelength coverage (1st order)	138 Å	895 Å
Instrument function	2.38 pixels	Not applicable
100 mm	0.45 Å	
at 2296 Å	430 eV	

performance plasma experiments, the ion heating efficiency is determined by the beam deposition profile, which is derived from the same subroutine. Distinctive changes of the power deposition in the pre-divertor (Mark 0) and divertor phases (Mark I and Mark II) have emphasised even more the need for high data quality, to investigate the differences of central- and off-axis-heating. Moreover, all of the non-thermal processes depend crucially on the neutral beam source rate profile.

In spite of early proof-of-principle results in 1991, beam emission spectroscopy as a direct tool for the local measurements of fast particle density profiles is still not routinely available. The complexity of the motional Stark spectrum in the heating beams, which is the basis for the deduction of local beam densities from observed line emission intensities, and, remaining uncertainties in atomic physics data have caused problems. During high power neutral beam heating, up to 54 spectral components contribute to the motional Stark spectrum. The successful deduction of line intensities was limited in the past to the exceptional case of pulses with a single neutral beam, or at most, a single bank operation.

High Resolution Divertor Visible Spectroscopy

The Active Phase CX Spectroscopy System (KT3D) is actually two separate spectrometers sharing the same optical path and viewing areas. The optical path images the outer divertor tiles onto the entrance slit of each spectrometer with a magnification of 1/20. With this magnification and restrictions of the port size and optics used, it allows 150 mm of the divertor to be imaged in the radial direction. The optical layout is shown in Fig.82. KT3A is dedicated to observation of the near-UV with a spectral coverage of about 135 Å (using a 1200 lines/mm grating) although it can observe emission lines up to 7000Å. KT3B is limited to visible operation from 4000 to 7500Å with ~900 Å (using a 300 lines/mm grating). The standard capabilities of the two systems are outlined in Table XII. Typically, the two spectrometers collect data along 12 lines-of-sight with radial size of 12.6 mm and radial resolution of less than 5mm (full width of 90% to 10% wing). The viewed area is remotely moveable so that different areas of the outer divertor and wall

Progress towards a Useful Divertor Diagnostic

In 1996, the KT3D system was upgraded to correct for several imaging defects. Optics were designed that formed the final image on the entrance slits from the achromatic lens telescope to a mirror-based Newtonian telescope. The next modification was to improve the poor imaging qualities of the spectrometers themselves. Although the spectrometers, when introduced ~15 years ago, were

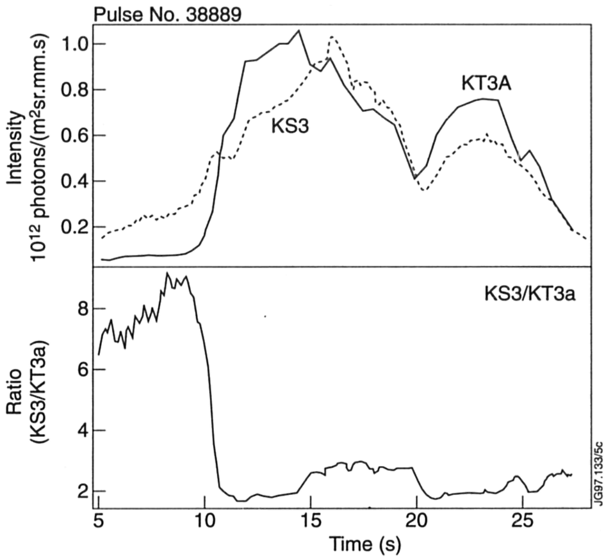

Fig.83: Comparison of KT3A and KT3 bremsstrahlung signals and the true ratio of KS3 to KT3 for Pulse No. 38889

meant to be imaging devices, it became obvious from the visible images of the divertor that there was a significant aberration in their imaging qualities. A third modification to the system was to change both CCD cameras.

The KT3A system operated from the start of 1996 and work was begun to commission the diagnostic. The KT3B diagnostic was awaiting the arrival of a new camera.

Firstly, the imaging characteristics and the amount of vignetting were evaluated. It was believed that the vignetting occurs mainly from mirrors B and C (Fig.82) but also from the turning mirror in the telescope. The plasma light was used to determine the vignetting of the system. During the ohmic, non-diverted phase of the discharge, the bremsstrahlung emission was assumed to be uniform across the line-of-sight. The bremsstrahlung was measured for each of the tracks across several of wavelengths.

A cross-calibration in intensity of KT3A in the near-UV with the KS3 diagnostic in the visible using bremsstrahlung signals was undertaken. A comparison of the bremsstrahlung signals for Pulse No.38889 is shown in Fig.83. The ratio of the bremsstrahlung signals for two different wavelengths but identical lines-of-sight is given by the inverse ratio of the different wavelengths.

In 1996, KT3A measured emission of CI, CII, CIV and BeI routinely in the outer divertor. In addition, NeIII and NeII lines were monitored during the neon retention experiments. A scan of the outer divertor was performed to assess carbon emission during CD4 puffing. Most of the data is awaiting a more complete analysis which will continue when the absolute calibration data is analysized and calibration files produced.

KT3B came on line in November 1996. PPF's have not been created yet as the system is being commissioned and the track-to-track calibration and absolute calibration are under-way. In addition to the standard wavelength setting, which observes D_β, D_γ and D_δ as well as CII, CIII and BeI and BeII, KT3B successfully observed the thermal helium beam at Octant No.8.

Divertor Periscopes and Penning Discharge Spectroscopy

The KT6D system has been used to study visible radiation from the divertor plasma under a variety of operating conditions. Using periscopes to overcome problems of restricted access, two vertically-aligned arrays collect light, respectively, from between the X-point and the inner strike zone, and the X-point and the outer strike zone. Each array comprises ten optical fibres of core diameter 300mm, covering a total height of ~ 60cm with spatial resolution ~ 2.5cm. Analysis and detection, in the range 400 to 750nm and with time resolution 50ms, is accomplished using grating spectrometers with CCD cameras. One instrument has pass band of 8nm with wave-length resolution 0.01nm, whilst the respective parameters for the other are 95nm and 0.13nm. Both instruments are calibrated absolutely.

Radiating divertor plasmas, produced by injecting Ar, Ne or N_2, have been studied, and the distribution and retention of these impurities determined. A thermal He beam has been employed to measure n_e and T_e in the divertor, from HeI line ratios. During L-mode operation, from an attached to a detached plasma, at the strike point Te drops from ~20eV by a factor of 3, whilst simultaneously n_e increases from ~ $5 \times 10^{18} m^{-3}$ by a factor of 5 or more. Doppler line broadening permits ion temperature evolution to be followed. The line shape of the injected species is characterised by two energy components, one of a few eV from electron-impact excitation of the cold influx, and a hotter component of 10 - 100eV from passive charge-exchange excitation in the divertor chamber.

The light collection and detection systems for KT5P have been installed and commissioned. This diagnostic will analyse the divertor exhaust gas by spectroscopically monitoring the discharge in a Penning gauge. The detection system comprises a high resolution spectrometer and CCD camera, with characteristics similar to the KT6D system, and four photomultiplier/filter combinations. In

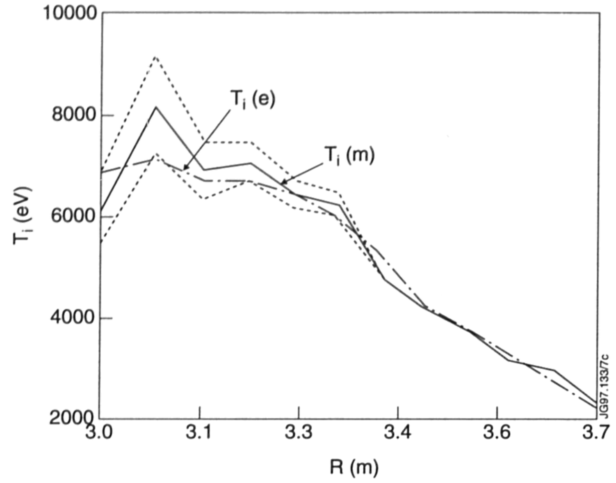

Fig.84: Neural network estimate of ion temperature, $T_i(e)$, and maximum liklehood analysis, $T_i(m)$, together with neural net photon statistics error laws (dotted line) (Pulse No. 38882)

particular, low thermal broadening of the gaseous species facilitates the separation of the deuterium and tritium components, using the spectrometer, when operating with a D-T mixture. A number of measurements have been made with the system on a test rig. The data has been used to simulate the sensitivity of the system in detecting tritium in the presence of deuterium as majority species. Results indicate that accurate measurements can be made down to the 5% level.

In preparation for the D-T campaign, heated optical fibre jumpers have been installed in the Torus Hall - as well as the controlling electronics in the Basement - for a number of diagnostics. This will improve the radiation resistance of the fibres by thermal annealing of the damage. The installation is close to completion and commissioning is under-way.

Neural Network Analysis of Charge Exchange Spectra

A system of neural networks have been trained and installed for automatic intershot analysis of charge exchange carbon spectra. This provides profiles for ion temperature, rotation velocity and total active charge exchange emission automatically after each pulse. The system consists of 28 different networks, one per viewing line and output parameter. The training data for the networks have been collected from a large range of scenarios from pulses analysed during two years of previous campaigns. This dataset consists of about 250,000 analysed spectra, of which about 150,000 have been extracted as suitable for the neural net training. The performance of the neural networks has been tested for several different scenarios (hot-ion modes, reversed shear experiments, etc.) and gives an accuracy comparable to the traditional maximum-likelihood analysis (Fig.84).

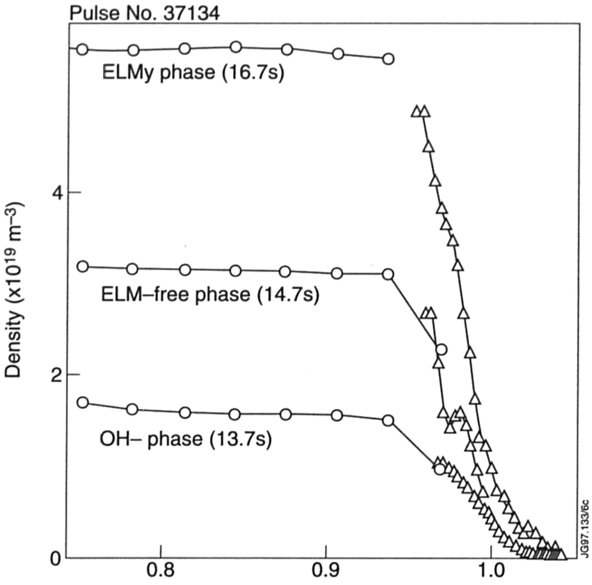

Fig.85: Comparison of edge electron density profiles for Li-beam diagnostic and LIDAR for three different plasma states

When the density is high, the accuracy in the central plasma is limited by the photon statistics caused by the attenuated beam. The accuracy in the neural network estimate will also be limited by this and to estimate this error a local linear approximation of the neural net is used to estimate the standard deviation of the neural net output. This calculation is done in a very efficient way using the results from the preceding feed-forward, thus cutting the time taken to evaluate these error bars down to about the same as one single feed-forward through the network (Fig.84).

The neural net evaluation of a spectrum does not involve any iterations or conditional branches and is very fast, the time taken to calculate a complete ion temperature profile is about 5ms, with error bars and novelty detection ~15ms, still well within the 50ms time window of the diagnostic. Thus, it will be possible to provide a real-time estimate of the ion temperature which could be used for the control of high performance plasmas or to simulate ignition and burn in D-T plasmas.

Li-beam Plasma Edge Diagnostic

A number of improvements have been made to the Li-beam diagnostic. The incorporation of an additional spectrometer system has enhanced the Li light collection efficiency and improved the signal-to-background ratio. Implementation, early in the new campaign, of remote optical alignment enabled more reliable imaging of the beam. New atomic data governing the collision processes

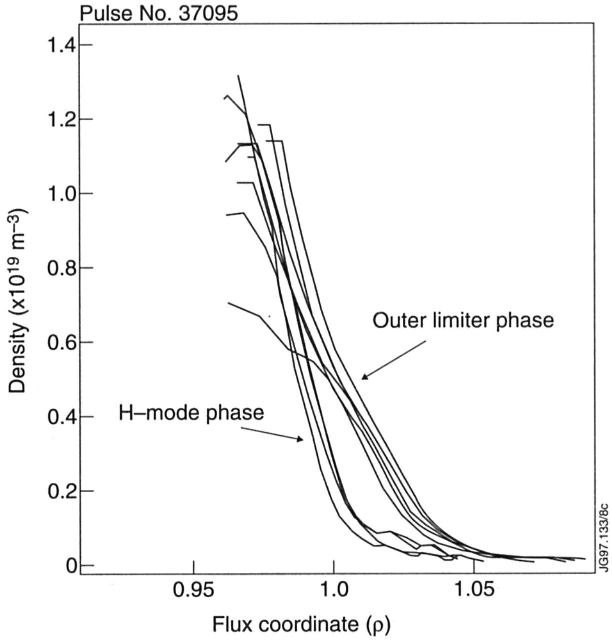

Fig.86: Comparison of edge density profiles from an outer limiter plasma and the subsequent hot-ion H-mode

between impurity ions and Li-atoms has been incorporated into the beam attenuation and emission evaluation code, and evaluated density profiles now include effects of impurities in the plasma edge. Recent results confirmed the good agreement obtained in the 1994/95 campaign of the Li-beam with LIDAR (Fig.85).

The main course of investigation was the change of edge density gradients during L and H-modes. Data was obtained for a series of similar discharges with a long outer limiter period followed by a neutral beam heated hot-ion H-mode phase. A steepening of the edge density gradient at the transition into H-mode (Fig.86) is observed. Whilst the electron density inside the separatrix rises with the increase in central density, the density outside the separatrix is little affected by central density changes.

Previous developments of Abel inversion of passive line emissions collected by the Li-beam line-of-sights have been extended to Bremsstrahlung signals, as well as to include the multi-chord system of the CXRS diagnostic. A new algorithm for emissivity determination has been developed and Z_{eff} profiles have been obtained. The good agreement obtained from inversion methods with those from CXRS analysis suggests that a self-consistent Z_{eff} determination in the edge region is possible for the Li-beam diagnostic in the future.

Conceptual Design of a MSE Diagnostic

The Motional Stark Effect (MSE) (the Stark splitting of a spectral line produced by the electric field associated with an atom's motion across a magnetic field) is used in several fusion devices to gain information about the internal magnetic field structure, in particular the *q*-profile. MSE emission features were first observed in the D_α spectrum from the JET heating beams [4]. Subsequently, measurements were made of the polarisation of line emission [5-7] and the magnitude of the Stark splitting [8], to provide input to the calculations of internal magnetic fields in JET. Developments in high resolution polarimetry for astronomical purposes were applied to the measurement of the polarisation angle of beam emission from TFTR [9] and DIII-D.

The components of the spectral lines in the Stark spectrum are polarised either parallel or perpendicular to the electric field, which itself is perpendicular to the plasma magnetic field. Applied to the neutral beams (deuterium) injected into a tokamak for plasma heating, the direction of polarisation of radiation yields information about the direction of the magnetic field vector in the plasma. Such information is essential for the calculation of the plasma magnetic field structure.

The use of the MSE technique in JET poses particular problems involving the geometry of the neutral heating beams and the vacuum ports available. A study was made of the feasibility of using this technique which showed that it would be possible to make use of this type of measurement, and that such a diagnostic could be constructed within the constraints imposed by the geometry. Work is now underway in collaboration with PPPL, USA and UKAEA Culham Laboratory to construct such a diagnostic with the aim of installing the first components on JET during the remote tile exchange shutdown, following DTE1.

Spectroscopy and Impurity Physics

Operation and Development of Bolometric Detectors.

The old JET bolometer (KB1) was used throughout the 1996 experimental campaign. Its cooling was modified from air to water as it was considered to be more reliable. In emergencies, the air cooling could be brought in naturally. This apparatus has been made available for real-time calculation of the total radiation and the radiated power fraction. For that purpose, the frequency modulated pulse train output from the bolometer amplifiers is converted into an analogue signal using a set of frequency voltage converters. The first step of data treatment of these analogue signals in the real-time signal server (RTSS) is to emulate in a digital filter the relation $\int Edl=C.(dU/dt+U/\tau)$ where U is the zero adjusted bolometer bridge voltage signal, t is the integration time constant of the bolometers, typically 0.2s, and C is the conversion factor into line-of-sight (LOS) integrated radiation $\int Edl$. The individual LOS measurements are combined with fixed weights, determined by analysis of a representative subset of pulses, to calculate the total radiation without making use of the magnetic surface reconstruction. The error is small, at around 3%. The ohmic heating and the additional heating powers, also available in the RTSS, are used to derive the radiated power fraction. There are two main applications: (a) real-time radiation control via feedback control of the flow of additional gaseous impurities; and (b) interpret a high level of radiated power fraction, close to the density limit, as a disruption precursor that may be used to trigger an automatic disruption avoidance scheme.

For the first time since installation in 1993/4, the full set of the 84 high temperature bolometer channels could be used. In the October shutdown, the four-channel camera on the inner wall was removed, since it had suffered too much plasma interaction. The set of seven cameras, newly installed for the Mark II divertor, was successfully commissioned and used throughout the year. Typically 50 to 60% of all installed channels worked well. Other channels suffer from various problems, which manifested themselves as moving baselines, large noise levels or no signal at all. The causes were erratic or broken in-vessel contacts and electromagnetic interference. Possible further influences are the heating up of the detector itself during the pulse and the influence of neutral gas on the measurement [10]. The interference from the 3GHz LHCD system was found to be smaller than previously, since some shielding had been installed, but quite a few channels were still affected significantly. An investigation in the LHCD test-bed revealed the mechanism by which the LHCD can still perturb the measurements despite considerable screening at the front face.

This investigation brought about a design change for the next generation of bolometers for the Mark II Gas-box, when three of the divertor cameras will be replaced. For these bolometers, the copper reference window shield has been removed. An additional design feature provides shielding from stray light. Another expected benefit from this design change is that the influence of neutral gas will be reduced since both the reference and the measurement bolometers will be exposed to the neutral gas.

One of the possibilities, exploited for the first time on the new system, has been the highly time resolved measurement of the radiation evolution during ELMs. Within the maximum signal bandwidth of 2kHz, it can be deduced that the total emitted radiation is similar in its temporal evolution to the D_α emission from the divertor; with a time lag that is accounted for by the heat pulse delay through the detector foil of about 0.7^{-1}ms and an electronic delay of about 0.25-5ms.

ITER work concentrated on the lines-of-sight (LOS) radiation related issues and initial research in a novel bolometer type. The criteria for the new LOS proposal were to make maximum use of the ports and the divertor, while maintaining the possibility of tomographic reconstructions, even in the presence of energetic neutral particle losses in the divertor [11]. The most urgent radiation concern for ITER bolometers is that at the proposed installation location, the radiation doses are 100 times higher than tolerable values, for mica foils which are presently used as substrates for the JET thermoresistive detectors. One of the most promising candidate materials to substitute for mica is Al_2O_3. The novel bolometer type under development promises higher sensitivity with fewer cables. Instead of relying on a relatively small change of electrical resistance with temperature, the new proposal uses the strong change of the dielectric constant of ferroelectric materials near their Curie-temperature. A high quality tuned circuit using a ferroelectric capacitor has a resonance frequency changing with temperature that can be tracked very accurately with phase-locked loop techniques. First measurements of the basic effect on samples of such capacitors have been encouraging. The next step is to proceed to first prototypes with high quality tuned circuits.

Bolometer Tomography

Analysis of bolometer measurements during the Mark I campaign, by means of tomographic reconstructions has continued. The algorithm used is a constrained optimization method which imposes smoothness as regularization. A different degree of smoothness can be chosen parallel or perpendicular to the flux surfaces and between the bulk plasma and divertor region. This method

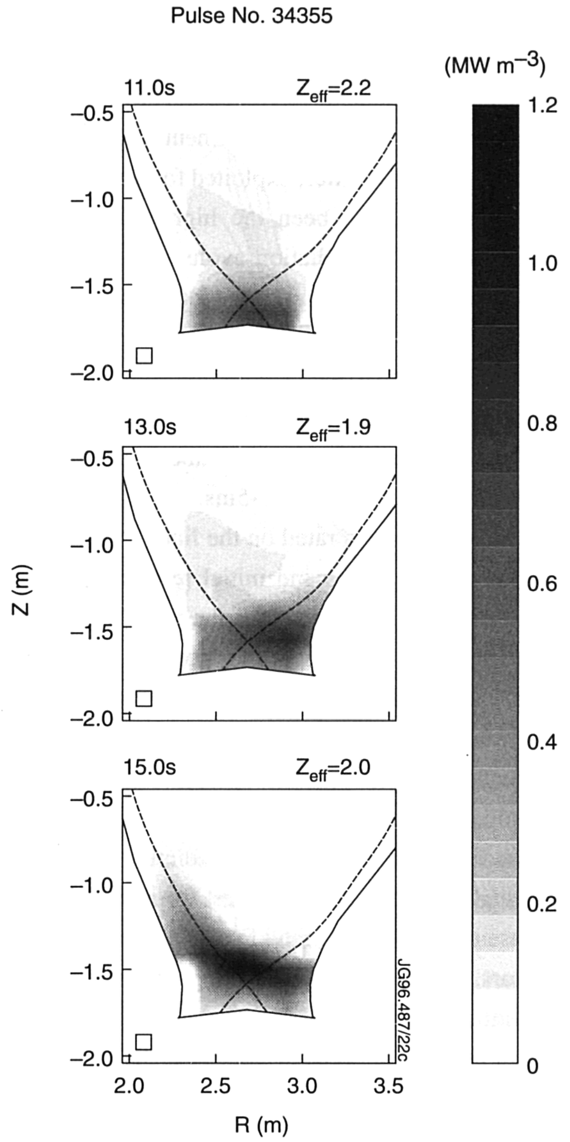

Fig.87: Tomographic reconstructions of the total emitted power during detachment (Pulse No. 34355)

works satisfactorily in many cases (Fig.87). The method has also been applied very successfully to soft X-ray tomography.

Complications that have to be taken into account in the analysis are the presence of neutral particles which give rise to an increased signal on some divertor bolometers and the small size of some emitting structures. These complications seem to be more severe in the Mark II divertor than in Mark I. Therefore, satisfactory reconstructions are harder to obtain in Mark II, despite the increased number of bolometers in this campaign. The algorithm has been, and is being, extended with several features to address these complications: (a) a convergence criterion that causes less oversmoothing in difficult cases has been implemented; (b) the actual beam widths of the views of the bolometers are taken into account instead of the approximation of thin lines; (c) the excess signal due to neutral particles is dealt with inside the algorithm and; (d) an efficient algorithm to impose positive values in the reconstructions has been added, which is needed to avoid negative values that often occur in regions poorly covered by views.

X-ray Spectroscopy

During 1996, several developments were made to the soft X-ray monitor spectrometer. A critical component of the soft X-ray survey spectrometer is its large-area proportional counter, which requires a thin polymer window to give useful transmission at wavelengths around 3nm. The aluminium-coated polyester film has been reduced in thickness from 2mm to 1.5mm, giving a factor four increase in sensitivity to the CVI Ly-a line at 3.374nm (the most important line monitored) as well as significant increases for Be IV and O VIII lines.

An upgraded detector has been designed and built to incorporate several improvements, the most significant being to replace the original woven window support mesh by a photo-etched mesh. The new mesh has a more regular hole pattern (useful in determining its transmission), is simpler to assemble, and has a much reduced tendency to puncture the thin window during assembly.

During 1996, the data storage capacity of the instrument was doubled, allowing faster sampling of the (scanning monochromator) spectrum, and an improved quality of spectral fitting. The increased sensitivity of this instrument, combined with background noise reductions due to a smaller detector volume and improved pulse processing, results in a signal-to-noise ratio improvement of a factor 10 relative to the configuration used during the preliminary tritium experiments (PTE) in 1991.

A new spectral fitting code has been implemented, using least-squares fits of multiple Gaussians, and giving a better treatment of weak and blended lines than the earlier programme. The line fits are combined with the instrument sensitivity functions to give absolutely-calibrated central-chord intensities of lines from all the major impurities.

Spatially Scanning VUV Spectrometers

The three spatially scanning VUV-spectrometers (KT1) (wavelength range: $200 \geq l(\text{Å}) \geq 2000$) have been put into operation. The instruments view the plasma cross-section and the divertor region. Two VUV-wavelengths can be monitored at a time by each instrument.

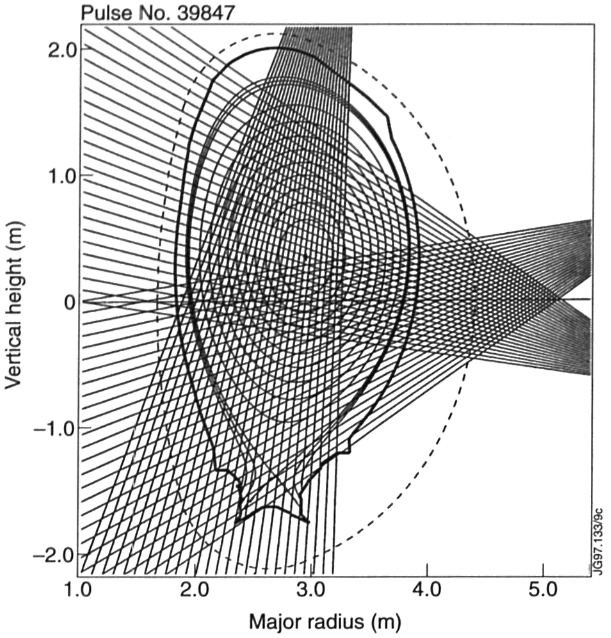

Fig.88: Viewing regions of the spatially scanning VUV spectrometers

Despite comprehensive testing on a prototype, some problems were encountered with operation of the diagnostic by the newly developed tritium compatible rotary feedthroughs. These drive multi-faceted (4 and 8 faces) mirrors inside the torus vacuum, and so provide the spatial scan. They tend to seize and two of them had to be replaced, when the torus was vented in October. The number of discharges where data were acquired is limited. Nevertheless, a good overview of radiation related plasma phenomena could be obtained.

During recent experiments, the main emphasis was on spectral emission of deuterium and carbon; as graphite is the major plasma-facing material. High fluxes of the two species were observed in the divertor region, with pronounced peaks close to the separatrix strike points. The maximum is typically higher at the inner separatrix leg. When detachment occurs, the peaks are moving up towards the X-point.

Figure 88 shows the viewing regions of the instruments. Typical profiles of CII- and DI-emission in the lower half of the plasma cross-section during an ohmic phase are depicted in Fig.89. Figure 89(a) shows, versus the lines-of-sight poloidal angle, the emission profiles in the divertor, as monitored by the top instrument. The prominent peaks occur where the separatrix hits the target. The side view into the same region is displayed in Fig.89(b). The divertor region can only be seen in part.

The fluxes in the main chamber depend sensitively on the width of the gaps between the scrape-off layer (SOL) and the wall. Where the SOL comes close to or hits inner structures, local maxima of carbon emission are observed, indicating enhanced carbon fluxes. During ELMs, the emission of carbon and deuterium increases significantly and can even exceed the emission in the divertor.

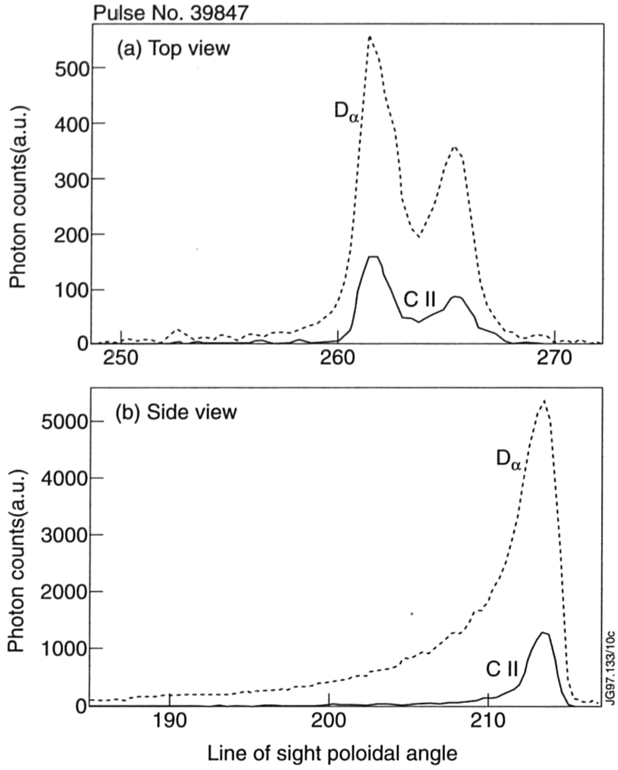

Fig.89: Emission profiles versus lines-of-sight poloidal angle for (a) top view and (b) side view

As two instruments are scanning the lower half of the plasma cross-section with two different viewing directions and allows resolution radiation profiles two-dimensionally, KT1 is particularly useful for transport studies, when tracer impurities are injected into the discharge. When neon is introduced, radiation from lower ionisation stages peaks in the divertor, while Ne-VIII radiation is confined to the plasma cross-section and peaks close to the X-point.

Divertor VUV/XUV Spectroscopy

Line radiation of the main plasma impurities emitted from the divertor region has been observed using the VUV/XUV spectroscopy diagnostic (KT7D). The instrument consists of three spectrometers, a double SPRED, which combines two VUV spectrometers in one instrument, and a SOXMOS for the measurement of XUV/VUV emission. A visible line-of-sight through the diagnostic has been used to obtain an absolute calibration of the VUV spectrum by means of branching ratios.

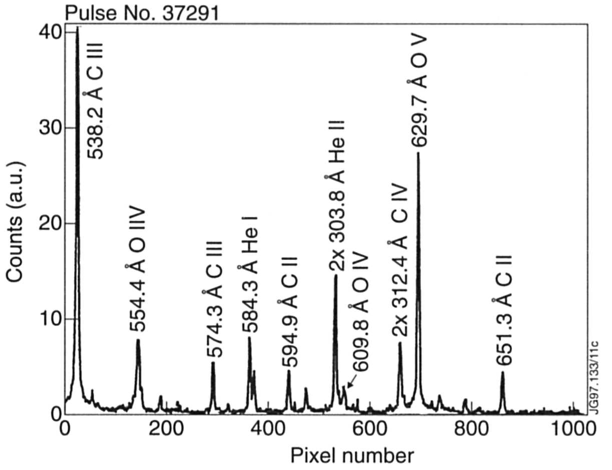

Fig.90: Example of SOXMOS spectrum (with line identification)

During 1996, the SOXMOS detector system was re-installed on the double SPRED. After careful alignment, the SOXMOS has started to produce data (see Fig.90). Further progress was made on the automated control of the instrument and the automatic analysis of the obtained data.

Bulk Impurity VUV/XUV Spectroscopy

VUV and XUV emission from the bulk plasma was monitored using two grating spectrometers during 1996. These were available from the start of the Mark II divertor programme.The SPRED spectrometer is a VUV instrument providing coverage of the wavelength region from 100 to 1100Å with a spectral resolution of ~ 40Å and can be moved remotely to record the spectrum at positions between 15 and 340Å. The SPRED has a near horizontal line-of-sight close to the vessel midplane, while the SOXMOS can be tilted to look at angles between the horizontal and a near divertor view.

Time histories of the line intensities of all the major intrinsic impurities (Be, C, O, Cl, Fe, Cr, Ni) were produced for the intershot analyses providing valuable information on the impurity content (and level) of a given plasma. Impurity influxes from elements such as Mn and Cu were also monitored routinely, as were impurities added for experimental purposes, such as nitrogen and neon for radiative divertor studies and various elements injected via the laser system.

A sensitivity calibration of these instruments was produced towards the end of the 1996 operations. This enabled the derivation of absolutely calibrated line intensity time histories and radiated power components for the major impurity species. By the end of the operational phase, a total of 37 spectral lines from 14 different elements were being recorded for each discharge. The temporal resolution of these data was typically 20 to 50ms over the entire pulse with 11ms resolution being available for intervals of a discharge of particular significance.

Both systems use the same PC based data acquisition system which was introduced, along with new detectors, at the beginning of the 1994-95 operational phase. A custom designed, stand-alone Windows software package was installed at the start of the Mk II operations; giving improved reliability and ease of use. The new software incorporates an initial real-time impurity intensity output via the PC ethernet connection. Work is progressing to upgrade this output to a dedicated I/O card and interface the system to the RTSS. This will enable these outputs (specified at eight per system at 11ms resolution) to be used for control/feedback application, an example being the potential use of the FeXXIII line at 132.9Å as an interlock for the Lower Hybrid Launcher movement relative to the plasma.

Remote control of the hydraulic movement of the XUV was successfully commissioned during the latter part of 1996. This uses a closed loop motion controller to drive a hydraulic ram which changes the viewing angle of the spectrometer from slightly below horizontal to a near-divertor line-of-sight. The controller allows a variety of movements including simple positioning between pulses, movement during a pulse to view different plasma regions during different phases of the discharge and continuous spatial scanning during a pulse. A closed circuit camera system has also been installed to observe the movement of the assembly from the diagnostic hall control cubicle.

Calibration of the XUV and Soft X-ray Spectrometers

Absolute sensitivity calibrations have been determined for the VUV, XUV and soft X-ray survey spectrometers. This includes the XUV SPRED spectrometer that observes the bulk plasma along a line-of-sight close to the machine's horizontal midplane, the SOXMOS spectrometer, whose line-of-sight can scan from the horizontal midplane down to a near-divertor view and a double SPRED instrument that observes the divertor plasma. The XUV region of the electromagnetic spectrum is one of the more difficult to calibrate and, consequently, it is of value to include the Bragg Rotor Monitor spectrometer in the suite of instruments whose calibration is being determined. This uses crystal and multilayer diffractors to observe the bulk plasma along a horizontal midplane and the photon counting detector employed in this device allows additional calibration techniques to be used. By using the available calibration methods and confirming the consistency of the sensitivities of the different instruments by cross-calibrations, sensitivities to within a factor of 2 have been determined.

A common technique used to extend a known calibration from one spectral region to another relies on the ability to calculate the branching ratio of atomic transitions from the same upper state with a good accuracy. Suitable transitions to connect the visible region with the VUV and XUV spectral regions occur in the elements D, He, and C. A standard source provides a calibration for the visible spectrum and this allows calibration points to be found for the VUV SPRED instruments. Despite the very different lines-of-sight of these spectrometers, a cross-calibration was possible and allowed confirmation of the branching ratio calibrations. It also enabled the sensitivity of the single SPRED to be extended to longer wavelengths, the use of the D branching ratio to a wavelength of 1025Å proving to be unsatisfactory for this instrument with its horizontal line-of-sight.

The SOXMOS instrument uses a blazed, ruled grating in a standard Rowland circle mount and the general shape of the sensitivity curve is known. After a cross-calibration from the single SPRED instrument in the wavelength range 100-150Å, the calibration could, therefore, be extended to shorter wavelengths and further comparisons made with the Bragg Rotor monitor channels, which routinely observe the Lyman transitions of Be, C and O.

The Bragg Rotor spectrometer offers advantages over VUV and XUV grating instruments in the determination of an absolute calibration, both because of its geometry and its photon-counting detector. The observation of near-parallel radiation from the plasma means that the transmission, reflectivity or efficiency of each component in the instrument can be characterized and used to derive an overall sensitivity for the instrument. Further, it is possible to measure the background emission in the spectrum and relate this to a calculated "free-free" and "free-bound" continuum emission from the plasma, electron temperature and density profiles being routinely available, thereby obtaining a second measurement of the sensitivity. The use of the background emission was found to be valuable for the shorter wavelength channels; however, signal-related noise made a significant contribution to the background for the longer wavelength channels, thus making the arrangements less reliable. Finally, the observation of absorption edges in the spectrum, such as the Ar K-edge at a wavelength of 3.9Å, which arises because of the use of this gas in the detector, provides yet another confirmation of the sensitivity calibration for this spectrometer.

Particle Dynamics

Far-infrared Interferometer and Polarimeter (KG1/KG4)

During 1996, the interferometer and polarimeter system has seen continuous improvement concerning reliability and ease of operation. In preparation for DTE1, the ducts connecting the Diagnostic and Torus Halls, through which the laser beams traverse, have now been completely sealed, so that environmental influences on KG1 operation have been minimized. The system performs well the key task of measuring absolute electron density, and in conjunction with the LIDAR Thomson scattering system, measuring the electron density profile.These measurements are indispensable for analysis and physics interpretation of all experiments.

Measurements of Faraday rotation angle using the polarimeter system are now regularly incorporated, together with soft X-ray camera determination of the magnetic axis, magnetic field measurements at the plasma edge, and measured kinetic pressure profiles in a Grad-Shafranov equilibrium computation, in which the best consistent magnetic configuration is identified using EFIT. The resulting q-profile is now well enough determined for systematic investigations to be made of effects of q-profile shape on plasma confinement behaviour.

Low Energy Neutral Particle Analyzer (KR2)

This instrument was refurbished early in 1996 by replacing all thirty channeltron detectors. The overall availability and reliability have also been greatly improved in preparation for forthcoming DTE1 experiments. KR2 will be the key instrument for measuring fluxs of atoms of H, D, T and He^4 from the plasma and thus in determining the plasma composition.

A persistent worry in JET deuterium plasmas with high power NBI heating is the inability to fully account for the measured neutron yield in terms of measured plasma composition, temperature profiles, and heating parameters. One conjecture is that there are sources of hydrogen in the torus and that the neutron shortfall is due to dilution of deuterium plasmas by hydrogen. The NPA measurements have addressed the question of hydrogen behaviour in much detail. A large increase in the relative concentration of hydrogen was observed during the ELM-free phase of hot-ion H-mode deuterium plasmas [12]. Subsequent to the first giant ELM, the relative hydrogen concentration reverted to its initial target plasma value. At the time, this behaviour was attributed to increased desorption of hydrogen from exposed metal inner wall of the torus during the ELM-free hot-ion H-mode. Subsequent cladding of the inner torus wall with graphite has reduced but not eliminated the effect. The question of why there is hydrogen enrichment of the plasma during ELM-free hot-ion H-mode remains outstanding.

Prospects of measuring Tritium Content (n_T/n_D)

The determination of any ion concentration ratio of two different species can only be based on the assumption of a thermal plasma with the same $T_i(r)$ for the species in question. This is well justified during ohmic phases. In this case, sufficient intensity of the neutral particle fluxes is obtained only for $E<10$keV, which means that, roughly, the outer half of the plasma column is actually monitored. During NB injection, the non-thermal component has proven to be appreciable beyond 10keV, leading to the same restriction for the useful energy range. In this case of additionally heated plasmas, however, this means monitoring a rather narrow edge region only.

The data delivered by the NPA is the charge exchange neutral flux ratio. Its conversion into a concentration ratio requires the calculation of a conversion factor C. A simple procedure, applicable to ohmic plasmas, which uses the measured electron density and temperature profiles, has proven successful with respect to H/D, where $C=0.5 - 0.8$. It can be applied to T/D as well, where C will be larger than unity but $|C-1|$ will be smaller than in the case of H/D. Unfortunately, no simple routine procedure like that is available for additionally heated plasmas, but in this case C can be expected to be close to unity anyway.

High Energy Neutral Particle Analyzer (KF1)

This NPA is intended for measurement of perpendicular velocity distribution function $f(v_\perp)$ of hydrogenic ions and alpha-particles in the plasma; the line-of-sight geometry determining that the measured ions are trapped and have pitch-angle $\pi/2$. During 1996, the NPA was equipped with a neutron shield in readiness for DTE1. In addition to preparation for alpha-particle measurements, a vigorous programme of measurement and interpretation of MeV energy hydrogenic ion interactions in ICRF heating and LH current drive regimes has been pursued. This activity has proven valuable in understanding the meaning of the measurement and in testing and improving physics models, which are used in numerical codes to simulate existing experiments and to model and develop application of ICRF heating and LH current drive in future experiments.

This has included: (a) interpretation of ICRF-heated minority proton distribution function [13]; (b) two-dimensional time-dependent solution for minority ICRF heating [14]; (c) dissipation of lower hybrid waves by MeV energy ICRF driven protons [15,16]; (d) neutralization of alpha-particles in deuterium-tritium plasmas during DTE-1 [17, 18]; (e) modelling of NPA measurements of high energy alpha-particle distribution functions.

References

[1] Cherubini A et al, Plasma Phys. & Contr. Fusion, **38**, 1421 (1996)

[2] Gill R D et al, 23rd Conf. on Plasma Phys. & Contr. Fusion, (Kiev, Ukraine 1996)

[3] Conway G D, Schott L and Hirose A , (1996) Rev. Sci. Instrum. **67**, 3861

[4] A. Boileau et al., J. Phys. B, At. Mol. Opt. Phys. **22** (1989) L145

[5] W. Mandl, R. Wolf, M von Hellermann, Plasma Phys. Contr. Fusion, **35**, 1373, 1993, JET-P(92)93

[6] R Wolf, J O'Rourke, A.W. Edwards, M. von Hellermann, Nuclear Fusion Lett., **33**, 663(1993)

[7] R.C. Wolf, L-G Eriksson, M. von Hellermann, R. König, W. Mandl, F. Porcelli, Nuclear Fusion, 33, 1835(1993)

[8] A. Howman, Private Communication.

[9] F. M. Levinton, Rev. Sci. Instrum. **63** 10 (1992) 5158

[10] "Bolometer for ITER" R Reichle et al in "Diagnostics for Experimental Thermonuclear Fusion Reactors, ed. P.E. Stott, G. Gorini, E. Sindoni, Plenum Press New York, 1996

[11] "Low energy neutral particle fluxes in the JET divertor, R. Reichle et al., Contr. to 12th PSI, Saint Raphael, France, 20-24 May 1996, to be publ. in Journ. of Nuclear Materials

Table XIII: Breakdown of Days in 1996

	Days	%
Restart (March - June)		
Restart	41.5	57.6
Access	20.5	28.5
No Access	10	13.9
Total	**72**	
Operations (June - September)		
Operations	76	70.4
Commissioning	6	5.5
Access	14	12.9
Maintenance	2	1.9
PDFA Intervention	8	7.4
No Access or Operations	2	1.9
Total	**108**	
Restart (October - November)		
Restart	17	77.3
Access	5	22.7
Total	**22**	
Operations (November - December)		
Operations	16	53.3
Access	3	10.0
NB Intervention	11	36.7
Total	**30**	
Overall Total	**232**	

[12] K.Gunther, G.Bracco, R.Konig, M.F.Stamp and K-D.Zastrow, Journal of Nuclear Materials, Proceedings of the 12th International Conference on Plasma Surface Interactions, May 1996.

[13] K.G.McClements, R.O.Dendy and A.Gondhalekar, Proceedings of the 23rd EPS Conference, June 1996, JET Report JET-P(96)50, and Nuclear Fusion, to be published.

[14] S.Dalla and N.N.Ljepojevic, JET Report JET-P(96)56, and submitted for publication in Physics of Plasmas.

[15] Y.F.Baranov, A.Ekedahl, P.Froissard, C.Gormazeno, M.Lennholm, F.Rimini, F.X.Soldner, Nuclear Fusion, 36(1996)1031.

[16] D.Testa, A.Gondhalekar, L.-G.Eriksson, C.Lashmore-Davies, M.J.Mantsinen and T.Martin, Contribution to the 24th EPS Conference, June 1997.

[17] A.A.Korotkov, A.Gondhalekar and A.J.Stuart, JET Report JET P-(95)47, and Nuclear Fusion, 37(1997) in press.

[18] A.A.Korotkov and A.M.Ermolaev, 22nd EPS Conference Abstracts, 19C(1995)III-389.

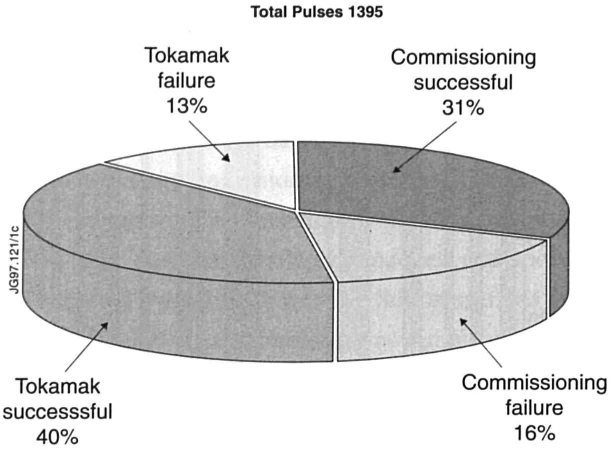

Fig.91: Restart Pulses - 1996

Summary of Operations

The shutdown for the installation of the Mark II divertor ended on the 28th March 1996. The Restart period then started and was completed on 10th June 1996. Mark II divertor operations continued until 28th September 1996. At this time, a further shutdown occurred until 26th October for the divertor bypass filling. Restart after this minor shutdown was much shorter and took place until 22nd November. Task Force Operations on the Mark II divertor with bypass filling lasted until 10th December 1996, and was curtailed due to a water leak, which developed in the Octant No. 8 Neutral Beam system.

The breakdown of days during the four periods of operation (two of Restart and two of Task Force operation) are shown in Table XIII. During the year, out of the 232 days available 150.5 days of operation were achieved (64%).

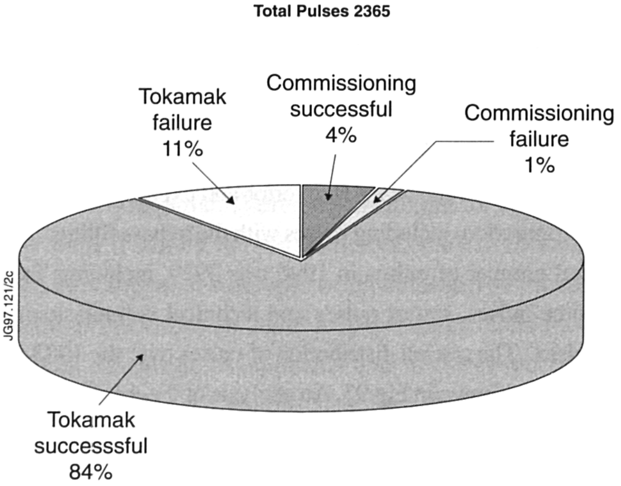

Fig.92: Task Force Pulses - 1996

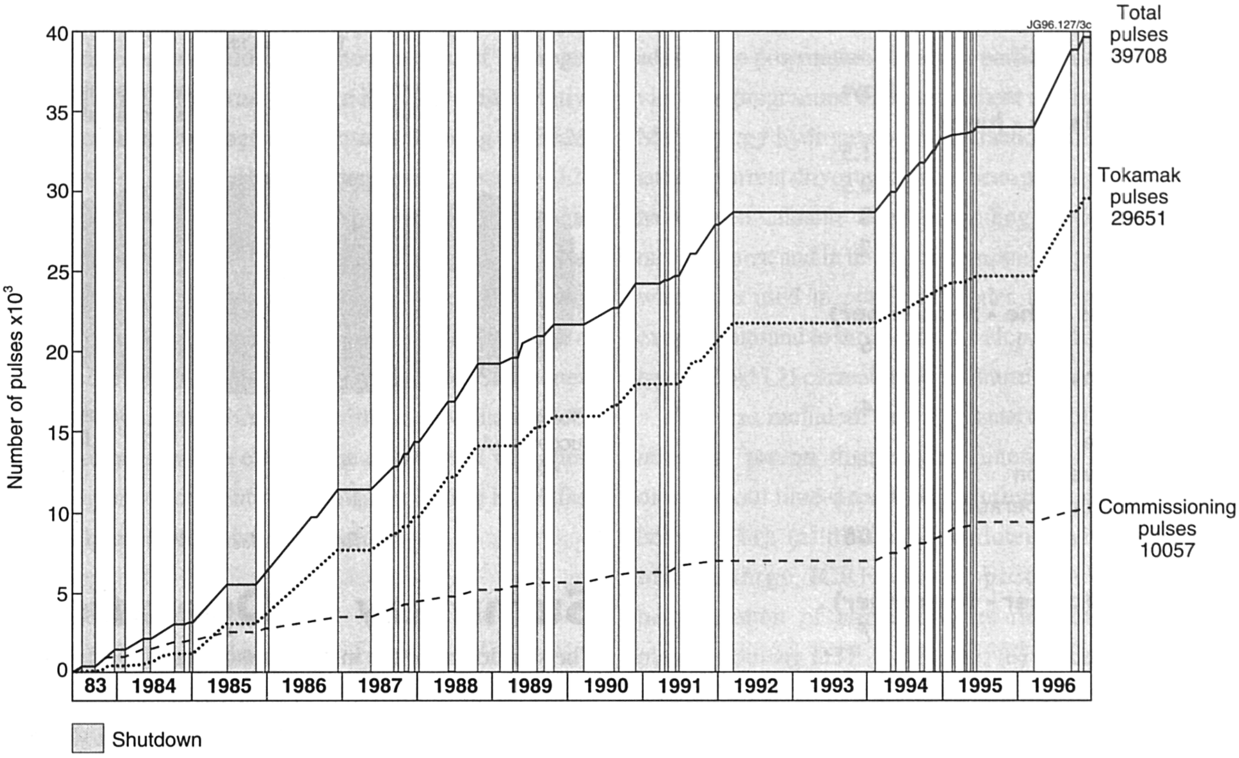

Fig.93: Culminative total of JET Pulses: 1983-1996

Breakdown of Pulses

Restart Pulses

During the two restart periods, 1395 pulses were run and the distribution of these pulses is shown in Fig.91. These were successful restarts with no major problems and a successful pulse rate of 71%.

Task Force Pulses

There were 2365 Task Force pulses during the year and these were distributed as shown in Fig.92, with a success rate of 84%. The distribution between the Task Forces was: Divertor Physics Task Force (D) - 34.9%; High Fusion Performance Task Force (H) - 30.6%; and ITER Physics and Performance Optimisation Task Force (P) - 34.5%.

Overall Summary

1996 was a good year for JET, with completion of the installation of the Mark II divertor and experiments in this configuration, including pulses with the bypass filling. The total number of pulses in 1996 was 3929, including Task Force pulses, restart pulses and technical commissioning pulses. The overall distribution of pulses over the 1983-96 period is shown in Fig.93. An analysis of the distribution of the plasma current shows that operations in the range 2-3MA continued to be routinely established and represented 64% of all plasma pulses (Fig.94).

Summary of Technical Achievements

One of the advantages of the JET machine is its capability to adapt flexibly to new scientific requirements. During the years, JET has undergone a number of modifications and upgradings suggested by results and those considered necessary for further progress to be achieved. These engineering developments were implemented without replacing any of the major tokamak components (vacuum vessel, toroidal and poloidal field coils), and by making use of the UK's 400kV Grid for further power and energy requirements.

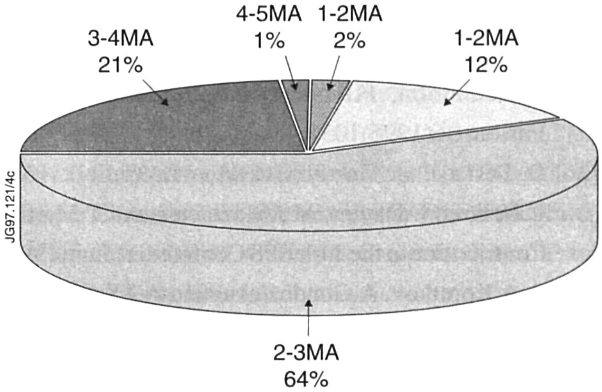

Fig.94: Plasma current distribution for 1996

The high performance results achieved during the first few years of JET operation, clearly indicated that passive control of impurities was not sufficient to maintain high performance for more than one or two seconds duration, due to the detrimental effect of the combination of MHD instabilities and excessive accumulation of impurities in the X-point region. Active control of the impurity influx into the plasma has proved necessary for a tokamak reactor. To implement active impurity control in a tokamak, the machine must be equipped with a pumped divertor to control impurity levels and particle and energy exhaust.

Therefore, the divertor programme has become the focus of JET physics and engineering activities, and implied a further major upgrading of the JET machine. This involved installation of new poloidal coils, power supplies, ICRF antennae, diagnostics, a completely new configuration of the vacuum vessel first-wall and new plasma control and coil protection systems. Three divertor configurations were foreseen to study optimum divertor performance for the benefit of the ITER design: Mark I, Mark II and Mark IIGB (Gas Box) providing progressively "more-closed" configurations. Mark I, installed in 1992-94, operated successfully in 1994-95, and then this configuration was replaced with the Mark II divertor for the following 1996-97 experimental campaign.

Mark II Divertor Design and Installation

The Mark II divertor was conceived to provide a "more-closed" configuration, leading to enhanced particle and impurity retention in the divertor chamber. It was designed to minimise the modifications required to install different divertor configurations at later stages (such as Mark IIGB).

Mark II consists of a new inconel continuous water-cooled toroidal tray, which acts as support structure on top of the divertor coils (unlike Mark I, it has independent supports). The tray is formed from three concentric rings, consisting of a base plate, and an inner and an outer ring. The structure was made up of 24 modules, consisting of a honey-comb with 4mm vacuum and water retaining walls, manufactured with stringent specifications for vacuum tightness, mechanical properties, dimensional stability and corrosion resistance. On top of this structure, tile carriers and CFC tiles were installed to match the Mark II divertor configuration and could be subsequently replaced with different divertor configurations by means of remote handling. The restricted space and the hostile environment (radiation and beryllium contamination) effected design, requirements, and assembly procedures. As part of the overall shutdown preparation, an accurate full size mock up of the vessel, using the spare machine octant as a central element, was set up (In-Vessel Training Facility, IVTF). Three dummy load modules were used to prove the handling inside the vessel, both hands-on and with remote handling techniques. The dummy modules were also used to develop techniques and tools for assembling a joint while wearing full pressurised suits.

The Mark II installation work was completed in March 1996 and after an extensive sub-system and machine integrated re-commissioning without and with plasma, the experimental programme started in June 1996.

Further Engineering Development

The necessity to move from Mark II divertor to Mark IIGB divertor configuration, immediately after completion of the first deuterium-tritium experiment (DTE1) (foreseen for Spring 1997), has required the replacement of tiles by remote handling techniques (6000mSv/hr expected inside the vessel at the end of DTE1). The remote handling tools developed at JET over the years, to carry out routine maintenance, repairs and replacements, are centred around the Mascot servomanipulator. The Mascot can be positioned where desired by large transporters: in-vessel by the Articulated Boom and ex-vessel by the Telescopic Articulated Remote Mast. The operator performs the job from a remote control room, through the master-slave device. Complex planned and unplanned operations can be performed, as the sophisticated servo and control systems of Mascot give the operator the tactile sensation of actually doing the job with his hands. Navigation and pre-positioning is performed automatically, using teach-and-repeat computerised techniques.

Extensive work has been performed to adapt the JET remote handling system to the tasks associated with the installation of Mark IIGB in active conditions. The IVTF has been used extensively to perform all operations eventually required. The remote operations for the removal of Mark II and for the installation of Mark IIGB involve the handling of seven types of modules at 144 locations around the torus. In addition, other tasks related to in-vessel diagnostic components and to interventions for possible failure of remote handling components in the vessel have been tested. To further ensure the operability of the system, a number of Mark II modules have actually been installed by remote handling.

The new Plasma Control System, (Plasma Position and Current Control, PPCC), played a key role in the success of the Mark I campaign. Its accuracy and flexibility in controlling plasma discharges have been further enhanced to better meet the requirements of operation with Mark II, by redesigning both the Shape Controller (SC) and the Vertical Stabilisation System (VS), including both hardware and software. The updated SC controller shows better control of the poloidal flywheel generator, leading to a greater accuracy in plasma current control. The number of plasma-wall distances (gaps) to be controlled has been increased, since this type of control is preferred as plasma shape and position do not change during the experiment, unlike other plasma parameters such as β and current profile. The vertical stabilization system upgrading was dictated by the necessity of attaining more information to study plasma behaviour during fast events, such as ELM's and by the decision to explore the possibility of using a Soft X-ray diagnostic to control plasma vertical speed. The Mark II support structure is a continuous conducting toroidal tray, and induced currents would not allow the magnetic field null formation for breakdown. Therefore, this system now has the capability of generating a current proportional to the current induced in this structure, re-establishing the magnetic field null at the centre of the vacuum vessel.

The AC-DC Converters of the Poloidal Divertor Field Amplifiers (PDFA) supplying the four divertor coils generate harmonics at a frequency of multiples of 600Hz. These coils are strongly coupled to the (bottom) magnetic field measurement detectors used for plasma control. The amplitude of the coupled signals were so large that these detectors could not be properly used during the Mark I campaign. Since attempts to compensate the magnetic signals were not successful, harmonic power tuned filters were installed, capable of 32dB attenuation for 600 and 1200Hz harmonics and 20dB for other harmonics. The filters were successfully commissioned without plasma. However, the current induced in the divertor coils and circulating in the filters at plasma breakdown prevented plasma initiation. The filters have been modified successfully by adding a 10 W resistor in series with each filter, to be switched off 100-200ms after breakdown.

The Coil Protection System (CPS), already operational with Mark I, has been extended to include ampere-turn protection for both the toroidal coils (supplementing the existing hardware protection, based on voltage comparison between coils, DMSS) and the divertor coils. Work is underway to implement additional protecting functions, such as the measurement of radial and vertical expansion of the toroidal coils, as a linear combination between the magnetic expansion, due to the interaction between the coil current and the self generated magnetic field and the thermal expansion, due to the dissipated energy. The algorithm for the measurement of the forces on the supporting ring and collar teeth of the mechanical structure and of the shear stress on the coil insulation, calculated in real-time from the measurement of the coil current and the (normal) flux loops, has been successfully tested.

The basic configuration of two Neutral Beam Injectors (eight beam-lines each) has not been modified. However, operational flexibility has been enhanced by further alleviation of limitations arising from 'shine-through' exposure of in-vessel structures and from deposition of re-ionised beam particles on torus entry duct surfaces, by installing CFC tiles at appropriate locations. The beam-line calorimeters have been replaced with new ones of enhanced capability in power density loading ($20MWm^{-2}$), thus allowing longer pulses in asynchronous operation (no beam into the plasma). All 16 beam lines have been made compatible with tritium and the AGHS (Active Gas Handling System) can now supply the injectors with deuterium and/or tritium. During DTE1, eight beam-lines will be operated at 80kV, 55A and supplied with deuterium (13.6MW) and eight beam lines supplied with tritium, will be operated at 160kV, 30A (12MW).

During the 1994-95 campaign, the average power coupling to the plasma from the ICRF antennae was significantly less than anticipated. Therefore, the antennae were removed during the shutdown to incorporate a number of modifications. Additional capacitance was added to the cross-over straps linking the inner conductors to the incoming vacuum transmission lines, the antennae were displaced 6mm inwards and the lower straight section of the limiter sections were modified to better follow the plasma curvature. Moreover, several modifications were introduced in the electronic circuitry, such as the addition of a conditioning mode, to maximise energy deposition without risking antenna damage. As a result, 15MW of coupled power to H-mode plasmas was achieved in dipole phasing.

Work on pellet injection concentrated on the Pellet Centrifuge, designed to deliver strings of 2-3mm deuterium pellets of up to 1 minute duration at a repetition rate of

$40s^{-1}$ and velocities from 50 to 600m/s. The system is now installed and operational and 5Hz strings of pellets have been launched into the plasma for pellet windows up to 5s.

The Active Gas Handling System (AGHS) is a full gas reprocessing plant, built to collect the gases from the torus, to remove impurities from hydrogen, to isotopically separate the hydrogen gas into streams of protium, deuterium and tritium, to store the deuterium and tritium in U-beds for re-use and to inject D and T back into the torus. Isotope separation makes use of cryo-distillation and gas chromatography. It was designed for a maximum daily throughput of up to 5 moles of tritium, 15 moles of deuterium and 150 moles of protium. It was installed in compliance with a strict quality assurance programme and went through an extensive phase of inactive testing. Tritium commissioning was performed in two steps. Trace tritium commissioning with about (~ 0.08g) was performed with a tritium-hydrogen gas mixture. Full tritium commissioning with about 3g of tritium is underway, to test the complete process using all sub-systems.

The design of the Mark IIGB di*vertor* tile carriers has been completed and manufacturing is well advanced. The requirement to accept $2MW/m^2$ anywhere on the tile carrier structure led to the decision to use carbon-carbon fibre composite (CFC) plates for both the tiles and the structural supports. This represents a new feature for JET and therefore thermal and mechanical tests have been performed, including tests on a representative septum at 250°C. The structure was subject to vibration, pulse and steady state loads, proving that the copper bolts retained the original torque.

Machine Upgrading

Further machine upgrading has been considered for increasing global fusion performance. In the late 1980's, JET had increased plasma current capability from the design value of 4.8MA to 7MA in limiter mode and, more recently with the divertor, to 6.0MA in H-mode plasmas. Extensive studies have now been performed to assess the possibility of increasing the toroidal magnetic field from 3.45T to 4.0T.

Finite element stress analysis has shown that for a variety of high performance scenarios, the shear stresses on the interturn insulation and tension on the copper brazed joints are well within their design capability and the evaluation of the manufacture documentation, including tests on insulation and on brazed joint samples and on the prototype coil, indicate an acceptable margin of safety at 4.0T.

Between 1989 and 1991, three TF coils developed interturn electric shorts due to water leaks. The water coolant was replaced by Freon and no more faults became apparent. It has been decided to use these coils to perform further tests. One of the coils has been cut for inner visual inspection and to extract samples, now under testing for shear stress in the interturn insulation. Another coil will be used for repeating some of the tests performed on two occasions on the prototype coil, during manufacture in 1979 and in 1987 as part of the assessment for 7.0MA operation. If these results support the finite element calculations, operations above 3.45T should be approved. To avoid any delay, the order for the upgrading of the TF power supplies has been already placed.

The effects of a 4.0T field on the P1 coil, which transfers the inward force of the toroidal magnet to the inner support steel cylinder have also been studied. The analysis has shown that the P1 coil temperature is the most critical feature for high toroidal field operation, as a raised temperature in P1 transfers load from the inner support cylinder to the coil. This can be prevented by limiting the I^2t of P1 to $2.8 \times 10^9 A^2s$, which still allows the proposed plasma operation scenarios.

The strongest contribution to the out-of-plane forces on the toroidal coils are the magnetic field created by the shaping coil P2 and P3, which have an essential function in establishing X-point configurations, plasma elongation and triangularity. Therefore, there is an apparent conflict between physics requirements and the desire to limit the forces exercised on the machine and, in particular, on the toroidal coils. Ways to maintain high triangularity and good ICRF heating power coupling, which reduce the lateral forces on the toroidal coils are being investigated.

Experiments conducted in the Neutral Beam Test-bed, using a prototype modified accelerator structure have demonstrated the capability to increase the ion beam current from the present 30A to 60A at 140kV. This would lead to an enhancement of injected power from 4 to 6MW per box (eight injectors). While minor modification would be required of the NB injectors, additional power supplies are required, since the present supplies are for 60A at 80kV (or for 30A at 160kV). Taking into account cost considerations it has been decided to upgrade the power supplies to 60A at 120kV (which would somewhat reduce the delivered beam power).

Studies are well advanced on a power upgrading of the ICRF heating system: in fact, the RF generators cannot provide full power in the presence of ELMs, due to the rapid change of coupling resistance with which the present automatic tuning system cannot cope. A new scheme has been designed, based on rapid change of generator frequency. This is achieved with a sliding impedance tuner, consisting of a section of transmission line with characteristic impedance of 105Ω, whose position and length can be varied.

Effects of Plasma Behaviour on Structural Components

Since early operation, JET experienced vertical instabilities and disruptions (Vertical Displacement Events (VDEs)). These caused vessel forces and displacements well beyond the levels considered in the original design , (ie, forces up to several hundred tonnes and displacements of several millimetres). Initially, the vacuum vessel was only supported by vertical elastic suspensions at each octant joint and at each main horizontal port (MHP). Therefore, the vacuum vessel has been progressively provided with new supports. New measurements of vessel radial and vertical forces and associated vessel displacements have been measured. These supports could only be installed on the MHP and on the main vertical ports (MVP) due to non-accessibility of the vessel main body.

Following the installation of the divertor, new phenomena were noticed. It had always been assumed, that the vertical forces were essentially toroidally symmetric. Therefore, analysis of a VDE event in May 1994 showed that these forces were toroidally asymmetric. Previous disruptions with and without the divertor were then re-assessed and a number of similar asymmetries were found, but these were more significant, with divertor plasmas. In June 1995, vertical stabilisation was lost at a plasma current of 3.5MA. The vertical force was only ~ 1.8MN, but not uniform toroidally and the most striking observation was that the radial displacement measured indicated that the whole vessel was displaced sideways, (in the direction of Octant No.1 to No.5) by 5.6mm. The toroidal asymmetries in vessel forces corresponded to asymmetries in the toroidal distribution of halo currents, measured at the graphite mushroom tiles installed at the top of the vessel.

During the subsequent shutdown, it was discovered that these sideways motions caused damage to the seals of the two rotary valves connecting the MHP to the neutral beam injection boxes. A new system of hydraulic lateral restraints linking the MHP to mechanically fixed bridges between the mechanical structure the transformer limbs was installed. These formed a complete belt surrounding the vessel, and was expected to lead to an appreciable reduction of radial displacement during VDEs.

The same type of VDE continues to occur with the Mark II divertor with a radial displacement of 7mm, in spite of the fact that the lateral restraints worked according to design specifications. The lateral force was higher than anticipated (~ 400 tonnes instead of ~ 150 tonnes), and therefore, another dumping mechanism must be present. Preliminary calculations showed that magnetic dumping of the vessel moving across magnetic field lines is far more effective than the installed hydraulic restraints. Further work is underway to better assess the mechanism of these events.

It was obvious that the appropriate way to counteract these forces and displacements, would be to support the vessel directly and not through the ports. Unfortunately, the engineering relevance of VDEs was not known to the original JET designers and the other large tokamaks in the mid seventies. Therefore, when the first serious event occurred in 1984, the vessel was not accessible and the only choice was to support the vessel through the MHPs and the MVPs.

In conclusion, the knowledge acquired so far is insufficient to devise means to prevent such events. This understanding and intuition suggest that, as an electrical machine, the tokamak should not be compared to a transformer, but better to a motor (or a generator) where the plasma (rotor) is moving. As in an electrical machine, both a good mechanical and magnetic accuracy is needed to limit the so called 'unbalance magnetic pull'. which make the rotor oscillating around the mechanical axis. Therefore, VDEs should reduce in importance in a tokamak, if the vessel walls were smooth and toroidally symmetric and if 'error' magnetic fields were reduced as much as possible.

This type of interaction between plasma and structures should be considered as a problem to be seriously addressed both in present tokamaks and in ITER.

Scientific Achievements during 1996

Introduction

For 1996, the operation system of the scientific programme was similar to that employed since 1989. The programme operated for a series of campaign periods, the standard being of eight weeks duration (composed of six weeks tokamak operation and two weeks of maintenance/ commissioning). Two Programme Leaders had responsibility for formulating near programme proposals (one campaign ahead) and out-line plans (two periods ahead). This was carried out in collaboration with the Head of Operations Division (A Tanga). These proposals were within the broad outline of the Development Plan and subject to guidelines provided by the Experiments Committee. These proposals were presented to the Experiments Committee for discussion and approval before implementation. The Programme Leaders, Task Forces and the Topic Groups for 1996, were as follows:

Programme Leaders for 1996 were:

PR Thomas and M L Watkins.

Three Task Forces implemented the programme, as follows:

H) High Performance and High Q in ELM-free H-modes

(With the objective of producing high fusion performance and high Q in ELM-free H-modes in the Mark IIA pumped divertor configuration with currents up to 6MA: including, optimization of configuration; progressive to high Q and high fusion power; disruption assessment and control; and preparation for D-T operation).

(Task Force Leader: P J Lomas)

D) Divertor Physics and High Performance ITER Modes of Operation

(With the objective of assessing divertor performance in the Mark IIA pumped divertor and otpimizing main plasma performance in ITER relevant conditions: including, power and particle handling in the Mark II divertor; divertor and SOL physics; optimization of main plasma performance in ITER relevant conditions; helium transport and exhaust; and preparation for D-T performance).

(Task Force Leader: LD Horton)

P) ITER Physics and Performance Optimization

(With the objective of studying physics and optimizing plasma performance in those areas in which JET can make important contributions to ITER and DEMO: including; dimensionless scaling experiments; performance optimization through profile control; effect of rotation; fast-particle confinement; reactor relevant RF scenarios; and preparation for D-T operations).

(Task Force Leader: C Gormezano)

Task Force Leaders had responsibility for (i) interacting with and advising Programme Leaders on programme requirements within that task area; (ii) devising and setting out a detailed programme for allocated time within a campaign period; (iii) driving through that task programme (including acting as a Control Room representative); (iv) analysing data (in conjunction with Topic Leaders, if appropriate); (v) disseminating information in the task area through internal meetings and publications (in conjunction with Topic Leaders, if appropriate).

In addition, Topic Groups were formed, as follows:

Topic Group	*Topic Leader*
(a) Performance limitations	D J Campbell
(b) Divertor Physics	G C Vlases
(c) ITER physics	J G Cordey

During 1996, the work of the three Topic Groups was mainly, but not exclusively, aligned with the work of each Task Force. However, the Topic Group subjects were of longer term interest than the immediate tasks undertaken by the Task Force Groups. The Topic Groups were responsible for analysis of results within many areas across the Task Force spectrum, but they also had responsibility for advising Programme Leaders on programme requirements which were topical and relevant to the Groups areas of activity. In addition, the Groups disseminated information through a number of internal meetings and in external publications and journals.

Programme Execution and Analysis

The main objectives of the 1996 campaign period were: to assess divertor performance of the Mark IIA divertor; to demonstrate the high performance capability of the pumped divertor; and to study and optimize plasma performance in those physics areas in which JET could make important contributions to ITER and DEMO.

The main themes of the programme were:

- to assess the performance of the Mark IIA pumped divertor configuration and to compare with the Mark I performance;
- to optimize main plasma performance in ITER relevant conditions;
- to study divertor pumping and exhaust, especially helium exhaust;
- to generate and understand high performance modes of operation in the Mark IIA divertor configuration, including optimization of configuration;
- to progress to high Q and high fusion power in specific configurations and scenarios;
- to analyse and introduce methods to avoid disruptions;
- to develop "advanced tokamak scenarios" based on stable, long pulse discharges with a "high-bootstrap" component to the total plasma current;
- to develop and establish transiently enhanced confinement and fusion performance with reversed magnetic shear;
- to develop reactor relevant RF scenarios, including fundamental resonance of deuterium and second harmonic of tritium.

The scientific achievements for 1996 are described in the following sections, within the Task Force, and Topic Group headings.

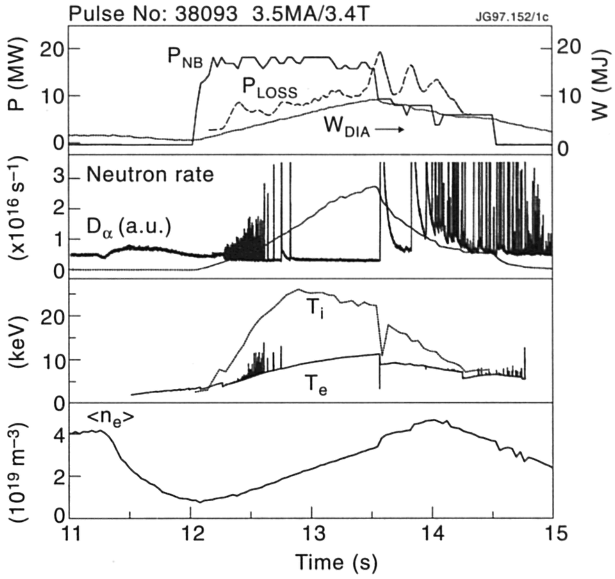

Fig.95: Typical time traces for a hot-ion plasma showing neutral beam power P_{NB}, loss power P_{Loss}, diamagnetic stored energy W_{DIA}, D-D neutron rate, D_α ion and electron temperatures (T_i and T_e) and volume averaged density $<n_e>$

High Fusion Performance in ELM-Free H-Modes

Introduction

The objective of this Task Force was to produce high fusion performance and high Q in ELM-free H-modes in the Mark IIA pumped divertor. The highest fusion yield in JET was obtained in the hot ion H-mode regime, with D-D neutron rates up to 4.65×10^{16}n/s demonstrated, equivalent to Q_{DT}~1 (similar to the PTE-1 series). The new results obtained are described in the following sections.

Basic Features of the Regime

Figure 95 shows a typical hot-ion H-mode plasma obtained with the Mark II divertor.After formation of the X-point, the density was allowed to pump out to ~$1\times10^{19}m^{-3}$ before the application of high power neutral beam (NB) heating. After a period of threshold ELMs, the plasma became ELM-free, during which time both stored energy and D-D neutron rate increased steadily. The ion temperature, on the other hand, reached a maximum and then declined somewhat as the density continued to increase. The loss power, $(P_{NB}-dW/dt-P_{SH})$, where P_{SH} corresponds to the calculated shine-through power, increased with time as did the stored energy, indicating approximately constant confinement time. The high performance phase was limited in this case by beam switch-off followed 50ms later by a giant ELM and sawteeth (coincident to

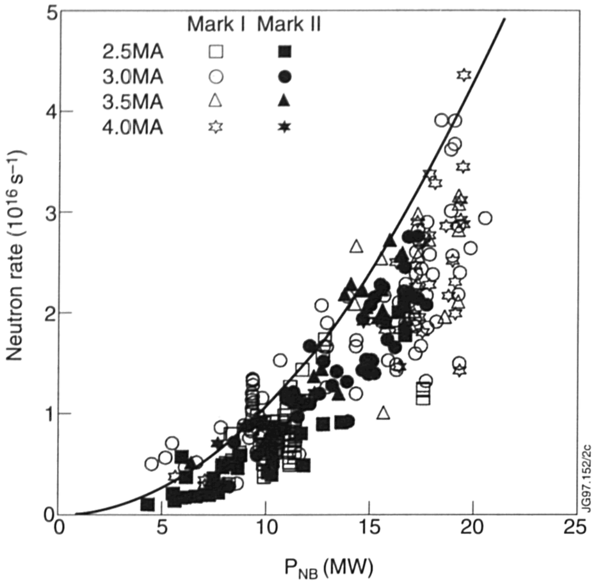

Fig.96: Neutron rate plotted against total neutral beam power. Open symbols refer to Mark I and closed symbols refer to Mark II. The shape of the symbols indicate plasma current: squares-2.5MA, circles-3MA, triangles-3.5MA and stars-4MA

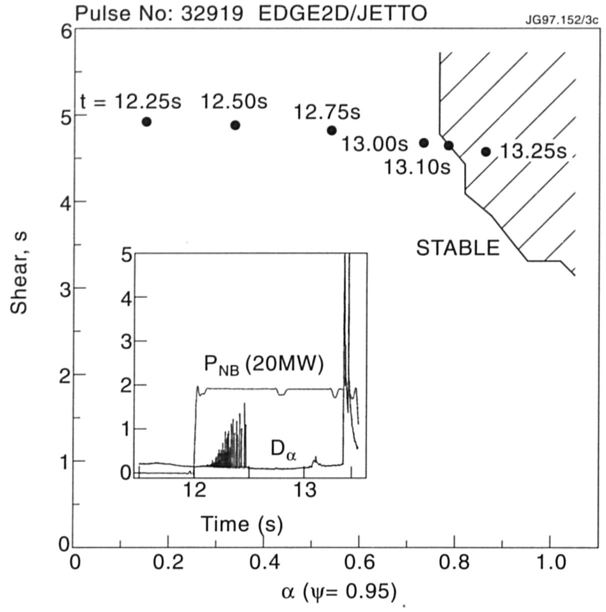

Fig.97: Trajectory of model simulation of Pulse No.32919 in the shear versus normalised pressure gradient diagram. The ballooning unstable region is shaded. Ballooning instability is predicted at 13.1s which is compared with the ELM time of 13.4s in the inset

within 100μs). These and other limitations to performance have been published [1].

The duration of the ELM-free phase is similar on both Mark I and Mark II for similar core plasma shapes, edge shear, S_{95}≥3.5, and triangularity, δ≥0.3. Higher triangularity configurations were tested up to δ~0.6, S_{95}~4.0 at 2.5MA but did not demonstrate any significant improvement in confinement quality. Configurations with low edge shear S_{95}≥3 and low triangularity δ≤0.2 showed repetitive giant ELM's with frequencies ≥5Hz.Given the similarities in plasma behaviour in Mark I and Mark II, it was not surprising that the fusion performance of the NB-only data was also similar at the same beam power and showed the same strong scaling with NB power as illustrated in Fig.96. So far, for technical reasons, the NB power on Mark II was limited to <17MW, but this deficiency has been corrected, and is expected to restore the Mark I performance. The steady neutron yields could be maintained for about 1s by step-down of the beam power to the level of the loss power in the preceding transient phase.

The Transport Barrier

A model has been developed [2] which accounts for many of the features observed in ELM-free H-modes. The model assumes: (a) transport inside the barrier region is ion neoclassical together with anomalous terms including both Bohm (global) and gyro-Bohm terms; (b) transport coefficients within the transport barrier $D \sim \chi_i \sim \chi_e \sim \chi_i^{neoc}$ are given by the ion neoclassical diffusivity; and (c) the width of the transport barrier is given by the ion poloidal banana width $\Delta \sim \varepsilon^{1/2} \rho_{\theta i}$. The Bohm terms dominate the transport in the outer regions up to the transport barrier and the gyro-Bohm terms dominate the central confinement.

With these assumptions, it was possible to construct a complete set of transport equations for n_e, T_e, T_i and J which could be solved self consistently. A single free parameter remained, which could be the edge density (or alternatively the net recycling coefficient), which was adjusted to match the observed density evolution. When applied to hot-ion plasmas the time evolution of plasma parameters and profiles were well reproduced. In particular, the initial linear rise in stored energy was well described, and was followed by a progressive saturation, which the model suggested was due to the density rise. The model described accurately the evolution of power step-down pulses and the effect of strong gas puffing, and could account qualitatively for the temporary degradation of confinement following a sawtooth crash. The code predicted the time when ballooning modes became unstable, which was consistent with the experimentally observed appearance of giant ELM's, as shown in Fig.97. Indeed, this confirmed, in a satisfying manner, that the transport was close to ion neoclassical in the barrier region, since an increase in transport would lead to ballooning modes always being stable.

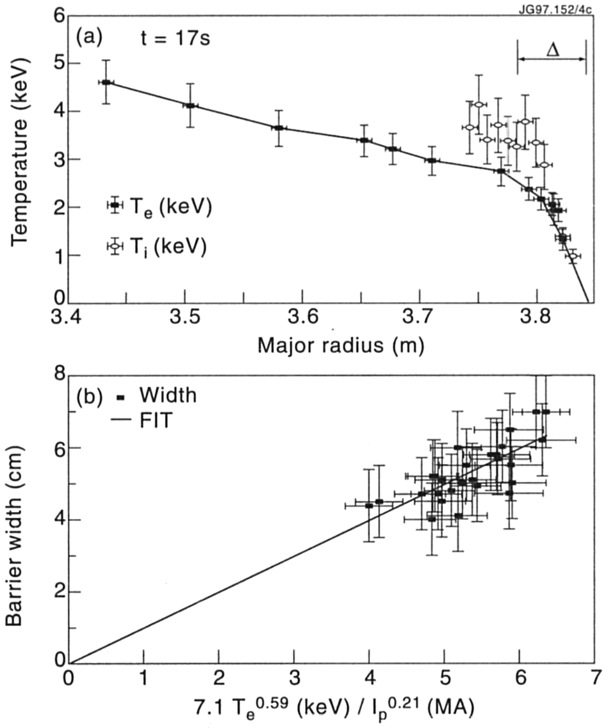

Fig.98: (a) Ion and electron temperature profiles for Pulse No.37444 (2.6MA/2.54T) from which the transport barrier width Δ is determined; (b) barrier width against fitted dependence of temperature and plasma current. Note the weak dependence on I_p

Measurements of both ion and electron temperature profiles across the transport barrier are shown in Fig.98(a). The transport barrier is most clearly defined in the electron temperature data and this width is plotted against the best fit in Fig. 98(b). This result did not conform to the expected scaling $T_i^{1/2}/I_p$. Further analysis is in progress which may resolve these discrepancies, but it may be necessary to include more physics elements such as the penetration depth of cold neutrals. The first attempt to self consistently compute the scrape-off layer (SOL) and core transport together with neutral penetration has been described [3].

Role of Recycling

The main chamber recycling plays an important role influencing both ELM-free period and performance [4]. Simulations with the model described above confirm this sensitivity. The distribution of the D_α light clearly shows the brightest signals from the divertor strike zones but reveals some contribution from the inboard (small major radius) plasma edge.

Measurements of Zeeman split D_α radiation on a horizontal chord indicates about four times the light from the small major radius side of the plasma compared to the large major radius side.

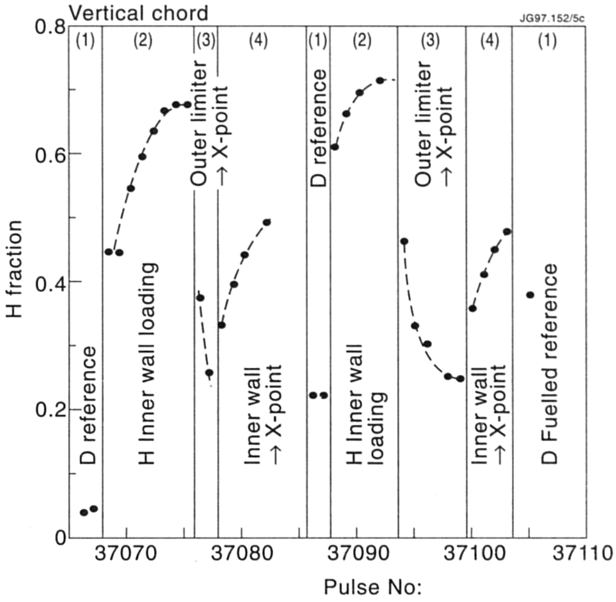

Fig.99: Ratio of H/(H+D) from H_α, D_α light measured on a vertical chord for a series of pulses from the selective hydrogen loading experiment. Where the plasma pulse includes both limiter and X-point phases, the measurement is taken during the deuterium beam fuelled H-mode in the X-point phase. The figure shows two cycles of experiments Pulse Nos.37066-37084 and Pulse Nos.37086 - 37105 repeated on successive days.

To quantify the relative contribution of recycling in the main chamber compared to the divertor, a selective hydrogen loading experiment was performed. The measured H/(H+D) fraction determined from vertical chord H_α and D_α radiation is shown in Fig.99, as a function of pulse number for four sequences of pulses repeated on two successive days.

The sequence of pulses are as follows (as labelled on Fig.99): (1) reference pulse with deuterium gas fuelled inner limiter phase followed by deuterium beam fuelled H-mode; (2) inner wall limited pulses with hydrogen gas fuelling; (3) pulses with deuterium gas fuelled outboard limiter phase followed by deuterium beam fuelled H-mode; (4) pulses with hydrogen gas fuelled inner wall limiter phase followed by deuterium fuelled H-mode. For clarity, the data points in Fig.99 represent the X-point phase, when there was more than one phase. Generally, the hydrogen concentration was low during the outboard limiter phases of sequences (1) and (3). The H/(H+D) ratio during the inner wall hydrogen loading pulses of (2) behaved in a similar manner to previous isotope exchange experiments [5]. The sequence in (3) had no direct contact with the inner wall and its inventory of hydrogen, and yet the X-point phase started with a high concentration of hydrogen, which decreased pulse by pulse. In sequence

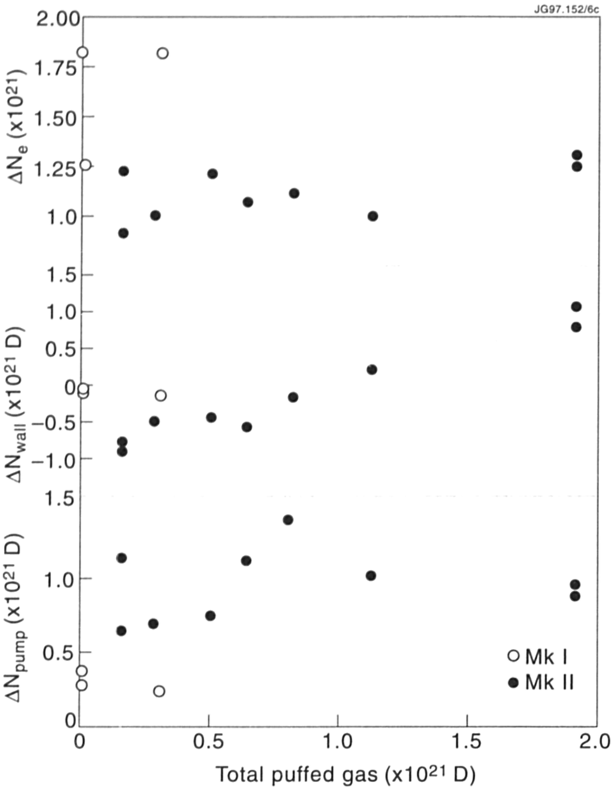

Fig.100: Particle balance over the first second of neutral beam heating for a series of ELM-free H-modes. The change in plasma particle inventory, wall inventory and pump inventory are shown as a function of total gas puffed in the same interval. Open symbols refer to Mark I and closed symbols to Mark II. The neutral beams inject 17MW and 1.4×10^{21} particles per second

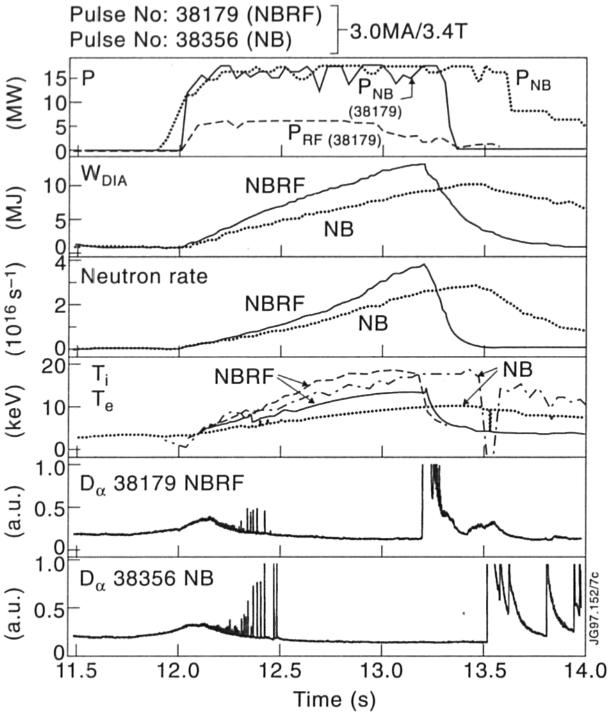

Fig.101: Typical time traces comparing NB-only (Pulse No.38356) and combined heating NBRF (Pulse No.38179). The traces shown are input powers, P_{NB}, and P_{RF}, diagmagnetic stored energy, W_{DIA}, neutron rates, ion and electron temperatures and D_a

(4), where the hydrogen concentration was topped up during the inner wall phase, the concentration during the X-point phase increased pulse by pulse. These results demonstrated that there was significant exchange, during the H-mode phase only, of hydrogen from the inner wall to the divertor target and of deuterium from the divertor target to the inner wall. Thus, a significant fraction (0.25 - 0.5) of the recycled particles originated from the inner wall, demonstrating the importance of the main chamber recycling during diverted H-modes.

The more closed Mark II divertor was predicted to increase the pressure of neutrals in the diverted region and hence increase pumping. The data in Fig.100 clearly show the increase in pumping during ELM-free H-modes in Mark II compared with Mark I. Indeed in Mark II the density rise during the ELM-free H-modes was reduced by ~ 30%, such that it was necessary to add gas to optimise the fusion yield (minimise NB shine-through losses and Z_{eff}). At low gas puff, there was a clear net source of particles from either walls or target, whereas at sufficiently high gas flow these surfaces provided a net pump. Alternatively, these results could be thought of as a decrease in gas fuelling efficiency (from ~50% to ≤10%). This strong divertor pumping reduced the need for extensive conditioning for access to the hot-ion regime and increased the reproducibility of the performance achieved but did not, significantly improve the performance or confinement quality.

Combined Heating

Ion cyclotron resonance frequency (ICRF) heating was coupled in conjunction with NB heating to produce ELM-free H-modes with combined heating (NBRF). The coupling resistance fell during the ELM-free H-mode from about 2Ω to 1.5Ω. Nevertheless, it was possible to couple up to 9.5MW. Together with NB, a total power up to 25MW was applied for plasma currents up to 3.8MA, generating stored energies up to 14MJ. The diamagnetic energy confinement time $\tau=W_{dia}(P_{NB}+P_{RF}-dW/dt)$ was about 1s in these cases, similar to the NB-only cases, suggesting no strong effect according to different proportions of electron and ion heating.

Figure 101 compares high D-D yield pulses at similar NB power with and without 6.5MW of ICRF resonant on-axis heating with hydrogen and second harmonic deuterium. The increase in stored energy, D-D neutron yield, ion and electron temperatures are clear, and the shorter ELM-free phase is as expected. The high energy neutral particle analyser clearly shows the generation of a deuteron tail with energies up to 1MeV, as expected from PION code calculations. Neutron accounting using kinetic data suggested increased neutron production from both thermonuclear and non-thermal reactions. With added hydrogen or mixed frequency (multiple resonance position) ICRF heating, the observed tail could be smaller by an order of magnitude and yet still the D-D neutron rate increased over and above the NB-only cases. These results suggested a useful increase in fusion yield when ICRF heating was applied to D-T plasmas, but it is too early to make quantitative predictions.

D-T Expectations

The best NB-only plasma in Mark I demonstrated $n_D(0)\tau_E T_i(0)$~$8.8\mathrm{x}10^{20}\mathrm{m}^{-3}$skeV and TRANSP analysis indicated Q_{DT}(equiv)~1 (with the definition in [6]). High performance could be sustained for about 1s by stepping down the NB power to about the loss power and in such cases Q_{DT}(equiv)>0.8 for 1s. Similar results are expected with Mark II, when the full beam power is restored.

These extrapolations assume that 50:50 D:T mix can be achieved. By operation of the tritium beams at full power and the deuterium beams at reduced power, 20MW could be delivered with comparable deuterium and tritium fluxes. Provided that the core was dominated by beam fuelling, a 60:40 mix should be readily achievable. Contributions to the core D-T mix from recycling could be offset by tritium beam prefuelling or gas puffing. Operation of the deuterium beams at full power would deliver ~23MW and would be expected to increase the D-T neutron yield by up to 30%, provided that the shortfall in tritium fuelling could be made up (by gas puffing or prefuelling).

Conclusions

The behaviour of the hot ion ELM-free H-mode regime was reassuringly similar in the Mark I and Mark II divertor. Improved pumping reduced the characteristic density rise and increased operational flexibility, but did not as yet lead to any significant improvement in performance. Similar high fusion performance, as already demonstrated on Mark I, is expected on Mark II when the neutral beam power is restored. Improved performance has been demonstrated with the addition of ICRF power to the hot ion ELM-free regime. The transport model continues to describe the main features of this regime and recently detailed edge temperature measurements have been made which should enable a refinement of the physics of the transport barrier.

The rapid progress achieved with the Mark II divertor shows great promise for the forthcoming D-T experiments.

References

[1] The JET Team (presented by P. R. Thomas), IAEA-CN-64/A3-2, Plasma Physics and Controlled Fusion Research, 1996 (Proc. 16th Int. Conf. Montreal, 1996).

[2] Bak, P., et al., Nucl. Fusion **36** (1996) 321.

[3] The JET Team (presented by A. Taroni), IAEA-CN-64/D3-3, Plasma Physics and Controlled Fusion Research, 1996 (Proc. 16th Int. Conf. Montreal, 1996).

[4] The JET Team (presented by P. J. Lomas) in Plasma Physics and Controlled Nuclear Fusion Research 1994 (Proc. 15th Int. Conf. Seville, 1994) Vol. 1, IAEA, Vienna (1996) 211.

[5] Horton, L.D., et al., J. Nucl. Mater. **196-198** (1992) 139.

[6] Balet, B., et al., Nucl. Fusion **33** (1993) 1345.

Performance Limitations

Limitations in the Hot-Ion H-Mode

Introduction

Hot-ion H-modes, heated by high power neutral beams and supplemented in some cases by ICRF heating, have produced high fusion yields in JET [1] and will form a cornerstone of the forthcoming DTE1 experiments. However, the high performance phase is short-lived and decays, usually irreversibly, to a lower level of performance after 1-2s. This performance deterioration is due to a fall in energy confinement, which is associated with a variety of MHD activity. Development of understanding of both the transport processes, which lead to a continuous rise in energy confinement time during the ELM-free period of hot-ion H-modes and of the processes, which terminate the high performance phase, is an essential element of the JET programme, as these control the peak fusion output and its duration. Also, these phenomena introduce variability in the fusion performance, which is a concern for DTE1.

High Performance Hot-Ion H-mode and Performance Limitation

High power neutral beam heating is applied to a low recycling, low density divertor plasma. After a short

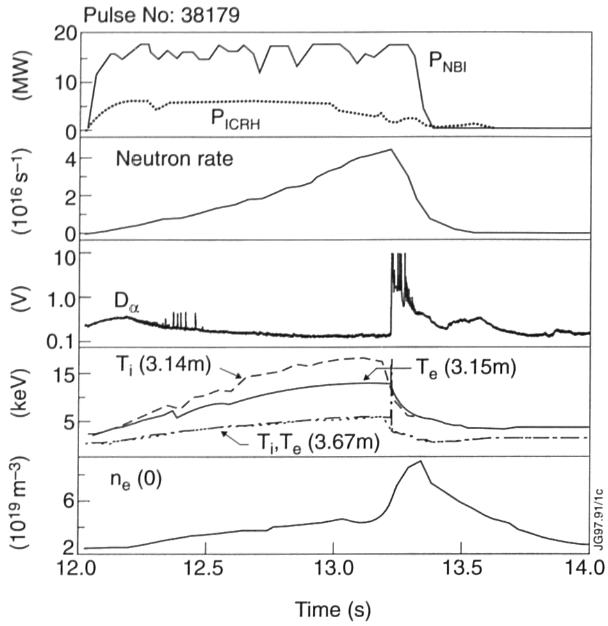

Fig.102: The time history of a hot-ion H-mode, heated with NB and ICRF heating, which terminates with an ELM. Shown are the heating powers, the neutron rate, the D_α rate, temperatures near the axis and half minor radius and central electron density

period of threshold ELMs, an ELM-free period starts in which the energy, density, fusion power as well as energy confinement time rise continuously until a terminating event occurs; after which the confinement is degraded, usually irreversibly. The period of the high performance is characterised by the formation of a very pronounced transport barrier near the separatrix, particularly in the ion and electron temperature, which rises steadily with time. Shortly before the terminating event, the plasmas are characterised by energy confinement up to 1.4 times the ITER93-P value and central ion temperatures up to 30keV. The formation of the transport barrier leads to a development of a significant bootstrap and ohmic current flow at or near to the separatrix, which can excite the kink instability. Pressure gradients approach $1MPa.m^{-1}$ in the barrier region and have a profound effect on plasma ballooning stability.

The termination of the high performance phase is often triggered by a global MHD event such as an ELM or a sawtooth collapse plus an ELM. The ELM is used unambiguously to mean Type I [2] or giant ELM. Many terminations do not show such global MHD but instead have low m/n activity close to the edge called "outer modes" [3]. The outer modes are associated with a relatively mild reduction in confinement and a rapid fall in fusion rate (Fig.102).

The distribution between the various kinds of MHD is rather uniform (Fig.103). More than half the terminations involve two or more kinds of MHD instability together. The MHD do not always cause a termination but their ability to do so increase throughout the ELM-free phase. In view of this and the small amplitude of outer modes, compared with the resulting transport, it is supposed that the MHD is coupling to the underlying transport mechanism to trigger a change of state [4,5].

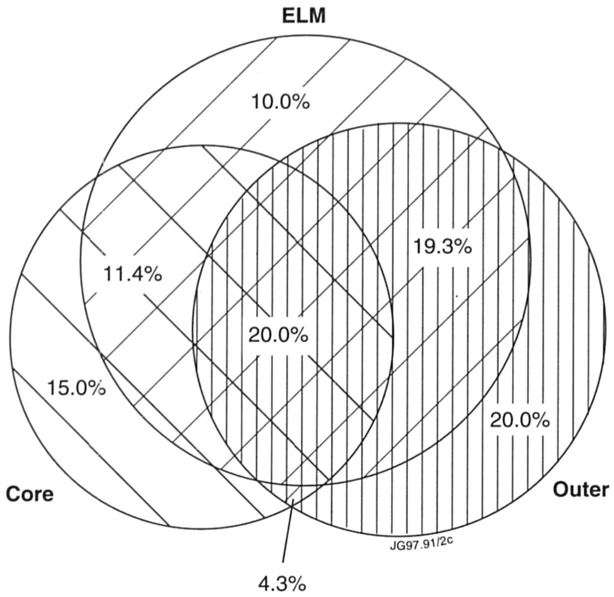

Fig.103: Statistical analysis of main MHD modes observed to grow at the start of the neutron rate collapse. In discharges where a sequence of events is seen, the MHD event with the fastest change in R_{DD} has been taken. The total sample size is 142 pulses chosen on the basis of $R_{DD}>10^{16}s^{-1}$

A termination which is triggered by an ELM is shown in Fig.102. The D_α spike at the terminating ELM lasts tens to hundreds of milliseconds and corresponds to ionisation of order of the plasma ion inventory, of up to 10^{22} ionisations. This is reflected in an increase in plasma density, which can double in a few hundred milliseconds. The outer half of the pressure profile is eaten away by the ELM (see Fig.104). After this a cold wave propagates to the core and the central pressure starts to decline. The fusion rate falls due to the propagation of the cold wave to the core and the cooling due to the density increase.

A sawtooth or other core MHD, becomes an effective cause of confinement limitation above $\beta_N \sim 1.5$, or so, because a large proportion of the plasma cross-section is affected and a strong coupling to ELMS and outer modes occurs. The core pressure collapses and the energy is distributed in the outer regions of the plasma column. When the core MHD triggers an ELM or outer mode, the decrement of the core energy is able to propagate through the outer regions of the plasma, with little or no change to the pressure or temperature profiles there. This implies

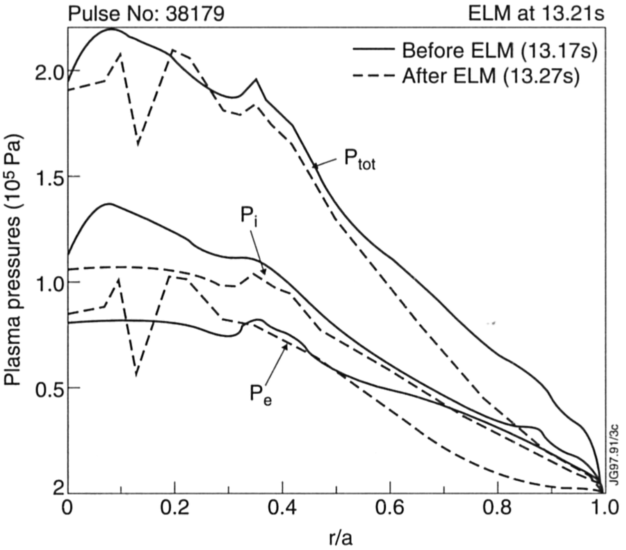

Fig.104: The pressure profiles before and after a terminating giant ELM. P_{tot}, P_i and P_e are the total, ion and electron pressures, respectively. Note that the ELM has eaten away the outer half of the electron profile

that a plasma, in these conditions, must be able to support different levels of transport.

Outer modes are observed in the outer regions of the plasma; typically near the q=3 surface, as shown in Fig.105. Toroidal mode numbers 1-4 and poloidal mode numbers 3-12 are observed. Modes with n=1 typically have a frequency of around 10kHz. A noticeable signature of the outer mode is a small, slow increase in the D_α emission which indicates a loss of confinement. As well as an immediate deterioration of edge confinement, a cold pulse propagates promptly into the plasma core and together cause the degradation of fusion performance. Evidently, the irreversible performance limitation due to an outer mode alone arises from the particle influxes which are rapidly transported inwards through the region affected by MHD. Note, however, that the plasma can recover from the effects of outer modes which occur early in the ELM-free period. Often this recovery is triggered by the isolated Type I ELM, which significantly reduces pressure gradient and current near the separatrix. Typical example of such a recovery is shown in Fig.106. It is worthwhile to note that cooling of the plasma edge by an additional radiation, caused by laser impurity ablation [6], can also lead to a cessation of the roll-over.

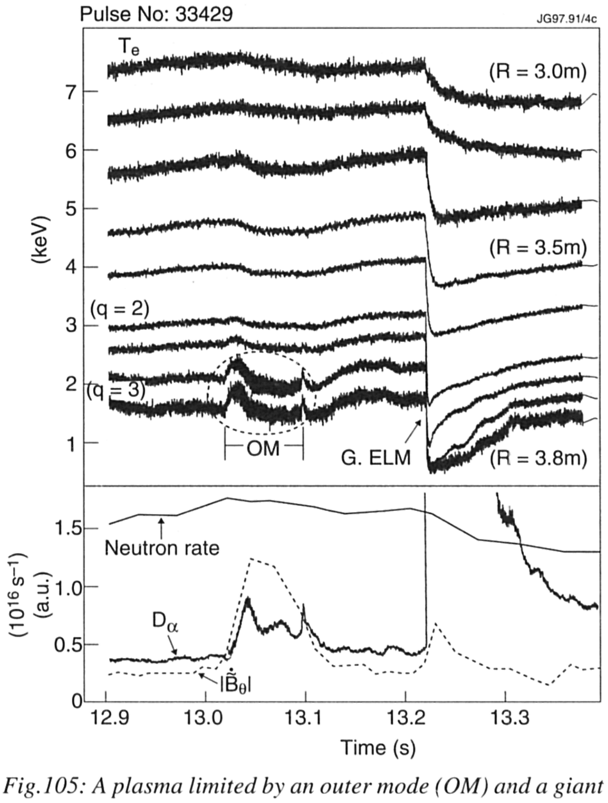

Fig.105: A plasma limited by an outer mode (OM) and a giant ELM (G.ELM). A range of electron temperature traces are shown from the axis to the plasma periphery, together with the neutron rate, D_α and magnetic pick-up coil signals

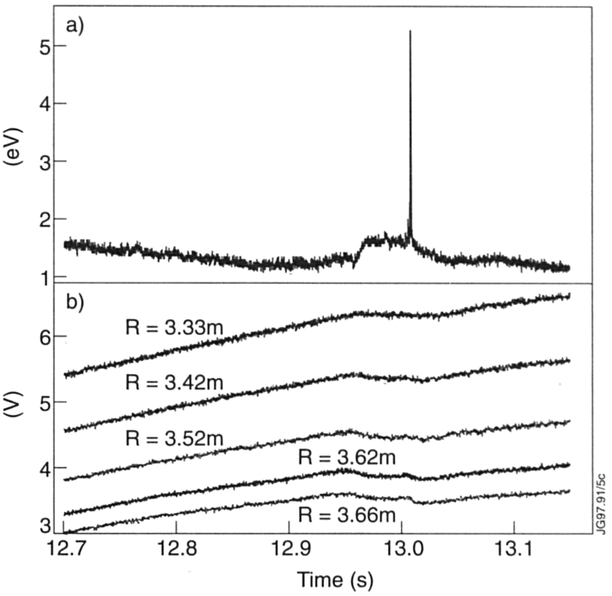

Fig.106: Recovery triggered by the isolated Type I ELM, which significantly reduces pressure gradient and current near the separatrix

Prior to the installation of the pumped divertor, the loss in confinement generated a heat pulse which caused a rise in target tile temperature and generated a carbon bloom. The resultant influx of impurities, coupled with the rise in core transport, prevented any recovery in performance and confused the analysis of the core behaviour. The improved design of the pumped divertor target has eliminated the carbon bloom. However, the link between the MHD instabilities and the loss of core confinement remain unclear and the resulting change in performance continues to be irreversible, for the reasons described

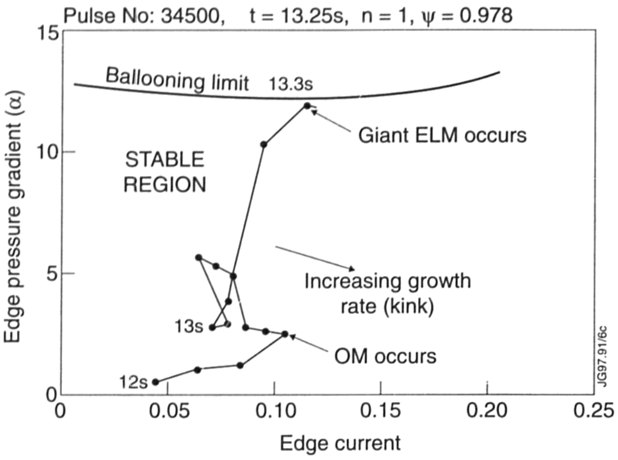

Fig.107: Edge stability diagram of normalised pressure gradient versus normalised edge current. The lines to the right of the stable region are contours of the ideal kink growth rate. The trajectory of Pulse No. 34500, which showed outer modes and ELMs can be seen

above. Even without the carbon bloom, impurity influxes increase during the terminating MHD activity, as does the main plasma Z_{eff}. It seems, that although impurities might contribute to the performance deterioration, they are not fundamental to the observed behaviour.

Magnetic fluctuations, identified as TAE modes [7], are often observed during performance limitations ascribed to outer modes. It is found that their onset is coincident with the plasma density rising to the point where some of the slowing-down NB particles are resonant with $v_A/3$. Some improvement in the comparison between the measured neutron yield and that estimated from the profiles can be obtained, if it is assumed that this resonance causes ejection of the fast ions. However, plasmas have been obtained where TAE modes should have been excited but which have good agreement between experimental and simulated neutron yields. Thus, definitive experiments and measurements will have to be devised before the role of TAEs in these plasmas can be clarified and the fast ion losses demonstrated.

MHD Stability Analysis

The ideal MHD stability of the hot-ion H-modes has been studied both against low m,n kinks and ballooning modes. The edge pedestals are very important for determining MHD stability. The pressure gradient is such that, before the terminating events, it is close to or at the ballooning limit. The pressure gradient also drives a bootstrap current which is close enough to the separatrix surface to drive the kink instability. This is illustrated in Fig.107, which shows a plot of the trajectory of plasmas in the edge pressure gradient versus normalised edge current density space. The stable region is bound from above by the ballooning limit and on the right by kink instability. Different hot ion H-modes appear to limit at both boundaries and suffer ELMs where the boundaries meet. An important determinant of the trajectory is the recycling level or edge density. When these are high, the ballooning boundary is encountered first.

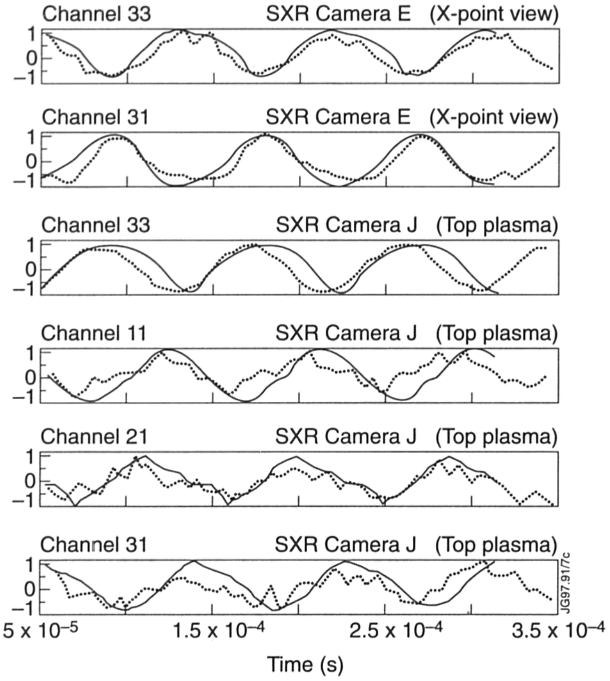

Fig.108: Comparison of the phases of a number of soft X-ray camera signals (dotted) with the simulation (full lines). The top two panels are particularly significant for showing the 180°C phase shift between adjacent channels, looking towards the X-point

Analysis, using the CASTOR code [8], shows that ideal external kinks, with n=1-4 are linearly unstable when outer modes are present. The JET vessel wall is too far from the plasma to have any significant stabilising effect. That outer modes are observed when instability is predicted and, with n values from 1 to a least 4, encourages the identification of outer modes with saturated kinks.

The structure of outer modes, measured with the internal soft X-ray cameras, has been compared with the computed kink eigenmodes. This was carried out by distorting the equilibrium soft X-ray emission profile by the kink displacements and recomputing the signal, which should be seen in the individual detectors. The approach is suited to identifying kink modes because the concentration of lobes around the X-point and the top of the plasma leads to phase inversions in the fluctuations between adjacent detectors. This is what is observed and the observed phases show excellent agreement with the kink mode simulations, as seen in Fig.108. The fluctuating amplitudes

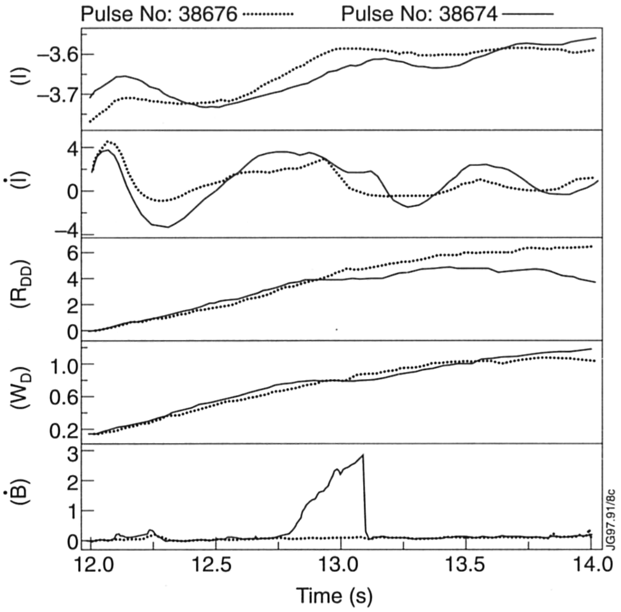

Fig.109: Example of the stabilisation of the Outer Mode by reducing the edge current density through a current ramp down

are in a reasonable agreement. The predicted displacement amplification, of ~1.2cm in the midplane to ~15cm at the X-point, due to the poloidal flux expansion, is confirmed by the data.

Tearing modes have also been simulated and compared with the outer mode soft X-ray signals, using the same method. Extra structure appears in the simulated signals because of the phase inversion within the resonant surface. The data show no signs of this structure, so securing the identification of the outer mode with ideal kinks.

To test the link between the edge current density and the occurrence of the Outer Mode, current ramp experiments have been carried out. Ramping the current up increases the edge current density and the Outer Mode should occur earlier as compared to no current ramp. Ramping the current down should delay the Outer Mode.

In a series of three hot-ion H-mode discharges, one reference discharge and two discharges with a current ramp-up with different timing of the ramp, it was shown that the Outer Mode could be destabilised by a current ramp-up. Adding a 400kAs^{-1} current ramp up 250ms before the occurrence of the Outer Mode in the reference discharge, destabilised the Outer Mode 150ms earlier. In a discharge where the current ramp-up was started earlier, (550ms before), the Outer Mode also occurred earlier (at 250ms) compared to the reference discharge.

Figure 109 shows an example of successfully stabilising the Outer Mode through a current rampdown. A large Outer Mode is observed in Pulse No. 38674, between t=12.8s and t=13.1s during which the R_{dd} saturates. Avoiding the small ramp up of the current at t=12.3s and adding a stronger ramp-down starting at 12.6s, avoided the onset of the larger outer mode in Pulse No. 38676, leading to a larger R_{dd}. These experiments show that the stability of the Outer Mode is linked to the edge current density as predicted by the identification of the Outer Mode as an external kink mode.

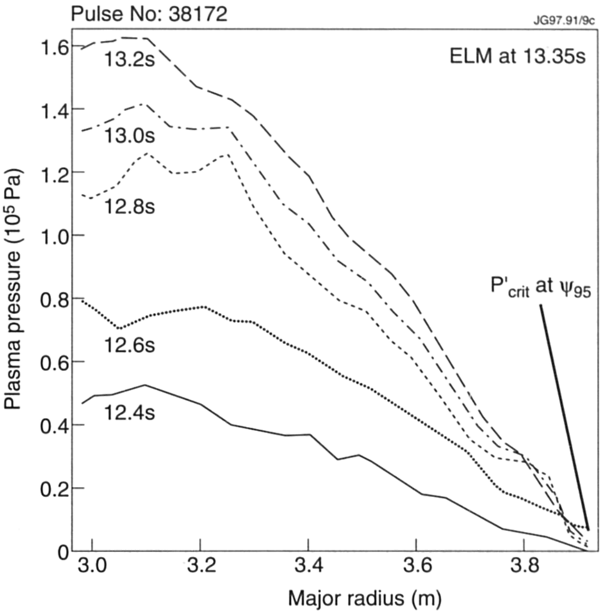

Fig.110: A sequence of pressure profiles, obtained from Thomson scattering and charge exchange recombination spectroscopy, for a pulse which had an ELM at 13.35s. Also shown is the critical pressure gradient for ideal ballooning at the 95% flux surface

In discharges limited by an ELM, the edge pressure gradient, evaluated at the 95% flux surface, is at or close to the ideal ballooning limit. A range of different plasma conditions confirm this and the experimental dependence on shear and poloidal field strength correspond to theoretical expectations.

Unfortunately, there is still no direct experimental evidence for ballooning modes at or near the termination of hot-ion H-modes in JET. The difficulty of detecting them is probably the determining factor here. Not only is the current bandwidth of the data acquisition system smaller than is desirable for this purpose but the predicted unstable region is also in the low emissivity part of the plasma.

However, the pressure profile has been observed to saturate at the ballooning limit for hundreds of milliseconds before the terminating ELM, as shown in Fig.110. Whilst not definitive, this does indicate that ballooning modes are playing a role in ELM terminations.

Plasmas limited by ELMs are also predicted to be unstable to kinks. Soft X-ray cameras show precursors to many giant ELMs with the same characteristics as outer modes and lasting tens of milliseconds. In these cases, the degradation of fusion power starts with the outer mode and is not greatly perturbed by the ELM. Given the identification described above, it is likely, therefore, that kinks are also observed in conjunction with ELMs.

It seems possible that the combination of ballooning and kink instability is needed for ELMs to occur, although it should be stressed that there is no evidence to support this and that there are ELMs with no detectable precursor activity. Nonetheless, the conjunction between predicted instability of both modes and their observation in conjunction with ELMs does seem compelling.

Transport Effects during Termination

Although there is a clear relation between the time of the deterioration in the hot-ion H-mode performance and the appearance of the MHD activity, it is difficult to understand how relatively low-level MHD activity can quantitatively explain the losses of heat and particles. The MHD activity is short lived, with timescales 100μs-100ms. However, the global energy confinement, which usually increases throughout the high performance phase, falls at the termination, by as much as a factor of three, and the neutron yield declines thereafter, usually irreversibly. The irreversibility is likely to be due both to the deteriorated confinement and the density increase, which results from ELMs particularly, preventing a rebuilding of central pressure and a separation of the ion and electron temperatures.

The predictive TRANSP and JETTO simulations confirm that, even without the MHD activity, the hot-ion H-mode character will eventually be lost due to the increasing ion-electron equipartition and the reduced heating to the central region of the plasma. Thus, even in the absence of MHD events there would be a gradual rollover in the neutron rate related to the density increase, which approximately matches the beam fuelling rate at low recycling. In the presence of MHD activity, the transition from a hot-ion H-mode to an H-mode with high density and equal electron and ion temperatures is accelerated. As mentioned before, earlier in the discharge, before the high densities are reached, MHD activity like single ELMs outer MHD modes and sawteeth do not seriously affect the plasma performance. The relaxation in the neutron rate towards one of a non hot-ion H-mode becomes irreversible when the mode activity occurs "late" into the heating phase. Which plasma parameter should define the word "late" is not entirely clear. Present analysis indicates that the irreversibility is probably due to a gradual deterioration of the effective heat conduction, a gradual decrease of the power deposition in the plasma centre and an increasing ion-electron equipartition due to the density build-up.

However, this gradual degradation is insufficient itself to explain a sudden increase in transport coefficients in the region one quarter to one half of the outside of the plasma cross-section and in the core as well at the beginning of the termination.

A number of potential mechanisms responsible for the link between MHD and transport have been investigated:

(a) Loss of the confinement barrier alone is not sufficient to reproduce the observed behaviour. The sudden change in confinement at termination, or during an outer mode, clearly encompasses to one half of the outside of the plasma cross-section;

(b) ELMs generate as much ionisation in a few tens of milliseconds as the plasma ion content. A hypothesis that the neutral cloud could penetrate to the core and so cause enhanced charge exchange losses there, is not borne out either by modelling or by experiments involving large gas puffs. In these experiments, a gas puff, of 100ms duration and magnitude to match the D_α spikes of terminations in similar pulses, was injected late in the ELM free phase of high performance plasmas. The edge cooled somewhat and that the cold pulse propagated to the plasma core on a timescale consistent with transport which was not degraded.

(c) Transport models which connect edge conditions to core transport [9] give a satisfactory account of most termination events. Further evidence for these models is found in their ability to reproduce the gas puff experiments, and the ability of laser ablation injection of impurities to cause changes in transport which propagate rapidly to the core. Also, the propagation of the L-H transition is reproduced. These observations encourage the belief that the transport mechanism is in some way extensive and that edge conditions are able to affect core transport.

(d) Magnetic activity, identified as TAE modes, is seen during the fusion rate roll-over associated with outer modes. Unlike the other mechanisms, (i)-(iii), TAE modes would cause confinement degradation by reducing the input power density, rather than acting

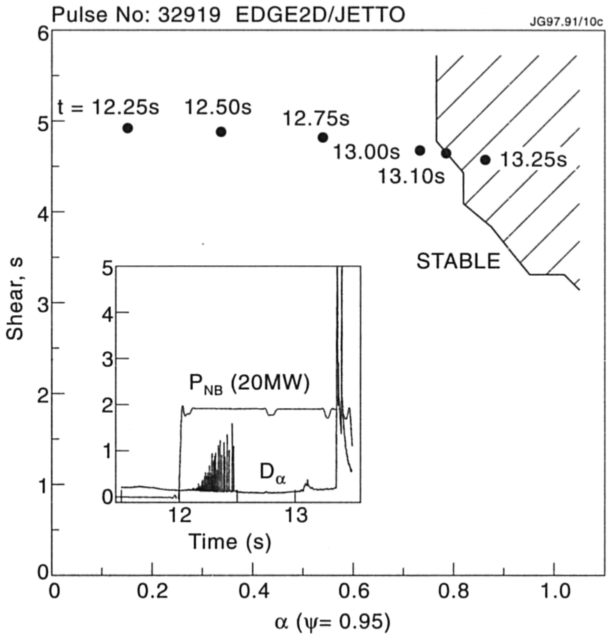

Fig.111: Trajectory of the model simulation of Pulse No.32919 in the s-α (shear versus normalised pressure gradient) diagram. The ballooning unstable region is shown shaded. Ballooning instability is predicted at 13.1s, which should be compared with the ELM time of 13.4s shown in the inset

on the plasma losses. The TAE modes could be triggered by the outer mode induced density rise dropping the Alfvén velocity to match the resonance condition with the beam ions. Instability requires a sufficiently fast ion pressure gradient. It might be that this lies behind the variability in the observation of shortfalls in fusion yield which could be ascribed to TAE modes and underwrites the need to verify that TAEs cause fast ion losses at all.

The data might be interpreted as showing that MHD can directly modulate the turbulence causing transport. Except for TAE modes, as described in (iv), there do not seem to be any candidates for interactions of this kind. Since there is other evidence which indicates that the edge temperature can affect the core plasma transport, this seems the most natural mechanism for connecting MHD with the loss of confinement in the terminating events. Success in simulations encourages this view. However, unambiguous corroboration of this model is likely to be very difficult to obtain and will have to await further progress in understanding transport in general.

Predictive Modelling

A transport model has been developed [10] which accounts for many of the features observed in JET-ELM-free H-modes. The model assumes: (1) transport inside the barrier region is given by ion neo-classical together with anomalous terms inducing both Bohm (global) and gyro-Bohm terms; (2) transport coefficients within the transport barrier are controlled by the ion neo-classical diffusivity; and (3) the width of the transport barrier is given by the ion poloidal banana width $D\sim\varepsilon^{1/2}\rho_{\theta i}$. Note that the Bohm terms dominate the transport in the outer regions of the plasma up to the transport barrier and the gyro-Bohm terms dominate the central confinement.

With these assumptions, it is possible to construct a complete set of transport equations for n_e, T_e, T_i and J which can be solved self-consistently. A single free parameter remains which can be the edge density (or alternatively the net recycling coefficient), which is adjusted to match the observed density evolution.

Recently, transport code JETTO, which solves transport equations inside the separatrix in the 1D approximation, was coupled to the EDGE2D code, which solves transport equations for plasma and neutrals outside the separatrix in 2D geometry [11]. This combination significantly improved predictive capability of the transport model, which now allows a direct comparison between measured and simulated plasma parameters not only inside the separatrix but in the SOL as well.

When applied to hot-ion plasmas, the time evolution of plasma parameters and profiles were well reproduced. In particular, the initial linear rise in stored energy was well described, and was followed by a progressive saturation, which the model suggested was due to the density rise. The model described accurately the evolution of power step-down pulses and the effect of strong gas puffing, and could account qualitatively for the temporary degradation of confinement following a sawtooth crash. The code predicted the time when ballooning modes became unstable, which was consistent with the experimentally observed appearance of giant ELM's, as shown in Fig.111. Indeed, this confirms, in a very satisfying manner, that the transport is close to ion neo-classical in the barrier region because an increase in transport would lead to ballooning modes always being stable.

Recently, the JETTO code was used in combination with MHD code, CASTOR, to assess the relative importance of ideal kink and ballooning modes as a cause of the hot-ion H-mode termination. The newly proposed and tested experimentally current ramp down scenario (to postpone the onset of the ideal kink mode) was used in numerical simulations. The result of such an analysis is

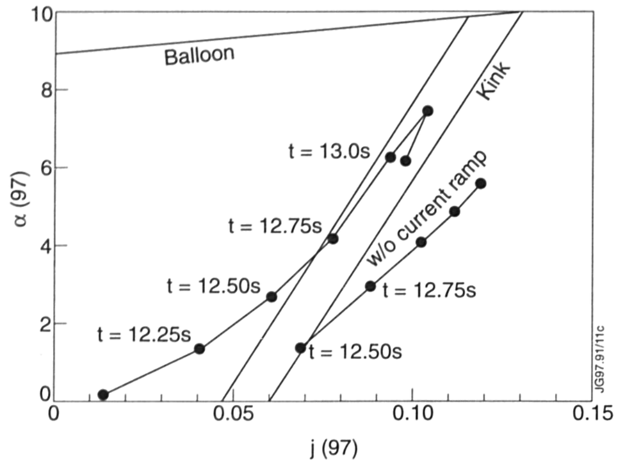

Fig.112: Assessment of the importance of the ideal link and ballooning modes as a cause of hot-ion H-mode termination

shown in Fig.112 and allows us to conclude that in typical hot-ion H-mode edge plasma parameters approach simultaneously both the ballooning and kink instabilities. The current ramp down indeed allows the postponement of the onset of the kink: in this situation ballooning stability start to play a dominant role.

The mixed Bohm/gyro-Bohm transport model, coupled to the neo-classical transport barrier model, has been also successfully used to simulate both 1.7MA and 3.8MA hot-ion H-mode pulses. The termination of the high performance phase was represented by ideal ballooning and ideal kink modes. It is known experimentally fact that the maximum achievable normalised β_N in the hot-ion H-mode is a decreasing function of the toroidal magnetic field. For example, hot-ion H-modes at 1.7MA/1.5T are able to reach the Troyon limit and profile analysis shows that they approach 60% of the ballooning limit across the entire plasma, as seen in Fig.113(a). In contrast, their 3.8MA/3.4T counterparts (Fig.113(b)) achieve only $\beta_N \sim 1.7$ and are far from the ballooning limit, except in the outer region of the plasma. This seems to be a transport effect and modelling has been able to reproduce the difference. It is a feature of the two components of the confinement model that the barrier improves more rapidly with magnetic field that in the core confinement. Thus, in the 3.8MA pulses, the ratio of the edge pressure gradient to that in the core is such that the MHD limits are encountered in the edge region long before the core. In contrast, the 1.7MA pulses limit more or less uniformly across the plasma cross-section. The density scale length in the barrier region has so far proven to be smaller than JET's diagnostics have been able to resolve. Thus, it has not been possible to confirm the modelling results directly.

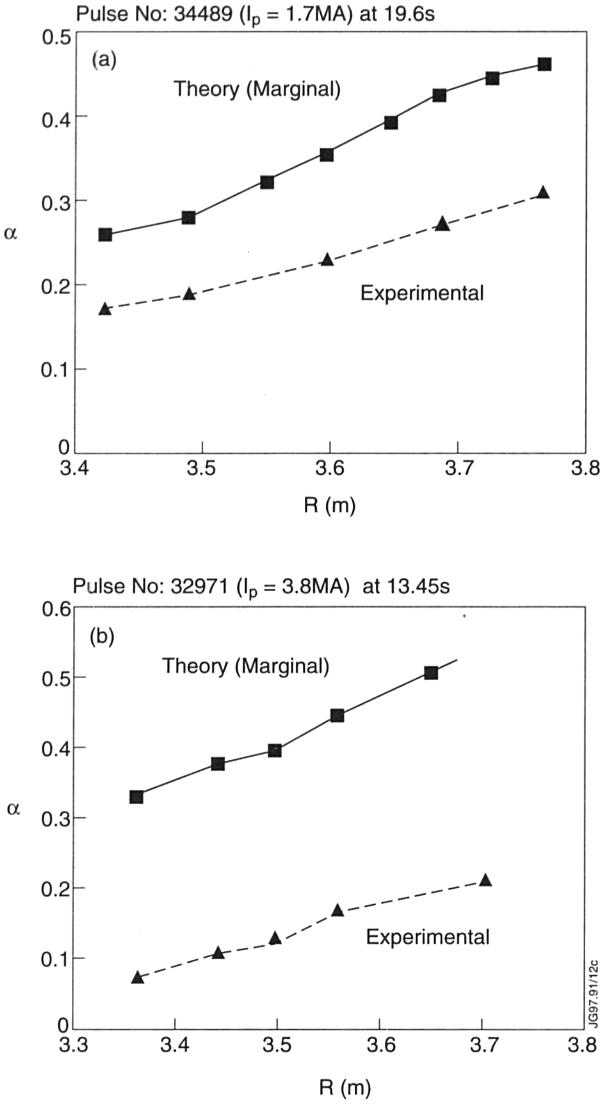

Fig.113: Comparison of the experimental profile of plasma pressure gradient compared with the ballooning threshold for (a) 1.7MA/1.5T and (b) 3.8MA/3.4T discharges.

However, the model edge pressure profiles are consistent with experiment, particularly in respect of the magnitude of the pedestal, so it is feasible that the relatively poor performance at high current is due to a transport effect. The only clear way forward is to increase the central power density at the start of the high power heating, so that more energy is placed in the core before the heat wave arrives at the boundary and triggers the observed MHD instabilities.

References

[1] The JET Team (presented by P. Lomas), IAEA-CN-64/A1-1, Montreal, Canada, 1996.

[2] Zohm, H. et al., in Controlled Fusion and Plasma Physics (Proc. 19th Eur. Conf. Innsbruck, Austria, 1992), Vol. I, European Physical Society, Geneva (1992) 243.

[3] Nave, F. et al., JET Report JET-P(96)14, submitted to Nuclear Fusion.

[4] Wesson, J., Balet, B., "Abrupt Changes in Confinement in the JET Tokamak", JET Report, JET-P(96)19.

[5] Parail, V.V., et al., 22nd EPS Conference, Bournemouth, UK, 1995, V19c, part 1, p1-013.

[6] The JET Team (presented by R. Gianella) IAEA-CN-60/A-2-111-1, 15th IAEA Conference, Seville, Spain, 1994.

[7] The JET Team (presented by D. Start), IAEA-CN-64/A2-6, Montreal, Canada, 1996.

[8] Huysmans, G., Goedbloed, J. and Kerner, W., Phys. Fluids **B5** (1993) 1545.

[9] Erba, M., et al., "Development of a Non-Local Model for Tokamak Heat Transport in L-Mode, H-Mode and Transient Regimes", JET-P(96)10, to be published in Plasma Physics and Controlled Fusion, 1997.

[10] Cherubini, A., et al,. Plasma Physics and Controlled Fusion **38** (1996) 1421.

[11] The JET Team (presented by A. Taroni), IAEA-CN-64/D3-3, Montreal, Canada 1996.

Divertor Physics and High Performance ITER Modes of Operation

The JET Mark IIA divertor was installed to test the influence of divertor geometry on the combined performance of the divertor and the core plasma. It is one of a sequence of JET divertors which are progressively "more-closed" to the escape of neutral particles from the divertor into the main plasma chamber. Detailed experiments have been performed to map out the available operating space in the Mark II divertor and to compare this space to that obtained in the previous divertor configuration (Mark I). The Mark II divertor has been operated both with significant leakage paths for neutrals from the divertor pumping plenum into the main chamber and with these leaks plugged (Mark IIAP).

The term "closure" in this context refers to the degree to which neutrals recycling from the target plates escape from the divertor region. Closure depends on the divertor plasma temperature, density, and magnetic geometry as well as on the geometry of the divertor components. In general, a "geometrically closed" divertor will have a larger effect on closure in the low recycling and detached plasma limits, where the ionisation mean free path becomes larger, than in the intermediate high recycling regime. The reasons for increasing closure are: (a) to provide easier access to the regime of high volumetric losses in the divertor, thus reducing target heat loading; (b) to reduce the neutral density in the main chamber, which may improve main plasma confinement quality and reduces sputtering of impurities; and (c) to increase neutral pressure in the divertor chamber, thus facilitating pumping. At the same time, improved closure generally leads to reduced flow in the scrape-off layer (SOL) which results in poorer flushing out of impurities and ash from the main chamber; this can be partly offset by increased pumping. The problem of choosing the correct geometrical closure for a divertor, which must operate with Type I ELMs is particularly difficult due to the great disparity in effective SOL width between and during ELMs.

It is not sufficient to evaluate the performance of different divertor geometries solely on the basis of parameters in the divertor (pumping speed, erosion rates, etc.). The performance of the core plasma must simultaneously be maintained at the levels required for a reactor. The ITER reference point requires a core confinement of 0.85 times the ELM-free H-mode scaling (ITER93H), a core density about 10% greater than the Greenwald value [1] and a core Z_{eff} value of approximately 1.6, excluding helium ash. Considerable emphasis has been placed in the divertor programme on studying the compatibility of the various reactor requirements and to mapping the available operating space which can be achieved simultaneously.

Divertor Closure

Recycling and neutral pressure measurements show that the modifications to the divertor geometry have indeed resulted in a more closed system. The neutral pressure at the divertor cryopump and thus the neutral pumping speed increased by a factor of 2 to 6 in going from Mark I to Mark IIA, depending on the operating regime. On closing the Mark IIA divertor bypasses, the main chamber neutral pressure decreased by about a factor of two, but, unexpectedly, the pressure at the cryopump remained unchanged (Fig.114). The neutral deuterium compression ratio, defined as the ratio of the pump to midplane neutral pressures, increased by at least a factor of two when the bypass leaks were closed. A similar improvement in

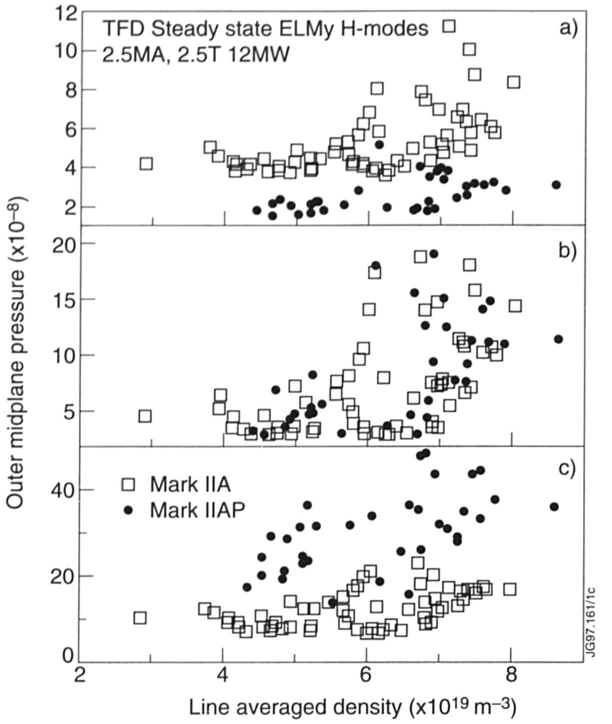

Fig.114: (a) Neutral pressure measured at the outer midplane in Mark IIA and Mark IIAP (2.5 MA, 2.5 T, 12 MW, ELMy H-modes); (b) neutral pressure next to the divertor cyropump for the same pulses in (a); and (c) neutral compression factor, defined as the ratio of subdivertor pressure to outer midplane pressure, as a function of line-averaged core electron density

retention is found when the deuterium recycling (D_α) from the inner wall is used as the upstream measurement instead of the pressure measurements, which are on the outer midplane (i.e. the improvement in closure applies equally the inside and outside of the machine).

Using the three divertor geometries, Mark I, Mark IIA, and Mark IIAP, a series of dedicated experiments was performed to study impurity exhaust using neon as a trace, recycling impurity. In these experiments a small quantity of neon was puffed into the SOL, introducing an intial neon concentration in the core plasma which then decayed with an e-folding time, τ_{Ne}. This decay time was measured as a function of the plasma density, the divertor magnetic configuration, the fuelling and pumping rates, and the fuelling location. τ_{Ne} was infinite without the cryopump activated, indicating that neon is a fully recycling impurity. Otherwise, τ_{Ne} varied from 3-5s in Mark I to around 1s in Mark IIA. The most notable effect in any of the three series of experiments is that τ_{Ne} decreased by a factor of two with increasing plasma density over the range accessible in L-mode plasmas. The neon exhaust rates for Mark IIA and Mark IIAP followed the same trend, when the decay time was plotted as a function of divertor plenum pressure or, equivalently, of

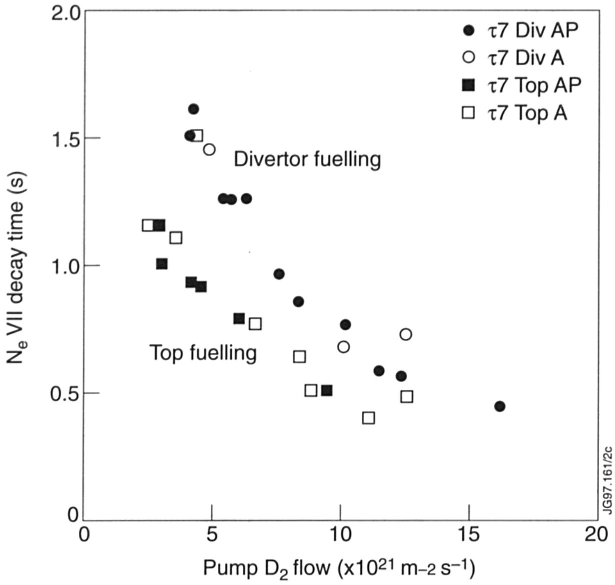

Fig.115: The decay time of Ne VII emission after the neon source is removed as a function of deuterium exhaust rate. Data are plotted for both the Mark IIA (open points) and Mark IIAP (solid points) divertors. The squares correspond to cases where the deuterium fuelling is from the top of the main chamber and the circles to cases where the deuterium fuelling was into the divertor

deuterium exhaust rate (Fig.115). In this way, it can be seen that the neon exhaust rate is proportional to the deuterium exhaust rate from the divertor. This result might be expected at low plasma density as it reflects the proportionality of the pumping speed of neon to that of deuterium. At high plasma density, the pumping of deuterium is expected to be assisted by the process of charge exchange, whereas neon should not be similarly affected. Therefore, the experimental observation that neon and deuterium are pumped at proportional rates even at high density is surprising. Further analysis, including 2-D modelling of the neon transport in the edge and SOL is underway to try to shed light on the reason for this behaviour.

One of the aims of the series of neon experiments was to investigate the influence of controlled convection on the retention of neon in the divertor. This was undertaken by changing the position of the deuterium fuelling between the top of the machine and the divertor. Once the influence of the deuterium exhaust rate was recognised, it was possible to see the improved neon exhaust resulting from top fuelling and the increased SOL flows (Fig.115). The influence of externally induced SOL flows is at its highest at low density (and low deuterium exhaust rate in the figure), where the flow due to recycling deuterium in the divertor is minimised.

Particle Exhaust Efficiency

Understanding neutral pumping in divertor tokamaks is of great importance for the design of tokamak reactors

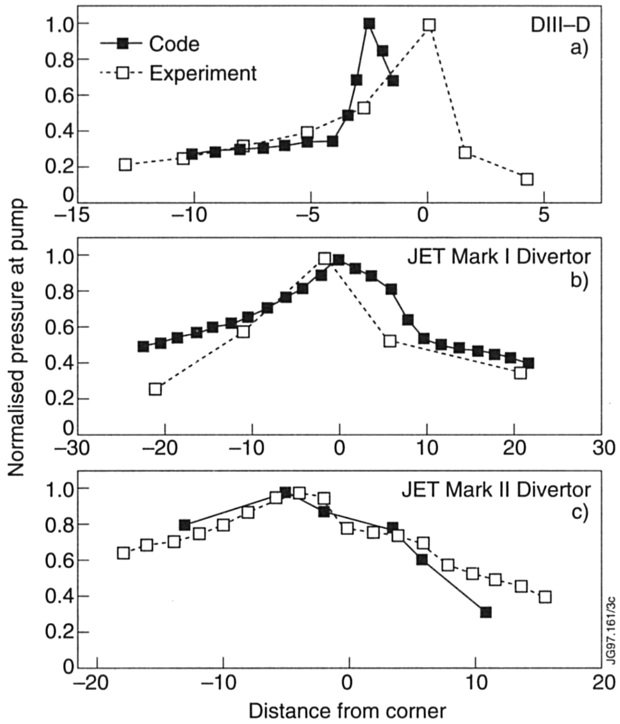

Fig.116: Comparison of measured (solid curves) and modelled (dashed curves) pressure in the pumping plenum as a function of the distance of the strike point from the entrance to the plenum for (a) DIII-D, (b) the JET Mark I divertor, and (c) the JET Mark IIA divertor

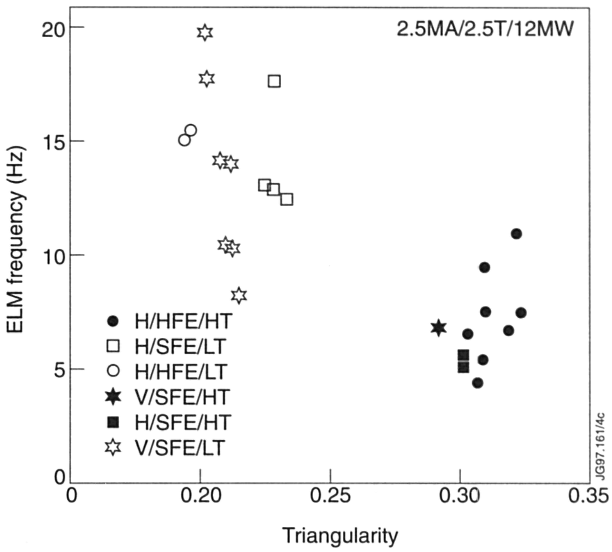

Fig.117: ELM frequency versus triangularity for Mark IIA pulses with beam fuelling only. The designation of the equilibria A/BBB/CC indicates target orientation, flux expansion (high or standard), and triangularity (high or low), respectively. All pulses were run at 2.5MA, 2.5T, and 12MW NB power

such as ITER. Neutral pumping determines the amount of plasma convection in the SOL and the rate of helium removal from the core plasma, which are critical for the performance of the device. Existing results from divertor tokamak experiments display apparently contradicting features, in particular with respect to the dependency of pumping (or neutral pressure in the pumping plenum) on the divertor geometry and proximity of the strike zone to the plenum. DIII-D has reported a strong decay of the pressure (a factor of 2-3) in the plenum when the strike point is moved 2-3 cm from the pumping baffle [2] (Fig.116(a)) for low density H-modes and a somewhat smaller drop at high densities. However, for discharges in JET with the Mark I and Mark IIA divertors (Fig.116(b) and (c)) a plenum neutral pressure variation of a factor of 2 can only be obtained by moving the strike points over distances of 20 cm (i.e. the whole divertor target) [3, 4].

Multi-machine simulations with the 2-D EDGE2D/U-NIMBUS code for the SOL plasma have successfully reproduced the features of these experimental results (Fig.116) and have allowed the identification of the physical process responsible for the above discrepancy. The physical basis for this behaviour lies in the transport of the neutrals that arrive at the pumping plenum across the SOL. In the JET Mark I and Mark IIA divertors, the computed neutral flux arriving at the plenum is dominated by multiply-scattered neutrals. However, in DIII-D the direct first flight recycled neutral flux dominates the computed flux at the plenum. This leads to a strong dependency of the plenum pressure on the effective solid angle of the pumping port to the neutral flux as seen in experiment (Fig.116(a)).

Dependence of ELMy H-mode Performance on Plama Configuration

To isolate the effects arising from configurational changes, a series of Mark IIA discharges was carried out with fixed plasma current, magnetic field, and neutral beam power (2.5 MA, 2.5 T, and 12 MW, respectively), in which the target orientation, flux expansion (horizontal target only), and main plasma triangularity were varied. These discharges reached nearly steady state conditions within about 3s of applying the beam power and that this state was characterised by regularly spaced Type I ELMs. In the absence of gas puffing, the ELM frequency depended most strongly on triangularity, without reproducible dependencies on target orientation or flux expansion, as shown in Fig.117. Although the ELM frequency, f_E, varies by a factor of 6 for these pulses, the confinement quality, as measured by H_{93}, was nearly independent of both f_E and configuration as shown in Fig.118. However, the "natural" density at which these beam-fuelled discharges run decreases with increasing f_E. Z_{eff} also

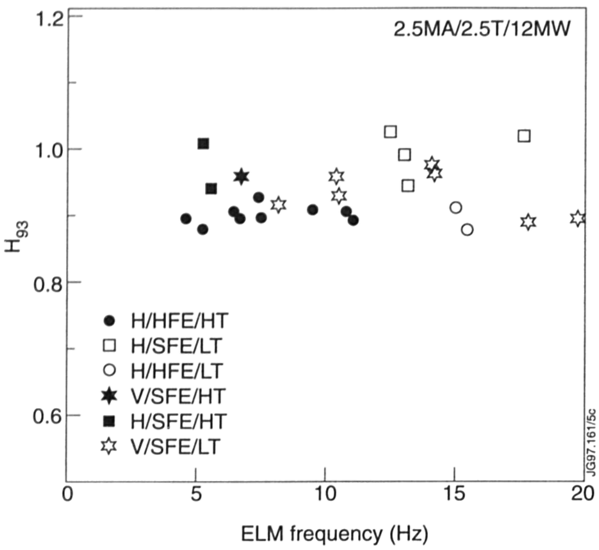

Fig.118: Variation of confinement quantity, H_{93}, with ELM frequency for beam-fuelled pulses in Mark IIA

reduces as f_E increases, illustrating the importance of ELMs in purging the edge plasma of impurities. The total radiated power fraction in these discharges was quite low for the high ELM frequency configurations, around 25%, increasing at lower ELM frequencies to about 40%.

The above series of discharges was systematically repeated with deuterium puffing, which was varied in strength and location. The ELM frequency increased with the addition of heavy fuelling (>2 x 10^{22} s^{-1}). As puffing increased the particle and energy confinement quality declined, so that there was a maximum density which could be obtained before the confinement degradation outweighed the increased puffing, and the fuelling efficiency became effectively negative (Fig.119).The highest densities were achieved in triangular plasmas which seem to maintain somewhat higher confinement at a given gas fuelling rate. Little difference was found in either confinement or attainable density between horizontal and vertical target discharges.

Experiments were also performed to raise the core density using shallow pellet fuelling (v<600 ms^{-1}). At the penetration available with the present injector, it was not possible to raise the density of an ELMy H-mode; each pellet was followed immediately by an ELM, which expelled the injected material.

ELM Physics

The major difficulty with standard ELMy H-mode operation produced by neutral beam injection was the presence of large amplitude Type I ELMs, which deposited high power levels repetitively onto the divertor

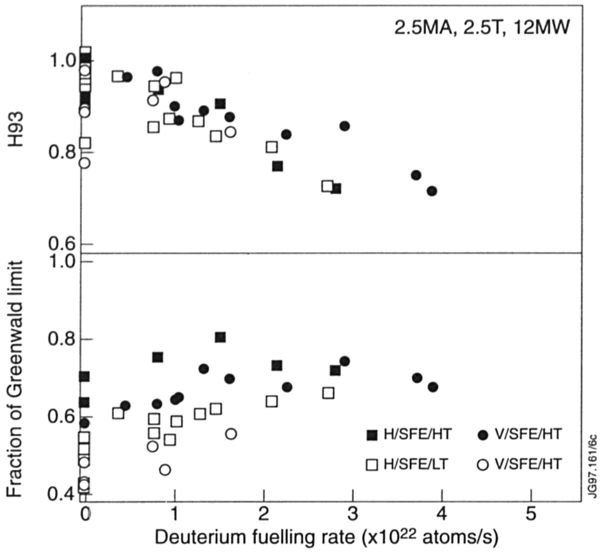

Fig.119: (a) Confinement enhancement relative to the ITERH93-P scaling law (H93) as a function of deuterium gas fuelling in the various Mark IIA configurations; (b) Plasma density achieved (as a fraction of the Greenwald limit) against deuterium gas fuelling for the discharges in (a)

components, coupled with low SOL density between ELMs. Sublimation of the graphite tiles due to ELMs was expected to be the main limit to the lifetime of the ITER divertor. Statistical analysis has been performed for the step changes in the diamagnetic energy and core density, which occur due to ELMs. The results indicated that the percentage change in energy and density decreased approximately as the square root of the ELM frequency (Fig.120). Futhermore, the percentage change in energy due to ELMs is about 20% greater than the percentage change in density in the Mark I divertor and about 50-70% greater in Mark IIA and Mark IIAP. The values of

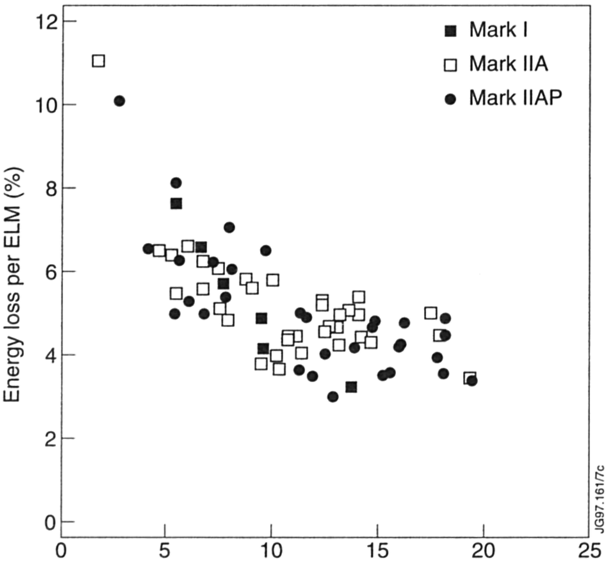

Fig.120: Percentage of the plasma stored energy lost during an ELM as a function of ELM frequency.

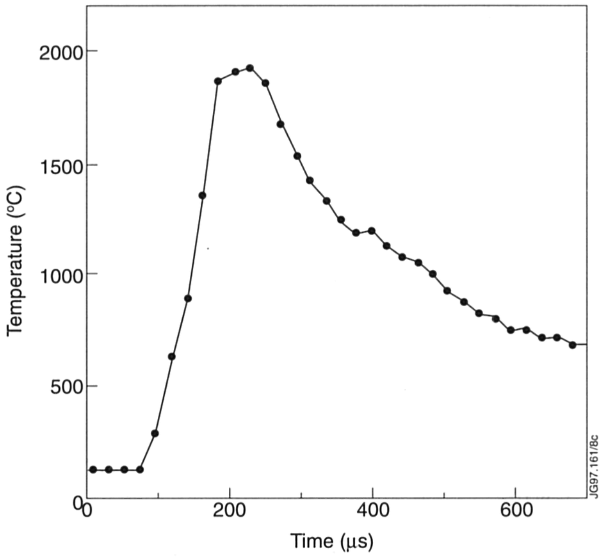

Fig.121: Temperature evolution as a function of time during an ELM on a divertor tile. Assuming toroidal symmetry, the peak power flux is about 2GW/m²

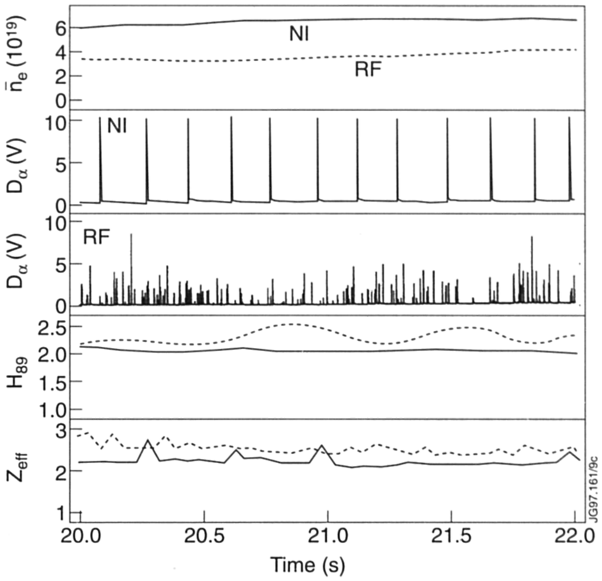

Fig.122: Example of comparable ELMy H-mode pulses (11MW, 2.5MA, 2.5T) produced by NB heating and RF heating illustrating the changed character of the ELMs (D_α signal)

energy drops are rather larger than those planned for in ITER (3%). How this translates into surface heating of the divertor tiles depends on the duration of the heat pulse, the area of interaction, and how much of the ELM energy is radiated. The dynamics of surface power deposition by Type I ELMs are crucial for extrapolation to ITER.

For the first time, direct high time resolution (20ms) measurements of the power flux to the divertor during the ELM have been obtained on JET using a fast 2D infrared camera, working in the 3-5mm range. The duration of the peak power deposition for typical Type I ELMs is about 120±20ms and the peak temperature is in excess of 1500°C (Fig.121). Fast interferometer measurements show that particles are lost on a much longer time scale of 3 to 4ms. Preliminary estimates show a typical peak power flux of ~2GWm^{-2}; the scaling with ELM frequency is being evaluated. The measured time dependence of the power deposition is consistent with that obtained by 1-D modelling of the SOL response to an ELM [5]. New modelling results show that the ELM duration has a very weak scaling with machine size, which has important implications for ITER.

During a Type I ELM, a fast displacement of the plasma occurred, with the strike zones moving from their initial positions with characteristic times ranging from 50ms to a few ms [5]. Code simulations indicate that ballooning modes alone are not sufficient to explain this behaviour and that the ELM may be also associated with an external kink limit. The new infra-red measurements support these conclusions. For typical Type I ELMs, the peak power deposition occurs at the inner divertor. This is where the largest motion of the strike points is observed but the movement does not ameliorate the heat load due to the relative timing of the movement and the power deposition. During an ELM, the peak power flux to the inner strike zone is first shifted by about 20cm to a smaller major radius in less than 20ms, with no measurable temperature increase of the scanned region. The strike zone then moves around this new position inwards or outwards by ~5cm during the next 120ms, where the largest power deposition takes place. Fast bolometer data show that radiative losses are a consequence of the power deposition and hence do not reduce the peak rate.

The ELM behaviour of discharges heated with ICRF waves rather than NB power is significantly different (Fig.122). ELMs in RF H-modes are smaller in amplitude and more frequent. Two reasons have been postulated for this observed difference: the low rotation in RF pulses and the lower density due to a lack of central (beam) fuelling. Determining which is the dominant cause of the large amplitude ELMs has important implications for ITER since, while the rotation is potentially avoidable, high density is required. Experiments attempting to raise the density of RF-heated H-modes were unsuccessful, both with gas fuelling and using pellets. This led to the conclusion that central fuelling, at least past the radius strongly affected by ELM losses, was essential to attain the necessary density in ITER.

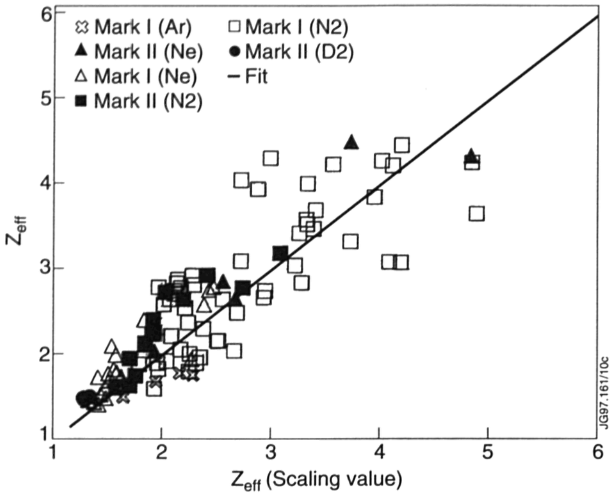

Fig.123: Measured effective charge (Z_{eff}) versus the scaling law for a number of discharges in Mark I and Mark IIA with seeded impurity gas as indicated. The solid line is a fit to the data

Radiative Plasma Operation

One method for reducing the power load on the divertor was to introduce an impurity seed to increase the radiant losses. Experiments were performed using either nitrogen or neon as the radiating species, with similar results in both cases. The maximum radiated power fraction achievable in these pulses decreased as the divertor closure was increased: from 80% in Mark I to 70% in Mark IIA and 60% in Mark IIAP. This difference appeared to be due to divertor charge exchange losses which were higher in more closed geometries, with the total power flow to the divertor tiles remaining small [6]. A further advantage of highly radiating discharges is that the ELMs are much more frequent and have smaller amplitudes, thus reducing dramatically the peak power loading.

To be attractive for a fusion reactor, radiative discharges must combine high volume power losses with relatively low core pollution. For ITER, the core impurity content is limited by bremsstrahlung losses and must result in a Z_{eff} smaller than 1.6, excluding helium ash, which is assumed to contribute little to radiative losses. Comparison of radiative discharges from different machines around the world [7] has shown that there is a robust relationship between the radiative power and the in the Z_{eff} core. This relationship is shown in Fig.123 for Mark I and Mark IIA discharges covering a variety of different impurities and for pure deuterium fuelling. Numerically, $Z_{eff}=1+7P_{rad}/(S\langle n_e\rangle^2)$, where S is the main plasma surface area and $\langle n_e\rangle$ is the line-averaged plasma density in units of $10^{20}m^{-3}$. Such a scaling predicts a Z_{eff} of 1.9 for ITER if 150 MW of power were radiated with $\langle n_e\rangle \sim 1x10^{20}m^{-3}$ and $S=1200m^2$. It might be possible to simultaneously match ITER's impurity content and radiation needs by using a somewhat higher Z impurity (such as argon). Present day experiments tend to use lighter impurities such as nitrogen and neon, which are better suited to their lower edge temperatures.

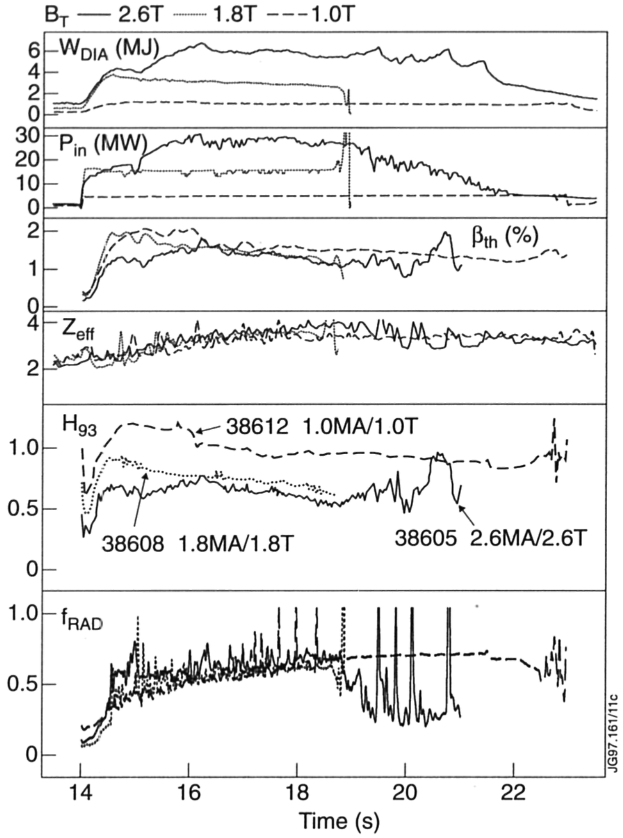

Fig.124: Comparative time evolution of stored energy, input power, thermal β, Z_{eff}, H_{93} and radiated power fraction for three discharges in the (ρ, ν*) scan of radiative divertor plasmas.*

The scaling of energy confinement in discharges with a high fraction of radiated power was studied in a series of plasmas which are dimensionally similar, except for the variation in normalised Larmor radius (ρ*) and collisionality (ν*) [8]. The aim of these experiments was to ascertain whether these ITER-relevant discharges were consistent with a gyro-Bohm scaling, such as ITERH93-P.

The time development of H-mode discharges at 1 MA/1T, 1.8 MA/1.8T, and 2.6 MA/2.6T is shown in Fig.124. The discharges had the same q_{95} (=3.1), triangularity (δ~0.3), minor radius, elongation and were all seeded by a mixture of N_2 and D_2 gas such that these reached a radiated power fraction of ~60%. These attained a Z_{eff} of about 3.5. The input powers were adjusted so that the same thermal β_T was obtained (~1.3%). This involved scaling the input powers approximately by B^2. Since the plasma Z_{eff} follows the scaling described above, it was not possible to keep the collisionality constant in such a scan. Since the collisionality scaling of ITERH93-P (gyro-

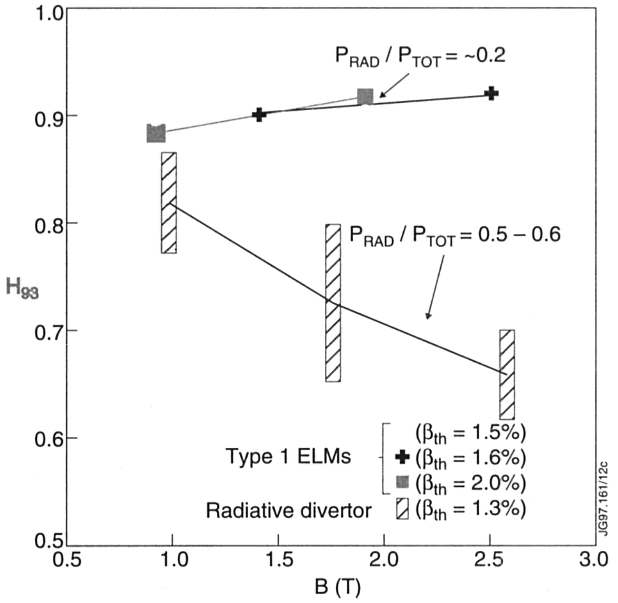

Fig.125: H_{93} as a function of toroidal field for the JET radiative divertor plasmas at similar (β, q, δ, κ, a, Z_{eff}, f_{RAD}). Also plotted are the Type I ELMy H-modes from the ρ scan in JET*

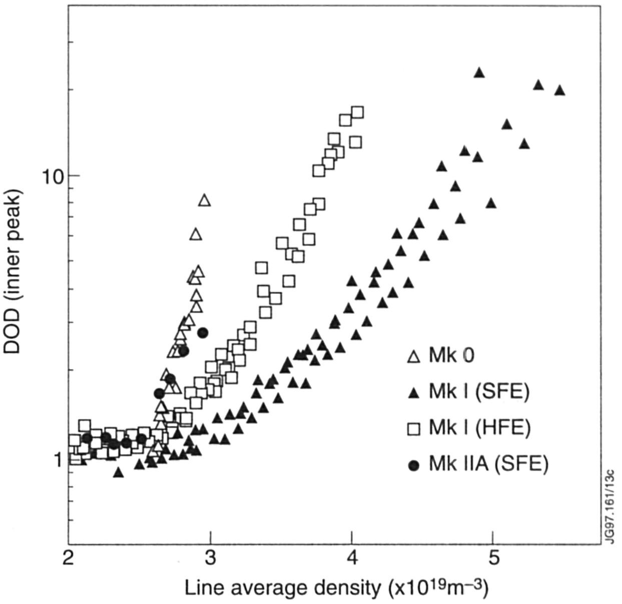

Fig.126: Degree of detachment of inner divertor leg as a function of density for Mark 0 (no divertor), Mark I in standard flux expansion, Mark I in high flux expansion, and Mark IIA with standard flux expansion configuration

Bohm like) and Bohm like scalings such as ITER89P are very weak, the measurements should be capable of distinguishing the ρ* scaling. The variation of ρ* across the dataset is close to a factor 2.

The plot of H93 as a function of toroidal field in Fig.125 shows that confinement progressively decays relative to ITERH93-P as B increases. This is in contrast to Type I ELMy H-mode discharges in JET which satisfy gyro-Bohm scaling [9]. These data suggest that radiative discharges are not consistent with a gyro-Bohm scaling law. Preliminary transport analysis of radiative discharges, using the TRANSP code, indicate that the thermal diffusivity of the core retains its gyro-Bohm like scaling whilst the outer region is degraded. Similar results have been obtained from analysing discharges whose global confinement is degraded by strong deuterium puffing.

Density Limits and Divertor Detachment

When operating at very low divertor temperatures, either due to high core densities or to large radiated power fractions, the flux of ions to the divertor target plates is dramatically reduced from what would be expected from a simple high recycling divertor model, where the ion flux increases with the square of the upstream (separatrix) density. This phenomenon is commonly referred to as divertor detachment. Operating in a detached regime is potentially an important benefit to a fusion reactor in which the lifetime of divertor components can have a strong impact on the overall cost of electricity.

To allow the quantitative comparison of detachment experiments, a new method of evaluating the degree and operating window of detachment has been introduced using the ion flux measurements at the divertor target. In this new definition, the degree of detachment is defined as the inverse ratio of the measured ion flux to that which one would expect in a high recycling divertor. In Fig.126, the degree of detachment is plotted as function of the core density for L-mode discharges in the various divertor configurations. In the Mark IIA divertor, it was found that the main plasma density threshold for the onset of detachment was reduced by a factor of ~2 relative to Mark I, a somewhat larger reduction than was predicted by the codes.

During ELMy H-modes with D_2 fuelling, it was possible to obtain plasma detachment in between the ELM events but not during them. However, as fuelling was added to increase the degree of detachment, the global confinement degraded before detachment became significant (Fig.127). In JET, it was not possible to maintain high core confinement while simultaneously achieving a high degree of detachment.

To reach ignition, ITER needs to operate in a high confinement regime with low Z_{eff} and at a plasma density of about 1 to 1.5 times the Hugill-Greenwald density limit (HGDL). Experiments were carried out in the Mark IIA campaign to determine the maximum density compatible with H_{93}>0.8 in steady state, partially detached discharges.

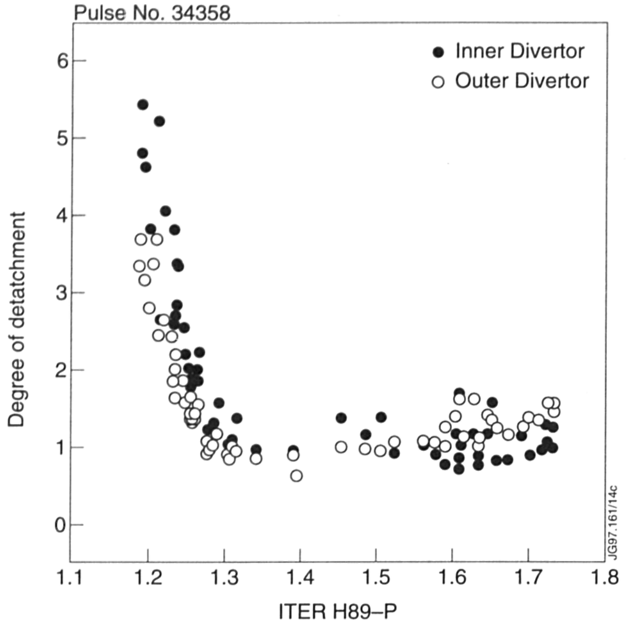

Fig.127: Degree of detachment versus core plasma confinement for a 2MA, 2.4T, 10MW discharge showing incompatibility between strong detachement and high confinement enhancement factors

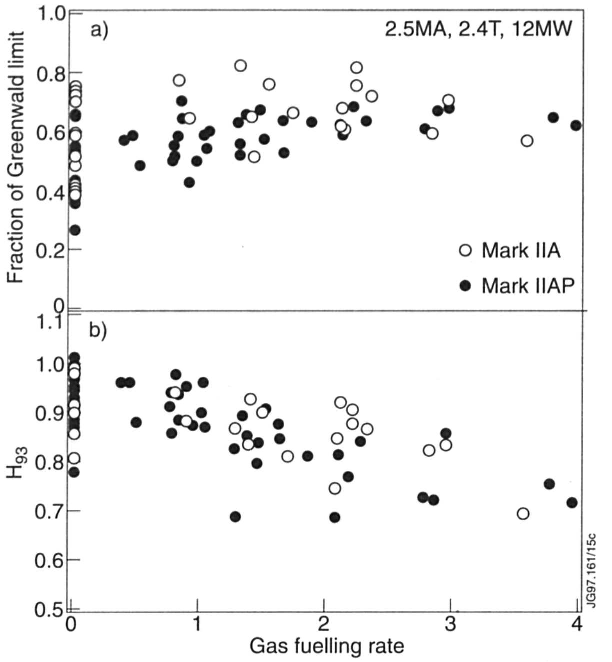

Fig.128: (a) Plasma density achieved (as a fraction of the Greenwald limit) versus deuterium gas fuelling in Mark IIA and Mark IIAP; (b) Confinement enhancement relative to the ITERH93-P scaling law (H_{93}) as a function of deuterium gas fuelling for the discharges in (a)

High density ELMy H-modes were obtained with gas and pellet fuelling, although the database for pellet fuelled discharges was more limited than that for gas fuelling. The line-averaged density and core plasma confinement are shown in Fig.128 for a series of discharges at 2.5MA and 2.4T as a function of the deuterium fuelling rate. The closure of the bypass leaks (Mark IIAP) has increased the maximum density achievable by ~5% and that the degradation of confinement is somewhat less at a given fuelling rate. At the same time, the midplane neutral pressure was substantially reduced by plugging the bypass leaks. Indeed, the close correlation between core confinement and neutral pressure seen in Mark IIA has shifted by a factor of two to lower pressures in Mark IIAP (Fig.129), suggesting that increased midplane pressure is a consequence of the confinement deterioration rather than a cause of it.

The maximum density achieved in steady state conditions with $H_{93}>0.85$ is 0.8-0.9 times the Hugill-Greenwald limit. In this regime, the divertor is partially detached. Attempts to exceed this density limit by increased puffing were characterised by a progressive deterioration of the energy confinement, accompanied by a decrease in particle confinement, which more than compensated for the additional fuelling. As the density (and/or power) increased, both the frequency and particle loss per ELM increase, leading to an effective saturation of the achieved electron density. The H-mode density limit was not disruptive and was not associated with MARFE formation. As observed in other machines, the maximum density was independent of input power and scaled with plasma current, in agreement with the Hugill-Greenwald formulation.

Impurity Behaviour in Mark IIA

The intrinsic carbon density in the plasma core and the impurity influxes have been studied over the wide range

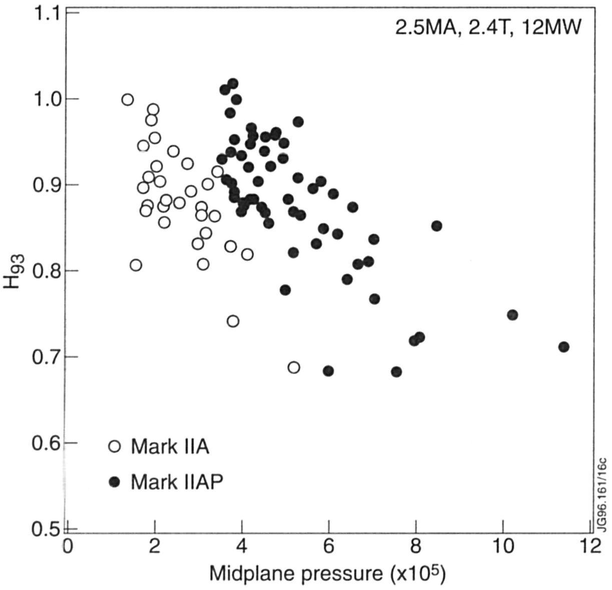

Fig.129: Dependence of the confinement enhancement factor on mid-plane neutral pressure for Mark IIA and Mark IIAP

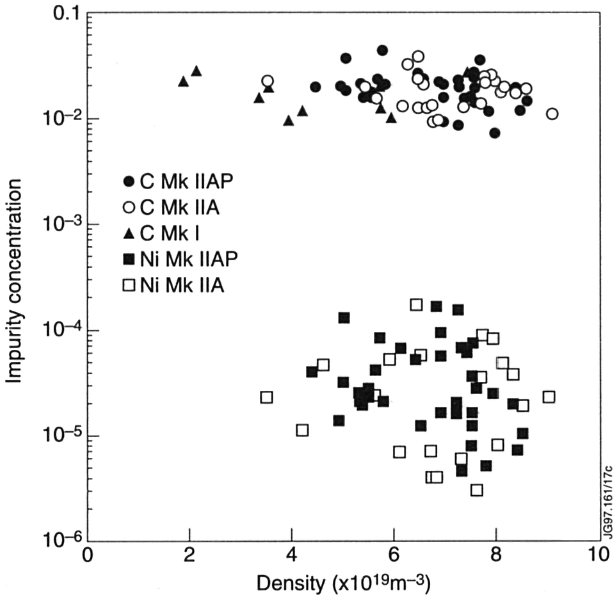

Fig.130: Concentrations of carbon and nickel in the core plasma for various JET divertors as a function of volume-averaged density

of plasma shapes available in Mark II. In ELMy H-modes, over the range of conditions studied, the core impurity density tends to increase with electron density keeping the impurity concentration constant (Fig.130). This behaviour, combined with the fact that the carbon influxes do not decrease at high density, suggests that chemical sputtering, which does not decrease at low edge temperature, as opposed to physical sputtering may be the predominant source of carbon in Mark II. In general, higher triangularity tends to produce higher core concentrations, but there is little variation with divertor flux expansion. The higher triangularity configurations are associated with lower ELM frequencies, the impurity density decreasing as the ELM frequency increases. For a given triangularity, the core carbon density does not change when the strike point is varied from the horizontal to the vertical target.

The impurity influxes have been studied with a range of spectrometers including one with a rotating mirror giving the poloidal distribution of the fluxes from the divertor and the inner wall, and one with a detailed view, spatially and spectroscopically resolved, of the outer divertor. The combined instrumentation allows CI to CV species to be viewed with good spatial resolution over a large poloidal distribution of the vessel walls. The deuterium and carbon influxes have been compared. Unlike the core densities, there are no obvious trends of the impurity influxes with triangularity. The carbon influx increases by a factor of ~2 for both the inner wall and the target when the strike point is moved from the horizontal to the vertical target.

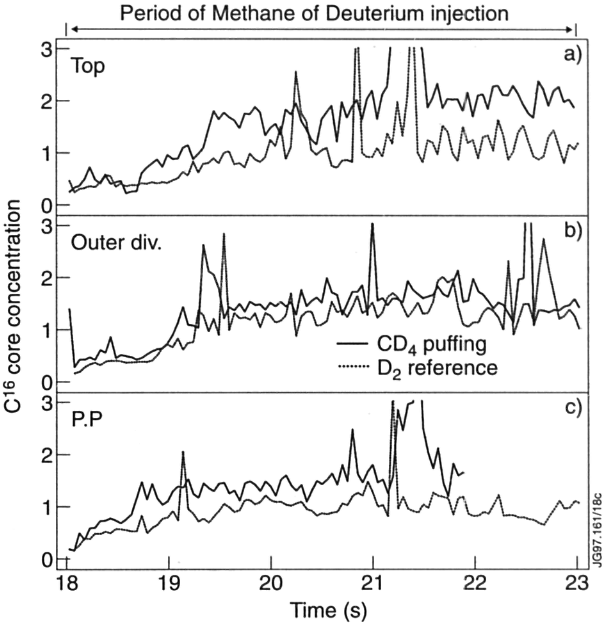

Fig.131: Core carbon concentrations in pairs of discharges to compare methane (solid curves) and deuterium (dotted curves) gas puffing: (a) fuelling into the top of the main chamber, (b) fuelling in the outer divertor plasma leg, and (c) fuelling into the private plasma region of the divertor. The fuelling was at a steady value from 18 to 23s

Since the impurity density increases with triangularity while the influx does not, this effect may be attributed to an increase in particle confinement. A similar increase in the nickel content is observed. It is speculated that the low ELM frequency in triangular discharges is reducing the flushing action of the ELMs, which normally controls the core impurity content.

The impurity content of high density Mark IIA and Mark IIAP discharges is similar to that in Mark I (Fig.130). This is despite the fact that reduced neutral pressure in the main chamber should lead to lower levels of sputtering in the region where impurities most efficiently contaminate the core. One explanation is that ion impact on components forming the narrow entrance of the closed divertor, especially during ELMs, is the dominant source of impurities at high density. A second possibility is that the chemical sputtering in Mark IIA is higher than in Mark I due to higher tile temperatures in the non-wetted areas of the divertor. A third effect is the cladding of the inner wall with carbon tiles which took place at the time of the plugging of the bypass leaks (Mark IIA to Mark IIAP).

To test the fuelling efficiency of chemically-sputtered carbon a series of dedicated experiments was performed in which methane was puffed into the plasma boundary.

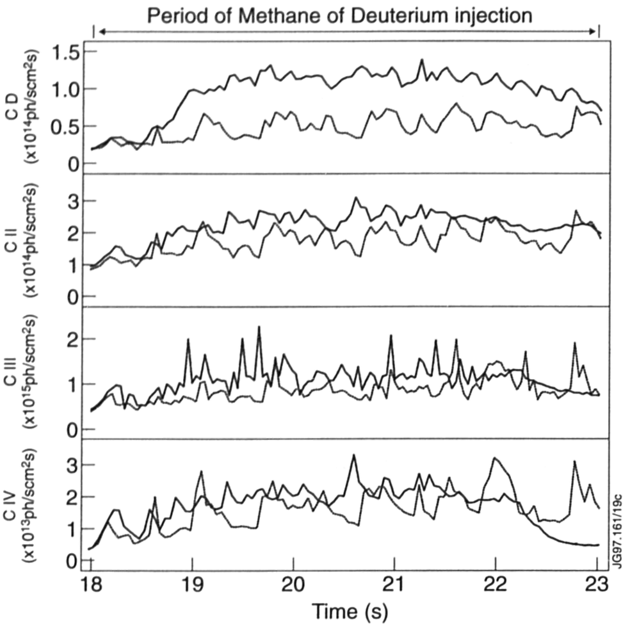

Fig.132: Emission from a molecular band of CD and from three different ionisation states of carbon for a pair of otherwise identical discharges fuelled with methane (solid curves) and deuterium (dotted curves). The fuelling for this pair of discharges was into the private plasma region of the divertor. The fuelling was at a steady value from 18 to 23s

Three pairs of discharges were performed: one pair with fuelling from the top of the vacuum vessel, one with fuelling into the outer leg of the divertor scrape-off layer, and one with fuelling into the private plasma region in the divertor. For each fuelling location, two discharges were carried out, one with methane fuelling and one with molecular deuterium fuelling at a rate such that the total rate of deuterium atoms was the same as in the methane shot. All pulses were performed at 2.5MA, 2.5T, and with 12MW of NB heating, so that these were ELMy H-mode plasmas.

The core carbon content is compared for the three pairs of discharges in Fig.131. It can be seen that top fuelling was the most efficient at contaminating the plasma core. An impurity penetration factor can be defined by dividing the incremental core carbon content by the external fuelling rate. This penetration factor, which is in units of time, is ~25ms for top fuelling. The corresponding number is <12ms for fuelling into either the private plasma region or directly into the divertor plasma and is within the uncertainty of the measurement. This last result reflects the good impurity retention expected in the flow generated by recycling deuterium.

The emission from a CD molecular band and from various ionisation stages of carbon are shown in Fig.132 for the pair of pulses with fuelling into the private plasma region. While the emission from the CD band is more than doubled by the addition of the methane puff, the emission from CII, III, and IV is only slightly increased, by a factor roughly the same as the increase in the core carbon concentration (Fig.131). This difference can be explained if a large fraction of the injected methane is being ionised before completely dissociating, with the resultant molecular ion being swept back to the divertor target plates.

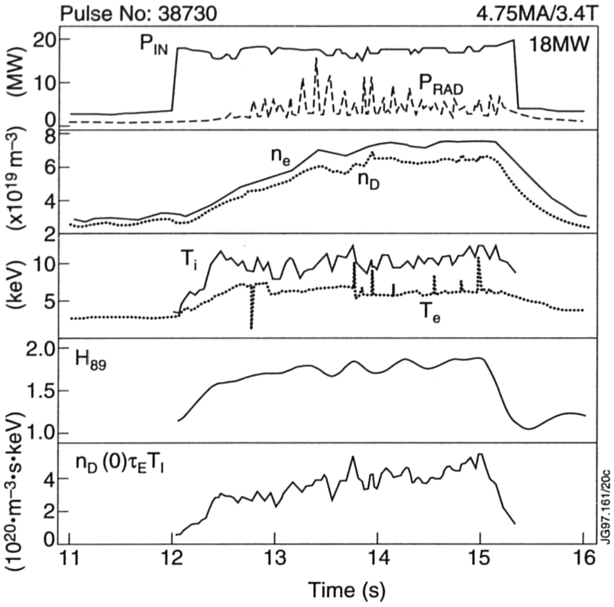

Fig.133: Time traces of a high power 4.7MA discharge, where the fusion triple product reaches a value of $4x10^{20}m^{-3}skeV$. $P_{L-H} \propto nBS$ *represents an L- to H-mode threshold power scaling*

High Current Operation

The JET tokamak, due to its large size and similar shape, is in a position to produce plasmas which most closely resemble those required for ITER. The confinement and fusion performance of steady state Type I ELMy plasmas have been studied at plasma currents up to 5MA. The highest stored energies and equivalent QD_T are achieved at the highest plasma current but with a confinement somewhat lower than the prediction of 0.85 times the ITER ELM-free confinement scaling. In fact, while at 2.5MA H_{93}~0.9, at 4MA H_{93}~0.85 and above 4MA H_{93}~0.75. The confinement quality does not seem to depend on q_{95}. Steady state equivalent fusion power of approximately 3.5MW has been achieved at 4.7MA with 17MW of NB power (see Fig.133) and at 3.5MA with 24MW of combined heating (16MW NB + 8MW of ICRF). The optimisation of plasma performance is underway in order to identify the scenario to be chosen for the forthcoming demonstration of steady state high fusion power in D-T plasmas.

At I_p>3.5MA, most discharges suffer from a spontaneous H-L "back-transition" (see, for example, the high current discharge in Fig.133 where the stored energy begins to drop before the end of the high power phase). The loss of confinement (sometimes after several energy confinement times) is often followed by a nondisruptive mode lock. In some cases, the confinement recovers a few seconds after the loss; up to three cycles have been observed in pulses with long duration additional heating. On a given day, the H-L transition tends to occur at a constant value of P/n_eB_T. There is variation of this value from day to day, suggesting that vessel conditions may also be important. At 2.5MA, where normally H-modes can be maintained for all of the available heating length (up to 10s), a similar H-L transition is seen in pulses with NB heating powers near the threshold power, in particular, if the vacuum vessel is not very well conditioned. On the other hand, the addition of up to 8MW of ICRF heating in high current discharges causes an earlier H-L transition, making it impossible to establish a clear link between the H-L transition and the level of heating power.

Conclusions

A central issue for ITER is the degree to which the integrated performance of the plasma/edge/divertor can be influenced by choice of divertor geometry. A general summary of the changes seen in going from Mark I to Mark IIA and then reducing the bypass leakages (Mark IIAP) is as follows. Increasing closure has produced three expected effects: the density for the onset of detachment, for a given P_{sol}, was reduced; the pumping speed was increased (Mark I → Mark IIA); and the main chamber neutral pressure was reduced (Mark IIA→ Mark IIAP). It had also been expected that the intrinsic impurity level of the core plasma would be reduced, which did not occur. The explanation seems to lie in the fact that: (a) there is more direct ion impact on the divertor shoulders of the narrower Mark II; (b) the higher tile operating temperature of Mark II leads to increased chemical sputtering from the non-wetted areas; and (c) the carbon cladding of the inner wall was increased. The pump-out time for injected trace neon was reduced considerably in going from Mark I to Mark IIA.

The influence of these observed changes on global confinement was generally small, but in some cases significant. In particular, the more closed configurations appear to be able to maintain good confinement to a slightly higher normalized density in ELMy H-modes at given power, current, and field, which is very important for ITER. The H-mode density limit was unchanged, and to be close to the Greenwald value. The L→ H threshold was independent of divertor closure or target orientation, but more investigation is needed on this point. As the divertor closure increased, the maximum radiated power fraction attainable decreased, but there was evidence that divertor charge exchange losses increased correspondingly.

For ELMy Type I H-mode operation, the ELM frequency has a stronger effect on performance than either target orientation or flux expansion, and the ELM frequency is determined (at a given power and density) primarily by triangularity and gas puff rate.

In going from Mark IIA to Mark IIAP, it was possible to separate the effects of neutral pressure in the divertor and the midplane. Experiments showed that the confinement quality of ELMy H-modes was correlated with divertor neutral pressure rather than midplane neutral pressure. The divertor neutral pressure controlled the divertor plasma density for a given SOL power, and hence the core edge density. For discharges operating at the ballooning limit, increased edge density implies reduced edge temperature, which was believed to adversely affect confinement.

Implications for ITER

To operate successfully, ITER requires an "integrated scenario" in which the confinement quality is good enough ($H_{93} \geq 1$, $Z_{eff} \leq 1.8$ for $\tau_{He*}/\tau_E = 5$), the temperature of the divertor and first wall components remained below melting/ablation temperatures at all times (even during transients such as ELMs), and the erosion rate was low enough to ensure reasonable component lifetimes.

It was possible to routinely produce long pulse, quasi steady ELMy H-modes at fairly high densities, as have been adopted by ITER for its baseline operating scenario. When high radiated power fractions (and correspondingly high density, cold edges) were produced, the ELMs became Type III and the heat load to the divertor, and target erosion, were very low. However, the confinement deteriorates and scaling experiments suggest that such discharges do not follow the gyro-Bohm scaling law. The Z_{eff} of such discharges, when scaled to ITER, appeared marginally satisfactory.

When the ELMy H-modes were operated with hot, medium density edges, the confinement quality was good and followed gyro-Bohm scaling. In addition, the Z_{eff} resulting from intrinsic impurities was quite low and well within the ITER requirements. The Type I ELMs which occurred in the neutral beam heated H-modes had amplitudes in the range $\Delta W/W \sim 3\% - 8\%$ and characteristic energy deposition times of 100μsec. Such ELMs, when extrapolated to ITER, would result in unacceptable heating and erosion of the target plates if all the energies were to fall on them; this is the principal objection to this mode of operation. On the other hand, the Type I ELMs produced in comparable RF heated ELMy H-modes were much smaller in amplitude and higher in frequency, while the confinement remained very good. It is not yet understood whether the changed ELM character resulted from lack of a central particle source and reduced momentum input, or from some other cause. However, these results give room for optimism in that they show that Type I ELMs can be controlled and their effects mitigated. The relatively low densities achievable in RF heated discharges, however, suggest that some degree of deep fuelling will probably be required in ITER.

Thus, it appears that either the Type III or Type I scenarios may be further developed to the point where these can satisfy ITER's requirements for an integrated scenario. The Type III scenario requires better understanding of the scaling of the edge region to be able to scale to ITER, while the Type I scenario needs further development of ELM control techniques.

References

[1] M. Greenwald et al., Nucl. Fusion **28** (1988) 2199.

[2] C.C. Klepper et al., Nucl. Fusion **33** (1993) 533.

[3] G. Saibene et al., 22nd Eur. Conf. Contr. Fusion and Plasma Phys. Vol. 19C, Part II (1995) 121.

[4] JET Team (Presented by G. Vlases), IAEA-CN-64/A4-1, 16th IAEA Conf., Montréal, Canada (1996).

[5] H Lingertat Proceedings of the 12th PSI Conference, to be published in J. Nucl. Mater.

[6] R. Reichle *et al.*, 12th PSI Conf., to be published in J. Nucl. Mater.

[7] G Matthews Proceedings of the 12th PSI Conference, to be published in J. Nucl. Mater.

[8] JET Team (Presented by D. Stork), IAEA-CN-64/A1-1, 16th IAEA Conf., Montréal, Canada (1996).

[9] JET Team (Presented by J.G. Cordey), IAEA-CN-64/AP1-2, 16th IAEA Conf., Montréal, Canada (1996).

ITER Physics and Performance Optimisation

The main briefs of the Task Force and the Topic Group who have worked very closely together addresses the general aspect of ITER physics and performance optimisation, mainly through current profile control. JET's contribution to the dimensionless scaling laws, which are the basis of scaling of ITER is outstanding, in particular for dimensionless scaling experiments including similarity experiments with DIII-D and C-Mod, ρ^* scaling, beta scaling, L-H and H-L threshold transitions.

A significant part of the experimental time has also been devoted to the simulation of ITER plasmas using ICRF fast ions as a simulation of alpha-particles and assessing some effects of fast particles on rotation and the study of Toroidal Alfven Eigen Modes (TAE).

Good results have been achieved with performance optimisation through current profile control with proper tuning of the plasma current ramp and of the power waveforms: high fusion yield has been achieved with the establishment of large Internal Transport Barriers, central ion temperature in excess of 30keV and central pressure up to 3bar.

ITER Physics

Energy Confinement Scaling With ITER Dimensionless Parameters

Introduction

A series of ELMy H-mode experiments has been undertaken in which the values of the dimensionless physics parameters are close to ITER values. The dependence of the confinement scaling upon the dimensionless parameters, ρ^* (dimensionless Larmor radius $\equiv T^{1/2}/aB$), ν^* (collisionality $\equiv na/T^2$) and β ($\equiv nT/B^2$) is examined in turn. The dependence of energy confinement with the parameter ρ^* is obtained for a larger range of ρ^* and at higher β's than studied previously [1], [2]. The dependence of τ_E is again found to be close to gyro-Bohm and in agreement with the ITERH93-P [3] scaling expression which is being used to predict the ITER confinement time. A similar behaviour was first

Table XIV: ρ* Scans

a) $\beta_{nth} \sim 2$ $\nu^*/\nu^*_{ITER} = 2.8$

Pulse No.	B	I	n	P	τ_{th}	$B\tau_{th}/\rho^{*-2.7}$
37380	1	1	2.2	7	0.14	1
37375	2	2	5.6	15	0.26	1.04

b) $\beta_{nth} \sim 1.6$ $\nu^*/\nu^*_{ITER} = 1$

Pulse No.	B	I	n	P	τ_{th}	$B\tau_{th}/\rho^{*-2.7}$
38429	1.5	1.5	2.5	10	0.20	1
38427	2.6	2.6	5.0	21	0.30	0.97

c) $\beta_{nth} \sim 1.5$ $\nu^*/\nu^*_{ITER} = 2.3$

Pulse No.	B	I	n	P	τ_{th}	$B\tau_{th}/\rho^{*-2.7}$
37379	1	1	2	4.4	0.19	1
38047	2	2	4.8	10	0.34	1.03
37944	2.6	2.6	6.8	12.5	0.43	1.05

found on DIII-D for low q ELMy H-modes [4]. The dependence of τ_E with ν*, the collisionality is also found to be in agreement with the ITERH93-P expression whilst the scaling with β is found to be very weak in contrast to the strong scaling with β of ITERH93-P. The reasons for this discrepancy and the implications of the results are discussed later.

Dependence of τ_E on the Dimensionless Parameters ρ, ν* and β*

Three separate groups of experiments were carried out to determine the dependence of confinement on ρ*, ν* and β. The ITER like plasma geometry was the same as in reference [1], R = 2.9m, a = 0.92m, κ = 1.7, $q_{\psi 95} = 3.2$, δ=0.2 and the current and toroidal fields ranged from 1MA/1T to 2.6MA/2.6T. To adjust the density only moderate gas puffing was used, the main particle source was from the neutral beams, which was also the main heating source.

The results were compared with the ITERH93-P scaling expression, which can be written in dimensionless form as follows:

$$B\tau_E \propto \rho^{*-2.7}\,\nu^{*-0.28}\,\beta^{-1.2} \qquad (1)$$

where the parameters ρ*, ν* and β are defined in terms of their average values as $\rho^* \equiv W_{th}^{1/2}/n^{1/2}a^{5/2}B$, $\nu^* \equiv n^3a^7/W_{th}^2$ and $\beta \equiv W_{th}/B^2a^3$, with W_{th} being the total thermal stored energy, n the volume average density and a is the minor radius.

ρ Scaling Experiments*

Table XV: ν* and β scans

	ν* scan		β scan	
Pulse No.	37718	37728	38407	38415
B (T)	2	2.6	1.5	1.7
I (MA)	2	2.6	1.5	1.7
<n> 10^{19}	5	5	2.7	4.1
P (MW)	10	16	6.5	16.5
W_{th} (MJ)	3.0	4.8	1.5	3.4
τ_{th} (s)	0.3	0.3	0.24	0.21
$B\tau_{th}$	0.6	0.78	0.36	0.35
ν^*/ν^*_{ITER}	3.4	1.3	2.1	1.5
β_{nth}	1	1	1.2	2.2

Three sets of experiments have been completed at different β's and collisionalities, close to those expected in ITER, these are listed in Table XIV and typical time traces are shown in Fig.135. To keep ν* and β fixed, the density should be proportional to $B^{4/3}$ and the stored energy proportional to B^2. From Table XIV, it can be seen that this has been approximately achieved and that the resulting dimensionless confinement $B\tau_{th}$ follows the $\rho^{*-2.7}$ scaling of ITERH93-P, that is the scaling is close to gyro-Bohm. The three ρ* scans are shown against the scaling expression in Fig.134, the H_{93} factor is greater than 0.9 for all of the pulses.

ν Scaling Experiments*

Here β and ρ* were kept fixed and this means that n = const. and W ∝ B^2. The results are shown in Table XV, and the profiles of ρ* and β which are also well matched for these two pulses can be seen in Fig.136. From Table XV it can be seen that $B\tau_{th}$ scales as $\nu^{*-0.27}$ in close agreement with the ITERH93-P scaling.

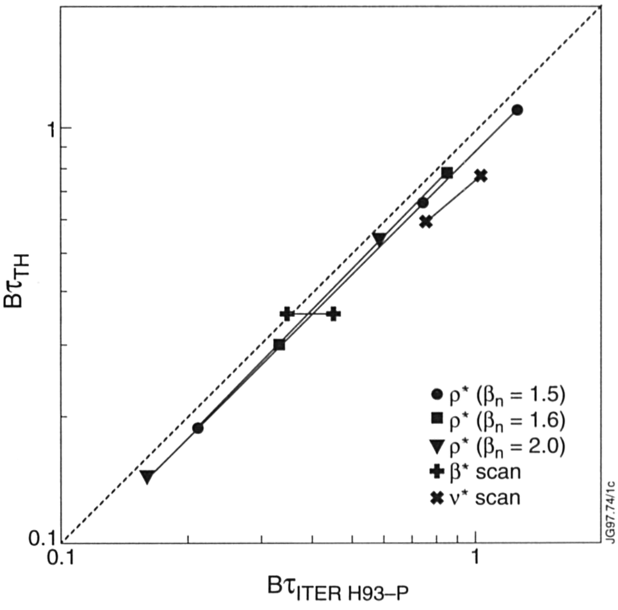

Fig.134: The normalised confinement time $B\tau_E$ versus $B^*\tau_{ITERH93P}$. The three ρ scans are indicated by solid triangles, squares and ellipses. The β scan is crosses and ν* scan is diagonal crosses*

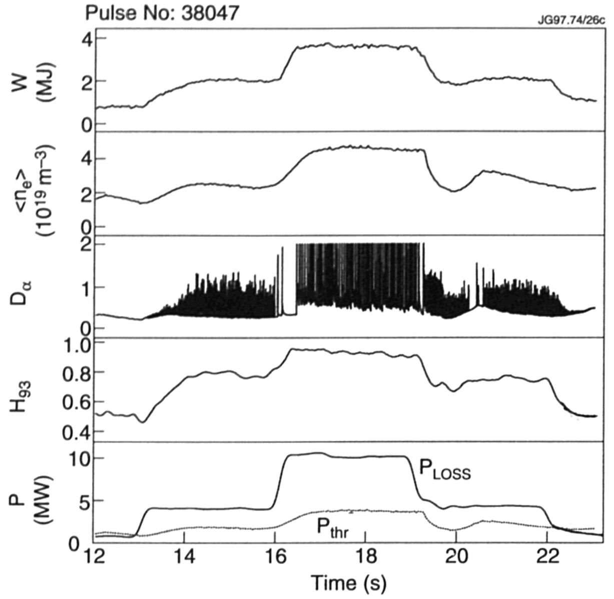

Fig.135: Typical time traces of ρ^* scaling experiments showing the variation of W, $<n_e>$, D_α, H_{93} and P

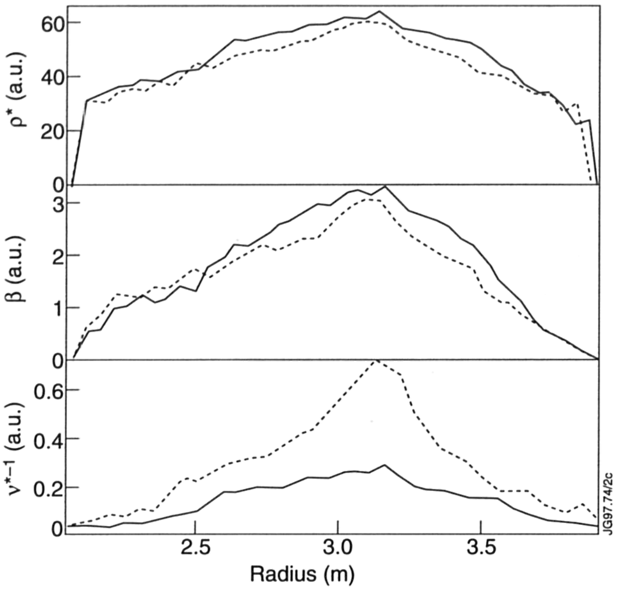

Fig.136: Radial profiles of ρ^*, β, and ν^* for pulses in the ν^* scan

β Scaling Experiments

ρ^* and ν^* were kept fixed, which meant that $\nu \propto B^4$ and $W \propto B^6$. The results of these experiments are given in Table XV. A preliminary analysis of the data gives a weak dependence of τ_e upon β with $B\tau_e \propto \beta^{-0.05}$ in marked contrast to the strong dependence of the ITERH93-P scaling expression. A similar result was recently found on DIII-D [5].

A comparison of both the ν^* and β dependence with the ITERH93-P scaling expression is given in Fig.134. The ν^* dependence follows the scaling expression whilst this is clearly not the case for the β dependence.

Discussion

The dimensionless physics parameter scans in ρ^*, ν^* and β confirm the validity of the ITERH93-P scaling expression as far as its ρ^* and ν^* dependence are concerned. However the β dependence is very different. There are several possible explanations for this discrepancy and these are currently being investigated. One obvious difference between determining the β scaling as compared with the ρ^* and ν^* scaling is that the range in β is much narrower than either the ρ^* or ν^* range. It is also possible that data close to the MHD β limit has been included in the ITER database by some of the machines.

If this lack of β scaling is confirmed with other experiments, then the prediction of the ITER confinement time will be increased by about 10% at the ignition point.

H-Mode Power Threshold (L-H and H-L Transitions)

Introduction

During 1996, a significant effort was made to further investigate the characteristics of the transition to H-mode. This was already started in 1991/92 (before the installation of the Pumped Divertor) when the Threshold Database was first compiled, and carried on during the 1994/95 Mark I divertor experimental campaign. For the first time, the study of the transition back to L-mode was also undertaken. Both issues are critical to the ITER design: knowledge of the scaling of the power threshold for the L-H transition with quantities like density and toroidal field are essential to correctly estimate the amount of additional heating necessary to trigger the H-mode in ITER. Information about the H-L transition is on the other hand necessary to keep ITER in the H-mode, while on its route to ignition. Initial reports from other machines showed that the minimum power necessary to keep the plasma in the H-mode was slightly over half that necessary for the L-H transition (the so-called "hysteresis effect"). During 1996, one of the main objects was to study the H-L transition and the hysteresis effect on H-modes.

Experimental Data

At the beginning of the experimental campaign, different configurations were used to test their influence on the H-mode power threshold. Standard Fat, Super Fat and Gas-box configurations were compared.No significant

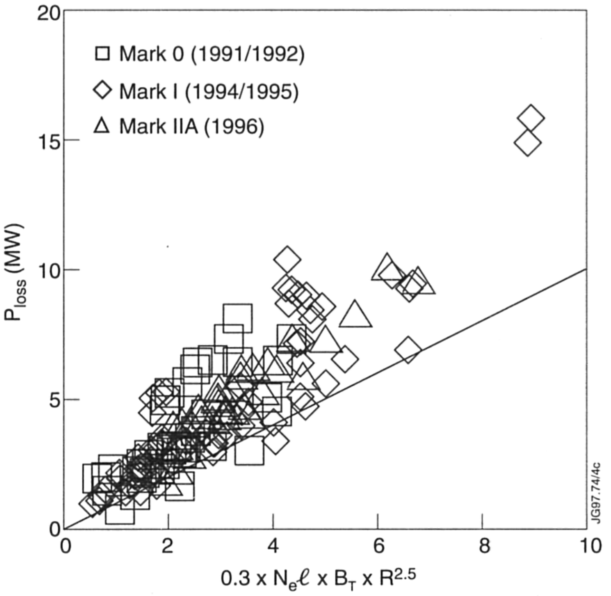

Fig.137: The threshold power, expressed as loss power $P_{LOSS}=P_{TOT}-\Delta W_{DIA}$, with P_{TOT} total coupled power and ΔW_{DIA} rate of change of the diamagnetic energy, is plotted for the complete Threshold Database against the global scaling law that fits best JET data. The other variables defined in the picture are the central line averaged density n_{el} (in units of $10^{20}m^{-3}$), magnetic field B_T (in T) and geometrical major radius R (in m)

difference was found. Different phasings of the ICRF antennae during auxiliary heating were also used to see if these had an influence on the transition to H-mode. The results confirmed previous observations, namely that with 0π0π and 0ππ0 phasings the power necessary for the H-mode transition is as expected (and equivalent to that obtained with NB heating only), while at 00ππ phasing the threshold power is about 30% higher, and finally that with pure monopole (0000) phasing the plasma remains in L-mode. Comparison between systems shows that ICRF and NB heating are equivalent in obtaining the H-mode.

Throughout the period of restart of the machine and the campaign, a Standard Fat discharge was used to scan as much as possible the density range obtainable on JET. The deviation from the linear density scaling observed at high density during the 1994/95 Campaign [6] was confirmed at 3MA/3.1T, while at very low density ($<1x10^{19}$ m^{-3}), the H-mode required more power to be triggered. This result is in agreement with those from other machines, like JT60-U [7], where a minimum density is required to obtain the H-mode, below which the power threshold sharply increases again. In JET, however, such a sharp increase of the threshold power has not been observed, but rather a gradual flattening and then a mild increase of the threshold power as a function of decreasing density. The difference could be simply due to the fact that, on JET, it is almost impossible to operate below $0.8x10^{19}m^{-3}$ due to the formation of locked modes and, therefore, such a sharp increase in the power threshold cannot be observed.

There is also strong evidence that radiation coming from the X-point region could strongly influence the transition to H-mode. Until now it is generally recognised that radiation coming from the bulk plasma should be included in the power balance at the separatrix to determine the power threshold. However, new results show clearly that excess radiation, coming from the X-point but not necessarily inside the separatrix, contributes to cool the scrape-off layer and prevent the transition to H-mode. This clearly demonstrates the importance that phenomena originating outside the separatrix, but influencing the edge and the scrape-off layer, have on the H-mode transition.

Measurements of toroidal rotation during RF-only H-modes have also been carried out using the X-ray crystal spectrometer. Results show [8] that ICRF heating does not actively induce rotation, but that the plasma starts to accelerate in the same direction as the plasma current at the L-H transition. Increased toroidal rotation during the H-mode has been found to be associated with increased ion pressure gradient. Toroidal rotation during RF-only H-modes is a factor 2-3 below that measured during NB H-modes, in similar conditions.

Discussion

To summarise the L-H transition database on JET, the threshold data taken from 1991 to 1996 can be compared (Fig.137). Such a comparison shows that in general the threshold power for the transition to H-mode has not changed substantially since the installation of the pumped divertor. All data follow quite well the global scaling expressions derived from the multi-machine threshold database, although for values of the central line averaged density $n_e>5x10^{19}m^{-3}$ the deviation from the linear density scaling is evident for both the 1994/95 and 1996 data.

At the other end of the discharge, characterisation of the the H-L back transition poses just as many problems as that of the L-H transition. In the past and also recently, it was claimed that hysteresis of the H-L transition existed, and that therefore it was possible to decrease the input power up to a factor of two with respect to that necessary for the L-H transition without losing the H-mode. This phenomenon has been extensively studied on JET during 1996, using both ICRF and NB heating and exploiting different techniques to induce the H-L transition. The first method used a fast power step-down from values of P_{TOT} well above the threshold power P_{LH} to either P_{LH} itself or below, as in Fig.138. In both cases, the H-mode was maintained only for approximately a fast ion slowing down-time. Alternatively, the power input was kept constant above P_{LH} and the density was ramped up until the H-mode was lost, a scenario more representative of what could happen in ITER. In this case, as well, the H-L transition occurred at values of the density such that hysteresis could be excluded. Until further experiments can be carried out, it must be concluded that on JET there is no hysteresis in the H-L transition.

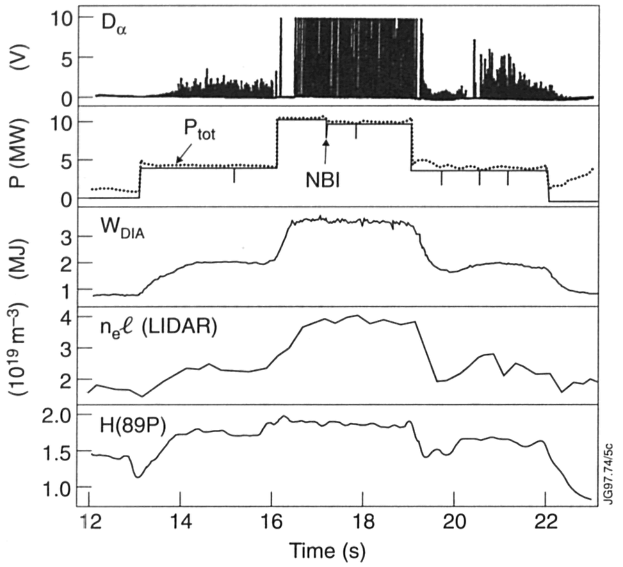

Fig.138: An example of power step-down experiment with NB power to study the hysteresis of the H-L transition shows that the H-mode behaviour is the same if the total power is the same. Thus, during the first power step, near the threshold, the H-mode is dithering with Type III ELMs, then the power is raised well above the threshold and Type I ELMs appear. When the power is stepped down to the threshold level Type III ELMs reappear. If hysteresis existed, Type I ELMs would have been maintained after the power step-down.

TAE Excitation and Analysis

Introduction

In a tokamak reactor, the slowing down alpha-particles will provide the main source of plasma heating. Over the alpha slowing down time from 3.5MeV to the ion thermal energies (10-20keV), the fast particle radial cross-field transport due to neo-classical or turbulence effects is in general negligible. Significant transport and losses of suprathermal particles can only occur in the presence of waves which resonate with their speed before thermalisation. Weakly damped collective modes with phase velocities of the order of the fusion generated alpha-particle speed, such as the Alfvèn Eigenmodes (AE), are therefore a danger for an ignited plasma. Resonant wave-particle interaction can in fact take place and produce an effective energy and momentum exchange between the alpha pressure gradient and the modes. The balance between the alpha-particle drive and the background damping determines the stability limits for the modes, as well as, indirectly, their non-linear saturation level. For large mode amplitudes, strong modifications to the alpha-particle orbits can arise, potentially leading to enhanced transport and losses. In addition to the alphas in tokamaks, AE can be driven unstable by fast particles produced by additional heating. The neutral beam produced ions may resonate with the Alfvèn waves in their untrapped trajectories along the B-field lines, whilst for the ICRF heated ions, the wave can resonate with the bounce and precessional frequencies associate with their trapped orbits.

Systematic experimental studies of weakly-damped Alfven Eigenmodes were continued during 1996 along three main routes, corresponding to the three main critical issues for the AE-fast particle physics in ITER: the mode stability, which introduces the question of which classes of AE are most unstable, and in particular which damping mechanisms one should rely upon to avoid or weaken AE activity; the direct observation of fast particle drive in high performance plasmas; the effects of relatively large amplitude AE on the fast particle orbits. These three issues have been addressed using three complementary AE excitation methods.

The first and most fundamental question, that of the AE stability, motivated the development of a dedicated active diagnostic system, aimed at directly measuring the AE spectrum, both in terms of frequencies and damping rates, in the frequency range 30-500kHz. An external exciter connected to the saddle coils drives low toroidal mode number AE (n=1,2,3), which are detected synchronously by a number of diagnostic channels, including magnetic probes, reflectometer and electron cyclotron emission detectors [9]. AE have been extensively driven and detected during the 1993-1995 campaign. An AE damping rate database for comparison with theoretical models has been established and continues to be filled with more reactor relevant plasma conditions.

Active Measurements of TAE Modes

In 1996, a new AE resonance tracking scheme, based on real-time mode detection and digital control of the frequency, has been implemented. The exciter frequency

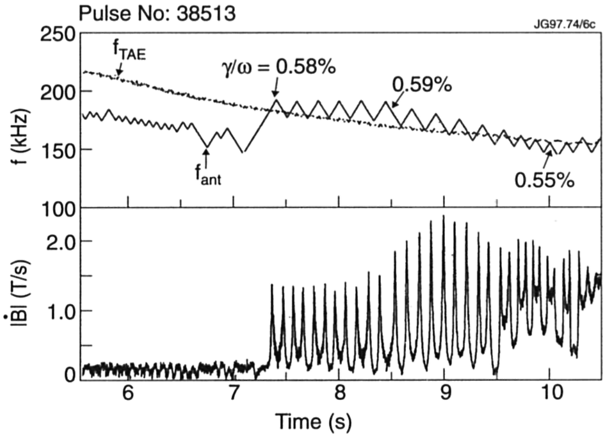

Fig.139: AE excitation with mode-locked saddle coil frequency

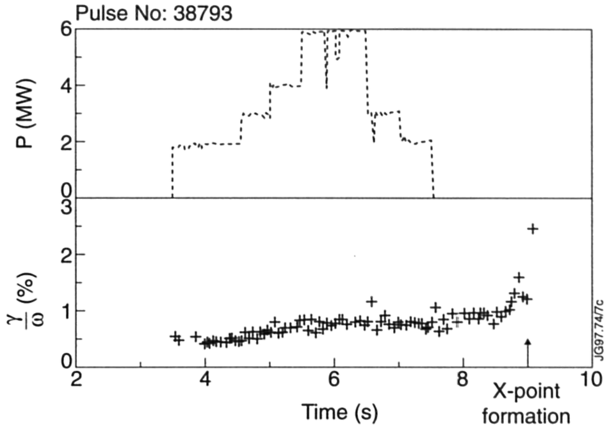

Fig.140: Damping rates of |n|=1 TAE tracked with 140keV NB ($v_{\parallel}/<v_A>$~0.24; β_{fast} (at max β_{fast}')~1.5%; $<\beta_t><0.4\%$)

is locked on to the AE resonance, with a small sweep of few kHz superimposed to enable the damping to be measured as a function of time. This allows one to follow the evolution of a single AE throughout several seconds within a discharge, hence measuring the dynamical evolution of the mode frequency, spatial structure and damping rate. An example is shown in Fig.139, where an AE driven by the saddle coil system is detected and followed for more than 3s. In this purely ohmic case the small variations in the plasma conditions such as equilibrium profiles and temperatures did not produce strong variations in the observed damping rate, which is consistent with radiative damping all throughout.

Along with the damping, it is possible to obtain quantitative information on the fast particle drive and its variations during the additional heating phase of a discharge.The evolution of the measured effective damping rate of the driven mode, resulting from the difference between the total damping and the fast particle drive, both before and after the creation of fast particles and for toroidal Fourier components with opposite mode numbers, yields information on the mode marginal stability. In specific conditions, this technique allows a direct evaluation of the critical fast particle pressures and pressure gradients for instability, and/or of the minimum unstable toroidal mode number. These studies have been performed so far in limiter plasmas with fast ions produced by ICRF and non-resonant NB heating, with $v_{\parallel}<v_A/3$ [10]. An example is given in Fig.140, where a |n|=1 TAE is tracked while a few MW of NB power at 140keV was injected into a limiter plasma. The mode damping only increased (by about a factor of two) when the additional heating was introduced. These experimental results agree with the predictions of the CASTOR-K code [11] that the NB produced fast ions play a stabilising role for AE of low toroidal mode numbers (n<3) and that, for β_{fast} of about 1%, only AE with n>~8-10 can be driven unstable.

In addition to the Toroidal Alfven Eigenmodes and Kinetic Toroidal Alfven Eigenmodes, for which an extensive database of spectra and damping was accumulated during 1993-96 experimental campaigns [12], other classes of AE were studied. Systematic measurements of AE in the low frequency range (30-80kHz) have been performed during 1996 to investigate the existence and the characteristics of the Beta-induced Alfven Eigenmodes (BAE). Although first observations of NB-driven BAE have been reported by the DIII-D group in 1992 [13], only few theoretical considerations have been devoted to the BAE, with no self consistent explanation found so far for the scaling of the observed BAE frequency on the DIII-D and TFTR tokamaks. The low-frequency global AE, if they do exist, may be of special interest as they can affect, along with the resonant fast particle orbits, the global transport properties of the tokamak plasma [14]. Direct measurements of the low-frequency AE were performed in different high beta scenarios, including hot ion H-modes and optimised shear configurations, by combining saddle-coil excitation with coherent detection of various probing signals. The analysis of the externally driven MHD spectra in high beta and in the BAE frequency range is complicated by the combination of intrinsic drive from fast particles created by additional heating and the fast plasma rotation inducing Doppler shifts to the mode frequencies of the same order of the expected frequencies in the plasma frame. However, in some cases, weakly damped modes are excited by the saddle-coils and detected unambiguously. In plasmas heated only by ICRF, with negligible toroidal rotation, modes have been observed whose frequency does not scale with the Alfvèn frequency ($B/n^{1/2}$), but shows a direct dependence upon ion temperature

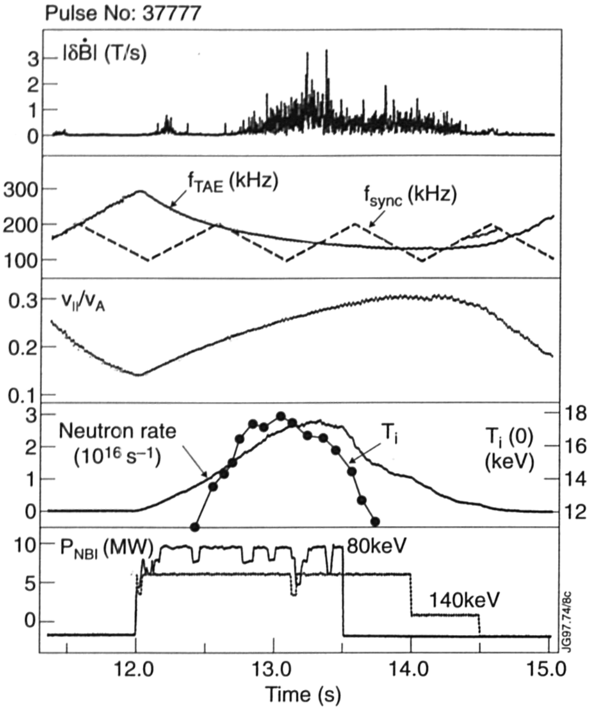

Fig.141: MHD modes in the TAE frequency range excited by NB power when $v_{\parallel} \sim <v_A>/3$ *in a hot-ion H-mode*

($f \sim T_i^{1/2}$ or T_i). This preliminary observation seems to agree with calculations from the CASTOR code, which predicts a temperature dependence for the BAE frequency, $f_{BAE} \sim T_i^{1/2}$ [15], but can also be consistent with the interpretation in terms of kinetic ballooning modes ($f_{KBM} \sim T_i$) [16].

The damping of Ellipticity Induced AE (EAE) was also measured and compared with theoretical models. Low values of γ/ω were found in a number of cases (γ/ω <0.5%), similarly to the case of weakly damped TAE. Low damping was also experimentally observed to characterise the saddle coil driven n=0 AE, identified as the first poloidal harmonic components of Global AE. Due to their small absorption by the background plasma, both these modes can in principle be destabilised by fast particles. These observations motivate careful analysis of the role that wave-particle interaction related to these two classes of AE, the EAE and the low-m GAE, can play in ignited tokamaks.

TAE Issues for ITER

The second issue for ITER is the fast particle drive of AE in reactor relevant plasmas. Direct measurements of electromagnetic fluctuations in the AE frequency range revealed the appearance of high-n unstable modes driven by fast particles created by NB and ICRF heating in high performance plasmas. Particularly, in the NB case, broad band activity in the TAE frequency range was observed, when the second order fast particle - wave resonance $v_{\parallel}=v_A/3$ was satisfied [10]. An example of these observations is given in Fig.141. The AE system was in detection mode (no saddle-coil excitation), in which the reference frequency for the synchronous detection is derived from the calculated TAE frequency plus a modulation of the order of the expected shear Alfvèn gap width. The TAE frequency decreases during beam heating since the density is increased by the combined effect of beam fuelling and the onset of an ELM-free H-mode. There is a tendency for the neutron rate to saturate and even decrease. Such an effect is often, but not always, clearly due to strong MHD events such as sawtooth crashes or giant ELMs. A number of observations similar to that shown in Fig.141 suggest that unstable AE modes should also be considered as possible causes for this 'rollover' effect, as these may affect the overall fusion performance hot ion H-modes via modification of the beam power deposition profile, which is the main source of plasma heating. The amplitudes observed at the plasma edge via magnetic pick-up coils correspond, in the case of high-n kinetic TAE, to perturbations in the plasma core of the order of the threshold for generating stochastic particle orbits.

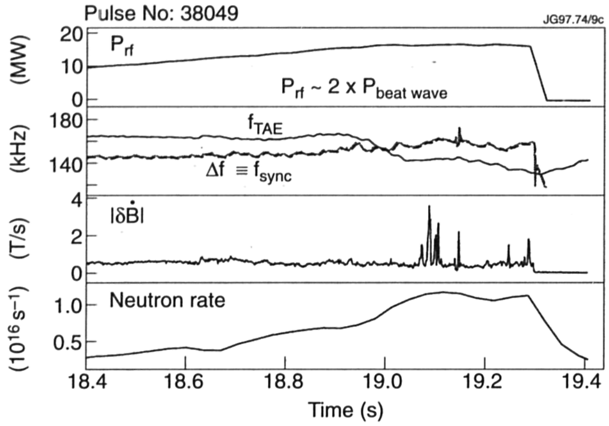

Fig.142: ICRF beat wave drive of TAE modes

TAE induced by ICRH Beat Waves

The third method for studying AE is based upon the non-linear interaction of two fast waves in the ion cyclotron frequency range [17]. TAE can be excited by the beating of the two ICRF waves, whose difference frequency coincides with that of the eigenmodes. The excitation takes place in the plasma core, at the ICRF resonant layer, is not limited by the antenna geometry to low toroidal mode numbers and can yield relatively large amplitude modes due to the high power available in the ICRF plant. This method, which has been demonstrated experimentally, is therefore suitable for assessing the effect of AE on fast particle orbits. Figure 142 shows the

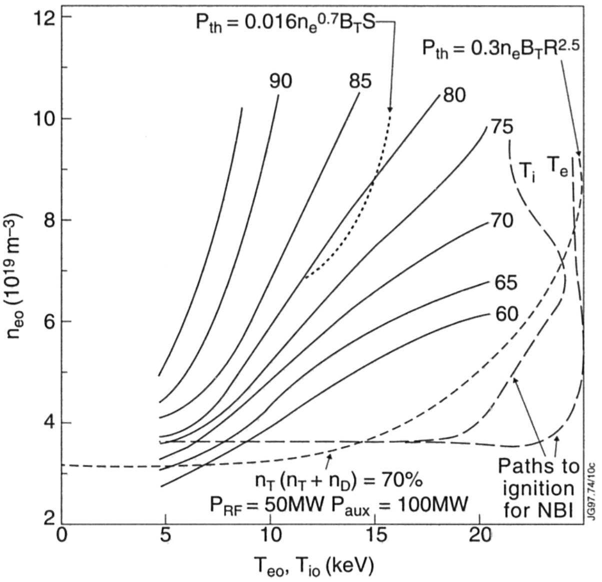

Fig.143: Contours of constant fraction of bulk ion heating for the second harmonic tritium ICRF scenario. Also shown are typical theoretical paths to ignition

excitation of a relatively large amplitude n=3 TAE when the difference frequency of two ICRF modules is close to the expected TAE frequency. A complete assessment of the effect of the driven TAE on the neutron rate, suggested by the raw data shown in the figure, requires further diagnostic investigations. Optimisation studies indicate that the most efficient configuration for AE excitation encompasses two adjacent RF modules with dipole phasing, corresponding to a high ICRF absorption per pass and a greater overlap of the RF fields.

Discussion

In summary, the JET saddle coils have been used to excite and track low-n AE. The dynamical evolution of AE damping rates has been measured in a variety of plasma conditions. Comparisons with theoretical models are under-way, to establish the quantitative understanding of the different AE absorption mechanisms required for meaningful extrapolation to ITER plasmas. Excitation and detection of stable AE in the presence of NB generated fast ions has proved experimentally that beams are stabilising for low n-modes, but can drive high n (n > 8-10) unstable, in accordance with theoretical expectations. Direct passive observations in high performance plasmas confirm the conclusion that high-n modes in the TAE frequency range are excited when the beam ion-Alfvèn wave resonance ($v_{\parallel} \sim v_A/3$) is satisfied. Effects of large amplitude AE on fast particle transport are studied by using ICRF beat wave excitation.

These experiments will be continued during the forthcoming D-T campaign, to investigate the effect of the alpha-particles on the mode stability and to establish the significance of alpha-particle drive for ITER thermonuclear plasmas.

ITER-Relevant RF Scenarios

The ITER reference operation scenarios involves applying about 100MW of auxiliary power at low density to access the H-mode, raising the density to $1.3 \times 10^{20}m^{-3}$ on a timescale of one minute and switching down the additional power as the alpha-heating builds to a sufficient level to maintain the H-mode. Recent calculations with the PION code have shown that, for reasonable evolution of the electron temperature, both second harmonic tritium and fundamental deuterium ion cyclotron heating can transfer typically 50% of the input power to the bulk ions. Since the exact ITER path is not known, these results are best expressed as contours of fixed ion heating fraction in the $n_e(0)$, $T_e(0)$ plane as shown in Fig.143. Any proposed ITER path can then be overlayed on this plot to access the electron/ion heating partition. Such a path will begin with $n_e \cong 3 \times 10^{19}m^{-3}$, $T_e(0) \cong T_i(0) \cong 5$kev and end with $n_e \cong 1.3 \times 10^{20}m^{-3}$, $T_e(0) \cong 25 - 30$keV and $T_i(0) \cong 20$keV. The exact trajectory in between will depend on the magnitude, type and time evolution of the additional heating power, the density rise and the confinement scaling. The trajectory to ignition must also pass below the appropriate H-mode threshold curve to remain in the H-mode. Two curves of the H-mode threshold, in the $n_e(0)$, $T_i(0)$ plane, are shown in Fig.143 for 100MW of additional power and different threshold power scalings. These calculations take account of the additional heating, the alpha-heating, the ohmic heating and the bremstrahlung losses. In the more optimistic case, it is possible to construct a trajectory for which 75% of the RF power would be directed to ion heating.

Examples of calculated trajectories in n_e, T_e space and n_e, T_i space are also shown in Fig.143.These were obtained by Kinsey [18] for neutral beam injection, which predominately heats electrons, and the Weiland/Guzdar-Drake transport model which gives an optimistic confinement for ITER and produces ignition for only 50MW of additional heating power. A consequence of the good confinement is the closeness of the T_e and T_i trajectories: models predicting poorer confinement will produce more separated trajectories since equipartition is less effective in such cases. Calculations giving trajectories which are self-consistent with the heating profiles and the ion/electron heating partition appropriate to the ICRF heating will be made in the near future, particularly when the PRAETOR transport code is linked to the PION code.

Fundamental deuterium minority heating in a 30%/ 70% D-T plasma also gives substantial ion heating as shown in Fig.144. The contours are somewhat different in shape than those of Fig.143 due to the stronger competition from TTMP damping in this scheme. The ion heating is strongest at the beginning of the trajectory but is decreased by the TTMP absorption as n_e and T_e increase.

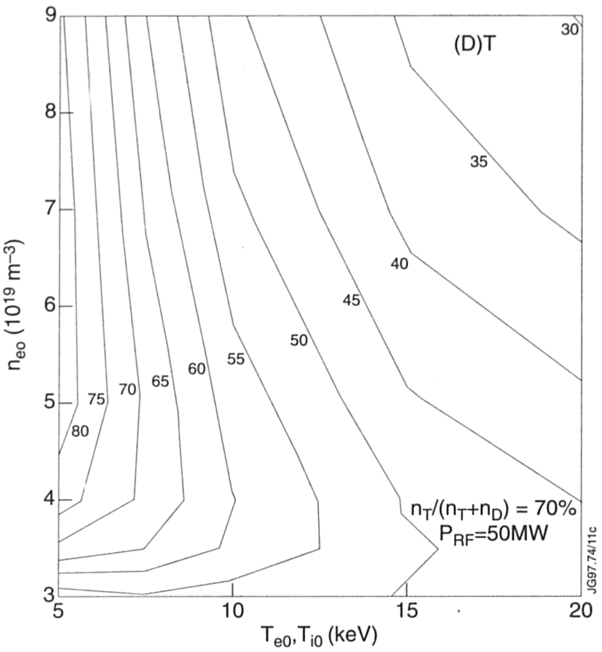

Fig.144: Contours of constant fraction of bulk ion heating for fundamental deuterium ICRF in a 30:70 D-T plasma

Optimisation of JET Plasmas with Current Profile Control

Introduction

Operating a tokamak with higher confinement than predicted by the usual confinement scaling laws [19] has several advantages. One of them is to maximise the fusion yield for a given input power allowing access to regimes in D-T operation, where the alpha-power can play a significant role. Another advantage is to operate a fusion reactor at lower plasma current. This opens the possibility of steady state operation, especially at high poloidal beta, high bootstrap current, by reducing the demand on non-inductive current drive. These so-called advanced scenarios require the demonstration of improved confinement not merely transiently but for a long time duration.

Current profile control has proved to be an important technique to optimise confinement of tokamak plasmas. For example, in JET, current profile modification has produced high confinement with reversed shear magnetic configuration in the pellet enhanced performance mode (PEP + H-mode) [20] and also in high β_p, high bootstrap current plasmas [21]. Ion minority current drive has been used to stabilise or destabilise sawteeth by local modifications of the current profile. Lower Hybrid Current Drive (LHCD) has been used to modify the current profile before the formation of a hot-ion H-mode [22], to raise q(0) above unity and provide sawtooth suppression during the high power heating phase resulting in an increase of the overall neutron yield. This technique has also allowed application of ICRF and NB power at high power levels in the hot-ion H-mode which, in the absence of sawteeth, benefits from increased power deposition in the plasma core and a 30% increase in confinement [23].

Substantial effort has been made to develop discharges with reversed shear either by using LHCD (Tore Supra) [24] achieving high confinement quasi steady-state discharges or by making use of heating in the current ramp phase to freeze the current profile to achieve an optimised q profile resulting in good central confinement [25-27].

In current ramp experiments in JET in the 1994/95 campaign, where a few MW of LHCD power was applied during a fast current ramp (1MA/s), a substantial increase of the electron temperature was observed during the initial phase of the reversed shear: up to 10keV. Transport analysis has shown that the electron thermal diffusivity coefficient during this phase was reduced by an order of magnitude to values close to the level of neo-classical thermal conductivity. This phase of enhanced confinement was not maintained when heavy gas puffing was used to raise the density to allow NB with low shine-through. A broad density profile resulted and an ELMy H-mode was produced with 12MW of NB power.

New hardware has allowed operation of the NB system at lower density. With proper current ramp and power waveforms, Internal Transport Barriers (ITB) have been obtained with a combination of NB and ICRF power resulting in high performance plasmas. Up to 28MW of combined power has been used for discharges with I_p - 2.5 to 3MA and B_t = 3.4T with low target density. Internal barriers at a radius of r/a = 0.55 have been achieved resulting in:

- high confinement L-modes (H_{89} = 2);
- simultaneous high T_i (32keV) and T_e (15keV);

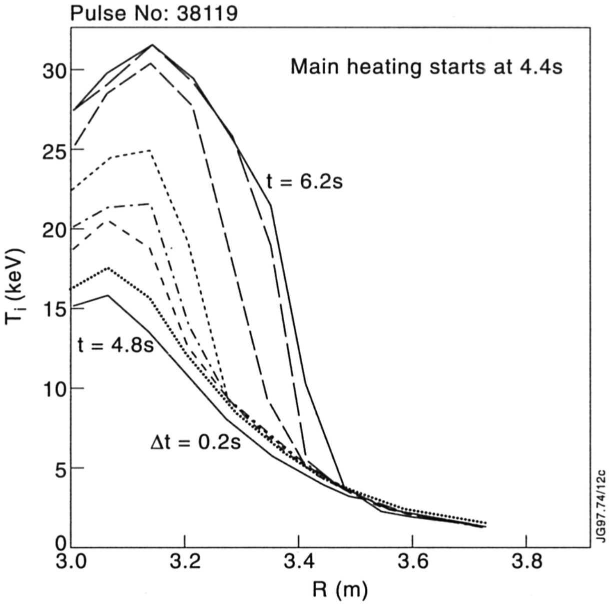

Fig.145: Ion temperature profiles from charge exchange recombination (B_t = 3.4T, 2.5<I_p<3MA) with early power waveform and 1MW (ICRF) of preheating

- high neutron yield (R_{DD} = 7.8x$10^{16}s^{-1}$) comparable to best hot-ion H-modes for time duration longer than the energy confinement time;
- no apparent accumulation of impurities;
- a high ratio of neutron yield to stored energy.

Internal Transport Barrier

In JET, the core transport is reduced when the main power waveform is applied during the current ramp phase of the plasma, with or without a preheating phase. The main evidence of an internal barrier can be seen from the ion temperature profile as shown in Figs.145 and 146 for two different timings of the power application. With early power application, a barrier is formed very close to the plasma core, about 1.2s after the start of the heating. This barrier then moves outwards to r/a = 0.45. The discharge remains in an L-mode during the whole development of the ITB and is generally terminated by a disruption, which has been attributed to the growth of n = 1 modes, indicating that q(0) was close to unity.

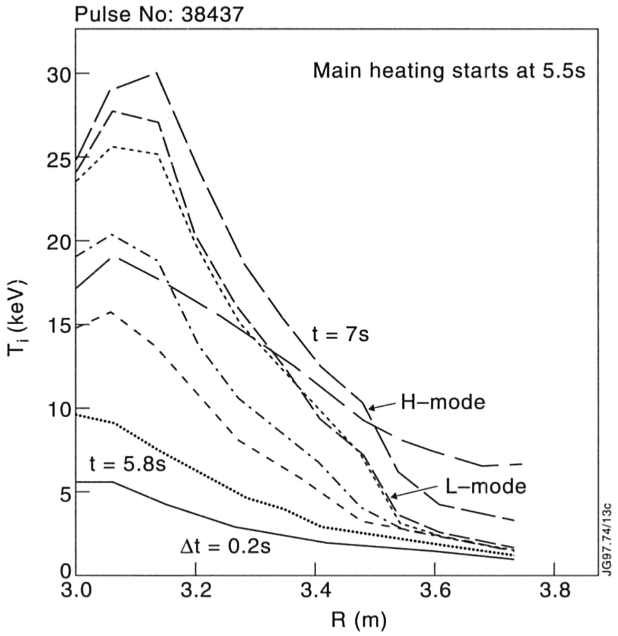

Fig.146: Ion temperature profiles from charge exchange recombination (B_t = 3.4T, 2.5<I_p<3MA) with late power waveform and no preheat

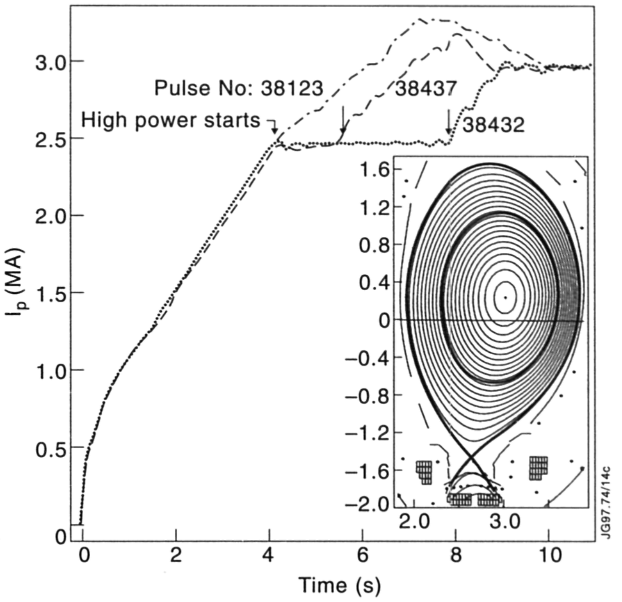

Fig.147: Typical current waveforms and flux contour for internal transport barrier (ITB). In the absence of heating, sawteeth appear at about t = 9s

ITBs have also been established when power is applied later in time and with no preheating as shown in Fig.146. The barrier is established almost immediately with a slow expansion up to r/a ~ 0.55. In this case, the L-mode phase is followed by an H-mode with central pressure up to 3bar. A pedestal was formed at the plasma periphery and the whole ion temperature profile is raised by about 2keV. These profiles are quite different from profiles of equivalent hot-ion H-modes with similar power and neutron yield, which shows significantly lower central temperature and much higher edge temperature. Similar transport barriers can be seen on the electron temperature profiles and to a lesser extent on the density profiles.

ITBs are very sensitive to the timing of the high power waveform as illustrated in Fig.147. The ramp rate of the discharge to 2.5MA is adjusted to the highest rate compatible with the absence of MHD activity during the ramp. The second ramp in current is used to delay the onset of the H-mode. If H-modes appear too early, the

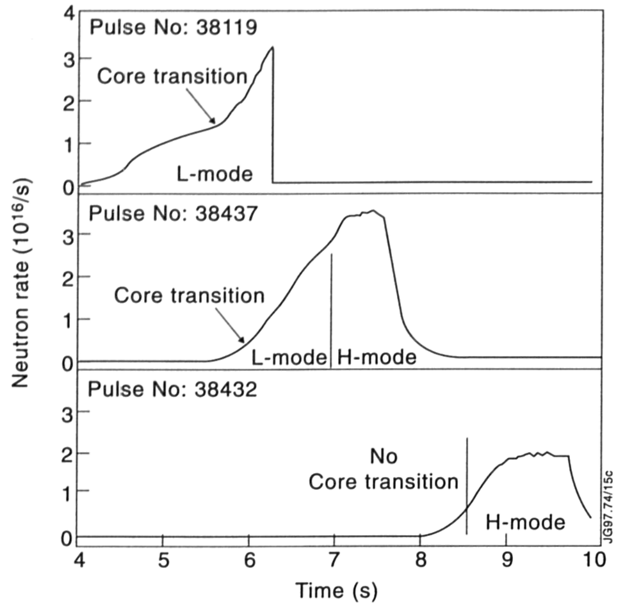

Fig.148: Time evolution of the neutron yield for different timing of the power waveform with a total power of 25MW. No ITB is observed when power is injected after 6s from the start of discharge

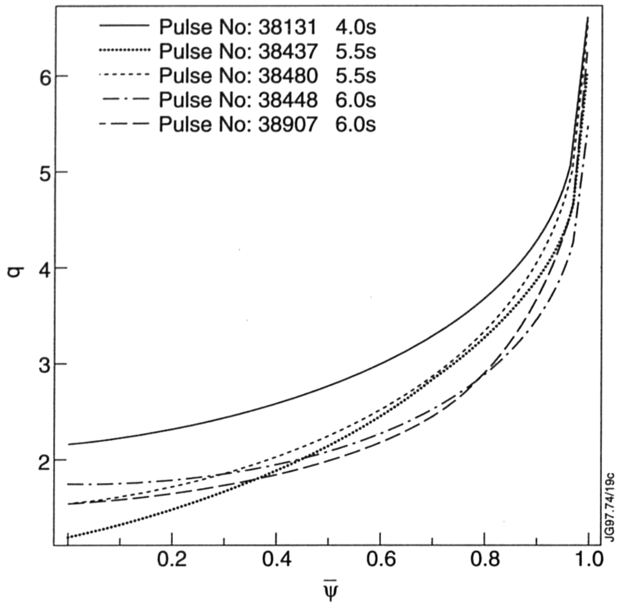

Fig.150: Central safety factor from EFIT equilibrium reconstruction using Faraday channels 2, 3 and 4 and comparison with electron temperature indicating sawteeth (Pulse No. 37551)

L-mode peaked pressure profile is not yet fully established and NB penetration is compromised by the building up of the edge pedestal. In addition, the strike points of the last closed surface are maintained close to the divertor pump entrance to prevent the edge density from building up quickly. This also delays the onset of the H-mode. As shown in Fig.148, early heating results in a late core transition. Late heating leads to an early H-mode which prevents the establishment of an ITB. The best performance (without disruption) has been obtained when the power is applied 5.5s after the beginning of the discharge. Note that discharges with an ELMy H-mode obtained with late heating still have peaked density profile because q(0) remains above unity and sawteeth are absent. An example of such a discharge, where a quasi-steady state is achieved for the time duration of the full additional heating power, is shown in Fig.149. An ion temperature of 18keV together with electron temperature of 10keV at central densities of $4x10^{19}m^{-3}$ is maintained for several seconds. The neutron yield is about double that corresponding to sawteething discharges with similar power.

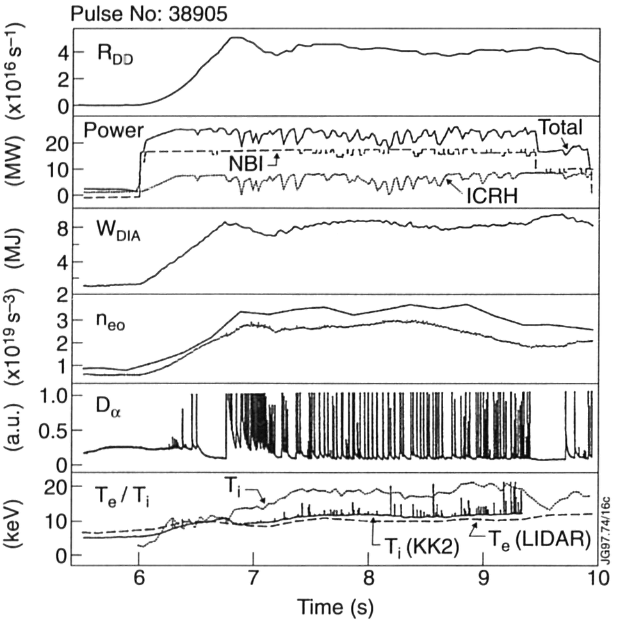

Fig.149: Time history of a sawteeth-free ELMy H-mode in a shear optimised configuration (3MA, 3.4T with a 0.35 triangularity)

Current Profile Measurements

An accurate determination of the current and safety factor profile is of fundamental importance for advanced tokamak optimised shear experiments. The profile reconstruction is carried out with the full equilibrium code EFITJ. A reliable profile determination for the core plasma requires internal data in addition to the magnetic diagnostic data. Another prerequisite is reducing the bias from the choice of profile parameterization used in the equilibrium reconstruction. Various choices of profile parameterization and regularization have been tested and the results compared with independent measurements. A high resolution profile with fourth order polynomials was chosen as appropriate. An example is given in Fig.150, which gives the time development of q on axis, using data from three Faraday rotation channels in the equilibrium reconstruction. The onset of sawtooth oscillations coincides with the central safety factor falling below unity.

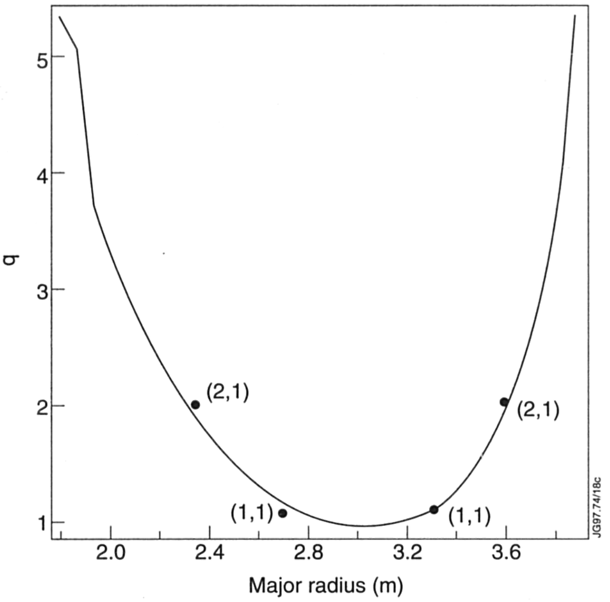

Fig.151: Comparison of equilibrium using Faraday data as input to resonant MHD surfaces detected by CATS (Pulse No. 38119, t = 16.2s)

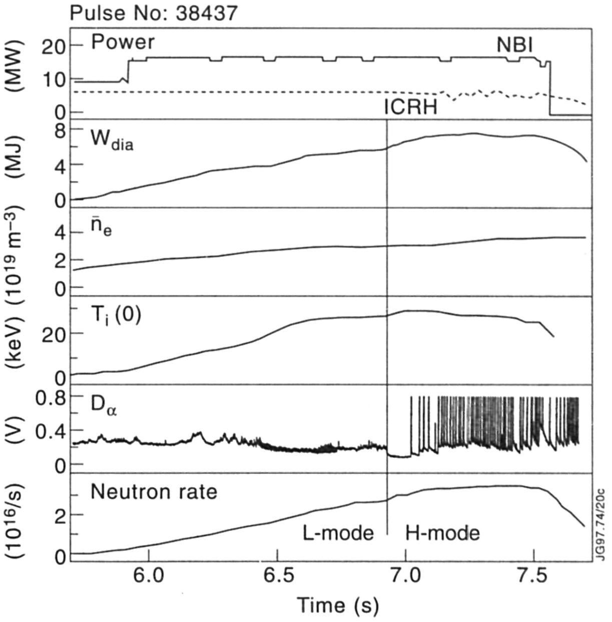

Fig.153: Time history of a high fusion yield pulse with shear optimisation (B_t=3.4T, 2.5 < I_p <3MA). ICRF frequency (51MHz) corresponds to resonance (H minority or second harmonic D) close to the centre

Another example is Pulse No. 38119, with strong MHD activity, where the rational q surfaces can be inferred independently and observations using soft X-ray measurements. Figure 151 compares the q values obtained from SXR with the safety factory of the equilibrium reconstruction. Although there is only one Faraday channel available, good agreement was obtained. A Monte-Carlo analysis of the same pulse shows the confidence interval of the central q value to be about 30%, using data from one reliable Faraday channel. Subsequent analysis with artificial data shows, that this value can be reduced to 10% or less by adding at least one other Faraday channel. After the assessment of profile parameterization, selected optimised shear discharges were analysed. Figure 152 shows the resulting target q profile at the onset time of heating. Within the confidence interval, shear reversal can neither be deduced nor excluded from the data. It should be emphasised, however, that more internal data is required for a reliable profile analysis, e.g. an improved Faraday diagnostics, a Motional Start effect measurement system, or at least a measurement giving the position of the magnetic axis. It is not yet possible to have a very precise q profile, but it appears that a strong reversed shear is not necessary to trigger an ITB, in agreement with observations on DIII-D. The location of the barrier at the onset of the H-mode appears to be in the vicinity of a q=2 surface.

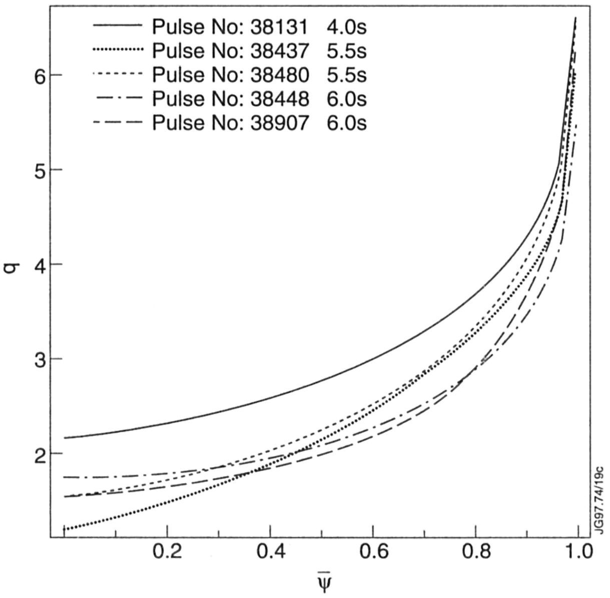

Fig.152: Q profiles for selected optimised shear discharges, time taken for target plasma

High Performance Discharges with Shear Optimisation

An example of a high performance discharge where the L-mode phase is followed by an H-mode is shown in Fig.153. The H_{89} factor reaches 2 during the L-mode phase and 2.5 during the H-mode phase. These discharges have about 30% less stored energy than a comparable hot-ion H-mode but a similar neutron yield because of the peaked profiles. There is no evidence of impurity accumulation on this time scale, Z_{eff} remaining constant at about 1.7. In the case shown in Fig.153, the neutron yield remains about constant during the ELMs for as long as the

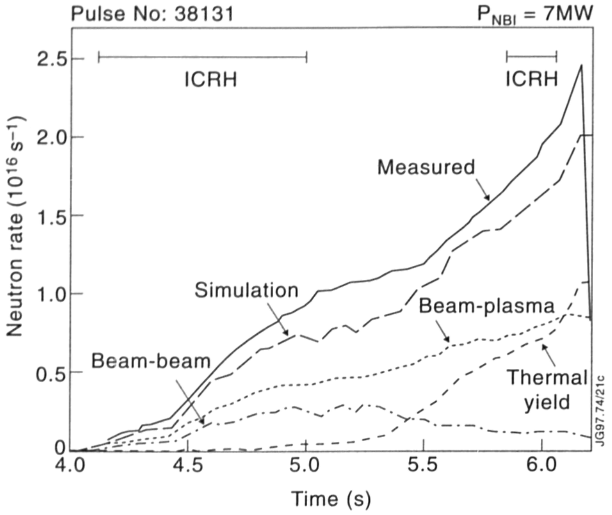

Fig.154: TRANSP simulation of Pulse No.38131. NB (14MW) is on from 4s and ICRF (7MW) is off for 1s

power was applied, i.e. for time duration longer than the energy confinement time (0.4s). However, often, in similar pulses a giant ELM leads to a degradation of performance. The largest neutron yield which has been achieved in such discharges equals the highest yield in the hot-ion H-mode achieved on JET in the present campaign.

Several experimental observations such as: no significant flux of gammas, an increase of only 2 to 3 keV in electron temperature when comparing NB-only and combined heating shear optimised discharges, together with numerical simulations indicate that a substantial part of the ICRF wave is coupled to fast deuterons at energies lower than a few hundred keV leading to ion heating, especially at high electron temperature.

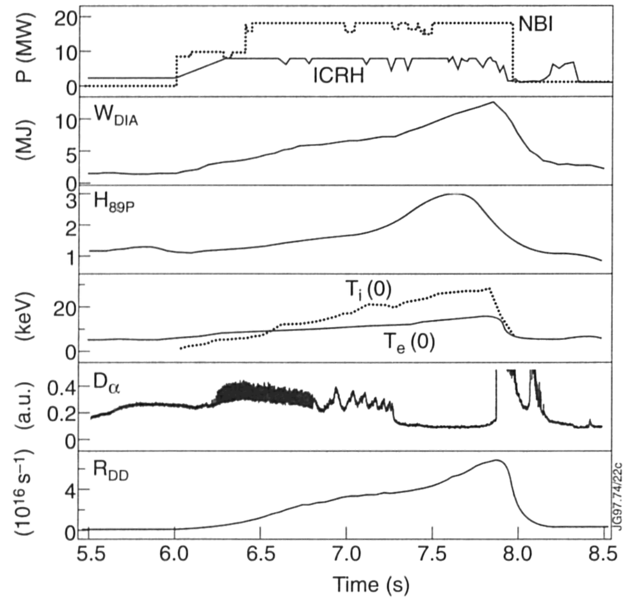

Fig.155: Time history of a high fusion yield with shear optimisation and increased triangularity during the H-mode phase (Pulse No. 39515)

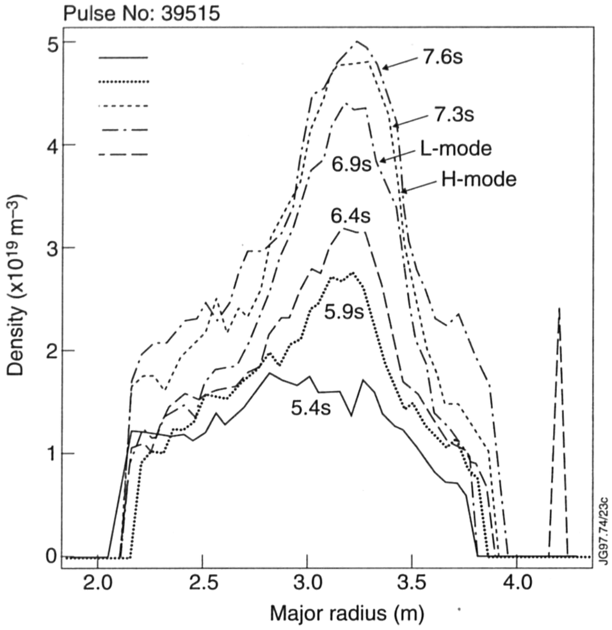

Fig.156: Time evolution of density profiles for Pulse No.39515. The high power L-mode phase ends at t = 17s

In the absence of a proper simulation of the damping and heating of the ICRF wave in such plasmas, a TRANSP simulation has been made for a discharge with shear optimisation where the ICRF power was off for 1s and is shown in Fig.154. Good agreement between experimental values and simulation is obtained with significant thermal yield reaching more than 50% of the total yield.

Experiments have also been carried out where triangularity can be varied. A low triangularity has to be used during the high power L-mode phase to avoid an early H-mode. As shown in Fig.155, when triangularity is increased during the pulse up to 0.4, a long ELM-free H-mode phase can be achieved with high neutron yield following the high power L-mode phase. For this pulse, peaked density profiles have been achieved, as shown in Fig.156. A TRANSP simulation for this pulse indicates that the thermal yield corresponds to 80% of the total yield.

Power Dependence and Discussions

A minimum power is required to obtain an ITB in JET, as shown in Fig.157, where the database of R_{DD} versus total injected power is given for all discharges where a sustained core transition has been achieved. A substantial part of the data scattering is due to the large range of power, density and configuration waveforms investigated for shear optimisation, in particular, R_{DD} is very sensitive to target density. The low range of power corresponds to power step-down experiments, similar to Fig.154, where 6 to 8MW of ICRF power was switched off after about 1s,

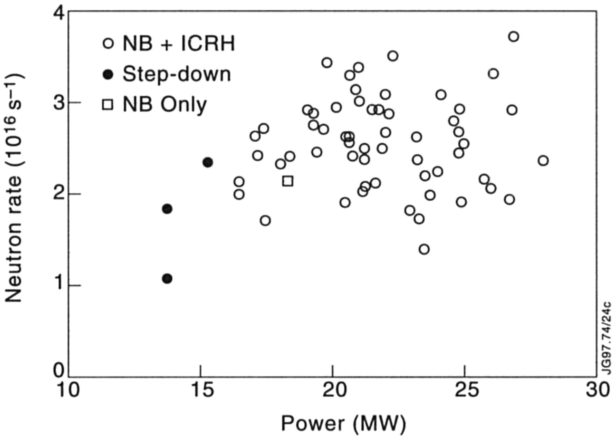

Fig.157: Neutron rate versus power for discharges with sustained core transitions

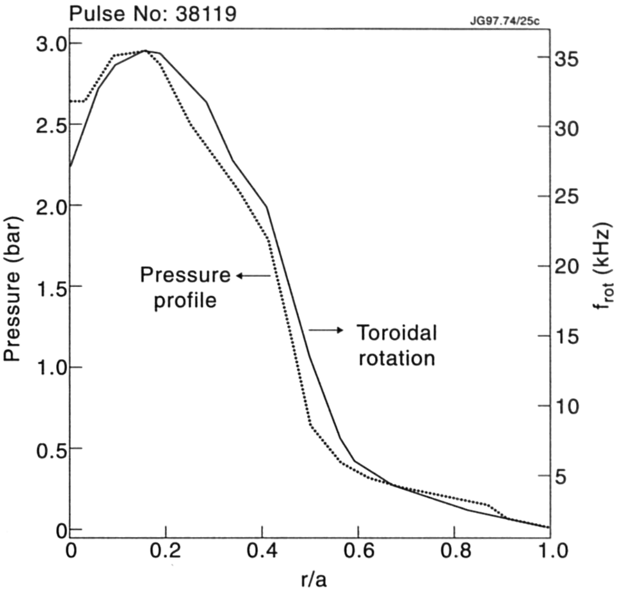

Fig.158: Radial profiles of pressure profile and toroidal rotation at the end of an high power L-mode phase (early heating)

when an ITB was already established. The dependence of this minimum power versus various parameters such as magnetic field and plasma current has not yet been carried out. At higher combined power, the performance during the L-mode phase was often limited by low frequency, n=1 modes hardly rotating, sometimes locked, located near the q = 2 surface. These modes are very different from the modes appearing during pulses with early heating with an n=1 structure rotating at very high frequency and leading to a disruption. The low frequency modes are not disruptive but limit the increase of neutron yield.

As shown in Fig.158, very peaked pressure profiles and high toroidal rotation have been achieved. As a consequence, large radial electric fields may occur in these plasmas:

Although u_ϕ is not measured, reasonable assumptions indicate that the electric fields in such plasmas are comparable to the values which, it is suggested, may reduce turbulence. Optimisation of overall performance is being prepared.

Acknowledgements

Specific contributions from C. Greenfield, E. Lazarus, T.Luce, B.Rice, E.Strait (GA), M Zarnstorff, G.Schmidt (PPPL) and from B.Lloyd, C.Warwick, and C. Hunt are gratefully acknowledged.

References

[1] B. Balet, D.J. Campbell, J.P. Christiansen et al. 23rd EPS Conference on Controlled Fusion and Plasma Physics, Kiev, Ukraine, (1995) Vol I-009.

[2] J.G. Cordey et al. Proceedings of the H-mode Workshop PPPL, USA (1995).

[3] ITER H-mode Database Working Group, in Controlled Fusion and Plasma Physics (Proc. 20th Eur. Conf. Lisbon, 1993). Vol. 17C, Part I, EPS Geneva (1993) 15.

[4] C.C. Petty, et al. Phys. Plasmas **2** (1995) 2342.

[5] C.C. Petty, et al. to be published in Controlled Fusion and Plasma Physics (Proc. 23rd EPS Conf. Kiev, 1996).

[6] E Righi et al. Proc. 22nd EPS Conference on Controlled Fusion and Plasma Physics, Bournemouth (UK), (1995) 19C, II-73.

[7] M Sato et al. (1996), Plasma Phys. and Controlled Fusion 38(8),(1996) 1283.

[8] L-G Eriksson, E Righi and K-D Zastrow, Plasma Phys. and Controlled Fusion 38 (1997), 24.

[9] A.Fasoli et al., *Phys. Rev. Lett.* **74**, 645 (1995).

[10] The JET Team (presented by D.Start), IAEA Conf., Montreal, Paper IAEA-CN-64/A2-6 (1996)

[11] D.Borba et al., Proceed. of Int. Workshop on Theory of Fusion Plasmas, Varenna, Italy 26-30 August 1996; JET Preprint JET-P(96)35 (1996).

[12] A.Fasoli et al., Nuclear Fusion 35, 1485 (1995)

[13] A.D.Turnbull et al., Phys. Fluids B 5, 2546 (1993).

[14] J.G.Cordey et al., Nuclear Fusion 35, 505 (1995).

[15] G.T.A.Huysmans et al., Phys. Plasmas 2, 1605 (1995).

[16] S.T.Tsai and L.Chen, Phys. Fluids B 5, 3284 (1993).

[17] A.Fasoli et al., Nuclear Fusion 36, 258 (1996).

[18] M F Turner, private communication.

[19] The JET Team (presented by J.G. Cordey), IAEA-CN-64/AP1-2.

[20] Tubbing, B, et al., Nucl. Fusion, 31 (1991) 839.
[21] Challis, C., et al., Nucl.Fusion, 33 (1993) 1097.
[22] Bhatnagar, V.P., et al., Nucl. Fusion, 34 (1994) 1579.
[23] Ekedahl, A., et al., to appear in Controlled Fusion and Plasma Physics (Proc. 23rd Eur.Conf.Kiev, 1996).
[24] Cottrell, G., et., ibid.
[25] Litaudon, X., et al., ibid.
[26] JET Team (presented by C. Gormezano), in Plasma Physics and Controlled Nuclear Fusion Research (1994) (Proc.15th Int.Conf.Seville, 1994) Vol.1, IAEA, Vienna (1996) 633.
[27] Levington, F.M., et al., Phys.Rev.Letters (1995) 417.

Data Analysis and Modelling

The work on data analysis and modelling can be divided into three areas: Analytic Theory; Numerical Simulation; and Data Processing and Analysis. However, there is a very strong interaction among these areas. The ultimate goal is to improve the modelling of the many physics processes taking place in both the core and edge regions of a tokamak. There is a strong interaction with the experimental programme through Task Force and Topic Groups.

Analytic Theory

The Analytic Theory Group has supported the experimental programme by detailed interpretation of JET discharges and by predictive studies. Analytic theory was applied to the development of new models relevant for tokamak stability and transport with emphasis on scaling. Macroscopic MHD models in conjunction with large-scale computer codes were applied to the equilibrium reconstruction, to the MHD modelling of JET discharges including energetic particle effects, to alpha-particle transport, to current drive and RF studies and to turbulence models. In a collaborative effort together with UKAEA Culham Laboratory and IFS University of Texas, USA, a formulation in the context of weak turbulence was developed and implemented numerically for the self consistent evolution of the unstable Alfvén Eigenmode amplitudes and the fast ion distribution.

Equilibrium Reconstruction

The equilibrium code EFIT continues to play a pivotal role during operations and for subsequent scientific analysis. To increase the accuracy of the reconstruction, the code incorporates the fitting to Faraday, diamagnetic, pressure profile and motional Stark data.The Faraday diagnostic data has been used routinely for the intershot analysis of reversed shear experiments. The gain in accuracy achieved by using Faraday or Motional Stark diagnostic data has been assessed by a sensitivity study. The safety factor was determined by magnetic measurements with good accuracy close to the boundary. In the core plasma, the uncertainty became large and was strongly influenced by the choice of profile parameterization and regularisation. Using Faraday diagnostic data, the reconstruction was improved considerably, provided sufficient channels were used. By including measurements of the electric field angle through the motional Stark effect, the accuracy was even more enhanced.

Collaboration with General Atomics, USA, has been intensified to unify the versions of the EFIT code used on different tokamaks. A global machine-independent version of EFIT is now being developed, from which all other versions, in particular the JET version EFITJ, will be derived. The EFITJ code has been implemented on a dedicated workstation for intershot analysis. The boundary reconstruction code XLOC has been modified to explicitly take account of the flux due to the currents in the divertor coils. This extension of the code gives a more accurate and robust reconstruction utilising a specific set of small and reliable magnetic sensors. It has been used in all magnetic configurations.

Edge Plasma Physics

Ideal Interchange Instabilities near the Separatrix in the SOL

The linear stability of the scrape-off-layer (SOL) with respect to interchange-type modes was studied using the reduced MHD model and applying a ballooning approximation to the perturbations. 'Line-tying' boundary conditions were implemented at the target plates. Employing a metric determined by the magnetic field geometry, the influence of the X-point on stability was assessed. The effect of relevant parameters like X-point height, magnetic shear and plasma shaping was qualitatively determined. It was demonstrated that the calculations for experimental configurations and those based on an analytical equilibrium model yield good qualitative agreement. It was shown that the SOL plasma just outside the separatrix can become unstable more easily (i.e. for lower pressure gradients) than the plasma

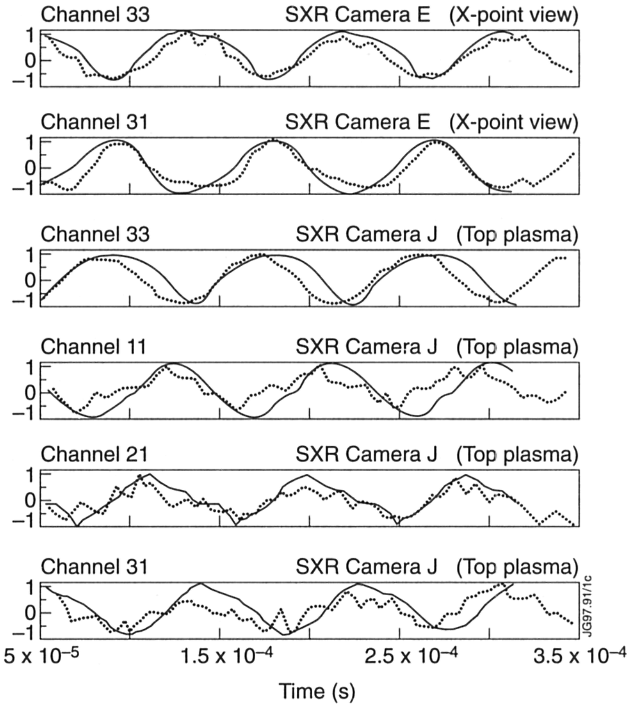

Fig.159: Comparison of Soft X-ray data with predictions based on the mode structure of an ideal external kink mode

just inside the separatrix where the magnetic well is stabilising. These findings can be important for the explanation of the onset of giant ELMs. The interchange instability in the SOL may act as a precursor and is mainly localised near the X-point, but may also have a strong signature just above the midplane.

Some tokamak experiments exhibit a dependence of the L-H power threshold on the ion drift direction. This experimental result could be explained by interchange instabilities in the SOL. The sheath resistance near the target plates depends on the direction of the longitudinal SOL current and alters the boundary condition at the target plate. In conjunction with the curvature of the toroidal magnetic field and the ion drift direction, these effects lead to an asymmetry in the turbulence near the plasma edge requiring a different L-H power threshold for reducing this turbulence.

A different physical mechanism by means of a local, non-homogeneous resistivity was studied for the onset of MHD instabilities below the ideal MHD threshold. The main result was that a small and localised cold plasma (e.g. generated by impurities or neutrals), can play the same role as a uniform cold plasma periphery. In addition, the energy can be released by this mechanism even if the plasma is in the second ballooning stable regime, i.e. completely stable against ideal MHD modes inside the separatrix.

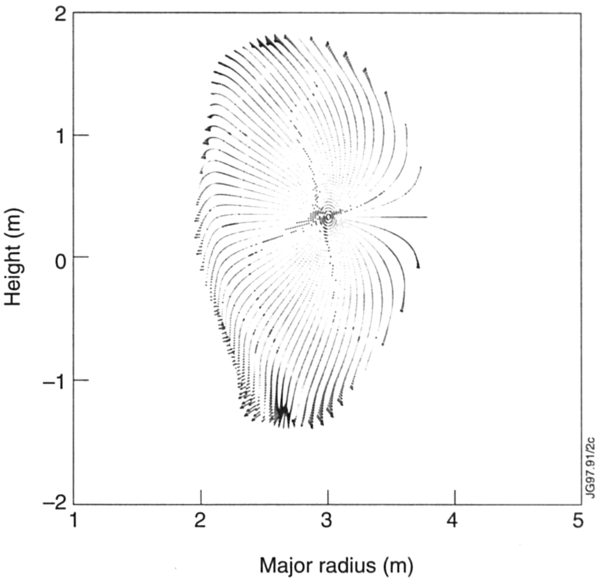

Fig.160: The mode structure of the n=1 external kink mode

MHD Stability Analysis

The Outer Mode is one of the instabilities that limits the performance of the hot-ion H-mode discharges. Previously, it was proposed that the Outer Mode was a non-linearly saturated external kink mode.This was based on the localisation of the perturbation close to the edge. In addition, MHD stability calculations showed that the plasma edge was close to the ideal external kink stability boundary at the time when the Outer Mode was observed.

To further investigate the link between the Outer Mode and the external kink mode, the SXR data of the Outer Mode was compared with predicted soft X-ray signals based on the external kink mode structure. An example was Pulse No. 37431, where an Outer Mode was observed before an ELM. The newly developed MISHKA-1 code was used to calculate the n=1 external kink mode structure using the equilibrium as reconstructed by EFIT. This mode structure was then added to the equilibrium to obtain the perturbed flux surfaces. Assuming a SXR emmisivity profile, the line integrals of all the SXR channels were calculated at 16 different toroidal angles, which corresponded to 16 time points in one period of the mode frequency (assuming the mode frequency is due to the plasma rotation).

The results are shown in Fig.159 which compares the actual soft X-ray data with the predictions based on the external kink mode. The amplitudes are normalised, so that only the phase is relevant. Excellent agreement was found and all the phase changes observed were reproduced by the predictions. The phase change in two adjacent channels E33 and E31 (first and second trace in Fig.159) can be understood from the external kink mode structure (Fig.160). Around the

X-point, the external kink mode had very small convective cells, but on the outboard side the convective cells were very large. Channels E31 and E33 look from the outboard side to the X-point. These see the same phase of the mode as they pass the outboard side but an opposite phase as the line of sight crosses the X-point. The same phase inversion is seen on the vertical camera which looks from the top down to the X-point at the bottom. The amplitude of the mode can be determined if the equilibrium emissivity profile is calculated from an inversion of the soft X-ray data. The amplitude of the external kink mode which is added to the equilibrium flux surfaces, can then be varied to obtain a best fit with the absolute value of the soft X-ray data. This yields an amplitude of 15cm at the X-point which corresponds to a movement of the plasma boundary at the midplane of about 1.5cm. In conclusion, the excellent agreement between the soft X-ray data and the predictions based on the n=1 external kink mode structure confirms that the outer mode can be identified as an external kink mode.

Alfvén Eigenmodes (AE) Studies

Systematic theoretical studies of toroidicity-induced Alfvén Eigenmodes (AE) were continued during 1996. In addition to the MHD normal-mode code CASTOR [1], a new optimised code MISHKA-1 [2] was developed for fast computation of the ideal MHD spectrum in toroidal geometry. Due to the high computational efficiency of MISHKA-1, a wide set of tokamak equilibria could be considered. In particular, the existence of the multiple ideal Low-Shear Toroidal AE (LSTAE), predicted recently [3], was demonstrated for JET and DIII-D low-shear equilibria, as well as for tight aspect ratio tokamaks [4, 5]. In the analytical theory [3], the spectrum of multiple ideal LSTAE exists inside the TAE gap if the local magnetic shear $S = rq'/q$ is smaller than the local inverse aspect ratio $\varepsilon = \rho/R_0$, $|S|<\varepsilon$. As the ratio, $\varepsilon/|S|$, decreases, the spatial width of the LSTAE-modes $\Delta\omega \propto \varepsilon/|S|$ decreases while the non-ideal parameter characterising the Kinetic TAE-modes [6], $\lambda \propto \rho_i |S|/\varepsilon^{3/2}$ increases (ρ_i is the Larmor radius of thermal ions). Thus, the LSTAE-type mode is expected to change into a KTAE-type mode and vice versa at varying equilibrium parameter, $\varepsilon/|S|$; this effect might be important for typical ITER equilibria, where the low-shear region is expected to cover a broad central part of the discharges. For typical JET equilibria, the condition $|S| < \varepsilon$ was found to be restrictive. Therefore, multiple ideal LSTAE were not found in cold JET plasmas, as reported earlier [7]. However, multiple ideal LSTAE's exist in some low-shear DIII-D discharges. In addition the multiple ideal LSTAE's were particularly ubiquitous in tight aspect ratio tokamaks [4,5], where the condition $|S|<\varepsilon$ was easily satisfied, due to the large value of $a/R_0 \approx 1$.

For the general treatment of the AE stability and AE-induced anomalous transport of energetic ions in JET and ITER plasmas, the guiding centre HAGIS code was extended towards a self-consistent nonlinear code [9, 10]. In collaboration with UKAEA, Culham Laboratory and IFS University of TEXAS, USA, a novel df - method [11] was implemented and validated in the HAGIS code and in the FAC code [12]. In both HAGIS and FAC codes this approach produced superior results in the Monte-Carlo simulations without the need to use excessive numbers of Monte-Carlo points. Due to this fact, the very complicated five dimensional problem of the nonlinear AE interaction with energetic ions could be treated sufficiently accurately using about 500 particles for the linear stage of the instability and about 20000 particles for the nonlinear stage.

A hybrid magnetrohydrodynamic-gyrokinetic model was developed for the stability analysis of global Alfvén waves in the presence of energetic ions. The ideal MHD model was extended by including the effect of the perturbed parallel electric field and of the finite Larmor radius both being relevant for high temperature plasmas. The core localised modes did exist in the plasma core with very small damping in addition to the global toroidicity-induced Alfvén modes, which extended across the entire plasma. The analysis of the interaction of the Alfvén modes with the energetic particles was performed using a gyro-kinetic model based on a Lagrangian formalism for the particle motion in the toroidally symmetric magnetic field. The power transfer between the energetic particles and the waves was expressed by a five dimensional phase space integral dW_{hot}, evaluated in the CASTOR-K code, which included the wave eigenfunction and the unperturbed particle orbits. It is emphasised that this form was self-consistent and allowed the treatment of passing and trapped particles.

The non-linear models (FAC and HAGIS codes) were applied to the stability analysis of the JET fusion experiments, where a large amount of energetic particles were present, as well as for future fusion reactor experiments (ITER) with a significant fraction of alpha-particles. The finite orbit effects reduced the destabilising influence of the alpha-particles on JET and that the most unstable Alfvén waves were kinetic

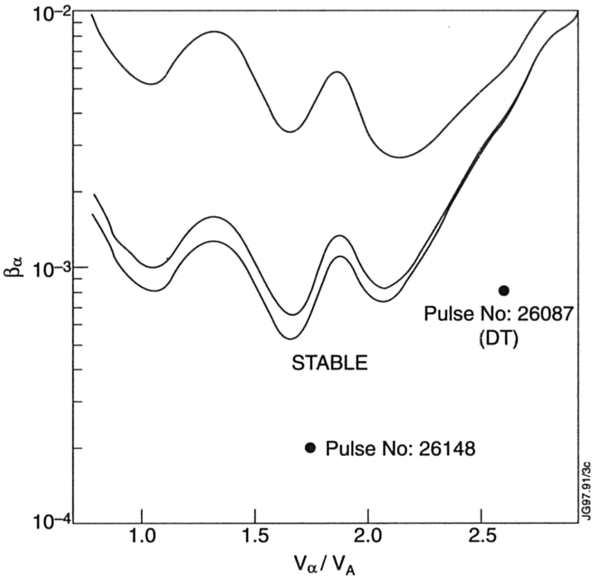

Fig.161: Stability diagram for KTAE's in high performance discharges: for the preliminary tritium experiments (PTE1) Pulse No. 26148; and a future 50% T discharge based on Pulse No. 26087

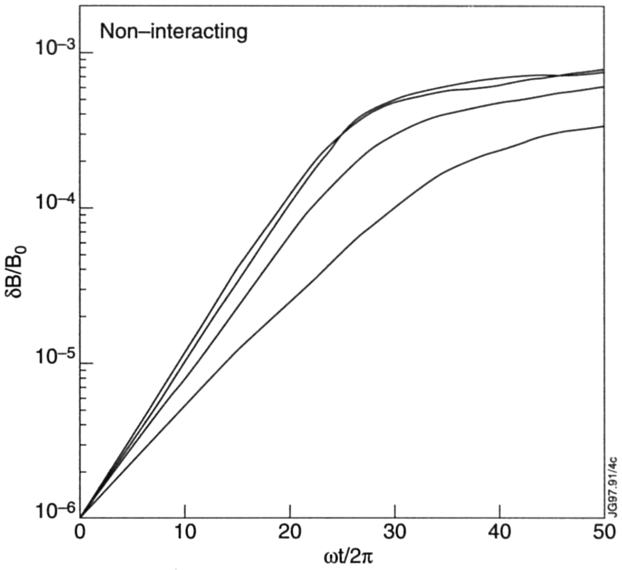

Fig.162: Nonlinear evolution of unstable KTAE modes with n=5 to n=8 for β_α=1%

Alfvén Eigenmodes (KTAE) with toroidal mode numbers ranging from n=5 to n=10. Taking into account the alpha-particle pressures feasible in the JET tritium experiments, $<\beta_\alpha> \le 10^{-3}$, and the various damping mechanisms these modes are expected to be marginally stable as shown in Fig.161.Further analysis involving non-linear simulations, shown in Fig.162, revealed that for linearly unstable KTAEs the saturation amplitude scales as $dB/B \approx 0.5(\gamma/\omega)^2$. From this relation between the saturation amplitude and the linear growth rate, it is concluded that for the unstable KTAE scenarios the saturation amplitude of the KTAEs is small, $\delta B/B \approx 10^{-5}$. Furthermore, the non-linear simulations indicated that, in the presence of unstable TAEs, an anomalous particle diffusion is expected only for values of the amplitude perturbation larger than $\delta B/B \approx 10^{-4}$. It is concluded that in JET tritium experiments, low-n KTAEs should not be destabilised by the alpha-particles. However, if the electron density can be reduced, the experimental domain should fall into the unstable region with $n_\alpha/n_A \approx 1.5$.

ρ* Scaling of Turbulent Ion Conductivity

It is generally accepted that the anomalous transport observed in tokamaks is caused by some form of small scale turbulence. What has not been clear, both theoretically and experimentally, is how the anomalous transport coefficients scale with the separation parameter ρ^*, the ratio of the ion Larmor radius to the machine size. Understanding this scaling is particularly crucial for the extrapolation of the confinement database of the present experiments to future devices such as ITER.

Besides dedicated experiments, the ρ^*-scaling problem has been addressed with a specially designed code, which directly solves the relevant equations of ion-temperature-gradient-driven turbulence, (the leading candidate for anomalous ion transport) in toroidal geometry [12]. By comparing the input power required to maintain the same temperature profile with different values of ρ^*, it has been possible to conclude that the effective ion thermal conductivity is proportional to ρ^* (so-called gyro-Bohm scaling).

Ion Cyclotron Resonance Heating

The distribution function of ions in the presence of Ion Cyclotron Resonance Frequency (ICRF) heating has been studied with the Finite Drift Orbit width code (FIDO code), which has been developed under a JET contract [13]. The code solves an orbit averaged 3D Fokker-Planck equation with a Monte Carlo method. There are two important effects included in the FIDO code which are not taken into account in standard 2D bounce averaged Fokker-Planck codes, namely finite orbit width and wave induced spatial diffusion. The latter of these effects depends strongly on the toroidal mode number n of the wave; in fact the diffusion coefficient in real space is proportional to n^2.

The relative importance of the two effects has been studied for scenarios relevant to JET. A major finding is that for dipole phasing of JET antennae (i.e. when the antennae radiate waves with predominantly high toroidal mode numbers) wave induced spatial diffusion tends to play an equally or even more important role than the finite orbit width for the evolution of the distribution function. In the case of dipole phasing, the resonating ions are diffused outwards resulting in a broader fast ion pressure profile and a lower peak for the averaged energy. The total fast ion energy contents for the two phasings are, however, almost the same. Consequently, the experimentally determined saturation of the fast ion energy content with power [14,15], which in the past has been mainly attributed to the finite orbit width of the fast ions, seems in the case of dipole phasing to be caused to a large extent by wave induced diffusion rather than finite orbit width.

Numerical Simulation

The activities of the Simulation Group were directed along two main lines:

- Development and validation of models of energy transport inside the separatrix (JETTO code);
- Predictive and interpretive study of plasma in the boundary region (EDGE2D/U-NIMBUS codes).

The predictive transport codes JETTO and EDGE2D/NIMBUS have been extensively used, both in stand alone versions and combined into a single code [16, 17]), to study energy and particle transport. The mixed Bohm-gyro-Bohm transport model developed at JET [18, 19], has been tested in a variety of cases including heat pulse propagation, [20, 21], the time evolution of hot-ion H-modes and experimental results from several tokamaks available in the profile ITER data base [22, 23].

The results obtained so far, while certainly not sufficient to claim that the model provides a complete and accurate description of transport in tokamaks, show that the model provides a good description of many important observations. Therefore, it can be considered as a useful guide for the interpretation and planning of experiments and for further development of theoretical transport models. Moreover, the combined EDGE2D/NIMBUS - JETTO code has provided for the first time a tool to study transport in a consistent way across the entire plasma region, including the effect of the boundary region on the global plasma performance which is an important issue.

Predictive work on the performance, of the JET divertors and on the ITER divertor was also carried out [24, 25], as well as development of theoretical transport models and upgrading for the EDGE2D code.

Simulation of Heat Pulses and Optimised Shear Experiments

A predictive numerical modelling of selected JET discharges with different kinds of heat pulses has been performed [20, 21]. The selection includes "hot" pulses initiated from the plasma core and caused by a sawtooth crash and cold pulses from the plasma edge due to ELMs and impurity laser ablation.

The results of simulations compared with experimental results have showed that:

- The mixed Bohm-gyro-Bohm model, together with a non-local dependence of the Bohm term on the electron temperature profile in the boundary region (inside the transport barrier in the core of H-modes) is consistent with both the diffusive and the non-local aspects of transport observed in the experiments;
- The model predicts an asymmetry between pulses originated in the boundary region and pulses originated in the centre. This asymmetry has also been observed in experiments and might rule out other models, such as those based on ion temperature gradient driven instabilities (ITG modes).

There are however open problems, many of them related to lack of sufficient experimental information, that do not permit firm conclusions to be drawn on this subject. A related problem that needs further investigation is the appearance of internal transport barriers (or regions) of reduced transport.

Simulations of these important regimes have been carried out by including in the model a dependence of the Bohm term on the magnetic shear. However, the results of the simulations are not fully consistent with observations. In cases when the ion heating is dominant, it appears that the gyro-Bohm term should also be reduced or eliminated within the good confinement region. Work is in progress to improve the model in these cases.

ELM-free H-modes in terms of a Neoclassical Edge Transport Barrier

The inclusion of a neoclassical transport barrier inside the separatrix in the mixed Bohm-gyro-Bohm model [17, 18], has been shown to provide a reasonable description of the time evolution of ELM-free H-modes. For this reason, it has provided a useful guide for the optimisation of the performance of this regime by predicting that in this regime:

- the best confinement require low edge density and low recycling conditions;

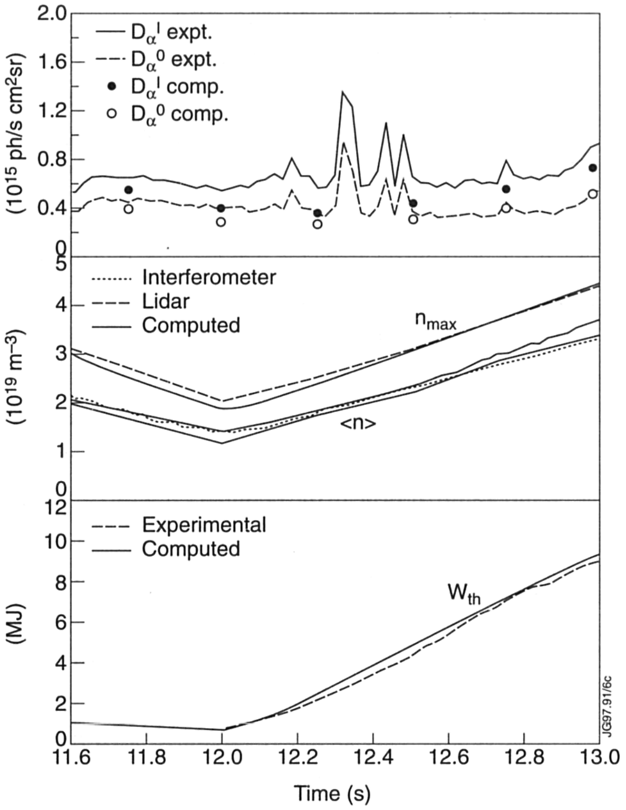

Fig.163: Experimental and computed time evolution of D_α emissivities averaged and peak core plasma densities, and thermal energy content

- good performance in quasi-steady state can be reached by stepping down the input power;
- any degradation of confinement in the boundary region is reflected in an increase of transport coefficients in the entire plasma cross section;
- while the density in the boundary region remains low and the neoclassical heat loss across the separatrix is small compared to the input power, the energy content increases almost linearly as the pressure gradient in the transport barrier increases. This leads the plasma to hit some instability limit (ballooning, external kink, or a combination of both) and to the end of the good performance phase.

Not only these general predictions have been substantiated by experimental results, but the model has shown good simulation of individual hot-ion discharges. In particular, with the JETTO-EDGE2D/NIMBUS combined code, simulations have been undertaken describing simultaneously the edge and core region (Fig.163) and providing a consistent evaluation of the particle sources in the core. Based on these simulations, an effective particle diffusion coefficient has been developed consistent with experimental observations and strongly suggesting the presence of an inward particle pinch term in the boundary region.

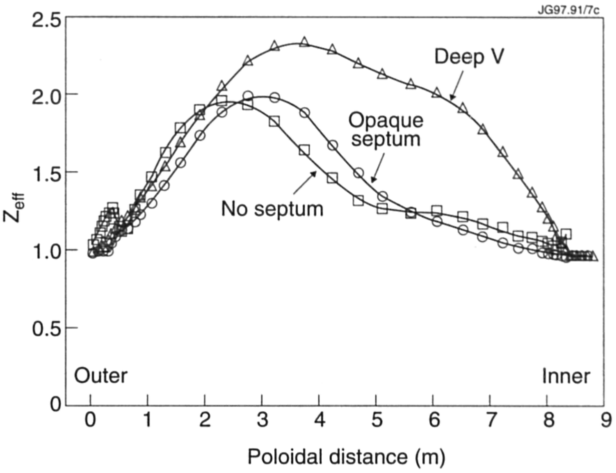

Fig.164: Poloidal profiles of Z_{eff} at separatrix with carbon as the radiating impurity for the three septum configurations $n_s=2x10^{19}m^{-3}$, $P_i=P_e=5MW$ in the Gas-box divertor

Predictive Studies of Mark II Gas-box Divertor and ITER Divertor

The Mark IIGB divertor incorporates a flexible design which allows several configurations to be tested. These include horizontal and vertical targets, and an optional septum of as yet unspecified conductance to neutrals. A third possible variant is one which uses a broad, opaque septum to form a double slot divertor.

EDGE2D/NIMBUS modelling has been carried out to compare the various configurations from an overall performance standpoint [24]. Results of simulations indicate that none of these configurations seems to have a clear advantage over the others. In particular, for a given density at the separatrix and radiated power, most of the parameters of the main plasma are practically the same.

The type of the septum also has little effect on recycling impurities introduced to increase radiation: the impurity content required for a given radiated power is practically independent on the presence and shape of the septum. The shape of the septum has however some effect on the content of intrinsic impurities such as carbon. The carbon content results to be somewhat higher in the deep configuration (Fig.164).

Little difference is found between carbon and nitrogen for fixed radiated power, P_{rad}, except for the fact that more carbon than nitrogen is required to radiate the same amount of power. There is not enough deuterium flow, resulting from pumping and leakage, for impurity entrainment in the divertor. The low level of carbon retention, in particular, is mainly due to transport and not to the sputtering from the vessel wall outside the divertor. These conclusions hold for both vertical and horizontal targets, but in addition the horizontal targets have to sustain a much higher peak heat load. In any case, no solutions have been found with simultaneous detachment, high radiated power fraction and retention of impurities for the Mark IIGB.

EDGE2D/NIMBUS simulations were also carried out to study the performance of an ITER divertor in a partly detached regime with intrinsic or recycling impurities [25]. The results indicate that adopting a relatively low radiated power fraction (≤ 50% of input power), a partly detached divertor operating scenario for ITER may make it possible to maintain the required confinement quality and purity in the main plasma while providing satisfactory divertor target plate lifetimes against erosion. However, the viability of this approach requires more information on the scaling of ELMs and the H-mode threshold, as well as better characterisation of the perpendicular SOL transport and sputtering and radiation data. This approach (and all ITER divertor scenarios) depend rather critically on the upstream SOL density which can be achieved.

Implementation of Particle Drift Fluxes into the EDGE2D Transport Code

The implementation of particle drift fluxes into the EDGE2D transport code has been completed for all particle species. The divergence-free component of the diamagnetic fluxes (the $B\times\nabla p$ and $B\times\nabla T$ terms) has been shown not to contribute either to the continuity, collisionless parallel momentum or energy equations or to the plasma boundary conditions. This has been used in the implementation of the drift fluxes into the EDGE2D code, giving a significant simplification and removing possible sources of numerical errors. All components of the ∇B and curvature drifts, the centripetal force drifts and the $E\times B$ drifts have been implemented. The target boundary conditions have been modified to take account of poloidal and radial particle drifts using boundary conditions proposed in [26].

To calculate the electric potential and parallel current density, full account is taken of radial currents arising from the drift term. Inside the separatrix, the radial electric field is obtained iteratively by requiring that the surface-averaged radial current is ambi-polar. Results obtained for a typical divertor plasma show that the $E\times B$ drifts are largely dominant and flow as expected for the two cases of forward and reserve magnetic field. The drifts also appear to have the greater effect on the inner divertor region.

Implementation into EDGE2D of a 21 Moment Description of Classical Parallel Transport

Modelling the transport in the scrape-off-layer of a confined plasma, continous efforts have been made to improve the calculation of the coefficients for the transport parallel to the magnetic field lines. Very accurate results were obtained in [27, 28]. The calculation is based on a fluid approach and collisions are assumed to be dominant. The collision integrals are calculated following Grad's moment approximation to the distribution function, truncating at 21 moments.

The resulting system of equations is then to be solved for the higher moments as functions of the lower moments density, momentum, temperature and their gradients. If an analytical solution is attempted, rather crude approximations have to be made. To obtain transport coefficients that are valid for arbitrary impurity masses and densities, the equations have to be solved by direct matrix inversion. If N is the total number of impurity species, this would amount to two (2N+2)x(2N+2) matrices to be inverted at each iteration step. This problem has been overcome by employing the reduced charge state (RCS) method [29] which requires no further approximation apart from common ion temperature and Coulomb logarithm. The RCS method allows all the charge states of an impurity species to be dealt with simultaneously, thus reducing the number of equations in a system from (2N+2) to (2S+2), with S being the number of impurity elements. For example, in the case of carbon thus reduces the number from 14x14 to 4x4.

The full calculation of the parallel transport has been implemented into the EDGE2D code, already providing for the option of modelling a multi-impurity elements plasma. The RCS method has shown to significantly reduce the computing time compared to that needed for direct calculation. In the above example, the RCS method brings down the computing time to 20% of the direct matrix inversion.

Data Processing and Analysis

Multi-machine Database Collaboration

The ITER Confinement Database and Modelling Expert Group is in charge of the ITER L-mode Database, the ITER H-mode Database, the ITER H-mode Threshold Database and the ITER Profile Database. The official Expert Group (three members from each of the four ITER Parties) acts as a Steering Committee for the activities, whereas the actual Working Group is much larger. All the

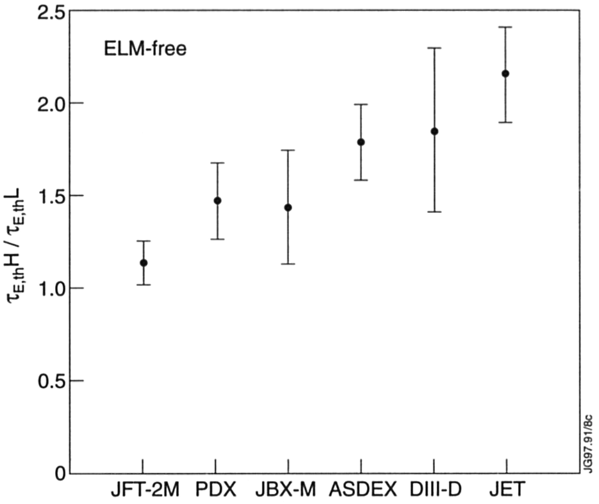

Fig.165: Ratios of the ELM-free H-mode thermal confinement time to the L-mode scaling. The error bars correspond to the standard deviations of the ratios

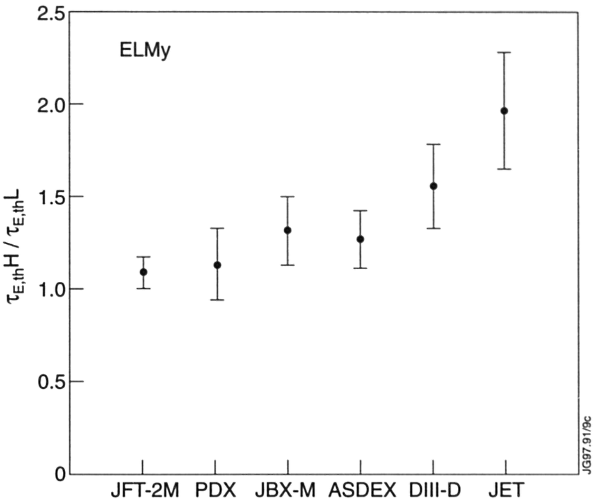

Fig.166: Ratios of the ELMy H-mode thermal confinement time to the L-mode scaling. The error bars correspond to the standard deviations of the ratios

participating Tokamaks, i.e.. ASDEX, ASDEX-UPGRADE, C-MOD, COMPASS-D, DIII, DIII-D, FTU, JET, JFT-2M, JT-60, JT-60U, PBX-M, PDX, RTP, START, TCV, TDEV, TEXTOR, TFTR, TORE SUPRA and T-10, are represented in the Working Group. The Working Group also includes modellers participating in the ITER 1-D modelling activity for which the Expert Group also is responsible. Two official Workshops were held in 1996: in Moscow (R.F.) during April 15-17 and in Montreal (Canada) October 13-16 1996. Progress made with each database and the data analysis is described in detail below.

ITER L-mode Database

The current version of the L-mode database consists of data from the following 14 tokamaks: ASDEX, C-MOD, DIII, DIII-D, FTU, JET, JFT-2M, JT-60, PBX-M, PDX, TEXTOR, TFTR, TORE SUPRA and T-10. Thermal energy confinement data are now available from all tokamaks, except DIII. The database also contains a large amount of ohmic data and some enhanced L-mode data from TORE SUPRA and TEXTOR. The database documentation [30] and the data are now publicly available. The thermal L-mode confinement scaling determined from this database is [30,31] :

$$\tau_{th} = 0.023 x I^{0.96} B^{0.03} R^{1.83} \varepsilon^{-0.06} \kappa^{0.64} n^{0.40} M^{0.20} \rho^{-0.73}$$

in units of MA, T, m, -, -, $10^{19}m^{-3}$, AMU and MW. This scaling can also be written in terms of dimensionless parameters as:

$$B\tau \propto \rho^{*-1.98} \nu^{*0.19} \beta^{-1.39} \varepsilon^{-4.26} \kappa^{0.87} M^{0.74} q^{0.14},$$

which corresponds to a Bohm scaling. Comparisons with the data in the ITER H-mode database [32] show that the H-mode enhancement factor, defined by the thermal L-mode scaling, increases with machine size (decreasing ρ^*) for both the ELM-free and ELMy H-mode data, see (Figs.165 and 166).The total confinement scaling [30] determined from this database is very close to the ITER89-P scaling [33]. The main difference a weaker isotope dependence, i.e. $\tau_E \sim M^{0.26}$. The ohmic data have also been analysed and the confinement of the data in the saturated ohmic confinement regime is in agreement with the thermal L-mode scaling. It is planned for next year to extend the L-mode database with more dedicated ohmic data and do a more detailed analysis of the ohmic confinement.

ITER H-mode Database

The public version of the H-mode database [32] consists of data from the following six Tokamaks: ASDEX, DIII-D, JET, JFT-2M, PBX-M and PDX. The log-linear thermal ELM-free H-mode confinement scaling, determined from this database, is ITERH93-P [32, 34]. The current ELM classification in the database does not allow for a determination of scalings for the various types of ELMs. The thermal ELMy H-mode scaling, ITERH92-P(ELMy) [35], is the best log-linear fit to the ELMy standard subset of this database. The assumption that Type I ELMs degrade the underlying ELM-free H-mode confinement by a constant fraction leads to the log-linear thermal Type I ELMy H-mode scaling 0.85xITERH93-P. However, the H-mode data can also be represented by other functional forms, such as offset-linear scaling for energy [35, 36] or log-linear scalings with quadratic interaction terms [35, 37] for the confinement time. Extrapolation using such scalings should be treated with caution as the physics in the scalings may change drastically. Work has also started on the next version of the H-mode database. The next version will include new data from DIII-D and JET as well as data from ASDEX-Upgrade, C-MOD, COMPASS-D, JT-60U, TCV and TEXTOR (for comparison with radiative cooled I-mode data).

ITER H-mode Threshold Database

The public version of the H-mode Threshold database [38, 39] consists of data from the following nine Tokamaks: ASDEX, ASDEX-UPGRADE, COMPASS-D, C-MOD, DIII-D, JET, JFT-2M, JT-60U and PBX-M. This version has now been extended with data from TCV as well as with new data from dedicated threshold experiments on the other machines [31]. A subset of this data, representing the lowest achieved threshold in each tokamak, support a range of dimensionally correct H-mode power threshold scalings. This range can be written in the condensed form

$$P_{thr}=2.53\ B\ n_{19}^{0.75}\ R^2\ [6.0 n_{19} R^2]^{\pm 0.25}$$

in units of MW, T, $10^{19}m^{-3}$ and m. It is the (unknown) proximity to the threshold of each data point in the database which makes it impossible to be more definite. Unfortunately, $n_{19} R^2$ is very large for ITER, resulting in a point prediction for P_{THR} at $n_{19} = 5.0$, ranging from 50 to 200MW for ITER. This range should not be interpreted as a confidence interval for the prediction. In another approach, discriminant analysis techniques have been used to establish the threshold scaling [39]. If a simple power law is assumed, this approach gives

$$P_{thr} = S\ n_{19}^{0.06}\ B^{1.11}\ R^{-1.23}\ \varepsilon^{-0.46}\ \kappa^{-0.51}$$

where S is the plasma surface area in units of m^2. Notice the lack of density dependence in this expression. If a model with interaction terms is assumed the following scaling is obtained:

$$P_{thr}= S^{i+a}\ n_{19}^{b}\ B^{0.95}\ R^{1.27}\ I^{-0.68}$$

where $a=1-0.2\ln(S)$ and $b=-1.84+0.45\ln(n_{19})+0.17\ln(S)$, respectively. Both these two scaling expressions predict a threshold power of 80MW for ITER, at $n_{19} = 5$.

Ohmic Confinement

The analysis of the global energy confinement for the ohmic data obtained in the 1994, 1995 and 1996 experimental campaigns can be summarised as follows [40]: a comparison of this data with the 1984-1992 data [41] shows that the reduction in the plasma volume, due to the introduction of the divertor, has reduced the value the confinement time in the same proportion. The energy transport in the plasma seems to have adapted itself so that the peak electron temperature and the loop voltage have not been changed by the reduction of the volume. Between the Mark I and the Mark II divertor configurations, no strong difference in global energy confinement can be detected. It can be observed that the latter configuration has apparently reduced the available density range at least in the part of the Mark II campaign completed up to the time of this analysis. The dependence of global confinement on elongation is still uncertain because it is correlated with configuration and Z_{eff}.

Data Processing

During 1996, the intershot processing CHAIN1 has analysed JET data for more than 2000 pulses. The pulses, grouped into campaigns of three Task Forces, feature new data; (i) charge exchange normal network analysis; (ii) infrared temperature measurements of the divertor heat load; (iii) edge density from reflectometer are some examples of data types now regularly available between JET pulses. These data types, together with the existing data are intended to facilitate experimental progress during sessions as is the small subsets of data being analysed in real time.

During 1996, the entire data has been reprocessed as part of an ongoing effort to improve on the quality of data. As in earlier years, this reprocessing is a consequence of discussion by the Data Coordination Committee which meets regularly during the year. During 1996, a particular effort on cross calibration of electron density and temperature diagnostics has been undertaken.

The consistency between data from various diagnostics is also examined in calculations by the transport analysis code TRANSP. The checking for consistency is a lengthy process involving iterations as part of the data can be subjected to reprocessing.

TRANSP Code Calculations

Different JET regimes have been analysed by TRANSP and therefore different physics issues have been addressed. The dimensionless parameter scaling studies in ELMy H-modes (ρ^*, ν^* and beta scans as well as radiative ρ^* scan) addressed whether the bulk transport is Bohm or Gyro-Bohm and whether or not the local analysis confirm the global scaling laws.

The hot-ion H-modes were extensively analysed to study the links between MHD events (Outer Modes, ELM's and sawteeth) and confinement to clarify the causes of the limitation in performance. An MHD stability study using TRANSP current and pressure profiles shows that some hot-ion H-modes exhibit edge conditions marginally unstable for the external kink throughout the high performance phase and eventually reach the ballooning limit. However, some other cases did not show this behaviour and hence the abrupt change in confinement must be explained. Several other causes have been investigated by TRANSP, such as influx of neutrals associated with ELMs or sudden loss of fast ions; none was convincing.

In preparation for the D-T campaign, NB step-down scenarios were analysed, as well as some optimised shear pulses and other ITER relevant pulses such as high current, long ELMy H-modes.

All these analyses were first tested for data consistency. There was still a data inconsistency problem for the high performance hot-ion H-modes. TRANSP was used to test possible data problems (or solutions); comparisons with the neutron profile data suggest that the deuterium density derived by CXRS is probably overestimated in the outer part of the plasma. For other JET regimes, the quality of the data consistency was variable, often suffering of a lack of experimental data (about recycling, particle mixing, measured radiation profiles, time resolution of some diagnostics ...) and/or of limits in the modelling capabilities of TRANSP (RF package, neutral treatment ...).

TRANSP was also used in a predicative mode, mainly to explore possible scenarii to demonstrate alpha-heating during the forthcoming D-T campaign. Possible D-T fusion performances were also assessed; under present circumstances fusion powers from 5.6MW to 8MW, corresponding to Q_{DT} from 0.31 to 0.44, could be obtained depending on the D, T mixing ratio.

TRANSP Code Development

The joint project continues between JET and PPPL, (USA) to enable TRANSP to run in a fully free boundary mode of operation. Two "free boundary" equilibrium reconstruction codes VMEC and EFIT have been linked to TRANSP by UNIX pipes.

Previously, a fixed boundary equilibrium model was used to time evolve the magnetic geometry and the current profile then calculated using neoclassical resistivity. The free boundary equilibrium directly reconstructs the plasma current profile from external magnetic data while fitting to internal data such as pressure profiles, diamagnetic flux, Faraday measurements (on JET) and MSE data (on TFTR).

First results have been obtained using VMEC on selected TFTR pulses [42], and work is continuing at PPPL to make the operation more robust and add the possibility of using EFIT. At JET, preliminary runs have been completed for Pulse No. 33643 using EFIT. Further work is required in the area of the EFIT to TRANSP equilibrium representation interface.

The ITER Profile Database now contains data for pulses from nine major world tokamaks together with ITER simulations. JET has updated data on the seven pulses previously contributed and added five more. All are ELMy H-mode plasmas: Pulse No. 33131 (3.1T, 2.8MA); Pulse No. 33465 (1.0T, 1.0MA); and Pulse No. 35174 (1T, 1MA) are all D plasmas and are additional members of a group of pulses of a ρ^* scaling experiment. Pulse No. 32745 (2.8T, 2.9MA) is a 80%D 20% He^3 plasma and Pulse No. 34340 (2.0T, 2.0MA) is a high beta plasma 95%D 5%H relevant for ITER scaling.

Diagnostic Software

The Diagnostic Software Section is responsible for the design and maintenance of diagnostic control, data acquisition, calibration and display-software for a considerable number of diagnostics. It also provides support to diagnoticians with the commissioning of diagnostics and trouble-shooting during operations. The Section maintains some general purpose software products, such as: a JPF data retrieval and display package; a General Data Acquisition and Control package; and various subroutine libraries. It also supplies data analysis support on the IBM mainframe computer system, mainly for the KS1, KS2 and KS6 spectroscopy diagnostics. The section is responsible for the Chain-1 Intershot Analysis data processing. This involves a considerable amount of PPF reprocessing.

In 1996, considerable effort went into the further development of the Central Acquisition and Trigger System (CATS) and the Real Time Plasma Boundary Display (XLOC-RT), while it has continued to support existing PC-based diagnostics and their network file-servers, the Diagnostic Data network. Calibration software has been developed for the new 14MeV Time-of-Flight Neutron Spectrometer. The space and time resolved velocity distribution of alpha-particle diagnostic (KE4) is now producing some data and a suite of control programs has been built up to allow the physicist to control this diagnostic. A new commitment is the development of control software for the two Gas Collection System Mass spectrometers (GCS-A and GCS-B). This system will become operational before the start of the DTE1 campaign. The section continued to provide consultancy support to the Data Management Group (DMG) towards the design and implementation of the new JET Office network.

References

[1] G.T.A. Huysmans, J.P. Goeldbloed, W. Kerner, Phys. Fluids **B5**, 1545 (1993).

[2] A.B. Mikhailovskii, G.T.A. Huysmans, W. Kerner, S.E. Sharapov, Optimisation of the computational MHD normal-mode analysis in tokamaks, JET Preprint, JET-P(96)25 (1996).

[3] J. Candy, B.N. Breizman, J.W. Van Dam, T. Ozeki, Phys. Lett. A **215**, 299 (1996).

[4] H.L. Berk et al., Alpha Particle Transport due to Alfvén Wave Excitation, IAEA Conf., Montreal, Canada, IAEA-CN-64/D2-5 (1996).

[5] S.E. Sharapov, In Proceed. of the 1996 ST Workshop, 4-6 December 1996, Culham, UK.

[6] A. Fasoli et al., Phys. Rev. Letters **76**, 1067 (1996).

[7] A. Fasoli et al., Phys. Rev. Letters **75**, 645 (1995).

[8] L. Appel et al., Nuclear Fusion **35**, 1697 (1995).

[9] S. Pinches, Nonlinear Interaction of Fast Particles with Alfvén Waves in Tokamaks, PhD Thesis, University of Nottingham, UK, November 1996.

[10] S.E. Parker and W.W. Lee, Phys. Fluids **B5**, 77 (1993).

[11] J. Candy, to appear in Journal Comput. Physics (1996).

[12] G. Manfredi and M. Ottaviani, Global numerical simulation of ion-temperature-gradient turbulence in three dimensions, to appear in the Proceedings of the 1996 Joint Varenna-Lausanne Fusion Theory Workshop (Varenna, August 1996).

[13] "FIDO, a code for computing the resonant-ion distribution function during ICRH" Carlsson, J., H., L.-G. Eriksson, Alfvén Laboratory report ALF-1996-104, Royal Institute of Technology, Sweden.

[14] Cordey, J.G., et al., Proc. 18th European Conf. on Controlled Fusion and Plasma Physics (Berlin 1991) Vol. 15c, Part III, p. 385.

[15] Cottrell, G.A. Start, D.F.H. Nucl. Fusion 32 (1991) 61.

[16] A Taroni, et al., Transport Modelling with a Combined Core and Edge Code, 23rd EPS Conference on Plasma Fusion, Kiev, Ukraine, 28-28 June, 1996.

[17] The JET Team (presented by A. Taroni), Energy and Particle Transport Modelling with a Time Dependent Combined Core and EDGE Transport Code, 16th IAEA Fusion Energy Conference, Montreal, Canada, 7-11 October 1996, IAEA-CN-64/D3-3.

[18] M. Erba, et al., Development of a Non-Local Model for Tokamak Heat Transport in L-mode, H-mode and Transient Regimes, JET Report, JET-P(96)10, to appear in Plasma Physics and Controlled Fusion.

[19] M. Erba, et al., Validation of a Mixed Bohm-gyro-Bohm Transport Model on Discharges of the ITER Data-base, JET Report, JET-R(96)07.

[20] V.V. Parail, et al., Numerical Analysis of Heat Pulses in JET, 23rd EPS Conference on Plasma Physics and Controlled Fusion, Kiev, Ukraine, 24-28 June 1996.

[21] V.V. Parail, et al., Transport Analysis of Transient Phenomena in JET, accepted for publication in Nuclear Fusion.

[22] A Cherubini, et al., A Description of ELM-free H-modes in Terms of a Neoclassical Edge Barrier and a "Mixed' Model for Energy and Particle Transport, 23rd EPS Conference on Plasma Physics and Controlled Fusion, Kiev, Ukraine, 24-28 June 1996.

[23] J. Connor, et al., Validation of 1-D Transport and Sawtooth Models for ITER, 16th IAEA Fusion Energy Conference, Montreal, Canada, 7-11 October 1996, IAEA-CN-64/EP-21.

[24] R. Simonini, et al., A Predictive Study of the JET Mark II Gas-box Divertor, ibidem.

[25] G. Vlases, G. Corrigan and A. Taroni, Lightly or Non-Seeded, Partially Detached ITER Divertor Operation, 12th Plasma Surface Interaction in Conference on Controlled Fusion Devices, St. Raphael, France, 20-24 May 1996.

[26] A.V. Chankin and P.C. Stangeby, Plasma Phys. Cont. Fusion **36** (1994) 1485.

[27] G.J. Radford, Contrib. to Plasma Phys. **32** (1992) 297.

[28] G.J. Radford, Classical Parallel Transport in a Multi-Species Plasma from a 21 Moment Approximation, JET report JET-R(93)05.

[29] C.D. Boley, E.M. Gelbard, S.P. Hirshman, Phys. Fluids, **22** (1979) 1280.

[30] Kaye, S.M., et. al., Submitted to Nuclear Fusion.

[31] Takizuka, T., et. al., IAEA-CN-64/F-5. 16^{th} IAEA, Montreal, Canada, (1996).

[32] Thomsen, K., et al., Nuclear Fusion **34** (1994) 131.

[33] Yushmanov, P.N., et al., Nuclear Fusion **30** (1990) 1999.

[34] Schissel, D.P., et al., in Controlled Fusion and Plasma Physics (Proc. 20th Eur. Conf. Lisbon, 1993), Vol. 17C, Part I, European Physical Society, Geneva (1993) 103.

[35] Kardaun, O., et al., in Plasma Physics and Controlled Nuclear Fusion Research (Proc. 14th Int. Conf. Wurzburg, 1992), Vol. 3, IAEA, Vienna (1993) 251.

[36] Kardaun, O., et al., in Controlled Fusion and Plasma Physics (Proc. 21st Eur. Conf. Montpellier, 1994), Vol. 18B, Part I, European Physical Society, Geneva (1994) 90.

[37] Dorland, W., Kotschenreuther, M., Private Communication.

[38] Ryter, F., et al., Plasma Physics and Controlled Fusion **38** (1996) 1279.

[39] Ryter, F., et al., Nuclear Fusion **36** (1996) 1217.

[40] Bracco, G., Thomsen, K., 'A Preliminary Analysis of a Global Energy Confinement Database for JET Deuterium Ohmic Plasma from 1994, 1995 and 1996 Campaigns', to be published.

[41] Bracco, G., Thomsen, K., JET Report, JET-R(96)03, accepted for publication in Nuclear Fusion.

[42] R.M. Wieland, D.C. McCune, D.P. and P.M. Stubberfield presented at the 38th Annual Meeting of the Division of Plasma Physics, 11-15 November 1996, Denver, Colorado, USA.

Summary of Scientific Progress

Introduction

The 1996 Experimental Campaign had three overall objectives: to characterise plasma behaviour with the Mark IIA pumped divertor; to undertake a number of physics studies for ITER; and to prepare plasma scenarios for the JET D-T experiments (DTE1, scheduled for the summer of 1997). Specifically, the campaign concentrated on ITER-relevant issues related to the more closed Mark IIA divertor and, because of their importance for predicting ITER's ignition margin and fusion power output, the scaling of the threshold power for access to the H-mode regime and energy confinement in this regime. The preparation of high performance scenarios for DTE1 was also a high priority.

Following a five week shutdown in September/October 1996 to plug divertor by-pass leakage paths, to clad the inner wall of the vacuum vessel with graphite tiles and to replace the three (of sixteen) NB PINIs which were faulty, the experimental programme recommenced in November with the aim of optimising performance in preparation for DTE1. However, the Programme was again interrupted during the second half of December to repair a water leak in the Octant No.8 NB injection box, ready for operations to restart in early January 1997.

Characterisation of Plasma Behaviour with the Mark IIA Divertor

Mark IIA behaved as expected for a more closed divertor. It offered improved power handling over the Mark I divertor, withstanding JET's full heating power without overheating or localised sublimation of the graphite target material. In comparison with the Mark I divertor, the neutral pressure at the pump increased by a factor of ≈3, the plasma was pumped 2-3 times more rapidly and the need to position the strike point over the pump throat was obviated. In the divertor region, the effects of increased closure were clear from signs of increased neutral recycling and detachment of the divertor plasma from the target at significantly lower main plasma density than with Mark I, a trend which was in agreement with code predictions. On the other hand, the effect of closure on main plasma confinement was, in general, small, although the more closed configuration appeared to maintain good confinement to a slightly higher density normalised to the Greenwald density. With Mark IIA, the time for injected trace neon to be pumped out was observed to be shorter, but the expected reduction in the level of intrinsic impurities in the plasma core did not occur, perhaps because of stronger interactions with the tile shoulders of the divertor, higher tile operating temperatures or greater tile coverage of the inner wall.

The frequency of Edge Localised Modes (ELMs), which is determined by plasma triangularity and gas puff stength, had a greater effect on performance than either target orientation or magnetic flux expansion in the divertor. The further closure of the by-pass leakage paths in October 1996 resulted in a further reduction in neutral recycling in the main chamber, but did not significantly change plasma performance or purity (perhaps because of the increased carbon tile coverage of the inner wall). A comparison of the behaviour before and after plugging the bypass leakage paths showed that the confinement of the main plasma was correlated with the divertor neutral pressure, rather than the mid-plane neutral pressure which had previously been assumed.

Physics Studies for ITER

ITER-relevant Scaling Studies

Studies for ITER have concentrated on the heating power required to make the transition from L-mode to H-mode and back to L-mode confinement, and the scaling of energy confinement. Both of these scaling studies are of crucial importance for the prediction of ITER's ignition margin and fusion power output.

The threshold power for access to the H-mode has not changed substantially since the introduction of the pumped divertor. It is independent of the magnetic configuration and the type of additional heating (NB or ICRF) and exhibits no hysterisis in either edge temperature or, probably, heating power. The data follows quite well the global scaling expressions derived from a multi-machine threshold data base, although a deviation from the linear density scaling is evident at densities above $5x10^{19}m^{-3}$.

In conjunction with DIII-D, confinement in the plasma core of ELMy H-mode discharges with ITER dimensionless parameters has been shown to depend on three dimensionless parameters (normalised Larmor radius, ρ^*, collisionality, ν^* and plasma pressure, β). Similarity experiments with DIII-D and C-Mod have validated the approach. Precise experiments on JET have shown that confinement is close to a gyro-Bohm scaling, with the ρ^* and ν^* dependences confirming the ITERH93-P scaling law used at present to predict the ITER confinement time. However, a very weak but favourable dependence on β is found, in contrast to the strong and unfavourable scaling with β of the ITERH93-P scaling.

The effect of different types of ELMs on confinement in high power, long pulse quasi-steady H-mode discharges has also been studied. Type III ELMs (conditions close to the L-H threshold) are found to be significantly worse for confinement than Type I "Giant" ELMs (conditions well above the L-H theshold). Specifically, with increasing radiated power to reduce the heat load to the divertor target plates, Type III ELMs are produced and confinement degrades progressively, no longer following the ITERH93-P scaling law. It is clear that somewhat better confinement will be required for ITER operations with a high radiated power fraction.

Preparation of an Integrated Operating Scenario for ITER

JET has studied the effect of increased divertor closure on the establishment of long pulse quasi-steady H-mode discharges with sufficiently high confinement for ignition in ITER and with edge conditions which allow sufficiently good energy and particle exhaust and low erosion (even with ELMs) for reasonably long component lifetimes.

Type I ELMy H-modes at high density have sufficient confinement, and Z_{eff} from intrinsic impurities is quite low and well within ITER requirements. However, Type I ELMs deposit high powers repetitively on divertor components and the scrape-off layer plasma density is low between ELMs. When extrapolated to ITER, operation with such ELMs would result in unacceptable heating and erosion of the target plates. It should be noted, however, that with ICRF rather than NB heating, the ELMs are much more frequent and have a lower amplitude, but this may be due to the lower particle and momentum sources associated with ICRF heating.

In Type III ELMy H-modes, the maximum radiated power fraction decreases with increasing divertor closure, from 80% with Mark I to 60% with Mark IIA after plugging the divertor by-pass leakage paths. None-the-less, the total power flow to the targets remains small since charge-exchanged neutral losses from the divertor appear to be higher with the more closed geometries. Plasma purity in such radiative discharges in Mark IIA has been found to fit the empirical scaling law between radiated power loss and Z_{eff} in the plasma core which was established from a multi-machine data base. This scaling shows that impurity control will have to be slightly better for ITER operations with radiative plasmas. On the other hand, as pointed out above, confinement deteriorates with increasing radiated power fraction and the scaling becomes less favourable than the gyro-Bohm scaling of ITERH93-P.

It is clear that further development is needed if ITER is to use either of these modes of operation.

Preparation of High Performance Scenarios for DTE-1

The preparation of scenarios for DTE-1 has concentrated on three high performance regimes: the hot ion ELM-free

H-mode; the high current ELMy H-mode and the optimised magnetic shear regime. The first two, being well developed before the present campaign, have continued to make progress. The last, building on developments on DIII-D, TFTR and JT-60U, has now achieved a fusion performance in deuterium equal to that of the hot ion ELM-free H-mode during 1996. In spite of considerable progress, further work is still required to raise the operating density (in order to maximise the D-T fusion performance) and to improve discharge reliability. In the longer term, the optimised shear regime must demonstrate the steady-state capability for which it is of so much potential interest to reactor designers.

Hot-ion ELM-free H-modes

Hot-ion ELM-free H-modes, heated by high power NB injection and augmented by ICRF heating, have produced high fusion yields and will form a cornerstone of DTE1 in 1997. Strong pumping with the Mark IIA divertor has reduced the need for extensive conditioning for access to this regime, but has not improved confinement or performance significantly. The improved design of the pumped divertor target has eliminated the carbon "bloom", but MHD instabilities and a loss of confinement in the plasma core remain and ultimately limit performance and reproducibility.

Fusion performance in hot ion ELM-free H-modes is similar with the Mark I and Mark IIA divertors. The same strong dependence on NB heating power is seen, but neutron rates were restricted during 1996 to less than $3x10^{16}$ neutrons per second by the available NB heating power (≈17MW). Improved performance has been demonstrated when ICRF is combined with NB heating. Up to 9.5MW of ICRF power has been coupled and, together with NB heating, 25MW of additional heating power has raised the stored plasma energy up to 14MJ, with plasma currents up to 3.8MA.

The period of high performance is characterised by the formation of a very pronounced transport barrier near the separatrix, particularly in the electron and ion temperatures. Pressure gradients and bootstrap and ohmic currents in the barrier region can be significant and can have a profound effect on plasma stability. "Outer modes" close to the plasma edge produce a relatively mild reduction in confinement and a rapid fall in fusion rate, while "giant" ELMs eat away the outer half of the plasma pressure profile. The phase and amplitude of soft X-ray camera measurements during the outer mode matches the predicted behaviour of an ideal external kink mode, rather than a tearing mode. The appearance of a "giant" ELM corresponds to the prediction that the edge plasma becomes unstable to ideal ballooning modes. At high current and toroidal magnetic field, the edge plasma reaches a limiting pressure gradient before the core plasma and the normalised β_N is thus reduced below the Troyon value.

Many features of the hot ion ELM-free H-mode have been described by a model which includes both neoclassical and anomalous transport losses inside a neoclassical edge transport barrier of width equal to the ion poloidal Larmor radius. This model also confirms the sensitvity of performance to particle recycling in the main chamber and the duration of the ELM-free phase prior to the onset of MHD instabilities, and accounts satisfactorily for most of the termination events. The JETTO code incorporates this model and has been coupled successfully to the EDGE2D/NIMBUS code for the self-consistent computation of the scrape-off layer and core plasma transport, and with the MHD code CASTOR for the assessment of the relative importance of ideal ballooning and kink modes in the termination of hot ion ELM-free H-modes.

Alfvèn Eigenmode Experiments

Systematic studies of weakly damped Alfvèn eigenmodes have concentrated on the three issues of mode stability, direct observation of fast particle drive in high performance plasmas and the effects of relatively large amplitude Alfvèn eigenmodes on fast particle orbits. Both the JET saddle coils and the non-linear interaction of two fast waves in the ICRF range of frequencies have been used. A novel technique based on real-time mode detection and digital control of the frequency allows the exciter frequency to be locked to the mode frequency. A small sweep of a few kHz superimposed enables the damping rate also to be determined. This technique has been proven with NB injection and will be used during DTE-1 to measure the intrinsic excitation by alpha-particles. Furthermore, magnetic fluctuations, identified as toroidal Alfvèn eigenmodes, have often been observed during performance limitations ascribed to outer modes. However, agreement between experimental and simulated neutron yields can be obtained even when toroidal Alfvèn eigenmodes are expected to be present.

High Current ELMy H-mode Operation

With plasma currents up to 5MA, JET has studied the high confinement, high performance steady-state, ELMy H-mode plasmas which most closely resemble those considered for ITER. A steady-state equivalent fusion power of ≈3.5MW has been produced at 4.7MA with 17MW of NB heating and at 3.5MA with 24MW of combined heating (16MW NB and 8MW ICRF). At 2.5MA, an ELMy H-mode can be maintained for the whole of the heating pulse (≈10s) but above a current of ≈3.5MA, most discharges suffer a spontaneous H-L back transition where the stored plasma energy begins to fall (and sometimes recovers, with up to three cycles) before the end of the high power phase.

Optimised Shear Modes of Operation

Current profile control has proved to be an important technique for optimising confinement in tokamaks. Of particular significance during 1996 was the development of the high performance optimised shear plasmas. Following JET's pioneering work in achieving enhanced performance with deep pellet fuelling to reverse the magnetic shear in the central plasma, and building on the results obtained recently in DIII-D, TFTR and JT-60U, proper control of the current rise and power waveforms has resulted, for power levels above ≈17MW, in the formation of an internal transport barrier (which expands to about half the plasma radius) and high fusion performance.

Under these conditions, high confinement L-modes (H_{89}≈2) with simultaneously high ion (32keV) and electron (15keV) temperatures and high neutron rates ($3.9x10^{16}$ neutrons per second, 80% of which are computed to be thermal in origin) have been produced with up to 28MW of combined NB and ICRF power for longer than an energy confinement time (0.4s). There is no apparent accumulation of impurities (Z_{eff} remains constant at ≈1.7) and the ratio of neutron yield to stored plasma energy is high. Fusion performance is already comparable to that achieved in the best hot ion ELM-free H-modes of 1996 and there is promise for further improvement, but the diagnostic capability for measuring the current profile is a limiting factor. In fact, an accurate determination of the current profile is of fundamental importance for optimising performance and improving understanding. In JET, the current profile has to be inferred from a combination of magnetic reconstruction and observations using soft X-ray measurements. While a strong reversed magnetic shear appears not to be necessary for triggering an internal transport barrier, shear reversal can neither be deduced or excluded from the data. Clearly, more internal data is required for a reliable profile measurement. This could be provided by a Motional Stark Effect diagnostic.

Developments and Future Plans

In 1978, the original objectives of JET were set out in the JET Design Proposal, EUR-JET-R5, as follows:

> *'The essential objective of JET is to obtain and study a plasma in conditions and dimensions approaching those needed in a thermonuclear reactor. These studies will be aimed at defining the parameters, the size and the working conditions of a Tokamak reactor. The realisation of this objective involves four main areas of work:*
>
> *i) the scaling of plasma behaviour as parameters approach the reactor range;*
> *ii) the plasma-wall interaction in these conditions;*
> *iii) the study of plasma heating; and*
> *iv) the study of α-particle production, confinement and consequent plasma heating.*
>
> *The problems of plasma-wall interaction and of heating the plasma must, in any case, be solved in order to approach the conditions of interest.*
>
> *An important part of the experimental programme will be to use JET to extend to a reactor-like plasma, results obtained and innovations made in smaller apparatus as a part of the general tokamak programme. These would include: various additional heating methods, first wall materials, the control of the plasma profiles and plasma formation.'*

At the beginning of 1996, JET had entered the ITER-EDA Support Phase of its ITER Support Programme, and started the year in shutdown for installation of the Mark II support structure. This will be the basis for all future divertor work at JET and is the key to the programme to 1999. In addition, the "more-close" Mark IIA divertor target assembly was installed. During the shutdown, work was also undertaken on various systems in preparation for the next period of D-T operation (DTE-1), scheduled for early 1997, and for the Remote Tile Exchange shutdown after DTE-1.

The 1996 experimental campaign then concentrated on specific ITER-relevant issues related to the more closed Mark IIA divertor and, due to their importance for predicting ITER's ignition margin and fusion power output, the scaling of the H-mode threshold power and the energy confinement. In addition, the preparation of high performance scenarios for DTE-1 was a high priority of the campaign.

Since the beginning of its experimental campaign, extensive studies had been made in the first and third areas of work of JET's objectives: reactor relevant temperatures (up to 30 keV), densities (up to $4\text{x}10^{20}\text{m}^{-3}$) and energy confinement times (up to 1.7s) had been achieved in separate discharges. The second area of work had been well covered in the limiter configuration for which JET was originally designed. However, the highest performance JET discharges had been obtained with a 'magnetic limiter', (or X-point configuration).The duration of the high performance phase of these discharges exceeded 1.5s; this was achieved by careful design of the targets and specific operation techniques, but is limited, ultimately, by an unacceptably high influx of impurities, characterized by a rapid increase in electron density, effective ionic discharge and radiated power (referred to as the 'bloom').

The fourth area of work had been started by earlier studies of energetic particles produced as fusion products or by ion cyclotron resonance heating (ICRH). It was addressed further during 1991 by the first tokamak plasma experiments in deuterium-tritium mixtures. The high performance achieved in deuterium discharges, together with the experience gained in making substantial modifications to JET in a beryllium environment and with significant vessel activation, gave confidence that an experiment with about 10% tritium in the plasma could be performed. A further campaign of deuterium-tritium experiments is now planned for early-1996.

During 1991, the JET Council had approved the policy of a step-wise approach to the introduction of tritium in advance of the full D-T phase of JET operations. As a first such step, after having obtained all necessary regulatory approvals, JET successfully carried out a preliminary tritium experiment (PTE-1) in November 1991 (as already described). A release of fusion energy in the megawatt range in a controlled fusion device had been achieved for the first time in the world.

In the 1991/92 campaign, JET achieved plasma parameters approaching breakeven values for about a second, resulting in large bursts of neutrons. However, in spite of the plasma pulse continuing for many seconds after reaching peak plasma values, the neutron count fell away rapidly as impurities entered the plasma and lowered its performance. This limitation on the time for which the near-breakeven conditions could be maintained was due to the poisoning of the plasma by impurities (the 'bloom'). This further emphasised the need to provide a scheme of impurity control suitable for a Next Step device.

In late 1991, the Council of Ministers approved a modification to the JET Statutes, which prolonged its statutory lifetime by four years until 31st December 1996. The extension will allow JET to implement the new Pumped Divertor Phase of operation, the objective of which is to establish the effective control of plasma impurities in operating conditions close to those of the Next Step. This programme of studies will be pursued before the final phase of full D-T operations in JET.

During 1993, a large proportion of JETs effort was devoted to shutdown work for the pumped divertor phase of operations. The first stage of the shutdown in 1992 had involved removal of components and replacement of faulty toroidal magnetic field coils. The second stage in 1992/93 involved assembly of the four divertor coils and casings inside the vacuum vessel. The third stage of the shutdown began in mid-1993, with the final positioning of the coils. The shutdown was successfully completed with pumpdown of the torus in January 1994. The first plasma in the Pumped Divertor Characterisation Phase was produced in mid-February and by mid-March successful 2MA diverted plasmas had been established. During 1994, the plasma current was increased to 5MA, the total heating power to 26MW, the stored energy to 11.3MJ and the neutron rate to 4x10^{16} neutrons/s.

1994 saw significant progress in optimising peak fusion performance and extending operation to the reactor relevant steady-state ELMy H-mode, which has now been obtained under a variety of conditions (plasma currents up to 4MA, power levels up to 26MW, in the high β_p regime, in discharges with negative central magnetic shear, and at high β_N). The high β_p regime has also been extended to steady-state and to the reactor relevant domain.

The high power handling capability of the Mark I divertor target was demonstrated and the severe impurity influxes (carbon "blooms"), which previously terminated high performance plasmas, have been eliminated.The cryopump reduces recycling, eliminates the effects of wall saturation (observed in previous long pulse operation), allows effective particle control, and generally allows higher performance.

The 1995 experimental programme had addressed the central problems of the ITER divertor: efficient dissipation of the exhausted power, control of particle fluxes and effective impurity screening, using both carbon fibre composite and beryllium as the power handling material.

During this phase, the plasma current was increased to 6MA (a world record in an X-point configuration), the total heating power to 32MW, plasma stored energy to 13.5MJ (the highest energy recorded in a JET plasma) and the neutron rate to a new JET record in deuterium of 4.7 x 10^{16} neutron/s (comparable to the best achieved prior to the installation of the pumped divertor and was achieved even though the plasma volume was 20% smaller). ITER-relevant quasi-steady state ELMy H-modes were also studied at high power, high current, high β and in combination with detached divertor plasmas and radiative power exhaust.

The campaign with CFC tiles on the first-wall was successfully completed in early-1995. This was followed by experiments to assess the performance of beryllium as a divertor target tile material and to compare it with CFC. In response to a request from the ITER Joint Central Team, beryllium melting was induced at ITER-relevant heat fluxes to see whether a protective radiative shield was established.

In 1996, the Mark IIA Pumped Divertor behaved as expected. It offered improved power handling over the Mark I divertor, pumped the plasma 2-3 times more rapidly and showed signs of increased neutral recycling in the divertor region. The latter feature showed up particularly well in the detachment of the divertor plasma from the target at significantly lower main plasma density than Mark I configuration, in agreement with code predictions. Closure of the divertor to reduce the leakage of neutrals from the divertor to the main plasma has proved to have little effect on plasma purity or performance. The initial results following the further closure of the bypass leaks did not lead to significant differences in plasma behaviour.

On ITER-relevant scaling studies, the threshold power for the H-mode was found to be independent of the type of additional heating (NBI or ICRF), no hysterisis was found, but the data dispersion remained large. Steady-state ITER-like plasmas were achieved at high current and heating power reached an equivalent Q_{DT}~0.3.

Overall, these achievements show that the main objectives of JET are being actively addressed and substantial progress is being made.The overall aim for JET can be summarised as a strategy "to optimise the fusion product ($n_i T_i \tau_E$)". For the energy confinement time, τ_E, this involves maintaining, with full additional heating, the values that have already been reached. For the density and ion temperature, it means increasing their central values $n_i(0)$ and $T_i(0)$ to such an extent that D-T operation would produce alpha-particles in sufficient quantities to be able to analyse their effects on the plasma.

In parallel, preparations continued for the next phase of D-T operations (DTE-1), which is scheduled for early-1997. JET has continued the commissioning the sub-systems of the active gas handling system in accordance with the JET programme for D-T operations.

In mid-1996, the lifetime of the Project was officially extended to the end of 1999, to enable the Project to provide further data of direct relevance to ITER. In particular, the Project should contribute significantly to the development and demonstration of a viable divertor concept for ITER. It should undertake experiments using D-T plasmas in an ITER like configuration, which should provide a sound basis for the D-T operation of ITER In addition, the extension would permit key ITER relevant technology activities to be carried out, such as the demonstration of remote handling and tritium handling.

JET is now continuing its programme of operations to demonstrate effective methods of power exhaust and impurity control in operational conditions close to those envisaged for ITER before the final phase of full D-T operations. ITER relevant studies will provide stimulation to JET and JET's results will make an important contribution to the development of the ITER design.

The following sections describe various developments underway on JET to implement these systems.

Tritium Handling

The JET Active Gas Handling System (AGHS) was constructed to pump the torus, to recover deuterium and tritium and to re-inject these gases into the torus during the tritium phase at JET. A schematic of the system is shown in Fig.167. The AGHS is located in Building J25, with its own ventilation system, and is connected to the torus via long pumping lines and gas transfer lines.

Gases collected from the torus and the other systems are mainly the six hydrogen molecules, helium, other gases added to the plasma for research purposes, and impurities such as hydro-carbons (mainly methane and higher hydro-carbons) generated by the interaction of the plasma with the first wall or by the interaction of the atomic tritium (generated by the tritium decay) with carbon on the surfaces of the primary containment, and water, nitrogen, oxygen from leaks.

The main processing steps of the gases in the AGHS are:

i) to pump the gases;

ii) to remove impurities (all gases with the exception of protium, deuterium and tritium);

iii) to detritiate the tritiated impurities with the purpose of regaining the tritium atoms from the gas species;

iv) to enrich tritium and deuterium and to discharge protium (H_2);

v) to store isotopically pure deuterium and tritium in uranium beds for further re-use;

vi) to re-inject deuterium and tritium into the torus.

Processing of Tritium in the AGHS

Normal pumping of the torus is undertaken by the Cryogenic Forevacuum (CF) system which consists of six separate cryo-pumps. All gases except helium are pumped by cryocondensation at 4K. Four cryopumps contain charcoal which pumps helium by cryoadsorption.

A controlled warm-up of the cryopump allows the separation of the pumped gases into the streams of i) helium, ii) six hydrogen molecules, and iii) impurities. Helium and the impurities are sent to the Impurity Processing (IP) system where small residual amounts of hydrogen and tritiated gas species are oxidised to water by the addition of small batches of oxygen in the presence of a platinum based catalyst. Hydrogen and tritium are re-gained by cracking water on warm uranium beds. The residual gas left contains mainly helium, CO and CO_2 and can be discharged via the Exhaust Detritiation (ED) system.

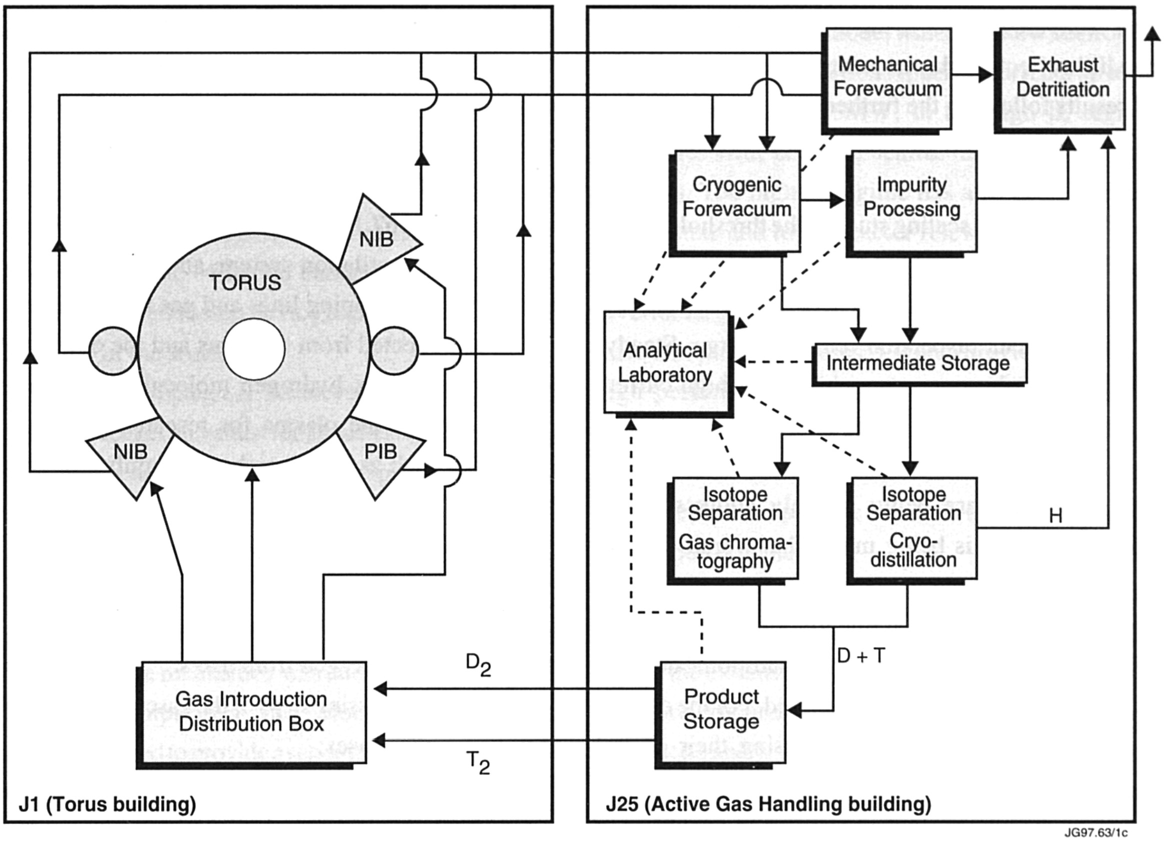

Fig.167: Schematic of the Active Gas Handling System

The hydrogen from Cryogenic Forevacuum and Impurity Processing is sent to the Intermediate Storage (IS) system for temporary storage prior to their injection into one of two isotope separation systems. Intermediate storage consists mainly of four JET uranium beds (U-beds) which are located in an evacuated secondary containment. JET U-beds can contain up to 4.284kg of uranium and can store up to 27moles or 605NL of hydrogen if loaded fully.

Gases (hydrogen) from intermediate storage can be sent via two feed lines to the Cryogenic Distillation (CD) system. Three product lines exist where the products (protium, deuterium, tritium) can be withdrawn with very high purity. For the protium (H_2) product the contamination level of tritium is in the low ports per billion (ppb) range, which makes direct discharge of this gas into the environment possible. The deuterium and tritium products are sent to the Product Storage (PS) system.

Displacement gas chromatography (GC) is used to gain tritium and deuterium from the six hydrogen molecules. The packing material is palladium which shows a large isotopic effect of the solubility of protium, deuterium and tritium. It is a batch process; at the end of every run the hydrogen molecule (H_2) which has the highest affinity to palladium has to be desorbed. This is done by heating the columns to about 200°C.The deuterium and tritium products are sent to the Product Storage (PS) system.

The isotopically pure gas products of cryogenic distillation or gas chromatography are collected and stored in U-beds of the Product Storage (PS) system. In the case of the U-beds, in-situ determination of the tritium inventory can be performed by quasi-adiabatic calorimetry. In addition, the gas content of the U-beds can be determined by gas desorption into 100ℓ or 700ℓ reservoirs. Deuterium and tritium are then supplied from the product storage system via the Gas Introduction (GI) system to the various users: NIB Octant No.4, NIB Octant No.8, and GIM15.

The purpose of the Mechanical Forevacuum (MF) system is to pump the torus and NIB cryopumps from atmosphere, to pump the torus and the NIB cryopumps during normal operation when Cryogenic Forevacuum is not available, to supply the necessary backing pressure for the torus turbopumps during helium glow discharge, and to discharge gases from the various AGH subsystems via the Exhaust Detritiation (ED) system. Almost all gases (except the protium product of the cryogenic distillation system) are sent through the exhaust detritiation system before their discharge into the environment. Also in case of incidents such as a window rupture on the torus, the air from the torus is pumped into the exhaust detritiation system and detritiated during the once-through clean-up process.

The exhaust detritiation system is a conventional tritium removal system where tritium and tritium containing gas species are oxidised to water. The water is trapped on one of three dry molecular sieves arranged in a parallel configuration. Wet molecular sieve beds are regenerated by heating, the desorbed humidity is collected in coolers and finally stored in drums for disposal or reprocessing.

The Analytical Laboratory is connected via small bore pipe work to most other subsystems of the AGHS. In this way samples from almost all other subsystems can be analysed by the three analytical techniques available in Analytical Laboratory:

i) analytical gas chromatography;
ii) mass spectroscopy (omegatron and quadrupole);
iii) ionisation chambers.

In addition, the cryogenic distillation product streams of protium and deuterium are analysed by sensitive katharometers. A typical chromatogram for a protium-deuterium-tritium gas mixture is shown in Fig 168.

Commissioning of the AGHS

The commissioning of the AGHS plant was performed in three steps:

i) Inactive commissioning: the performance of the sub-systems was checked with inactive gases, the functioning of tritium specific equipment was tested with gamma sources wherever possible;
ii) Trace tritium commissioning: trace tritium commissioning was performed with the tritium gas used during the first PTE experiment in 1991 and stored in U-beds. The total tritium amount was about 30TBq (800Ci or 0.08g);
iii) Full tritium commissioning: full tritium commissioning was performed with about 3g of tritium supplied in an Amersham transport U-bed.

Inactive Commissioning

Some systems (eg cryogenic forevacuum, gas introduction, gas distribution, and partly mechanical forevacuum), are still in the phase of inactive commissioning. Trace tritium and full tritium commissioning with these systems will not be performed separately because these systems do not contain any tritium specific equipment and these systems can be considered as buffer systems between the AGHS and the torus. These systems will see the first tritium during the 1% tritium gas mixture shots at the beginning of DTE1 and will then be progressively commissioned with tritium during DTE1.

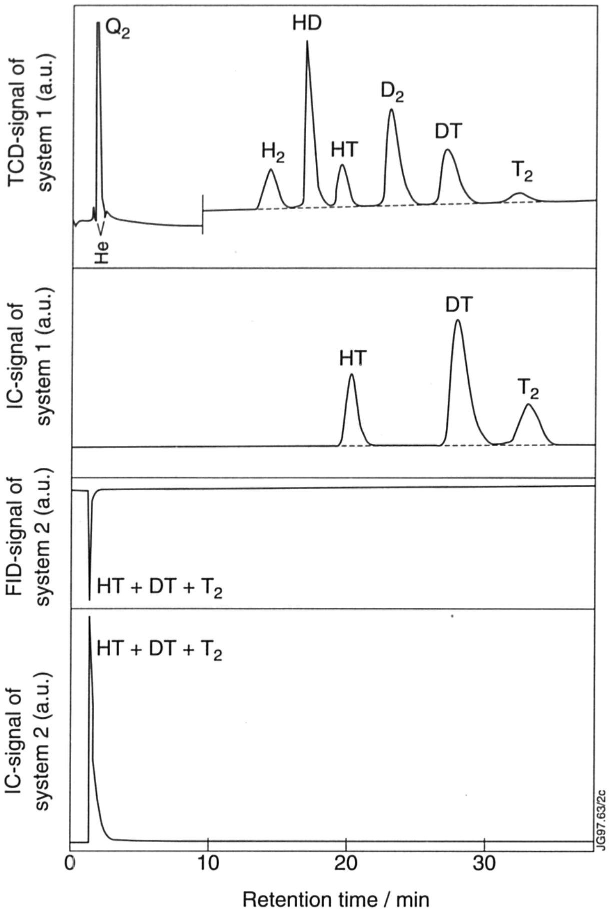

Fig.168: A typical chromatogram for protium-deuterium-tritium gas mixture

Mechanical forevacuum and cryogenic forevacuum were used to provide the necessary backing pressure for the torus turbo pumps for a test of about one week. Both systems worked very well, permitting torus operation to be performed as usual. The AGHS pumping systems coped with an unintended warm-up of the divertor cryopump. The four pumps of mechanical forevacuum have been demonstrated to supply enough pumping speed during helium glow discharge cleaning. Deuterium gas is now routinely supplied to the Neutral Beam Injection (NBI) systems through the gas introduction system.

Trace Tritium Commissioning

Trace tritium commissioning was performed with the tritium gas collected during and after the Preliminary Tritium Experiment (PTE). The tritium gas mixture was moved through the various systems in the following sequence: analytical laboratory, product storage, intermediate storage, impurity processing, gas chromatography, analytical laboratory, cryogenic distillation, gas chromatography.

The main purpose of the trace tritium gas commissioning was to check the leak tightness of the whole pipework and to test tritium specific equipment (ionisation chambers, flow proportional counter detectors, flame ionisation detector, etc) in the presence of tritium.

The trace tritium commissioning was successfully completed in June 1996. Details of the trace tritium commissioning results for the impurity processing, cryogenic distillation and gas chromatography systems are shown below.

Impurity Processing System

The performance of the recombiner and the cold trap was tested with trace tritium gas and methane added to the helium in the 2m^3 reservoir of impurity processing.

The tritium activity was monitored via the ionisation chamber in the tank. A reduction in activity demonstrated the oxidation of the tritiated gas species with oxygen (which was added in small batches to avoid explosive gas mixtures) to water and the subsequent trapping of the water (with the activity) in the cold trap. The tritium activity in the tank was finally so small that discharge of the gas in the process lines to exhaust detritiation could be permitted.

The cold trap was warmed up and the water vapour was allowed to enter a heated uranium bed. The hot uranium was oxidised by the water vapour and the generated hydrogen gas was absorbed in a second cold uranium bed. This process worked well, but has the disadvantage that uranium is consumed during the cracking process of the water. Exchange of a fully oxidised uranium bed with a fresh uranium bed is possible, but is there sufficient capacity to permit DTE1 to be performed without U-bed exchange.

Cryogenic Distillation System

The cryogenic distillation system was filled with the gas amount stored in the four uranium beds of the gas collection trolley used during PTE and cooled down to about 18K. The various operating modes were tested.

Small sample batches were taken via the product lines and analysed with the Analytic Laboratory diagnostics. The main results were that the tritium concentration in the H_2 product was about 3ppb and in the D_2 product about 18ppb and that the maximum tritium concentration in the T_2 product was about 4% DT in almost pure D_2 gas. Higher tritium concentrations can only be achieved with higher tritium inventory in the cryogenic distillation system (the cryogenic distillation system was designed for an inventory of about 33g of tritium, but the tritium amount used for the tests was only about 0.08g).

Finally the cryogenic distillation-system was operated with the two feed-lines and the three product-lines open and the system operated on a continuous feed and extraction mode. A good balance of the total gas amount in the cryogenic distillation system was achieved using flow meter totalisers which means that overfilling of the system can be avoided. Before warming up the system, tritium from the bottom of column No.3 was extracted. All the gas left in the cryogenic distillation system could be discharged within the daily discharge limits.

Gas Chromatography System

In the first separation runs the whole column was filled with the trace tritium gas (no eluant gas was used). A clear and sharp peak was seen by the ionisation chamber mounted next to the column exit and a small peak in the katharometer signal. These signals were large enough to check the gas chromatography diagnostics. The tritium concentration in the peak was estimated to be about 20% tritium in deuterium gas.

After the cryogenic distillation runs had been performed, about 20NL of cryogenic distillation enriched tritium-deuterium gas mixture were injected into the gas chromatography columns and displaced with eluant gas (protium) through the columns. This time the katharometer signal showed large tritium peak as well as the ionisation chamber. The tritium concentration in the peak was estimated to be about 90% tritium in deuterium gas. These runs showed clearly that the diagnostics were working but the tritium inventory was still too small to check the correct opening and closing of valves with the various products and interfractions (see Fig.169).

Gas Collection Trolley

A further by-product of the trace tritium commissioning was that the total gas inventory in the four U-beds of the gas collection trolley used during PTE was moved into the AGHS and processed. Most of the inactive gases deuterium and protium were discharged and a large part of the tritium activity was stored in an Amersham bed. In this way four further U-beds were made available for further storage.

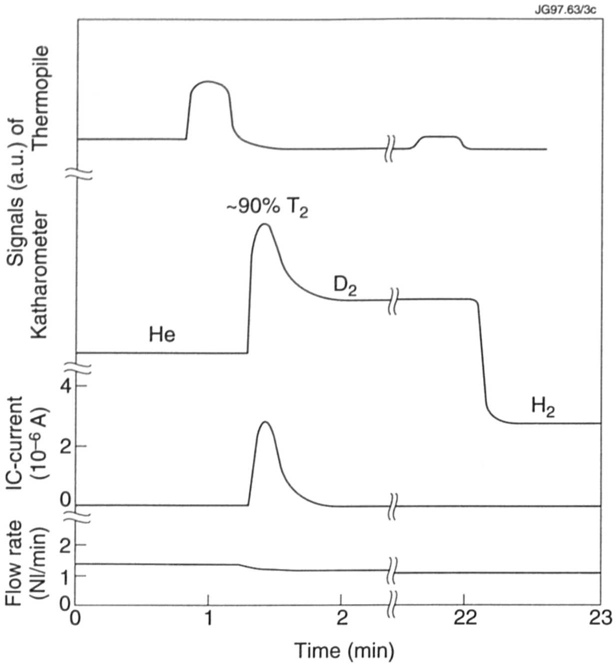

Fig.169: Output of diagnostics on the Gas Chromatography System during trace tritium commissioning

Full Tritium Commissioning

Full tritium commissioning commenced in September 1996 with 3g of tritium.The tritium gas was supplied in an Amersham U-bed and transferred to the AGHS in the Analytical Laboratory make-up box.The almost 100% pure tritium gas was moved through the AGH sub-systems: analytical laboratory, product storage, intermediate storage, gas chromatography, analytical laboratory.

The purpose of the full tritium commissioning was to check the leak tightness of part of the pipe work with pure tritium which gives a leak sensitivity 2000 times higher than with the trace tritium gas and to check various diagnostics in the presence of pure tritium, and to test the gas chromatography with bypassed D_2/T_2 mixtures.

Product Storage System

The 3g of tritium were moved through the PS-T_2 U-beds to check the in-situ calorimeters. The U-bed calorimeters responded as expected, but temperature changes of the room and of the nitrogen gas used for cooling and the thermal history of the U-beds influenced the results. The long waiting/cooling times (some days) were necessary after heating a U-bed to high temperatures to achieve thermal stability. The averaged accuracy achieved was ±8%.

Gas Chromatography System

Deuterium was added to 1g of tritium to achieve a gas mixture of about 20% tritium-80% deuterium. This gas was injected into the four columns of the gas chromatography system which were filled with helium and displaced with eluant gas (protium). The results are shown in Fig 170. A clear plateau for the enriched tritium is seen in the katharometer as well as the ionisation chamber signals. The interfractions are sharp. It is also clearly visible that the interfraction from T_2 to D_2 is not as sharp as the one between D_2 and H_2. This is due to the fact that it is more difficult to separate tritium from deuterium than deuterium from protium with a palladium filled column. With this gas mixture, the correct switching of the valves to cut only tritium and deuterium was checked. Valve switching is now performed fully automatically. The protium concentration in the tritium gas produced with the gas chromatography system was finally lower than that in the T_2 gas supplied to JET.

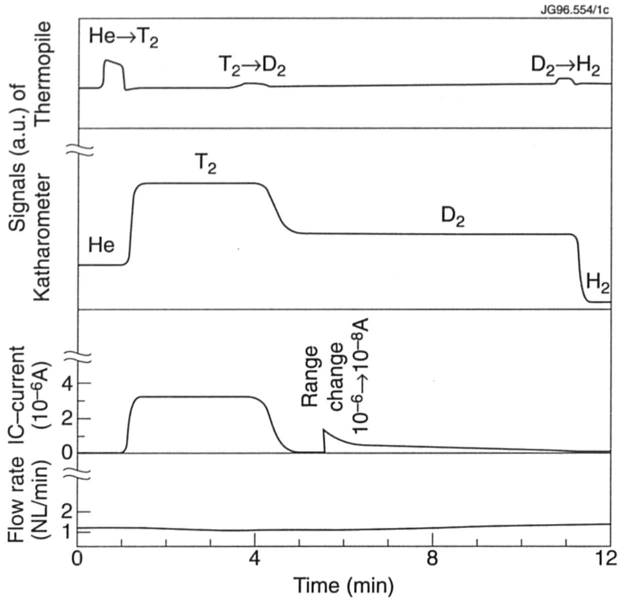

Fig.170: Output of diagnostics on the Gas Chromatography System during full tritium commissioning;

Analytical Laboratory

The various diagnostics were checked with the almost pure tritium and performed satisfactorily.

Developments

Water Detritiation

Trace and full tritium commissioning has shown that to minimise atmospheric discharges of tritium using the exhaust detritiation system, significant quantities of tritiated water may be generated. To provide an alternative to the current route for disposal, a system to recover tritium from water with a capacity of ~10 tonnes per year is under development.

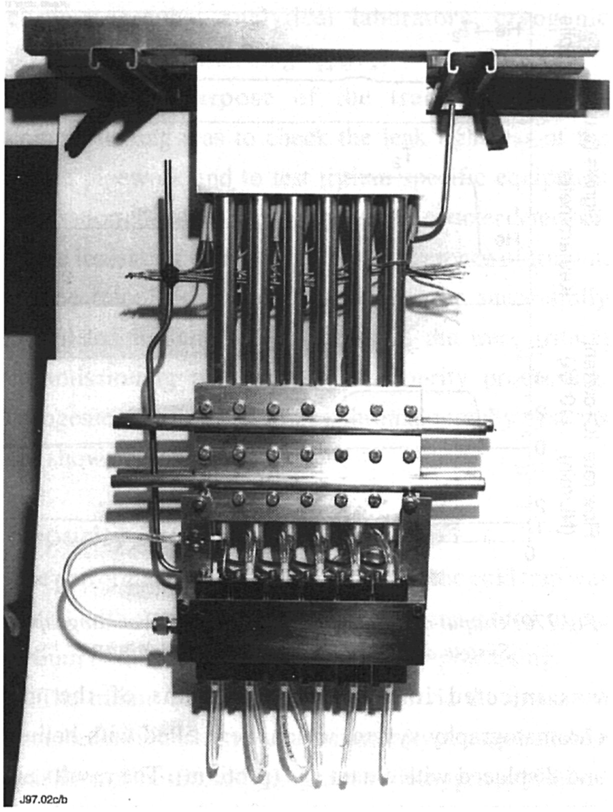

Fig.171: Six-stage vapour-phase catalytic exchange prototype for a water detritiation system

Tests on a prototype (Fig 171) for a 6-stage Vapour Phase Catalytic Exchange (VPCE) have shown promising results: this device is capable of reducing deuterium concentration in an H_2-D_2 mixture in exchange with an equimolar flow of H_2O by a factor of 170. Tritium removal, being more efficient is expected to result in detritiation factors of ~4000 in the same six-stage configuration. The test system, designed for water flows of 0.22kg/h, can be readily scaled up to 2.2kg/h required for a plant capable of processing 10 tonnes of tritiated water per year.

Preparations for D-T Operation

The scientific plans for D-T operation during the DTE1 period were presented in the 1995 Progress Report. These were based on the report of the Working Group established under the Chairmanship of Dr A Gibson. These plans have not been changed significantly since that time.

The experimental campaign in deuterium during 1996 had an objective of undertaking the necessary preparatory experiments. The main results of the experimental campaign is that the types of discharges for carrying out the broad objectives of DTE1 have been established, but the details of the experimental campaign will rely on the results and analysis of experiments carried out at the end of 1996 and the beginning of 1997, to assess the effects of changes carried out to the divertor gas bypass structure and inner wall modifications in the Autumn 1996 shutdown.

The DTE1 experiments will take place in early 1997. The major work undertaken for DTE1 during 1996 was on the technical level, with extensive work on equipment preparation, safety assessments and operating procedures.

JET was designed from the outset for D-T operation, and, consequently, the major design provisions such as the biological shield, the double wall vacuum vessel, and the provision of remote handling features on critical components, are an integral part of the installation. Furthermore, the Project has experience in carrying out D-T experiments gained during the first experiments with tritium (PTE) in 1991.

The technical preparations required for DTE1 consisted essentially of bringing existing systems to full tritium readiness and producing the necessary documentation to fulfil JET's obligation for tritium operation to satisfy the UKAEA (the Host Organisation) that the arrangements conform to the standards in force in their own organisation.

The main areas in which work has been required are:

- Preparation of the Safety Case;
- Completion and commissioning of the tritium plant;
- Completion of installed systems to full tritium specification;
- Commissioning of tritium related safety systems;
- Establishing written operational procedures for tritium related systems;
- Training of staff for operation of tritium related systems.

The status of these main areas of work has been described in the earlier sections of the report (in the chapter on Fusion Technology Systems).

Studies for Machine Performance Enhancement

In the light of the approved extension to the end of 1999, studies have been undertaken on possible enhancement options of some JET subsystems. In particular, it has been considered that, the toroidal magentic field could be increased from the present 3.45T to a value of 4T. Improvements to the neutral beam injectors from 80kV, 60A to 120-140kV at 60A operation were also considered

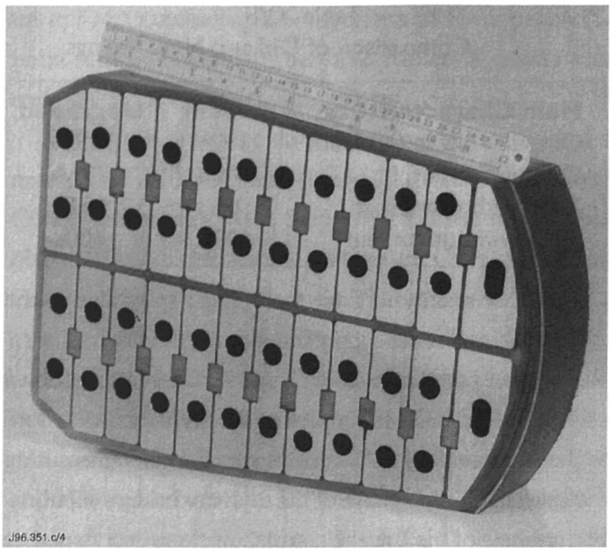

Fig.172 : Slice cut out of TF coil 3.1 for inspection and for test sample production

and these were described in some detail in the 1995 Progress Report.

Upgrading Toroidal Field to 4T

Mechanical Tests on Fibre-epoxy Insulation

Tests on small shear samples cut from TF Coil No.3.1 (Fig.172) were made at ENEA Association, Frascati, Italy. These showed an average shear strength of 38 MPa with a standard deviation of 8 MPa.

Samples cut from the same coil were also tested by JET using a different design of sample, which allowed the key to be tested (Fig 173). These tests show similar results for the basic insulation and also show the effect of the key in both static and fatigue conditions.

Inspection of Coil Insulation

When TF Coil No.3.1 was cut for preparation of the shear test samples, the insulation was also inspected at ENEA and JET. This inspection showed that the coil had been well impregnated and that the insulation was in good condition. There was no sign of deterioration due to ageing or stress, although, as this coil had suffered a water leak and internal short circuit, there was damage due to water and carbonisation due to short circuit currents.

Forces on Mechanical Structure Teeth

The out of plane forces acting on the TF coils were measured using flux loops attached to the coils. These loops measured the poloidal flux crossing the coil. This enables the average perpendicular field to be calculated, which can be multiplied by the TF coil current to give the magnetic force in the region of the flux loop. Discrepancies between these measurements and magnetic calculations (with the MAXFEA code) were investigated, and found to be basically due to the ferromagnetic effect of the teeth. Consequently the flux values given by the magnetic loops is approximately correct and corresponds to a reduction of 10% of the stresses in the coils predicted by magnetic calculations.

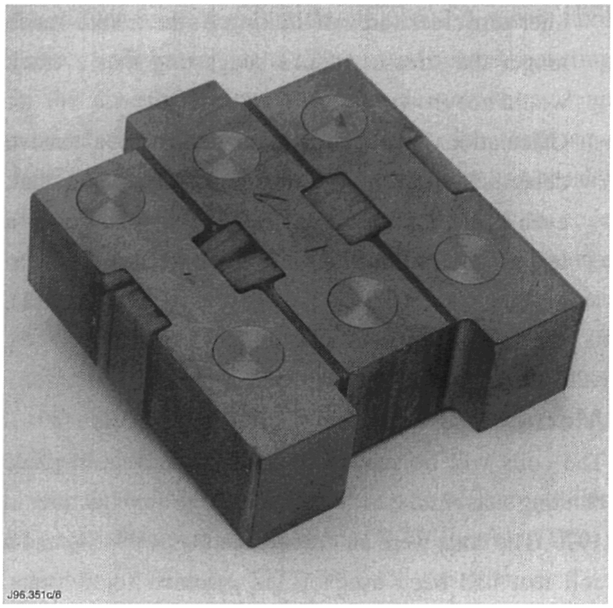

Fig.173: Samples from TF Coil 3.1 for shear tests including the interturn keys

Stress Analysis of TF Coils in Collar Region

The allowable force on the collar tooth is based on a calculation made in 1988, which showed that 50 tonnes collar tooth force corresponds to 17MPa peak or <15MPa average stress in the coil. This calculation has been repeated using a much more detailed model, where the insulation is modelled explicitly. (In 1988, average properties for a copper and insulation mixture were used.). This new calculation has shown that the peak shear stress is less than previously calculated. The value achieved depends on the shear modulus of the insulation, which has been reassessed on the basis of recent tests. The 1988 results can be reproduced with this new model by reverting to "average" properties for all elements. This new result is significant in that it shows increased factors of safety over previous assumptions.

Crack Growth and Effects of Delamination

Two assessments have been made:

- The stresses at the end of an inter-turn crack in the collar region have been calculated to determine whether inter-turn cracks are self limiting. As the crack is made longer the stresses reduce suggesting that a crack would not grow;

- Calculations have been made on the effect of extensive delamination in the collar region. These show that, even if the coil was completely delaminated over a length of 200 mm (i.e. only the inter-turn key was available to transmit shear forces between conductors), stresses and deflections would be acceptable.

Mechanical Tests on Complete Coils

The coils will be subject to in-plane and out-of-plane bending tests similar to those made by the manufacturer in 1979. The coils were an unused spare coil (No. 4) and a coil that had been used on the machine for 7 years, production (No. 23). The coils will be subjected to in-plane and out-of-plane bending. Stresses and deflections for all proposed tests have been calculated to determine the forces required to give suitable stress levels (i.e. significant but not excessive).

Upgrade of TF Static Units for 4T Operation

To further enhance the performance of the JET, it has been decided to upgrade the toroidal field power supplies to allow a TF field up to 4T for ~10s flat top. Major engineering work started in 1996 to upgrade the voltage and current ratings of two Toroidal Field Static Units so that the required level of field could be reached. The comparison between the present and future of characteristics of the static units are shown in Table XVI.

Table XVI
Comparison of Old and New Ratings

Main Characteristics	Present	Upgraded
Output Voltage (no load)	2192V	3055V
Output current, I_n	67kA	78kA
Time with current at I_n	20s	14.8s
Time without current	600s	600s

The main actions for the upgrade are the following:

- replacement of the four Static Unit transformer units by four new transformer units;
- modifications of the transformer pens (civil work consisting in the enlargement towards the north of the transformer pens and modification of the plinth supporting the new transfomers);
- replacement of AC/DC thyristor converter fuses (for the protection of the rectifier supply AC cables and fuses for the individual protection of the rectifier thyristors);
- implementation of a combined snubber consisting of the addition of an individual snubber across each thyristor as protection against voltage spikes generated when the thyristors are forced to turn-off, and upgrade of the existing "bucket" type snubber to match new Static Unit voltage ratings (used in combination with the individual snubber mainly to limit the voltage spike due to the switching-off the supply transformer);
- upgrade of the water cooling unit flow used to cool down the copper busbars supporting the thyristors;
- replacement of AC current transformers measuring current on each phase of the thyristor bridges input;
- upgrade of the Local Control Cubicle to accommodate the new additional signals.

Together with the water cooling upgrade, the combination of the existing upgraded "bucket" snubber and new individual snubbers will enable to keep in place the existing thyristors and save the cost of replacement.

At the end of 1996, the general progress of the engineering work was:

- parameters for the new transformer unit had been determined, the technical specifications issued and the Contract had been been awarded;
- the transformer pens had been enlarged during the summer 1996 shutdown, and modification of the plinth will be carried out during the summer of 1997 once the existing transformers are removed;
- the design of the combined snubber has been completed and the different components are ready to be ordered;
- the replacement ACCTs have been defined and ordered in November 1996.

The upgrade of the water cooling unit and of the local control cubicle will be carried out at the beginning of 1997 and the full installation should be completed during the 1997 summer shutdown.

Future Plans

The JET Programme was divided into phases governed by the availability of new equipment and fitting within the accepted life time of the Project. Phase I (Ohmic Heating Studies) was completed in September 1984, and Phase II (Additional Heating Studies) in October 1988. Phase III (Full Power Optimization Studies) ended in February 1992. The scientific aims of Phase III were to obtain maximum performance in limiter configuration (currents up to 7MA) and to optimize X-Point Operation (currents up to 6MA) including a comparison of H-modes in X-point configuration using beryllium (lower X-point) with carbon (upper X-point) dump plates.

JET future plans are dominated by the insertion of a new phase of the Project (Phase IV: Pumped Divertor Configuration and Next-Step Oriented Studies). This phase is subdivided into a Divertor Characterization Plasma and an ITER Support Phase. This new phase extended the lifetime of the Project up to the end of 1996.

The Pumped Divertor Characterisation Phase began in February 1994 and ended in June 1995. During this period, the Mark I pumped divertor was very effective and allowed a broad-based and highly ITER-relevant research programme to be pursued. It had addressed the central problems of the ITER divertor: efficient dissipation of the exhausted power, control of particle fluxes and effective impurity screening, using both carbon fibre composite (CFC) and beryllium as the power handling material.

During this phase, the plasma current was increased to 6MA (a world record in an X-point configuration), the total heating power to 32MW, plasma stored energy to 13.5MJ (the highest energy recorded in a JET plasma) and the neutron rate to a new JET record in deuterium of 4.7 x 10^{16} neutron/s (comparable to the best achieved prior to the installation of the pumped divertor and was achieved even though the plasma volume was 20% smaller).

The campaign with CFC tiles on the first-wall was successfully completed in mid-March. The CFC tiles were then removed and replaced by beryllium, and experiments were performed to assess the performance of beryllium as a divertor target tile material and to compare it with CFC. In response to a request from the ITER Joint Central Team, beryllium melting was induced at ITER-relevant heat fluxes to see whether a protective radiative shield was established.

In June 1995, installation of the Mark IIA divertor and the modification of the ICRH antennae was started, and was completed in March 1996.The 1996 experimental campaign concentrated on specific ITER-relevant issues related to the more closed Mark IIA divertor and, due to their importance for predicting ITER's ignition margin and fusion power output, the scaling of the H-mode threshold power and the energy confinement. In addition, the preparation of high performance scenarios for DTE-1 was a high priority of the campaign.

In 1996, the Mark IIA Pumped Divertor behaved as expected. It offered improved power handling over the Mark I divertor, pumped the plasma 2-3 times more rapidly and showed signs of increased neutral recycling in the divertor region. The latter feature showed up particularly well in the detachment of the divertor plasma from the target at significantly lower main plasma density than Mark I configuration, in agreement with code predictions. Closure of the divertor to reduce the leakage of neutrals from the divertor to the main plasma has proved to have little effect on plasma purity or performance. The initial results following the further closure of the bypass leaks did not lead to significant differences in plasma behaviour.

Preparations were also continuing on various systems in preparation for the next period of D-T operation (DTE1) scheduled for early 1997, and for the Remote Tile Exchange shutdown after DTE1.

Objectives in support of ITER

The extension of JET to the end of 1999 was officially approved in mid-1996. The purpose of the extension is to provide further data of direct relevance to ITER, especially for the ITER-EDA, before entering into a final phase of D-T operation. In particular, the extension:

i) will make essential contributions to the development and demonstration of a viable divertor concept for ITER, and
ii) carry out experiments using D-T plasmas in an ITER-like configuration, which will provide a firm basis for the D-T operation of ITER;

while allowing key ITER-relevant technology activities, such as the demonstration of remote handling and tritium handling, to be carried out.

Divertor studies

The divertor must fulfil three main functions:

(i) exhaust plasma power at acceptable erosion rates;
(ii) control plasma purity; and
(iii) exhaust helium "ash" and provide density control.

For ITER, successful divertor operation must also be compatible with high confinement (H-mode) operation with Edge Localised Modes (ELMs).

Erosion can be reduced by decreasing the plasma temperature at the target plates which can be achieved with high density and high recycling near the target plates. However, the exhausted plasma power conducted to the targets in this high recycling regime is not reduced and must be distributed over a large surface area. To some extent, this can be achieved by inclining the targets in order to project a larger surface area to the conducted heat flux which flows along the magnetic field.

An alternative approach is to reduce the conducted power to the targets by atomic physics processes (charge exchange, hydrogen and impurity radiation) in the divertor channel. These power losses can be enhanced byseeding the divertor plasmawith impurities which must then be retained in the divertor by plasma flows. This requires sufficient pumping and recirculation of the plasma in the divertor. Of course, the divertor conditions must not affect adversely the main plasma performance and this requires that the divertor plasma must be as decoupled as much as possible from the main plasma. In particular, the leakage of neutrals from the divertor to the main plasma must be reduced as far as possible. Such "closure" of the divertor can be achieved by introducing baffle structures at the entrance to the divertor or maintaining a sufficiently dense plasma to attenuate neutrals within the divertor (plasma "plugging"). The geometry of the divertor is thus important in providing the necessary degree of closure, and several different divertor configurations must be tested.

The JET divertor programme is based on three divertor configurations (Mark I, Mark IIA and an ITER-specific Mark IIGB) which it is planned to test sequentially in the period up to the middle of 1998 (end of the ITER-EDA).

The relatively "open" Mark I divertor which was used for the 1994/95 Experimental Campaign was replaced during the 1995/96 shutdown by the Mark II divertor, which comprises a common base structure capable of accepting various target assemblies. This allows the divertor geometry (degree of closure and target configuration) to be varied and its effect on divertor and main plasma performance to be studied.

Due to the need to test various divertor geometries for ITER, the Mark II divertor has been designed so that its target assembly can be exchanged by remote handling, but it does not lend itself to the use of active cooling.

The first target assembly (Mark IIA), which is being used for the 1996/97 experimental campaign, is a moderate "slot" divertor which is significantly more closed than the Mark I divertor. Mark IIA allows operation under a wide range of plasma configurations and conditions and makes high power, high current operation possible on both the horizontal and vertical target plates.

The second target assembly (Mark IIGB) will be a deep divertor with a well baffled entrance. The aim of the Mark IIGB configuration is to distribute the exhaust power over the length of the divertor. This is assisted by free recirculation of neutrals below the baffle on one or both sides of the divertor plasma legs. Recirculation also allows greater flows, better pumping and better impurity retention in the divertor.

The various options for an ITER divertor will be studied in a timely and co-ordinated way by the investigation of these three generically different divertor configurations. This is designed to lead to a solution giving compatibility between power exhaust, purity control and high performance (H-mode). A major part of the strategy is the development and validation of numerical codes for the edge and divertor plasma so that they may be used for extrapolation to the geometry, dimensions and operating conditions of ITER. The experimental results from the three JET divertor configurations, together with those from smaller tokamaks and model calculations, will allow the ITER divertor design to be validated. This should be possible by the middle of 1998, in line with the ITER-EDA schedule.

D-T Plasma Studies

JET performed the first magnetic confinement experiments using a mixture of 10% tritium in deuterium in 1991. These experiments produced significant fusion power (peaking at 1.7MW and averaging 1MW over 2 seconds). The US tokamak TFTR has since produced some 10MW of fusion power, using 50% tritium in deuterium, and has shown that, with their particular operating conditions and geometry, D-T plasmas have more favourable confinement properties than deuterium plasmas (isotopic effect). Two further periods of D-T operation (DTE-1 and DTE-2) are foreseen for the JET programme to the end of 1999.

The physics mission of DTE-1 will have as its main objective study of the isotopic effect on confinement scaling and H-mode threshold power in D-T plasmas. These will be the first experiments of this kind in the geometry appropriate to ITER and including a divertor, and will be essential to determine whether the D-T performance improvements observed in the circular cross-section TFTR tokamak are also realised in the D-shaped cross section of JET, and ITER. Furthermore, the H-mode threshold power in D-T plasmas will be determined for the first time in these JET experiments. This will allow more accurate assessments of the ignition margin and the heating requirements for ITER.

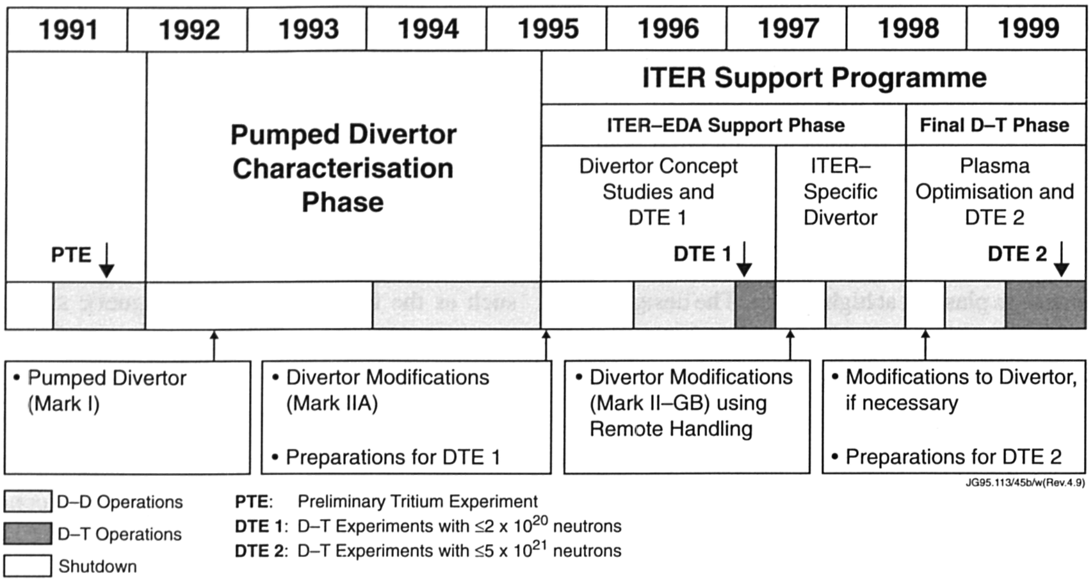

Fig.174: JET Programme to end of 1999

In addition, JET's capability for long pulse operation and impurity control should permit some 10MW of fusion power for several seconds (typically with 50% tritium). The alpha-particle heating will then make a significant contribution to the plasma power balance and this will allow the effects of alpha-particle heating (confinement and thermalisation of alpha-particles and stability of toroidal Alfven eigenmodes in the presence of alpha-particles) to be studied and experience gained for ITER. The operating conditions foreseen for ITER, namely long pulse ELMy H-mode plasmas, could also be studied in D-T, albeit at reduced levels of fusion power. These results could provide important information for the design of the ITER divertor.

As well as a physics mission, DTE-1 will also have a technology mission to carry out and demonstrate key ITER and reactor-relevant technologies, such as tritium handling and processing, remote handling and control, and heating systems operating in D-T. Specifically, DTE-1 will provide a first test of a large scale technology for processing tritium through an operating tokamak.

Operation in TFTR and detailed preparations for DTE-1 on JET have shown that a longer phase of D-T operation than DTE-1 is needed for a thorough study of the physics and technology of D-T plasmas. This is provided for by DTE-2, with substantial alpha-particle heating, capitalising on the performance improvements achieved in the preceding experimental campaigns with deuterium. This further period of D-T operation will also provide a full evaluation of the technology of processing tritium in support of an operating tokamak.

Programme Plan

The programme to the end of 1999 is illustrated in Fig.174. It covers all the agreed objectives for the JET extension. Its main aspects are summarised below.

The first period of D-T operation (DTE-1) is scheduled for early 1997, following an intervention to make the necessary final adjustments for D-T operations. The content and duration of DTE-1 has been defined to take account of the developing needs of ITER and the experience gained in JET and TFTR. The extent of DTE-1 is a compromise between studying essential D-T physics for the ITER-EDA and minimising the delays in the experimental programme that could result from certain component failures during DTE-1.

The physics mission of DTE-1 as defined above will last about four months and could produce up to $2x10^{20}$ neutrons. In this case, the activation of the JET vessel would prevent normal manned in-vessel intervention for up to one year after D-T operation. However, in-vessel components which are accessible could be repaired using the remote handling equipment developed for the Mark IIGB target assembly change. This equipment has demonstrated a very high level of reliability and is now fully proven for the planned remote handling tasks. Its versatility and ability to perform a wide variety of other tasks has also been demonstrated, provided access can be obtained. Normal manned access for ex-vessel repairs will be possible after DTE-1.

In a five month shutdown planned to commence in June 1997, the Mark IIA target structure will be exchanged for a second target structure, the ITER-specific Gas-box divertor (Mark IIGB). The exchange will be made by remote handling without manned intervention. This remote handling operation will demonstrate, for the first time, one of the central technologies required both for ITER and for a fusion reactor.

During the remainder of 1997 and the first half of 1998, the Mark IIGB divertor will be tested experimentally with deuterium plasmas at high power. The design of the Mark IIGB provides flexibility to modify the target geometry with relative ease. The Programme Plan provides for two target geometries for Mark IIGB, together with a septum which may, or may not, be included to limit the communication between the inner and outer divertor legs and to absorb energy from energetic neutrals and photons.

Possible ways of improving JET's performance which are under consideration include increasing the toroidal magnetic field (to 4T), increasing the heating power (by ≈30%) and overcoming the performance limitations due to MHD instabilities.

Final Phase of D-T Operation (mid-1998 to end-1999)

A four month shutdown in 1998 will permit any necessary modifications to the divertor and final preparations for a further period of D-T operation (DTE-2). Normal manned in-vessel interventions will again be possible in this shutdown. The Mark IIGB divertor target structure is less flexible than Mark IIA with respect to the variety of equilibria which can be accommodated. Furthermore, its power handling capability in attached divertor operation is somewhat lower. Therefore, it may not be compatible with the highest plasma performance obtained in JET, such as the low density, high magnetic shear, hot-ion H-mode of operation. This must be tested experimentally and, if it proves to be the case, it will be possible to re-install Mark IIA (for DTE-2) following the completion of the Mark IIGB studies. During late-1998 and early-1999, the experimental programme will continue by optimising plasma performance in deuterium in preparation for DTE-2.

DTE-2 is scheduled to take place during the remainder of 1999. DTE-2 experiments could last up to eight months and could produce up to 5 x 10^{21} neutrons. Actual neutron production, within this upper limit, will be reassessed in the light of the experience with D-T operations on JET and TFTR. Every effort will be made to reduce this upper limit, while still satisfying JET's role in supporting ITER and the world fusion programme. In this way the activation of the JET structure would be kept as low as possible compatible with fulfilling the required objectives.

Appendix I

JET Task Agreements 1996

Title	*Association*	*JET Responsible Officer*
RF HEATING DIVISION		
Wave induced current drive experiments on JET	EUR-CEA, Cadarache, France	C. Gormezano
RF transport code development	EUR-IPP Garching, Germany	C. Gormezano
Fast ion and electron kinetic effects on JET	EUR-UKAEA Culham, UK	C. Gormezano
Confinement studies in profile control experiments	EUR-ENEA Frascati, Italy	F.X. Soldner
Tokamak Optimisation	EUR-UKAEA Culham, UK	C. Gormezano/ P.Thomas
Study of MHD Limits of JET relevant current and pressure profiles	EUR-NFR Sweden	F.X. Soldner/ W. Kerner
EXPERIMENTAL DIVISION I		
Plasma wall interactions	EUR-IPP Garching, FRG	P.E. Stott
Neutron production related physics and associated diagnostics	EUR-NFR Sweden	P.E. Stott
Turbulent studies in the divertor and scape-off layer regions in the JET tokamak	EUR-CIEMAT Spain	G. Matthews

Title	*Association*	*JET Responsible Officer*
Neutron production related physics	EUR-UKAEA Harwell, UK	P.E. Stott
Microwave reflectometry	EUR-CFN/IST Lisbon, Portugal	P.E. Stott
Neutron production related physics and associated diagnostics	EUR-ENEA Frascati, Italy	P.E. Stott
Work on collector probes	EUR-NFR Sweden	P.E. Stott
EXPERIMENTAL DIVISION II		
Dynamics of ions and of neutral particles in tokamak plasmas	EUR-ENEA Frascati, Italy	R. Gianella
Impurity analysis and plasma diagnostics using spectroscopic measurements	EUR-NFR Sweden	P.R. Thomas
DATA ANALYSIS & MODELLING		
Plasma stability	EUR/UKAEA Culham, UK	W. Kerner
Modelling of anomalous transport and study of energetic particle collective effects	EUR-ENEA Frascati, Italy	A. Taroni
Transient transport analysis in JET	EUR-ENEA CNR-Milan, Italy	A. Taroni
Comparison between JET profile data and the predictions of a transport model based on ITG and trapped electron modes	EUR-NFR Sweden	J.P. Christainsen
MHD spectroscopy and stability	EUR-FOM The Netherlands	W. Kerner

Title	*Association*	*JET Responsible Officer*
OPERATIONS		
Alfven eigenmodes	EUR-CRPP Lausanne, Switzerland	J. Jacquinot
Feedback stabilization of disruptions	EUR-ENEA CNR-Milan, Italy	D.J. Campbell
The control of instabilities and disruptions	EUR-UKAEA Culham, UK	D.J. Campbell
Study of density evolution and recycling of JET plasmas during (pumped) divertor operation as a function of fuelling method and wall conditioning state	EUR-ENEA Frascati, Italy	G. Saibene
Scenario studies of plasma breakdown	EUR-ENEA CNR-Milan, Italy	P.J. Lomas
Geodesic curvature and enhanced confinement in JET	EUR-ENEA Frascati, Italy	P.J. Lomas

Appendix II

List of Articles, Reports and Conference Papers Published in 1996

1. The model and experimental basis for the design parameters of the JET divertor cryopump protection system including variations in divertor geometry and first wall materials.
   Ageladarakis P Papastergiou S Stork D Van der Beken H
   JET Joint Undertaking, October 1996 (JET Papers presented at the 19th Symposium on Fusion Technology (SOFT) Lisbon, Portugal, 16-20 September 1996). p.81. Report JET-P(96)44

2. The model and experimental basis for the design of the JET divertor cryopump protection system including variations in divertor geometry and first wall materials.
   Ageladarakis P Papastergiou S Stork D van der Beken H
   JET Joint Undertaking, September 1996 (JET Posters presented at the 19th Symposium on Fusion Technology (SOFT) Lisbon, Portugal, 16-20 September 1996). p.111. Report JET-P(96)45

3. Overview of magnetic diagnostics planned for ITER.
   Ali-Arshad S Stott P E Todd T and others
   Diagnostics for Experimental Thermonuclear Fusion Reactors: Proceedings of the International Workshop on Diagnostics for ITER, September 1, 1995, Varenna, Plenum Press, New York, 1996. p.71.

4. Plasma movement at ELMs in JET.
   Ali-Arshad S Edwards A Lingertat J Puppin S Wesson J
   JET Joint Undertaking, July 1996. (JET Posters presented at the 23rd EPS Conference Kiev, Ukraine, 24-28 June 1996). p.1. Report JET-P(96)30

5. Plasma movement at ELMs in JET.
   Ali-Arshad S Edward A Lingertat J Puppin S Wesson J
   JET Joint Undertaking, August 1996. (JET Papers presented at the 23rd EPS Conference on Plasma Physics and Controlled Fusion, Kiev, Ukraine, 24-28 June 1996). p.1. Report JET-P(96)33

6. The JET soft X-ray diagnostic systems.
   Alper B Dillon S Edwards A W Gill R D Robins R Wilson D J
   JET Joint Undertaking, 1996. (JET Papers presented at the 11th APS Conference on High Temperature Plasma Diagnostics, Monterey, CA, USA, 12-16 May 1996) p.1. Report JET-P(96)18

7. Sawtooth crashes at high beta on JET.
   Alper B Nave M F F Huysmans G T A Sips A C C
   21st EPS Conference on Controlled Fusion and Plasma Physics, Montpellier, 27 June - 1 July 1994, Contributed papers, Part I. European Physical Society, 1994. p.202.

8. Strong asymmetries in impurity distributions of JET plasmas.
   Alper B Edwards A E Gill R D Ingesson L C Romanelli M Wesson J Zastrow K-D
   JET Joint Undertaking, July 1996. (JET Posters presented at the 23rd EPS Conference Kiev, Ukraine, 24-28 June 1996). p.7. Report JET-P(96)30

9. Strong asymmetries in impurity distributions of JET plasmas.
   Alper B Edwards A W Giannella R Gill R D Ingesson C Romanelli M Wesson J Zastrow K-D

JET Joint Undertaking, August 1996. (JET Papers presented at the 23rd EPS Conference on Plasma Physics and Controlled Fusion, Kiev, Ukraine, 24-28 June 1996). p.11. Report JET-P(96)33

10. The MKII gas box divertor - a new design concept.
Altmann H Deksnis E Froger C Lawson S Lowry C Peacock A Pick M
JET Joint Undertaking, October 1996 (JET Papers presented at the 19th Symposium on Fusion Technology (SOFT) Lisbon, Portugal, 16-20 September 1996). p.1. Report JET-P(96)44

11. The MKII gas box divertor - a new design concept.
Altmann H Deksnis E Froger C Lawson S Lowry C Peacock A Pick M
JET Joint Undertaking, September 1996 (JET Posters presented at the 19th Symposium on Fusion Technology (SOFT) Lisbon, Portugal, 16-20 September 1996). p.1. Report JET-P(96)45

12. Monte Carlo simulations of fast particle confinement during a sawtooth crash.
Appel L C Hender T C Gimblett C G Marcus F Huysmans G T A Pinches S D
JET Joint Undertaking, July 1996. (JET Posters presented at the 23rd EPS Conference Kiev, Ukraine, 24-28 June 1996). p.13. Report JET-P(96)30

13. Excitation and ionization of neutral Cr and Mo, and the application to impurity influx.
Badnell N Gorczyca T Pindzola M S Summers H P
Journal of Physics B: Atomic, Molecular and Optical Physics, vol.29 no.16 28 August 1996. p.3683.

14. Physics of L and H-mode confinement in JET.
Bak P Balet B Cherubini A Cordey J G Deliyanakis N Erba M Parail V V Porte L Springmann E M Taroni A Vayakis G
Nuclear Fusion, vol.36 no.3 March 1996. p.321.

15. Fusion performance and alpha heating in future JET D-T plasmas.
Balet B Cordey J G Gibson A Lomas P Stubberfield P M Thomas P
21st EPS Conference on Controlled Fusion and Plasma Physics, Montpellier, 27 June - 1 July 1994, Contributed papers, Part I. European Physical Society, 1994. p.58.

16. MHD related transport analysis in JET.
Balet B Huysmans G Nave M F F Smeulders P Wesson J
JET Joint Undertaking, July 1996. (JET Posters presented at the 23rd EPS Conference Kiev, Ukraine, 24-28 June 1996). p.19. Report JET-P(96)30

17. MHD related transport analysis in JET.
Balet B Huysmans G Nave M F F Smeulders P Wesson J A
JET Joint Undertaking, August 1996. (JET Papers presented at the 23rd EPS Conference on Plasma Physics and Controlled Fusion, Kiev, Ukraine, 24-28 June 1996). p.17. Report JET-P(96)33

18. Modelling of lower hybrid current drive and comparison with experimental results in JET.
Baranov Yu F Ekedahl A Froissard P Gormezano C Lennholm M Rimini F G Soldner F X
Nuclear Fusion, vol.36 no.8 August 1996. p.1031.

19. Applications of X-ray spectroscopy to ITER.
Barnsley R Giannella R M Lawson K D Peacock N J
Diagnostics for Experimental Thermonuclear Fusion Reactors: Proceedings of the International Workshop on Diagnostics for ITER, August 28 - September 1, 1995, Varenna, Plenum Press, New York, 1996. p.353. Report JET-P(96)01

20. Physics issues of ECE and ECA for ITER.
Bartlett D V
Diagnostics for Experimental Thermonuclear Fusion Reactors: Proceedings of the International Workshop on Diagnostics for ITER, August 28 - September 1, 1995, Varenna, Plenum Press, New York, 1996. p.183.

21. Identification of the physical mechanism of low-m, n=1 MHD mode control in JET.
Benedetti M De Ali Arshad S Campbell D J D'Antona G Edwards A M Fishpool G La Haye R J Lazzaro E Santagiustina A Sartori F Savrukhin P
JET Joint Undertaking, August 1996. (JET Papers presented at the 23rd EPS Conference on Plasma

Physics and Controlled Fusion, Kiev, Ukraine, 24-28 June 1996). p.57. Report JET-P(96)33

22. Collective Thomson scattering of millimetre waves in JET.
Bindslev H Egedal J Fessey J Hoekzema J Hughes T
JET Joint Undertaking, 1996. Report JET-P(96)47

23. The effect of an ion beam on fluctuations in a hot, magnetized plasma
Bindslev H Lashmore-Davies C N
Bulletin of the American Physical Society, vol.41 no.7 November 1996 (Program of the Thirty-Eighth Annual Meeting of the Division of Plasma Physics, 11-15 November 1996, Denver, Colorado). p.1543.

24. On the applicability of the fluid approach to the description of bilinear interaction and scattering of waves in plasmas.
Bindslev H
Plasma Physics and Controlled Fusion, vol.38 no.4 April 1996. p.639. Report JET-P(96)07

25. Recent developments in theory of wave scattering in plasmas.
Bindslev H
JET Joint Undertaking, 1996. Report JET-P(96)41

26. The harmonic power filters of the JET poloidal divertor field amplifiers.
Bonicelli T Huart M Doyle P Rouleau M Zullo G
JET Joint Undertaking, October 1996 (JET Papers presented at the 19th Symposium on Fusion Technology (SOFT) Lisbon, Portugal, 16-20 September 1996). p.5. Report JET-P(96)44

27. The harmonic power filters of the JET poloidal divertor field amplifiers.
Bonicelli T Huart M Doyle P Rouleau M Zullo G
JET Joint Undertaking, September 1996 (JET Posters presented at the 19th Symposium on Fusion Technology (SOFT) Lisbon, Portugal, 16-20 September 1996). p.7. Report JET-P(96)45

28. Alfven eigenmodes in JET high performance plasmas
Borba D Candy J Cherubini A Gormezano C Sadler G Sharapov S and others
Bulletin of the American Physical Society, vol.41 no.7 November 1996 (Program of the Thirty-Eighth Annual Meeting of the Division of Plasma Physics, 11-15 November 1996, Denver, Colorado). p.1520.

29. Linear and nonlinear dynamics of Alfven eigenmodes in JET plasmas.
Borba D Candy J Fasoli A Kerner W Muir D Sharapov S
JET Joint Undertaking, July 1996. (JET Posters presented at the 23rd EPS Conference Kiev, Ukraine, 24-28 June 1996). p.25. Report JET-P(96)30

30. Linear and nonlinear dynamics of Alfven eigenmodes in JET plasmas.
Borba D Candy J Fasoli A Kerner W Muir D Sharapov S
JET Joint Undertaking, August 1996. (JET Papers presented at the 23rd EPS Conference on Plasma Physics and Controlled Fusion, Kiev, Ukraine, 24-28 June 1996). p.27. Report JET-P(96)33

31. Linear and nonlinear dynamics of Alfven eigenmodes in JET plasmas
Borba D Sharapov S Pinches S Candy J
Bulletin of the American Physical Society, vol.41 no.7 November 1996 (Program of the Thirty-Eighth Annual Meeting of the Division of Plasma Physics, 11-15 November 1996, Denver, Colorado). p.1609.

32. Non-standard alpha particle orbit effects on the stability of Alfven eigenmodes in JET.
Borba D Candy J Kerner W Sharapov S JET Joint Undertaking, October 1996. (JET Papers presented at the International Workshop on Theory of Fusion Plasmas, Varenna, Italy, 26-30 August 1996). p.1. Report JET-P(96)35

33. Analysis of a global confinement database for JET ohmic plasmas.
Bracco G Thomsen K
JET Joint Undertaking, 1996. 14p. Report JET-R(96)03

34. H/D measurement by neutral particle analysis at JET.
Bracco G Guenther K

JET Joint Undertaking, 1996. 22p. Report JET-R(96)04

35. An adaptive plasma density controller at JET.
Brelen H E O Budd T Ehrenberg J Gadeberg M Ryle C
JET Joint Undertaking, September 1996 (JET Posters presented at the 19th Symposium on Fusion Technology (SOFT) Lisbon, Portugal, 16-20 September 1996). p.13. Report JET-P(96)45

36. Implementation and initial operation of an adaptive plasma density controller at JET.
Brelen H Budd T Ehrenberg J Gadeberg M Ryle C
JET Joint Undertaking, October 1996 (JET Papers presented at the 19th Symposium on Fusion Technology (SOFT) Lisbon, Portugal, 16-20 September 1996). p.9. Report JET-P(96)44

37. Remote sensing of a capacitance manometer pressure measurement head.
Browne A Cooper D Davies J F Hackett L Svensson L Young D
JET Joint Undertaking, October 1996 (JET Papers presented at the 19th Symposium on Fusion Technology (SOFT) Lisbon, Portugal, 16-20 September 1996). p.13. Report JET-P(96)44

38. Remote sensing of a capacitance manometer pressure measurement head.
Browne A Cooper D Davies J F Hackett L Svensson L Young D
JET Joint Undertaking, September 1996 (JET Posters presented at the 19th Symposium on Fusion Technology (SOFT) Lisbon, Portugal, 16-20 September 1996). p.19. Report JET-P(96)45

39. An in-vessel inspection system (IVIS) for ITER
Businaro T V Consano L
JET Joint Undertaking, 1996. Report JET-R(96)05

40. Axisymmetric and non-axisymmetric structural effects of disruption-induced electromechanical forces on the JET tokamak.
Buzio M Noll P Raimondi T Riccardo V Sonnerup L
JET Joint Undertaking, October 1996 (JET Papers presented at the 19th Symposium on Fusion Technology (SOFT) Lisbon, Portugal, 16-20 September 1996). p.17. Report JET-P(96)44

41. Axisymmetric and non-axisymmetric structural effects of disruption-induced electromechanical forces on the JET tokamak.
Buzio M Noll P Raimondi T Riccardo V Sonnerup L
JET Joint Undertaking, September 1996 (JET Posters presented at the 19th Symposium on Fusion Technology (SOFT) Lisbon, Portugal, 16-20 September 1996). p.25. Report JET-P(96)45

42. The density limit in JET diverted plasmas.
Campbell D J Clement S Gottardi N Gowers C Harbour P Loarte A Horton L Lingertat H Lowry C G Monk R Saibene G Stamp M Stork D
21st EPS Conference on Controlled Fusion and Plasma Physics, Montpellier, 27 June - 1 July 1994, Contributed papers, Part I. European Physical Society, 1994. p.2.

43. Experimental comparison of carbon and beryllium as divertor target materials in JET.
Campbell D J and the JET Team
JET Joint Undertaking, June 1996. (JET Papers presented at the 12th International Conference on Plasma Surface Interaction in Controlled Fusion Devices, St Raphael, France, 20-24 May 1996) p.1. Report JET-P(96)22

44. H-mode confinement and fusion performance in JET.
Campbell D J and the JET Team
JET Joint Undertaking, 1996. Report JET-P(96)42

45. Studies of reactor-relevant H-mode regimes in the JET-pumped divertor.
Campbell D J Bickley A Chankin A Clement S Davies S J Ehrenberg J Erents S K Guo H Y Harbour P J Horton L Lintertat J Loarte A Lowry C G McCormick K Maggi C Matthews G F Monk R O'Brien D Reichle R Righi E Saibene G Stamp M Start D F H Stork D Vlases G C von Hellermann M
Plasma Physics and Controlled Fusion, vol.38 no.8 August 1996 (Papers from the 5th IAEA Technical Committee Meeting/US-Japan Workshop on H-mode Physics, Princeton, 18-20 September 1995). p.1497

46. Electron Landau damping of toroidal Alfven eigenmodes.
Candy J
Plasma Physics and Controlled Fusion, vol.38 no.6 June 1996. p.795.

47. Multiplicity of low-shear toroidal Alfven eigenmodes.
Candy J Breizman B N Van Dam J W Ozeki T
Physics Letters A, vol.215 nos.5,6 10 June 1996. p.299

48. A numerical method for solution of the generalized liouville equation.
Candy J
Journal of Computational Physics, vol.129 no.1 November 1996. p.160.

49. JET/DIII-D size scaling of the H-mode power threshold.
Carlstrom T N Campbell D J Cordey J G DeBoo J C Groebner R J Righi E Saibene G Schissel D P Start D Thomsen K
Plasma Physics and Controlled Fusion, vol.38 no.8 August 1996 (Papers from the 5th IAEA Technical Committee Meeting/US-Japan Workshop on H-mode Physics, Princeton, 18-20 September 1995). p.1231. Report JET-P(95)50

50. Toroidal Field Reversal Effects on Divertor Asymmetries in JET
Chankin A V Campbell D K Clement S Davies S J Horton L D Lingertat J Loarte A Matthews G F Monk R D Reichle R Saibene G Stamp M Stangeby P C
Report JET-P(96)05

51. Classical drifts in the tokamak SOL and divertor: models and experiment.
Chankin A V
JET Joint Undertaking, 1996. (JET Invited Papers presented at the 12th International Conference on Plasma Surface Interaction in Controlled Fusion Devices, St Raphael, France, 20-24 May 1996). p.1.

52. Toroidal field reversal effects on divertor asymmetries in JET.
Chankin A V Campbell D J Clement S Davies S J Horton L D Lingertat J Loarte A Matthews G F Monk R D Reichle R Saibene G Stamp M Stangeby P C
Plasma Physics and Controlled Fusion, vol.38 no.9 September 1996. p.1579. Report JET-P(96)23

53. Toroidicity in the tokamak SOL: effects on poloidal asymmetries, radial current and the L-H transition.
Chankin A V Stangeby P C
Plasma Physics and Controlled Fusion, vol.38 no.11 November 1996. p.1879. Report JET-P(96)12

54. A description of ELM-free H-modes in terms of a neoclassical edge barrier and a “mixed” model for energy and particle transport.
Cherubini A Balet B Deliyanakis N Erba M Giannella R Hawkes N Parail V V Porte L Rookes A Springmann E Taroni A
JET Joint Undertaking, July 1996. (JET Posters presented at the 23rd EPS Conference Kiev, Ukraine, 24-28 June 1996). p.31. Report JET-P(96)30

55. A description of ELM-free H-modes in terms of a neoclassical edge barrier and a ‘mixed’ model for energy and particle transport.
Cherubini A Balet B Deliyanakis N Erba M Giannella R Hawkes N C Parail V V Porte L Rookes A Springmann E Taroni A
JET Joint Undertaking, August 1996. (JET Papers presented at the 23rd EPS Conference on Plasma Physics and Controlled Fusion, Kiev, Ukraine, 24-28 June 1996). p.33. Report JET-P(96)33

56. Numerical simulation of ELM-free H-mode and hot-ion H-mode JET plasmas.
Cherubini A Erba M Parail V Springmann E and Taroni A
Plasma Physics and Controlled Fusion, vol.38 no.8 August 1996 (Papers from the 5th IAEA Technical Committee Meeting/US-Japan Workshop on H-mode Physics, Princeton, 18-20 September 1995). p.1421. Report

57. The ρ^* scaling experiments for ELMy H-modes in JET.
Christiansen J P Cordey J G Balet B Campbell D Challis C D Ehrenberg J Gianella R Gormezano C Gowers C de Haas J Harbour P Lowry C Nielsen

P Porte L Righi E Saibene G R Start D F H Stamp M P M Thomsen K von Hellermann M
JET Joint Undertaking, 1995. (JET Posters presented to the 37th Annual Meeting, APS Division of Plasma Physics, Louisville, USA, 6-10 November 1995). p.1. Report JET-P(95)72

58. Beam properties of the enhanced JET PINIs.
Ciric D Challis C D de Esch H P L Falter H-D Godden D Holmes A J T Stork D Thompson E
JET Joint Undertaking, October 1996 (JET Papers presented at the 19th Symposium on Fusion Technology (SOFT) Lisbon, Portugal, 16-20 September 1996). p.21. Report JET-P(96)44

59. Beam properties of the enhanced JET PINIs.
Ciric D Challis C D de Esch H P L Falter H D Godden D Holmes A J T Stork D Thompson E
JET Joint Undertaking, September 1996 (JET Posters presented at the 19th Symposium on Fusion Technology (SOFT) Lisbon, Portugal, 16-20 September 1996). p.31. Report JET-P(96)45

60. Effects of density and plasma configuration on the divertor asymmetries.
Clement S Chankin A Davies S Lingertat J Monk R Sartori R Stamp M
JET Joint Undertaking, 1996. (JET Posters presented at the 23rd EPS Conference Kiev, Ukraine, 24-28 June 1996). p.37. Report JET-P(96)30

61. Effects of density and plasma configuration on the divertor asymmetries.
Clement S Chankin A Davies S Lingertat J Monk R Sartori R Stamp M
JET Joint Undertaking, August 1996. (JET Papers presented at the 23rd EPS Conference on Plasma Physics and Controlled Fusion, Kiev, Ukraine, 24-28 June 1996). p.41. Report JET-P(96)33

62. The amount and distribution of deuterium retained in the JET divertor after the C and Be phases in 1994-5.
Coad J P Wu C H
JET Joint Undertaking, June 1996. (JET Papers presented at the 12th International Conference on Plasma Surface Interaction in Controlled Fusion Devices, St Raphael, France, 20-24 May 1996) p.63. Report JET-P(96)22

63. Deuterium content of material redeposited in tokamaks.
Coad J P
JET Joint Undertaking, 1996. 37p. Report JET-R(95)10

64. Hydrogen isotope analysis of thick layers deposited in tokamaks.
Coad J P Skorodumov B G Ulanov V G Wu C H
Vacuum, vol. 47 nos.6-8 June-August 1996 (Proceedings of the 13th International Vacuum Congress and the 9th International Conference on Solid Surfaces, 25-29 September 1995, Yokahoma, Japan) p.985.

65. Cl XV and Cl XVI in the JET and Compass-D tokamaks.
Coffey I H Barnsley R Keenan F P Melnick I McGinnity P O'Mullane M G Peacock N J
JET Joint Undertaking, 1995. (JET Papers presented to 11th Colloquium on UV and X-Ray Spectroscopy of Astrophysical and Laboratory Plasmas, Nagoya, Japan, June 1995.) p.1. Report JET-P(95)54

66. Stability of m=1 mode with energetic particles, sawtooth relaxation and locked modes in tokamaks.
Connor J W Dendy R O Gimblett C G Hastie R J Hender T C Martin T J McClements K G Fitzpatrick R Sharapov S E
Plasma Physics and Controlled Nuclear Fusion Research 1994, 15th International Conference, Seville, 26 September-1 October 1994. Vol.3. p.211.

67. Energy confinement and H-mode power threshold scaling in JET with ITER dimensionless parameters.
Cordey J G and the JET Team
JET Joint Undertaking, October 1996. (JET Papers presented at the 16th IAEA Fusion Energy Conference, Montreal, Canada, 7-11 October 1996). p.37. Report JET-P(96)51

68. ITER simulation experiments on JET of the H-mode power threshold, confinement scaling and beta saturation.

Cordey J G Balet B Campbell D Challis C D Christiansen J P Ehrenberg J Giannella R Gormezano C Gowers C de Haas J Harbour P Lowry C Nielsen P Porte L Righi E Saibene G R Start D F H Stamp M Stubberfield P M Thomsen K von Hellermann M
Plasma Physics and Controlled Fusion, vol.38 no.8 August 1996 (Papers from the 5th IAEA Technical Committee Meeting/US-Japan Workshop on H-mode Physics, Princeton, 18-20 September 1995). p.1237.

69. On the dependence of the L-H power threshold on the ion drift direction.
Cordey J G Kerner W Pogitse O Nassigh A
Plasma Physics and Controlled Fusion, vol.38 no.11 November 1996. p.1905. Report JET-P(96)09

70. A review of the dimensionless parameter scaling studies.
Cordey J G Balet B Campbell D Challis C D Christiansen J P Gormezano C Gowers C Muir D Righi E Saibene G R Stubberfield P M Thomsen K
Plasma Physics and Controlled Fusion, vol.38 no.12A December 1996 (Invited papers from the 23rd European Physical Society Conference on Controlled Fusion and Plasma Physics, Kiev, Ukraine, 24-28 June 1996). p.A67. Report JET-P(96)32

71. Efficient time dependent modelling of the physics of NBI heating in JET.
Core W G F Zastrow K-D
JET Joint Undertaking, 1996. 25p. Report JET-R(96)01

72. Requirements for ITER diagnostics.
Costley A E Bartiromo R de Kock L Marmar E Matoba T Mukhovatov V Muraoka K Nagashima A Orlinski D V Petrov M Stott P E Strelkov V Yamamoto S Young K M
Diagnostics for Experimental Thermonuclear Fusion Reactors: Proceedings of the International Workshop on Diagnostics for ITER, August 28 - September 1, 1995, Varenna, Plenum Press, New York, 1996. p.23.

73. ICRH in hot-ion H-modes in JET.
Cottrell G A Gormezano C Howman A Jones T Lomas P J Rimini F Sartori R Sips G Start D F H
JET Joint Undertaking, July 1996. (JET Posters presented at the 23rd EPS Conference Kiev, Ukraine, 24-28 June 1996). p.43. Report JET-P(96)30

74. ICRH in hot-ion H-modes in JET.
Cottrell G A Gormezano C Howman A Jones T Lomas P J Rimini F Sartori R Sips G Start D F H
JET Joint Undertaking, August 1996. (JET Papers presented at the 23rd EPS Conference on Plasma Physics and Controlled Fusion, Kiev, Ukraine, 24-28 June 1996). p.49. Report JET-P(96)33

75. A new comb reflectometer for the JET divertor plasma.
Cupido L Prentice R Bartlett D V Manso M E Nunes I Serra F Silva A
JET Joint Undertaking, 1996. 13p. Report JET-P(96)79

76. The implementation and operation of a full size mock-up facility in preparation for remote handling of JET divertor modules.
Cusack R Brown P Haist B Loving A Stokes R
JET Joint Undertaking, October 1996 (JET Papers presented at the 19th Symposium on Fusion Technology (SOFT) Lisbon, Portugal, 16-20 September 1996). p.25. Report JET-P(96)44

77. The implementation and operation of a full size mock-up facility in preparation for remote handling of JET divertor modules.
Cusack R Brown P Haist B Loving A Stokes R
JET Joint Undertaking, September 1996 (JET Posters presented at the 19th Symposium on Fusion Technology (SOFT) Lisbon, Portugal, 16-20 September 1996). p.37. Report JET-P(96)45

78. Two-dimensional time-dependent solution of Stix's equation for the distribution function of minority ions during ion cyclotron resonant heating.
Dalla S Ljepojevic N N
JET Joint Undertaking, 1996. Report JET-P(96)56

79. Structural integrity assessment of the JET neutral beam components.
Daniels B Papastergiou S
JET Joint Undertaking, 1996. Report JET-P(96)20

80. The JET reciprocating probe systems - performance and data analysis.
Davies S J Erents K Guo H Y Loarte A Matthews G F McCormick K Monk R D
JET Joint Undertaking, 1995. (JET papers presented to 2nd workshop on electrical probes in magnetised plasmas, Berlin, Germany, 4-6 October 1995). p.9. Report JET-P(95)68

81. Parallel electron temperature and density gradients measured in the JET MkI divertor using thermal helium beams.
Davies S J Morgan P D Ul'Haq Y Maggi C F Erents S K Fundamenski W Horton L D Loarte A Matthews G F Monk R D Stangeby P C
JET Joint Undertaking, June 1996. (JET Papers presented at the 12th International Conference on Plasma Surface Interaction in Controlled Fusion Devices, St Raphael, France, 20-24 May 1996) p.101. Report JET-P(96)22

82. Identification of the physical mechanism of low-m, n=1 mode control in JET.
De Benedetti M Ali-Arshad S Campbell D J D'Antona G Edwards A M Fishpoll G La Haye R Lazzaro E Santaguistina A Sartori R Savrukhin P Tanga A
JET Joint Undertaking, July 1996. (JET Posters presented at the 23rd EPS Conference Kiev, Ukraine, 24-28 June 1996). p.49. Report JET-P(96)30

83. Simulations of JET hot-ion H-modes with a predictive code.
de Esch H P L Cherubini A Cordey J G Erba M Jones T T C Parail V V Stork D Taroni A
JET Joint Undertaking, July 1996. (JET Posters presented at the 23rd EPS Conference Kiev, Ukraine, 24-28 June 1996). p.55. Report JET-P(96)30

84. Simulations of JET hot-ion H-modes with a predictive code.
de Esch H P L Cherubini A Cordey J G Erba M Jones T T C Parail V V Stork D Taroni A
JET Joint Undertaking, August 1996. (JET Papers presented at the 23rd EPS Conference on Plasma Physics and Controlled Fusion, Kiev, Ukraine, 24-28 June 1996). p.65. Report JET-P(96)33

85. Langmuir probes and optical diagnostics for ITER divertor.
de Kock L Ando T Antipenkov A Janeschitz G Martin E Matthews G Monk R
Diagnostics for Experimental Thermonuclear Fusion Reactors: Proceedings of the International Workshop on Diagnostics for ITER, August 28 - September 1, 1995, Varenna, Plenum Press, New York, 1996. p.591.

86. Sawtooth heat pulse propagation in tokamaks: ballistic response and Fourier analysis.
de Luca F Galli P Gorini G Jacchia A Mantica P Deliyanakis N Erba M Porte L
Nuclear Fusion, vol.36 no.7 July 1996. p.909.

87. Marfes: a magnetohydrodynamic stability study of two-dimensional tokamak equilibria.
De Ploey A Van der Linden R A M Huysmans G T A Goossens M Kerner W Goedbloed J P
JET Joint Undertaking, 1996. Report JET-P(96)49

88. Mechanical study of JET Mark I beryllium divertor tiles after ELMs and deliberate melting.
Deksnin E Chankin A Hurd F Parsons W Tubbing B
JET Joint Undertaking, September 1996 (JET Posters presented at the 19th Symposium on Fusion Technology (SOFT) Lisbon, Portugal, 16-20 September 1996). p.43. Report JET-P(96)45

89. Mechanical study of JET MKI beryllium tiles after ELMs and deliberate melting.
Deksnis E Chankin A Hurd F Parsons W Tubbing B
JET Joint Undertaking, October 1996 (JET Papers presented at the 19th Symposium on Fusion Technology (SOFT) Lisbon, Portugal, 16-20 September 1996). p.29. Report JET-P(96)44

90. Thermal fatigue of beryllium.
Deksnis E B Ciric D Falter H Ibbott C Peacock A
JET Joint Undertaking, November 1995. (JET papers presented to the 2nd IEA International Workshop on Beryllium Technology for Fusion, 6 September 1995, Jackson Hole, USA.) p.9. Report JET-P(95)59

91. Reply to the comment by Lazzaro and Minardi on 'Minimum entropy production principle due to ohmic

dissipation and determination of non-inductive current profiles on JET'.
DiVita A Brusati M
Plasma Physics and Controlled Fusion, vol.38 no.7 July 1996. p.1085.

92. The JET high voltage power distribution, analysis of present and future operational requirements.
Dolgetta N Berolini E Huart M Murphy G
JET Joint Undertaking, October 1996 (JET Papers presented at the 19th Symposium on Fusion Technology (SOFT) Lisbon, Portugal, 16-20 September 1996). p.33. Report JET-P(96)44

93. The JET high voltage power distribution, analysis of present and future operational requirements.
Dolgetta N Bertolini E Huart M Murphy G
JET Joint Undertaking, September 1996 (JET Posters presented at the 19th Symposium on Fusion Technology (SOFT) Lisbon, Portugal, 16-20 September 1996). p.49. Report JET-P(96)45

94. Study of matching systems and schemes for ITER (design of fast tuning elements).
Durodie F Crawley P Kaye A
Next European Torus (NET), Brussels, Belgium 1996. 105p. Report NET REPORT 109

95. The control system for the disruption stabilisation experiment in JET.
D'Antona G Campbell D J Santagiustina A Savrukhin P
IEEE Transactions on Nuclear Science, vol.43 no.1 part 1, 1996, (Selected papers from the Ninth Conference on Real-time Computer Applications in Nuclear, Particle, and Plasma Physics (Real-time '95)). p.207.

96. Neutral particle compression in the JET MK I divertor.
Ehrenberg J K Campbell D J Harbour P J Horton L D Loarte A McCormick G K Monk R D Saibene G R Simonini R Taroni A Stamp M F
JET Joint Undertaking, June 1996. (JET Papers presented at the 12th International Conference on Plasma Surface Interaction in Controlled Fusion Devices, St Raphael, France, 20-24 May 1996) p.75. Report JET-P(96)22

97. Profile control in JET with off-axis lower hybrid current drive.
Ekedahl A Baranov Y Dobbing J Fischer B Gormezano C Lennholm M Pericoli-Ridolfini V Rimini F Romero J Schild P Soldner F
JET Joint Undertaking, July 1996. (JET Posters presented at the 23rd EPS Conference Kiev, Ukraine, 24-28 June 1996). p.61. Report JET-P(96)30

98. Profile control in JET with off-axis lower hybrid current drive.
Ekedahl A Baranov Y Dobbing J Fischer B Gormezano C Lennholm M Pericoli-Ridolfini V Rimini F Romero J Schild P Soldner F
JET Joint Undertaking, August 1996. (JET Papers presented at the 23rd EPS Conference on Plasma Physics and Controlled Fusion, Kiev, Ukraine, 24-28 June 1996). p.73. Report JET-P(96)33

99. Ion temperature profile measurements by means of neutron spectroscopy.
Elevant T Brelen H Linden P Scheffel J
Diagnostics for Experimental Thermonuclear Fusion Reactors: Proceedings of the International Workshop on Diagnostics for ITER, August 28 - September 1, 1995, Varenna, Plenum Press, New York, 1996. p.445.

100. Scintillating fibre neutron spectrometer.
Elevant T Chakarova R Karlsson J
Diagnostics for Experimental Thermonuclear Fusion Reactors: Proceedings of the International Workshop on Diagnostics for ITER, August 28 - September 1, 1995, Varenna, Plenum Press, New York, 1996. p.451.

101. Development of a non-local model for tokamak heat transport in L-mode, H-mode and transient regimes.
Erba M Cherubini A Parail V V Springmann E Taroni A
JET Joint Undertaking, 1996. Report JET-P(96)10

102. Validation of a new mixed Bohm/gyro-Bohm transport model on discharges of the ITER data-base.
Erba M Cherubini A Parail V V Springmann E Taroni A
JET Joint Undertaking, 1996. Report JET-R(96)07

103. Assessment of the DIVIMP 'onion-skin' model in the JET Mark I divertor.
Erents S K Breger P Davies S J Elder J D Guo H Y Horton L D Matthews G F Monk R D Stangeby P C Summers D D R
JET Joint Undertaking, June 1996. (JET Papers presented at the 12th International Conference on Plasma Surface Interaction in Controlled Fusion Devices, St Raphael, France, 20-24 May 1996) p.137. Report JET-P(96)22

104. Analysis of fast minority ion distribution and current generation for ICRF and LH heating.
Eriksson L-G Heikkinen J A Kiviniemi T P Mantsinen M J Saveliev A Pattikangas T J H Sipila S K Piliya A
Plasma Physics and Controlled Fusion, vol.38 no.12 December 1996. p.2063.

105. Topological transitions of fast ion orbits in toroidal plasmas.
Eriksson L-G Porcelli F Furno I
JET Joint Undertaking, October 1996. (JET Papers presented at the International Workshop on Theory of Fusion Plasmas, Varenna, Italy, 26-30 August 1996). p.9. Report JET-P(96)35

106. Toroidal rotation in ICRF heated H-modes on JET.
Eriksson L-G Righi E Zastrow K-D
JET Joint Undertaking, 1996. Report JET-P(96)28

107. Runaway electron measurements in the JET tokamak.
Esposito B Martin-Solis R van Belle P Jarvis Marcus F B Sadler G Sanchez R Fischer B Froissard P Adams J M Cecil E Watkins N
Plasma Physics and Controlled Fusion, vol.38 no.12 December 1996. p.2035.

108. Performance of Hypervapotron Beam Stopping Elements in JET
Falter H D Ibbott C
Report JET-P(96)37

109. High heat flux exposure tests on 10mm beryllium tiles brazed to an actively cooled vapotron made from CuCrZr.
Falter H D Ciric D Godden D J Ibbot C Celentano A
JET Joint Undertaking, 1996. 44p. Report JET-R(96)02

110. Performance of hypervapotron beam-stopping elements at JET.
Falter H-D Thompson E
Fusion Technology, vol.29 no.4 July 1996. p.584.

111. Vapotron as heat sink for flat high-conductivity undirectional carbon-fiber- composite tiles.
Falter H-D Ciric D Celentano A Ibbott C M Watson M J Araki M suzuki S Sato K
Fusion Technology, vol.29 no.4 July 1996. p.571.

112. ITER alpha-particle diagnostics using knock-on ion tails.
Fisher R K Barnes C W Gondhalekar A Parks P B McChesney J M Roquemore A L Rosenbluth M N
Diagnostics for Experimental Thermonuclear Fusion Reactors: Proceedings of the International Workshop on Diagnostics for ITER, August 28 - September 1, 1995, Varenna, Plenum Press, New York, 1996. p.485.

113. Comparison between JET profile data and the predictions of a transport model based on ITG and trapped electron modes: interpretative comparison of heat fluxes and predictive comparison of profiles.
Frojdh M and others
Plasma Physics and Controlled Fusion, vol.38 no.3 March 1996. p.325.

114. The command and control system for JET remote handling equipment.
Galbiati L Carter P Haist B
JET Joint Undertaking, October 1996 (JET Papers presented at the 19th Symposium on Fusion Technology (SOFT) Lisbon, Portugal, 16-20 September 1996). p.37. Report JET-P(96)44

115. The command and control system for JET remote handling equipment.
Galbiati L Carter P Haist B
JET Joint Undertaking, September 1996 (JET Posters presented at the 19th Symposium on Fusion Technology (SOFT) Lisbon, Portugal, 16-20 September 1996). p.55. Report JET-P(96)45

116. Characterization of fluctuations in the JET divertor plasmas with langmuir probes.
Garcia-Cortes I Hidalgo C Martin-Solis J R Ali-Arshad S Clement S Davies S J Lingertat J Loarte A Matthews G F Monk R D
Plasma Physics and Controlled Fusion, vol.38 no.12 December 1996. p.2051.

117. Quantitative simulation of non-thermal charge exchange spectra during helium neutral beam injection.
Gerstel U Horton L Summers H P von Hellermann M Wolle B
JET Joint Undertaking, 1996. 21p. Report JET-P(96)31

118. Negative snakes in JET: evidence for negative shear?
Gill R D Alper B Edwards A W Pearson D
21st EPS Conference on Controlled Fusion and Plasma Physics, Montpellier, 27 June - 1 July 1994, Contributed papers, Part I. European Physical Society, 1994. p.198.

119. Properties of giant ELMs.
Gill R D Alper B Ali-Arshad S Cheetham A Deliyanakis N Edwards A W Fishpool G M Garcia-Cortez I Ingesson L C Lingertat J Mayaux L Menicot O Monk R Porte L Rochard F Romanelli M Rookes A
JET Joint Undertaking, July 1996. (JET Posters presented at the 23rd EPS Conference Kiev, Ukraine, 24-28 June 1996). p.67. Report JET-P(96)30

120. Properties of giant ELMs.
Gill R D Alper B Ali-Arshad S Cheetham A Deliyanakis N Edwards A W Fishpool G M Garcia-Cortez I Ingesson L C Lingertat J Mayaux L Menicot O Monk R Porte L Rochard F Romanelli M Rookes A
JET Joint Undertaking, August 1996. (JET Papers presented at the 23rd EPS Conference on Plasma Physics and Controlled Fusion, Kiev, Ukraine, 24-28 June 1996). p.79. Report JET-P(96)33

121. Non-uniform rotation and the resistive wall mode.
Gimblett C G Hastie R J van der Linden R A M Wesson J A
Physics of Plasmas, vol.3 no.10 1996. p.3619.

122. Impurity induced neutralization of MeV energy protons in JET plasmas.
Gondhalekar A Korotkov A A
21st EPS Conference on Controlled Fusion and Plasma Physics, Montpellier, July 1994, Contributed papers, Part I. European Physical Society, 1994. p.266.

123. RF Systems for heating and current drive in fusion experiments
Gormezano C
Report JET-P(96)57

124. Ion cyclotron resonance heating of H-modes in the JET Mark I divertor configuration
Gormezano C et al
Report JET-P(96)60

125. Optimisation of JET plasmas with current profile control.
Gormezano C and the JET Team
JET Joint Undertaking, October 1996. (JET Papers presented at the 16th IAEA Fusion Energy Conference, Montreal, Canada, 7-11 October 1996). p.91. Report JET-P(96)51

126. A Thomson scattering scheme for obtaining T_e and n_e profiles of the ITER core plasma.
Gowers C Nielsen P Orsitto F Pijper F J Salzmann H Schunke B
Diagnostics for Experimental Thermonuclear Fusion Reactors: Proceedings of the International Workshop on Diagnostics for ITER, August 28 - September 1, 1995, Varenna, Plenum Press, New York, 1996. p.249.

127. Analysis of VUV Ne radiation in the JET divertor during Ne injections.
Guirlet R Giannella R Horton L Lawson K Maas A Maggi C O'Mullane M
JET Joint Undertaking, July 1996. (JET Posters presented at the 23rd EPS Conference Kiev, Ukraine, 24-28 June 1996). p.73. Report JET-P(96)30

128. Analysis of VUV Ne radiation in the JET divertor during Ne injections.
Guirlet R Giannella R Horton L Lawson K Maas A Maggi C O'Mullane M

JET Joint Undertaking, August 1996. (JET Papers presented at the 23rd EPS Conference on Plasma Physics and Controlled Fusion, Kiev, Ukraine, 24-28 June 1996). p.85. Report JET-P(96)33

129. Behaviour of hydrogen in JET deuterium plasmas.
Gunther K Bracco G Konig R Stamp M F Zastrow K-D
JET Joint Undertaking, June 1996. (JET Papers presented at the 12th International Conference on Plasma Surface Interaction in Controlled Fusion Devices, St Raphael, France, 20-24 May 1996) p.15. Report JET-P(96)22

130. Erosion/redeposition at the JET MKI divertor.
Guo H Y Coad J P Davies S J Elder J D Horton L D Li X L Lingertat J Loarte A Matthews G F Monk R D Simonini R Stamp M F Stangeby P C Tabasso A
JET Joint Undertaking, June 1996. (JET Papers presented at the 12th International Conference on Plasma Surface Interaction in Controlled Fusion Devices, St Raphael, France, 20-24 May 1996) p.115. Report JET-P(96)22

131. Evolution of edge electric field at the L to H transition in JET.
Hawkes N C Bartlett D V Campbell D J Deliyanakis N Giannella R M Lomas P J Peacock N J Porte L Rookes A and Thomas P R
Plasma Physics and Controlled Fusion, vol.38 no.8 August 1996 (Papers from the 5th IAEA Technical Committee Meeting/US-Japan Workshop on H-mode Physics, Princeton, 18-20 September 1995). p.1261. Report JET-P(95)50

132. Measurements of edge electric field, electron and impurity ion profiles during H-modes in the new JET divertor configuration.
Hawkes N C Bartlett D V Campbell D J Deliyanakis N Erents S K Giannella R M Lomas P J O'Mullane M G Peacock N J Porte L Rookes A Thomas P R Vayakis G
JET Joint Undertaking, 1995. (JET Posters presented to the 37th Annual Meeting, APS Division of Plasma Physics, Louisville, USA, 6-10 November 1995.) p.33. Report JET-P(95)72

133. Analysis of fast minority ion distribution and current generation for ICRF and LH heating.
Heikkinen J A Kiviniemi T P Mantsinen M J Saveliev A Eriksson L-G Pattikangas T J H Sipila S K Piliya A
JET Joint Undertaking, 1996. 22p. Report JET-P(96)34

134. Advances in temperature derivative control and calorimetry.
Hemmerich J L Loos J-C Miller A Milverton P
Review of Scientific Instruments, vol.67 no.11 November 1996. p.3877. Report JET-P(96)21

135. Comparison of helium transport and exhaust in JET and DIII-D
Hillis D L Von Hellermann M Horton L Hogan J T Wade M R Ehrenberg J Morgan P Campbell D Saibene G
Bulletin of the American Physical Society, vol.41 no.7 November 1996 (Program of the Thirty-Eighth Annual Meeting of the Division of Plasma Physics, 11-15 November 1996, Denver, Colorado). p.1520.

136. Collective Thomson scattering using a gyrotron from JET plasmas.
Hoekzema J A Bindslev H Egedal J Fessey J A Hughes T P
JET Joint Undertaking, JET, 1996. 6p. Report JET-P(96)69

137. First results of collective scattering on JET.
Hoekzema J A Bindslev H Egedal J Fessey J A Gatcombe C P Hammond N P Hughes T P Machuzak J S Oosterbeek J W Roberts P J Stevens A L Stott P E
JET Joint Undertaking, 1996. Report JET-P(96)40

138. Dependence of the MHD Spectrum on the Safety Factor Profile
Holties H A Goedbloed J P Huysmans G T A Kerner W
JET Joint Undertaking, 1996. Report JET-P(96)58

139. Tokamak instability threshold for low-shear alfven eigenmodes
Holties A Huysmans G T A Sharapov S and others

Bulletin of the American Physical Society, vol.41 no.7 November 1996 (Program of the Thirty-Eighth Annual Meeting of the Division of Plasma Physics, 11-15 November 1996, Denver, Colorado). p.1612.

140. MHD stability of advanced tokamak scenarios.
Holties H A Huysmans G T A Kerner W Goedbloed J P Soldner F X Parail V V
21st EPS Conference on Controlled Fusion and Plasma Physics, Montpellier, 27 June - 1 July 1994, Contributed papers, Part I. European Physical Society, 1994. p.234.

141. Stability of internal and ballooning modes in advanced tokamak scenarios.
Holties H A Huysmans G T A Goedbloed J P Kerner W Parail V V Soldner F X
Nuclear Fusion, vol.36 no.8 August 1996. p.973.

142. Atomic and molecular data needs for fusion research.
Horton L D
Physica Scripta, vol. T65 1996 (The 5th International Colloquium on Atomic Spectra and Oscillator Strengths for Astrophysical and Laboratory Plasmas, Meudon, France, August 28-31, 1995). p.175.

143. High-density divertor operation in JET.
Horton L D and the JET Team
Plasma Physics and Controlled Fusion, vol.38 no.12A December 1996 (Invited papers from the 23rd European Physical Society Conference on Controlled Fusion and Plasma Physics, Kiev, Ukraine, 24-28 June 1996). p.A269. Report JET-P(96)32

144. Gamma-ray emission profile measurements during JET ICRH discharges.
Howarth P J A Adams J M Bond D S Jarvis O N Marcus F B Sadler G van Belle P Watkins N
21st EPS Conference on Controlled Fusion and Plasma Physics, Montpellier, 27 June - 1 July 1994, Contributed papers, Part I. European Physical Society, 1994. p.262.

145. Parametric upconversion of scattered CO_2 laser radiation for an ITER alpha and fast particle diagnostic.
Hughes T P
JET Joint Undertaking, 1996. Report JET-P(96)73

146. Similarity in divertor studies.
Hutchinson I H Vlases G C
Nuclear Fusion, vol.36 no.6 June 1996. p.783.

147. SOL-One: a one-D scrape-off-layer transport code.
Huysmans G T A Borrass K
JET Joint Undertaking, 1996. Report JET-R(96)06

148. H-mode profile parameterization for extrapolation and control.
Imre K Riedel K S Schissel D P Schunke B
JET Joint Undertaking, 1995. (JET papers presented to the IAEA H-mode Workshop, Princeton, 1996) p.17. Report JET-P(95)50

149. Features of JET plasma behaviour in two different divertor configurations.
Jacquinot J and the JET Team
JET Joint Undertaking, October 1996. (JET Papers presented at the 16th IAEA Fusion Energy Conference, Montreal, Canada, 7-11 October 1996). p.1. Report JET-P(96)51

150. Gamma ray emission profile measurements from JET ICRF-heated discharges.
Jarvis O N Adams J M Howarth P J A Marcus F B Righi E Sadler G J Start D F H Van Belle P Warrick C D Watkins N
Nuclear Fusion, vol.36 no.11 1996. p.1513.

151. Neutron profile measurements in JET.
Jarvis O N Adams J M Marcus F B Sadler G J
JET Joint Undertaking, 1995. 17p. Report JET-P(95)67

152. 15-MeV proton emission from ICRF-heated plasmas.
Jarvis O N Conroy S W Hone M Sadler G J van Belle P
21st EPS Conference on Controlled Fusion and Plasma Physics, Montpellier, 27 June - 1 July 1994, Contributed papers, Part I. European Physical Society, 1994. p.270.

153. Upgrading of the neutral beam power supplies from 80kV/60A to 140kV/60A.
Jensen F Claesen R McBryan H Mills J Ostrom R Vadgama A P

JET Joint Undertaking, October 1996 (JET Papers presented at the 19th Symposium on Fusion Technology (SOFT) Lisbon, Portugal,
16-20 September 1996). p.41. Report JET-P(96)44

154. Upgrading of the neutral beam power supplies from 80kV/60A to 140kV/60A.
Jensen F Claesen R McBryan H Mills J Ostrom R Vadgama A
JET Joint Undertaking, September 1996 (JET Posters presented at the 19th Symposium on Fusion Technology (SOFT) Lisbon, Portugal, 16-20 September 1996). p.61. Report JET-P(96)45

155. Design and development of a new remote handling transporter facility for JET.
Jones L P D F Irving M Palmer J Hamilton D
JET Joint Undertaking, October 1996 (JET Papers presented at the 19th Symposium on Fusion Technology (SOFT) Lisbon, Portugal, 16-20 September 1996). p.45. Report JET-P(96)44

156. Design and development of a new remote handling transporter facility for JET.
Jones L P D F Irving M Palmer J Hamilton D
JET Joint Undertaking, September 1996 (JET Posters presented at the 19th Symposium on Fusion Technology (SOFT) Lisbon, Portugal, 16-20 September 1996). p.67. Report JET-P(96)45

157. High performance JET plasmas for DT operation with the Mk II divertor
Jones T T C
Bulletin of the American Physical Society, vol.41 no.7 November 1996 (Program of the Thirty-Eighth Annual Meeting of the Division of Plasma Physics, 11-15 November 1996, Denver, Colorado). p.1418.

158. VH mode accessibility and global H-mode properties in previous and present JET configurations.
Jones T T C Ali-Arshad S Bures M Christiansen J P de Esch H P L Fishpool G Jarvis O N Konig R Lawson K D Lomas P J Marcus F B Sartori R Schunke B Smeulders P Stork D Taroni A Thomas P R Thomsen K
21st EPS Conference on Controlled Fusion and Plasma Physics, Montpellier, 27 June - 1 July 1994, Contributed papers, Part I. EuropeanPhysical Society, 1994. p.54.

159. Additions to the spectrum of Be II observed at the JET divertor.
Jupen C Beringer M Meigs A Granzen A
JET Joint Undertaking, 1996. 12p. Report JET-P(96)53

160. Extended and revised analysis of the spectrum and term system of Be III.
Jupen C Beringer M Meigs A Morsi H W von Hellermann M
JET Joint Undertaking, 1996. 26p. Report JET-P(96)52

161. Spectral and correlation analysis of soft X-ray signals from the JET tokamak.
Karlsson J Pazsit I Gill R D
JET Joint Undertaking, 1996. Report JET-P(96)03

162. RF voltage measurements on ICRF antennas
Kaye A S and others
Bulletin of the American Physical Society, vol.41 no.7 November 1996 (Program of the Thirty-Eighth Annual Meeting of the Division of Plasma Physics, 11-15 November 1996, Denver, Colorado). p.1427.

163. Alfven eigenmodes and alpha-particle losses in JET.
Kerner W Appel L C Cox M Hender T C Huysmans G T A O'Brien M R Pinches S D Sharapov S E Zaitsev F S
Plasma Physics and Controlled Nuclear Fusion Research 1994, 15th International Conference, Seville, 26 September-1 October 1994. Vol.3. p.575.

164. The effect of finite sheath conductivity on the interchange instability in the SOL.
Kerner W Nassigh A Pogutse O
JET Joint Undertaking, 1996. 18p. Report JET-P(96)43

165. ELMs as ideal interchange instabilities near the separatrix.
Kerner W Pogutse O van der Linden R Schnuke B
JET Joint Undertaking, 1996. 33p. Report JET-P(96)17

166. Influence of X-point on edge plasma MHD stability.
Kerner W Pogutse O Van der Linden R A M
JET Joint Undertaking, 1995. (JET Papers presented to the 6th European Fusion Theory Conference, Utrecht, The Netherlands, 2-4 October 1995) p.1. Report JET-P(95)64

167. The scaling of the giant ELM frequency.
Kerner W Pogutse O
JET Joint Undertaking, 1996. Report JET-P(96)24

168. Recycling in JET high performance hot-ion H-modes
Konig R W T Lawson K D Lomas P Maas A C Andrew P Breger P Davies S Fasoli A Gowers C Guo H Jones T T C Kubo H McCormick K Marcus F B Stamp M F Thomas P R Zastrow K-D
Bulletin of the American Physical Society, vol.41 no.7 November 1996 (Program of the Thirty-Eighth Annual Meeting of the Division of Plasma Physics, 11-15 November 1996, Denver, Colorado). p.1520.

169. Capacitance of an array of thick rods parallel to the ground - application to the ion cyclotron resonance frequency antenna of the Joint European Torus.
Lamalle P U
Journal of Physics D: Applied Physics, vol.30 no.1 7 January 1997. p.78. Report JET-P(96)06

170. Commissioning tests and enhancements to the JET active gas handling plant.
Lasser R Bell A Bainbridge N Brennan D Grievson B Hemmerich J L Jones G Knipe S Lupo J Mart J Perevezentsev A Skinner N Stagg R Walker K Warren R Yorkshades J
JET Joint Undertaking, October 1996 (JET Papers presented at the 19th Symposium on Fusion Technology (SOFT) Lisbon, Portugal, 16-20 September 1996). p.49. Report JET-P(96)44

171. Upgrading the JET toroidal field to exceed 3.45 Tesla.
Last J R Bertolini E Buzio M Presle P Raimondi T Riccardo V
JET Joint Undertaking, October 1996 (JET Papers presented at the 19th Symposium on Fusion Technology (SOFT) Lisbon, Portugal, 16-20 September 1996). p.57. Report JET-P(96)44

172. Upgrading the JET toroidal field to exceed 3.45T.
Last J R Bertolini E Buzio M Presle P Raimondi T Riccardo V
JET Joint Undertaking, September 1996 (JET Posters presented at the 19th Symposium on Fusion Technology (SOFT) Lisbon, Portugal, 16-20 September 1996). p.73. Report JET-P(96)45

173. Impurity transport of high performance discharges in JET.
Lauro-Taroni L Alper B Giannella R Lawson K Marcus F Mattioli M Smeulders P von Hellerman M
21st EPS Conference on Controlled Fusion and Plasma Physics, Montpellier, 27 June - 1 July 1994, Contributed papers, Part I. European Physical Society, 1994. p.102.

174. Correlations between locked modes and impurity influxes.
Lawson K D Fishpool G M
21st EPS Conference on Controlled Fusion and Plasma Physics, Montpellier, 27 June - 1 July 1994, Contributed papers, Part I. European Physical Society, 1994. p.194.

175. Density scaling of the threshold for locked mode instability in presence of toroidal field ripples in a tokamak.
Lazzaro E de Benedetti M Campbell D Savrukhin P Smolyakov A I
JET Joint Undertaking, 1996. 15p. Report JET-P(96)54

176. Studies of giant ELM interaction with the divertor target in JET.
Lingertat J Tabasso A Ali-Arshad S Alper B van Belle P Borrass K Clement S Coad J P Monk R
JET Joint Undertaking, June 1996. (JET Papers presented at the 12th International Conference on Plasma Surface Interaction in Controlled Fusion Devices, St Raphael, France, 20-24 May 1996) p.87. Report JET-P(96)22

177. Understanding the edge physics of divertor experiments by comparison of 2-D edge code calculations and experimental measurements.
Loarte A

JET Joint Undertaking, 1996. (JET Invited Papers presented at the 12th International Conference on Plasma Surface Interaction in Controlled Fusion Devices, St Raphael, France, 20-24 May 1996). p.33. Report JET-P(96)23

178. High fusion performance ELM-free H-modes and the approach to steady operation.
Lomas P J and the JET Team
JET Joint Undertaking, October 1996. (JET Papers presented at the 16th IAEA Fusion Energy Conference, Montreal, Canada, 7-11 October 1996). p.29. Report JET-P(96)51

179. High fusion performance plasmas in JET.
Lomas P J Ali-Arshad S Alper B Bures M Balet B Christiansen J P Cordey G Deliyanakis N De Esch H Fishpool G Giannella R Hender T Huysmans G Jarvis O N Jones T T C Konig R Lawson K McCormick K Maas A Marcus F Nave F Parail V Porte L Sartori R Schunke B Smeulders P Taroni A Thomsen K Thomas P R
JET Joint Undertaking, 1995. (JET Posters presented to the 37th Annual Meeting, APS Division of Plasma Physics, Louisville, USA, 6-10 November 1995.) p.81. Report JET-P(95)72

180. Initial operation of an ITER compatible lost alpha detector at JET.
Loughlin M J Cecil F E Hone M Jarvis O N Sadler G J van Belle P Whitfield G
Diagnostics for Experimental Thermonuclear Fusion Reactors: Proceedings of the International Workshop on Diagnostics for ITER, August 28 - September 1, 1995, Varenna, Plenum Press, New York, 1996. p.477.

181. Simulation of triton burn-up in JET plasmas.
Loughlin M J Balet B Jarvis O N Stubberfield P M
21st EPS Conference on Controlled Fusion and Plasma Physics, Montpellier, 27 June - 1 July 1994, Contributed papers, Part I. European Physical Society, 1994. p.258.

182. Divertor configuration studies on JET.
Lowry C G Campbell D J Davies S Guo H Harbour P J von Hellermann M Horton L D Loarte A Maggi C Matthews G Mohanti R Monk R Radford G J Reichle R Saibene G Spence J Stamp M Taroni A Vlases G C
JET Joint Undertaking, June 1996. (JET Papers presented at the 12th International Conference on Plasma Surface Interaction in Controlled Fusion Devices, St Raphael, France, 20-24 May 1996) p.187. Report JET-P(96)22

183. Ion temperature anisotropy in high power helium neutral beam fuelling experiments in JET.
Maas A C Core W G F Gerstel U C von Hellermann M G Konig R W T Marcus F B
21st EPS Conference on Controlled Fusion and Plasma Physics, Montpellier, July 1994, Contributed papers, Part I. European Physical Society, 1994. p.254.

184. Developments towards remote metrology for component alignment under conditions of restricted access in JET's toroidal vacuum vessel.
Macklin B Brade R Celentano G Tait J van Lente E
JET Joint Undertaking, 1996. Report JET-P(96)13

185. Measurement and analysis of radiated power components in the JET MkI divertor using VUV spectroscopy.
Maggi C F Elder J D Fundamenski W Giannella R Horton L D Lawson K D Loarte A Maas A Reichle R Stamp M Stangeby P C Summers H P
JET Joint Undertaking, June 1996. (JET Papers presented at the 12th International Conference on Plasma Surface Interaction in Controlled Fusion Devices, St Raphael, France, 20-24 May 1996) p.51. Report JET-P(96)22

186. Enhancement of JET machine instrumentation and coil protection systems.
Marchese V Businaro T Buzio M De Marchi E Dolgetta N Howie J Last J Raimondi T Scibile L van Veen J
JET Joint Undertaking, October 1996 (JET Papers presented at the 19th Symposium on Fusion Technology (SOFT) Lisbon, Portugal, 16-20 September 1996). p.61. Report JET-P(96)44

187. Enhancement of JET machine instrumentation and coil protection systems.

Marchese V Businaro T Buzio M De Marchi E Dolgetta N Howie J Last J Raimondi T Scibile L van Veen J
JET Joint Undertaking, September 1996 (JET Posters presented at the 19th Symposium on Fusion Technology (SOFT) Lisbon, Portugal, 16-20 September 1996). p.79. Report JET-P(96)45

188. Effects of sawtooth crashes on beam ions and fusion product tritons in JET.
Marcus F B Adams J M Bond D S Hone M A Howarth P J A Jarvis O N Loughlin M J Sadler G Watkins N
21st EPS Conference on Controlled Fusion and Plasma Physics, Montpellier, July 1994, Contributed papers, Part I. European Physical Society, 1994. p.274.

189. A neutron camera for ITER: conceptual design.
Marcus F B Adams J M Batistoni P Elevant T Jarvis O N Johnson L C de Kock L Sadler G Stott P E
Diagnostics for Experimental Thermonuclear Fusion Reactors: Proceedings of the International Workshop on Diagnostics for ITER, August 28 - September 1, 1995, Varenna, Plenum Press, New York, 1996. p.385.

190. A neutron camera for ITER.
Marcus F B Adams J M Bond D S Batistoni P Elevant T Hawkes N P Jarvis O N Johnson L de Kock L Loughlin M Rapisarda M Sadler G Stott P Walker C Watkins N
JET Joint Undertaking, 1996. (JET Papers presented at the 11th APS Conference on High Temperature Plasma Diagnostics, Monterey, CA, USA, 12-16 May 1996) p.7. Report JET-P(96)18

191. A power step-down approach to high performance, steady-state operation with ELM-free H-mode deuterium plasmas in JET.
Marcus F B Balet B Deliyanakis N Giannella R Gowers C Jarvis O N Jones T T C Konig R Lomas P Rimini F Smeulders P Thomas P
JET Joint Undertaking, 1996. Report JET-P(96)59

192. Scaling radiative plasmas to ITER.
Matthews G F Allen S Asakura N Goetz J Guo H Kallenbach A Lipschultz B McCormick K Stamp M Samm U Stangeby P C Steuer K-H Taroni A Unterberg B West P
JET Joint Undertaking, June 1996. (JET Papers presented at the 12th International Conference on Plasma Surface Interaction in Controlled Fusion Devices, St Raphael, France, 20-24 May 1996) p.165. Report JET-P(96)22

193. Technical performance of fixed langmuir probe system in the JET pumped divertor.
Matthews G F Davies S J Monk R D
JET Joint Undertaking, 1995. (JET papers presented to 2nd workshop on electrical probes in magnetised plasmas Berlin, Germany, 4-6 October 1995). p.1. Report JET-P(95)68

194. Interpretation of measurements of ICRF-heated minority proton distributions in JET.
McClements K G Dendy R O Gondhalekar A
JET Joint Undertaking, 1996. Report JET-P(96)50

195. Derivation of SOL transport coefficients using 2D modelling for hot-ion ELM-free H-modes in JET.
McCormick G K Chankin A Clement S Davies S Ehrenberg J Loarte A Monk R Simonini R Spence J Stamp M Taroni A Vlases G
JET Joint Undertaking, June 1996. (JET Papers presented at the 12th International Conference on Plasma Surface Interaction in Controlled Fusion Devices, St Raphael, France, 20-24 May 1996) p.149. Report JET-P(96)22

196. Ar XVII and Ar XVIII in the JET Tokamak.
McGinnity P Barnsley R Coffey I H Keenan F P O'Mullane M G Peacock N J
JET Joint Undertaking, 1995. (JET Papers presented to the 11th Colloquium on UV and X-Ray Spectroscopy of Astrophysical and Laboratory Plasmas, Nagoya, Japan, 29 May - 2 June 1995) p.7. Report JET-P(95)54

197. Optimisation of computational MHD normal-mode analysis in tokamaks.
Mikhailovskii A B Huysmans G T A Kerner W O K Sharapov S E
JET Joint Undertaking, 1996. 28p. Report JET-P(96)25

198. Enhancement of the JET vacuum vessel supports.
Miller A Hemmerich J L
JET Joint Undertaking, October 1996 (JET Papers presented at the 19th Symposium on Fusion Technology (SOFT) Lisbon, Portugal, 16-20 September 1996). p.65. Report JET-P(96)44

199. Enhancement of the JET vacuum vessel supports.
Miller A Hemmerich J L
JET Joint Undertaking, September 1996 (JET Posters presented at the 19th Symposium on Fusion Technology (SOFT) Lisbon, Portugal, 16-20 September 1996). p.85. Report JET-P(96)45

200. Design and development of RH tools for the JET divertor exchange.
Mills S F Loving A B
JET Joint Undertaking, October 1996 (JET Papers presented at the 19th Symposium on Fusion Technology (SOFT) Lisbon, Portugal, 16-20 September 1996). p.69. Report JET-P(96)44

201. Design and development of RH tools for the JET divertor exchange.
Mills S F Loving A B
JET Joint Undertaking, September 1996 (JET Posters presented at the 19th Symposium on Fusion Technology (SOFT) Lisbon, Portugal, 16-20 September 1996). p.91. Report JET-P(96)45

202. Divertor langmuir probe measurements in JET.
Monk R D Loarte A Chankin A Clement S Davies S J Gunther K Guo H Y Lingertat J Maggi C F Matthews G F Stamp M F Tabasso A
JET Joint Undertaking, 1995. (JET papers presented to 2nd workshop on electrical probes in magnetised plasmas Berlin, Germany, 4-6 October 1995). p.15. Report JET-P(95)68

203. Interpretation of ion flux and electron temperature profiles at the JET divertor target during high recycling and detached discharges.
Monk R D Loarte A Chankin A Clement S Davies S J Ehrenberg J K Guo H Y Lingertat J Matthews G F Stamp M F Stangeby P C
JET Joint Undertaking, June 1996. (JET Papers presented at the 12th International Conference on Plasma Surface Interaction in Controlled Fusion Devices, St Raphael, France, 20-24 May 1996) p.41. Report JET-P(96)22

204. An overview of MHD activity at the termination of JET hot-ion H-modes.
Nave M F F Smeulders P Hender T C Lomas P J Alper B Bak P Balet B Christiansen J P S de Esch H P L Hawkes N Huysmans G T A Jones T T C Konig R Lawson K Lingertat J Maas A Marcus F B O'Brien D P Rookes A Sartori R Stamp M Schunke B Thomas P R Thomsen K
JET Joint Undertaking, 1996. 21p. Report JET-P(96)14

205. Present understanding of electromagnetic behaviour during disruptions in JET.
Noll P Andrew P Buzio M Litunovsky R Raimondi T Riccardo V Verrecchia M
JET Joint Undertaking, October 1996 (JET Papers presented at the 19th Symposium on Fusion Technology (SOFT) Lisbon, Portugal, 16-20 September 1996). p.73. Report JET-P(96)44

206. Present understanding of electromagnetic behaviour during disruptions in JET.
Noll P Andrew P Buzio M Litunovsky R Raimondi T Riccardo V Verrecchia M
JET Joint Undertaking, September 1996 (JET Posters presented at the 19th Symposium on Fusion Technology (SOFT) Lisbon, Portugal, 16-20 September 1996). p.97. Report JET-P(96)45

207. Drift wave transport simulations of dimensionally similar JET discharges
Nordman H et al
Report JET-P(96)02

208. Flexible corrugated cryotransferlines, long term experience at JET and the experience with supercritical helium flow conditions.
Obert W Mayaux C
JET Joint Undertaking, 1996. Report JET-P(96)26

209. JET experience with the large scale cryogenic system.
Obert W
JET Joint Undertaking, 1996. Report JET-P(96)27

210. Performance of the supercritical helium cooling loop for the JET divertor cryopump.
Obert W Mayaux C Barth K Herblin L
Advances in Cryogenic Engineering, vol.41, 1996 (Proceedings of the 1995 Cryogenic Engineering Conference, July 17-21, 1995, Columbus, Ohio). p.751.

211. Non-linear collisionless magnetic reconnection and fast relaxations.
Ottaviani M Porcelli F
Plasma Physics and Controlled Nuclear Fusion Research 1994, 15th International Conference, Seville, 26 September-1 October 1994. Vol.3. p.417.

212. Thermal transport from a phenomenological description of ion-temperature-gradient-driven turbulence.
Ottaviani M Horton W Erba M
JET Joint Undertaking, 1996. Report JET-P(96)16

213. Unanswered questions in ion-temperature gradient-driven turbulence.
Ottaviani M Beer M A Cowley S Horton W Krommes J
JET Joint Undertaking, 1996. Report JET-P(95)70

214. Magnetic reconstruction of TFTR and JET current profiles with TRANSP.
O'Brien D Stubberfield P and others
Bulletin of the American Physical Society, vol.41 no.7 November 1996 (Program of the Thirty-Eighth Annual Meeting of the Division of Plasma Physics, 11-15 November 1996, Denver, Colorado). p.1515.

215. Effect of shear in the radial electric field on confinement in JET.
O'Brien D P Balet B Deliyanakis N Cordey J Stubberfield P M
21st EPS Conference on Controlled Fusion and Plasma Physics, Montpellier, 1 July 1994, Contributed papers, Part I. European Physical Society, 1994. p.346.

216. Analysis of emission spectra from Marfes in JET.
O'Mullane M G Coffey I H Peacock N J Giannella R Reichle R
JET Joint Undertaking, 1995. (JET Papers presented to the 11th Colloquium on UV and X-Ray Spectroscopy of Astrophysical and Laboratory Plasmas, Nagoya, Japan, 29 May - 2 June 1995.) p.13. Report JET-P(95)54

217. Monitoring of detachment and the edge using XUV impurity spectra from the Mk1 divertor phase of JET.
O'Mullane M G Coffey I H Giannella R
JET Joint Undertaking, July 1996. (JET Posters presented at the 23rd EPS Conference Kiev, Ukraine, 24-28 June 1996). p.79. Report JET-P(96)30

218. Monitoring of detachment and the edge using XUV impurity spectra from the Mark I divertor phase of JET.
O'Mullane M G Coffey I H Giannella R
JET Joint Undertaking, August 1996. (JET Papers presented at the 23rd EPS Conference on Plasma Physics and Controlled Fusion, Kiev, Ukraine, 24-28 June 1996). p.95. Report JET-P(96)33

219. Variation of impurity transport during ELMy H-modes in JET plasmas.
O'Mullane M G Chen H Flewin C Hawkes N C von Hellermann M Lauro-Taroni L Peacock N J
JET Joint Undertaking, July 1996. (JET Posters presented at the 23rd EPS Conference Kiev, Ukraine, 24-28 June 1996). p.85. Report JET-P(96)30

220. Variation of impurity transport during ELMy H-modes in JET plasmas.
O'Mullane M G Chen H Flewin C Hawkes N C von Hellermann M Lauro-Taroni L Peacock N J
JET Joint Undertaking, August 1996. (JET Papers presented at the 23rd EPS Conference on Plasma Physics and Controlled Fusion, Kiev, Ukraine, 24-28 June 1996). p.103. Report JET-P(96)33

221. Effects of high frequency disruptions on the JET divertor cryopump, including potential JET toroidal field upgrades.
Papastergiou S Ageladarakis P
JET Joint Undertaking, October 1996 (JET Papers presented at the 19th Symposium on Fusion Technology (SOFT) Lisbon, Portugal, 16-20 September 1996). p.77. Report JET-P(96)44

222. Effects of high frequency disruptions on the JET divertor cryopump, including potential JET toroidal field upgrades.

Papastergiou S Ageladarakis P
JET Joint Undertaking, September 1996 (JET Posters presented at the 19th Symposium on Fusion Technology (SOFT) Lisbon, Portugal, 16-20 September 1996). p.105. Report JET-P(96)45

223. Optimisation of support positions for fusion in-vessel components to minimise eddy current stresses.
Papastergiou S Ageladarakis P
JET Joint Undertaking, 1996. Report JET-P(96)48

224. On the problem of the transient transport in a tokamak.
Parail V Cherubini A Cordey J G Erba M Galli P Romanelli F Springmann E Taroni A
JET Joint Undertaking, 1995. Report JET-P(96)08

225. Numerical analysis of the heat pulses in JET.
Parail V V Cherubini A Erba M Galli P Giannella R Porte L Rookes A Romanelli F Springmann E Taroni A
JET Joint Undertaking, August 1996. (JET Papers presented at the 23rd EPS Conference on Plasma Physics and Controlled Fusion, Kiev, Ukraine, 24-28 June 1996). p.111. Report JET-P(96)33

226. Plasma transport properties at the L-H transition and high performance phase of JET discharges.
Parail V V Balet B Cordey J G Erba M Jones T T C Lomas P J Smeulders P Springmann E M Stubberfield P M Taroni A Thomsen K
21st EPS Conference on Controlled Fusion and Plasma Physics, Montpellier, July 1994, Contributed papers, Part I. European Physical Society, 1994. p.106.

227. Development of silver-free bonding techniques and an investigation of the effect of cadmium in brazed joints made with silver based brazing alloys.
Peacock A T Harrison M R Jacobson D M Pick M Sangha S P S Vieider G
JET Joint Undertaking, October 1996 (JET Papers presented at the 19th Symposium on Fusion Technology (SOFT) Lisbon, Portugal, 16-20 September 1996). p.85. Report JET-P(96)44

228. Development of silver-free bonding techniques and an investigation of the effect of cadmium in brazed joints made with silver based brazing alloys.
Peacock A T Harrison M R Jacobsen D M Pick M Sangha S P S Vieider G
JET Joint Undertaking, September 1996 (JET Posters presented at the 19th Symposium on Fusion Technology (SOFT) Lisbon, Portugal, 16-20 September 1996). p.117. Report JET-P(96)45

229. The experience with JET'S combined DC/RF glow discharge cleaning (GDC) system.
Pearce R J H Andrew P Bryan S Claesen R Harling J How J Jensen H McBryan H Orchard J Saibene G Vadgama A
Vacuum, vol. 47 nos.6-8 June-August 1996 (Proceedings of the 13th International Vacuum Congress and the 9th International Conference on Solid Surfaces, 25-29 September 1995, Yokahoma, Japan) p.665. Report JET-P(95)52

230. Tritium extraction from gases by isotopic exchange with molecular hydrogen.
Perevezentsev A N
JET Joint Undertaking, 1996. 13p. Report JET-P(96)04

231. Functional dependence of the lower hybrid power absorption coefficient in JET.
Pericoli-Ridolfini V Ekedahl A Baranov Y Dobbing J A Fischer B Gormezano C Lennholm M Rimini F Romero J Schild P Soldner F X
JET Joint Undertaking, 1996. Report JET-R(96)08

232. Functional dependence of the lower hybrid power absorption coefficient in JET.
Pericoli-Ridolfini V Ekedahl A Baranov Y Dobbing J A Fischer B Gormezano C Lennholm M Rimini F Romero J Schild P Soldner F X
JET Joint Undertaking, 1996. 13p. Report JET-P(96)55

233. JET's latest technical and scientific results and engineering development.
Pick M A and the JET Team
JET Joint Undertaking, 1996. Report JET-P(96)29

234. Operational aspects of using beryllium - safety and decontamination.
Pick M A Haigh A D

JET Joint Undertaking, November 1995. (JET papers presented to the 2nd IEA International Workshop on Beryllium Technology for Fusion, 6 September 1995, Jackson Hole, USA.) p.1. Report JET-P(95)59

235. Modelling the sawtooth period at JET.
Porcelli F
JET Joint Undertaking, 1995. Report JET-IR(95)02

236. Evolution of edge electron temperature and density in JET H-mode plasmas.
Porte L Bartlett D V Deliyanakis N Rookes A
JET Joint Undertaking, 1995. (JET Posters presented to the 37th Annual Meeting, APS Division of Plasma Physics, Louisville, USA, 6-10 November 1995.) p.91. Report JET-P(95)72

237. Real-time control of plasma boundary in JET.
Puppin S Angoletta M E Campbell D J Ellis J J Garibba M Lennholm M Milani F O'Brien D Sartori F Sartori R
JET Joint Undertaking, October 1996 (JET Papers presented at the 19th Symposium on Fusion Technology (SOFT) Lisbon, Portugal, 16-20 September 1996). p.89. Report JET-P(96)44

238. Real-time control of plasma boundary in JET.
Puppin S Angoletta M E Campbell D J Ellis J J Garribba M Lennholm M Milani F O'Brien D Sartori F Sartori R
JET Joint Undertaking, September 1996 (JET Posters presented at the 19th Symposium on Fusion Technology (SOFT) Lisbon, Portugal, 16-20 September 1996). p.123. Report JET-P(96)45

239. The particle and heat drift fluxes and their implementation into the EDGE2D transport code.
Radford G J Chankin A V Corrigan G Simonini R Spence J Taroni A
Contributions to Plasma Physics, vol.36 nos.2/3 1996, (5th International Workshop on Plasma Edge Theory in Fusion Devices, December 4-6, 1995, Asilomar, CA.) p.187

240. Bolometer for ITER.
Reichle R and others
Diagnostics for Experimental Thermonuclear Fusion Reactors: Proceedings of the International Workshop on Diagnostics for ITER, August 28 - September 1, 1995, Varenna, Plenum Press, New York, 1996. p.559.

241. Low energy neutral particle fluxes in the JET divertor.
Reichle R Ehrenberg J K Gottardi N A C Horton L D Ingesson L C Jackel H J McCormick G K Loarte A Simonini R Stamp M F
JET Joint Undertaking, June 1996. (JET Papers presented at the 12th International Conference on Plasma Surface Interaction in Controlled Fusion Devices, St Raphael, France, 20-24 May 1996) p.175. Report JET-P(96)22

242. Fast wave studies in JET.
Rimini F and the JET Team
Plasma Physics and Controlled Nuclear Fusion Research 1994, 15th International Conference, Seville, 26 September-1 October 1994. Vol.2. p.221.

243. The assessment and improvement of JET remote handling equipment availability.
Rolfe A C Scott E Smith D
JET Joint Undertaking, October 1996 (JET Papers presented at the 19th Symposium on Fusion Technology (SOFT) Lisbon, Portugal, 16-20 September 1996). p.93. Report JET-P(96)44

244. The assessment and improvement of JET remote handling system availability.
Rolfe A C Scott E Smith D
JET Joint Undertaking, September 1996 (JET Posters presented at the 19th Symposium on Fusion Technology (SOFT) Lisbon, Portugal, 16-20 September 1996). p.129. Report JET-P(96)45

245. Reaching JET's remotest parts.
Rolfe A C
Nuclear Engineering International, vol.41 no.503 June 1996. p.24.

246. First measurements of gas balance and chemical composition in the MK1 pumped divertor phase of JET using the gas collection system.
Rossi A Saibene G Kupschus P

JET Joint Undertaking, July 1996. (JET Posters presented at the 23rd EPS Conference Kiev, Ukraine, 24-28 June 1996). p.91. Report JET-P(96)30

247. First measurements of gas balance and chemical composition in the Mk I pumped divertor phase of JET using the gas collection system.
Rossi A Saibene G Kupschus P
JET Joint Undertaking, August 1996. (JET Papers presented at the 23rd EPS Conference on Plasma Physics and Controlled Fusion, Kiev, Ukraine, 24-28 June 1996). p.117. Report JET-P(96)33

248. Results from the ITER H-mode threshold database.
Ryter F Snipes J A Granetz R S Greenwald M Kardaun F Kus A Ryter F Stroth U Ryter F Kollermeyer J Fielding S J Valovic M DeBoo J C Carlstrom T N Schissel D P Thomsen K Campbell D J Christiansen J P Cordey J G Righi E Miura Y Suzuki N Mori M Matsuda T Tamai H Fukuda T Kamada Y Matsuda T Sato M Takizuka T Tsuchiya K Kaye S M
JET Joint Undertaking, 1995. (JET papers presented to the IAEA H-mode Workshop, Princeton, 1995.) p.27. Report JET-P(95)50

249. The comparative analysis of the different mechanisms of toroidal rotation in tokamaks.
Sabot R Parail V
21st EPS Conference on Controlled Fusion and Plasma Physics, Montpellier, 27 June - 1 July 1994, Contributed papers, Part I. European Physical Society, 1994. p.350.

250. Influence of active pumping on density and confinement behaviour of JET plasmas.
Saibene G Campbell D Horton L D Loarte A Monk R D Righi E Stork D
JET Joint Undertaking, June 1996. (JET Papers presented at the 12th International Conference on Plasma Surface Interaction in Controlled Fusion Devices, St Raphael, France, 20-24 May 1996) p.197. Report JET-P(96)22

251. Operational experience with the JET saddle coil system.
Santagiustina A Altmann H Buzio M Campbell D J Claesen R D'Antona G Benedetti M De Fasoli A Israel G Ostrom R Peruzzo S Raimondi T Rossi L Sartori F Tabellini M Tanga A Zullo G
JET Joint Undertaking, October 1996 (JET Papers presented at the 19th Symposium on Fusion Technology (SOFT) Lisbon, Portugal, 16-20 September 1996). p.97. Report JET-P(96)44

252. Operational experience with the JET saddle coil system.
Santagiustina A Altmann H Buzio M Campbell D J Claesen R D'Antona G Benedetti M De Dobbing J A Fasoli A Israel G Ostrom R Raimondi T Rossi L Sartori F Tabellini M Tanga A Zullo G
JET Joint Undertaking, September 1996 (JET Posters presented at the 19th Symposium on Fusion Technology (SOFT) Lisbon, Portugal, 16-20 September 1996). p.135. Report JET-P(96)45

253. Numerical simulations of feedback control of magnetic field perturbations in JET tokamak.
Savrukhin P Campbell D J D'Antona G Santaguistina A
IEEE Transactions on Nuclear Science, vol.43 no.1 part 1, February 1996, (Selected papers from the Ninth Conference on Real-time Computer Applications in Nuclear, Particle, and Plasma Physics (Real-time '95)). p.238.

254. Pfirsch-Schluter currents in the JET divertor.
Schaffer M J Chankin A V Guo H-Y Matthews G F Monk R
JET Joint Undertaking, 1996. Report JET-P(96)11

255. Operation of high power ICRH with ELMy plasmas at JET.
Schmid M Bhatnagar V Gormezano C Lamalle P U Sibley A Simon M Timms M Wade T
JET Joint Undertaking, October 1996 (JET Papers presented at the 19th Symposium on Fusion Technology (SOFT) Lisbon, Portugal, 16-20 September 1996). p.101. Report JET-P(96)44

256. Operation of high power ICRH with ELMy plasmas at JET.
Schmid M Bhatnagar V Gormezano C Lamalle P U Sibley A Simon M Timms M Wade T

JET Joint Undertaking, September 1996 (JET Posters presented at the 19th Symposium on Fusion Technology (SOFT) Lisbon, Portugal, 16-20 September 1996). p.143. Report JET-P(96)45

257. Log-additive parameterization of JET electron temperature and density profiles.
Schunke B Imre K Riedel K S
JET Joint Undertaking, 1996. Report JET-P(95)80

258. A predictive study of the JET Mark II gas box divertor.
Simonini R Corrigan G Radford G Spence J Taroni A Vlases G
JET Joint Undertaking, July 1996. (JET Posters presented at the 23rd EPS Conference Kiev, Ukraine, 24-28 June 1996). p.97. Report JET-P(96)30

259. A predictive study of the JET Mark II gas box divertor.
Simonini R Corrigan G Radford G Spence J Taroni A Vlases G
JET Joint Undertaking, August 1996. (JET Papers presented at the 23rd EPS Conference on Plasma Physics and Controlled Fusion, Kiev, Ukraine, 24-28 June 1996). p.125. Report JET-P(96)33

260. Beta limits in H-modes and VH-modes in JET.
Smeulders P Hender T C Huysmans G Marcus F Ali-Arshad S Alper B Balet B Bures M Deliyanakis N de Esch H Fishpool G Jarvis O N Jones T T C Kerner W Koenig R Lawson K Lomas P Nave M F O'Brien D Sadler G Stork D Stubberfield P Thomas P Thomsen K Wesson J
21st EPS Conference on Controlled Fusion and Plasma Physics, Montpellier, 27 June - 1 July 1994, Contributed papers, Part I. European Physical Society, 1994. p.206.

261. Extension of high-performance NCS operating regimes to low-triangularity plasmas, with implications for JET/ITER
Soldner F Sips G and others
Bulletin of the American Physical Society, vol.41 no.7 November 1996 (Program of the Thirty-Eighth Annual Meeting of the Division of Plasma Physics, 11-15 November 1996, Denver, Colorado). p.1386.

262. JET/DIII-D similarity experiments on shear optimization
Soldner F X Cherubini A Fischer B Gormezano C Parail V V Sips A C C Tubbing B J D and others
Bulletin of the American Physical Society, vol.41 no.7 November 1996 (Program of the Thirty-Eighth Annual Meeting of the Division of Plasma Physics, 11-15 November 1996, Denver, Colorado). p.1520.

263. Radial electric fields induced by poloidal ponderomotive forces of LH waves.
Soldner F X and others
Bulletin of the American Physical Society, vol.41 no.7 November 1996 (Program of the Thirty-Eighth Annual Meeting of the Division of Plasma Physics, 11-15 November 1996, Denver, Colorado). p.1428.

264. Modelling impurity injection edge experiments.
Stangeby P C
JET Joint Undertaking, 1996. 38p. Report JET-IR(96)03

265. Simple models for the radial and poloidal E x B drifts in the scrape-off layer of a divertor tokamak: effects on in/out asymmetries.
Stangeby P C Chankin A V
Nuclear Fusion, vol.36 no.7 July 1996. p.839.

266. Alfven eigenmodes and fast particle physics in JET reactor relevant plasmas.
Start D F H and the JET Team
JET Joint Undertaking, October 1996. (JET Papers presented at the 16th IAEA Fusion Energy Conference, Montreal, Canada, 7-11 October 1996). p.43. Report JET-P(96)51

267. The H-mode power threshold in JET.
Start D F H Bhatnagar V P Campbell D J Cordey J G De Esch H P L Gormezano C Hawkes N Horton L Jones T T Lomas P J Lowry C Righi E Rimini F G Saibene G Sartori R Sips G Stork D Thomas P Thomsen K Tubbing B J D von Hellermann M Ward D J
21st EPS Conference on Controlled Fusion and Plasma Physics, Montpellier, 27 June - 1 July 1994, Contributed papers, Part I. European Physical Society, 1994. p.314.

268. Optimisation of JET steady-state ELMy discharges with ITER-relevant divertor conditions.
Stork D and the JET Team
JET Joint Undertaking, October 1996. (JET Papers presented at the 16th IAEA Fusion Energy Conference, Montreal, Canada, 7-11 October 1996). p.21. Report JET-P(96)51

269. Reflectometry for ITER density profiles.
Stott P E and others
Diagnostics for Experimental Thermonuclear Fusion Reactors: Proceedings of the International Workshop on Diagnostics for ITER, August 28 - September 1, 1995, Varenna, Plenum Press, New York, 1996. p.133.

270. Comparison between JET profile data and the predictions of a reactive drift wave model for anomalous transport.
Strand P Nordman H Frojdh M Weiland J Christiansen J P
JET Joint Undertaking, 1995. (JET Papers presented to the 6th European Fusion Theory Conference, Utrecht, The Netherlands, 2-4 October 1995). p.9. Report JET-P(95)64

271. Edge density profiles in high-performance JET plasmas.
Summers D D R Breger P Erents K Pietrzyk Z A Viaccoz B Vince J
JET Joint Undertaking, June 1996. (JET Papers presented at the 12th International Conference on Plasma Surface Interaction in Controlled Fusion Devices, St Raphael, France, 20-24 May 1996) p.127. Report JET-P(96)22

272. Disruptions and vertical displacement events in JET.
Tanga A and the JET Team
JET Joint Undertaking, October 1996. (JET Papers presented at the 16th IAEA Fusion Energy Conference, Montreal, Canada, 7-11 October 1996). p.63. Report JET-P(96)51

273. Energy and particle transport modelling with a time dependent combined core and edge transport code.
Taroni A and the JET Team
JET Joint Undertaking, October 1996. (JET Papers presented at the 16th IAEA Fusion Energy Conference, Montreal, Canada, 7-11 October 1996). p.83. Report JET-P(96)51

274. Transport modelling with a combined core and edge code.
Taroni A Cherubini A Corrigan G Guo H McCormick G K Radford G J Simonini R Spence J Springmann E
JET Joint Undertaking, July 1996. (JET Posters presented at the 23rd EPS Conference Kiev, Ukraine, 24-28 June 1996). p.103. Report JET-P(96)30

275. Transport modelling with a combined core and edge code.
Taroni A Cherubini A Corrigan G Guo H McCormick G K Radford G J Simonini R Spence J Springmann E
JET Joint Undertaking, August 1996. (JET Papers presented at the 23rd EPS Conference on Plasma Physics and Controlled Fusion, Kiev, Ukraine, 24-28 June 1996). p.131. Report JET-P(96)33

276. Bifurcations and intermittent magnetic activity.
Tebaldi C Ottaviani M Porcelli F
Plasma Physics and Controlled Fusion, vol.38 no.4 April 1996. p.619.

277. Divertor diagnostics for JET.
Thomas P R
Diagnostics for Experimental Thermonuclear Fusion Reactors: Proceedings of the International Workshop on Diagnostics for ITER, August 28 - September 1, 1995, Varenna, Plenum Press, New York, 1996. p.531.

278. Performance limitations in JET hot-ion H-modes.
Thomas P R and the JET Team
JET Joint Undertaking, October 1996. (JET Papers presented at the 16th IAEA Fusion Energy Conference, Montreal, Canada, 7-11 October 1996). p.51. Report JET-P(96)51

279. Plasma performance on solid and molten beryllium divertor targets in JET.
Tubbing B J D and the JET Team
JET Joint Undertaking, 1995. (JET Posters presented to the 37th Annual Meeting, APS Division of

Plasma Physics, Louisville, USA, 6-10 November 1995.) p.101. Report JET-P(95)72

280. Spectroscopic investigation of C IV.
Tunklev M Engstrom L Jupen C Kink I Martinson I Meigs A
JET Joint Undertaking, 1996. Report JET-P(96)15

281. Ballooning instabilities in the scrape-off layer of diverted tokamaks as giant ELM precursors.
van der Linden R A M Kerner W Pogutse O Schunke B
JET Joint Undertaking, July 1996. (JET Posters presented at the 23rd EPS Conference Kiev, Ukraine, 24-28 June 1996). p.109. Report JET-P(96)30

282. Ballooning instabilities in the scrape- off-layer of diverted tokamaks as giant ELM precursors.
Van der Linden R A M Kerner W Pogutse O Schunke B
JET Joint Undertaking, August 1996. (JET Papers presented at the 23rd EPS Conference on Plasma Physics and Controlled Fusion, Kiev, Ukraine, 24-28 June 1996). p.137. Report JET-P(96)33

283. Movement of the radiative zone from target to X-point in radiative divertor scenarios.
Van der Linden R A M Huysmans G T A Kerner W Reichle R Wesson J A
JET Joint Undertaking, 1995. (JET Papers presented to the 6th European Fusion Theory Conference, Utrecht, The Netherlands, 2-4 October 1995). p.21. Report JET-P(95)64

284. Geometry free of singularities for fusion duplex components.
Viola R Deksnis E B
Fusion Engineering and Design, vol.31 no.1 April 1996. p.17.

285. Effect of divertor configuration on plasma performance in JET.
Vlases G and the JET Team
JET Joint Undertaking, October 1996. (JET Papers presented at the 16th IAEA Fusion Energy Conference, Montreal, Canada, 7-11 October 1996). p.71. Report JET-P(96)51

286. Lightly-or non-seeded, partially detached ITER divertor operation.
Vlases G Corrigan G Taroni A
JET Joint Undertaking, June 1996. (JET Papers presented at the 12th International Conference on Plasma Surface Interaction in Controlled Fusion Devices, St Raphael, France, 20-24 May 1996) p.29. Report JET-P(96)22

287. Feasibility of quantitative spectroscopy on ITER.
von Hellermann M G Core W G F Howman A Jupen C Konig R W T Stamp M F Summers H P Thomas P R Zastrow K-D
Diagnostics for Experimental Thermonuclear Fusion Reactors: Proceedings of the International Workshop on Diagnostics for ITER, August 28 - September 1, 1995, Varenna, Plenum Press, New York, 1996. p.321.

288. LH transition theories and theory of H-mode.
Ward D J
Plasma Physics and Controlled Fusion, vol.38 no.8 August 1996 (Papers from the 5th IAEA Technical Committee Meeting/US-Japan Workshop on H-mode Physics, Princeton, 18-20 September 1995). p.1201. Report JET-P(95)50

289. The Joint European Torus (JET) pumped divertor results and their significance for the International Thermonuclear Experimental Reactor (ITER).
Watkins M L and the JET Team
Physics of Plasmas, vol.3 no.5 pt.2 May 1996 (Special issue: Invited and Review Papers from the 37th Annual Meeting of the Division of Plasma Physics of the American Physical Society, 6-10 November 1995, Louisville, Kentucky). p.1881.

290. Abrupt changes in confinement in the JET tokamak.
Wesson J A Balet B
Physical Review Letters, vol.77 no.26 23 December 1996. p.5214. Report JET-P(96)19

291. Poloidal distribution of impurities in a rotating tokamak plasma.
Wesson J A
JET Joint Undertaking, 1996. 10p. Report JET-P(96)36

292. Engineering design of the JET edge Thomson scattering system.
Wilson D J Nielsen P Gowers C W Eagle R J
JET Joint Undertaking, October 1996 (JET Papers presented at the 19th Symposium on Fusion Technology (SOFT) Lisbon, Portugal, 16-20 September 1996). p.105. Report JET-P(96)44

293. Engineering design of the JET edge Thomson scattering system.
Wilson D J Nielsen P Gowers C W Eagle R J
JET Joint Undertaking, September 1996 (JET Posters presented at the 19th Symposium on Fusion Technology (SOFT) Lisbon, Portugal, 16-20 September 1996). p.149. Report JET-P(96)45

294. The ITER diagnostic programme.
Young K M Costley A E Matoba T Orlinski D V Stott P E
Diagnostics for Experimental Thermonuclear Fusion Reactors: Proceedings of the International Workshop on Diagnostics for ITER, August 28 - September 1, 1995, Varenna, Plenum Press, New York, 1996. p.13.

295. Plasma heating by Langmuir probe.
Yu Q Wesson J
JET Joint Undertaking, 1996. 5p. Report JET-P(96)39

296. Experimental results using the JET real-time power control system.
Zornig N H Brelen H E O Browne A Browne M L Gormezano C Dobbing T How J A Jensen F A Jones T T C Marcus F B King Q A Rimini F G Romero J A Sibley A G H Soldner F Tubbing B J D
JET Joint Undertaking, October 1996 (JET Papers presented at the 19th Symposium on Fusion Technology (SOFT) Lisbon, Portugal, 16-20 September 1996). p.109. Report JET-P(96)44

297. Experimental results using the JET real-time power control system.
Zornig N H Brelen H E O Browne A Browne M L Gormezano C Dobbing T How J A Jensen F A Jones T T C Marcus F B King Q A Rimini F G Romero J A Sibley A G H Soldner F Tubbing B
JET Joint Undertaking, September 1996 (JET Posters presented at the 19th Symposium on Fusion Technology (SOFT) Lisbon, Portugal, 16-20 September 1996). p.155. Report JET-P(96)45

298. Alpha-physics and measurement requirements for ITER.
Zweben S J Putvinski S Petrov M P Sadler G Tobita K Young K M
Diagnostics for Experimental Thermonuclear Fusion Reactors: Proceedings of the International Workshop on Diagnostics for ITER, August 28 - September 1, 1995, Varenna, Plenum Press, New York, 1996. p.467.

299. JET Annual Report 1995.
JET Joint Undertaking 1996. Edited and compiled by B.E.Keen and G.W.O'Hara. 97p. EUR-16872-EN-C (EUR-JET-AR 18).

300. JET Progress Report 1995.
JET Joint Undertaking 1996. Edited and compiled by B.E.Keen. 241p. EUR 16873-EN-C (EUR-JET-PR 13).